The Effect of Carbon Nanofibers on the Mechanical Performance of Composite Laminates

Paulo Sérgio Pina dos Santos

Tese para obtenção do Grau de Doutor em
Engenharia Mecânica
(3º ciclo de estudos)

Orientador: Prof. Doutor Paulo Nobre Balbis dos Reis
Co-orientador: Prof. Doutor Abílio Manuel Pereira da Silva

dezembro de 2025

Provas públicas realizadas em 11 de novembro de 2025

Composição do júri

Presidente

Doutor José Carlos Páscoa Marques
Professor Catedrático na área de Engenharia Mecânica da Universidade da Beira Interior

Vogais

Doutor Paulo Nobre Balbis dos Reis
Professor Associado da Universidade de Coimbra

Doutor Alfredo Manuel Balacó de Morais
Professor Associado da Universidade de Aveiro

Doutor Luís Miguel Marques Ferreira
Professor Titular da Universidade de Sevilha

Doutor José Luís Soares Esteves
Professor Auxiliar da Faculdade de Engenharia da Universidade do Porto

Doutor André Ferreira Costa Vieira
Professor Auxiliar da Universidade da Beira Interior

Declaração de Integridade

Eu, Paulo Sérgio Pina dos Santos, que abaixo assino, estudante com o número de inscrição D1259 de/o Engenharia Mecânica da Faculdade de Engenharia, declaro ter desenvolvido o presente trabalho e elaborado o presente texto em total consonância com o **Código de Integridades da Universidade da Beira Interior**.

Mais concretamente afirmo não ter incorrido em qualquer das variedades de Fraude Académica, e que aqui declaro conhecer, que em particular atendi à exigida referenciação de frases, extratos, imagens e outras formas de trabalho intelectual, e assumindo assim na íntegra as responsabilidades da autoria.

Universidade da Beira Interior, Covilhã 19 / 12 / 2025

Assinado por: **PAULO SÉRGIO PINA DOS SANTOS**
Num. de Identificação: 11769115
Data: 2025.12.19 11:47:25+00'00'

Dedication

This thesis is dedicated to my grandparents and to my much missed friend Bruno Lopes.

Acknowledgment

During the realization of this thesis, there were several supports, aids and stimuli that would contribute to its elaboration. I would like to express my gratitude to all the people and institutions that made this work possible, namely:

- Advisor, Professor Paulo Nobre Balbis dos Reis for believing in me and for his invaluable guidance and support during my graduate studies;
- To the scientific co-advisor, Professor Abílio Manuel Pereira da Silva for all his availability, patience, encouragement and collaboration in carrying out this research work;
- Dr. Alberto Maceiras, from the BCMaterials - Basque Center for Materials, Applications and Nanostructures, for all his support and help in the interpretation of results;
- Engineer Carlos Coelho, from the Instituto Politécnico de Abrantes, for all his support and availability in carrying out the impact tests;
- To the University of Beira Interior, in particular to the "Centre for Mechanical and Aerospace Sciences and Technologies" (C-MAST, UID/00151/2020), for hosting during the execution of the work plan and for funding participation and dissemination of the work at conferences;
- To the Department of Electromechanical Engineering of the University of Beira Interior for the support and collaboration provided throughout the execution of this thesis;
- To my wife, Ana Catarina Ramos Paiva, for always being by my side, especially in my most discouraging moments;
- To my parents, Manuel Faustino dos Santos and Maria Eugénia Amaro Caramona Pina dos Santos, for everything;
- To all my friends, for their support and friendship;
- To my family for all.

Abstract

Carbon fibre reinforced polymer composites are now widely used in various industries/sectors of activity, replacing traditional materials due to their ease of processing, excellent specific resistance, excellent fatigue behaviour, durability and low specific weight. However, the development and optimisation of these materials is faced with new challenges every day, either by optimising their properties or by changing the paradigm in terms of energy consumption. The incorporation of nanofillers significantly improves the mechanical response by reinforcing the polymer matrices and the fibre/matrix interface. This improvement is due to several synergistic mechanisms operating at the nanoscale. In addition, the dispersion of these nanoscale reinforcements within the matrix can inhibit crack propagation and increase the resistance of the material to deformation and fracture. At the fibre/matrix interface, nanofillers can bridge gaps and promote stronger adhesion, resulting in more effective load transfer between the reinforcing fibres and the surrounding polymer. The use of carbon nanofibres (CNFs) offers advantages over other nanofillers such as graphene and carbon nanotubes (CNTs), primarily due to their comparatively lower specific surface area, which facilitates the implementation of accessible and cost-effective manufacturing processes. The lower specific surface area of CNFs, in contrast to the high surface areas of graphene and CNTs, results in reduced interparticle interactions and a lower tendency to agglomerate. In this work, the manufacturing process and the fraction of CNFs that maximises mechanical response, viscoelastic behaviour and impact and fracture resistance were optimised for two commercial epoxy matrices. To assess the improvements, an extensive static mechanical characterisation was carried out, studied the viscoelastic behaviour in bending, interlaminar fracture, low-velocity impact, multi-impact and residual strength and viscoelastic behaviour after impact. The results obtained show that even with small amounts by weight of CNFs (0.5 and 0.75) added to the epoxy resins, significant benefits were obtained, for example: improvements of more than 10% in bending stress and bending stiffness of the matrices and laminates. As a result, the resistance under different strain rates and the interlaminar shear strength were higher in the additive matrices and laminates. In terms of multiple impacts and for an impact energy of 3 J, approximately 66 - 89 impacts are required to achieve full perforation for the nano-enhanced laminate with CNFs, whereas only 17 - 20 impacts are required for the control laminates.

Keywords

Nano-reinforced epoxy; Carbon nanofibres; Nano-reinforced carbon fibre laminates; Bending strain rate; Stress relaxation and creep; Interlaminar fracture; Low-velocity impact; Damage mechanism.

Resumo

Os compósitos poliméricos reforçados com fibras de carbono são hoje amplamente utilizados em diversas indústrias/sectores de atividade, substituindo os materiais tradicionais devido à sua facilidade de processamento, excelente resistência específica, excelente comportamento à fadiga, durabilidade e baixo peso específico. No entanto, o desenvolvimento e otimização destes materiais depara-se todos os dias com novos desafios, quer pela otimização das suas propriedades, quer pela alteração do paradigma em termos de consumo energético. A incorporação de nano cargas melhora significativamente a resposta mecânica através do reforço das matrizes poliméricas e da interface fibra/matriz. Esta melhoria deve-se a vários mecanismos sinérgicos que operam à nanoescala. Além disso, a dispersão destes reforços à nanoescala na matriz pode inibir a propagação de fissuras e aumentar a resistência do material à deformação e à fratura. Na interface fibra/matriz, as nano cargas podem colmatar lacunas e promover uma adesão mais forte, resultando numa transferência de carga mais eficaz entre as fibras de reforço e o polímero circundante. A utilização de nanofibras de carbono (CNFs) oferece vantagens em relação a outras nanocargas, como o grafeno e os nanotubos de carbono (CNTs), principalmente devido à sua área superficial específica comparativamente mais baixa, o que facilita a implementação de processos de fabrico acessíveis e económicos. A menor área de superfície específica das CNFs, em contraste com as elevadas áreas de superfície do grafeno e dos CNTs, resulta em interações interpartículas reduzidas e numa menor tendência para a aglomeração. Neste trabalho, o processo de fabrico e a fração de CNFs que maximiza a resposta mecânica, o comportamento viscoelástico e a resistência ao impacto e à fratura foram otimizados para duas matrizes epoxídicas comerciais. Para avaliar as melhorias, foi realizada uma extensa caraterização mecânica estática, estudado o comportamento viscoelástico em flexão, fratura interlaminar, impacto a baixa velocidade, multi-impacto e resistência residual e comportamento viscoelástico após impacto. Os resultados obtidos mostram que, mesmo com pequenas quantidades em peso de CNFs (0,5 e 0,75) adicionadas às resinas epoxídicas, foram obtidos benefícios significativos, por exemplo: melhorias de mais de 10% na tensão de flexão e rigidez à flexão das matrizes e laminados. Como resultado, a resistência a diferentes taxas de deformação e a resistência ao corte interlaminar foram maiores nas matrizes e laminados aditivados. Em termos de multi-impacto e para uma energia de impacto de 3 J, são necessários cerca de 66 - 89 impactos para obter a perfuração total do laminado nano-reforçado com CNFs, ao passo que são necessários apenas 17 - 20 impactos para os laminados de controlo.

Palavras-chave

Epóxi nano-reforçado; Nanofibras de carbono; Laminados de fibra de carbono nano-reforçados; Taxa de deformação por flexão; Relaxamento de tensões e fluência; Fratura interlaminar; Impacto de baixa velocidade; Mecanismo de dano.

Contents

List of Figures

List of Tables

Acronym List

0D	Zero-dimensional
1D	One-dimensional
2D	Two-dimensional
3D	Three-dimensional
3PB	Three-point bending
AAO	Anodic aluminium oxide
ABS	Acrylonitrile butadiene styrene
AC	Alternating current
AF	Aramid fibre
ASTM	American society for testing and materials
BBs	Buckyballs
BF	Boron fibre
BMI	Bismaleimide
BVID	Barely visible impact damage
BR	(Poly)butadiene rubber
C60	Fullerenes
CAGR	Compound annual growth rate
CC	Compliance calibration method
CCVD	Catalytic chemical vapor deposition
CCM	Compliance calibration method
CF	Carbon fibre
CFRPs	Carbon fibre reinforced polymers
CNFs	Carbon nanofibres
CNHs	Carbon nanohorns
CNOs	Carbon nano-onions
CNPs	Carbon nanoparticles
CNTs	Carbon nanotubes
Co	Cobalt
CR	(Poly)chloroprene rubber (neoprene)
CSNFs	Cup-stacked carbon nanofibres
CT	Computed tomography
CTE	Coefficient of thermal expansion
CVD	Chemical vapor deposition
DBT	Direct beam theory
DC	Direct current
DCB	Double cantilever beam
DDS	4,4'-diaminodiphenyl sulfone
DDM	4,4'-diaminodiphenyl methane
DETDA	Diethyl toluene diamine
DGEBA	Bisphenol A diglycidyl ether
DGEBF	Bisphenol F
DM	Direct dispersion method
DMA	Dynamic mechanical analysis
DMTA	Dynamic mechanical thermal analysis

DSC	Differential scanning calorimetry
DWCNTs	Double-walled carbon nanotubes
ECM	Experimental compliance method
ECNFs	Electrospun carbon nanofibres
ECNFs	Expanded carbon nanofibres
ENF	End notched flexure
EP	Epoxy resin
ESPI	Electronic speckle pattern interferometry
FC	Floating catalyst
Fe	Iron
FPCs	Fibre polymer composites
FRPs	Fibre-reinforced polymers
GF	Glass fibre
GFRPs	Glass-fibre-reinforced plastics
GNFs	Graphitic carbon nanofibres
GNPs	Graphene nanoplatelets
GP	Graphene powder
HCl	Hydrochloric acid
HDPE	High-density polyethylene
HLu	Hand lay-up process
HM	Higher modulus
HS	High strength
IDM	Indirect dispersion method
IDVARTM	Injection double vacuum-assisted resin transfer moulding
ILFT	Interlaminar fracture toughness
ILSS	Interlaminar shear strength
Jeffamine	Polypropylene ether amine
KWW	Kohlrausch-Williams-Watts
LDPE	Low-density polyethylene
LVI	Low-velocity impact
MBT	Modified beam theory method
MCs	Mesoporous carbons
MCC	Modified compliance calibration method
MDA	4,4'-methylenedianiline (diaminodiphenylmethane)
MLRFI-CM	Multilayer resin film infusion-compressive moulding
MPP	Mesophase pitch
M-FRCs	Multiscale fibre-reinforced composites
MRFs	Multiscale-reinforcement fabrics
MWCNTs	Multi-walled carbon nanotubes
NaOH	Sodium hydroxide
NDT	Non-destructive technique
NMs	Nanomaterials
NPs	Nanoparticles
O-CNFs	Oxidized carbon nanofibres
ODA	3,4'oxydianiline
PA	Polyamide
PAN	Polyacrylonitrile
PC	Polycarbonate
PE	Polyethylene

PECVD	Plasma-enhanced chemical vapor deposition
PEEK	Polyetheretherketone
PEI	Polyetherimide
PET	Polyethylene terephthalate
PF	Phenolic
PL	Polyester
PMCs	Polymer matrix composites
PMMA	Poly(methyl methacrylate)
PNCs	Polymer nanocomposites
PP	Polypropylene
PrP	Prepreg (pre-impregnated mixture of uncured resin and fabric)
PS	Polystyrene
PTFE	Polytetrafluoroethylene
PU	Polyurethane
PVC	Polyvinyl chloride
PZTs	Lead zirconate titanate
RFI	Resin film infusion
RT	Room temperature
RTM	Resin transfer moulding
SAN	Styrene/acrylonitrile
SBS	Short beam shear
SBSS	Short beam shear strength
SBT	Simple beam theory method
SCFs	Short carbon fibres
SEM	Scanning electron microscopy
SENT	Single edge notch tension
SHPB	Split Hopkinson pressure bar
Stdev	Standard deviation
SWCNTs	Single-walled carbon nanotubes
TDW	Triple-distilled water
TETA	Triethylene tetramine
TGA	Thermogravimetric analysis
TRM	Three-roll milling
UP	Unsaturated polyester
UV	Ultraviolet
VARIM	Vacuum assisted resin infusion moulding
VARTM	Vacuum assisted resin transfer moulding
VE	Vinylester resin
VGCFs	Vapor-grown carbon fibres
VGCNFs	Vapor-grown carbon nanofibres
WLu	Wet lay-up process
wt.%	Weight contents percentage

Symbology

Lowercase Latin letters

Symbol	Description	Unit
a	Delamination length	[mm]
b	Specimen width	[mm]
c	Constant	N/A
d	Constant	N/A
$\dot{e}$	Logarithm of strain rate	[s^{-1}]
h	Thickness of the specimen	[mm]
m	Correction factor	N/A
n	Constant independent of the stress	N/A
t	Time	[s]
u	Bending displacement	[mm]
w	Width	[mm]
x	Displacement rate	[mm/min]

Capital Latin letters

Symbol	Description	Unit
A	Amplitude of transient creep	N/A
B	Constant	N/A
C	Constant	N/A
D	Displacement at any moment of the test	[mm]
D_0	Displacement of the first value of the test	[mm]
E	Bending stiffness modulus (Young modulus)	[GPa]
E_a	Absorbed energy	[kJ]
E_e	Elastic energy	[kJ]
E_i	Impact energy	[kJ]
F	Constant	N/A
G_c	Critical energy release rate	[J/m^2]
G_{Ic}	Mode I critical energy release rate	[J/m^2]
$G_{Ic,\mathrm{init}}$	Fracture initiation energy in Mode I	[J/m^2]
$G_{Ic,\mathrm{prop}}$	Fracture energy propagation in Mode I	[J/m^2]
G_{IIc}	Mode II critical energy release rate	[J/m^2]
$G_{IIc,\mathrm{prop}}$	Fracture energy propagation in Mode II	[J/m^2]
H	Constant	N/A
I	Moment of inertia	[mm^4]
IBS	Impact bending stiffness	[kN/mm]
ILSS	Interlaminar shear strength	[MPa]
J	Constant	N/A
K	Constant	N/A
L	Span length	[mm]
Ls	Sample length	[mm]

N	Number of layers	N/A
N_f	Number of impacts	N/A
P	Load	[N]
P_{max}	Maximum load	[N]
S	Deflexion	[mm]
R	Correlation coefficient	N/A
T_g	Glass transition temperature	[°C]
V_T	Crosshead speed	[mm/min]
W_t	Total fracture work	kJ/mm^2

Greek letters

Symbol	Description	Unit
β	Fractional power exponent	N/A
Δ	Range	N/A
ε	Strain	[mm]
$\varepsilon(t)$	Strain at time t	[mm]
ε_0	Initial displacement	[s^{-1}]
$\dot{\varepsilon}$	Stain rate	[s^{-1}]
ε_f	Bending strain	[%]
σ	Bending strength	[MPa]
$\sigma(t)$	Stress at time t	[MPa]
σ_0	Stress at time t = 0	[MPa]
τ	Relaxation or creep time	N/A
ϕ	Relaxation	[MPa]
ΔD	Difference between initial and final bending displacement	[mm]
ΔP	Load range	[N]
Δu	Bending displacement range in the middle span for an interval in the linear region of the load versus displacement plot	[mm]
$\Delta\sigma$	Difference between initial and final bending stress	[MPa]
δ	Load point deflection	[mm]

Chapter 1

Introduction

1.1. Fundamental concepts

The concept of composite materials was not created by humanity, but by nature. An example is wood, which is a composite of cellulose fibres in a matrix of natural glue called lignin. Another is the bone consisting of a high elastic modulus mineral "fibres" of hydroxyapatite embedded in a low elastic modulus organic collagen matrix, permeated with pores filled with liquids. Composite materials began their successful path in the mid-twentieth century, and since then their development and application at an industrial level have been exponential. According to ASTM D 3878, a definition of composite material is given:

"Composite material - a substance consisting of two or more materials, insoluble in one another, which are combined to form a useful engineering material possessing certain properties not possessed by the constituents."

Nowadays, composites are widely used across industries like aerospace and aeronautics, wind produces energy, automotive, marine, transportation and extraction of oil and gas. Their choice, to the detriment of materials from other families, is a trade-off between cost and performance. For example, they are more expensive than some metals but have made their impact in the application in high-performance vehicles and racing cars, jet fighters, spacecraft and large commercial aircraft and yachts, due to the ease of processing, the high stiffness and mechanical strength and the low specific weight, in particular the polymeric matrix components. The effort to produce economically attractive composite components involves the development of innovative manufacturing techniques, advanced software tools, production technology and attractive and environmentally friendly raw materials.

Fibre polymeric composites (FPCs) are typically fabricated using a polymer matrix, such as epoxy, vinyl ester, or polyester and reinforced with fibres, organic fibres, or inorganic fibres like carbon, glass, aramid, boron, basalt and/or natural fibres. Reinforcing fibres are commercially available in the shape of, short fibres, discontinuous fibres, long continuous fibres in the form of woven fabric, chopped fibres and mat. Woven fabrics are produced by interlacing fibres in perpendicular directions and may have varied patterns. In chopped fibres and mats, the fibres are randomly distributed and aggregated with a special binder in emulsion or powder form that provides stability and must be soluble in the impregnation.

Two-dimensional (2D) composites, fabricated of unidirectional or woven plies, are the most types used in industrial applications. They are marketable in various widths, thicknesses, orientations, and mechanical strengths and their properties vary greatly depending on the fibre material, fabric weaving, fibre orientation, fibre stacking sequence, particle size, volume of short fibres, and matrix type. Although they possess substantially high strength and stiffness in the in-plane direction, they are characterized by poor transverse "out-of-plane" properties especially when subjected to impact loading [1].

In terms of matrices, these are divided into two categories: thermoplastics and thermosets, constituted by polymers in which the molecules form very rigid three-dimensional structures. The most commonly used thermosetting resins in the manufacture of composites for non-structural and semi-structural applications are unsaturated polyesters, vinylester resins, and phenolic resins. In advanced high-strength and structural composites, epoxides, bismaleimides, and polyimides are the most common choices. Epoxy matrices are low molecular weight organic liquid resins containing several epoxide groups (difunctional to polyfunctional), which are simply three-membered rings with one oxygen and two carbon atoms. After their reaction with the curing agents, they yield high-performance systems with a combination of high rigidity, solvent resistance, and elevated temperature behaviour [2].

Epoxy resins are characterized by being easily manipulated and do not require sophisticated equipment, in a system can be observed a wide variety of properties, such as: low shrinkage during cure (lowest within thermosets), good resistance to most chemicals, good adhesion to most of the fibres, good fillers, good resistance to creep and fatigue, and good electrical properties. But like any other system, they also have their disadvantages, such as: sensitivity to moisture, difficulty in combining toughness and high-temperature resistances, high coefficient of thermal expansion (CTE) as compared to other thermosets, susceptibility to ultraviolet (UV) degradation, and cost [2].

One of the reasons for the excellence of composite materials is the fact that the fibres present mechanical properties superior to those of identical materials in solid form. For example, carbon fibre reinforced polymer (CFRP) composites are light or low-density composite materials high-tech which, through the application of carbon fibre (CF), provide the strength and stiffness while the polymer provides a cohesive matrix to protect and hold the fibres together and promotes some toughness. CF provide highly directional properties, much different from the metals most used in a variety of industrial applications [3].

Meantime, the need arose to optimize the mechanical, thermal and electrical response of composite materials already applied in a focused way to various requests and with optimized properties. In 1974, Japanese scientist Norio Taniguchi was the first person to use the term "nano-technology" in her paper, which refers to the improvement of mechanical processing and precision of materials. Nowadays, it can be defined as an emerging engineering discipline that applies methods from nanoscience to create usable, marketable, and economically viable products

[4]. Nanotechnology refers to technology at the nanoscale level in which materials, devices, or systems are developed via controlling matter at the nanoscale length to stimulate the unique properties of the material at the nano-level [5]. Nanofillers for polymer composite applications are mainly classified according to their dimensions [6].

Generally, nanoparticles (NPs) can be classified into organic, including polymer NPs, dendrimers, micelles, liposomes, lipid-based NPs, and ferritin; inorganic, including metal and metal oxide NPs (i.e., silver, gold, iron oxide, zinc oxide, and silica); and carbon-based nanoparticles (CNPs), including fullerenes, graphene, and carbon nanotubes [7].

Since carbon is one of the most plentiful elements on the planet, it is found in nature as graphite, diamond, and coal in its basic form. In the last two decades, the various hybridization states of CNPs have been extensively studied. The chemical, mechanical, thermal, and electrical characteristics of various allotropic forms are closely connected to their structure and hybridization state, allowing the same material to be used for a variety of applications [8]. Carbon has around 500 allotropes of sp^2, varying from a zero- (0D) to three-dimensional (3D) structure: 0D-CNPs (i.e., fullerenes, onion-like carbon, particulate diamonds, carbon dot and graphene dot), 1D-CNPs (i.e., carbon nanotubes (CNTs), single-walled carbon nanotubes (SWCNTs), double-walled carbon nanotubes (DWCNTs) and multi-walled carbon nanotubes (MWCNTs)), CNFs, and diamond nanorods), 2D-CNPs (i.e., graphene nanoplatelets (GNPs), graphite sheets, and diamond nanoplatelets), and 3D-CNPs (i.e., diamond, graphite and hybrid assemblies).

Among all these CNPs, CNFs have been considered as promising means for enhancing mechanical properties of advanced composites, including high strength, stiffness, and improved toughness. In the last decades, numerous studies have been carried out, with promising results in the incorporation of CNFs in composite materials and thus somehow optimizing their properties.

1.2. Objectives of current research

The present work intends to increase the mechanical strength of carbon/epoxy laminates nano-enhanced with CNFs, thus expanding the field of application of these materials.

In light of the above, the following questions should be asked and answered throughout the development of the work:

- Taking the hand lay-up technique as a starting point, a low cost technique that is easily transferable to industry, can various variables such as mixer speed, CNFs dispersion time, vacuum time and ultrasonic bath application, both in the matrix and in the laminate after manufacture, influence the final mechanical properties of these materials? What is the optimum weight percentage (wt.%) of CNFs to be added to two epoxy matrices with different properties to improve both the mechanical properties (quasi-static and viscoelastic) of the matrices and the carbon laminates?

- Regardless of the epoxy matrix, is the amount of CNFs added to maximise mechanical and viscoelastic properties always the same?

- After applying the optimum percentage by weight of CNFs, either in the matrices or in the carbon laminates, how much was improved in terms of quasi-static properties and viscoelastic behaviour?

- How do these new materials nano-enhanced with CNFs behave in terms of mechanical strength and viscoelastic behaviour compared to the neat matrices and control laminates? In the long term, does the use of CNFs extend the service life of matrices and carbon laminates?

- What is the interlaminar shear strength (ILSS) response of nano-enhanced laminates when exposed to aggressive environments, such as hydrochloric acid (HCl), sodium hydroxide (NaOH), water and temperature?

- Is it possible to estimate its mechanical properties by means of mathematical and predictive models, which have already been extensively discussed in the bibliography?

- Will the Mode I and Mode II interlaminar fracture toughness (ILFT) of carbon laminates nano-enhanced with CNFs improve compared to control laminates?

- In terms of low-velocity impact (LVI), what is the response and relationship between the percentage of nano-reinforcement of CNFs added to the epoxy matrix in terms of impact properties such as impact energy, impact load, elastic recuperation and absorbed energy?

- Does the addition of CNFs to epoxy matrices improve the multi-impact performance of carbon laminates?

- What is the residual strength after LVI in carbon-epoxy laminates? And what is the stress relaxation and creep behaviour compared to the control laminate?

1.3. Mechanical characterization

In this study an extensive experimental work was carried out, developed to compare the benefits of enhancing epoxy matrices and carbon laminates with different of weight percentages of CNFs, compared to respective neat matrices and control laminates. Initially, a quasi-static characterization was performed, to identify the composite mechanical properties and the damage and rupture mechanisms that occur during loading, first of the matrices and then of the nano-enhanced laminates, to determine the optimal weight percentage in terms of CNFs. Quasi-static characterization was adopted because it allows for determining the displacements, stresses, strains, and forces in structures or components caused by loads that do not induce significant inertia and damping effects. It was studied the behaviour of materials when subjected to various viscoelastic behaviour and based on the experimental results, applied predictive models that give

us an indication of the long-term behaviour with great precision. It is known how sensitive composite materials are to ILSS and impact, especially LVI, mechanical characterization that was also not forgotten, in order to understand the behaviour of laminates when requested by a quasi-static load and simulate the impact of foreign objects, as well as the study of Mode I and Mode II interlaminar fracture in order to determine the respective critical rates of energy release. Figure 1.1 summarizes the mechanical characterization performed throughout the work.

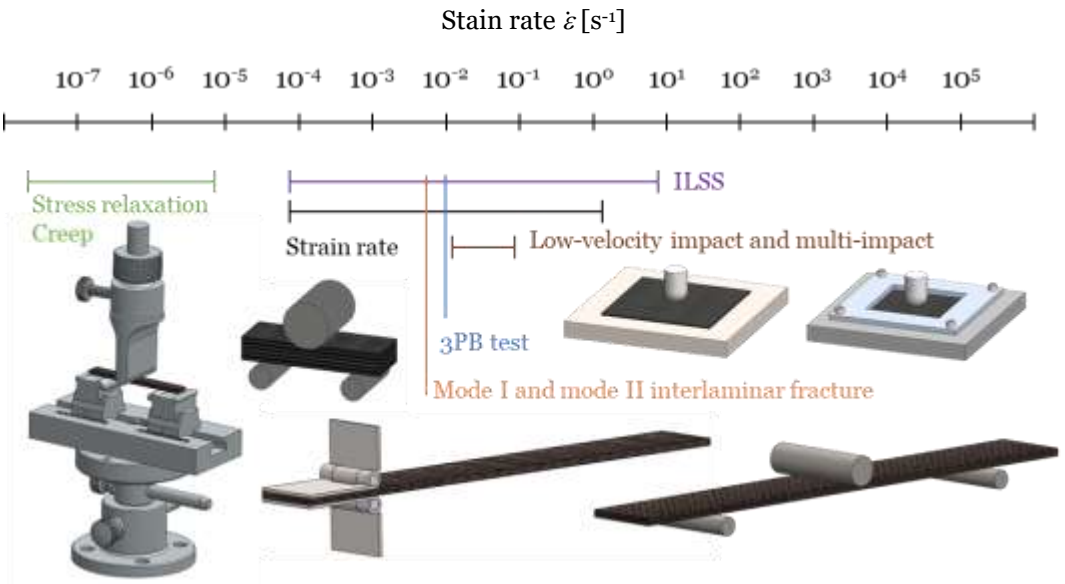

Figure 1.1: Relevant experiments and respective loading.

A comprehensive mechanical characterization allows us to understand how beneficial the addition of CNFs in an epoxy matrix or in a CFRP laminate is in improving the mechanical properties. In this regard, the following tests were carried out and with the following objectives:

- The three-point bending (3PB) test is applied in the mechanical characterization of brittle materials to determine the stress and deflection at failure, as is the case with epoxy matrices and CFRP composites. The test measures key parameters, including bending strength, bending modulus, and strain at failure, which are essential for characterizing the bending behaviour and mechanical performance of the composite material. A great advantage is the use of specimens with simple geometry and easy production. This technique consists of supporting the sample between two points spaced on one length (L) and at a controlled and constant speed applying a bending load (P) in the centre of it. The application of 3PB tests has the following advantages: bending strength determination, bending modulus measurement, standardized testing and material characterization. In engineering, the 3PB tests are widely used to assess the bending properties of FPCs for structural engineering applications in the most varied areas and industries.

- CFRP composites exhibit intense viscoelastic behaviour, even under stable and controlled environmental conditions. When a CFRP is mechanically requested, part of the energy is dissipated in the form of heat or acoustic emission and another part is stored in the form of elastic

energy. Key aspects of the viscoelastic behaviour of CFRP composites include time-dependent deformation, stress relaxation, temperature sensitivity, loading rate dependency, frequency dependency and time-dependent recovery. Understanding the viscoelastic behaviour of composites is crucial for various engineering applications, particularly in situations where long-term durability, creep resistance, and time-dependent deformation are critical considerations. The knowledge of viscoelastic properties helps in predicting the material's behaviour over its service life and aids in the design of structures that can withstand time-dependent loads effectively. Engineers employ various experimental and analytical techniques, such as strain rate, creep and stress relaxation tests, to characterize and predict the viscoelastic behaviour of CFRP composites. This understanding contributes to the safe and efficient utilization of CFRP composites in a wide range of industries.

- ILSS is a critical mechanical property of CFRP composites that measures the resistance of the material to interlaminar shear forces. It is an important parameter that characterizes the bond strength between adjacent fibre layers and the polymer matrix in a composite laminate. ILSS testing involves applying a shear force perpendicular to the fibre orientation, causing the layers to slide relative to each other. The purpose of ILSS testing in CFRP composites from a practical point of view includes structural integrity, delamination resistance, design and optimization, material selection and quality control. Some practical applications where ILSS testing is essential include the aerospace industry (in aircraft components, ensuring the reliability of composite structures subjected to various loads), the automotive industry (is critical in automotive parts, ensuring structural integrity and safety), the marine industry (ensuring the ability of the composite to withstand water-induced stresses and environmental conditions), wind energy production (is crucial for evaluating the material's resistance to fatigue and cyclic loading) and the construction industry (ensuring its long-term performance and durability). Overall, ILSS testing plays a vital role in ensuring the reliability, safety, and performance of FPCs in a wide range of practical applications across different industries.

- ILFT is a crucial mechanical property of laminated composites that characterizes the material's resistance to crack propagation between adjacent layers of fibres and the polymer matrix. CFRP composites manufacture with high strength continuous fibres in a ductile or brittle matrix material are susceptible to delamination. Geometries such as free edge, notch (hole), ply drop, bonded joint, bolted joint, T-joint, buckling and impact, may give rise to the initiation of delamination if they exceed the through-thickness strength. The ILFT of laminated composites is normally expressed in terms of the critical energy release rate, which is usually represented by the symbol G_C. For Mode I, the most commonly used test is the double cantilever beam (DCB) specimen. The purpose of the test is to determine the opening mode ILFT G_{IC} of continuous fibre composites with a polymer matrix. For Mode II the method that has received the most attention is the three-point loaded end notched flexure (ENF) test. The purpose of the ENF specimen is to determine the critical strain energy release rate in pure Mode II loading, G_{IIC}, of composites. The ILFT test provides valuable information on the ability of the composite to resist crack propagation

and resist delamination, which are critical factors in the structural integrity and reliability of CFRP laminates. The purpose of ILFT testing of laminated composites from a practical point of view includes structural integrity, damage tolerance, delamination resistance, material selection and failure analysis. ILFT testing is applicable in various industries where laminated composites are used and where it is necessary to ensure the safety and reliability of critical components, components that are subjected to cyclic loading and environmental stresses, and where it is necessary to evaluate their resistance to fatigue and crack growth, to ensure durability and resistance to induced stresses and, is essential for assessing crashworthiness and impact resistance.

- Being the impact, in particular the low-velocity one, the major impact-induced damage mode not visible, which can occur at any time since the construction and during the service life of the CFRP composite, and it is responsible for the reduction of the service life and even the collapse of a structure. The LVI is a serious threat to their use in real life applications as it causes barely visible impact damage (BVID) and it is essential to understand the influence of this mode of occurrence. The impact energy is generally absorbed, in the form of damage, delamination between different oriented layers, matrix cracking, fibre breakage and fibre matrix debonding, leaving only small indentations on the impacted surface, resulting in the interaction of the several damage types without exterior signs detectable by visual inspection, it is necessary to resort to non-destructive techniques (NDT) to detect the same damages, such as ultrasonic C-scan techniques, electronic speckle pattern interferometry (ESPI), Shearography System and X-ray computed tomography (CT) to quantify the level of induced damage. On the other hand, the multi-impact can occur at the same point or on the same composite structure but at different locations and with the same energy (velocity) or happen with different energies (velocity). It is characterized by consecutive impacts on the same material specimen or part to be tested and makes it possible to predict its fatigue behaviour and residual strength when subjected to multiple impacts. The purpose of conducting low-velocity impact and multi-impact testing of laminated composites from a practical point of view includes damage assessment, structural design and optimization, material selection, safety and certification, damage tolerance assessment and failure analysis.

1.4. Thesis organization

According to the proposed objectives and the framework presented, this thesis is organized into eleven chapters, as shown in Figure 1.2:

Chapter 1 *Introduction*; The introductory chapter, includes the framing and motivation for writing this thesis, the objectives of the study and a general framework to quickly give an overview of the fabrication and characterization work of the matrices and carbon laminates nano-enhanced produced in the laboratory.

Chapter 2 *Mechanical behaviour of the epoxy polymer composites reinforced with carbon nanofibres*; Emphasis is given to CNFs pointing out perfectly consolidated application areas and

possible future applications. Its structure, the main fabrication techniques to produce CNFs, the main synthesis of polymer nanocomposites with CNFs and techniques applied in the manufacture of nano-enhanced epoxy composites are described. An intensive review of work already carried out using similar materials and the improvements achieved, summarised in tables, is presented. For the qualitative methodological analysis, the following scientific databases will be consulted: *Scopus*, *Science Direct* and *Institute of Electrical and Electronics Engineers (IEEE)*.

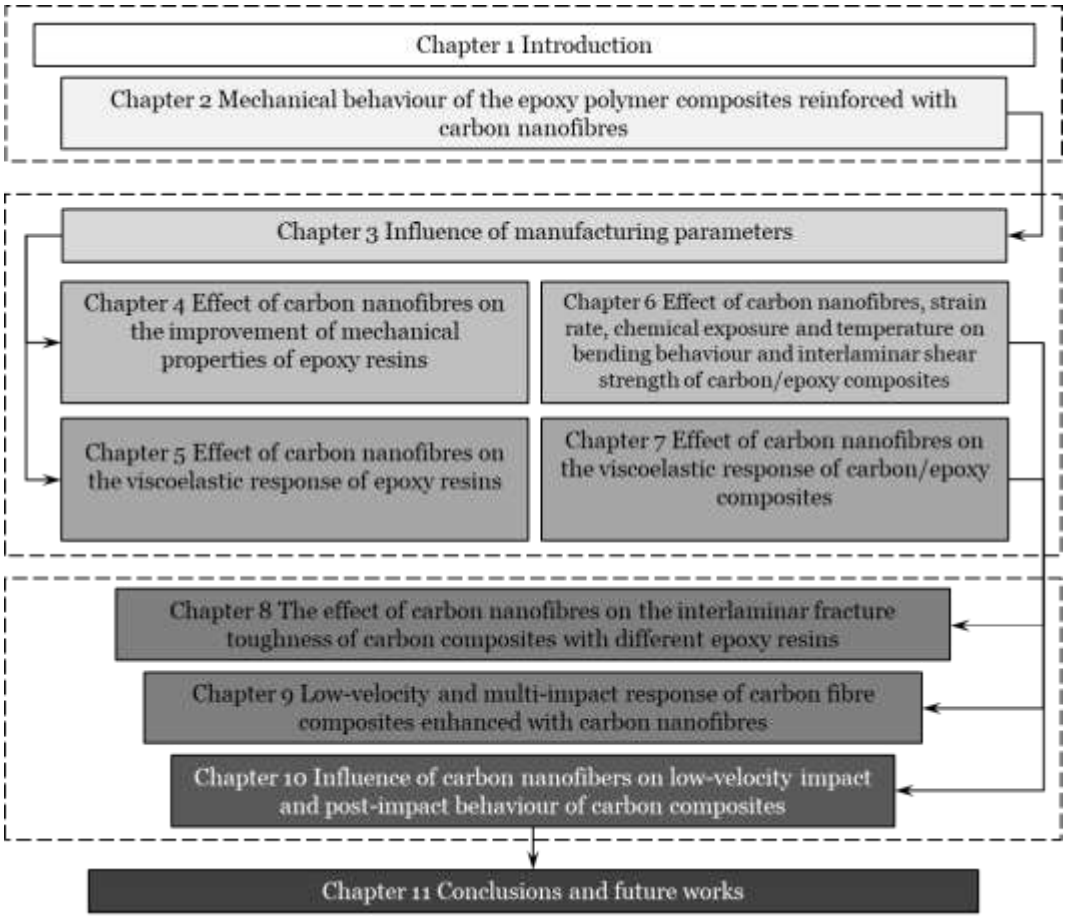

Figure 1.2: Diagram of the structure of this thesis.

Chapter 3 *Influence of manufacturing parameters*; In this chapter, it is addressed the influence of manufacturing parameters on the mechanical properties of nano-reinforced CFRP by CNFs. For this purpose, the manufacturing process is studied and variables like the mixer rotation speed, the dispersion time of the nanoparticles and the vacuum time applied to the system were analysed in detail, with the objective, and with the proposed materials for the accomplishment of the work, to implement a simple and optimized manufacturing process, easy to apply in an industrial environment and defect-free composites.

Chapter 4 *Effect of carbon nanofibres on the improvement of mechanical properties of epoxy resins*; This chapter compares the improvements, in terms of quasi-static and viscoelastic bending properties, of two epoxy resins reinforced with different wt.% of CNFs. These epoxy resins have different viscosities, and weight contents between 0.25% and 1% of CNFs that were used to

achieve the maximum mechanical properties. The sensitivity to strain rate and the viscoelastic behaviour, stress relaxation and creep, were then analysed for the best configurations obtained and compared with the corresponding neat epoxy resins.

Chapter 5 *Effect of carbon nanofibres on the viscoelastic response of epoxy resins;* Taking as starting points the nano-enhanced matrices with their respective weight percentages of CNFs and the quasi-static bending properties, the viscoelastic behaviour of each matrix was studied in detail and compared with the respective neat epoxy matrix. Stress relaxation tests were performed applying different bending stresses and creep tests applying different initial displacements. Applying predictive models, their predisposition to predict, from short-term mechanical tests, the viscoelastic behaviour of resins when subjected to unknown bending stresses and long periods was studied.

Chapter 6 *Effect of carbon nanofibres, strain rate, chemical exposure and temperature on bending behaviour and interlaminar shear strength of carbon/epoxy composites*; As in chapter 4, are studied, the quasi-static bending properties, of composite laminates manufactured in the laboratory by the technique hand lay-up technique applying the two epoxy resins reinforced with different wt.% of CNFs (i.e., 0.25, 0.5, 0.75 and 1). Subsequently, for the best configurations obtained, was studied and the sensitivity response to the strain rate and the effect of the ILSS behaviour from aggressive environments and compared with the respective control laminates.

Chapter 7 *Effect of carbon nanofibres on the viscoelastic response of carbon/epoxy composites*; From the quasi-static bending properties of the previous chapter, the viscoelastic behaviour of each composite laminate (control and nano-enhanced) was studied in detail. The influence of the carbon fibres used as reinforcement on the viscoelastic behaviour and the results obtained by mechanical tests of stress relaxation and creep were compared with the respective neat matrices. Were performed, stress relaxation tests were performed applying different bending stresses and creep tests applying different initial displacements. Predictive models were also applied to study their ability to predict, from short-term mechanical tests, the viscoelastic behaviour of the laminates over time when subjected to unknown bending stresses and long periods of time.

Chapter 8 *The effect of carbon nanofibres on the interlaminar fracture toughness of carbon composites with different epoxy resin*; One of the problems of the composites manufactured with two-dimensional (2D) smooth tissues (reinforcements) is the propensity to delamination when subjected to bending, shear, impact loads. To study the improvement of Mode I and Mode II ILFT values of nano-enhanced laminates with different wt.% CNFs, double cantilever beam (DCB) tests and end-notch flexure (ENF) tests were prepared to study their toughening mechanism.

Chapter 9 *Low-velocity and multi-impact response of carbon fibre composites enhanced with carbon nanofibres*; It is studied the impact response of CFRP laminates whose matrix has been modified with different of wt.% of CNFs on the LVI response, carried out drop-weight impact with a hemispherical impactor end, with five impact energy levels (i.e., 1 J, 3 J, 5 J, 7 J and 9 J). Impact

response of the different laminates under study was analysed in terms of peak load, absorbed energy, time and deflection at peak load. In a second part of this chapter, the damage tolerance of a nano-enhanced epoxy matrix to low-velocity multiple impacts is investigated. Low velocity multiple impact tests were carried out at different energy levels.

Chapter 10 *Influence of carbon nanofibres on low-velocity impact and post-impact behaviour of carbon composites*; For the Sicomin matrix, it was studied the impact response of CFRP laminates whose matrix has been modified with 0.75 wt.% CNFs. Five impact energies were considered in the study, carried out by drop-weight impact with a hemispherical impactor end. The impact response of the different laminates under study was analysed in terms of peak load, absorbed energy, time and deflection at peak load and the post-impact properties, such as, residual strength, the stress relaxation and in the creep behaviour, were also considered. The post-impact structural integrity and viscoelastic behaviour of the impacted laminates were evaluated by 3PB tests.

Chapter 11 *Conclusions and future works*; At the end, the main conclusions of the entire work are presented and a list of possible future works to be developed is presented.

Bibliography

[1] Saleh MN, El-Dessouky HM, Saeedifar M, De Freitas ST, Scaife RJ, Zarouchas D. Compression after multiple low velocity impacts of NCF, 2D and 3D woven composites. Composites Part A: Applied Science and Manufacturing 2019;125:105576. https://doi.org/10.1016/j.compositesa.2019.105576.

[2] Ghamarian N, Hanim MAA, Penjumras P, Majid DLA. Effect of Fiber Orientation on the Mechanical Properties of Laminated Polymer Composites. Encyclopedia of Materials: Composites, Elsevier; 2016, p. 746–65. https://doi.org/10.1016/B978-0-12-803581-8.04083-2.

[3] Fekete JR, Hall JN. Design of auto body. Automotive Steels, Elsevier; 2017, p. 1–18. https://doi.org/10.1016/B978-0-08-100638-2.00001-8.

[4] Barhoum A, Rasouli R, Yousefzadeh M, Rahier H, Bechelany M. Nanofiber Technologies: History and Development. Handbook of Nanofibers, Cham: Springer International Publishing; 2019, p. 3–43. https://doi.org/10.1007/978-3-319-53655-2_54.

[5] Baig N, Kammakakam I, Falath W. Nanomaterials: a review of synthesis methods, properties, recent progress, and challenges. Materials Advances 2021;2:1821–71. https://doi.org/10.1039/D0MA00807A.

[6] Akpan EI, Shen X, Wetzel B, Friedrich K. Design and Synthesis of Polymer Nanocomposites. Polymer Composites with Functionalized Nanoparticles, Elsevier; 2019, p. 47–83. https://doi.org/10.1016/B978-0-12-814064-2.00002-0.

[7] Spirescu VA, Chircov C, Grumezescu AM, Vasile B Ştefan, Andronescu E. Inorganic Nanoparticles and Composite Films for Antimicrobial Therapies. International Journal of Molecular Sciences 2021;22:4595. https://doi.org/10.3390/ijms22094595.

[8] Gaur M, Misra C, Yadav AB, Swaroop S, Maolmhuaidh FÓ, Bechelany M, et al. Biomedical Applications of Carbon Nanomaterials: Fullerenes, Quantum Dots, Nanotubes, Nanofibers, and Graphene. Materials 2021;14:5978. https://doi.org/10.3390/ma14205978.

Chapter 2

Mechanical behaviour of the epoxy polymer composites reinforced with carbon nanofibres[1]

2.1. Introduction

If a composite is defined as a combination of two or more materials that remain in separate phases, with one being the matrix and the other as the reinforcement, then nanocomposites can be defined as composites reinforced with a phase that possesses at least one dimension smaller than 100 nm. This subfamily of composites can be further subdivided into particle-reinforced and fibre-reinforced composites, as the interaction mechanisms between the reinforcement and the matrix are different at the nanoscale and result in significantly improved properties compared to those anticipated by scaling laws [1].

Composite materials have existed in nature since ancient times. In the terminology of modern mechanics, the earliest man-made composites date back to 4000 BC. Throughout history, the development and evolution of composite materials have aimed to meet human needs and fulfil increasingly demanding applications, in terms of mechanical and electrical stresses. Until recently, the strongest composite materials available for structural applications consisted of small diameter fibbers (in the range of 5 to 40 μm). These fibres were enhanced by their reduced defect size, fibre orientation aligned with the load direction, and reinforcement hybridization (woven or nonwoven textiles).

However, the application of composite materials faces several challenges, to highlight, their viscoelastic behaviour even at room temperature (RT), the negligible compressive strength of fibbers due to buckling, rapid strength degradation due to the generation of surface defects by fretting, environmental attack, permeability and the low-velocity impact (LVI) of foreign objects.

Recently, significant improvements in the properties of structural composites have been achieved by controlling the microstructure and properties at the μm and nm levels. This progress was achieved through the introduction of nanofillers, aiming to overcome the limitations mentioned

[1] Based on the work published in the Polymers journal, Santos, P.; Silva, A.P.; Reis, P.N.B. The Effect of Carbon Nanofibers on the Mechanical Performance of Epoxy-Based Composites: A Review. *Polymers* **2024**, *16*(15), 2152; https://doi.org/10.3390/polym16152152

[2]. In response to concerns regarding environmental conservation and sustainability, notable developments have been observed in the field of green composites, particularly through the advancement of bio composites produced from biofibres and biopolymers [3]. In addition, recycling and reusing are now widely recognized by both the scientific and industrial communities due to the increasing demand and the need to close the life cycle loop of composite materials, rather than resorting to landfill disposal.

Composite materials offer numerous advantages over traditional materials such as metals or polymers. They are lightweight and offer improved mechanical performance, increased specific strength and fatigue (durability). They contribute to energy efficiency through weight reduction, excellent energy absorption, and thermal insulation. Furthermore, they have high thermal stability, low thermal expansion, and efficient heat dissipation. Additionally, they can be adapted to specific chemical properties to obtain improved properties, such as resistance to environmental degradation, and offer versatility in applications, with fewer parts, manufacturing techniques, and design flexibility. These properties make composites highly beneficial in a wide range of industries [4,5].

Synthetic polymers are defined as polymers that are artificially produced in laboratories and are typically derived from petroleum oil [6]. Currently, in terms of volumetric output, the production of synthetic polymers exceeds the world production of crude steel (1,958.45 billion metric tons in 2021). This is primarily due to their lightweight nature, insulating properties for applications in the field of electricity conduction and thermal insulation, wide range of properties covering soft packaging materials to fibres stronger than steel, and their relative ease of processing [7]. Synthetic polymers can be classified into three main categories: thermoplastics, thermosets and elastomers.

The thermosets subfamily includes epoxy (EP), vinylester (VE), phenolic (PF), polyester (PL), and polyurethane resins (PU). The thermoplastics subfamily includes, among others, high-density polyethylene (HDPE), low-density polyethylene (LDPE), polyethylene terephthalate (PET), polypropylene (PP), polystyrene (PS), polyetheretherketone (PEEK), polyvinyl chloride (PVC), polyamide (PA), poly(methyl methacrylate) (PMMA), acrylonitrile butadiene styrene (ABS) and styrene/acrylonitrile (SAN) [8]. The elastomers subfamily includes polyisoprene, polybutadiene rubber (BR), polychloroprene rubber (CR) and polysiloxane (Silicone).

Since their discovery, polymers have greatly simplified life in numerous ways, and it is currently difficult to imagine a world without this family of materials. Engineers leverage their advantages and properties, such as flexibility, corrosion resistance, transparency, ease of construction, and, importantly, lightweight nature, to promote their application across a wide range, from simple objects to complex structures. In recent decades, there has been a noticeable shift from traditional materials to fibre polymer composites (FPCs) in applications requiring high strength and lightness [9]. Structural composites typically consist of a quasi-isotropic layer stack, and their strength and stiffness exhibit time-dependent behaviour due to the viscoelastic nature of the

polymers matrix [10]. These properties, which are already significant, can be further optimized through the addition of nanofillers. Even in small amounts, these nanofillers can significantly improve the mechanical, thermal, and electrical properties of the resulting polymer nanocomposites (PNCs) [11].

In a composite, the matrix acts as a binder that holds the reinforcement together and transfers loads between the reinforcement components. In the case of polymeric composites, epoxy matrices are a versatile class characterized by the presence of two or more oxirane rings or epoxy groups within their molecular structure [12,13]. They exhibit excellent properties, such as strong adhesion to a wide range of substrates, favourable mechanical properties (high strength, temperature resistance, durability, and resistance to extreme environmental conditions), dimensional stability, and design versatility, making them highly versatile for applications in structural materials and coatings. Despite these highly regarded properties, epoxy matrices have some limitations, such as very high viscosity, moisture absorption, low toughness, flammability, intrinsic brittleness after curing, poor fatigue strength, and low fracture energy, especially in high-end applications where better impact resistance and toughness are required. Another disadvantage of epoxy thermosets is that their stiffness and strength decrease significantly in the region of the glass transition temperature [14–16]. Their hardness and brittleness render them susceptible to cracking, which compromises their utility as structural adhesives, an area where epoxy matrices find significant application [17].

Among the various polymeric materials, epoxy resins are a versatile class of polymers characterized by the presence of two or more oxirane rings or epoxy groups within their molecular structure [12,13]. Aliphatic, aromatic amines, imides, and anhydrides are commonly available curing agents for epoxy resin. Among these, amine curing agents are the most widely used due to better understanding and control of epoxy-amine reactions [18]. The chemical structures of some commonly used curing agents are as follows: triethylene tetramine (TETA), 4,4´-diaminodiphenyl methane (DDM), 4,4`-diaminodiphenyl sulfone (DDS), diethyl toluene diamine (DETDA), and polypropylene ether amine (Jeffamine) [19]. The main physical, mechanical, and thermal properties of the polymers commonly used in composite manufacturing are provided in Table 2.1.

Epoxy matrices generally have higher modulus and strength than thermoplastics such as polyethylene (PE), polypropylene (PP), and polycarbonate (PC). This makes them more suitable for high-load applications. They maintain their mechanical properties at higher temperatures (120 °C) than most thermoplastics, which tend to soften and lose strength with heat [20]. They typically have higher surface hardness and abrasion resistance than thermoplastics, contributing to their durability in demanding applications. For example, epoxy matrices exhibit superior creep resistance compared to thermoplastics, maintain their shape and structural integrity over long periods of continuous loading, and are less susceptible to environmental stress cracking and UV degradation than many thermoplastics.

Table 2.1: Key properties of polymers used as matrix in composite materials.

Property	EP	VE	PF	PL	PP	PS	PEEK
Viscosity at 25°C, μ [mPa×s]	12000-13000[b]	200-700[e]	300[f]	250-350[b]	-	-	-
Density, ρ (×10³ [kg/m³])	1.1-1.4[a]	1.1-1.2[a]	1.2-1.5[a]	1.1-1.5[a]	0.9-0.91[a]	1,05[a]	1.32[a]
Young modulus, E [GPa]	2-5[a]	3.5-4[a]	2.5-4.5[a]	2-4.5[a]	1-1.5[a]	3.1-3.3[a]	3.7[a]
Tensile strength [MPa]	50-100[a]	65-85[a]	30-60[a]	40-90[a]	25-35[a]	35-65[a]	100[a]
Elongation at max. load [%]	2-8[a]	3-6[a]	1-3[a]	2-2.5[a]	20/800[a]	1.5/4[a]	50/300[a]
Bending strength [MPa]	60-120[b, c]	40-1310[d]	74.0-92.0[d]	53.8-265[d]	20.0-180[d]	7.35-106[d]	86.2-380[d]
Bending modulus [GPa]	2.8-3.4[c]	3.45-77.9[d]	8.60-10.5[d]	0.359-16.0[d]	0.0260-10.0[d]	1.58-106[d]	2.48-24.0[d]
Elongation at max. load [%]	3.9-6.2[c]	-	-	-	-	-	3.0-7.0[d]
Charpy impact strength [kJ/m²]	26-97[c]	-	-	5.0-45.0[d]	3.0[d]	6.0-17.0[d]	133-256[d]
Maximum service temperature in continuous, T [°C]	120[a]	98-300[d]	140[a]	100[a]	90[a]	80[a]	250[a]
Glass transition temperature, T_g [°C]	70-170[a]	118-200[d]	170-270[a]	150-200[a]	0-20[a]	90-100[a]	145[a]
Cost [€/kg]	3-20[a]	2-4[a]	1-2[a]	1[a]	1.5-2.8[a]	1.6-2.8[a]	70-80[a]

[a][20], [b][21], [c][22], [d][23], [e][24], [f][25]

Epoxies are widely used as adhesives because of their excellent bond strength to a wide variety of substrates, which is generally superior to thermoplastic adhesives. In terms of cost, epoxy matrices are about four times the price of polyester matrices and about twice the price of vinyl ester matrices. In summary, Table 2.2 compares the epoxy matrix with other common thermosetting and thermoplastic matrices used in the manufacture of composites for various performance criteria.

Regarding the type of fibre reinforcement, various options can be utilized. These include natural fibres, from a variety of sources, have garnered interest from researchers and industry, such as linen, hemp, jute, and cotton (plants), wool and silk (animals), and asbestos (minerals). Nevertheless, specific categories of natural fibres have faced prohibition in numerous nations owing to health-related apprehensions, asbestos, in particular, has been associated with the development of cancer [26].

Inorganic fibres, such as glass fibre (GF), carbon fibre (CF), aramid fibre (AF), and boron fibre (BF), are widely employed due to their favourable properties. The GF are the most popular due to their unique mechanical properties and low production cost. However, using synthetic fibres can harm human health and the environment, as they are associated with problems such as skin allergies and lung cancer [26]. Ceramic fibres are mainly two types, ceramic oxide fibres and ceramic nonoxide fibres. Ceramic oxide fibres, mostly consist of alumina (Al_2O_3) and alumina-silica (Al_2O_3-SiO_2) mixtures due to their high melting points, are generally used for high-temperature applications. Production of nonoxide fibres is difficult due to their high melting points and resistance to densification. Oxidation resistance tends to be their main deficiency. These ceramic fibres are either fine or thick diameter, such as, silicon carbide based fibres, SiCN

based fibres and boron-based fibres [27]. Finally, the metal fibres can be produced from conductive metals such as ferrous alloys, nickel, stainless steel, titanium, aluminium and copper. Although highly conductive, metallic fibres are expensive, brittle and heavier than most textile fibres, making it difficult to produce homogeneous blends. These can be applied in composite materials in different ways, fibres with conductive metals, semiconducting metal oxides and metal salts [28].

Table 2.2: Comparison of epoxy matrix with other common thermosetting and thermoplastic matrices on various performance criteria [20,29].

Property	Epoxy Matrix	Other Thermosets Matrix	Thermoplastic Matrix
Mechanical strength	High tensile and compressive strength	Moderate to high (e.g., polyesters: moderate, phenolics: high)	Generally lower than thermosets (varies by type, e.g., nylon: high, polyvinyl chloride (PVC): moderate)
Bending strength	High	Moderate to high	Varies, often lower than epoxies
Modulus of elasticity	High	Varies (phenolics and vinyl esters: high)	Lower than thermosets
Toughness	High, good fracture toughness	Moderate to high	Varies (e.g., acrylonitrile butadiene styrene (ABS): high, PE: moderate)
Adhesion	Excellent, bonds well to many substrates	Varies (polyesters: moderate, phenolics: high)	Generally lower, requires surface treatment
Chemical resistance	Excellent	Varies (phenolics: high, polyesters: moderate)	Good for specific chemicals (e.g., Polytetrafluoroethylene (PTFE): excellent)
Thermal stability	High, good heat resistance	Moderate to high (phenolics: high, polyesters: moderate)	Lower than thermosets (e.g., polyether ether ketone (PEEK): high, PP: low)
Electrical insulation	Excellent	Moderate to excellent (phenolics: high, polyesters: moderate)	Varies, some are good insulators (e.g., PE: excellent)
Thermal conductivity	Moderate, can be enhanced with fillers	Generally low, can be enhanced with fillers	Varies, some are low (e.g., PE: low)
Shrinkage	Low during curing	Moderate (polyesters: high, phenolics: low)	Low (due to lack of curing)
Dimensional stability	High	Moderate to high	Varies, often lower than epoxies
Water absorption	Low	Varies (polyesters: moderate, phenolics: low)	Varies (e.g., nylon: high, PP: low)
Ease of processing	Moderate, requires precise mixing and curing	Generally easier (polyesters: easy, phenolics: more complex)	High, often simpler processing methods
Recyclability	Not recyclable	Not recyclable	Recyclable
Cost	Moderate to high	Generally lower than epoxies	Varies, generally lower than thermosets

Comparing the typical properties of the three main types of structural fibres, namely CF, GF, and AF, it is concluded that, the density of CF is lower than that of GF, but is higher than that of AF, 1.76, 2.46 and 1.45 g/cm^3, respectively. The tensile modulus and the specific tensile modulus of

CF are higher than those of GF and AF. The tensile modulus of CF is much higher than GF or AF 230, 86.9 and 112 GPa, respectively. The tensile strength of CF is higher than AF but lower than GF, 3.53, 3.00, and 4.89, respectively. The compressive strength of CF is lower than that of GF, 0.87 and 1.6 GPa. For CF, the tensile strength is much higher than the compressive strength. The tensile strain at failure (the ductility) is considerably lower for CF than for GF or AF. The coefficient of thermal expansion (CTE) along the fibre axis is negative for CF and AF, but is positive for GF, -0.41, -6, and 2.9, $\times 10^{-6}$ K^{-1}, respectively. The negative CTE value of CF is due to the carbon in-plane interatomic bond distance increasing as the temperature increases [30].

Primarily due to their cost/properties ratio, carbon fibres are currently the most commonly used material in the production of carbon fibre reinforced polymers (CFRPs). Carbon fibres can be derived from polymeric precursor materials such as polyacrylonitrile (PAN), cellulose, pitch, and polyvinyl chloride. The preparation process typically involves three steps: the stabilization of precursor fibres in air (at 300 °C), carbonization at 1100 °C, and subsequent graphitization (>2500 °C). Fibres that undergo only the first two steps are commonly referred to as carbon fibres, while fibres that undergo all three steps are referred to as graphite fibres [31]. The predominant type of carbon fibres is PAN-based, as they exhibit high strength (HS) and good modulus properties. Other types of carbon fibres can be produced using pitch-based precursors, which offer higher modulus (HM) but lower strength [32–34].

Due to their unique combination of low density, high stiffness, strength, and toughness, the utilization of fibre-reinforced polymers (FRPs) composites as structural materials has steadily increased over the past 50 years. On the other hand, the global carbon fibre market was valued at USD 2.99 billion in 2022 and is projected to reach approximately USD 5.83 billion by 2032, with a compound annual growth rate (CAGR) of 6.9% between 2023 and 2032 [35]. The rapid growth of the wind turbine sector (30 kt to estimated 190–200 kt in 2030) and the demand for low-cost carbon fibres in pressure vessels (180 kt in 2030) and automotive applications (3–4 million fuel cell automotive vehicles globally in 2030) present significant research and development opportunities. CFRP composites are being used in various industries due to their fast processing and recyclability, while additive manufacturing techniques enable the production of complex carbon fibre composites. Large tow PAN fibres are replacing aerospace precursor fibres, catering to the needs of wind turbine blades, automotive, and rail transport. The application of carbon fibres in functional composites, such as C/C composites and fuel cells, is also expanding (50–60 kt in 2030). Despite challenges, recycled carbon fibres show promise in terms of price-performance ratio and circular economy benefits [36].

The properties of carbon fibres display a broad spectrum of variations determined by their structural attributes. Carbon fibres present numerous favourable traits, encompassing low density, high tensile modulus, and strength, a low coefficient of thermal expansion, outstanding thermal stability reaching up to 3000 °C in oxygen-depleted environments, exceptional resistance to creep, chemical stability (particularly in potent acids), biocompatibility, high thermal

conductivity, low electrical resistivity, consistent availability, and a decreasing cost trend over time. Nonetheless, carbon fibres do entail certain drawbacks, including anisotropic behaviour between the axial and transverse directions, limited strain-to-failure, lower compressive strength relative to tensile strength, susceptibility to oxidation above 400 °C in the presence of air, and vulnerability to alkaline-induced catalytic oxidation. These properties are interconnected, and specific trends often correlate, such as an augmented tensile modulus alongside reduced strain-to-failure and compressive strength. [30].

The success of FRP as a structural material can be attributed to its hierarchical structure, which consists of three levels of organization: ply, laminate, and structural element [2]. However, due to the anisotropic and heterogeneous nature of composites, several failure modes can occur. These include intra-ply cracking, interlaminar matrix delamination, and fibre failure, as depicted in Figure 2.1. Other forms of damage can simply shift the stress levels at which these failures occur. Of particular significance is the interlaminar matrix delamination, which is a subcritical failure mode. Its consequences may include stiffness loss, local stress concentration, and local instability, leading to further growth and ultimately, the failure of the laminate and the overall structure. Delamination is the most prevalent failure mode in composites and can be triggered by various factors, such as curved free edges, external ply drops, corners, skin stiffener interaction, solid-sandwich transition, internal ply drop, and straight free edge [37].

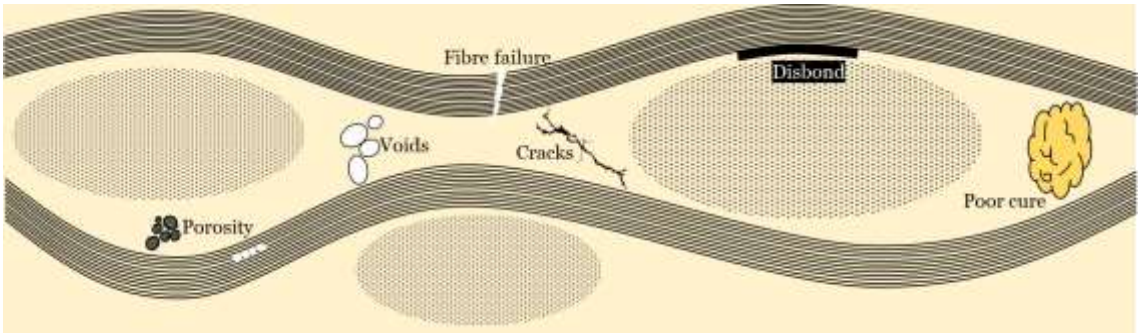

Figure 2.1: Typical failure modes that occur in a composite, fibre, matrix and interface.

The material properties of the FPC near the fibre surface play a pivotal role in stress transfer and failure mechanisms between the fibre and matrix. This zone undergoes varying thermal expansions during thermal processing, serving as a boundary between two dissimilar materials that diverge in their physical and chemical properties. A composite featuring a weak interface might display substantial degradation in both mechanical and thermal properties [38].

Moreover, specimens undergo chemical and thermal contractions during the curing process and cooling phase, resulting from variations in the mechanical attributes of the individual constituents. Residual stresses formed within the interphase can notably impact the adhesion between the fibre and matrix. The complex nature of this interphase is depicted in Figure 2.2, which, by coupling mechanics and surface chemistry approaches, enables a better understanding

of the structure and composition of the fibre-matrix interphase, as well as the state of stress, leading to a better comprehension of the composite's static and dynamic properties [39].

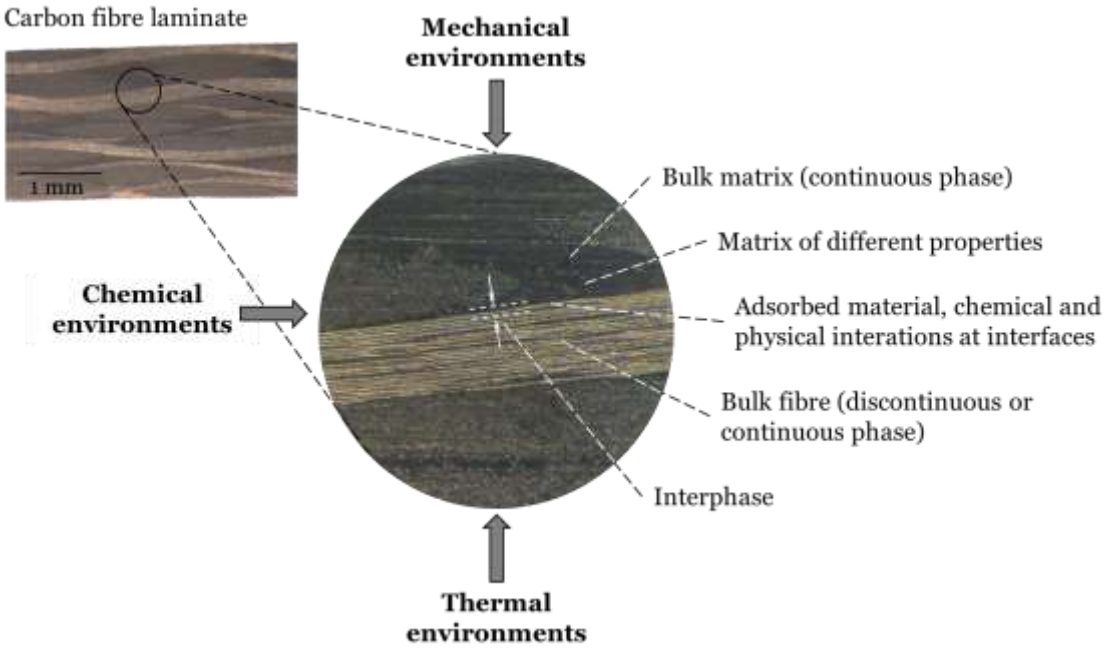

Figure 2.2: Elements that influence the properties of the fibre-matrix interface in a composite material. Adapted from [39–41].

The interphase exists from the points in the fibre where the local properties begin to change from the fibre bulk properties through the actual interface into the matrix, where the local properties again equal the bulk properties. Depending on the system, the interphase itself can extend from a few to a few thousand nanometres in depth [40]. There are different interfacial bonding mechanisms that occur at different fibre-matrix interfaces: (i) molecular entanglement; (ii) electrostatic adhesion; (iii) chemical bonding; and (iv) mechanical interlocking [42]. There are several phenomena that can occur simultaneously in the interphase region, can vary in magnitude and affect directly or indirectly on the performance of the composite in terms of its mechanical strength, chemical and thermal durability. When it comes to fibre: (i) can may have morphological variations close to surface that are not present in the fibre's volume; (ii) the surface area of the fibre can be much greater than its geometric value due to pores or cracks on the surface; (iii) the atomic and molecular composition of the fibre surface can be different from the bulk of the fibre; and (iv) surface treatments can add chemical groups and remove the original surface giving rise to a chemically and structurally different region. During and after the composite production process: (i) exposure to air can result in the adsorption of chemical species which may alter or eliminate certain beneficial surface reactivity; (ii) these adsorbed materials may also desorb at the increased temperatures seen in composite fabrication and be a source of volatiles which disrupt the interface if not removed; (iii) thermodynamic wetting of the fibre surface by the matrix is a necessary condition for fibre-matrix adhesion and is determined by the free energies of the components; (iv) both chemical and physical bonds exist at the interface and the number and type

of each strongly influences the interaction between fibre and matrix, i.e., the interaction between the fragile part and the reinforcing component; (v) changes in reactivity due to adsorption of matrix components can alter the local morphology; and (vi) unreacted matrix components and impurities can diffuse to the interphase region, altering the local structure [40].

When a composite is under external mechanical loading, the stress or load transfer across interfaces assumes a crucial role in maintaining material properties and extending its lifespan. The bonding or adhesion occurring between the fibre and matrix significantly influences the efficacy of stress transfer to adjacent fibres and the matrix. Strong adhesion between the fibre and matrix interfaces is essential for efficient stress distribution and load transfer between the matrix and neighbouring fibres. [41].

In the case of polymeric composites, extensively utilized in the design of composite structures, their properties are associated with their surface area rather than a single point. As a result, the composite should be designed to minimize stress concentration. The choice of composite geometry is, in turn, influenced by limitations of the manufacturing facility, production costs, and the desired final appearance of the component. The strength of a composite is primarily determined by: (i) the mechanical properties of the reinforcement and the matrix; (ii) the residual internal stresses; (iii) the degree of true interfacial contact; and (iv) the structure's geometry. Each of these factors significantly impacts the structural performance. Composite structures experience five types of stress: (i) compression; (ii) tension; (iii) peel; (iv) shear; and (v) cleavage. A combination of these stresses may be encountered in applications involving composite materials.

Another crucial aspect to consider when designing composite structures is understanding the factors that influence the impact strength and damage tolerance of FRP [43,44]. The impact response and damage in composite materials are influenced by four key groups of parameters: (i) material; (ii) geometry; (iii) event; and (iv) surrounding environment. By carefully selecting the fibre orientation or fibre architecture and material behaviour of each layer, an engineer/designer can configure a composite that effectively meets all load requirements while minimizing the number of layers. The matrix system in a composite material helps to protect, align, and stabilize the reinforcements, as well as ensure stress transfer between fibres. The mechanical performance of fibre-reinforced polymer matrix composites depends on the bond strength between the matrix and fibre. Geometrical parameters such as thickness and curvature are vital aspects that influence the impact behaviour of a composite structure, as they affect energy absorption modes and damage areas. The shape, mass, angle, and size of the impactor have a significant influence on impact resistance or energy absorption, which can result in property loss for the structural laminate. Exposure to different environmental conditions can cause both irreversible and reversible damage to composites, leading to premature damage during impact loading. The viscoelastic behaviour of polymers matrix in composites has a significant effect on the fracture strain, resistance to plastic deformation and fracture toughness of the matrix, particularly at elevated temperatures. [43,44].

The demand for materials with exceptional performance has become a reality, and numerous efforts have been applied over the last years to maximize the properties of polymers through the incorporation of specific nano-sized fillers. This approach provides a viable alternative, resulting in materials with improved mechanical properties, including tensile and bending strength, compression strength, Mode I and Mode II interlaminar fracture toughness, and impact properties. One of the most successful strategies for enhancing the chemistry, mechanics, and composition of epoxy resins has been the incorporation of fillers into their nanostructures [17]. However, the use of nanofillers as performance enhancers is a delicate process, and factors such as the resin-to-filler ratio and the uniformity of filler dispersion within the epoxy resins are critical determinants of the final properties of the composites.

In this context, nanomaterials (NMs) refer to chemical substances or materials produced and employed on a notably small scale, typically measuring between 1 to 100 nanometres in at least one dimension. The distinct physical properties of these materials can be influenced by their size and shape [45].

NMs exhibit diverse classifications based on several criteria, such as dimensionality, morphology, state, and chemical composition. Specifically, based on their dimensionality and overall structure, NMs can be categorized into four classes. Zero-dimensional (0D) NMs possess all dimensions within the nanoscale, typically below 100 nm. One-dimensional (1D) NMs have one dimension at the nanoscale while the other two dimensions are beyond that range. Two-dimensional (2D) NMs possess two dimensions at the nanoscale and the remaining dimension outside that scale. Three-dimensional (3D) materials encompass dimensions that exceed 100 nm across all axes. [45].

According to their structural makeup, NMs can be broadly divided into four groups: (i) organic/dendrimers NMs; (ii) inorganic NMs; (iii) carbon-based NMs; and (iv) composite NMs. Organic compounds transform into organic nanoparticles. Organic nanoparticles or polymers, such as liposomes, dendrimers, micelles and ferritin, exemplify this transformation. Nanocapsule micelles and liposomes are types of non-toxic and biodegradable nanoparticles, possessing hollow interiors and are sensitive to light, electromagnetic radiation and heat. Dendrimers have an exterior coated with numerous chain ends, which perform specific chemical reactions. Dendrimers are applied in identifying molecules, detecting tiny particles, producing light, and electronic chemical systems [46].

Inorganic nanoparticles are that lack carbon atoms. There are typically classified as those composed of metal-based or metal oxide-based NMs. Metal-based nanoparticles can be synthesized through destructive or constructive processes. These nanoparticles can be synthesized into metals such as aluminium (Al), cadmium (Cd), cobalt (Co), copper (Cu), gold (Au), iron (Fe), lead (Pb), silver (Ag), and zinc (Zn). Because of their quantum effects and huge surface-to-volume ratio, metal nanoparticles have excellent ultraviolet-visible sensitivity, as well outstanding as electrical, catalytic, thermal, antibacterial, and optical properties. Metal oxide nanoparticles or metal oxide NMs, are composed of positive metallic ions and negative oxygen

ions. As examples of metal oxide nanoparticles that are frequently synthesized include silicon dioxide (SiO_2), titanium oxide (TiO_2), zinc oxide (ZnO), and aluminium oxide (Al_2O_3). These NMs exhibit remarkable properties compared to their metal analogues. Ceramic nanoparticles are inorganic solids made up of carbides, carbonates, oxides, carbides, carbonates, and phosphates synthesized via heat and successive cooling. Lipid-based nanoparticles are generally spherical, with diameters ranging between 10 and 100 nm. It consists of a solid core made of lipids and a matrix containing soluble lipophilic molecules. Semiconductor NMs exhibit the same properties as metals and insulators [46].

Based on these weaknesses, in recent years, numerous efforts were made to maximize the properties of polymers by incorporating specific nano-sized fillers [47]. This approach provides a viable alternative, resulting in materials with improved mechanical properties, including tensile and bending strength, compression strength, Mode I and Mode II interlaminar fracture toughness (ILFT), and impact properties. One of the most successful strategies for enhancing the chemistry, mechanics, and composition of epoxy matrices is the incorporation of nanofillers into their nanostructures [17,47]. However, the use of nanofillers as performance enhancers is a delicate process, and factors such as the resin-to-filler ratio and the uniformity of filler dispersion within the epoxy matrices are critical determinants of the final properties of the composites.

The dispersion of nanofillers in epoxy resin is critical to achieving the desired improvements in mechanical and other properties. Common techniques for dispersing nano fillers in epoxy resins include mechanical agitation: use of high-speed stirrers to break up agglomerates and disperse nanofillers throughout the resin; ultrasonication: using ultrasonic waves to disperse nanofillers by breaking up agglomerates through cavitation; three-roll milling: passing the nanofiller/epoxy mixture through three rollers to achieve uniform dispersion; and solvent mixing: dissolving both the epoxy and nanofillers in a common solvent, followed by solvent evaporation to achieve a uniform mixture.

On the other hand, there are several mechanisms that affect epoxy performance, being (i) stress transfer: nanofillers with high aspect ratios, such as carbon nanotubes (CNTs) and graphene (GP), can efficiently transfer stress from the epoxy matrix to the nanofillers, significantly increasing the mechanical strength and stiffness of the composite; (ii) crack bridging and deflection: Nanofillers can act as barriers to crack propagation. They can bridge cracks and increase the energy required for crack growth, thereby improving the fracture toughness of the epoxy resin; (iii) interfacial interactions: Strong interfacial bonding between nanofillers and the epoxy matrix is essential for effective load transfer. Functionalization of nanofillers can enhance these interactions, resulting in improved mechanical properties; (iv) stress distribution: nanofillers can improve the stress distribution within the epoxy matrix, reducing stress concentrations and improving the overall strength and durability of the composite; (v) thermal stability: Nanofillers can improve the thermal stability of epoxy resins, allowing them to maintain their mechanical properties at higher temperatures. This is particularly important for applications involving thermal cycling or high

temperature environments; (vi) electrical and thermal conductivity: certain nanofillers, such as graphene and CNTs, can impart electrical and thermal conductivity to the epoxy resin, expanding its range of applications in electronics and thermal management; and (vii) viscosity modification. The addition of nanofillers can change the viscosity of the epoxy resin, which can be beneficial or detrimental depending on the application. Controlling filler dispersion and loading is key to maintaining processability [48–53].

The influence of carbon nanofillers on the mechanical properties of composites is multifaceted and can be attributed to several mechanisms. Allotropes of carbon improve the mechanical properties of composites through the following primary mechanisms: (i) load transfer: as they have high intrinsic strength and stiffness. When dispersed in a matrix, the load can be effectively transferred from the matrix to the nanofillers, thereby increasing the overall mechanical strength and stiffness of the composite. This load transfer is facilitated by strong interfacial bonding between the nanofillers and the matrix; (ii) stress distribution: Their high aspect ratio and large surface area allow them to act as stress concentrators, redistributing applied stresses more uniformly throughout the matrix. This leads to enhanced resistance to crack initiation and propagation; (iii) crack bridging and deflection: As a crack propagates, carbon nanofillers can bridge the crack by holding the two crack faces together, thereby increasing the energy required for crack propagation. In addition, nanofillers can cause crack deflection, increasing the crack path and hence the toughness of the composite; (iv) interfacial interactions: Strong interfacial interactions between the nanofillers and the matrix are critical. Covalent bonding, van der Waals forces, and mechanical interactions between the matrix and nanofillers can improve the efficiency of charge transfer. Functionalization of carbon nanofillers can enhance these interfacial interactions; (v) alignment and distribution of nanofillers: Proper alignment along the loading direction can maximize reinforcement efficiency. Homogeneous distribution prevents agglomeration and ensures that the nanofillers can interact effectively with the matrix; (vi) matrix reinforcement: Nanofillers can also affect the intrinsic properties of the matrix. For example, they can increase the modulus and strength of the matrix by introducing physical barriers to plastic deformation; and (vii) thermal stability and degradation resistance: Carbon nanofillers can improve the thermal stability of composites, which in turn can improve mechanical properties at elevated temperatures. They can also inhibit matrix degradation, thereby extending the mechanical performance of the composite over time [54–57].

For this purpose, for example, carbon-based nano-reinforcements garnered significant importance and interest within the scientific community due to their remarkable properties and diverse potential applications in various technologies [58]. They can be found in morphologies such as hollow tubes, ellipsoids or spheres, i.e., carbon nanofibres (CNFs), CNTs, carbon nano-onions (CNOs), carbon nanohorns (CNHs), graphene nanoplatelets (GNPs), fullerenes (C60), carbon black, buckyballs (BBs), mesoporous carbons (MCs), GP, and graphite [58–62].

Comparing the carbon-based nano-reinforcements, CNFs have the highest surface area ranging from 20 to 300 m^2/g, while CNTs, GP, graphite, and carbon black have surface areas of 50 to 1315, 500 to 2630, 1 to 132, and 10 to 1443 m^2/g, respectively. Diameter and length are crucial dimensions affecting variables such as dispersion, agglomeration, and property enhancements. CNFs exhibit the highest values with diameters of 10 to 500 nm and lengths of 0.5 to 200 μm, while CNTs have intermediate values (1 to 10 nm diameter, 1 to 100 μm length), and GP has the lowest values (6 to 9 nm diameter). In terms of density, GP has the highest values, followed by graphite, CNFs, CNTs, and carbon black (2 to 2.3, 1.9 to 2.3, 1.5 to 2.0, 0.8 to 1.8, and 0.13 to 2 g/cm, respectively). In general, CNFs have slightly lower electrical conductivities compared to CNTs and GP, with values ranging from 10−7 to 103, 102 to 106, and 106 S/cm, respectively. CNTs exhibit lower thermal conductivities compared to most carbon nanoallotropes, followed by GP and CNFs, with values ranging from 2000 to 6000, 600 to 5000, and 5 to 1600 W/(m × K), respectively. Regarding surface area, CNFs have higher values followed by GP, carbon black, CNTs, and graphite, with ranges of 20 to 2500, 500 to 2630, 10 to 1443, 50 to 1315, and 1 to 20 m^2/g, respectively [60,62].

The selection of the appropriate dispersion process in the manufacture of epoxy matrix nanocomposites is critical to the performance of the resulting composites. The challenge is to create sufficiently strong chemical bonds between the nanofiller and the matrix without causing significant damage to the mechanical properties of the nanofiller.

For epoxy matrix nanocomposites, the combination of high-performance dispersion methods, such as high shear mixing, and simultaneous application of an ultrasonic bath is the simplest and most convenient approach to improve the dispersion of nanosized fillers in an epoxy matrix. In this method, the nanofillers are first dispersed in the resin or dissolved in certain solvents, followed by dispersion based on the viscosity of the epoxy resin. Shear mixing can be achieved by magnetic or mechanical stirring. Higher shear forces are required to generate greater shear energies, resulting in more effective dispersion of the nanofillers.

While the primary focus of this chapter is on the performance enhancement of epoxy resins through the addition of nanofillers, in particular CNFs, it is important to recognize the cost implications associated with these advanced materials. The cost of nanofillers is a significant factor in their technical application and commercialization. Different types of nanofillers have different cost structures due to their raw materials, production methods, and market availability: CNTs are one of the most effective nanofillers for improving mechanical and electrical properties, but their production costs are relatively high, especially for high-purity, single-wall CNTs; GP offers excellent mechanical and conductive properties, but is also expensive due to complex production processes such as chemical vapor deposition or exfoliation; CNFs are generally less expensive than CNTs and GP, offering a good balance between cost and performance; nanoclays are relatively less expensive than carbon allotropes and offer good mechanical and barrier

properties; and silica nanoparticles, alumina nanoparticles, and other inorganic nanofillers tend to be less expensive but may offer different property enhancements [63].

Incorporating nanofillers into epoxy resins can affect overall production costs due to material costs. The direct cost of nanofillers is a significant component; for example, high-quality, functionalized nanofillers can be particularly expensive. Achieving uniform dispersion of nanofillers may require additional processing steps, such as ultrasonication, three-roll milling, or solvent mixing, which can increase manufacturing complexity and cost. Large-scale production can benefit from economies of scale, reducing the unit cost of nanofiller-enhanced epoxy composites. However, the initial investment in equipment and process development can be significant.

When considering the use of nanofillers, a cost–benefit analysis should be performed to evaluate the trade-offs between increased cost and improved properties of the final composite. The significant improvements in mechanical, thermal, and electrical properties provided by nanofillers may justify the higher material and processing costs, especially for high-performance applications as in the aerospace, automotive, defence industries, biomedical, electronics, and energy sector. Improved durability, thermal stability, and resistance to environmental degradation can lead to longer service life and reduced maintenance costs, providing long-term economic benefits [64].

There are several ways to potentially reduce the cost of nanofillers and make them more viable for widespread use. Improvements in the synthesis and functionalization processes for nanofillers can reduce their cost. For example, scalable methods to produce graphene and CNTs at lower cost are under active research. Efficient functionalization methods can improve the compatibility of nanofillers with epoxy resins, potentially reducing the amount needed to achieve desired properties. Combining different types of nanofillers or using a blend of nano- and micro fillers can balance cost and performance [65].

Composite NMs encompass multiphase nanoparticles and nanostructured materials. They consist of at least one phase within the nanoscale dimension, combining either nanoparticles among themselves or a combination of nanoparticles with larger or bulk-type materials. For instance, these composite structures might involve hybrid nanofibres or intricate formations like metal-organic frameworks. These composites can be formed from various combinations, such as carbon-based, metal-based, or organic-based NMs integrated with metal, ceramic, or polymer bulk materials. The synthesis of NMs can result in diverse morphologies, tailored according to the specific properties required for the intended application.

2.2. Carbon nanofibres

In recent decades, CNFs have garnered attention from engineers, scientists, and different industrial sectors due to their potential in revolutionizing material performance and capabilities.

These nanofibres exhibit exceptional properties, such as a high aspect ratio and molecular orientation, large specific surface area, small pore size, minimal defects, low density, high specific modulus and strength, excellent electrical and thermal conductivity, remarkable chemical resistance, high temperature tolerance, low thermal expansion, and outstanding mechanical performance. These remarkable attributes render CNFs highly desirable for a wide range of applications [66,67].

The list of potential applications for CNFs spans various industries and fields. These include energy (batteries, fuel cells, supercapacitors, energy conversion, sensors, and catalysts), electronics (electromagnetic field shielding, heat management, and conductors), biomedical (wound dressing materials, bone tissue engineering, biosensors), medicine (tissue engineering, drug delivery, and implants), composites (high-performance composite materials: polymers, ceramics, glass, plastics, and resins), agriculture and food safety, chemical applications, security, aeronautics, aerospace, automotive and railway industries, and optical applications, water filtration, air treatment, as well as sports and recreational activities [68].

Incorporating CNFs into nanocomposites offers several potential benefits, including the increase in mechanical properties without changing the mass. These improvements encompass various aspects, such as increased modulus [69–72], strength [69–72], fracture toughness [73–75], fatigue strength [73,76], delamination resistance and damage tolerance [77], impact strength [78], and structural damping [79]. Furthermore, the addition of CNFs can lead to improved electrical and thermal conductivity, heightened thermal stability, enhanced flame retardancy, superior barrier properties, and reduced susceptibility to environmental factors such as moisture absorption and degradation caused by irradiation [80].

These nano-reinforcements can be described as 1D carbonaceous filaments with nanometre-scale dimensions (ranging from 3 to 100 nm in diameter). They are composed of stacked graphene layers that exhibit a specific orientation with respect to the fibre axis. These materials are typically categorized into three groups based on the angle between the graphene layers and the growth axis: parallel (angle = 0°), fishbone (0° < angle < 90°), and platelet (angle = 90°). The synthesis of CNFs involves various methods, leading to diverse structures such as porous, hollow, helical, twisted, and stacked forms. Achieving these structural variations is possible through instrumental techniques and experimental design [81,82].

CNFs differ from CNTs in that they lack the tubular nanostructure typically found in nanotubes. Instead, CNFs exhibit a fishbone or platelet-shaped arrangement, where graphene planes are stacked to form a 1D fibre morphology, as shown in Figure 2.3. Similar to other carbon nanofilaments, CNFs are mainly produced by catalytic chemical vapor deposition (CCVD) from a carbon feedstock (light or aromatic hydrocarbons) using an elemental transition metal (Fe, Ni, Co, and Cu) as a catalyst, in a hydrogen atmosphere (partial) at temperatures ranging from 500 to 1200 °C [83]. Therefore, the only difference between the various forms of CNFs is their chemical structure:

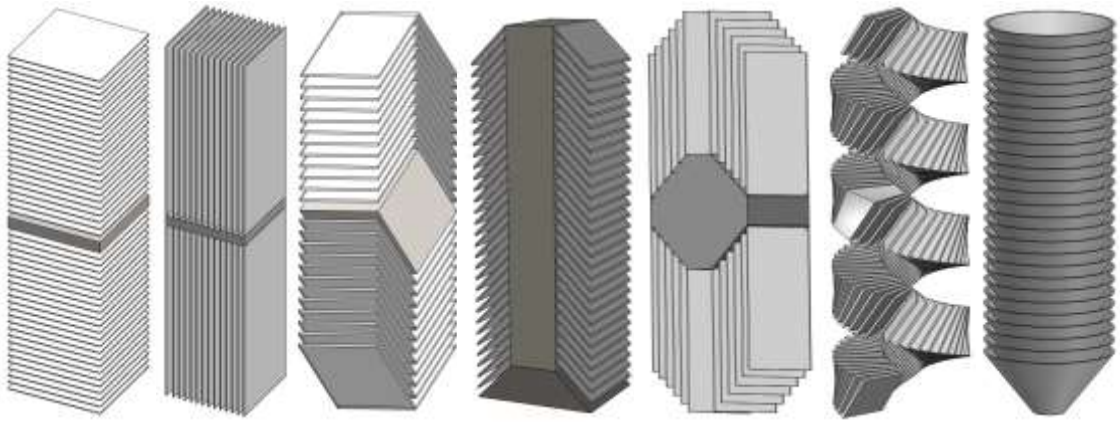

a) b) c) d) e) f) g)

Figure 2.3: Schematic representation of CNFs and their precipitated graphite platelets formed during the growth for the different morphologies: a) Platelet; b) Ribbon-type; c) Fishbone/herringbone with solid core; d) Fishbone/herringbone with hollow core; e) Ribbon/herringbone with solid core; f) Spiral type; and g) Stacked cup. Adapted from [58,83,86,87].

i) Platelet CNFs exhibit a structure where graphene layers are oriented perpendicular to the fibre axis, as shown in Figure 2.3.a). These fibrils typically have a width of around 100 nm, and the presence of hydrogen or other heteroatoms is necessary for stabilizing the plates [83]. In the case of bidirectional fibres, a solid particle is usually located in the middle of the fibre [84]. On the other hand, ribbon CNFs feature a stacked arrangement of graphene layers parallel to the fibre axis, as depicted in Figure 2.3.b).

ii) Fishbone CNFs are characterized by the inclination of graphene layers in relation to the fibril axis. The presence of hydrogen is necessary to stabilize the edges of these CNFs. There are two variations of fishbone CNFs: those with a hollow core, as shown in Figure 2.3.d), and those with a solid core, as depicted in Figure 2.3.c) [40].

iii) Ribbon CNFs consist of unrolled graphene layers that are straight and parallel to the fibril axis. They have non-cylindrical cross-sections, as shown in Figure 2.3.e). Regarding the position of the catalytic solid particle, there is agreement among researchers that it is located at one extreme. However, there is some discrepancy among authors regarding the orientation of the graphite layers in relation to the fibril axis. Some claim that the layers are completely parallel [84], while others suggest that they are slightly inclined [85].

iv) Stacked-cup CNFs exhibit a continuous layer of rolled (spiral) graphene along the fibre axis. This spiral orientation results in a truncated cone arrangement along the axis, with a wide internal hollow space, as shown in Figure 2.3.g).

Scanning electron microscope (SEM) image of the vapor-grown carbon nanofibres (VGCNFs) are presented in Figure 2.4. It is important to highlight that the VGCNFs were synthesized using the

floating catalyst method, exhibiting a discontinuous morphology and a high degree of graphitization.

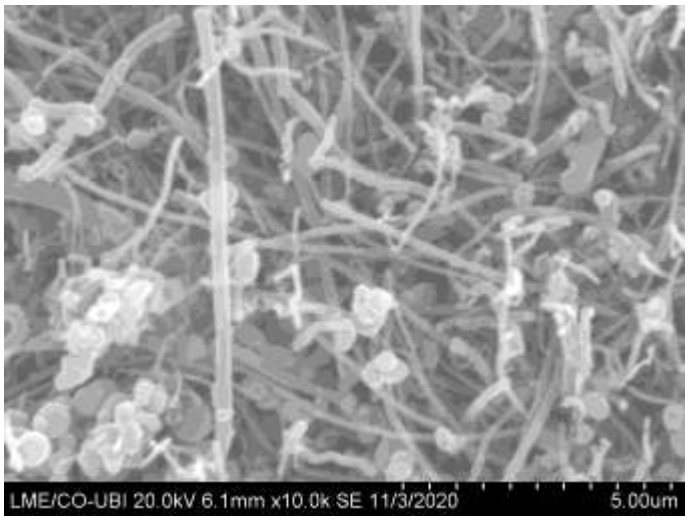

Figure 2.4: SEM image of CNFs VGCNFs manufacturing technology (magnification of 10k).

2.2.1. Synthesis of CNFs

In the production of different configurations of CNFs, different production techniques are applied according to their properties and applications. These include catalytic chemical vapor deposition (CCVD) [88], electrospinning/electrospun [89], plasma-enhanced chemical vapor deposition (PECVD) [90,91], gas-phase flow catalytic method [92], templating [93], phase separation [94], arc discharge deposition [95], and floating catalyst (FC) [96]. These fabrication techniques offer versatility in controlling the morphology, structure, and properties of CNFs, enabling their application in a wide range of fields.

CCVD is a widely used method for producing VGCNFs. This process, originating in the 1970s, was refined to specifically generate CNFs. In this technique, a catalytic thermal chemical vapor in a quartz tube electric furnace involves the use of C_2H_2 as the carbon source. Various metals or alloys, such as iron (Fe), cobalt (Co), nickel (Ni), chromium (Cr), and vanadium (V), act as catalysts to dissolve carbon into metal carbide. Carbon sources such as molybdenum (Mo), methane (CH_4), carbon monoxide (CO), synthesis gas (H_2/CO), or ethane (C_2H_6) are utilized within a temperature range of 700 to 1200 K. The CCVD procedure includes stages where catalyst powder is heated, carbon sources are introduced, and the temperature is controlled to synthesize CNFs (Figure 2.5.a)).

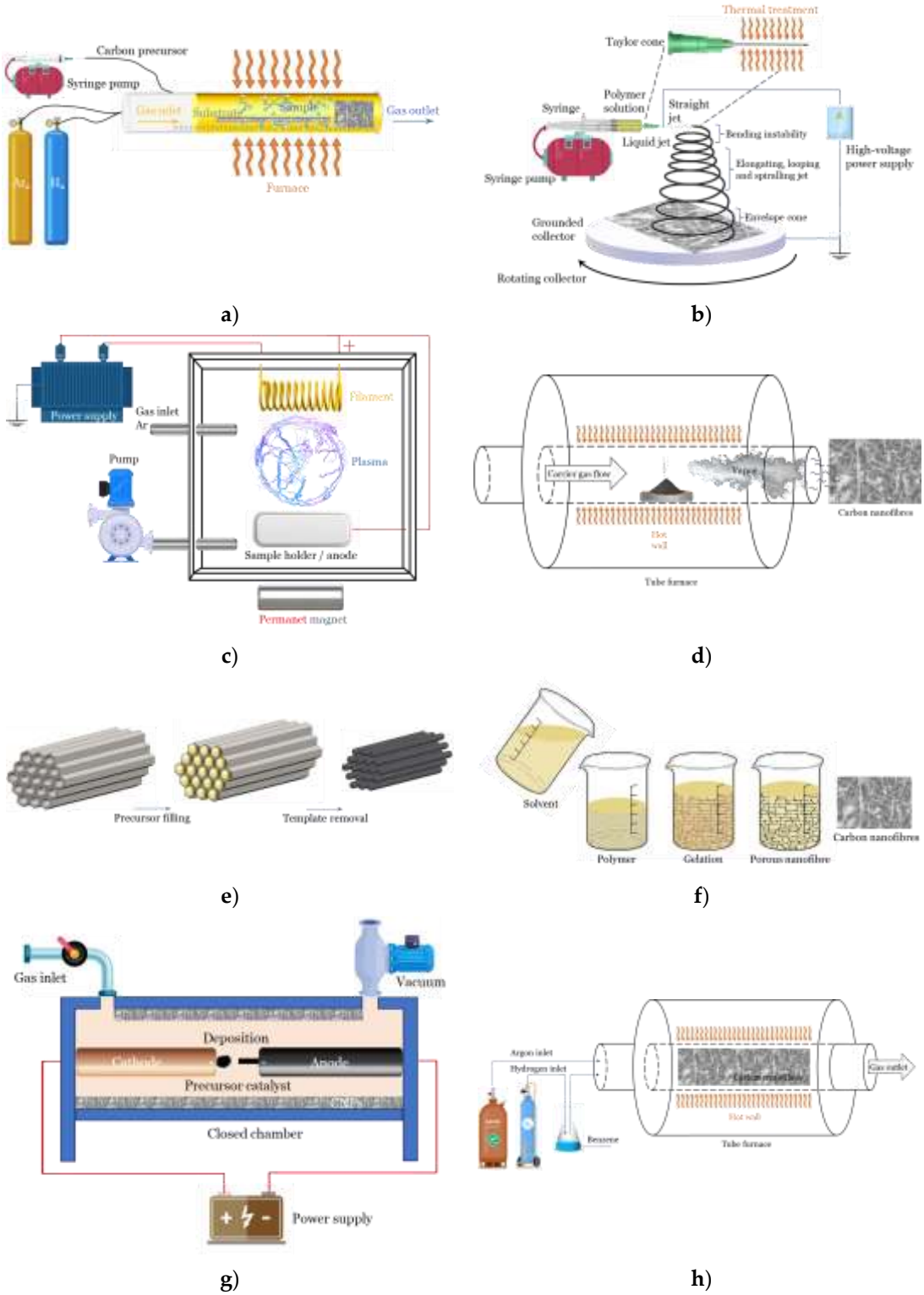

Figure 2.5: Schematic diagram setup of: a) CCVD [64,88]; b) Electrospinning/electrospun [60,64,89]; c) PECVD [99]; d) Gas-phase flow catalytic method; e) Templating [93,100]; f) Phase separation [64]; g) Arc discharge deposition [101]; and h) FC [96,102] (Schemes adapted from respective references indicated).

Post-processing involves purification steps in nitric acid (HNO_3) and hydrochloric acid (H_2O:HCl) solutions, followed by washing with distilled water and isopropyl alcohol. However,

CCVD has limitations in producing short, challenging-to-align fibres, hampering their use in applications. The growth mechanism of CNFs depends on the catalyst's surface geometry and the gaseous carbon feedstock during processing. The resulting CNF structures are influenced by manufacturing techniques. The size of catalyst particles typically dictates the CNF's outer diameter, with VGCNFs having unique structures resembling annular rings, characterized by sp2 graphite. Metal particle size affects fibre thickness, while growth temperature and metal type influence fibre orientation. Cup-stacked and platelet CNFs are two distinct types generated by CCVD, each exhibiting specific structures; cup-stacked CNFs have a helically folded graphene layer, forming a hollow core with cup-shaped appearances along the fibre axis. This unique structure differentiates VGCNFs from CNTs, which resemble single or multiple concentric cylinders formed by parallel-oriented graphene layers [81,97,98].

Electrospinning is a versatile technique that can be used to produce CNFs, where a polymer solution containing a carbon precursor, such as polyacrylonitrile (PAN) or a blend of PAN and other polymers, is electrospun. The resulting polymer nanofibres are then subjected to a thermal treatment process, known as carbonization, to convert them into CNFs (Figure 2.5.b)). Electrospinning is a widely utilized technique for synthesis of CNFs. This method enables the production of polymeric nanofibres, offering advantages such as ease of control and environmental compatibility. It is considered a flexible and robust method for large-scale production of organic polymer or composite nanofibrous mats, having diameters ranging from submicron to nanometre, and demonstrating good electrospinnability and stability.

The process involves a setup comprising a metallic spinneret, syringe pump, high-voltage power supply, and grounded collector within a controlled environment. A polymer solution is pumped through the spinneret while a high voltage is applied between the spinneret and the collector, resulting in fine filaments that deposit randomly on the collector, forming a nanofibre web. Improved techniques were developed to generate aligned nanofibre arrays, porous surfaces, and large-scale production. Rotating drum collectors enhanced homogeneity in fibre deposition, ensuring uniform thickness. Parameters such as polymer solution type, solvent, capillary size, flow rate, working distance, and applied potential significantly impact CNFs properties. A subsequent heat treatment carbonizes the polymer nanofibres to form CNFs. Solution concentration, viscosity, and temperature also influence fibre dimensions, with higher temperatures potentially inducing beta-phases and increased diameter correlating with solution concentration increment following a power law relationship [81,82,97,98].

PECVD is a technique in which plasma is utilized to enhance the deposition of thin films or nanostructures onto a substrate. In the case of CNFs, a carbon-containing precursor gas, such as methane or acetylene, is introduced into a PECVD chamber. The plasma dissociates the precursor gas, and the carbon species deposit and grow into CNFs on the substrate (Figure 2.5.c)). PECVD is an efficient alternative method for low-temperature production of CNFs as it provides improved control over synthesis parameters such as plasma power, reaction temperature, gas species, and

carbon source. Experimental results show that nanostructures produced via PECVD exhibit better alignment compared to nanostructures synthesized using thermal processes. PECVD-based methods offer advantages for CNF fabrication, including control over nanofibre diameter, length, and alignment, enabling the growth of individual, freestanding, and vertical carbon nanostructures. In contrast, thermal CVD typically yields either spaghetti-like films or ensembles resembling towers. Upon closer inspection, the individual nanostructures within the tower are found to be wavy [91,103].

In the gas-phase flow catalytic method, the catalyst precursor undergoes direct heating, followed by introduction into the reaction chamber alongside the hydrocarbon gas. This leads to decomposition of the hydrocarbon gas and the catalyst at two distinct temperature zones (Figure 2.5.d)). Consequently, the decomposed catalyst aggregates into nanoscale particles. Subsequently, CFs are synthesized utilizing these nanoscale catalyst particles [104]. Lastly, the decomposed catalyst particles resulting from the organic compound can be dispersed throughout a 3D space. This method enables straightforward management of volatilization quantities. Consequently, it allows for substantial production of CF in a shorter duration, facilitating uninterrupted carbon fibre fabrication [105].

Templating provides precise control over the size, shape, and distribution of carbon nanofibres, making it a versatile and powerful technique for their production. The hard template method uses solid templates, such as anodic aluminium oxide (AAO) or mesoporous silica, while the soft template method uses self-assembling structures, such as surfactant micelles or block copolymers. Both methods involve infiltration with a carbon precursor, followed by polymerization, carbonization, and template removal to produce high-quality CNFs (Figure 2.5.e)) [93,100].

In addition to these more industrial techniques, others were suggested in the literature, and duly accepted by the scientific community, with the aim of improving their physical and/or mechanical characteristics in order to obtain better adhesion to the matrix [98]. For example, phase separation is a technique involving dissolution, gelation, and extraction using varied solvents, freezing, and drying methods, leading to the creation of a nanoporous foam (Figure 2.5.f)). However, the entire transformation from solid polymer to nanoporous foam is time-consuming. Self-assembly, involving the spontaneous arrangement of dispersed components into an organized structure, occurs through local interactions among the components. This technique, akin to phase separation, is also time-consuming, especially in the continuous production of polymer nanofibres [105].

Arc discharge deposition is a method in which a graphite rod acts as the negative cathode and a positive anode when placed a few millimetres apart (Figure 2.5.g)). By applying a high current, the graphite rod is evaporated, resulting in the formation of carbon products that deposit on the chamber walls or the cathode substrate. Both CNTs and CNFs can be synthesized using arc discharge alternating current (AC) or direct current (DC) [106].

The FC method involves the production of VGCNFs through the catalytic decomposition of a hydrocarbon, such as benzene or methane, in a hydrogen atmosphere within a temperature range of 700 to 1200 °C (Figure 2.5.h)). During the FC method, the nanofibres float in the reactor space [96]. This method offers several advantages, including a relatively low cost, scalability, and the ability to produce large quantities of CNFs, making it suitable for industrial-scale implementation. However, achieving the desired properties of the nanofibres requires careful control of process parameters such as catalyst concentration, gas composition, temperature, and residence time. Insufficient contact time between catalyst particles and carbon sources can result in incomplete transformation of hydrocarbons into graphitic products [107].

Finally, Table 2.3 summarizes the main properties of CNFs produced by some processes available in the literature.

Table 2.3: Main properties for the different CNFs.

Property	CNFs [89]	CNFs [108]	VGCNFs [109]	VGCNFs [110–112]	VGCNFs [107]	VGCNFs [113]
Process	Electrospun	FC	-	-	FC	Gas-phase flow catalytic method
Diameter [nm]	106	60–150	50–200	150	20–80	200
Length [μm]	-	30–100	50–100	15 (10–20)	>30	10–20
Tensile modulus [GPa]	4806	400	240	516.5 (273–760)	-	-
Tensile strength [MPa]	206	2700	2920	3100 (2700–3500)	-	-
Strain to break [%]	1.46	1.5	-	-	-	-
Density [g/cm^3]	-	1.8	2.0	2.0	>1.97	2.1
Thermal conductivity [W/m×k]	-	20	1950	-	-	-
Electrical resistivity [Ω×cm]	-	-	1×10^{-4}	-	1×10^{-2}	-

2.2.2. CNFs in the production of polymer nanocomposites

In nano-enhanced composite materials, regardless of the nature of the NMs, it is essential that they are uniformly distributed within the matrix, and strong chemical bonds are formed between the nanofillers and the resin. This is crucial to maximize the reinforcing effect of the fillers, and it becomes more challenging as the size (weight or volume) of the load on the matrix increases. The size and geometry of the nanoparticles directly influence the uniformity of the distribution. While microscale fillers can be easily distinguished, nanofillers are extremely difficult to differentiate from each other. The interparticle distances between nanofillers are extremely close, resulting in significantly higher van der Waals or electrostatic interactions between nanoparticles. In practice, it is highly challenging, if not impossible, to insert closely spaced yet distinctly separated nanofillers within a polymer matrix. The tendency for agglomeration can be more severe for anisotropic nanofillers (e.g., nanotubes, nanowires, and nanoplatelets) that have 1D or 2D dimensions in the nanometre scale while the remaining fillers may be in the micrometre scale. As the amount of nanofillers increases, the surface area also increases, leading to a larger interface or interphase area with the polymers matrix [114]. This agglomeration relies on the

electromagnetic properties of NMs, magnetism and surface charge. Furthermore, their agglomeration in a liquid is based on morphology and functionalization [45].

The choice of the proper dispersion process in the synthesis of nanocomposites with polymers matrix is vital to the performance of the resulting materials. This is because creating sufficiently strong chemical bonds between the nanofiller and the resin, without causing significant damage to the mechanical properties of the nanofiller, presents a challenge. Currently, there are several synthesis techniques available. For instance, polymers with CNFs are effective nano-enhanced materials that can be prepared using easy mechanical methods that are also cost-effective. These methods include high-shear twin-screw extrusion [115], ultrasonication-assisted solution mixing [116], shear mixing [117,118], three-roll milling (TRM) [119–122], ball milling [123], and double-screw extrusion [124].

For polymer matrix nanocomposites, the combination of high-performance dispersion methods such as high shear mixing and simultaneously applying an ultrasonic bath is the simplest and most convenient approach to improving the dispersion of nanosized fillers in a polymer matrix. In this method, the nanofillers are initially dispersed in the polymer or dissolved in certain solvents, followed by dispersion based on the viscosity of the polymer. Shear mixing can be achieved using magnetic or mechanical stirring. Higher shear forces are required to generate greater shear energies, resulting in more effective dispersion of the nanofillers. This can be achieved using a high-shear mixer.

To achieve complete dispersal, ultrasound is used to agitate the bundles or agglomerates of nanoparticles. As ultrasound passes through the system in the form of high-frequency waves, smaller bundles are formed with increasing sonication time. Eventually, the nanoparticles reach a monodispersed state, where individual particles are completely separated from each other in the polymer matrix.

On the other hand, TRM also known as calendering, is a process that involves the application of shear forces between adjacent rollers rotating in opposite directions. This generates shear forces that are useful for mixing and dispersing materials with relatively high viscosities.

In the ball milling technique, rigid balls made of high-hardness materials such as ceramics, flint pebbles, and stainless steels collide with the powders within a closed chamber. This results in high shear or compressive forces acting on the powders at the interface, leading to the refinement of the powders and a decrease in particle sizes. These high shear and compressive forces are beneficial for the dispersion of nanofillers.

Chemical methods, such as surface oxidation [125], or the application of solvents during the exfoliation process [126], have been employed to enhance the adhesion of CNFs to polar polymers and resin matrix. Surface modifications of CNFs using surfactants [107], plasma treatment [127],

and branched polyols [128] have also been utilized to improve the CNFs-matrix interface adhesion.

The selection of an appropriate manufacturing process for a composite material, considering the type of matrix and reinforcement for a specific application, allows for the production of a material with excellent mechanical properties. These processes can be broadly classified into two types: open-mould processes and closed-mould processes. Closed-mould processes offer advantages such as superior finish, excellent reproducibility, and homogeneity in terms of constituent distribution and properties. Therefore, they are generally preferred over open-mould processes. Various manufacturing processes are available, each with its own specific characteristics. These include the hand lay-up method [129–132], vacuum bagging moulding [133], resin transfer moulding (RTM) [134], vacuum infusion or vacuum-assisted resin transfer moulding (VARTM) [112,135–138], vacuum-assisted resin infusion moulding (VARIM) [139], vacuum infusion [140], injection double vacuum-assisted resin transfer moulding (IDVARTM) [141], autoclave moulding [110,142–145], 3D printing/additive manufacturing [146], or combinations of two or more methods.

The hand lay-up method, also known as the wet lay-up method, is one of the simplest manufacturing methods for nano-enhanced composites and is relatively easy to implement on an industrial scale. In this method, the reinforcement is manually placed in the mould, and then resin is applied. The mould can be as simple as a flat plate. Release agents such as wax, silicone, and release paper are applied to facilitate the removal of the final part. A brush and roller are used to impregnate the fibres with the resin. However, due to the manual nature of the process, clumping of the nano-reinforcement can occur.

2.3. Static mechanical properties of epoxy matrix composites nano-enhanced with CNFs

The introduction of CNFs into an epoxy matrix can maximize various mechanical properties. CNFs, which consist of carbon atoms arranged in a fibrous structure, have exceptional mechanical properties such as high strength, stiffness and toughness. When dispersed in an epoxy matrix, CNFs can maximize the overall mechanical performance of the matrix, such as: increased strength, increased stiffness, increased toughness, increased fatigue resistance, increased wear resistance and improved thermal conductivity.

It is important to note that the specific mechanical improvements achieved by introducing CNFs into an epoxy matrix can depend on factors such as CNFs aspect ratio, filler dispersion and distribution quality, alignment, the adhesion and interface between filler and polymer matrix, the formation of CNFs agglomerates, voids between the CNFs surfaces and the matrix due to poor fibre to matrix adhesion, and processing techniques. On the other hand, one of their most effective uses is as interleaved reinforcement for composite laminate materials against delamination.

Additionally, the property enhancements may vary based on the particular application and the requirements of the composite material.

Subsequently, are present the main results achieved in recent years by various authors who aimed to maximize the mechanical properties in composite manufacturing such as bending properties of epoxy matrixes and epoxy matrixes composites, viscoelastic behaviour, Interlaminar shear strength, Mode I and Mode II interlaminar fracture and low-velocity impact properties. They achieved this by incorporating the optimal percentage of CNFs and various types of reinforcing fibres into the production of laminates using different epoxy matrix.

2.3.1. Bending properties of CNFs multiscale epoxy matrix

CNFs embedded in an epoxy matrix can create a multiscale composite material with enhanced mechanical properties, including bending properties. The multiscale nature refers to the combination of the macroscale epoxy matrix and the nanoscale CNFs, which interact synergistically to improve the overall performance of the composite.

The bending properties are crucial for evaluating a material's ability to resist bending or deformation under applied loads. In a three-point bending (3PB) test, the specimen is simultaneously subjected to compressive stresses (on the surface where the load is applied) and tensile stresses (on the opposite surface of the sample), along with shear stresses in the median plane (neutral axis). This combination of stresses results in typical cutting damage, delamination, and fibre breakage across the composite's cross-section. Due to the specific geometry of the specimens, this characterization is neither complex nor expensive, offering an advantage when compared to other destructive mechanical tests in terms of simplicity and cost-effectiveness.

It is well described in the literature that when an epoxy matrix is reinforced with CNFs, its mechanical performance can be improved significantly. However, these improvements depend on several factors, such as the aspect ratio of the CNFs, the dispersion and distribution quality, alignment, the adhesion and interface between the reinforcement and matrix, the formation of agglomerates, voids between the CNFs' surfaces and the matrix due to the weak adhesion of the fibre to the matrix, and processing techniques. In the specific case of laminated composite materials, their main advantage consists of delaying delamination (Figure 2.6). Therefore, the main results obtained with a view to maximizing the mechanical properties of composite materials are summarized below, with a special focus in this section on the static response in bending mode.

In this context, Table 2.4 summarizes the studies carried out on the effect of the CNF content on the bending response of epoxy resins, while Figure 2.7 quantifies the improvements achieved. For this purpose, the abscissa axis represents the percentage by weight of CNFs (wt.%), on a logarithmic scale, and on the ordinate axis the percentage improvement in bending strength and modulus. Figure 2.7.a) shows the increase in bending strength achieved by incorporating CNFs into the epoxy matrix. The studies show varying degrees of improvement, with some studies

showing significant improvements for specific CNFs loads. Similarly, the Figure 2.7.b) shows the percentage increase in bending modulus due to CNF reinforcement. The results evidence that the bending modulus is also improved with the addition of CNFs.

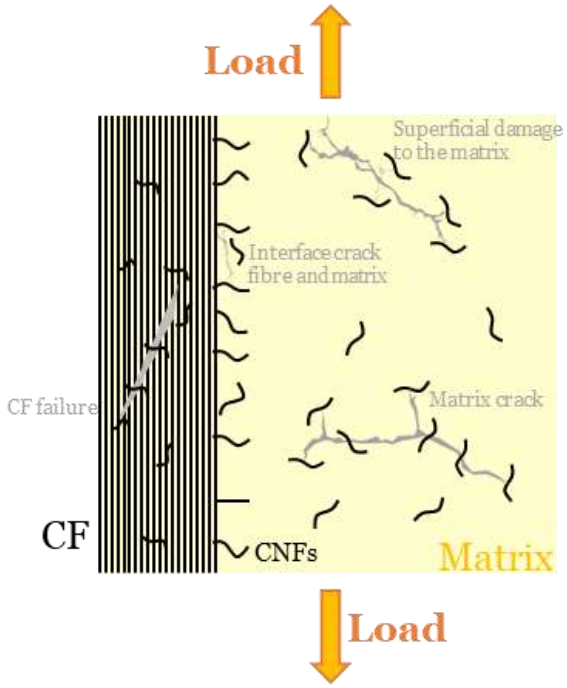

Figure 2.6: Effects of CNFs on the mechanical properties of epoxy matrix composites. Adapted from [147].

This analysis shows that it is possible to maximize the static properties of epoxy resins, regardless of their mechanical, physical, and chemical properties, by adding an optimum percentage by weight of CNFs. Patton et al. [148], who conducted one of the pioneering studies in this field, observed significant improvements in the bending modulus and strength of an epoxy matrix by incorporating a high quantity of CNFs (18.2 wt.%). They employed an acetone/epoxy solution infusion method through a CNFs mat under vacuum to prepare the nanocomposites. The results showed a 97.2% increase in bending modulus and a 36.7% increase in strength compared to the neat epoxy resin.

In another study Iwahori et al. [149], cup-stacked type carbon nanofibre (CSNFs) dispersed in epoxy resin were utilized at two different weight percentages (i.e., 5.0 wt.% and 10.0 wt.%), with two CSNFs aspect ratios of 10 and 50. The highest stress value in the stress-strain data was achieved by the 10.0 wt.% composite. This composite exhibited 42% and 38% higher bending modulus and strength, respectively, compared to the neat resin. Iwahori et al. also reported that increasing the weight content of CSNFs resulted in greater strength and modulus values in the bending tests.

Pervin et al. [150] introduced a novel technique for fabricating nanocomposite CNFs/epoxy by combining ultrasonic cavitation using a high-intensity ultrasonic liquid processor and high-speed

mechanical agitation. The results of bending tests demonstrated an enhancement in both modulus and strength as the loading percentage of CNFs increased. Specifically, the bending modulus and strength exhibited a progressive increase with higher weight percentages of CNFs. When 4.0 wt.% of CNFs were added, there was a 27% improvement in bending modulus and a 17% improvement in strength. This highlights the positive impact of incorporating CNFs into the epoxy matrix using their developed technique.

Zamu et al. [151] prepared nanocomposites with herringbone graphitic nanofibres (GNFs). Loadings of 0.15, 0.2, 0.3, 0.5, and 1.3.0 wt.% GNFs are compared with neat epoxy, and the highest mechanical properties were achieved by the nanocomposites containing 0.3 wt.% GNFs. At this filler amount, the bending strength, modulus, and breaking strain of the nanocomposite are increased by about 25.9, 20.6, and 30.8%, respectively. Bal [152] fabricated epoxy nanocomposites of different content of CNFs. The bending modulus increases 33%, 60% and 49% for composites with 0.5, 0.75 and 1 wt.% CNFs. As a result of CNFs' agglomeration at higher concentration, their high aspect ratio and Van der Waals attractive interactions, the bending property could be reduced.

Ardanuy et al. [153] prepared VGCNFs/trifunctional epoxy resin composites, and used different weight fractions of VGCNFs, between from 0.05 to 2.0 wt.%. The composite was prepared by directly mixing the VGCNFs and the epoxy resin using ultrasounds to improve dispersion. Compared to the neat epoxy, the maximum enhancement of the bending modulus was found for 0.1 wt.% VGCNFs composites, with 21.2% of improvement.

As shown in Table 2.4 and observing Figure 2.7.a), it can be concluded that the most results obtained for bending strength are concentrated at a very narrow range, from 0.25 to 1 wt.% CNFs content (area highlighted in blue) and the bending strength values are dispersed in a range of 76.9 to 424.6 MPa. Significant improvements have been achieved within this range, from tens to several hundred percentages. Other results were obtained for higher CNFs addition values, ranging between 3 and 19.2 wt.%.

It should be noted that, for the most part, these were the first published studies such as [148–150]. Less optimized production processes, commercial epoxy resins less likely to accept this type of nano reinforcement, with high viscosities and also larger nano particles are at the origin of these results. The bending strength values obtained in recent years mostly are in the range or above the reference values of bending strength for epoxy resins (dashed lines highlighted in gray), based on the values shown in Table 2.1 for epoxy matrix.

Table 2.4: Bending properties of CNFs multiscale epoxy matrix composites.

Autor, Ref.	CNFs Type	CNFs Integration Method	Optimum Loading (CNFs wt.%)	Bending Strength [MPa] (Increase (%))	Bending Modulus [GPa] (Increase (%))	Failure Strain [%] (Increase (%))
Patton et al., [148]	VGCNFs	Acetone/epoxy solution infusion.	18.2	123.0 (36.7%)	7.85 (97.2%)	-
		High shear mixing.	15.5	112.5 (29.3%)	6.18 (169.9%)	-
		Blender and two roll mill mixing.	19.2	146.4 (67.9%)	7.02	-
Xu et al., [154]	GCNFs	Mixed and sonicated.	0.3	139.6 ± 4.05 (28.25)	3.07 (0.52%)	3.93 (36.7%)
Iwahori et al., [149]	CSNFs	Mechanical mixing, passing through a vacuum chamber and post-cure in a hot press.	10.0	135.8 (37.7%)	3.277 (41.9%)	-
Pervin et al., [150]	CNFs	Ultrasonic cavitation.	4.0	99.4 ± 4.6 (17%)	2.81 ± 0.12 (27%)	-
Zhamu et al., [151]	GNFs	Mixed by low-power sonication and cured in a vacuum oven.	0.3	166.4 ± 2.0 (25.9%)	3.356 ± 0.056 (20.6%)	0.068 ± 0.005 (30.8%)
Sui et al., [155]	CNFs	Mechanical mixing.	0.3	137.7 ± 4.2 (32%)	2.92 ± 0.04 (9%)	7.5 ± 1.9 (70%)
Sancaktar et al., [156]	ECNFs	Non-woven ECNFs fabrics were impregnated with epoxy resin.	0.98	~220.0 (−33%)	-	-
Bal, [152]	CNFs	Dispersed in acetone by sonication, mixed with resin and sonicated at controlled power levels, and followed degassing process in vacuum oven.	0.75	-	2.69 (60%)	-
Ardanuy et al., [153]	VGCNFs	Mixing by hand and ultrasound bath.	0.1	105.0 ± 15 (4%)	4.0 ± 0.3 (21.2%)	3.8 ± 1.0 (−34.2%)
Zhang et al., [157]	VGCNFs	Ultrasonic and then mixing followed by ultrasonic again.	0.2	~120.0 (over 200%)	~2.7 (under 10%)	-
Zhang et al., [158]	CNFs	Ultrasonically dispersed, mixed, and rotary evaporator.	0.3	~80.0 (over 400%)	-	-
Shokrieh et al., [159]	VGCNFs	High speed mechanical mixing and sonicated via probe sonicator.	0.25	~121.0 (10%)	~3.18 (6%)	-
Chen et al., [125]	ECNFs VGCNFs GCNFs	Surfaces oxidation and functionalization. The nano-epoxy mixture was first subjected to ultrasonication, followed by mechanical stirring and degassing and finally post-curing.	0.5	412.3 (10%) 424.6 (13.3%) 418.7 (11.7%)	18.8 (14.6%) 18.2 (11.0%) 18.5 (12.8%)	- - -
Ahmadi et al., [160]	CNFs	Dispersed in acetone/epoxy resin under mechanical stirring by high-speed, sonicated, and vacuum oven.	1.0	213.6 ± 4.4 (97.8%)	5.14 ± 0.28 (143.6%)	-
Zeltmann et al., [161]	CNFs	Dispersing was accomplished using a mechanical mixer with a high shear impeller, and cured at RT and post-cured at 90 °C.	1.0	96.9 (−8.6%)	~2.3 (~5%)	-
Gao et al., [69]	CNFs	Rigorously agitation.	3.0	163.9 ± 7.8 (49.2%)	6.2 ± 0.4 (82.4%)	-
Danni et al., [89]	CNFs	Dissolution, magnetic stirring, and sonication to obtain CNF mats. Hand lay-up method to manufacture de composite.	3.0	122.58 (97.2%)	-	-
Nimbagal et al., [78]	CNFs	EP was preheated, mixed manually, and sonication and cured at RT.	0.3	76.9 (48.74%)	-	-

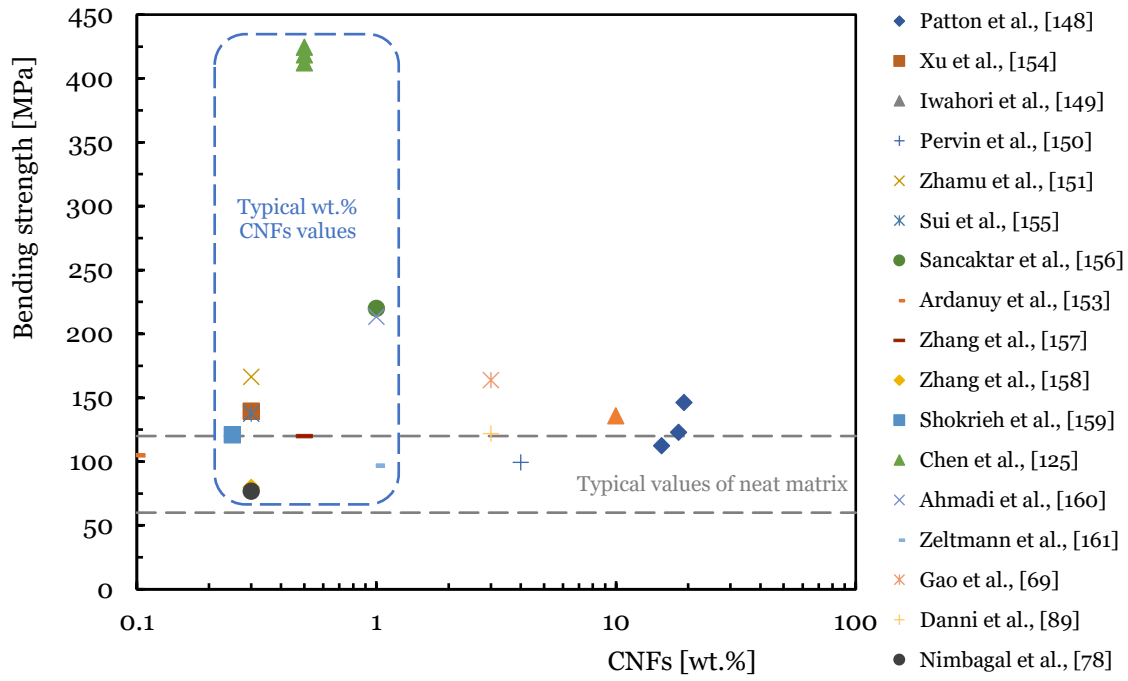

a)

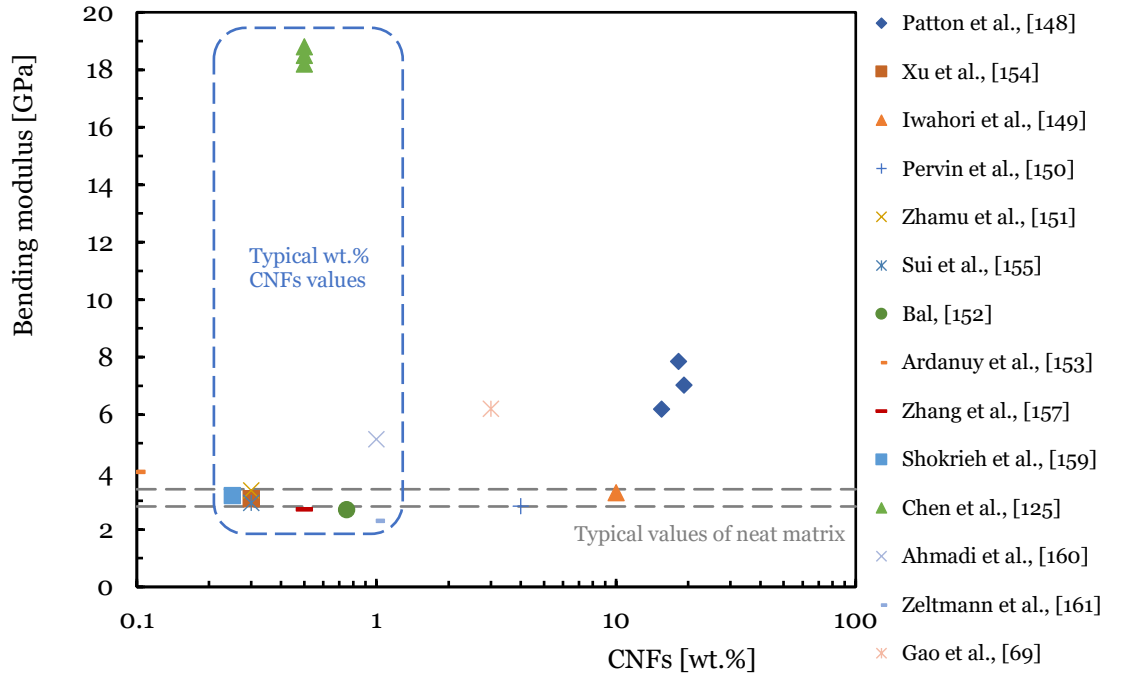

b)

Figure 2.7: Bending properties of various studies on epoxy matrix nano-enhanced with different wt.% CNFs: a) Bending strength; b) Bending modulus.

Similarly, Figure 2.7.b) show the results for the bending modulus, ranging from 2.3 to 18.8 GPa, being just added from 0.25 to 1 wt.% CNFs (area highlighted in blue). Other results were obtained for higher concentrations, from 3 to 19.2 wt.% CNFs, with notable improvements ranging from several tens to hundreds of percentages, Table 2.3. The majority are in the range or above the reference values of bending modulus for epoxy resins (dashed lines highlighted in gray), based on the values shown in Table 2.1. The application of proper dispersion techniques and optimizing

aspect ratios can result in improved bending modulus, strength, and overall performance of the epoxy matrix nanocomposites.

It is thus demonstrated that it is possible to maximize the static properties of epoxy resins, regardless of their mechanical, physical and chemical properties, by adding an optimal percentage of CNFs and optimizing the production process.

2.3.2. Bending properties of CNFs multiscale epoxy matrix composites

Regarding the benefits of the CNFs content on the bending response of epoxy matrix composite laminates, Table 2.5 provides an overview of the experimental work carried out on this subject, while Figure 2.8 summarizes the benefits obtained by each researcher reported above. One more time, the abscissa axis represents the percentage by wt.% CNFs, on a logarithmic scale, and on the ordinate axis, the percentage improvement in bending strength and modulus. Figure 2.8.a) shows the increase in bending strength for composite laminates with CNFs reinforcement, and Figure 2.8.b) illustrates the increase in bending modulus for composite laminates reinforced with CNFs. Different results show different degrees of improvement in mechanical properties, for example, the bending modulus improves significantly with the incorporation of CNFs.

Zhou et al. [135,136] conducted bending tests to investigate the effect of CNFs loading on the mechanical properties of the CF composites. The CNFs were infused into the epoxy resin through high-intensity ultrasonic irradiation and then mixed with a hardener using a high-speed mechanical stirrer. The test results revealed that incorporating 2 wt.% CNFs into the epoxy resulted in a 23.3% improvement in bending strength and a 2% improvement in bending modulus. At CNFs weight fractions below 2 wt.%, ultrasonic irradiations proved to be an effective method. However, when the fraction load exceeded 2 wt.%, CNFs agglomerates were observed.

In terms of static properties, Li et al. [110] observed that the addition of 20 g/m² of CNFs (approx. 12.7 wt.% CNFs) to carbon composites, prepared using a powder method for dispersing the nanofiller in the middle plane by hand lay-up of the laminate and manufactured by autoclave process, resulted in an approximate increase of 7.1% in bending strength and 10.1% in bending modulus compared to the control carbon composite. Too Green et al. [139] when adding 0.1 wt.% and 1 wt.% CNFs to produce multiscale GF reinforced composites applying the VARIM process, the bending strength increased by 17% and 20%, respectively, and the bending modulus increased 23% and 26%, respectively, when compared with the control composite. Miranda et al. [162], in your work, CNFs were grown in situ over the surface of a CF fabric by CVD, followed by laminate manufacturing by hot pressing. The results showed an overall reduction in mechanical properties as a function of added CNFs, for 1 wt.% CNFs the bending strength increased to 17% and the bending modulus had no influence by the deposition of CNFs over the surface of CF fabrics.

Chen et al. [125] used in your study small mass fractions (i.e., 0.1%, 0.3%, and 0.5%) of (expanded carbon nanofibres) ECNFs, VGCNFs and GCNFs surface-functionalized and oxidized with nitric acid and hexanediamine for the fabrication of hybrid multi-scale composites with woven fabrics of CF via the technique of VARTM and compared the mechanical properties. The results indicated that the incorporation of 0.5% ECNFs in the epoxy resin, resulted in the improvements of bending strength by 10.0%. In general, the reinforcement effect of ECNFs was like that of VGCNFs, while it was higher than that of GCNFs, as indicated in Table 2.3. The results of mechanical properties of hybrids multi-scale CFRPs allow us to conclude that the optimal mass fraction of ECNFs, VGCNFs, and GCNFs in the nano-epoxy resin is 0.3%. For example, the nano-epoxy resin with 0.3% VGCNFs resulted in a bending strength of 18.3%. In your study, Singer et al. [163] produced CFRP specimens were mechanically tested via a four-point bending test. The mechanical properties such as bending modulus and bending strength were improved by adding 0.7 wt.% CNFs to the resin compared to neat epoxy in 14%.

As the matrix is the most sensitive part to mechanical stress in a composite, the application of nano-enhanced matrix in the manufacture of polymer composites aims to maximize their already interesting mechanical properties. In this sense, and by observing Figures 2.8.a) and 2.8.b), it is worth highlighting a considerable group of works in which using an optimal quantity of CNFs, comprised between 0.3 and 1 wt.%, it was possible to maximize both the bending strength and the bending modulus (area highlighted in blue) in average values around 20% and 10% respectively, and in some cases it can be greater than 50%, as shown in Table 2.4. In other studies, the use of higher percentages of CNFs was also successful, with these values reaching up to 14.0 wt.% CNFs.

Different variables such as: the type of reinforcing fibre used, its properties and characteristics of the fabric (if applicable), fibre stacking sequence, number of composite layers and thickness, composite manufacturing process and post-curing process (if applied), type of epoxy resin and its properties (viscosity, polarity, among others), type of CNFs used, respective dimensions and additive amount of CNFs in an interlayer, test conditions (temperature, humidity) and mixing process used, contribute to final multiscale composite properties.

Overall, these studies highlight the potential of CNFs as reinforcing agents in FRP, with the optimal loading percentage depending on the specific application and type of reinforcement fibre. Careful selection of CNFs, dispersion methods, and processing techniques is crucial for achieving desired mechanical improvements in the resulting epoxy composites.

Table 2.5: Bending properties of CNFs multiscale fibre epoxy composites.

Autor, Ref.	Fibre/Matrix	CNFs Type	CNFs Integration Method	Manufacture Process	Optimum Loading (CNFs wt.%)	Bending Strength [MPa] (Increase (%))	Bending Modulus [GPa] (Increase (%))	Failure Strain [%] (Increase (%))
Iwahori et al., [149]	CF/EP	CSNFs	Mechanical mixing, passing through a vacuum chamber, and post-cure in a hot press.	Hand lay-up, vacuum application, and post-cure in a hot press.	10.0	789.5 (18.3%)	53.5 (4%)	-
Zhou et al., [135,136]	CF/EP	CNFs	High-intensity ultrasonic processing followed by high-speed mechanical mixing and high vacuum.	VARTM	2.0	597.0 ± 21 (22.3%)	49.4 ± 3.1 (1%)	1.27 ± 0.03 (8.5%)
Li et al., [110]	CF PrP/EP	VGCNFs	Powder method (applied in the middle plane by hand lay-up process).	Autoclave	12.7	1283.7 (7.1%)	114.1 (10.1%)	-
Green et al., [139]	E-GF/EP	CNFs	Mechanical mixer.	VARIM and compress	1.0	404.0 ± 18.6 (20%)	22.0 ± 0.5 (26%)	-
Bortz et al., [137]	CF/EP	CNFs	Hand mixing and TRM.	VARTM	1.0	~310 (over 9%)	~11.3 (over 10%)	-
Chen et al., [164]	CF/EP	ECNFs	Fabrication of mats of ECNFs.	VARTM with interlaminar regions containing mats of ECNFs.	~2.5	418.5 ± 11.7 (11%)	32.8 ± 7.8 (9%)	-
Miranda et al., [162]	CF/EP	CNFs	CNFs grown onto the surface of carbon fibre fabrics.	Hot pressed	1.0	~380.0 (17%)	31.5	-
Sarim et al., [165]	CF/EP	CNFs	CNFs dispersed using a high shear mix, sonicated in a bath ultrasonicator followed by a spray-up process.	VARTM	1.0	~160.0 (over 40%)	~30.0 (19%)	-
Chen et al., [166]	CF/EP	ECNFs	Thermal treatments of stabilization in air followed by carbonization in argon.	VARTM	14.0 (Collection time at 10 min)	465.6 ± 38.4 (23.5%)	24.8 ± 3.9 (105%)	-
Dhakate et al., [71]	CF PrP/EP	CNFs	Mixed and sonicated.	Impregnated and was applied temperature and pressure (hot plate).	1.1	730.0 (83.4%)	~40.0 (over 100%)	-
Chen et al., [125]	CF/EP	ECNFs VGCNFs GCNFs	Surfaces oxidation and functionalization. The nano-epoxy mixture was first subjected to ultrasonication, followed by mechanical stirring and degassing and finally post-curing.	VARTM	0.3	545.0 ± 9.5 (13.6%) 567.3 ± 21.8 (18.3%) 552.6 ± 44.8 (15.2%)	- - -	- - -
Jie. et al., [167]	CF/EP	CNFs	CVD	Manual stacking followed by heating at 2300 °C.	1.0	CF parallel CF vertical	- -	187.92 (45.6%) 11.23 (56.6%)	- -	- -
Singer et al., [163]	CF/EP	CNFs	TRM dispersion.	Infiltration and cure in a hot press.	0.7	~600.0 (14%)	~47.5 (14%)	-
Kattaguri et al., [168]	GF/EP	CNFs	EP resin was preheated, mechanical mixing at high speed, sonication, and degassing.	Hand lay-up followed by hot pressing.	1.0	~415.0 (29.0%)	~23.5 (~7%)	-
De et al., [132]	CF/EP	CNFs	Electrophoretic deposition (EPD) technique.	Hand lay-up, followed hot pressing.	0.5 [g/L]	191.0 ± 7.81 (6.7%)	13.0 ± 0.87 (30%)	3.14 ± 0.2 (36%)
Kar et al., [169]	GF/EP	CNFs	Magnetic stirring dispersion, ultrasonication, and degassing.	Hand lay-up, followed hot pressing.	1.0	~380 (~13%)	~20.0 (~8%)	-

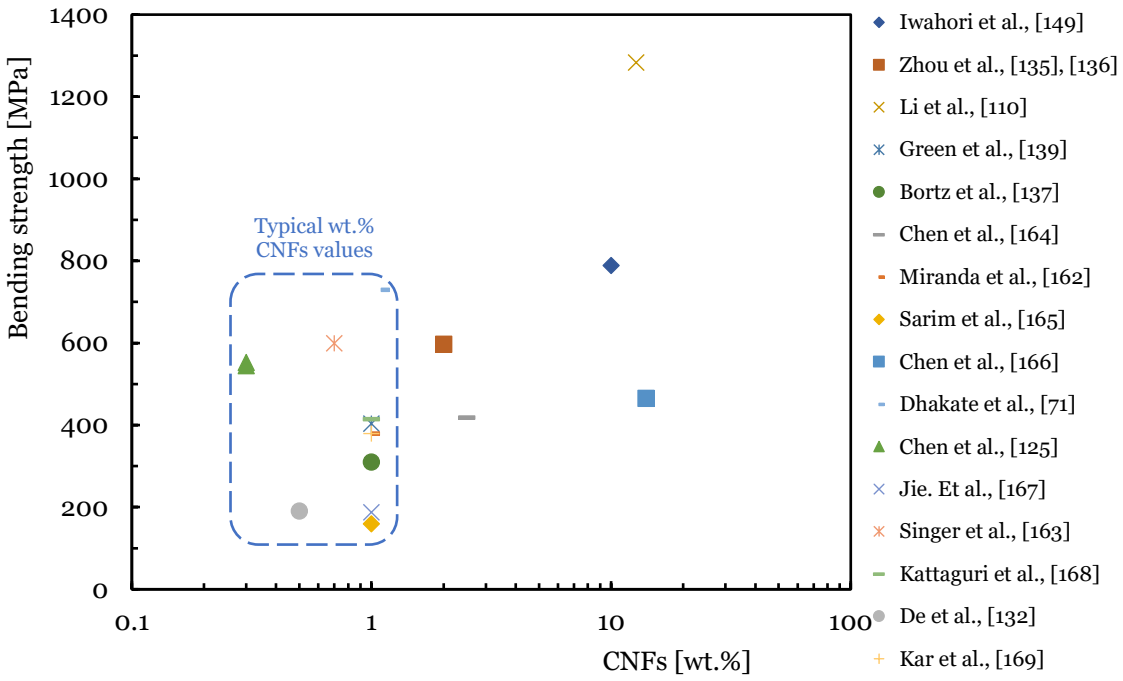

a)

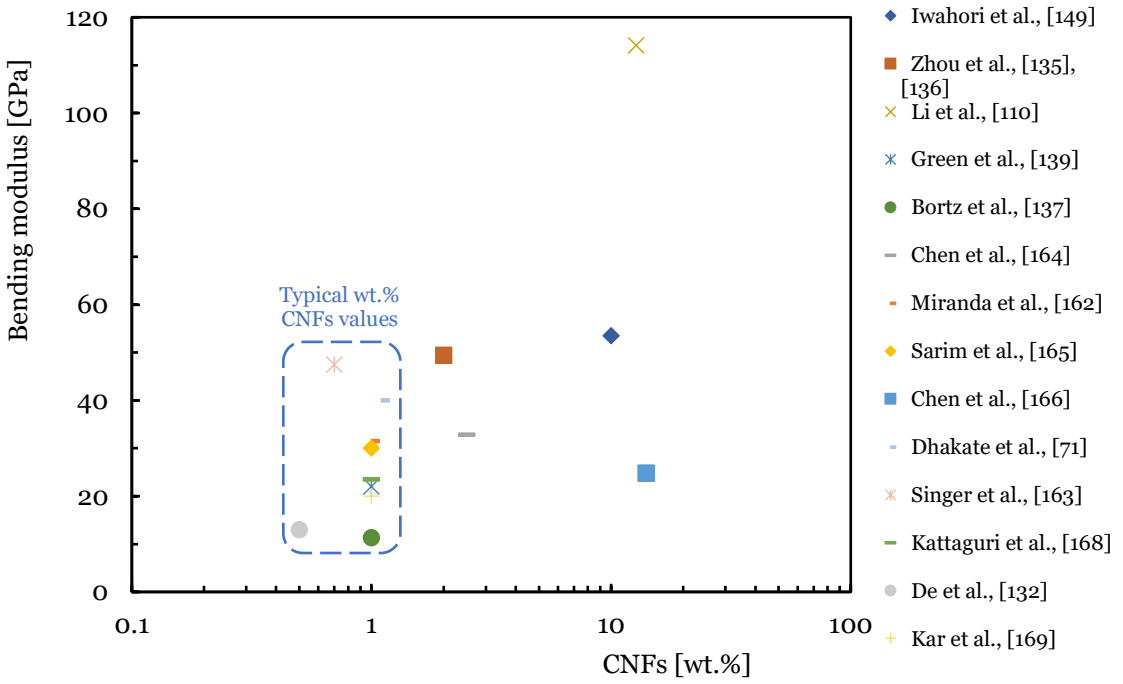

b)

Figure 2.8: Bending properties of various studies on epoxy composites nano-enhanced with different wt.% CNFs: a) Bending strength; b) Bending modulus.

2.3.3. Viscoelastic behaviour of CNFs multiscale epoxy matrix

2.3.3.1. Strain rate

Composites can behave differently under dynamic loading compared to static loading. The strain rate response helps to understand how a composite will perform under rapidly applied loads, which is critical in applications such as impact resistance and shock resistance. In industries such

as automotive, aerospace, and defence, where composites are often subjected to high strain rates during impacts or explosions, understanding strain rate response is essential to ensure safety and performance.

The mechanical properties of composites, such as yield strength, tensile strength, and ductility, can vary significantly with strain rate. For example, when composites are subjected to higher strain rates, their stress and modulus increase and their strain decreases. In the design phase, engineers must consider strain rate sensitivity when designing components that will experience different load rates. This will ensure that the selected composites will perform reliably under the expected service conditions.

The speed at which a material deforms is known as its strain rate, and varying strain rates can significantly affect a material's properties. In this context, the presence of CNFs may contribute to altering the sensitivity of the composite. Although there are not many studies on this topic in the literature, Table 2.6 summarizes the data in terms of strain rate effect on composites reinforced with CNFs, while Figures 9–10 quantify the benefits obtained with this nano-reinforcement in terms of strength and modulus.

Zhou et al. [76,170], for example, studied the tensile response of a nano-enhanced epoxy resin with different contents of CNFs (1, 2, and 3 wt.%) and for strain rates between 0.02 min^{-1} and 2 min^{-1}, observing that these nanocomposites are sensitive to the strain rate. For the range of strain rates studied, the authors observed a variation in tensile strength and modulus of around 13.0% and 20.3% for the neat resin and 21.6% and 20.5% for the nanocomposite reinforced with 2.0 wt.% of CNFs, respectively. Poveda et al. [171] studied the compressive response of syntactic foams reinforced with CNFs for strain rates between 1.7×10^{-6} and 50 min^{-1}, and observed that the strength and modulus increased by around 7.3% and 15.5%, respectively, compared to the values obtained for the control conditions.

According to Shokrieh et al. [172] the influence of adding 0.25 wt.% of VGCNFs on the tensile mechanical properties of the epoxy matrix at dynamic strain rates of 0.000028 min^{-1} leads to increases in tensile modulus and strength of 12.40% and 11.03%, respectively. Zhou et al. [173] studied the dynamic response to compression of epoxy composites functionalized with 0.75 wt.% CNFs for different loading rates (0.00005 to 60 min^{-1}) and obtained, for example, for a strain rate of 60 min^{-1}, an increase in Young's modulus and compressive strength of around 57% and 195.5%, respectively, compared to the neat epoxy matrix.

Kar et al. [169] studied the influence of loading rates on the bending performance for a temperature of 30 °C, and observed that adding 1 wt.% of CNFs to the laminate led to an increase in bending strength of around 13% and 14% and in bending modulus of around 9% and 18%, respectively, for 1 and 100 mm/min, due to the improvement promoted by CNFs in terms of stress transfer and a reduction in the rate of crack propagation.

Table 2.6: Strain rate of CNFs multiscale polymer composites.

Autor, Ref.	Fibre/Matrix	CNFs Type	CNFs Integration Method	Manufacture Process	Optimum Loading (CNFs wt.%)	Strain Rate
Zhou et al., [76,170]	-/EP	CNFs	High-intensity ultrasonic processing followed by high-speed mechanical mixing and high vacuum.	-	2.0	Tensile strength increase, tensile modulus increases, and failure strain decrease to neat and with 2.0 wt.% CNFs/EP to 0.02 min^{-1}, 0.2 min^{-1}, and 2 min^{-1} velocities.
Poveda et al., [171]	-/EP	CNFs	A mechanical mixer fitted with a high shear impeller was used, the mixture placed on a shaker for degassing and curing at RT.	-	1.0 to 10.0	The compressive strength and modulus under quasi-static testing increase.
Shokrieh et al., [172]	-/EP	VGCNFs	High speed mixing, sonication, and final degassing of the mixture.	-	0.25	Tensile strength and tensile modulus increase to neat EP and tensile strength decrease and tensile modulus increase to 0.25 wt.% CNFs/EP to 0.00167 min^{-1}, 0.1 min^{-1}, and 0.2 min^{-1} velocities.
Chanda et al., [174]	-/EP	CNFs	CNFs/epoxy were mixed by hand, sonicated and degassed in a vacuum oven. It was then placed between parallel aluminium electrodes and an electric field applied to produce a CNFs/epoxy composite aligned in the thickness direction.	-	0.4	The elastic modulus and tensile strength increased with increasing strain rates, to aligned composites and random composites, however, transversely aligned composites, compared to random composites, always exhibited lower modulus, strength and failure strain, under strain rates of 0.001, 0.01, 0.085, and 0.17 min^{-1}.
Zhou et al., [173]	-/EP	CNFs	Functionalization, mixture subjected to magnetic stirring and vacuum in an oven. Cured and post-cured at high temperatures.	-	0.75	To 0.00005 to 60 min^{-1} Young's modulus and compressive strength increases.
Kar et al., [169]	GF/EP	CNFs	Magnetic stirring dispersion, ultrasonication, and degassing.	Hand lay-up, followed hot pressing.	1.0	CNFs composite increases bending strength and bending modulus of GF with CNFs composite at 30 °C when tested at 1 and 100 mm/min loading rate

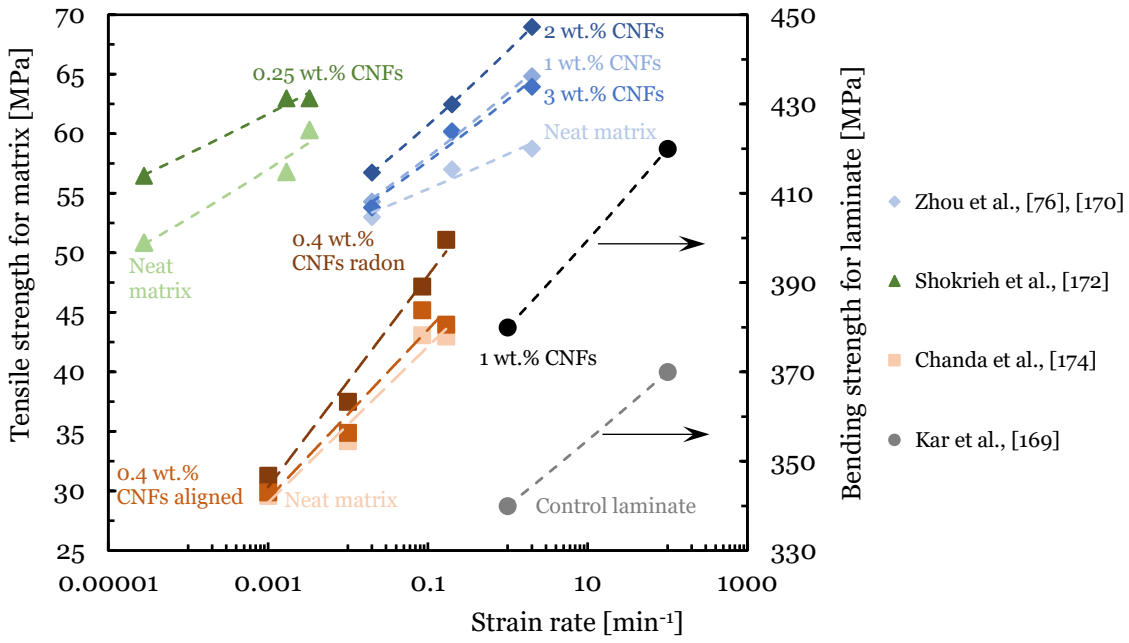

a)

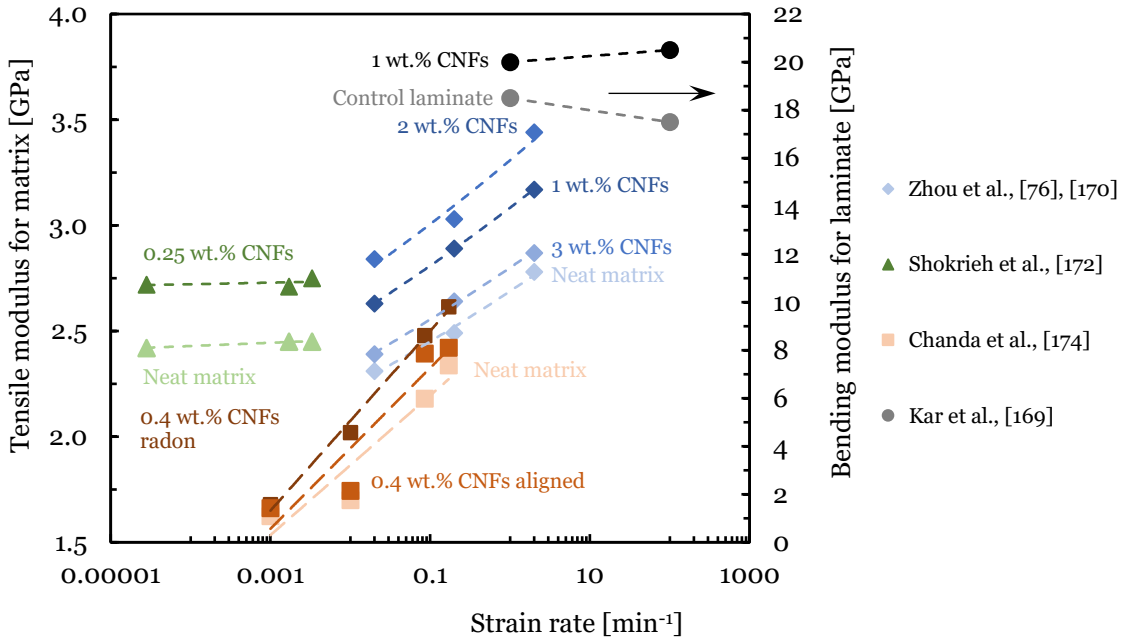

b)

Figure 2.9: Strain rate properties of various studies on epoxy matrix and epoxy composites nano-enhanced with different wt.% CNFs: a) Tensile strength and bending strength; b) Tensile modulus and bending modulus.

The neat and CNFs filled epoxy are strain rate-sensitive, as well reinforced with carbon long fibres. In general, the bending stress (Figure 2.9.a)) and modulus (Figure 2.9.b)) increase with the strain rate, while the strain at maximum bending stress decreases. Similar behaviour is observed for tensile studies, where bending (Figure 2.9.a)) and modulus (Figure 2.9.b)) increase with increasing strain rate. Finally, and taking into account the study of Figure 2.10, the neat epoxy

matrix and with various wt.% CNFs is also sensitive to the strain rate. Its compressive strength (Figure 2.10.a)) and its modulus (Figure 2.10.b)) increase as the strain rate increases.

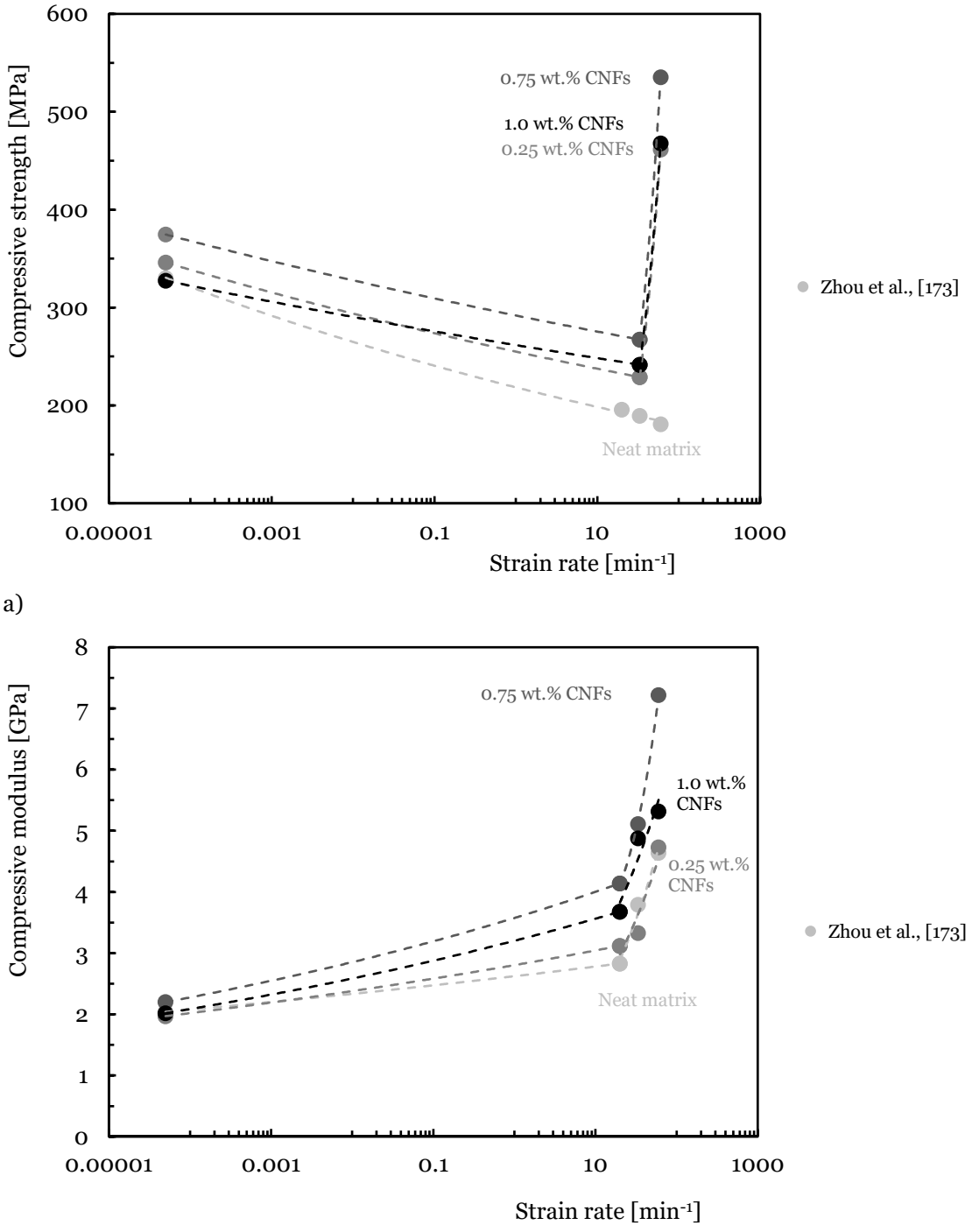

Figure 2.10: Strain rate properties of a study on epoxy matrix nano-enhanced with different wt.% CNFs: a) Compressive strength; b) Compressive modulus.

Given the gap in the literature, in terms of studying the mechanical characterization of the behaviour of epoxy polymers and fibre-reinforced composites when subjected to various strain rates, in particular, 3BP tests, it is therefore justified to carry out more experimental work, using

similar characterization conditions (at RT, range of strain rates), in order to better understand its behaviour when mechanically requested.

2.3.3.2. Stress relaxation and creep behaviour

In most engineering applications, understanding the stress relaxation and creep properties of polymer matrices and composites holds significant importance, especially concerning the need for long-term dimensional stability of structures/components. Nevertheless, the majority of published studies primarily focus on characterizing the mechanical behaviour of these complex systems at the quasi-static properties level, primarily examining tensile modes.

Based on existing literature, stress relaxation mechanisms in polymer systems are predominantly reliant on physical or chemical processes. Physical processes typically involve minimal formation or breakage of primary bonds, resulting in molecular rearrangements. Conversely, chemical processes encompass chain scission, crosslink scission, or crosslink formation [175]. However, when nanoparticles are added to the matrixes, these establish a network that contributes to restricting the mobility of the polymer chains [176].

Efficient load transfer, along with an optimal dispersion state, significantly influences the performance improvement of epoxy composites. When the dispersion state of nanoparticles is suboptimal or when nanoparticles exhibit random orientation during fabrication, the reinforcement effect may be inadequate or even lead to negative effects. Load transfer primarily depends on interfacial interactions, including weak fillers/polymer van der Waals interactions, potential chemical bonding through treatments, and mechanical interlocking due to irregular fibre surfaces.

However, when polymers are reinforced with long fibres, these obstruct molecular flow, leading to a delay in the relaxation process [177]. Additionally, interface properties play a crucial role because relaxation processes may arise from bond breakage and subsequent propagation. In composites, stress relaxation is a result of two mechanisms: relaxation within the matrix phase and the occurrence of fibre/matrix debonding zones followed by crack propagation [178].

In terms of creep, this phenomenon in polymers occurs even at room temperature and low stress levels due to the molecular motion within the backbone polymer arrangement [179]. For neat matrixes, creep results from a combination of viscous flow and elastic deformation [180]. Bouafif et al. [181] assert that molecular motions within the backbone polymer arrangement drive the creep phenomenon, influenced by stress levels. Jian et al. [182] propose a quantitative correlation between molecular mobility and macroscopic deformation. Inclusion of a relatively low amount of nanoparticles restricts the mobility of epoxy matrix polymer chains, impeding chain disentanglement and slippage. This hindered motion is suggested to enhance creep performance, although varying filler concentrations might elicit contradictory effects.

In this scenario, a substantial quantity of dispersed nanoparticles forms interphases that engage with the matrix through bridging segments and junctions, reinforcing load-bearing capability and reducing the polymer chain mobility [183]. CNFs contribute to this immobility by impeding slippage, realignment, and movement of polymeric chains [176]. This effect is attributed to three main mechanisms: (i) establishment of robust interfacial strength between CNFs and the matrix; (ii) CNFs functioning as obstruction sites; and (iii) the high aspect ratio of CNFs [184].

Increasing the filler weight fraction, while ensuring good dispersion, can notably decrease creep displacements. Nonetheless, at elevated weight fractions, the reinforcement efficacy diminishes due to agglomeration issues and deteriorating filler/epoxy adhesion [182].

In contrast, in composites reinforced with long fibres, the creep process is delayed or inhibited by these fibres due to their effect on elastic deformation and viscous flow. Consequently, as previously mentioned, the fibre/matrix interface plays a crucial role, governing the breakage of bonds and their propagation that ultimately controls creep displacement [185].

Almeida et al. [186] concluded that the fibre orientation of carbon/epoxy composites has influence on creep/recovery, stress relaxation. The laminate with longitudinally aligned fibres did not exhibit significant creep, and its storage modulus was the highest compared to the other angles studied (i.e., $[30^{o}]_4$ and $[60^{o}]_4$). The stress relaxation modulus was calculated using a 1% strain and showed a decrease with the fibre orientation angle. Reis et al. [187,188] investigated practical scenarios in which CFRPs are subjected to during their service life. These included the delamination effect on composite structures under bending loads and the impact of alkaline and acid solutions on stress relaxation behaviour. The most significant decrease in performance was observed when exposed to alkaline solutions, although this was strongly dependent on factors such as exposure time, temperature, and solution concentration. In addition to the viscoelastic nature of the matrix, operational conditions in harsh environments can degrade components made from composite materials. Therefore, for long-term applications, the tendency for the initial stress to be lost at higher rates should be appropriately considered in the design criteria.

At the moment, the literature on stress relaxation and creep studies of CNFs/epoxy matrix or CNFs/epoxy composites is not enlightening about their behaviour. However, there are numerous studies available that investigate the incorporation of other nanoparticles, such as carbon allotropes or nanoclays, into epoxy resin, a point worthy of further study.

2.3.4. Interlaminar shear strength of CNFs multiscale epoxy matrix composites

Composites with higher fibre-matrix adhesion, higher strength, and higher matrix toughness are desired because they can be subjected to high stresses during their service life, which can lead to crack propagation through the fibre-matrix interfaces. In order to evaluate this mechanical performance, it is usual to carry out short beam shear (SBS) tests to assess the interlaminar shear

strength (ILSS) of the composite. In this case, the shear force resulting from sliding between layers of the composite or its deformation between them is obtained.

Failure may not occur at the mid-plane, because it is difficult to ensure pure shear during [189]; however, failure results from a combination of different failure modes, such as microcracks in the resin, indentation, fibre breakage, micro-buckling, bending, and interlaminar shear cracking of the specimens [117,190]. It should be noted that the competition between failure mechanisms depends on the quality of the polymer matrix, the morphology of the fibre surface (smooth or rough), and the bonding mechanism between the fibre and the matrix [132].

CFRP composites have been widely used in various fields and industries, due to their exceptional weight-to-strength properties, but also show anisotropic behaviour and possible failure due to delamination. However, their ILSS and fracture toughness have been insufficient, which hinders their application in lightweight structures. According to the literature review, there are three methods to improve the ILSS and fracture toughness properties of CFRP composites:

i) Matrix toughening could improve the in-plane and interlaminar toughness of composites simultaneously, but it also introduces changes in the viscosity, T_g, and thermal properties of the resin, which would affect the manufacturing process of CFRP composites;

ii) Z-direction toughening, such as Z-pin and stitching, forms bridging structures in the interlaminar region of the composites to achieve an apparent toughening effect, but the in-plane properties would be reduced to some extent;

iii) The in-plane performance of composites using the 3D weaving method is significantly lower than that of typical laminates, but the long experimental process cycle, complex operating procedures and relatively high manufacturing costs limit their use in practical applications [147].

The reinforcement of the composites with CNFs, has the advantage that these have the interlocking and stress transfer capability of CNFs at the fibre/matrix interface [189]. The ILSS is expected to increase because of the improvement in epoxy matrix strength and fibre-matrix interface due to the good dispersion of the CNFs. The addition of the optimum percentage of CNFs results in a toughened epoxy matrix and promotes better interfacial bonding between the fibre and matrix, acting as a coupling between them. In addition, the high aspect ratio of the CNFs increases the interfacial area between the resin and the CNFs, resulting in improved mechanical properties. The high aspect ratio of CNFs can also prevent crack formation and crack propagation, resulting in improved performance. As the load on the CNFs increases beyond an optimum percentage, the CNFs have a tendency to agglomerate, and these agglomerations create stress concentrations that can act as crack initiation sites. These interfacial stress concentrations contribute to the debonding of the fibre from the matrix during loading and reduce the performance of the composite [116,189].

Table 2.7 provides a summary of published studies on the ILSS of multiscale composites of nano-enhanced epoxy resin with the ideal amount of CNFs by weight and reinforced with different types of fibres. Figure 2.11 show a summary of the ILSS results obtained by different researchers in recent years, as presented in Table 2.7.

Green et al. [139], for example, found increases of 23% when they nano-reinforced the matrix with 0.1 wt.% of CNFs in an E-glass/epoxy composite, but for 1 wt.%, the ILSS values obtained worsened due to the agglomerates formed or poor dispersion resulting from the manufacturing method used. Similarly, Bortz et al. [137] also observed a decrease compared to the control laminates, in this case of around 4%, when 1 wt.% of CNFs were added.

Chen et al. [164] found an increase in ILSS by incorporating ECNFs mats of around 86.2% compared to the control laminate, which represented an increase from 27.5 MPa to 51.2 MPa. Palmeri et al. [191] studied unidirectional and quasi-isotropic composites and observed that, in both cases, the ILSS increased when CNFs were added. In the case of unidirectional composites, the improvement was around 15% with the addition of 0.69 wt.% of CNFs, while in quasi-isotropic composites it was 22% with the addition of 0.67 wt.% of CNFs.

The studies carried out by Rodriguez et al. [192] showed that the incorporation of CNFs modified by deposition on the surface of the carbon fibre led to an improvement in the ILSS compared to composites reinforced with untreated fibres. In this case, the composite containing oxidized CNFs exhibited a 9.08% increase in ILSS, while the panels reinforced with amidized CNFs, deposited on both sized and unsized fibres using multiscale reinforcement fabrics (MRFs), showed even greater improvements. The ILSS increased by 10.01% for the panel with amidized CNFs deposited on sized fibres and by 12.44% for the panel with amidized CNFs deposited on unsized fibres. The addition of oxidized CNFs and amidized CNFs in these panels was 0.67 wt.% and 1 wt.%, respectively. Sarim et al. [165], obtained an increase of around 25% by incorporating 1 wt.% CNFs into laminates manufactured using the VARTM process.

In studies carried out by Khan et al. [193,194], the authors first impregnated the CNF sheets separately with the polymer and then integrated them into the composite. This method aimed to eliminate the weak wetting of nanofillers when present together with fibres/fabrics on a microscale in RTM or VARTM processes. By impregnating the CNFs sheets with polymer beforehand, the polymer could be infused throughout the bulk nanofiller–FRPCs composite, ensuring better compatibility and distribution of the nanofillers within the composite structure. Experimental studies developed by Chen et al. [166] showed that the deposition of electrospun precursor nanofibres on carbon fibre fabric leads to an improvement in ILSS of around 221.1% compared to the control laminates (i.e., an increase from 27.5 MPa to 88.3 MPa). Annad et al. [195] found that adding 0.5 wt.% CNFs to epoxy composites led to increases of 33% in ILSS, using the resin film infusion (RFI) technique.

Table 2.7: ILSS properties of CNFs multiscale composites.

Autor, Ref.	Fibre/Resin	CNFs Type	CNFs Integration Method	Manufacture Process	Optimum Loading (CNFs wt.%)	ILSS [MPa] (Increase (%))
Quaresimin et al., [129]	CF PrP/EP	VGCNFs	Dispersed in the EP system according to an attrition milling process.	Hand lay-up of prepreg. Curing performed using a vacuum bag and additional pressure.	7.5	~50.0 (~14%)
Green et al., [139]	E-GF/EP	CNFs	Mechanical mixer.	VARIM and compress.	0.1	43.85 ± 1.0 (23.6%)
Bortz et al., [137]	CF/EP	CNFs	Hand mixing and TRM.	VARTM	1.0	~50.0 (–4%)
Chen et al., [164]	CF/EP	ECNFs	Fabrication of mats of ECNFs.	VARTM with interlaminar regions containing mats of ECNFs.	~2.5	51.2 ± 4.9 (86.2%)
Palmeri et la., [191]	CF/EP	CNFs	Shear mixing.	hand placed	0.67	132.3.0 (15%)
Rodrigues et al., [192]	CF/EP	CNFs	Oxidized CNFs (O-CNFs) and amidized CNFs (A-CNFs).	VARTM	1.0	59.58 (12.4%)
Khan et al., [193]	CF/EP	CNFs	Simple soaking, hot compression moulding, and vacuum infiltration.	Bucky paper interleaves.	10.0	~70.0 (31%)
Miranda et al., [162]	CF/EP	CNFs	CNFs grown onto the surface of CF fabrics.	Hot pressed	0.2	~33.0 (–10%)
Arai et al., [143]	CF PrP/EP	VGCNFs	CNFs were inserted between prepregs layers using a sifter.	Autoclave	Area density of 10 [g/m^2]	52.2 (24.9%)
Sarim et al., [165]	CF/EP	CNFs	CNFs dispersed using a high shear mix, sonicated in a bath ultrasonicator followed by a spray-up process.	VARTM	1.0	~375.0 (25%)
Khan et al., [194]	CF/EP	CNFs	Simple soaking, hot compression moulding, and vacuum infiltration.	Bucky paper interleaves.	10.0	~69.0 (31%)
Chen et al., [166]	CF/EP	ECNFs	Thermal treatments of stabilization in air followed by carbonization in argon.	VARTM	14.0	88.3 ± 5.8 (221.1%)
Anand et al., [195]	E-GF/EP	CNFs	Mechanical probe sonicator and mechanical mixing.	RFI	0.5	83.6 ± 0.52 (33.1%)
Chen et al., [125]	CF/EP	ECNFs	Surfaces oxidation and functionalization. The nano-epoxy mixture was first subjected to ultrasonication, followed by mechanical stirring, and degassing and finally post-curing.	VARTM	0.3	45.8 ± 7.1 (42.2%)
		VGCNFs				38.3 ± 3.5 (18.9%)
		GCNFs				37.4 ± 1.3 (16.1%)
Zhou et al., [76]	CF/EP	CNFs	High-intensity ultrasonic processor and high-speed mechanical.	VARIM	2.0	41.6 ± 1.7 (15.9%)
Lake et al., [80]	CF/EP	CNFs	Producing a nanofibre mat composed of highly graphitic CNFs in an isotropic array.	VARTM	5.0	2250 (14.5%)
Ma et al., [196]	CF/EP	CNFs	High intensity ultrasonic atomizer probe and mechanical mixing.	Filter membrane assisted.	3.0	64.0 (50.9%)
				No filter membrane assisted.	1.0	45.5 (7.3%)
Srikanth et al., [123]	CF/EP	CNFs	Probe ultrasonicator followed by ball milling and aminofunctionalized.	Fabric layers were impregnated and compressed.	1.0	41.0 ± 1.1 (28.1%)

Table 2.7 (Continued)

Autor, Ref.	Fibre/Resin	CNFs Type	CNFs Integration Method	Manufacture Process	Optimum Loading (CNFs wt.%)	ILSS [MPa] (Increase (%))
Taheri-Behrooz et al., [197]	E-GF/EP	CNFs	Mixed and stirred, then sonicated using probe sonicator.	Vacuum-assisted hand lay-up.	0.25	44.76 ± 0.28 (19.5%)
Dhakate et al., [71]	CF PrP/EP	CNFs	Mixed and sonicated.	Impregnated and was applied temperature and pressure (hot plate).	1.1	55.0 (103.7%)
Kirmse et al., [144]	CF PrP/EP	CNFs	Flow-transferring a resin film containing electrical-field aligned CNFs.	Autoclave-vacuum bag.	1.0	53.93 (35.1%)
Yao et al., [198]	CF/EP	VGCNFs	Synthesis and spraying of the polymergrafted VGCNFs functionalized.	Degassed under vacuum, hot compressed.	0.4	83.0 ± 8 (72.9%)
Anjabin et al., [130]	Basalt/EP	CNFs	Functionalized and mixed using an overhead mechanical stirrer.	Hand lay-up, followed by static pressing.	0.3	80.2 (73.6%)
Kirmse et al., [199]	CF PrP/EP	CNFs z-threads	Shear mixing	Autoclave	0.85	44.81 (50.1%)
De et al., [132]	CF/EP	CNFs	Electrophoretic deposition (EDP) technique.	Hand lay-up, followed hot pressing.	0.5 [g/L]	~36.0 (16%)
Kirmse et al., [200]	CF PrP/EP	CNFs	High-sheared, sonicated, and degassed mixture.	Non-isothermal flow-transfer process.	1.0	69.72 ± 2.51 (7.4%)
Ranabhat et al., [201]	CF/EP	CNFs	Radial flow alignment technique.	Out-of-autoclave vacuum-bag-only (with 20% acetone in resin to create voids).	0.5	54.5 (24.2%)
Ravindran et al., [77]	CF/EP	CNFs	Hand-mixing followed by a TRM.	High pressure compression moulding process.	1.0	39.0 ± 1.9 (−5.6%)
He et al., [119]	CF/EP	CNFs	TRM	Multilayer resin film infusion-compressive moulding (with 10 min infusion).	0.3	53.65 (5.4%)
Yao et al., [147]	CF/EP	CNFs	Chemical vapor deposition.	Vacuum and temperature.	-	72.1 (18.6%)
Mrzljak et al., [202]	CF/EP	CNFs	Mechanical stirring under a vacuum and milled in a TRM and E-field was application to align the CNFs.	Hand-layup process and pressed in a hot press applied during curing.	0.7 random	55.5 ± 3.5 (6.1%)

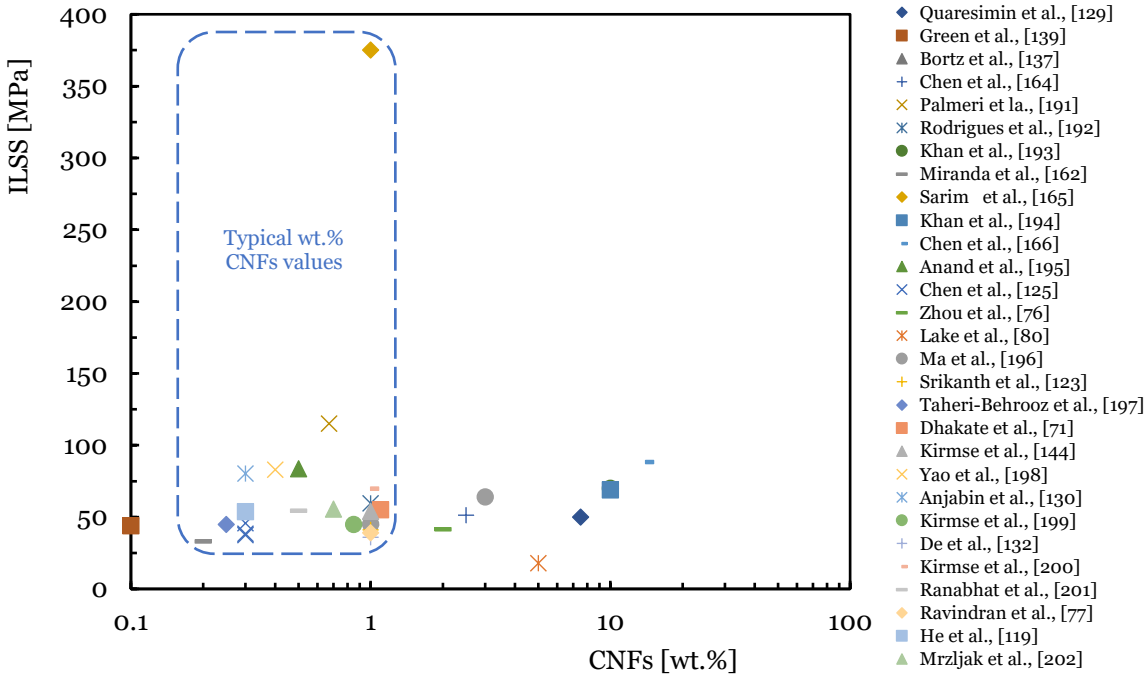

Figure 2.11: ILSS of various studies on epoxy composites nano-enhanced with different wt.% CNFs.

The studies performed by Chen et al. [125] showed that the inclusion of small contents of CNFs (between 0.1 wt.% and 0.3 wt.%) in the epoxy resin promotes significant improvements in the ILSS. Zhou et al. [76] used the VARIM technique to produce unidirectional composites with 2.0 wt.% CNFs and obtained an increase of around 15.8% in the ILSS compared to the control composites. Lake et al. [80] produced carbon/epoxy laminates, and the highest increase in ILSS, about 14.5%, was observed for the composite incorporating 5.0 wt.% of CNFs.

Ma et al. [196] used the filter membrane-assisted method to produce carbon/epoxy composites reinforced with CNFs and observed the highest increase in ILSS of around 55% for 3.0 wt.% of CNFs, while in the non-membrane-assisted method, the maximum increase in ILSS achieved was 11% and obtained for 1 wt.% of CNFs. Dhakate et al. [71], reinforced only the interlaminar region between the fabric layers with 1.1 wt.% of CNFs, which led to an increase in ILSS of around 190% compared to the control composite. Yao et al. [198] used 0.4 wt.%-modified CNFs and obtained a 73% increase in ILSS. Ranabhat et al. [201] showed that the ILSS can increase by around 24.2% when a CF/epoxy composite is reinforced with 0.5 wt.% CNFs.

Failure of composites is often caused by destruction of the interface. Improving the bond strength is critical to the preparation of high-performance composites. Incorporating CNFs into the epoxy matrix increases its strength and improves the interface, thereby increasing the stress transfer and consequently the ILSS of the composites. When CNFs are sufficiently and effectively oriented along the thickness direction and stitched into the interfibre space, they can modify the distribution of interlaminar shear stress and increase the ILSS. This improvement in interlaminar properties is driven by the roughness induced by the nanofillers, which increases the wettability

of the fibres and results in excellent mechanical interlocking between the fibre and the matrix. The improvement in ILSS with the addition of CNFs can be attributed to the nanoscale reinforcement provided by the presence of CNFs. These nanofibres bridge microcracks and prevent crack front propagation. The high aspect ratio and large surface area of CNFs facilitate effective stress transfer between the matrix and the fibres. In addition, CNFs can improve the toughness of the matrix, increasing its ability to absorb energy and delay delamination [119,132,147].

As shown in Table 2.7 and observing Figure 2.11 it can be concluded that the most results obtained for ILSS are concentrated at a very narrow range, where the CNFs reinforcement is approximately 0.65 ± 0.45 wt.% CNFs (area highlighted in blue) and the ILSS values are dispersed in a range of 33 to 375 MPa. Notably, significant improvements have been achieved within this range. Other results were obtained for higher CNFs addition values from 2 to 14 wt.%. The result that stands out is that obtained by Ali et al. [165], due to the manufacture of the laminate with 10 layers of CF and the application of a very efficient manufacturing process, VARTM, thus obtaining a control value of approximately 300 MPa, and consequently with the addition of 1 wt.% CNFs, an improvement of around 25%.

Variables such as the type of type and properties of the reinforcing fibre (density, fibre orientation), number of layers, CNFs/epoxy resin mixing method, laminate production process, physical/mechanical properties of the epoxy resin (viscosity, density) and test conditions contribute to the final response of the laminate to interlaminar fracture. It should be noted that the type of CNFs and the amount added have a direct influence on the final properties.

2.3.5. Mode I and Mode II interlaminar fracture of CNFs multiscale epoxy matrix composites

Continuous fibres reinforced polymer composites have excellent in-plane strength, but delamination damage is considered to be the most critical damage mode as the associated loss of stiffness can lead to catastrophic failure of the structure, particularly under compressive loading [203]. Fracture toughness, or the resistance of the composite interface to crack propagation, is an important material property to study. Mechanically, three different failure modes have been defined: Mode I is characterised by out-of-plane tensile crack initiation; Mode II is characterised by in-plane shear loading; and Mode III describes out-of-plane shear loading. For a composite material in service, pure mode loading is extremely rare and mixed Mode I/II loading is typical of the above scenarios.

In double cantilever beam laminates subjected to Mode I opening, the critical strain energy release rate (G_{IC}) of ILFT is a crucial factor monitored concerning slow, stable crack propagation. Generally, a characteristic R-curve behaviour is observed, wherein G_{IC} exhibits an increase during the initial crack propagation phase, attributed to translaminar failure mechanisms like fibre bridging. This increase continues until a stable state is achieved, after which G_{IC} reaches a point

of independence from further crack growth [191]. Conversely, Mode II ILFT (G_{IIC}) is a significant property influencing the resistance of laminated fibre composites against delamination and impact damage [194].

To enhance composite resistance against delamination cracking, numerous effective methods have been identified to bolster the delamination toughness in both Mode I and Mode II. Several exemplars of these strategies include: (i) incorporating high-toughness particles (such as elastomeric or thermoplastic fillers) or carbon allotropes into the polymer matrix can significantly enhance its properties. This enhancement is contingent upon the proportionate content of fillers, whether used singularly or in conjunction (in the instance of hybrid nano reinforcement); (ii) tailoring of the fibre types and orientation can be employed to encourage fibre bridging, alongside surface modifications applied to the fibres; (iii) insertion of interleaves or veils composed of thermoplastic, nanofibrous, aramid, or other high-toughness materials between the plies can be implemented; and (iv) macro-scale through the thickness fibre reinforcement methods, such as stitching, pinning, and orthogonal weaving, are employed to facilitate crack bridging within composite materials. These approaches prove effective in enhancing the delamination toughness of composites, supporting Mode I, Mode II, and mixed-Mode I/II interlaminar loading conditions. [204].

The results of several studies indicate that the use of higher aspect ratio CNFs placed in an interlayer between fibre reinforced plies is the most effective means of improving the fracture toughness of the laminated composite [145,205], due mainly to two factors acting complexly, one is that micro fibre bridging occurred at CNFs/epoxy matrix interface, and the other is that CNFs could control propagation of the delamination which occurred at CF/matrix interfaces.

Table 2.8 summarizes the recent experimental work on the study of multiscale composites with different types of fibres and epoxy matrix reinforced with CNFs and their effect on the Mode I, Mode II fracture mechanical properties of nanocomposite materials. The Figure 2.10 shows us in a summarized form these same results obtained, in terms of Mode I fracture toughness, G_{IC} (Figure 2.12.a)) and Mode II fracture toughness, G_{IIC} (Figure 2.12.b)).

According to Arai et al. [145], for example, incorporating 20 g/m² of CNFs into the interlayer of a unidirectional carbon/epoxy composite can increase the Mode I fracture toughness by around 50% compared to control laminates, while the Mode II fracture toughness was 2 to 3 times higher. Zhu et al. [205] carried out a similar study incorporating 0.5 wt.% of modified CNFs in specific areas of the resin layer, especially in the region surrounding the fracture plane and along the delamination growth path, and obtained improvements of 57% and 49% for Mode I and Mode II, respectively. In the study performed by Yokozeki et al. [206], authors obtained improvements in ILFT using modified CNFs. Gude et al. [207] used 0.25 wt.% CNFs and found improvements of around 10% in G_{IC}. Kostopoulos et al. [131] obtained a 100% increase in fracture energy by incorporating 1 wt.% CNFs into the composite matrix due to the extensive fibre bridging promoted by the CNFs.

Table 2.8: Mode I ILFT (G_{IC}) and Mode II ILFT (G_{IIC}) of CNFs multiscale composites.

Autor, Ref.	Fibre/Matrix	Fiber weight percentage (wt.%)	CNFs Type	CNFs Integration Method	Manufacture Process	Optimum Loading (CNFs wt.%)	G_{IC} [kJ/m²] (Increase (%))	G_{IIC} [kJ/m²] (Increase (%))
Kostopoulos et al., [208]	CF/EP	~ 42.5	CNFs	-	Hand lay-up followed autoclave process.	1.0	~0.8 (100% by MBT); ~1.0 (100% by areas method)	~2.6 (50% by MBT); ~2.2 (57% by areas method)
Kostopoulos et al., [209]	CF/EP	~ 52	CNFs	Mixing and vacuum.	Hand lay-up followed autoclave process.	1.0	0.91 (133.3% by MBT); 1.0 (100% by area method);	-
Tsantzalis et al., [210]	CF/EP	~ 52	CNFs	Temperature and vacuum.	Hand lay-up followed autoclave process.	1.0	~0.8 (100% by MBT); ~1.0 (100% by areas method)	-
Quaresimin et al., [129]	CF PrP/EP	~ 73	VGCNFs	Dispersed in the EP system according to an attrition milling process.	Prepreg hand lay-up. Curing using a vacuum bag between a platen press under vacuum and additional pressure.	7.5	~0.09 (initiation decrease ~ 55%); ~0.14 (propagation decrease ~ 70%)	~1.5 (over 100%)
Arai et al., [145]	VGCF PrP/EP	65	VGCNFs	VGCNFs/EP interlayer: VGCNFs/ethanol mixed manually and dispersed using a roller.	Autoclave	20 [g/m²]	~0.65 (23.8%)	~0.28 (100%)
Li et al., [110]	VGCF PrP/EP	~ 57	VGCNFs	Powder method (applied in the middle plane by hand lay-up process).	Autoclave	20 [g/m²]	0.432 (95.5% critical load); 0.616 (26% fracture resistance)	-
Yokozeki et al., [206]	CF/EP	67	CSCNFs	CSCNFs dispersed EP (sprinkle) and CSCNFs dispersed film between layers (planetary mixer and dispersed using the wet mill with ceramic beads).	Hand lay-up followed autoclave.	5.0 wt.% CSCNFs-dispersed EP with 10.0 wt.% CSCNFs-dispersed film between layers.	0.227 (167%)	1.753 (208.6%)
Bortz et al., [137]	CF/EP	~ 58 to 64	CNFs	Hand mixing and TRM.	VARTM	1.0	~0.42 (35%)	-
Gude et al., [207]	CF PrP/EP	~ 66	CNFs	Dispersion	Autoclave	0.5	0.0991 ± 0.0077 by area method; 0.096 ± 0.0087 by CBT; 0.0967 ± 0.0082 by ECM; (~15% for all methods)	-

Table 2.8 (Continued)

Autor, Ref.	Fibre/Matrix	Fiber weight percentage (wt.%)	CNFs Type	CNFs Integration Method	Manufacture Process	Optimum Loading (CNFs wt.%)	G_{IC} [kJ/m²] (Increase (%))	G_{IIC} [kJ/m²] (Increase (%))
Kostopoulos et al., [131]	CF/EP	~ 62.5	VGCNFs	Mixing and declassification by applying vacuum.	Hand lay-up and cured in an autoclave, using the vacuum bag technique.	1.0	0.79 (100% by MTB); 1.002 (100% by areas method)	2.626 (86.4% by MTB); 2.195 (55.8% by areas method)
Palmeri et la., [191]	CF/EP	~ 65	CNFs	Shear mixing	Hand placed	0.67	~1.40 (decrease ~ 20%)	-
Khan et al., [193,194]	CF/EP	~ 55	CNFs	Simple soaking, hot compression moulding and vacuum infiltration.	Bucky paper interleaves.	10.0	-	~2.49 (104%)
Hu et al., [111]	CF PrP/EP	-	VFCNFs	Manually dispersed (zigzag pattern) using the powder method.	Autoclave	20 [g/m²]	0.432 (95.5% critical load); ~0.62 (~30% fracture resistance)	-
Zhu et al., [205]	S2-GF/EP	~ 77	CNFs	Functionalized: magnetically stirred, sonicated in an ultrasonic bath with temperature.	Wet filament winding method and hot pressing.	Neat	0.165 ± 0.014 (onset 30%); 0.903 ± 0.0015 (propagation 47%)	0.783 ± 0.0037 (onset 39%); 0.996 ± 0.0067 (propagation 46%)
						0.5 Functionalized	0.176 ± 0.0084 (onset 39%); 0.968 ± 0.0041 (propagation 57%)	0.843 ± 0.011 (onset 49%); 0.963 ± 0.0023 (propagation 41%)
Koissin et al., [140]	CF/EP	-	CNFs	Infusion	Hand lay-up	2.6	~1.1 (crack start ~ 95%); ~0.9 (crack stop 140%)	-
Arai et al., [211]	CF/EP	-	VGCNFs	planetary centrifugal mixer.	VARTM	10 [g/m²]	~0 55 (20%)	-
Wang et al., [212]	CF/EP	-	CNFs	CNFs functionalized, sonication, and vacuum applied at the end.	Vacuum and hot pressure applied.	0.5	~0.30 (13.6%)	~0.51 (21.7%)
						1.0	~0.29 (9%)	~0.61 (45.3%)
Ma et al., [196]	CF/EP	~ 74 to 77	CNFs	High intensity ultrasonic atomizer probe and mechanical mixing.	Filter membrane assisted.	3.0	-	~0.815 (~90%)
Ladani et al., [213]	CF/EP	-	CNFs	TRM to disperse and E-field application.	Cured at RT.	1.6	2.345 (1650%)	-
Wu et al., [214]	CF/EP	-	VGCNFs	Magnetic stirring to functionalise the CNFs (ultraprobe sonication and simultaneous stirring). Sonication of the EP and subjected to a magnetic field.	Joints bonded using the Fe_3O_4 at CNFs/EP were cured at RT.	0.4	0.328 (144.8% aligned) 0.242 (80.6% random)	-

Table 2.8 (Continued)

Autor, Ref.	Fibre/Matrix	Fiber weight percentage (wt.%)	CNFs Type	CNFs Integration Method	Manufacture Process	Optimum Loading (CNFs wt.%)	G_{IC} [kJ/m²] (Increase (%))	G_{IIC} [kJ/m²] (Increase (%))
Gude et al., [127]	CF PrP/EP	~ 67	CNFs	EP adhesive was dispersed in chloroform and mixed by ultrasonication.	Two surface treatments applied to the laminates: grit blasting and atmospheric plasma and cured in the autoclave with vacuum bag.	0.5	~0.090 (~10% peel-ply) 0.2755 ± 0.0091 (26.5% grit blasted) 0.1739 ± 0.0361 (4.7% plasma)	-
Hsiao et al., [215]	CF PrP/EP	~ 63	CNFs	Magnetic stirrer, high shear mixing followed by agitation in a sonicator and then degassing.	Hand wet lay-up process and placed on a hot plate.	0.3	0.348 (14%)	-
Ladani et al., [216]	CF/EP	-	CNFs	TRM	Wet hand-layup process and cured at RT in the hydraulic press.	1.0	1.123 (67.6%)	-
Ladani et al., [217]	CF/EP	-	CNFs	TRM and E-field application.	DCB joints as a 2 mm thick adhesive layer bonding.	2.0	2.16 (1490% random) 2.27 (1570% aligned)	-
Wu et al., [121]	E-GF/EP	~ 60	VGCNFs	TRM, hand lay-up process and E-field application.	Vacuum bag, the matrix was then cured at RT.	0.7	Initiation toughness: ~0.6 (50% random) ~0.8 (100% aligned) Steady state toughness: ~1.5 (25% random); ~2.16 (80% aligned)	-
Ladani et al., [120]	CF PrP/EP	-	CNFs	TRM and E-field application.	Autoclave	1.0	1.29 ± 0.112 (862.7% random) 1.642 ± 0.161 (1125% aligned)	-
Ravindran et al., [122]	CF PrP + E-GF PrP/EP	-	CNFs	TRM and E-field application.	Autoclave	1.0	1.260 (830% random)	-
Ladani et al., [218]	CF PrP/EP	-	CNFs	TRM dispersion.	Nano EP adhesive layer was cured at RT.	2.0	~2.16 (1570%)	-
Ravindran et al., [219]	CF/EP	~ 60 to 65	CNFs	Hand mixing and TRM.	Liquid compression moulding.	1.0	1.40 ± 0.12 (91%)	2.88 ± 0.24 (42%)
Ravindran et al., [74]	CF/EP	~ 60 to 65	CNFs	CNFs hand-mixed into the EP and passed four times through a TRM.	Wet compression moulding process (consolidation in a hydraulic press).	5.0	0.84 ± 0.15 (240% initiation toughness) 2.04 (179.5% steady state toughness)	-
Ravindran et al., [204]	CF/EP	~ 60 to 65	CNFs	Hand-mixed into liquid EP, then passed four times through a TRM.	Liquid compression moulding approach.	5.0	-	3.39 ± 0.14 (66%)
Ekhtiyari et al., [220]	E-GF/EP	~ 65.4	CNFs	High speed mechanical stirring and ultrasonic agitation.	Hand lay-up process.	0.25	~0.70 (13.5%)	-
Ravindran et al., [75]	CF PrP/EP	-	CNFs	CNFs hand-mixed into the ER and passed four times through a TRM.	Wet-hand lay-up process and vacuum.	1.0	1.40 ± 0.12 (91.8%)	2.88 ± 0.24 (41.2%)

Table 2.8 (Continued)

Autor, Ref.	Fibre/Matrix	Fiber weight percentage (wt.%)	CNFs Type	CNFs Integration Method	Manufacture Process	Optimum Loading (CNFs wt.%)	G_{IC} [kJ/m²] (Increase (%))	G_{IIC} [kJ/m²] (Increase (%))
Gude et al., [127]	CF PrP/EP	~ 67	CNFs	EP adhesive was dispersed in chloroform and mixed by ultrasonication.	Two surface treatments applied to the laminates: grit blasting and atmospheric plasma and cured in the autoclave with vacuum bag.	0.5	~0.090 (~10% peel-ply) 0.2755 ± 0.0091 (26.5% grit blasted) 0.1739 ± 0.0361 (4.7% plasma)	-
Hsiao et al., [215]	CF PrP/EP	~ 63	CNFs	Magnetic stirrer, high shear mixing followed by agitation in a sonicator and then degassing.	Hand wet lay-up process and placed on a hot plate.	0.3	0.348 (14%)	-
Ladani et al., [216]	CF/EP	-	CNFs	TRM	Wet hand-layup process and cured at RT in the hydraulic press.	1.0	1.123 (67.6%)	-
Ladani et al., [217]	CF/EP	-	CNFs	TRM and E-field application.	DCB joints as a 2 mm thick adhesive layer bonding.	2.0	2.16 (1490% random) 2.27 (1570% aligned)	-
Wu et al., [121]	E-GF/EP	~ 60	VGCNFs	TRM, hand lay-up process and E-field application.	Vacuum bag, the matrix was then cured at RT.	0.7	Initiation toughness: ~0.6 (50% random) ~0.8 (100% aligned) Steady state toughness: ~1.5 (25% random); ~2.16 (80% aligned)	-
Ladani et al., [120]	CF PrP/EP	-	CNFs	TRM and E-field application.	Autoclave	1.0	1.29 ± 0.112 (862.7% random) 1.642 ± 0.161 (1125% aligned)	-
Ravindran et al., [122]	CF PrP + E-GF PrP/EP	-	CNFs	TRM and E-field application.	Autoclave	1.0	1.260 (830% random)	-
Ladani et al., [218]	CF PrP/EP	-	CNFs	TRM dispersion.	Nano EP adhesive layer was cured at RT.	2.0	~2.16 (1570%)	-
Ravindran et al., [219]	CF/EP	~ 60 to 65	CNFs	Hand mixing and TRM.	Liquid compression moulding.	1.0	1.40 ± 0.12 (91%)	2.88 ± 0.24 (42%)
Ravindran et al., [74]	CF/EP	~ 60 to 65	CNFs	CNFs hand-mixed into the EP and passed four times through a TRM.	Wet compression moulding process (consolidation in a hydraulic press).	5.0	0.84 ± 0.15 (240% initiation toughness) 2.04 (179.5% steady state toughness)	-
Ravindran et al., [204]	CF/EP	~ 60 to 65	CNFs	Hand-mixed into liquid EP, then passed four times through a TRM.	Liquid compression moulding approach.	5.0	-	3.39 ± 0.14 (66%)
Ekhtiyari et al., [220]	E-GF/EP	~ 65.4	CNFs	High speed mechanical stirring and ultrasonic agitation.	Hand lay-up process.	0.25	~0.70 (13.5%)	-
Ravindran et al., [75]	CF PrP/EP	-	CNFs	CNFs hand-mixed into the ER and passed four times through a TRM.	Wet-hand lay-up process and vacuum.	1.0	1.40 ± 0.12 (91.8%)	2.88 ± 0.24 (41.2%)

Table 2.8 (Continued)

Autor, Ref.	Fibre/Matrix	Fiber weight percentage (wt.%)	CNFs Type	CNFs Integration Method	Manufacture Process	Optimum Loading (CNFs wt.%)	G_{IC} [kJ/m²] (Increase (%))	G_{IIC} [kJ/m²] (Increase (%))
Kavosi et al., [138]	CF PrP/EP	-	CNFs	Functionalized	VARTM	2.0	~0.5 (25%)	-
Ravindran et al., [77]	CF/EP	-	CNFs	Hand-mixing followed by a TRM.	High pressure compression moulding process.	1.0	1.40 ± 0.12 (91% initiation toughness)	2.88 ± 0.24(42% initiation toughness)
							0.55 (~120% steady state toughness)	1.25 (~5% steady state toughness)

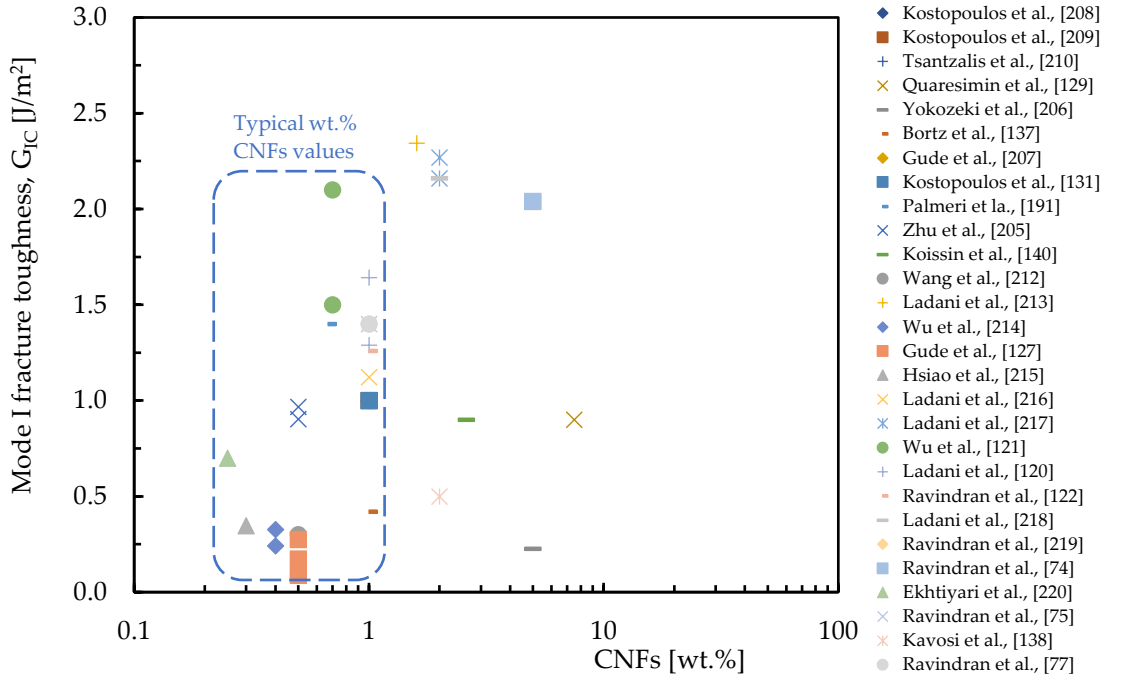

a)

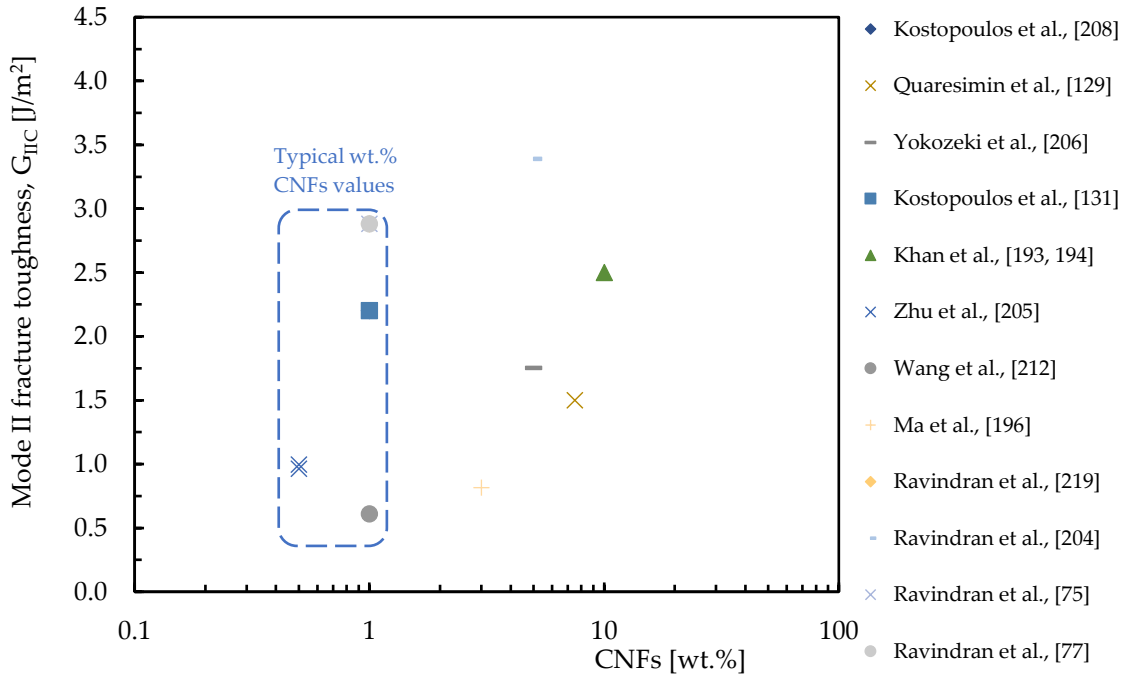

b)

Figure 2.12: Steady-state ILFT values of various studies on epoxy composites nano-enhanced with different wt.% CNFs: a) Mode I; b) Mode II.

Ladani et al. [213] and Ravindran et al. [74,219] observed that incorporating CNFs with through-thickness fibre rod reinforcements, such as z-pins, can promote synergistic effects on ILFT. In this case, the combination of multiple reinforcements can promote additional toughening mechanisms that are not present in the case of single reinforcements. In another study, Ladini et al. [120] also concluded that CNFs are effective in increasing delamination resistance with just 1 wt.% of CNFs.

Figures 2.12.a) and 2.12.b) show us numerous studies in which the addition of CNFs improvement the Mode I and Mode II ILFT of fibre reinforced epoxy composites without compromising their excellent in-plane mechanical properties. The use of CNFs as toughening agents in composite laminates offers several advantages, including multifunctional properties, minimal impact on the design and fabrication processes, and particularly significant increases in ILFT with small concentrations wt.% dispersed in the epoxy matrix, as demonstrated in the majority of published studies.

As shown in Table 2.8 and observing Figure 2.12.a) it can be concluded that the most results obtained for G_{IC} are concentrated at a very narrow range, where the CNFs reinforcement is approximately 0.75 ± 0.5 wt.% CNFs (area highlighted in blue) and the G_{IC} values are dispersed in a range of 0.09 to 2.1 J/m². Notably, significant improvements have been achieved within this range. Other results were obtained for higher CNFs addition values, ranging between 1.6 and 7.5 wt.%. Variables such as the type of epoxy resin applied and its matrix/CNFs and matrix/reinforcement fibre interface properties, viscosity, type of CNFs, their dimensions and properties, applied mixing method and test conditions contributed to these improvements.

Similarly, Figure 2.12.b) show the results for G_{IIC}, were that the reinforcement of CNFs ranges from 0.5 to 10 wt.%, with part of the results being just added 0.5 to 1 wt.% CNFs (area highlighted in blue), with notable improvements of several hundred percent, Table 2.7. The G_{IIC} values are dispersed in a range from 0.61 to 3.39 J/m², and the justification for such dispersion ranges from the properties of the laminate constituents (epoxy matrix, CNFs and reinforcing fibres types), manufacturing method and final characteristics of the laminates (mechanical, physical and chemical).

Depending on factors such as the type of CNFs, the method of CNFs incorporation into the epoxy resin, the type of reinforcing fibre utilized, and the specific manufacturing process employed for the laminates, these improvements can vary from tens to hundreds of percentage points.

2.3.6. Low-velocity impact of CNFs multiscale epoxy matrix composites

In service, composite structures can be subjected to out-of-plane impact loads, either by natural factors (e.g., falling branches from trees, hail, bird by strikes), or by other factors (e.g., tools falling during maintenance operations or impact of small foreign bodies) which can result in the separation of adjacent layers, known as delamination [203]. The dynamic behaviour of composites under impact loading, particularly low-velocity impact, is very complex, as many phenomena occur simultaneously during composite failure, such as, fibre breakage, delamination's, matrix cracking, plastic deformations due to the contact and large displacements [221]. Fibres reinforced composites nano-enhanced with CNFs, when subjected to low-velocity impact, exhibit several desirable properties: enhanced impact resistance, damage tolerance,

improved strength and stiffness, reduced energy absorption and residual denting and weight denting as well as, weight reduction.

In recent years, epoxy composites infused with nanoparticles like nano clay, CNTs, GP, different metal and metal oxides have gained interest due to improved mechanical response, in particular in improving low-velocity impact properties. Table 2.9 presents a compilation of recent studies that investigate the response of epoxy composites reinforced with CNFs under low-velocity impact loads. These studies focus on properties such as energy to peak load (Figure 2.13.a)), energy to maximum load, absorbed energy (Figure 2.13.b)) and damage area (Figure 2.13.c)). Thus, a visual comparison is made of the effect of adding CNFs.

CNFs have been shown to enhance the impact damage resistance of laminates. Bhuiyan et al. [222] investigated the reinforcement of foam cores in sandwich composites with CNFs and found that a 0.2 wt.% infusion of CNFs resulted in the highest improvement in fracture toughness, peak load, and reduction in damage area. The nanophased foam sandwich structures exhibited higher peak loads compared to neat foam sandwich structures. In their study, Ito et al. [223] inserted a 20 g/m^2 VGCNFs interlayer between unidirectional prepregs of carbon laminate for low-velocity impact testing. They concluded that the fibre orientation of carbon/epoxy composites has influence on the properties such as absorbed energy and damaged area and observed a significantly smaller damaged area due to the improved ILFT of VGCNFs/carbon laminate achieved through the addition of VGCNFs. Rahman et al. [224] investigated the response of CF prepreg/epoxy-CNFs composites to low-velocity impact loading by incorporating a small amount of CNFs in the matrix material. In the 1 wt.% CNFs-CF laminate manufactured via an out of autoclave and vacuum bag only (OOA–VBO), they observed an increase in peak load, while the absorbed energy decreased with the infusion of CNFs. Additionally, the use of oxidised CNFs led to a significant reduction in the impact damage area of a CFRP laminate. Specifically, the impact damage area was reduced by 30%, 70%, and 58% when impacted at incident energy levels of 10 J, 20 J, and 30 J, respectively.

The enhancements achieved about by incorporating CNFs in epoxy CFRPs under LVI conditions are evident, as observed in terms of energy to peak load, energy to maximum load, absorbed energy, and reduction of damage area, with the incorporation of a small amount of CNFs, which mostly varies between 0.2 and 1 wt.% CNFs, which is crucial for applications requiring structural integrity under dynamic loading conditions Table 2.9.

Peak load and damage initiation energy are related to each other in the sense that impact energy absorption up to maximum load exhibits higher values with the higher impact loads. As several studies have shown, the damage initiation energy was found to be lower in control samples for which ductility index becomes higher [224].

Table 2.9: LVI properties of CNFs multiscale composites.

Autor, Ref.	Fibre/Matrix	Fiber weight percentage (wt.%)	CNFs Type	CNFs Integration Method	Manufacture Process	Optimum Loading (CNFs wt.%)	Impact Energy [J]	Energy to Peak Load Increase [%]	Energy to Max Load Increase [%]	Absorbed Energy Increase [%]	Damage Area Characteristics
Bhuiyan et al., [222]	Polyurethane sandwich CF/EP face sheets	-	CNFs	Sonication, high-speed mechanical mixer.	VARTM	0.2	44	7.7	46.8	16.8	For 0.2 wt.% CNFs, 20.3% less base width damaged and 18.0% less indentation depth, compared to the control sandwich.
Ito et al., [223]	CF PrP/EP	~ 64 to 66	VGCNFs	VGCNFs interlayer.	Autoclave	20 [g/m^2]	8.69	-	-	−8.3	The damaged area is much smaller when VGCNFs interlayer is inserted between the carbon laminate layers.
Arai et al., [225]	CF/EP	~ 62	CNFs	Planetary centrifugal mixing.	Hand lay-up, vacuum, and hot cure.	2.5	8.69	-	-	−5.6	Less delamination area for the lamination with 2.5 wt.% CNFs
Rahman et al., [184]	CF PrP/EP	-	CNFs	CNFs oxidized, mechanical stirrer, sonicated, and degasification at RT.	OOA-VBO	1.0	30	~19.0	-	0	The damage area decreased with the incorporation of O-CNFs at all impact energy levels and a maximum reduction of 67% in damage area is obtained at 20 J.
Ivañez et al., [226]	Sandwich structures with woven CF/EP face-sheets and Nomex	~ 60 to 65	CNFs	Mechanical stirrer and simultaneously ultrasonic bath.	Manual filling of the damage.	0.75	10 to 30	In repaired sandwich structures with CNFs/EP is higher than in baseline specimens.	In repaired sandwich structures is less than in baseline specimens.		To the impact energy of 10 J no damage was identified on repaired sandwiches and at an impact energy of 30 J, some cracks appear around the area of impact.
Ravindran et al., [77]	CF/EP	~ 60 to 62	CNFs	Hand-mixing followed by a TRM.	High pressure compression moulding process.	1.0	10 to 50	~4.0 increase to 50 J impact energy	-	-	For impact energy of 10, 20, 30, 40 and 50 J there was a reduction in the damaged area in the order of 1.5%, 13%, 17% 9.9% and 11%, in the nano laminates reinforced with 1.0 wt.% CNFs in comparison with the control laminate.

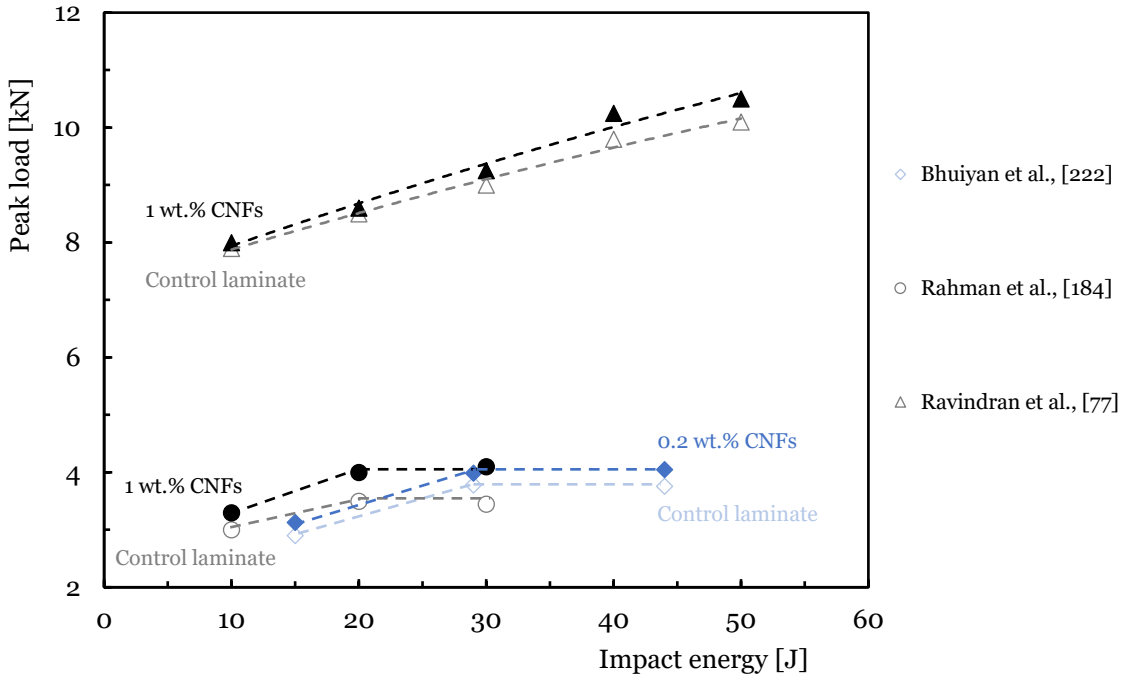
Peak load [kN]
Impact energy [J]
1 wt.% CNFs
Control laminate
0.2 wt.% CNFs
Control laminate
1 wt.% CNFs
Control laminate
Bhuiyan et al., [222]
Rahman et al., [184]
Ravindran et al., [77]

a)

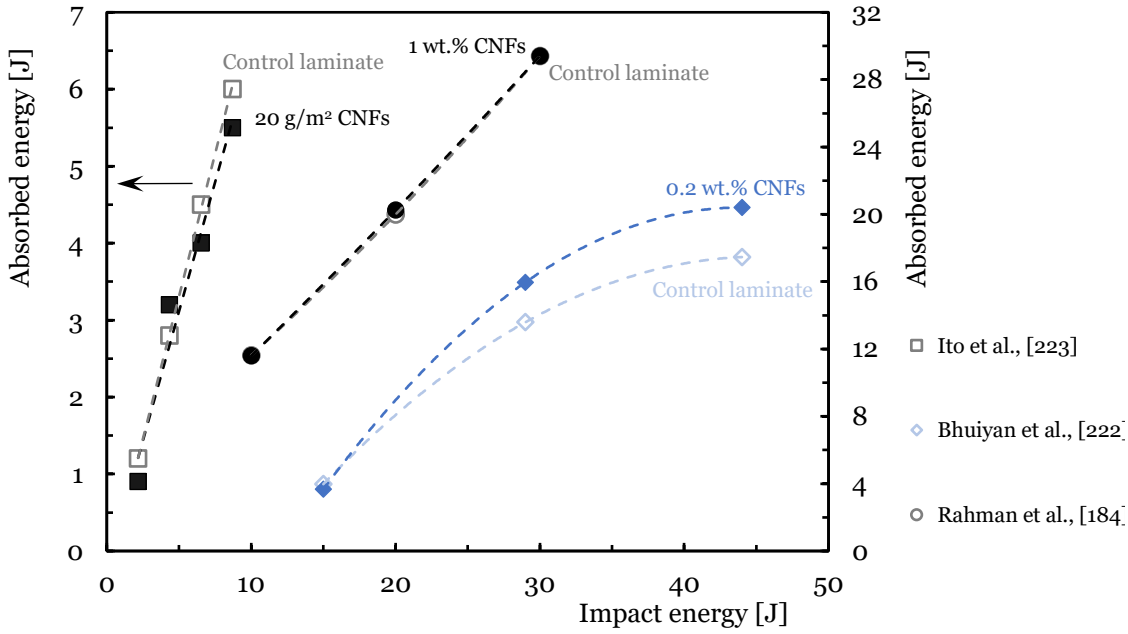
Absorbed energy [J]
Absorbed energy [J]
Impact energy [J]
Control laminate
20 g/m² CNFs
1 wt.% CNFs
Control laminate
0.2 wt.% CNFs
Control laminate
Ito et al., [223]
Bhuiyan et al., [222]
Rahman et al., [184]

b)

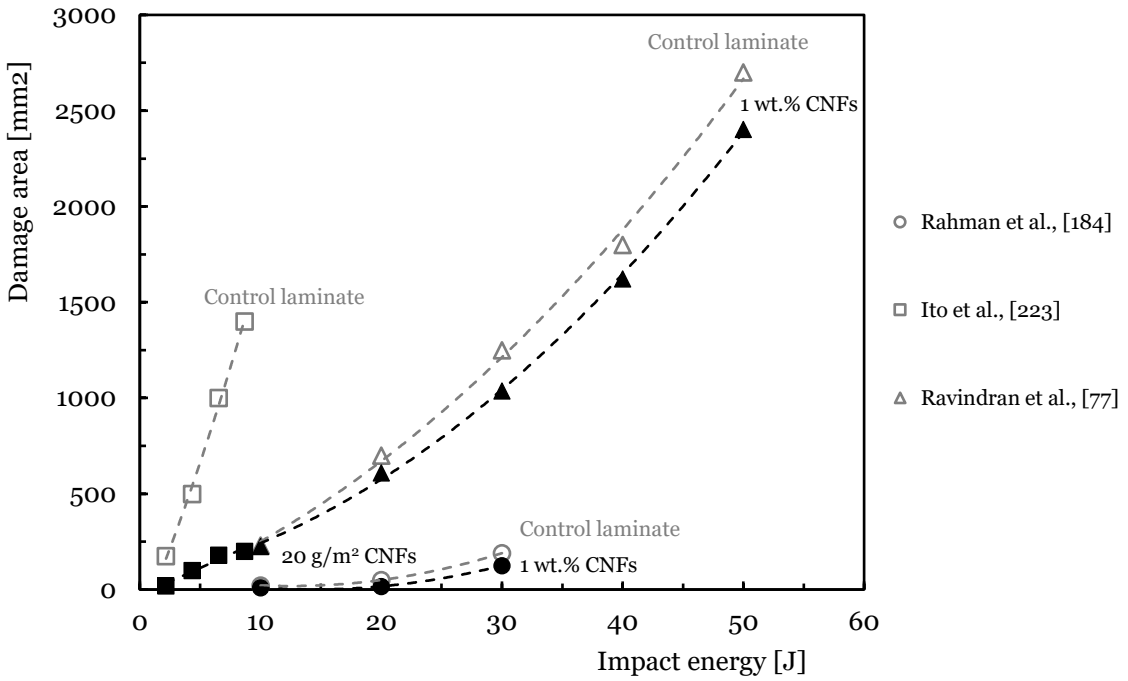

c)

Figure 2.13: LVI properties analysis of various studies on epoxy composites nano-enhanced with different wt.% CNFs.: a) Peak load; b) Absorbed energy; c) Damage area.

During crack propagation, energy is absorbed by various forms of damage, such as matrix cracking, delamination and more severe fibre-matrix debonding on impacted side, and fib fracture on the opposite side, with the optimum wt.% CNFs contributing to increased peak load and reduced damage area as shown in Figure 2.13.a) and Figure 2.13.c), respectively.

Absorbed energy also increases with the increase of impact energy level, Figure 2.13.b), however is functions of the stiffness and damage states of the samples, how the addition of CNFs contributes to increasing the stiffness of composites, consequently the absorbed energy was higher for the control samples, indicating relatively more indentation damage. The results of the various studies in Figure 2.13.b), and since the trend shown by the study by Bhuiyan et al. [222], tends to be curvilinear, both laminates are close to the penetration threshold, everything indicating that it will be bigger for the laminate with 0.2 wt.% CNFs. In the case of studies [223,224], as the trend of the results still to be linear for the energy levels studied, full penetration remains far from being achieved.

While significant progress has been made through several studies to enhance our understanding of this phenomenon, it is important to acknowledge that there remains a dearth of experimental research, particularly involving different types of reinforcements in addition to CF.

As with other mechanical properties, the characterization of composites subjected to low-velocity impacts reinforced with CNFs is limited and unclear. It is also important to highlight the gap in the literature concerning the study of properties such as fatigue resulting from low-velocity or

multi-impact impacts, static behaviour after impact, and viscoelastic behaviour after impact of CFRPs with optimal amount of CNFs. This justifies the need to carry out extensive experimental work on mechanical characterization to better understand the contribution of CNFs to maximizing these properties.

In the following chapters, the mechanical properties of two commercial epoxy resins with different percentages of CNFs by weight and their respective laminates reinforced with CF will be presented, employing mixing, manufacturing, and curing processes that are simple and easily implementable industrially. Simultaneously, analytical approaches, based on mathematical models will be applied to describe the response of these composites to a given mechanical request or in the long term. The primary goal is to maximize their properties, thereby expanding their range of applications and prolonging their service life.

2.4. Conclusions

The design of high-performance composites for structural liability applications with higher safety requirements led to the use of nano-reinforcements. In particular, the incorporation of a very small content of CNFs into the epoxy matrix showed significant potential for improving the mechanical properties of the composites.

In static response, even the addition of 0.25 and 1 wt.% of CNFs can delay crack initiation and reduce the crack propagation, improving the strength and the young modulus of the composite. This mechanical behaviour improvement is attributed to the CNFs, which can transfer a significant fraction of the load from the epoxy matrix (the lowest strength element of the composite) to the fibres of the reinforcing fabric. Thus, a homogeneous dispersion of CNFs forms a continuous network within the epoxy matrix and good interfacial adhesion between the CNFs and the epoxy resin can more effectively transfer the loads. In addition, this uniform CNFs network can effectively restrict the movement of the polymer chains.

The Interlaminar shear strength (ILSS), and fracture toughness are closely related to the fibre-matrix bond strength, the quality of the polymer matrix, and the surface morphology of the fibre (smooth or rough). The incorporation of up to 1 wt.% of CNFs results in improved mechanical response explained by fracture surfaces that reveal extensive fibre bridging (due to the addition of CNFs). Together with fibre-reinforced fabrics, they can even result in Z-shaped “pins”, promoting synergistic effects on the interlaminar fracture properties (both Mode I and Mode II) of CFRP composites. Furthermore, as a result of the different length scales of the (nano)reinforcements, additional toughening mechanisms are reported.

In addition, the composites showed improved resistance to low-velocity impact (LVI), and the damaged areas were significantly reduced with the incorporation of a small content of CNFs (typically up to 1 wt.%), which is beneficial for dynamic loading conditions. The addition of the CNFs increases the fracture energy, since crack propagation can be limited by the formation of

bridges between the epoxy matrix and the CNFs, and therefore better adhesion between them due to the interaction of cross-links. It is likely that the uniformly dispersed CNFs started out as a barrier to crack propagation under lower load conditions. During the crack propagation process, it is slowed down by the pulling force of the nanofibres well impregnated into the crack surface due to an energy dissipation phenomenon and, consequently, the energy of the crack tips is significantly reduced. In addition, there are reports that the crack tips are forced to stop or frequently change their crack line of propagation due to the presence of CNFs. As a result, crack initiation and propagation become difficult in the nano-reinforced matrix, which leads to greater strength and smaller areas of damage in the composites.

Regarding viscoelastic behaviour, the inclusion of CNFs reduces time-dependent deformation and improves the structural stability of the composite. Just 1 wt.% CNFs has a detrimental effect on the mobility of the polymer chain in the epoxy matrix, as well as in chain disentanglement and slippage. This way, in terms of stress relaxation and creep resistance, the CNFs can contribute to the reduction in their values. A relatively low amount of well-dispersed CNFs forms interphases that bind to the matrix through bonding segments and junctions, reinforcing the load-bearing capacity and improving the immobility of the polymer chains, preventing sliding and realignment

It is clear that the addition of the optimum content of CNFs in a given epoxy matrix, up to 1.0 wt.%, is advantageous, as observed in Figures 2.7 - 2.13. Industrial-scale production of composites with CNFs is more feasible than with CNTs or GP, but manufacturing technology, and especially dispersion, is a factor that cannot be neglected.

Bibliography

[1] Poveda RL, Gupta N. Introduction. Democratizing Innovation, 2016, p. 1–10. https://doi.org/10.1007/978-3-319-23787-9_1.

[2] González C, Vilatela JJ, Molina-Aldareguía JM, Lopes CS, LLorca J. Structural composites for multifunctional applications: Current challenges and future trends. Progress in Materials Science 2017;89:194–251. https://doi.org/10.1016/j.pmatsci.2017.04.005.

[3] Andrew JJ, Dhakal HN. Sustainable biobased composites for advanced applications: recent trends and future opportunities – A critical review. Composites Part C: Open Access 2022;7:100220. https://doi.org/10.1016/j.jcomc.2021.100220.

[4] Yu S, Huang M, Hao R, He S, Liu H, Liu W, et al. Recent advances in thermally conductive polymer composites. High Performance Polymers 2022;34:1081–101. https://doi.org/10.1177/09540083221106058.

[5] Kangishwar S, Radhika N, Sheik AA, Chavali A, Hariharan S. A comprehensive review on polymer matrix composites: material selection, fabrication, and application. Polymer Bulletin 2023;80:47–87. https://doi.org/10.1007/s00289-022-04087-4.

[6] Fonseca Machado AP da, Arruda HS, Reguengo LM, de Moura LD, de Carvalho FV, do Nascimento R de P, et al. Encapsulating products. Natural Plant Products in Inflammatory Bowel Diseases, Elsevier; 2023, p. 319–64. https://doi.org/10.1016/B978-0-323-99111-7.00004-0.

[7] Meyer T, Keurentjes JTF. Polymer Reaction Engineering, an Integrated Approach. Handbook of Polymer Reaction Engineering, Weinheim, Germany: Wiley; 2005, p. 1–15. https://doi.org/10.1002/9783527619870.ch1.

[8] Güven O, Gökdağ K, Jovanović B, Kıdeyş AE. Microplastic litter composition of the Turkish territorial waters of the Mediterranean Sea, and its occurrence in the gastrointestinal tract of fish. Environmental Pollution 2017;223:286–94. https://doi.org/10.1016/j.envpol.2017.01.025.

[9] Alberto M. Introduction of Fibre-Reinforced Polymers – Polymers and Composites: Concepts, Properties and Processes. Fiber Reinforced Polymers - The Technology Applied for Concrete Repair, InTech; 2013, p. 3–40. https://doi.org/10.5772/54629.

[10] Ornaghi HL, Almeida JHS, Monticeli FM, Neves RM. Stress relaxation, creep, and recovery of carbon fiber non-crimp fabric composites. Composites Part C: Open Access 2020;3:100051. https://doi.org/10.1016/j.jcomc.2020.100051.

[11] Basheer B V., George JJ, Siengchin S, Parameswaranpillai J. Polymer grafted carbon nanotubes—Synthesis, properties, and applications: A review. Nano-Structures & Nano-Objects 2020;22:100429. https://doi.org/10.1016/j.nanoso.2020.100429.

[12] Hodd K. Epoxy Resins. Comprehensive Polymer Science and Supplements, vol. 11, Elsevier; 1989, p. 667–99. https://doi.org/10.1016/B978-0-08-096701-1.00178-6.

[13] Unnikrishnan KP, Thachil ET. Toughening of epoxy resins. Designed Monomers and Polymers 2006;9:129–52. https://doi.org/10.1163/156855506776382664.

[14] Feng J, Guo Z. Temperature-frequency-dependent mechanical properties model of epoxy resin and its composites. Composites Part B: Engineering 2016;85:161–9. https://doi.org/10.1016/j.compositesb.2015.09.040.

[15] Xiong T, Wang N, Liao J, Zhang Y. Modified boron nitride-basalt fiber/epoxy resin composite laminates and their enhanced mechanical properties. Polymers for Advanced Technologies 2021;32:3621–32. https://doi.org/10.1002/pat.5370.

[16] Lee DY, Kim HJ, Kim H, Lim C, Chung I, Seo B. Polyol and polyurethane containing bisphenol- <scp>Z</scp> : Synthesis and application for toughening epoxy. Journal of Applied Polymer Science 2022;139:1–12. https://doi.org/10.1002/app.53013.

[17] Gonçalves FAMM, Santos M, Cernadas T, Alves P, Ferreira P. Influence of fillers on epoxy resins properties: a review. Journal of Materials Science 2022;57:15183–212. https://doi.org/10.1007/s10853-022-07573-2.

[18] Ammar S, Wonnie Ma IA, Ramesh K, Ramesh S. Polymers-based nanocomposite coatings. Nanomaterials-Based Coatings, Elsevier; 2019, p. 9–39. https://doi.org/10.1016/B978-0-12-815884-5.00002-8.

[19] Ratna D. Epoxy Composites: Impact Resistance and Flame Retardancy. iSmithers Rapra Pulishing, vol. 16, 2007, p. 3–28.

[20] Filipe L, Alves F, Marques A. Materiais de construção. Publindúst, Porto, Portugal: 2013, p. 271–310.

[21] Reis JML dos. Effect of temperature on the mechanical properties of polymer mortars. Materials Research 2012;15:645–9. https://doi.org/10.1590/S1516-14392012005000091.

[22] Sicomin. SR 8100 / SD 882X Infusion System. Available from: Http://SicominCom/Datasheets/Product-Pdf94Pdf [Accessed: 4 February 2022] 2019;33:1–9.

[23] Data FP. MatWeb , Your Source for Materials Information How to Find Property Data in MatWeb 2023:0–1. https://www.matweb.com/index.aspx.

[24] Vinyl Ester Resin Specification. Available from: Https://S3-Ap-Northeast-1AmazonawsCom/StaticIypTw/37629/Files/501f3e3c-D083-4bce-Bea5-9e8dea47ba15Pdf [Accessed: 4 February 2022] 2023:1.

[25] Maya MG, George SC, Jose T, Sreekala MS, Thomas S. Mechanical Properties of Short Sisal Fibre Reinforced Phenol Formaldehyde Eco-Friendly Composites. Polymers from Renewable Resources 2017;8:27–42. https://doi.org/10.1177/204124791700800103.

[26] Elfaleh I, Abbassi F, Habibi M, Ahmad F, Guedri M, Nasri M, et al. A comprehensive review of natural fibers and their composites: An eco-friendly alternative to conventional materials. Results in Engineering 2023;19:101271. https://doi.org/10.1016/j.rineng.2023.101271.

[27] Yalamaç E, Sutcu M, Basturk SB. Ceramic fibers. Fiber Technology for Fiber-Reinforced Composites, Elsevier; 2017, p. 187–207. https://doi.org/10.1016/B978-0-08-101871-2.00009-6.

[28] Xue P, Tao X, Leung M-Y, Zhang H. Electromechanical properties of conductive fibres, yarns and fabrics. Wearable Electronics and Photonics, Elsevier; 2005, p. 81–104. https://doi.org/10.1533/9781845690441.81.

[29] Deng S, Djukic L, Paton R, Ye L. Thermoplastic-epoxy interactions and their potential applications in joining composite structures - A review. Composites Part A: Applied Science and Manufacturing 2015;68:121–32. https://doi.org/10.1016/j.compositesa.2014.09.027.

[30] Chung DDL. Carbon Fibers, Nanofibers, and Nanotubes. Carbon Composites. Second Edi, Elsevier; 2017, p. 1–87. https://doi.org/10.1016/B978-0-12-804459-9.00001-4.

[31] Manivannan J, Kalaiselvan S, Padmavathi R. Vapor-Grown Carbon Fiber Synthesis, Properties, and Applications. Composite and Nanocomposite Materials - From Knowledge to Industrial Applications, vol. 11, IntechOpen; 2020, p. 13. https://doi.org/10.5772/intechopen.92300.

[32] Huang X. Fabrication and Properties of Carbon Fibers. Materials 2009;2:2369–403. https://doi.org/10.3390/ma2042369.

[33] Frank E, Steudle LM, Ingildeev D, Spörl JM, Buchmeiser MR. Carbon Fibers: Precursor Systems, Processing, Structure, and Properties. Angewandte Chemie International Edition 2014;53:5262–98. https://doi.org/10.1002/anie.201306129.

[34] Soulis S, Konstantopoulos G, Koumoulos EP, Charitidis CA. Impact of Alternative Stabilization Strategies for the Production of PAN-Based Carbon Fibers with High Performance. Fibers 2020;8:33. https://doi.org/10.3390/fib8060033.

[35] Based P, Tow L, Turbines W, Outlook R, Description R, Customization R, et al. Ask for sample 2023. https://www.precedenceresearch.com/carbon-fiber-market.

[36] Zhang J, Lin G, Vaidya U, Wang H. Past, present and future prospective of global carbon fibre composite developments and applications. Composites Part B: Engineering 2023;250:110463. https://doi.org/10.1016/j.compositesb.2022.110463.

[37] Palazzetti R, Zucchelli A. Electrospun nanofibers as reinforcement for composite laminates materials – A review. Composite Structures 2017;182:711–27. https://doi.org/10.1016/j.compstruct.2017.09.021.

[38] Lee CH, Khalina A, Lee SH. Importance of Interfacial Adhesion Condition on Characterization of Plant-Fiber-Reinforced Polymer Composites: A Review. Polymers 2021;13:438. https://doi.org/10.3390/polym13030438.

[39] Drzal LT, Herrera-Franco PJ, Ho H. Fiber–Matrix Interface Tests. Comprehensive Composite Materials, Elsevier; 2000, p. 71–111. https://doi.org/10.1016/B0-08-042993-9/00036-X.

[40] Drzal LT, Rich MJ, Koenig MF, Lloyd PF. Adhesion of Graphite Fibers to Epoxy Matrices: II. The Effect of Fiber Finish. The Journal of Adhesion 1983;16:133–52. https://doi.org/10.1080/00218468308074911.

[41] Cho D, Kim H, Drzal LT. Surface Treatment and Characterization of Natural Fibers: Effects on the Properties of Biocomposites. Polymer Composites, vol. 3, Wiley; 2013, p. 133–77. https://doi.org/10.1002/9783527674220.ch4.

[42] Amiandamhen SO, Meincken M, Tyhoda L. Natural Fibre Modification and Its Influence on Fibre-matrix Interfacial Properties in Biocomposite Materials. Fibers and Polymers 2020;21:677–89. https://doi.org/10.1007/s12221-020-9362-5.

[43] Andrew JJ, Srinivasan SM, Arockiarajan A, Dhakal HN. Parameters influencing the impact response of fiber-reinforced polymer matrix composite materials: A critical review. Composite Structures 2019;224:111007.

https://doi.org/10.1016/j.compstruct.2019.111007.

[44] Shah SZH, Karuppanan S, Megat-Yusoff PSM, Sajid Z. Impact resistance and damage tolerance of fiber reinforced composites: A review. Composite Structures 2019;217:100–21. https://doi.org/10.1016/j.compstruct.2019.03.021.

[45] Saleh TA. Nanomaterials: Classification, properties, and environmental toxicities. Environmental Technology & Innovation 2020;20:101067. https://doi.org/10.1016/j.eti.2020.101067.

[46] Mekuye B, Abera B. Nanomaterials: An overview of synthesis, classification, characterization, and applications. Nano Select 2023;4:486–501. https://doi.org/10.1002/nano.202300038.

[47] Tee ZY, Yeap SP, Hassan CS, Kiew PL. Nano and non-nano fillers in enhancing mechanical properties of epoxy resins: a brief review. Polymer-Plastics Technology and Materials 2022;61:709–25. https://doi.org/10.1080/25740881.2021.2015778.

[48] Ana MD. Handbook of Epoxy Blends. Cham: Springer International Publishing; 2015. https://doi.org/10.1007/978-3-319-18158-5.

[49] Atif R, Shyha I, Inam F. Mechanical, Thermal, and Electrical Properties of Graphene-Epoxy Nanocomposites—A Review. Polymers 2016;8:281. https://doi.org/10.3390/polym8080281.

[50] Kopsidas S, Olowojoba GB. Multifunctional epoxy composites modified with a graphene nanoplatelet/carbon nanotube hybrid. Journal of Applied Polymer Science 2021;138:1–19. https://doi.org/10.1002/app.50890.

[51] Yazman Ş, Uyaner M, Karabörk F, Akdemir A. Effects of nano reinforcing/matrix interaction on chemical, thermal and mechanical properties of epoxy nanocomposites. Journal of Composite Materials 2021;55:4257–72. https://doi.org/10.1177/00219983211037059.

[52] Periasamy K, Kandare E, Das R, Darouie M, Khatibi AA. Interfacial Engineering Methods in Thermoplastic Composites: An Overview. Polymers 2023;15. https://doi.org/10.3390/polym15020415.

[53] Białkowska A, Bakar M, Kucharczyk W, Zarzyka I. Hybrid Epoxy Nanocomposites: Improvement in Mechanical Properties and Toughening Mechanisms—A Review. Polymers 2023;15. https://doi.org/10.3390/polym15061398.

[54] Gojny F, Wichmann M, Fiedler B, Schulte K. Influence of different carbon nanotubes on the mechanical properties of epoxy matrix composites – A comparative study. Composites Science and Technology 2005;65:2300–13. https://doi.org/10.1016/j.compscitech.2005.04.021.

[55] Gojny FH, Wichmann MHG, Fiedler B, Bauhofer W, Schulte K. Influence of nano-modification on the mechanical and electrical properties of conventional fibre-reinforced composites. Composites Part A: Applied Science and Manufacturing 2005;36:1525–35. https://doi.org/10.1016/j.compositesa.2005.02.007.

[56] Singh S, Srivastava VK, Prakash R. Influences of carbon nanofillers on mechanical performance of epoxy resin polymer. Applied Nanoscience 2015;5:305–13. https://doi.org/10.1007/s13204-014-0319-0.

[57] Yang T, Lu S, Song D, Zhu X, Almira I, Liu J, et al. Effect of Nanofiller on the Mechanical Properties of Carbon Fiber/Epoxy Composites under Different Aging Conditions. Materials 2021;14:7810. https://doi.org/10.3390/ma14247810.

[58] Georgakilas V, Perman JA, Tucek J, Zboril R. Broad Family of Carbon Nanoallotropes: Classification, Chemistry, and Applications of Fullerenes, Carbon Dots, Nanotubes, Graphene, Nanodiamonds, and Combined Superstructures. Chemical Reviews 2015;115:4744–822. https://doi.org/10.1021/cr500304f.

[59] Feng L, Liu Z. Biomedical Applications of Carbon Nanomaterials. Biomedical Applications and Toxicology of Carbon Nanomaterials, Weinheim, Germany: Wiley; 2016, p. 131–62. https://doi.org/10.1002/9783527692866.ch5.

[60] Zhang B, Kang F, Tarascon J, Kim J. Recent advances in electrospun carbon nanofibers and their application in electrochemical energy storage. Progress in Materials Science

2016;76:319–80. https://doi.org/10.1016/j.pmatsci.2015.08.002.

[61] Adhikari J, Rizwan M, Keasberry NA, Ahmed MU. Current progresses and trends in carbon nanomaterials-based electrochemical and electrochemiluminescence biosensors. Journal of the Chinese Chemical Society 2020;67:937–60. https://doi.org/10.1002/jccs.201900417.

[62] Mokhena TC, Matabola KP, Mokhothu TH, Mtibe A, Mochane M., Ndlovu G, et al. Electrospun carbon nanofibres: Preparation, characterization and application for adsorption of pollutants from water and air. Separation and Purification Technology 2022;288:120666. https://doi.org/10.1016/j.seppur.2022.120666.

[63] Zaman I, Manshoor B, Khalid A, Araby S. From clay to graphene for polymer nanocomposites—a survey. Journal of Polymer Research 2014;21:429. https://doi.org/10.1007/s10965-014-0429-0.

[64] Rashid A Bin, Haque M, Islam SMM, Uddin Labib KMR. Nanotechnology-enhanced fiber-reinforced polymer composites: Recent advancements on processing techniques and applications. Heliyon 2024;10:e24692. https://doi.org/10.1016/j.heliyon.2024.e24692.

[65] Al-Saleh MH. Towards a cost-effective carbon nanofillers-based composites for EMI shielding applications. Synthetic Metals 2023;293:117271. https://doi.org/10.1016/j.synthmet.2022.117271.

[66] Jiang S, Chen Y, Duan G, Mei C, Greiner A, Agarwal S. Electrospun nanofiber reinforced composites: a review. Polymer Chemistry 2018;9:2685–720. https://doi.org/10.1039/C8PY00378E.

[67] Wang Z, Wu S, Wang J, Yu A, Wei G. Carbon Nanofiber-Based Functional Nanomaterials for Sensor Applications. Nanomaterials 2019;9:1045. https://doi.org/10.3390/nano9071045.

[68] Yadav D, Amini F, Ehrmann A. Recent advances in carbon nanofibers and their applications – A review. European Polymer Journal 2020;138:109963. https://doi.org/10.1016/j.eurpolymj.2020.109963.

[69] Gao X, Lan J, Jia X, Cai Q, Yang X. Improving interfacial adhesion with epoxy matrix using hybridized carbon nanofibers containing calcium phosphate nanoparticles for bone repairing. Materials Science and Engineering: C 2016;61:174–9. https://doi.org/10.1016/j.msec.2015.12.033.

[70] Santos P, Silva AP, Reis PNB. Effect of Carbon Nanofibers on the Viscoelastic Response of Epoxy Resins. Polymers 2023;15:821. https://doi.org/10.3390/polym15040821.

[71] Dhakate SR, Chaudhary A, Gupta A, Pathak AK, Singh BP, Subhedar KM, et al. Excellent mechanical properties of carbon fiber semi-aligned electrospun carbon nanofiber hybrid polymer composites. RSC Advances 2016;6:36715–22. https://doi.org/10.1039/C6RA02672A.

[72] Santos P, Silva AP, Reis PNB. Effect of Carbon Nanofibers on the Strain Rate and Interlaminar Shear Strength of Carbon/Epoxy Composites. Materials 2023;16:4332. https://doi.org/10.3390/ma16124332.

[73] Bortz DR, Merino C, Martin-Gullon I. Carbon nanofibers enhance the fracture toughness and fatigue performance of a structural epoxy system. Composites Science and Technology 2011;71:31–8. https://doi.org/10.1016/j.compscitech.2010.09.015.

[74] Ravindran AR, Ladani RB, Wang CH, Mouritz AP. Synergistic delamination toughening of composites using multi-scale carbon reinforcements. Composites Part B: Engineering 2019;161:18–28. https://doi.org/10.1016/j.compositesb.2018.10.031.

[75] Ravindran AR, Ladani RB, Wang CH, Mouritz AP. Strengthening of composite T-joints using 1D and 2D carbon nanoparticles. Composite Structures 2021;255:112982. https://doi.org/10.1016/j.compstruct.2020.112982.

[76] Zhou Y, Jeelani S, Lacy T. Experimental study on the mechanical behavior of carbon/epoxy composites with a carbon nanofiber-modified matrix. Journal of Composite Materials 2014;48:3659–72. https://doi.org/10.1177/0021998313512348.

[77] Ravindran AR, Ladani RB, Kinloch AJ, Wang C-H, Mouritz AP. Improving the delamination resistance and impact damage tolerance of carbon fibre-epoxy composites

using multi-scale fibre toughening. Composites Part A: Applied Science and Manufacturing 2021;150:106624. https://doi.org/10.1016/j.compositesa.2021.106624.

[78] Nimbagal V, Banapurmath NR, Umarfarooq MA, Revankar S, Sajjan AM, Soudagar MEM, et al. Mechanical and fracture properties of carbon nano fibers/short carbon fiber epoxy composites. Polymer Composites 2023;44:3977–89. https://doi.org/10.1002/pc.27371.

[79] Wang Y, Yao D, He Z, Wang D, Zheng Y. Enhanced mechanical and damping properties of epoxy using aggregated nanoparticles organic-inorganic hybrid as a filler. Composite Interfaces 2022;29:523–36. https://doi.org/10.1080/09276440.2021.1982334.

[80] Lake CL, Lake PD. Carbon Nanofiber Multifunctional Mat. Nanotube Superfiber Materials, Elsevier; 2014, p. 313–31. https://doi.org/10.1016/B978-1-4557-7863-8.00011-6.

[81] Ruiz-Cornejo JC, Sebastián D, Lázaro MJ. Synthesis and applications of carbon nanofibers: a review. Reviews in Chemical Engineering 2020;36:493–511. https://doi.org/10.1515/revce-2018-0021.

[82] Zhou X, Wang Y, Gong C, Liu B, Wei G. Production, structural design, functional control, and broad applications of carbon nanofiber-based nanomaterials: A comprehensive review. Chemical Engineering Journal 2020;402:126189. https://doi.org/10.1016/j.cej.2020.126189.

[83] Martin-Gullon I, Vera J, Conesa JA, González JL, Merino C. Differences between carbon nanofibers produced using Fe and Ni catalysts in a floating catalyst reactor. Carbon 2006;44:1572–80. https://doi.org/10.1016/j.carbon.2005.12.027.

[84] Rodriguez NM, Chambers A, Baker RTK. Catalytic Engineering of Carbon Nanostructures. Langmuir 1995;11:3862–6. https://doi.org/10.1021/la00010a042.

[85] Yoon S, Lim S, Hong S, Qiao W, Whitehurst DD, Mochida I, et al. A conceptual model for the structure of catalytically grown carbon nano-fibers. Carbon 2005;43:1828–38. https://doi.org/10.1016/j.carbon.2005.02.031.

[86] Guseva Canu I, Bateson TF, Bouvard V, Debia M, Dion C, Savolainen K, et al. Human exposure to carbon-based fibrous nanomaterials: A review. International Journal of Hygiene and Environmental Health 2016;219:166–75. https://doi.org/10.1016/j.ijheh.2015.12.005.

[87] Laurila T, Sainio S, Caro MA. Hybrid carbon based nanomaterials for electrochemical detection of biomolecules. Progress in Materials Science 2017;88:499–594. https://doi.org/10.1016/j.pmatsci.2017.04.012.

[88] Lu W, He T, Xu B, He X, Adidharma H, Radosz M, et al. Progress in catalytic synthesis of advanced carbon nanofibers. Journal of Materials Chemistry A 2017;5:13863–81. https://doi.org/10.1039/C7TA02007D.

[89] Danni N, Sasikumar T, Fazil AA. Mechanical Properties of Electrospun CNF / PVA Nanofiber Mats as Reinforcement in Polymer Matrix Composites. Nternational Journal of Applied Chemistry 12, 107-119 2016;12:107–19.

[90] Teo KBK, Lee S, Chhowalla M, Semet V, Binh VT, Groening O, et al. Plasma enhanced chemical vapour deposition carbon nanotubes/nanofibres how uniform do they grow? Nanotechnology 2003;14:204–11. https://doi.org/10.1088/0957-4484/14/2/321.

[91] Denysenko I, Ostrikov K, Cvelbar U, Mozetic M, Azarenkov NA. Carbon nanofiber growth in plasma-enhanced chemical vapor deposition. Journal of Applied Physics 2008;104. https://doi.org/10.1063/1.2986915.

[92] Bao Y, Zhan L, Wang C, Wang Y, Yang G, Yang J, et al. Synthesis of carbon nanofiber/carbon-foam composite for catalyst support in gas-phase catalytic reactions. New Carbon Materials 2011;26:341–6. https://doi.org/10.1016/S1872-5805(11)60086-3.

[93] Wang Y, Zheng M, Lu H, Feng S, Ji G, Cao J. Template Synthesis of Carbon Nanofibers Containing Linear Mesocage Arrays. Nanoscale Research Letters 2010;5:913–6. https://doi.org/10.1007/s11671-010-9562-9.

[94] Tan Y, Lin D, Liu C, Wang W, Kang L, Ran F. Carbon nanofibers prepared by electrospinning accompanied with phase-separation method for supercapacitors: Effect of thermal treatment temperature. Journal of Materials Research 2018;33:1120–30.

https://doi.org/10.1557/jmr.2017.373.

[95] Pacheco M, Pacheco J, Valdivi R. Synthesis of Carbon Nanofibers by a Glow-Arc Discharge. Nanofibers, InTech; 2010. https://doi.org/10.5772/8157.

[96] Ci L, Li Y, Wei B, Liang J, Xu C, Wu D. Preparation of carbon nanofibers by the floating catalyst method. Carbon 2000;38:1933–7. https://doi.org/10.1016/S0008-6223(00)00030-0.

[97] Ismar E, Sarac AS. Carbon Nanomaterials. vol. i, 2019, p. 1–33. https://doi.org/10.4018/978-1-5225-7921-2.ch001.

[98] Mohamed A. Synthesis, Characterization, and Applications Carbon Nanofibers. Carbon-Based Nanofillers and Their Rubber Nanocomposites, Elsevier; 2019, p. 243–57. https://doi.org/10.1016/B978-0-12-813248-7.00008-0.

[99] Ikuno T, Ryu J-T, Oyama T, Ohkura S, Baek Y-G, Honda S, et al. Characterization of low temperature growth carbon nanofibers synthesized by using plasma enhanced chemical vapor deposition. Vacuum 2002;66:341–5. https://doi.org/10.1016/S0042-207X(02)00141-0.

[100] Sacco LN, Vollebregt S. Overview of Engineering Carbon Nanomaterials Such As Carbon Nanotubes (CNTs), Carbon Nanofibers (CNFs), Graphene and Nanodiamonds and Other Carbon Allotropes inside Porous Anodic Alumina (PAA) Templates. Nanomaterials 2023;13:260. https://doi.org/10.3390/nano13020260.

[101] Arora N, Sharma NN. Arc discharge synthesis of carbon nanotubes: Comprehensive review. Diamond and Related Materials 2014;50:135–50. https://doi.org/10.1016/j.diamond.2014.10.001.

[102] Aziz S, Rashid S, Mohd Salleh MA. Theoretical Prediction of CNT-CF/PP Composite Tensile Properties Using Various Numerical Modeling Methods. Fullerenes, Nanotubes and Carbon Nanostructures 2013;21:411–6. https://doi.org/10.1080/1536383X.2011.629755.

[103] Meyyappan M. A review of plasma enhanced chemical vapour deposition of carbon nanotubes. Journal of Physics D: Applied Physics 2009;42:213001. https://doi.org/10.1088/0022-3727/42/21/213001.

[104] Bauman YI, Mishakov I V., Rudneva Y V., Plyusnin PE, Shubin Y V., Korneev D V., et al. Formation of Active Sites of Carbon Nanofibers Growth in Self-Organizing Ni–Pd Catalyst during Hydrogen-Assisted Decomposition of 1,2-Dichloroethane. Industrial & Engineering Chemistry Research 2019;58:685–94. https://doi.org/10.1021/acs.iecr.8b02186.

[105] Painuli R, Yadav PK, Raghav S, Kumar D. Synthesis of Carbon Nanofibers and Its Application in Environmental Remediation, 2021, p. 325–42. https://doi.org/10.1007/978-981-15-6699-8_15.

[106] Yang L. Carbon nanostructures. Nanotechnology-Enhanced Orthopedic Materials, Elsevier; 2015, p. 97–120. https://doi.org/10.1016/B978-0-85709-844-3.00005-7.

[107] Fernández A, Peretyagin P, Solís W, Torrecillas R, Borrell A. Functionalization of Carbon Nanofibres Obtained by Floating Catalyst Method. Journal of Nanomaterials 2015;2015:1–7. https://doi.org/10.1155/2015/395014.

[108] Rana S, Bhattacharyya A, Parveen S, Fangueiro R, Alagirusamy R, Joshi M. Processing and performance of carbon/epoxy multi-scale composites containing carbon nanofibres and single walled carbon nanotubes. Journal of Polymer Research 2013;20:314. https://doi.org/10.1007/s10965-013-0314-2.

[109] Al-Saleh MH, Sundararaj U. A review of vapor grown carbon nanofiber/polymer conductive composites. Carbon 2009;47:2–22. https://doi.org/10.1016/j.carbon.2008.09.039.

[110] Li Y, Hori N, Arai M, Hu N, Liu Y, Fukunaga H. Improvement of interlaminar mechanical properties of CFRP laminates using VGCF. Composites Part A: Applied Science and Manufacturing 2009;40:2004–12. https://doi.org/10.1016/j.compositesa.2009.09.002.

[111] Hu N, Li Y, Nakamura T, Katsumata T, Koshikawa T, Arai M. Reinforcement effects of MWCNT and VGCF in bulk composites and interlayer of CFRP laminates. Composites Part

B: Engineering 2012;43:3–9. https://doi.org/10.1016/j.compositesb.2011.04.022.

[112] Song JH. Manufacturing method of carbon and glass fabric composites with dispersed nanofibers using vacuum-assisted resin transfer molding. E-Polymers 2014;14:345–52. https://doi.org/10.1515/epoly-2014-0091.

[113] Endo M, Kim Y., Hayashi T, Nishimura K, Matusita T, Miyashita K, et al. Vapor-grown carbon fibers (VGCFs). Carbon 2001;39:1287–97. https://doi.org/10.1016/S0008-6223(00)00295-5.

[114] Akpan EI, Shen X, Wetzel B, Friedrich K. Design and Synthesis of Polymer Nanocomposites. Polymer Composites with Functionalized Nanoparticles, Elsevier; 2019, p. 47–83. https://doi.org/10.1016/B978-0-12-814064-2.00002-0.

[115] Yuksek M. Electromagnetic wave shielding and mechanical properties of vapor-grown carbon nanofiber/polyvinylidene fluoride composite fibers. Journal of Engineered Fibers and Fabrics 2020;15:155892502098595. https://doi.org/10.1177/1558925020985959.

[116] Hossain MK, Hossain ME, Hosur MV, Jeelani S. Flexural and compression response of woven E-glass/polyester–CNF nanophased composites. Composites Part A: Applied Science and Manufacturing 2011;42:1774–82. https://doi.org/10.1016/j.compositesa.2011.07.033.

[117] Subramaniyan AK, Sun CT. Enhancing compressive strength of unidirectional polymeric composites using nanoclay. Composites Part A: Applied Science and Manufacturing 2006;37:2257–68. https://doi.org/10.1016/j.compositesa.2005.12.027.

[118] Al-Sabagh A, Taha E, Kandil U, Nasr G-A, Reda Taha M. Monitoring Damage Propagation in Glass Fiber Composites Using Carbon Nanofibers. Nanomaterials 2016;6:169. https://doi.org/10.3390/nano6090169.

[119] He Y, Ju S, Duan K, Tang J, Bai S, Jiang D, et al. Tuning the through-thickness orientation of 1D nanocarbons to enhance the electrical conductivity and ILSS of hierarchical CFRP composites. Science and Engineering of Composite Materials 2021;28:453–65. https://doi.org/10.1515/secm-2021-0040.

[120] Ladani RB, Wu S, Kinloch AJ, Ghorbani K, Mouritz AP, Wang CH. Enhancing fatigue resistance and damage characterisation in adhesively-bonded composite joints by carbon nanofibres. Composites Science and Technology 2017;149:116–26. https://doi.org/10.1016/j.compscitech.2017.06.018.

[121] Wu S, Ladani RB, Ravindran AR, Zhang J, Mouritz AP, Kinloch AJ, et al. Aligning carbon nanofibres in glass-fibre/epoxy composites to improve interlaminar toughness and crack-detection capability. Composites Science and Technology 2017;152:46–56. https://doi.org/10.1016/j.compscitech.2017.09.007.

[122] Ravindran AR, Ladani RB, Wu S, Kinloch AJ, Wang CH, Mouritz AP. Multi-scale toughening of epoxy composites via electric field alignment of carbon nanofibres and short carbon fibres. Composites Science and Technology 2018;167:115–25. https://doi.org/10.1016/j.compscitech.2018.07.034.

[123] Srikanth I, Kumar S, Singh V, Rangababu B, Ghosal P, Subrahmanyam C. Effect of carbon nanofibre addition on the mechanical properties of different V f carbon-epoxy composites. Bulletin of Materials Science 2015;38:309–17. https://doi.org/10.1007/s12034-015-0841-z.

[124] Vaganov G, Yudin V, Vuorinen J, Molchanov E. Influence of multiwalled carbon nanotubes on the processing behavior of epoxy powder compositions and on the mechanical properties of their fiber reinforced composites. Polymer Composites 2016;37:2377–83. https://doi.org/10.1002/pc.23419.

[125] Chen Q, Wu W, Zhao Y, Xi M, Xu T, Fong H. Nano-epoxy resins containing electrospun carbon nanofibers and the resulting hybrid multi-scale composites. Composites Part B: Engineering 2014;58:43–53. https://doi.org/10.1016/j.compositesb.2013.10.048.

[126] Romero A, Lavin-Lopez MP, Sánchez-Silva ML, Valverde JL, Paton-Carrero A. Effects of oxidizing procedures on carbon nanofibers surface and dispersability in an epoxy resin. Materials Chemistry and Physics 2020;243:122571. https://doi.org/10.1016/j.matchemphys.2019.122571.

[127] Gude MR, Prolongo SG, Ureña A. Toughening effect of carbon nanotubes and carbon nanofibres in epoxy adhesives for joining carbon fibre laminates. International Journal of Adhesion and Adhesives 2015;62:139–45. https://doi.org/10.1016/j.ijadhadh.2015.07.011.

[128] Rhodes SM, Higgins B, Xu Y, Brittain WJ. Hyperbranched polyol/carbon nanofiber composites. Polymer 2007;48:1500–9. https://doi.org/10.1016/j.polymer.2007.01.038.

[129] Quaresimin M, Varley RJ. Understanding the effect of nano-modifier addition upon the properties of fibre reinforced laminates. Composites Science and Technology 2008;68:718–26. https://doi.org/10.1016/j.compscitech.2007.09.005.

[130] Anjabin R, Khosravi H. Property improvement of a fibrous composite using functionalized carbon nanofibers. Polymer Composites 2019;40:4281–8. https://doi.org/10.1002/pc.25289.

[131] Kostopoulos V, Karapappas P, Loutas T, Vavouliotis A, Paipetis A, Tsotra P. Interlaminar Fracture Toughness of Carbon Fibre-Reinforced Polymer Laminates With Nano- and Micro-Fillers. Strain 2011;47:e269–82. https://doi.org/10.1111/j.1475-1305.2008.00612.x.

[132] De S, Fulmali AO, Nuli KC, Prusty RK, Prusty BG, Ray BC. Improving delamination resistance of carbon fiber reinforced polymeric composite by interface engineering using carbonaceous nanofillers through electrophoretic deposition: An assessment at different in-service temperatures. Journal of Applied Polymer Science 2021;138:50208. https://doi.org/10.1002/app.50208.

[133] Movva S, Gang Zhou, Guerra D, Lee LJ. Effect of Carbon Nanofibers on Mold Filling in a Vacuum Assisted Resin Transfer Molding System. Journal of Composite Materials 2009;43:611–20. https://doi.org/10.1177/0021998308094546.

[134] Ghose S, Watson KA, Working DC, Siochi EJ, Connell JW, Criss JM. Fabrication and Characterization of High Temperature Resin/Carbon Nanofiber Composites. High Performance Polymers 2006;18:527–44. https://doi.org/10.1177/0954008306066538.

[135] Zhou Y, Pervin F, Rangari VK, Jeelani S. Fabrication and evaluation of carbon nano fiber filled carbon/epoxy composite. Materials Science and Engineering: A 2006;426:221–8. https://doi.org/10.1016/j.msea.2006.04.031.

[136] Zhou Y, Pervin F, Jeelani S, Mallick PK. Improvement in mechanical properties of carbon fabric–epoxy composite using carbon nanofibers. Journal of Materials Processing Technology 2008;198:445–53. https://doi.org/10.1016/j.jmatprotec.2007.07.028.

[137] Bortz DR, Merino C, Martin-Gullon I. Mechanical characterization of hierarchical carbon fiber/nanofiber composite laminates. Composites Part A: Applied Science and Manufacturing 2011;42:1584–91. https://doi.org/10.1016/j.compositesa.2011.07.002.

[138] Kavosi J, Sarikaya S, Creasy TS, Naraghi M. Identification of the effect of nanofiller morphology on interlaminar fracture toughness of hybrid composites. Journal of Composite Materials 2021;55:2899–910. https://doi.org/10.1177/00219983211002915.

[139] Green KJ, Dean DR, Vaidya UK, Nyairo E. Multiscale fiber reinforced composites based on a carbon nanofiber/epoxy nanophased polymer matrix: Synthesis, mechanical, and thermomechanical behavior. Composites Part A: Applied Science and Manufacturing 2009;40:1470–5. https://doi.org/10.1016/j.compositesa.2009.05.010.

[140] Koissin V, Warnet LL, Akkerman R. Delamination in carbon-fibre composites improved with in situ grown nanofibres. Engineering Fracture Mechanics 2013;101:140–8. https://doi.org/10.1016/j.engfracmech.2012.09.006.

[141] Chandrasekaran VCS, Advani SG, Santare MH. Role of processing on interlaminar shear strength enhancement of epoxy/glass fiber/multi-walled carbon nanotube hybrid composites. Carbon 2010;48:3692–9. https://doi.org/10.1016/j.carbon.2010.06.010.

[142] Yokozeki T, Iwahori Y, Ishiwata S, Enomoto K. Mechanical properties of CFRP laminates manufactured from unidirectional prepregs using CSCNT-dispersed epoxy. Composites Part A: Applied Science and Manufacturing 2007;38:2121–30. https://doi.org/10.1016/j.compositesa.2007.07.002.

[143] Arai M, Matsushita K, Hirota S. Criterion for interlaminar strength of CFRP laminates

toughened with carbon nanofiber interlayer. Composites Part A: Applied Science and Manufacturing 2011;42:703–11. https://doi.org/10.1016/j.compositesa.2011.01.005.

[144] Kirmse S, Hsiao KT. Enhancing the interlaminar shear strength of unidirectional carbon fiber reinforced plastic (CFRP) laminate using a nanofiber Z-threading strategy. Proceedings of CAMX 2018 (The Composites and Advanced Materials Expo), Dallas, TX, Oct 15-18, 2018, TP18-0499 2018.

[145] Arai M, Noro Y, Sugimoto K, Endo M. Mode I and mode II interlaminar fracture toughness of CFRP laminates toughened by carbon nanofiber interlayer. Composites Science and Technology 2008;68:516–25. https://doi.org/10.1016/j.compscitech.2007.06.007.

[146] Wu T, Huan X, Zhang H, Wu L, Sui G, Yang X. The orientation and inhomogeneous distribution of carbon nanofibers and distinctive internal structure in polymer composites induced by 3D-printing enabling electromagnetic shielding regulation. Journal of Colloid and Interface Science 2023;638:392–402. https://doi.org/10.1016/j.jcis.2023.02.014.

[147] Yao Z, Wang C, Wang Y, Qin J, Cui B, Wang Q, et al. Effect of Microstructures of Carbon Nanoproducts Grown on Carbon Fibers on the Interfacial Properties of Epoxy Composites. Langmuir 2022;38:2392–400. https://doi.org/10.1021/acs.langmuir.1c03459.

[148] Patton RD, Pittman, Jr CU, Wang L, Hill JR. Vapor grown carbon fiber composites with epoxy and poly(phenylene sulfide) matrices. Composites Part A: Applied Science and Manufacturing 1999;30:1081–91. https://doi.org/10.1016/S1359-835X(99)00018-4.

[149] Iwahori Y, Ishiwata S, Sumizawa T, Ishikawa T. Mechanical properties improvements in two-phase and three-phase composites using carbon nano-fiber dispersed resin. Composites Part A: Applied Science and Manufacturing 2005;36:1430–9. https://doi.org/10.1016/j.compositesa.2004.11.017.

[150] Pervin F, Zhou Y, Rangari VK, Jeelani S. Testing and evaluation on the thermal and mechanical properties of carbon nano fiber reinforced SC-15 epoxy. Materials Science and Engineering: A 2005;405:246–53. https://doi.org/10.1016/j.msea.2005.06.012.

[151] Zhamu A, Hou Y, Zhong W-H, Stone JJ, Li J, Lukehart CM. Properties of a reactive-graphitic-carbon-nanofibers-reinforced epoxy. Polymer Composites 2007;28:605–11. https://doi.org/10.1002/pc.20278.

[152] Bal S. Experimental study of mechanical and electrical properties of carbon nanofiber/epoxy composites. Materials & Design (1980-2015) 2010;31:2406–13. https://doi.org/10.1016/j.matdes.2009.11.058.

[153] Ardanuy M, Rodríguez-Perez MA, Algaba I. Electrical conductivity and mechanical properties of vapor-grown carbon nanofibers/trifunctional epoxy composites prepared by direct mixing. Composites Part B: Engineering 2011;42:675–81. https://doi.org/10.1016/j.compositesb.2011.02.006.

[154] Xu LR, Bhamidipati V, Zhong W-H, Li J, Lukehart CM, Lara-Curzio E, et al. Mechanical Property Characterization of a Polymeric Nanocomposite Reinforced by Graphitic Nanofibers with Reactive Linkers. Journal of Composite Materials 2004;38:1563–82. https://doi.org/10.1177/0021998304043758.

[155] Sui G, Zhong WH, Liu MC, Wu PH. Enhancing mechanical properties of an epoxy resin using "liquid nano-reinforcements." Materials Science and Engineering: A 2009;512:139–42. https://doi.org/10.1016/j.msea.2009.01.023.

[156] Sancaktar E, Aussawasathien D. Nanocomposites of Epoxy with Electrospun Carbon Nanofibers: Mechanical Behavior. The Journal of Adhesion 2009;85:160–79. https://doi.org/10.1080/00218460902881758.

[157] Zhang J, Niu H, Zhou J, Wang X, Lin T. Synergistic effects of PEK-C/VGCNF composite nanofibres on a trifunctional epoxy resin. Composites Science and Technology 2011;71:1060–7. https://doi.org/10.1016/j.compscitech.2011.03.008.

[158] Zhang J, Lin T, Cheung SCP, Wang CH. The effect of carbon nanofibres on self-healing epoxy/poly(ε-caprolactone) blends. Composites Science and Technology 2012;72:1952–9. https://doi.org/10.1016/j.compscitech.2012.08.017.

[159] Shokrieh MM, Esmkhani M, Vahedi F, Shahverdi HR. Improvement of mechanical and electrical properties of epoxy resin with carbon nanofibers. Iranian Polymer Journal

2013;22:721–7. https://doi.org/10.1007/s13726-013-0170-2.

[160] Ahmadi M, Masoomi M, Safi S. Mechanical property characterization of carbon nanofiber/epoxy nanocomposites reinforced by GMA-grafted UHMWPE fibers. Composites Part B: Engineering 2015;83:43–9. https://doi.org/10.1016/j.compositesb.2015.08.006.

[161] Zeltmann SE, Poveda RL, Gupta N. Accelerated environmental degradation and residual flexural analysis of carbon nanofiber reinforced composites. Polymer Degradation and Stability 2015;121:348–58. https://doi.org/10.1016/j.polymdegradstab.2015.09.022.

[162] Miranda AN de, Pardini LC, Santos CAM dos, Vieira R. Evaluation of carbon fiber composites modified by in situ incorporation of carbon nanofibers. Materials Research 2011;14:560–3. https://doi.org/10.1590/S1516-14392011005000083.

[163] Singer G, Rennhofer H, Sinn G, Unterlass MM, Wendrinsky J, Windberger U, et al. Processing of Carbon Nanotubes and Carbon Nanofibers towards High Performance Carbon Fiber Reinforced Polymers. Key Engineering Materials 2017;742:31–7. https://doi.org/10.4028/www.scientific.net/KEM.742.31.

[164] Chen Q, Zhang L, Rahman A, Zhou Z, Wu X-F, Fong H. Hybrid multi-scale epoxy composite made of conventional carbon fiber fabrics with interlaminar regions containing electrospun carbon nanofiber mats. Composites Part A: Applied Science and Manufacturing 2011;42:2036–42. https://doi.org/10.1016/j.compositesa.2011.09.010.

[165] Sarim A, Zhang BM, Wang CC. Mechanical Enhancement of Carbon Fiber/Epoxy Composites Based on Carbon Nano Fibers by Using Spraying Methodology. Applied Mechanics and Materials 2012;245:203–8. https://doi.org/10.4028/www.scientific.net/AMM.245.203.

[166] Chen Q, Zhao Y, Zhou Z, Rahman A, Wu X-F, Wu W, et al. Fabrication and mechanical properties of hybrid multi-scale epoxy composites reinforced with conventional carbon fiber fabrics surface-attached with electrospun carbon nanofiber mats. Composites Part B: Engineering 2013;44:1–7. https://doi.org/10.1016/j.compositesb.2012.09.005.

[167] Jie C, Long H, Peng X, Xiang X. Mechanical properties of carbon/carbon composites with the fibre/matrix interface modified by carbon nanofibers. Materials Science and Engineering: A 2016;656:21–6. https://doi.org/10.1016/j.msea.2016.01.013.

[168] Kattaguri R, Fulmali AO, Prusty RK, Ray BC. Effects of acid, alkaline, and seawater aging on the mechanical and thermomechanical properties of glass fiber/epoxy composites filled with carbon nanofibers. Journal of Applied Polymer Science 2020;137:1–13. https://doi.org/10.1002/app.48434.

[169] Kar RN, Fulmali AO, Ganesh Gupta K BNVS, Prusty RK, Ray BC. Effect of in-situ temperature and loading rate on the out-of-plane performance of carbon nanofiber embedded glass fiber / epoxy composite. Materials Today: Proceedings 2022;62:6115–9. https://doi.org/10.1016/j.matpr.2022.04.1020.

[170] Zhou Y, Pervin F, Jeelani S. Effect vapor grown carbon nanofiber on thermal and mechanical properties of epoxy. Journal of Materials Science 2007;42:7544–53. https://doi.org/10.1007/s10853-007-1618-6.

[171] Poveda RL, Gupta N. Carbon-Nanofiber-Reinforced Syntactic Foams: Compressive Properties and Strain Rate Sensitivity. JOM 2014;66:66–77. https://doi.org/10.1007/s11837-013-0791-0.

[172] Shokrieh MM, Kashani ARS, Mosalmani R. A dynamic constitutive-micromechanical model to predict the strain rate-dependent mechanical behavior of carbon nanofiber/epoxy nanocomposites. Iranian Polymer Journal 2016;25:487–501. https://doi.org/10.1007/s13726-016-0441-9.

[173] Zhou Z, Gao D, Lin G, Sun W. Static and dynamic mechanical properties of epoxy nanocomposites reinforced by hybridization with carbon nanofibers and block ionomers. Engineering Fracture Mechanics 2022;271:108638. https://doi.org/10.1016/j.engfracmech.2022.108638.

[174] Chanda A, Sinha SK, Datla N V. The influence of fiber alignment, structure and concentration on mechanical behavior of carbon nanofiber/epoxy composites: Experimental and numerical study. Polymer Composites 2021;42:1155–73.

https://doi.org/10.1002/pc.25890.

[175] Reis PNB, Silva MP, Santos P, Parente JM, Valvez S, Bezazi A. Mechanical performance of an optimized cork agglomerate core-glass fibre sandwich panel. Composite Structures 2020;245:112375. https://doi.org/10.1016/j.compstruct.2020.112375.

[176] Zhou TH, Ruan WH, Yang JL, Rong MZ, Zhang MQ, Zhang Z. A novel route for improving creep resistance of polymers using nanoparticles. Composites Science and Technology 2007;67:2297–302. https://doi.org/10.1016/j.compscitech.2007.01.015.

[177] Gugulothu D, Barhoum A, Nerella R, Ajmer R, Bechelany M. Fabrication of Nanofibers: Electrospinning and Non-electrospinning Techniques. Handbook of Nanofibers, Cham: Springer International Publishing; 2019, p. 45–77. https://doi.org/10.1007/978-3-319-53655-2_6.

[178] Reis PNB, Silva MP, Santos P, Parente JM, Bezazi A. Viscoelastic behaviour of composites with epoxy matrix filled by cork powder. Composite Structures 2020;234:111669. https://doi.org/10.1016/j.compstruct.2019.111669.

[179] Houshyar S, Shanks RA, Hodzic A. Tensile creep behaviour of polypropylene fibre reinforced polypropylene composites. Polymer Testing 2005;24:257–64. https://doi.org/10.1016/j.polymertesting.2004.07.003.

[180] Glaskova-Kuzmina T, Aniskevich A, Zarrelli M, Martone A, Giordano M. Effect of filler on the creep characteristics of epoxy and epoxy-based CFRPs containing multi-walled carbon nanotubes. Composites Science and Technology 2014;100:198–203. https://doi.org/10.1016/j.compscitech.2014.06.011.

[181] Bouafif H, Koubaa A, Perré P, Cloutier A. Creep behaviour of HDPE/wood particle composites. International Journal of Microstructure and Materials Properties 2013;8:225. https://doi.org/10.1504/IJMMP.2013.055385.

[182] Jian W, Lau D. Creep performance of CNT-based nanocomposites: A parametric study. Carbon 2019;153:745–56. https://doi.org/10.1016/j.carbon.2019.07.069.

[183] Yang J-L, Zhang Z, Schlarb AK, Friedrich K. On the characterization of tensile creep resistance of polyamide 66 nanocomposites. Part I. Experimental results and general discussions. Polymer 2006;47:2791–801. https://doi.org/10.1016/j.polymer.2006.02.065.

[184] Yang J, Zhang Z, Friedrich K, Schlarb AK. Creep Resistant Polymer Nanocomposites Reinforced with Multiwalled Carbon Nanotubes. Macromolecular Rapid Communications 2007;28:955–61. https://doi.org/10.1002/marc.200600866.

[185] Park B-D, Balatinecz JJ. Short term flexural creep behavior of wood-fiber/polypropylene composites. Polymer Composites 1998;19:377–82. https://doi.org/10.1002/pc.10111.

[186] Almeida JH, Ornaghi HL, Lorandi N, Marinucci G, Amico S. On creep, recovery, and stress relaxation of carbon fiber-reinforced epoxy filament wound composites. Polymer Engineering & Science 2018;58:1837–42. https://doi.org/10.1002/pen.24790.

[187] Reis PNB, Neto MA, Amaro AM. Effect of hostile solutions on stress relaxation of carbon/epoxy composites. Polymer Degradation and Stability 2019;165:60–7. https://doi.org/10.1016/j.polymdegradstab.2019.04.026.

[188] Reis PNB, Silva MP, Santos P. Stress Relaxation in Delaminated Carbon/Epoxy Composites. Fibers and Polymers 2019;20:1284–9. https://doi.org/10.1007/s12221-019-8916-x.

[189] Hossain MK, Hossain ME, Dewan MW, Hosur M, Jeelani S. Effects of carbon nanofibers (CNFs) on thermal and interlaminar shear responses of E-glass/polyester composites. Composites Part B: Engineering 2013;44:313–20. https://doi.org/10.1016/j.compositesb.2012.05.006.

[190] Fan Z, Santare MH, Advani SG. Interlaminar shear strength of glass fiber reinforced epoxy composites enhanced with multi-walled carbon nanotubes. Composites Part A: Applied Science and Manufacturing 2008;39:540–54. https://doi.org/10.1016/j.compositesa.2007.11.013.

[191] Palmeri MJ, Putz KW, Ramanathan T, Brinson LC. Multi-scale reinforcement of CFRPs using carbon nanofibers. Composites Science and Technology 2011;71:79–86.

https://doi.org/10.1016/j.compscitech.2010.10.006.

[192] Rodriguez AJ, Guzman ME, Lim C-S, Minaie B. Mechanical properties of carbon nanofiber/fiber-reinforced hierarchical polymer composites manufactured with multiscale-reinforcement fabrics. Carbon 2011;49:937–48. https://doi.org/10.1016/j.carbon.2010.10.057.

[193] Khan SU, Kim JK. Interlaminar shear properties of CFRP composites with CNF-bucky paper interleaves. ICCM International Conferences on Composite Materials 2011:1–6. https://doi.org/https://hdl.handle.net/1783.1/54411.

[194] Khan SU, Kim J-K. Improved interlaminar shear properties of multiscale carbon fiber composites with bucky paper interleaves made from carbon nanofibers. Carbon 2012;50:5265–77. https://doi.org/10.1016/j.carbon.2012.07.011.

[195] Anand A, Harshe R, Joshi M. On the processing and properties of carbon nanofiber reinforced hybrid structural composites. Journal of Composite Materials 2013;47:2937–43. https://doi.org/10.1177/0021998312459873.

[196] Ma L, Wu L, Cheng X, Zhuo D, Weng Z, Wang R. Improving the interlaminar properties of polymer composites using a situ accumulation method to construct the multi-scale reinforcement of carbon nanofibers/carbon fibers. Composites Part A: Applied Science and Manufacturing 2015;72:65–74. https://doi.org/10.1016/j.compositesa.2015.01.023.

[197] Taheri-Behrooz F, Esmkhani M, Yaghoobi-Chatroodi A, Ghoreishi SM. Out-of-plane shear properties of glass/epoxy composites enhanced with carbon-nanofibers. Polymer Testing 2016;55:278–86. https://doi.org/10.1016/j.polymertesting.2016.09.003.

[198] Yao H, Zhou G, Wang W, Peng M. Effect of polymer-grafted carbon nanofibers and nanotubes on the interlaminar shear strength and flexural strength of carbon fiber/epoxy multiscale composites. Composite Structures 2018;195:288–96. https://doi.org/10.1016/j.compstruct.2018.04.082.

[199] Kirmse S, Ranabhat B, Hsiao K. A Preliminary Study of the Electrical and Interlaminar Shear Properties of a Porous CFRP Composite Laminate Containing Carbon Nanofiber Z-Threads. CAMX 2019, NA SAMPE; 2019. https://doi.org/10.33599/nasampe/c.19.0773.

[200] Kirmse S, Ranabhat B, Hsiao K-T. Experimental and analytical investigation on the interlaminar shear strength of carbon fiber composites reinforced with carbon nanofiber z-threads. Materials Today Communications 2020;25:101512. https://doi.org/10.1016/j.mtcomm.2020.101512.

[201] Hsiao K, Johnson M, Kirmse S, Ranabhat B. Carbon Nanofiber Z-Threaded Carbon Fiber Reinforced Polymer Composite (ZT-CFRP) Laminate Parts Produced Using a Magnetic Compaction Force Assisted Additive Manufacturing (MCFA-AM) Technique. SAMPE 2020 | Virtual Series, vol. 2020- June, NA SAMPE; 2020. https://doi.org/10.33599/382/s.20.0256.

[202] Mrzljak S, Zanghellini B, Gerdes L, Helwing R, Schuller R, Sinn G, et al. Effect of carbon nanofibre orientation on fatigue properties of carbon fibre-reinforced polymers. Journal of Composite Materials 2023;57:1149–64. https://doi.org/10.1177/00219983221150496.

[203] May M, Hahn P, Manam BU, Imbert M. Mixed-Mode I/II Testing of Composite Materials—A Refined Data Reduction Scheme for the Wedge-Loaded Asymmetric Double Cantilever Beam Test. Journal of Composites Science 2022;6:319. https://doi.org/10.3390/jcs6100319.

[204] Ravindran AR, Ladani RB, Wang CH, Mouritz AP. Synergistic mode II delamination toughening of composites using multi-scale carbon-based reinforcements. Composites Part A: Applied Science and Manufacturing 2019;117:103–15. https://doi.org/10.1016/j.compositesa.2018.11.011.

[205] Zhu Y, Bakis CE, Adair JH. Effects of carbon nanofiller functionalization and distribution on interlaminar fracture toughness of multi-scale reinforced polymer composites. Carbon 2012;50:1316–31. https://doi.org/10.1016/j.carbon.2011.11.001.

[206] Yokozeki T, Iwahori Y, Ishibashi M, Yanagisawa T, Imai K, Arai M, et al. Fracture toughness improvement of CFRP laminates by dispersion of cup-stacked carbon nanotubes. Composites Science and Technology 2009;69:2268–73. https://doi.org/10.1016/j.compscitech.2008.12.017.

[207] Gude MR, Prolongo SG, Gómez-del Río T, Ureña A. Mode-I adhesive fracture energy of carbon fibre composite joints with nanoreinforced epoxy adhesives. International Journal of Adhesion and Adhesives 2011;31:695–703. https://doi.org/10.1016/j.ijadhadh.2011.06.016.

[208] Kostopoulos V, Tsotra P, Karapappas P, Vavouliotis A, Tsantzalis S, Friedrich K. Enhancement of the Mechanical Performance of Carbon Fiber Reinforced Epoxy Resin Composites by the Introduction of Carbon Nano-Fibers (CNF). 47th AIAA/ASME/ASCE/AHS/ASC Structures, Structural Dynamics, and Materials Conference
 14th AIAA/ASME/AHS Adaptive Structures Conference
 7th, vol. 5, Reston, Virigina: American Institute of Aeronautics and Astronautics; 2006, p. 3273–82. https://doi.org/10.2514/6.2006-1859.

[209] Kostopoulos V, Tsotra P, Karapappas P, Tsantzalis S, Vavouliotis A, Loutas TH, et al. Mode I interlaminar fracture of CNF or/and PZT doped CFRPs via acoustic emission monitoring. Composites Science and Technology 2007;67:822–8. https://doi.org/10.1016/j.compscitech.2006.02.038.

[210] Tsantzalis S, Karapappas P, Vavouliotis A, Tsotra P, Kostopoulos V, Tanimoto T, et al. On the improvement of toughness of CFRPs with resin doped with CNF and PZT particles. Composites Part A: Applied Science and Manufacturing 2007;38:1159–62. https://doi.org/10.1016/j.compositesa.2006.04.016.

[211] Arai M, Hirokawa J, Hanamura Y, Ito H, Hojo M, Quaresimin M. Characteristic of mode I fatigue crack propagation of CFRP laminates toughened with CNF interlayer. Composites Part B: Engineering 2014;65:26–33. https://doi.org/10.1016/j.compositesb.2014.02.025.

[212] Wang P, Liu W, Zhang X, Lu X, Yang J. Enhanced fracture toughness of carbon fabric/epoxy laminates with pristine and functionalized stacked-cup carbon nanofibers. Engineering Fracture Mechanics 2015;148:73–81. https://doi.org/10.1016/j.engfracmech.2015.09.010.

[213] Ladani RB, Wu S, Kinloch AJ, Ghorbani K, Zhang J, Mouritz AP, et al. Improving the toughness and electrical conductivity of epoxy nanocomposites by using aligned carbon nanofibres. Composites Science and Technology 2015;117:146–58. https://doi.org/10.1016/j.compscitech.2015.06.006.

[214] Wu S, Ladani RB, Zhang J, Kinloch AJ, Zhao Z, Ma J, et al. Epoxy nanocomposites containing magnetite-carbon nanofibers aligned using a weak magnetic field. Polymer 2015;68:25–34. https://doi.org/10.1016/j.polymer.2015.04.080.

[215] Hsiao K-T, Scruggs AM, Brewer JS, Hickman GJS, McDonald EE, Henderson K. Effect of carbon nanofiber z-threads on mode-I delamination toughness of carbon fiber reinforced plastic laminates. Composites Part A: Applied Science and Manufacturing 2016;91:324–35. https://doi.org/10.1016/j.compositesa.2016.10.022.

[216] Ladani RB, Ravindran AR, Wu S, Pingkarawat K, Kinloch AJ, Mouritz AP, et al. Multi-scale toughening of fibre composites using carbon nanofibres and z-pins. Composites Science and Technology 2016;131:98–109. https://doi.org/10.1016/j.compscitech.2016.06.005.

[217] Ladani RB, Wu S, Kinloch AJ, Ghorbani K, Zhang J, Mouritz AP, et al. Multifunctional properties of epoxy nanocomposites reinforced by aligned nanoscale carbon. Materials & Design 2016;94:554–64. https://doi.org/10.1016/j.matdes.2016.01.052.

[218] Ladani RB, Bhasin M, Wu S, Ravindran AR, Ghorbani K, Zhang J, et al. Fracture and fatigue behaviour of epoxy nanocomposites containing 1-D and 2-D nanoscale carbon fillers. Engineering Fracture Mechanics 2018;203:102–14. https://doi.org/10.1016/j.engfracmech.2018.04.033.

[219] Ravindran AR, Ladani RB, Wang CH, Mouritz AP. Hierarchical mode I and mode II interlaminar toughening of Z-pinned composites using 1D and 2D carbon nanofillers. Composites Part A: Applied Science and Manufacturing 2019;124:105470. https://doi.org/10.1016/j.compositesa.2019.05.038.

[220] Ekhtiyari A, Shokrieh MM, Alderliesten R. Loading rate effects on mode-I delamination in glass/epoxy and glass/CNF/epoxy laminated composites. Engineering Fracture Mechanics 2020;228:106908. https://doi.org/10.1016/j.engfracmech.2020.106908.

[221] Tita V, de Carvalho J, Vandepitte D. Failure analysis of low velocity impact on thin composite laminates: Experimental and numerical approaches. Composite Structures 2008;83:413–28. https://doi.org/10.1016/j.compstruct.2007.06.003.

[222] Bhuiyan MA, Hosur MV, Jeelani S. Low-velocity impact response of sandwich composites with nanophased foam core and biaxial braided face sheets. Composites Part B: Engineering 2009;40:561–71. https://doi.org/10.1016/j.compositesb.2009.03.010.

[223] Ito H, Arai M, Takeyama K, Hu N, Quaresimin M. Impact Damage and Residual Compression Strength of CNF/CFRP Hybrid Laminates. Journal of Solid Mechanics and Materials Engineering 2013;7:381–93. https://doi.org/10.1299/jmmp.7.381.

[224] Rahman MM, Hosur M, Hsiao K-T, Wallace L, Jeelani S. Low velocity impact properties of carbon nanofibers integrated carbon fiber/epoxy hybrid composites manufactured by OOA–VBO process. Composite Structures 2015;120:32–40. https://doi.org/10.1016/j.compstruct.2014.09.053.

[225] Arai M, Ito H, Nishimura M, Zakoji T, Quaresimin M. CAI strength of cfrp laminates toughened with multi-walled carbon nanofiber. 16th European Conference on Composite Materials, ECCM, Seville, Spain, 22–26 June 2014 2014:22–6.

[226] Ivañez I, Sánchez-Saez S, Garcia-Castillo SK, Barbero E, Amaro AM, Reis PNB. Impact response of repaired sandwich structures. Polymer Composites 2020;41:3014–22. https://doi.org/10.1002/pc.25593.

Chapter 3

Influence of manufacturing parameters[2]

Abstract

One of the most relevant problems of nano-reinforced resins is the uniform dispersion of nanoparticles. This problem is even more relevant when they are involved in the production of laminated composites. In this case, in addition to the agglomeration of nanoparticles, air bubbles are also very frequent during the manufacturing process of laminated composites with nano-reinforced resins. These air bubbles are even more frequent in the hand lay-up process. In this context, this study intends to study some manufacture parameters in order to maximize the mechanical properties. For this purpose, the mixer rotation speed, the dispersion time of the nanoparticles and the vacuum time applied to the system were analysed in detail. It was found that the mixing time is very dependent on the rotation speed used and there is an ideal vacuum time. A short vacuum time allows air bubbles to exist in the resin, while a long time promotes a decrease in mechanical properties due to the removal of resin in the laminates and, consequently, the fibres are not fully wet.

3.1. Introduction

Nowadays, polymer matrix composites (PMCs) are replacing, more and more, the traditional metallic materials and this trend extends to the most diverse industrial applications. This is consequence of their high specific strength and stiffness, good fatigue performance, corrosion resistance, and low processing costs [1].

The hand lay-up process, also called the wet lay-up method, is the simplest and oldest method and it is particularly suitable for large components/structures. In this process, each layer is handled manually, layer by layer, up to the desired thickness. Although brushes are often used to distribute the resin evenly onto the fibres, rollers are used to ensure complete wetting of the fibres and to remove air bubbles. However, the large amount of air bubbles that a laminate can present is the main drawback of this process. In this case, the vacuum bagging process proves to be a good alternative, because, as it is a closed mold process, it is able to manufacture components/structures with higher mechanical performance and low cost [2,3].

[2] Based on the work published in the IOP Conference Series: Materials Science and Engineering, Santos, P.; Maceiras, A.; Reis, P.N.B. Influence of Manufacturing Parameters on the Mechanical Properties of Nano-Reinforced CFRP by Carbon Nanofibers. *IOP Conference Series: Materials Science and Engineering* **2021**, *1126*, 012012, 10.1088/1757-899X/1126/1/012012

On the other hand, the open literature reports that the mechanical properties of nanocomposites are dependent on the content of nanoparticles, type of resin and manufacturing process. In this case, for example, in order to maximize mechanical properties, good dispersion is essential, which often involves great technical difficulties and high costs to achieve them. For example, Ferreira et al. [4] compared two dispersion processes, direct dispersion method (DM) and indirect dispersion method (IDM), in terms of mechanical properties, and they concluded that the nanocomposites obtained by the indirect method had lower mechanical properties than the neat resin due to the residual acetone.

Therefore, the present study intends to analyse the effect of some manufacturing parameters on the mechanical properties of nano-reinforced carbon fibre reinforced polymers (CFRPs) by carbon nanofibres (CNFs). The influence of the rotation speed, mixing time and vacuum application time will be analysed in detail for an epoxy resin. In fact, epoxy resins are thermosetting polymers used as matrices due to their chemical resistance, high specific strength, dimensional stability, and excellent adhesion to fillers, among others. Epoxies are two-component materials: resin and hardener, where resins are normally diglycidyl ethers of bisphenol-A and/or bisphenol-F; and hardeners are the curing agents. There are different types of hardeners, but the most commons are based on amines, and these amines when reacting with the epoxy rings are able to start the polymerization and subsequent crosslinking [5]. On the other hand, CNFs present superior mechanical and chemical properties over commonly used carbon fibres owing to their unique small-size characteristics. In addition, they have excellent electrical and high thermal conductivity. Therefore, CNFs can be considered for extending the physical and mechanical properties of conventional carbon fibre composites for lightweight structural applications.

3.2. Materials and experimental procedure

An SR 8100 epoxy resin and a SD 8822 hardener, both supplied by Sicomin, were used to produce nanocomposites and carbon/epoxy laminates reinforced with CNFs. Their average diameter is about 130 nm, length between 20 and 200 μm, and average specific surface area around 54 m^2/g. The SR 8100 epoxy is composed of a mixture of bisphenol A (DGEBA), bisphenol F (DGEBF) epoxy resins, and 1,6-bis(2,3-epoxypropoxy)hexane, as diluent. The hardener SD 8822 is a mixture of amines, 2-methylpentane-1,5-diamine, m-phenylenebis(methylamine), and trimethylolpropane tris[poly(propylene glycol), amine terminated] ether [5].

In terms of nanocomposites three different manufacturing processes were adopted, which are shown in Table 3.1.

Table 3.1: Manufacturing processes of nanocomposites.

Manufacturing Processes	Detail used during the manufacturing process
1	Resin and hardener mixed manually.
2	Resin and hardener mixed manually, followed by vacuum for 10 minutes.
3	The resin mixture with 0.5 wt.% CNFs was conducted at 1000 rpm for 3 hours and, at same time, submitted to an ultrasonic bath (frequency of 40 kHz). The hardener was subsequently added at 150 rpm for 10 minutes and, finally, the mixture was degassed for 10 minutes in a vacuum chamber.

After the manufacture process reported in Table 3.1, the mixture is carefully poured into a cardboard mold with dimensions of 100 × 130 × 3 ± 0.09 mm^3 and cured at room temperature (RT) for 24 hours. Finally, a post-cure at 40 °C was applied for 24 hours.

In terms of composite laminates, eight ply laminates of woven bi-directional carbon 195-1000P (195 g/m^2), all in the same direction, were prepared by hand lay-up and the overall dimensions of the plates were 150 × 150 × 1.5 ± 0.18 mm^3. The resin used was prepared by process 2. The system was placed inside a vacuum bag and a load of 2.5 kN was applied during 24 hours in order to maintain a constant fibre volume fraction and uniform laminate thickness. The bag remained attached to a vacuum pump to eliminate any air bubbles existing in the composite, and the vacuum time of 5 s, 1 min, 2 min, 3 min, 5 min and 10 min was analysed. Finally, the post-cure was followed according to manufacturer datasheet (epoxy resin) in an oven at 40 °C during 24 hours.

Finally, similar composites laminates were produced, but the epoxy resin was, in this case, enhanced by 0.5 wt.% of CNFs. Nine different manufacturing processes were studied, which are summarized in Table 3.2. In all conditions, the manufacturing process is completed with a post-cure in an oven at 40 °C for 24 hours.

Three-point bending (3PB) static tests were performed at RT and using specimens cut nominally to 60 × 10 × 3 mm^3 and 60 × 10 × 2 mm^3 from those plates, respectively, for resin and composite laminates as shown in Figure 3.1. The specimens were tested with a span of 50 mm and 40 mm, respectively, for resin and composite laminates, according to the European Standard EN ISO 178:2003. An Autograph AGS-X universal testing machine, from Shimadzu, with a 10 kN load cell and a displacement rate of 2 mm/min was used to test six different samples for each configuration.

The bending strength was calculated as the nominal stress in the middle span section obtained using maximum value of the load (Eq. 3.1), while the bending stiffness modulus was obtained by linear regression of the load-displacement curves considering the interval in the linear segment with a correlation factor greater than 95% according with Eq. 3.2 [6]. Finally, the bending strain is obtained according with Eq. 3.3:

Table 3.2: Manufacturing process of composite laminates.

Manufacturing Processes	Detail used during the manufacturing process
1	Control samples obtained by: Resin and hardener mixed manually, followed by vacuum for 10 minutes. The bag remained attached to a vacuum pump for 2 min.
2	Composite laminates were manufactured based on process 3, reported in Table 3.1, but conducted at 400 rpm for 3 hours. Thereafter, the system was placed in a vacuum bag, a 2.5 kN load was applied for 24 hours and vacuum for 2 min.
3	Composite laminates were manufactured based on process 3, reported in Table 3.1, but conducted at 700 rpm for 3 hours. Thereafter, the system was placed in a vacuum bag, a 2.5 kN load was applied for 24 hours and vacuum for 2 min.
4	Composite laminates were manufactured based on process 3, reported in Table 3.1, but conducted at 700 rpm for 4 hours. Thereafter, the system was placed in a vacuum bag, a 2.5 kN load was applied for 24 hours and vacuum for 2 min.
5	Composite laminates were manufactured based on process 3, reported in Table 3.1, but conducted at 700 rpm for 5 hours. Thereafter, the system was placed in a vacuum bag, a 2.5 kN load was applied for 24 hours and vacuum for 2 min.
6	Composite laminates were manufactured based on process 3, reported in Table 3.1, but conducted at 1000 rpm for 3 hours. Thereafter, the system was placed in a vacuum bag, a 2.5 kN load was applied for 24 hours and vacuum for 2 min.
7	Composite laminates were manufactured based on process 3, reported in Table 3.1, but conducted at 1000 rpm for 4 hours. Thereafter, the system was placed in a vacuum bag, a 2.5 kN load was applied for 24 hours and vacuum for 2 min.
8	Composite laminates were manufactured based on process 3, reported in Table 3.1, but conducted at 1000 rpm for 5 hours. Thereafter, the system was placed in a vacuum bag, a 2.5 kN load was applied for 24 hours and vacuum for 2 min.
9	Composite laminates were manufactured based on process 3, reported in Table 3.1, but conducted at 1000 rpm for 3 hours. The system, after 2 min in a vacuum chamber, was subsequently placed in a vacuum bag and a 2.5 kN load was applied for 24 hours. Finally, the bag remained attached to a vacuum pump for another 2 minutes.

$$\sigma = \frac{3\,P\,L}{2\,b\,h^2} \tag{3.1}$$

$$E = \frac{\Delta P\,L^3}{48\,\Delta u\,I} \tag{3.2}$$

$$\varepsilon_f = \frac{6\,S\,h}{L^2} \tag{3.3}$$

where P is the load, L the span length, b the width, h the thickness of the specimen, I the moment of inertia of the cross-section, ΔP and Δu are, respectively, the load range and bending displacement range in the middle span for an interval in the linear region of the load versus displacement plot and S is the deflexion.

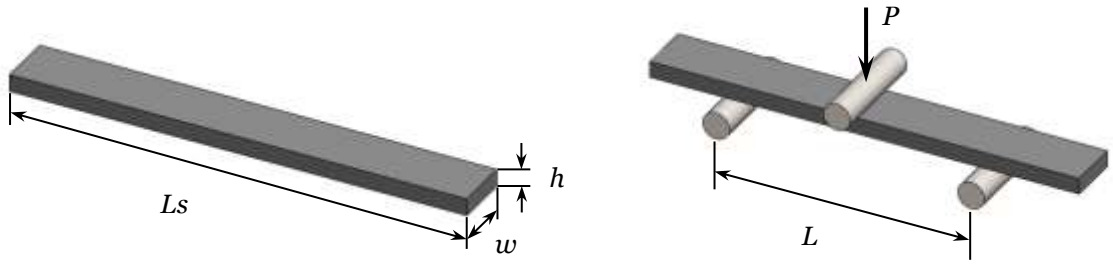

a) b)

Figure 3.1: a) Specimens geometry; b) Schematic view of the three-point bending apparatus.

3.3. Results and discussion

Bending static tests were performed to obtain the effect of some manufacture parameters on the mechanical performance. In this context, Figure 3.2 shows the stress-strain curves, and the results obtained for the procedures described in Table 3.1.

From Figure 3.2.a), it is possible to observe a linear increase of the bending stress with the bending strain, followed by a non-linear behaviour in which the maximum load is reached. It is also noticed that, when the resin is enhanced by CNFs, higher bending stress and modulus are achieved, while the bending strain decreases. After the peak load is reached, the bending stress decreases, arising the impending failure of the specimen. Figures 3.2.b) to 3.2.d) show the main bending properties in terms of average values (marks), and the bands represent, respectively, the maximum and minimum values for each condition. In terms of bending stress, Figure 3.2.b), it is noticed that the highest value was obtained with the resin enhanced by CNFs (114 MPa), reaching values around 12.6% higher than with the neat resin obtained without vacuum (process 1). However, when compared to the neat resin that involved vacuum, this improvement was only around 7.9%. Similar behaviour was observed for the bending modulus with values around 20.9% and 5.6%, respectively. Finally, the effect on the bending strain is not so evident due to the dispersion of the values observed. However, a small downward trend is observed for nano-enhanced resin. These results are in line with the open literature, because nanomaterials have a large surface area per volume unit compared to macro level materials and, in addition to their unique surface effects, increased chemical activity and particular physical properties, they promote synergy between constituents (polymer and CNFs) [6–8]. Simultaneously, the benefit of the vacuum is evident, where improvements in bending stress around 4.3% are obtained compared to the procedure that did not involve vacuum (process 1). Regardless of the resin/hardener mixture being made manually, and with particular care to avoid air bubbles, this process is not free from defects that need to be removed. In this context, the vacuum proved to be a viable technique for this purpose [2,3].

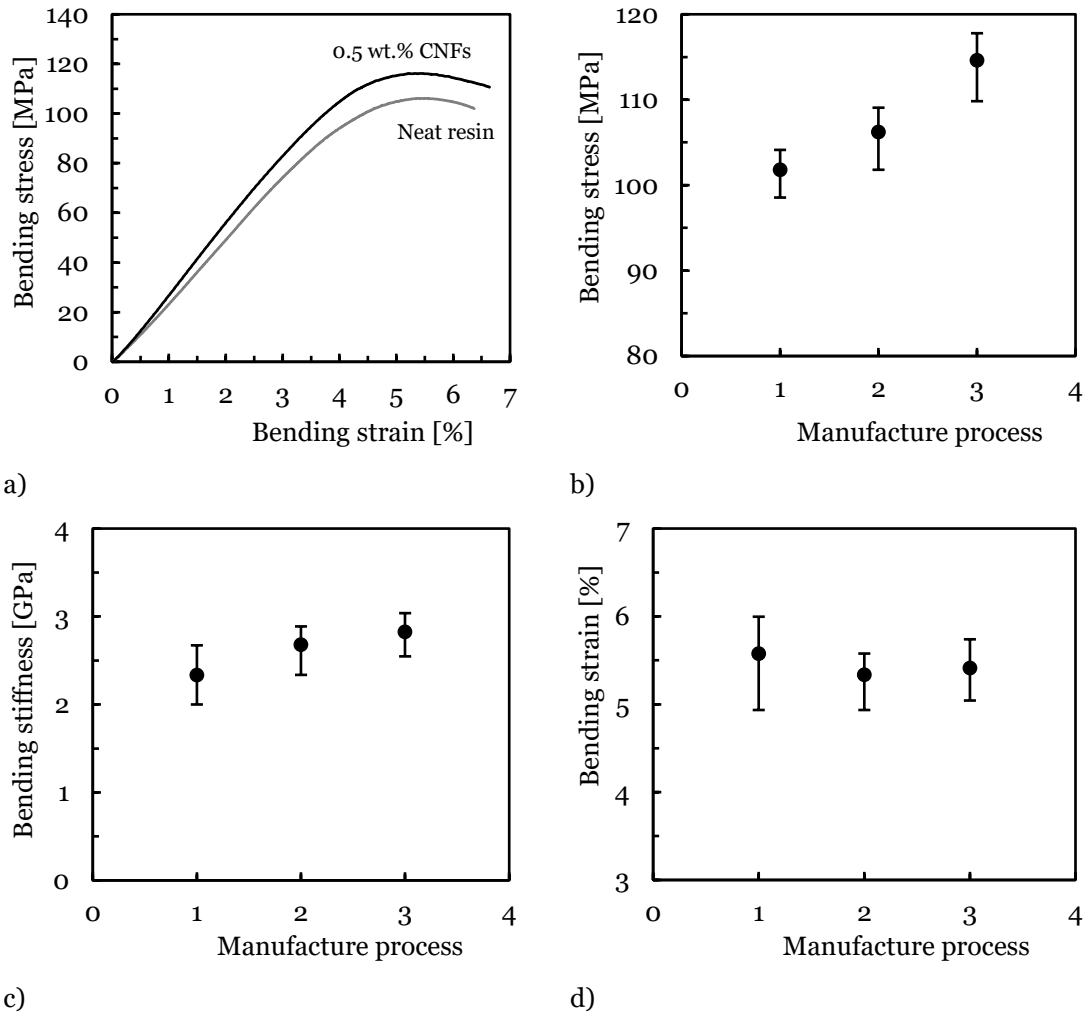

Figure 3.2: a) Representative bending stress-strain curves; b) Bending stress vs manufacture process; c) Bending modulus vs manufacture process; d) Bending strain vs manufacture process.

Figure 3.3 shows the fracture surface, showing a typical behaviour of brittle polymers with low resistance to crack propagation. On the other hand, the absence of air bubbles and a good dispersion of CNFs are also evident, confirming the benefits previously reported with the nanoparticles used.

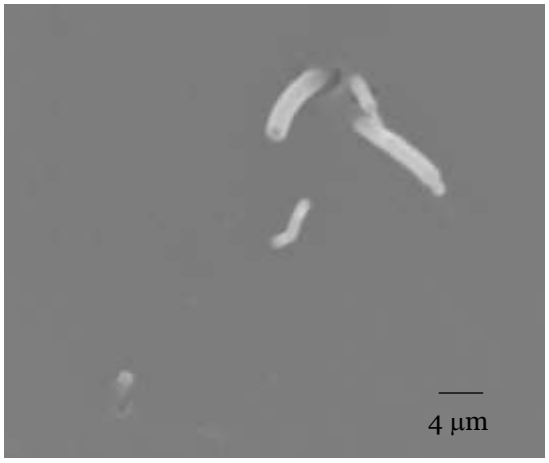

Figure 3.3: SEM image of the fracture surface.

In fact, according to the open literature, agglomerations/aggregations are responsible for stress concentrations in nanocomposites and reduce the interfacial area between the polymeric matrix and nanoparticles [8–11]. On the other hand, only a few polymer molecules are able to penetrate between the nanoparticles, which promotes an increase in viscosity [12].

In terms of composite laminates, Figure 3.4 shows the effect of the vacuum time on the bending properties. This study involved only laminates produced with neat resin obtained according to process 2 in Table 3.1. Therefore, the vacuum time is studied after the lamination of the composites. In fact, one of the most common defects of epoxy resins is the formation of air bubbles, so it is crucial to analyse the time for removing air by applying vacuum.

Figure 3.4.a) shows that all curves present a nearly fragile behaviour with a linear region up to the maximum load, followed by a significant drop after this value. Fibres breakage in compression side is the main damage mechanism observed, which is in line with the open literature [13,14]. According to Giancaspro et al. [14], carbon fibre composites fail mainly on the compression side, because this damage mechanism is consequence of the high compressive stress concentration in the pin load contact region associated to the low compressive strength of the carbon fibres [13,14].

From the other figures, Figures 3.4.b) to 3.4.d), it is possible to observe that the bending properties increase up to a vacuum time of 2 min, reaching their maximum values, after which they start to decrease. For example, compared to the values obtained for a vacuum time of 5 s, the bending stress increases around 14.1%, the bending modulus about 11% and the bending strain around 10.1%. On the other hand, the same comparison for the vacuum time of 10 min promotes decreases of 26.8% and 25.7%, respectively, for bending stress and bending strain, while the bending modulus remains very similar (comparisons in relation to the vacuum time of 5 s).

In order to explain this phenomenon, Figure 3.5 illustrates typical cross sections of specimens produced with vacuum times of 1 min and 2 min. As shown in Figure 3.5.a), it is possible to observe some voids, corresponding to air bubbles, in laminates that were produced with 1 min of vacuum, while for laminates subject to 2 min of vacuum, the absence of these voids is notorious (Figure 3.5.b)). Therefore, the increase in the mechanical properties previously reported up to 2 min of vacuum is a consequence of the decrease in voids. On the other hand, for higher vacuum times, the mechanical properties no longer decrease due to voids, but as a consequence of the lower amount of resin in the laminate. Vacuum suction was carried out at the end of the bag, and, in this case, the resin was sucked into the absorbent fabric that delimits the laminates. In this case, with the increase in the vacuum time, more resin is removed from the laminate and, consequently, the remaining resin is not enough to completely wet the fibres. Because the load transfer between fibres is not effective, due to the lack of resin, the mechanical properties of the laminates decrease. This can be justified by the lower thickness of the laminates that is observed with the increase in the vacuum time, because they were all subject to the same 2.5 kN load during the manufacturing process. For example, average thicknesses around 1.47 mm, 1.45 and 1.36 mm were measured for laminates subjected to vacuum times of 3 min, 5 min and 10 min, respectively,

which is a clear evidence of the lower resin content. In this context, the vacuum time of 2 min proved to be the ideal.

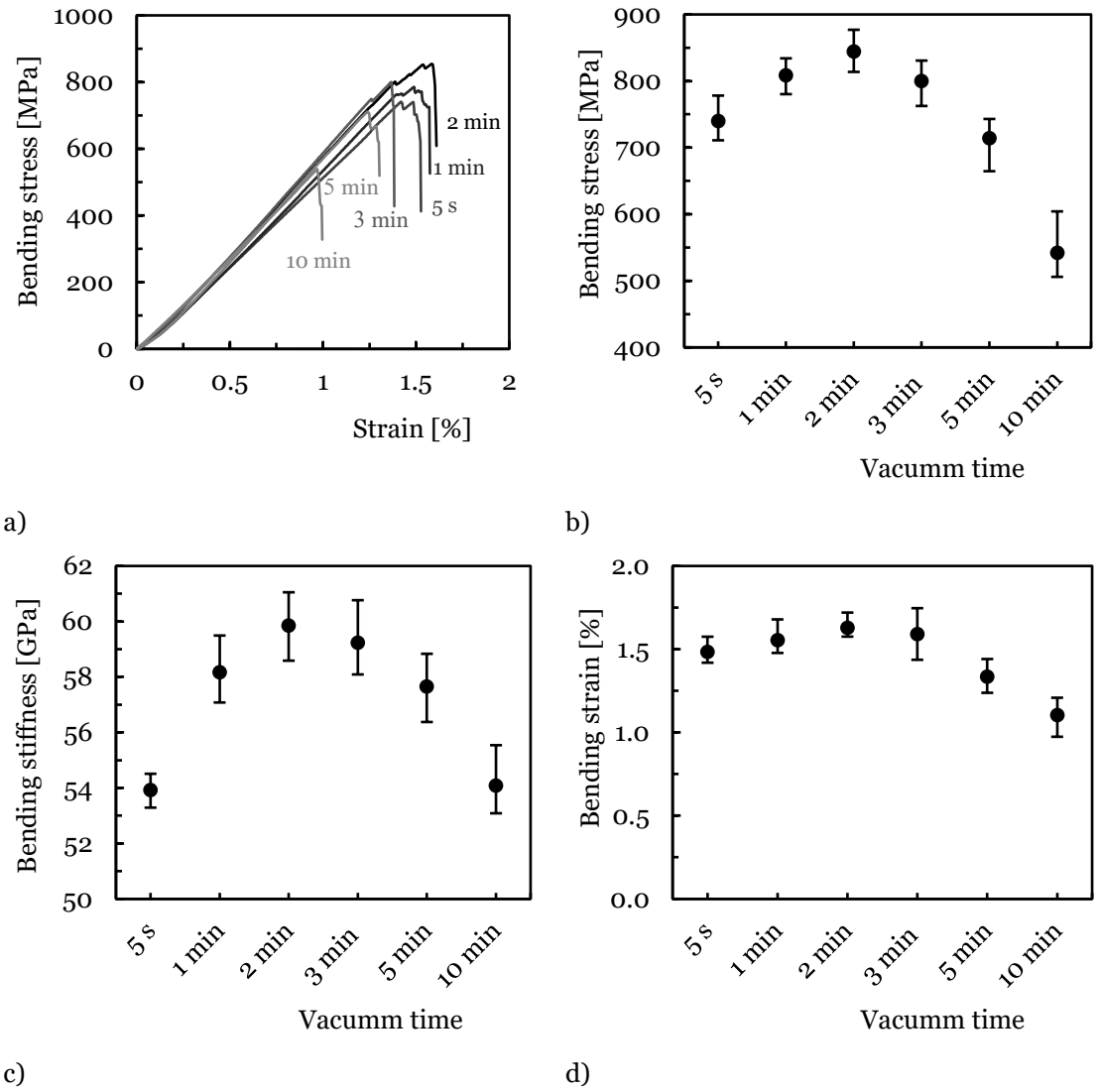

Figure 3.4: Effect of vacuum time on the: a) Bending stress-strain curves; b) Bending stress vs vacuum time; c) Bending modulus vs vacuum time; d) Bending strain vs vacuum time.

Finally, the effect of rotation speed and mixing time was analysed to obtain the best dispersion of CNFs in the resin and, consequently, in the composite laminates. For this purpose, nine different manufacturing processes were studied, which are summarized in Table 3.2, and the results obtained shown in Figure 3.6.

From Figure 3.6.a) it is possible to observe a typical profile to those obtained in Figure 3.4.a), where all curves present a nearly fragile behaviour with a linear region up to the maximum load, followed by a significant drop after this value. Only three curves are illustrated, but they are representative of all the others. As reported previously, fibres breakage in compression side is also the main damage mechanism observed.

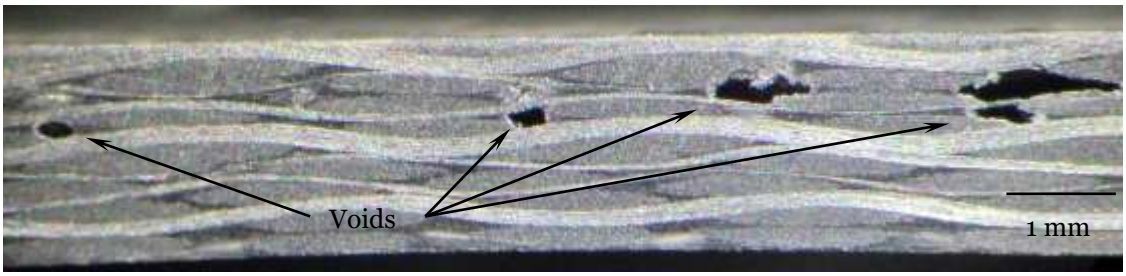

a)

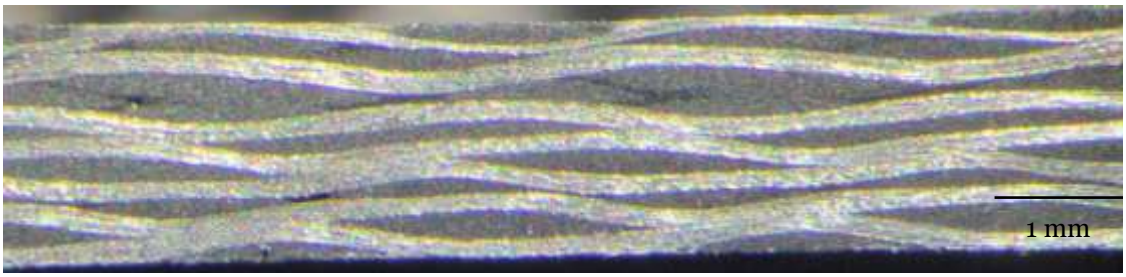

b)

Figure 3.5: a) Laminates with defects: air bubbles 1 min; b) Laminates without defects 2 min.

In terms of bending stresses, it is noticed that composite laminates produced according to process 5, reported in Table 3.2, show improvements about 11.3% higher than the value obtained for the control samples (resin and hardener mixed manually, followed by vacuum for 10 minutes, the bag remained connected to a vacuum pump for 2 min and a load of 2.5 kN was applied). This is clear evidence of the benefits obtained with CNFs, which were described in detail earlier when only the resin was analysed. In this context, CNFs have a large surface area per unit of volume, good physical and mechanical properties and promote synergy with the matrix [6–8]. However, the bending strength can be further improved by degassing the system (resin and fibres) after mixing with CNFs (beyond 2 min in the vacuum bag). In this case, for process 9, the bending stress is around 16.5% higher when compared to the control laminates (808.5 MPa). This benefit is related to the effect of the vacuum on the mechanical properties, as previously discussed [2,3]. It is worth mentioning that another vacuum step performed after mixing the resin with CNFs, in addition to the vacuum in curing, increased the bending strength by about 4.7%.

In terms of bending modulus, the same tendency was observed. In this case, the benefits obtained with CNFs, compared to the composites with neat resin, were around 15.6% higher, and the extra step of vacuum promoted improvements of 16.6%. In this example, comparing only the extra step of vacuum, it promoted an improvement around 6.4%. On the other hand, from Figure 3.6.d), it is possible to observe that the bending strain is not as affected as the bending stress and bending modulus, because the values are much more uniform. However, the processes that promoted higher bending stress and bending modulus were those that, as expected, presented lower values of bending strain. For example, compared to the control samples (1.57%), the bending strain decreased between 1.3% and 1.9%.

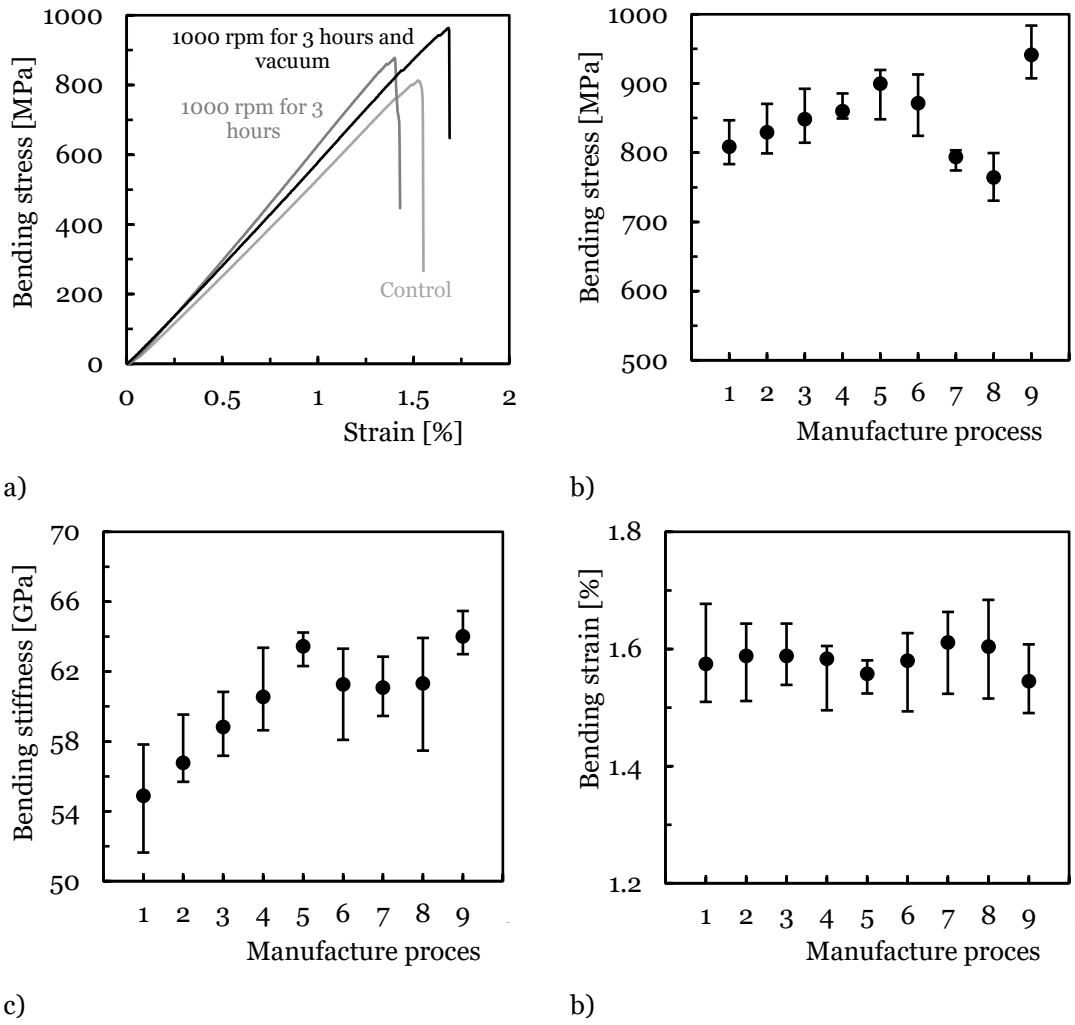

Figure 3.6: Effect of the manufacture parameters on: a) Typical bending stress-strain curves; b) Bending stress; c) Bending modulus; d) Bending strain.

3.4. Conclusions

CNFs were used to improve the mechanical properties of a commercial epoxy resin and a laminate composed by eight layers of bi-directional carbon woven prepared by hand lay-up process.

It was possible to conclude that the rotation speed of the mixer, dispersion time of the CNFs and vacuum time applied, both in the resin after its preparation and in the laminate after its manufacture, influence the mechanical properties of these materials.

In terms of resin, the best mechanical properties were obtained when 0.5 wt.% of CNFs were mixed at 1000 rpm for 3 hours, simultaneously using an ultrasound bath, followed by degassing for 10 minutes in a vacuum chamber. For example, the resin enhanced by CNFs reached values around 12.6% higher than the bending stress obtained for neat resin produced without vacuum. Finally, in relation to laminated composites, it was found that the manufacturing process that promoted the best mechanical properties involved two vacuum stages. In this case, resin and CNFs were mixed at 1000 rpm for 3 hours followed by 2 min in a vacuum chamber. The system

composed of fibres and nano-enhanced resin was, subsequently, placed in a vacuum bag and a 2.5 kN load was applied for 24 hours. Finally, the bag remained attached to a vacuum pump for another 2 minutes. The benefits obtained with CNFs, compared to the composites with neat resin, were around 15.6% higher, and the extra step of vacuum promoted improvements of 16.6%.

Bibliography

[1] Middleton B. Composites: Manufacture and Application. Design and Manufacture of Plastic Components for Multifunctionality, Elsevier; 2016, p. 53–101. https://doi.org/10.1016/B978-0-323-34061-8.00003-X.

[2] Sussmann M, Amirkhosravi M, Pishvar M, Altan M. Fabrication of High Quality, Large Wet Lay-Up/Vacuum Bag Laminates by Sliding a Magnetic Tool. Polymers 2018;10:992. https://doi.org/10.3390/polym10090992.

[3] Abdurohman K, Satrio T, Muzayadah NL, Teten. A comparison process between hand lay-up, vacuum infusion and vacuum bagging method toward e-glass EW 185/lycal composites. Journal of Physics: Conference Series 2018;1130:012018. https://doi.org/10.1088/1742-6596/1130/1/012018.

[4] Ferreira JAM, Reis PNB, Costa JDM, Capela C. Assessment of the mechanical properties of nanoclays enhanced low Tg epoxy resins. Fibers and Polymers 2014;15:1677–84. https://doi.org/10.1007/s12221-014-1677-7.

[5] Pina dos Santos PS, Maceiras A, Valvez S, Reis PNB. Mechanical characterization of different epoxy resins enhanced with carbon nanofibers. Frattura Ed Integrità Strutturale 2020;15:198–212. https://doi.org/10.3221/IGF-ESIS.55.15.

[6] H. Woldemariam M, Belingardi G, G. Koricho E, T. Reda D. Effects of nanomaterials and particles on mechanical properties and fracture toughness of composite materials: a short review. AIMS Materials Science 2019;6:1191–212. https://doi.org/10.3934/matersci.2019.6.1191.

[7] Reis PNB, Ferreira JAM, Zhang ZY, Benameur T, Richardson MOW. Impact response of Kevlar composites with nanoclay enhanced epoxy matrix. Composites Part B: Engineering 2013;46:7–14. https://doi.org/10.1016/j.compositesb.2012.10.028.

[8] Zare Y. The roles of nanoparticles accumulation and interphase properties in properties of polymer particulate nanocomposites by a multi-step methodology. Composites Part A: Applied Science and Manufacturing 2016;91:127–32. https://doi.org/10.1016/j.compositesa.2016.10.003.

[9] Oberdisse J. Aggregation of colloidal nanoparticles in polymer matrices. Soft Matter 2006;2:29–36. https://doi.org/10.1039/B511959F.

[10] Padmanabhan V, Frischknecht AL, Mackay ME. Effect of Chain Stiffness on Nanoparticle Segregation in Polymer/Nanoparticle Blends Near a Substrate. Macromolecular Theory and Simulations 2012;21:98–105. https://doi.org/10.1002/mats.201100048.

[11] Ma X, Zare Y, Rhee KY. A Two-Step Methodology to Study the Influence of Aggregation/Agglomeration of Nanoparticles on Young's Modulus of Polymer Nanocomposites. Nanoscale Research Letters 2017;12:621. https://doi.org/10.1186/s11671-017-2386-0.

[12] Shaffer MSP, Fan X, Windle AH. Dispersion and packing of carbon nanotubes. Carbon 1998;36:1603–12. https://doi.org/10.1016/S0008-6223(98)00130-4.

[13] Reis PNB, Ferreira JAM, Antunes FV, Costa JDM. Flexural behaviour of hybrid laminated composites. Composites Part A: Applied Science and Manufacturing 2007;38:1612–20. https://doi.org/10.1016/j.compositesa.2006.11.010.

[14] Giancaspro JW, Papakonstantinou CG, Balaguru PN. Flexural Response of Inorganic

Hybrid Composites With E-Glass and Carbon Fibers. Journal of Engineering Materials and Technology 2010;132:0210051–8. https://doi.org/10.1115/1.4000670.

Chapter 4

Effect of carbon nanofibres on the improvement of mechanical properties of epoxy resins[3]

Abstract

Epoxy with carbon nanofibres (CNFs) are effective nano-enhanced materials that can be prepared by easy and low-cost method. The present paper compares the improvements, in terms of bending and viscoelastic properties, of two epoxy resins reinforced with different weight percentages (wt.%) of CNFs. These epoxy resins have different viscosities, and weight contents between 0% and 1% of CNFs were used to achieve the maximum mechanical properties. Subsequently, for the best configurations obtained, the sensitivity to the strain rate and the viscoelastic behaviour (stress relaxation and creep) were analysed based on international standards. It was possible to conclude that, for both resins, carbon CNFs promote significant improvements in all the studied mechanical properties, even for different contents by weight.

4.1. Introduction

Epoxy resins are a class of thermosetting polymers frequently used as matrices in polymeric composites due to their interesting characteristics, such as dimensional stability, chemical resistance, good stiffness, high specific strength and good adhesion to various types of reinforcements [1,2]. Epoxy resin is a thermostable polymer consisted of two principal parts: resin and hardener. Diglycidyl ethers of bisphenol-F and/or bisphenol-A are the main elements of the most normal epoxy resins. Hardeners are curing agents that react with a resin and become part of the solid final epoxy through cross-linking chemical reaction when these two chemicals are mixed together [3]. These curing compounds can have different types of molecules such as amines, amideamines, anhydrides, carboxylic acids, polyamides or imidazoles. These molecules have in common that they are able to initiate the polymerization process when their reactive hydrogen or hydroxyl group that react with the oxirane (epoxy) rings.

Amines are one of the most frequent and important curing agents. The range of alternatives is huge since they are present in different chemical configurations. Amines can have two free

[3] Based on the work published in the Fracture and Structural Integrity, Pina dos Santos, P. S., Maceiras, A., Valvez, S., & Reis, P. Mechanical characterization of different epoxy resins enhanced with carbon nanofibers. *Fracture and Structural Integrity*, **2020**, *15*(55), 198–212. https://doi.org/10.3221/IGF-ESIS.55.15

hydrogens (primary amine), one free hydrogen (secondary) or no hydrogens (tertiary), and they may have a cyclic benzene structure (aromatic) or straight chains (aliphatic). In general, for low-temperature curing systems like adhesive or coatings, aliphatic primary and secondary are the most used, whereas, for fibre-reinforced composites, aromatic amines are chosen. Primary amines react speedily at room temperature (RT) with epoxies, through epoxy ring-opening, and the thermosetting results in highly cross-linked networks with short curing life and high curing rates. Aromatic curing agents react more slowly but impart higher general stability than their aliphatic amine counterparts. In his case, the resulting system needs longer curing time and higher temperature to reach optimum properties, but their chemical resistance, electrical, mechanical and heat resistance is better. Therefore, different types of amines that can be used present advantages and disadvantages, commercial hardeners contain a mixture of different types to broader its applicability [4]. Apart from the resin and the hardener, commercial epoxies present diluents as other important components. Diluents are low-viscosity and low-molecular-weight molecules applied to reduce the viscosity and enhance the resin-hardener solubility. Normally, these compounds do not leach or outgas during thermal-vacuum exposure because amid curing reactions are being combined and linked chemically with the resin [5].

Despite having many desirable properties, neat epoxies typically have low mechanical toughness. In the last few decades, a wide range of nano filers has been added to commercial epoxy resin to increase the mechanical properties, such as clays [6], alumina [7], graphene nanoplatelets (GNPs) [8], carbon nanotubes (CNTs) and CNFs [9,10]. Enhancement in mechanical properties of CNFs based epoxy composites have been well illustrated in the literature by the achievement of good dispersion of additives within the matrix and maximized interfacial adhesion is required to ensure uniform stress distribution, [11–13]. CNFs are carbon-based materials that present good compatibility with many polymer matrixes, and they can be disseminated following anisotropic and isotropic distributions. Their chemical structure, good qualities, and versatility are responsible for the outstanding thermal and electrical conductivity, a mechanical performance that can be introduced in a huge variety of matrices of different origins such as metals, ceramics and polymers.

If literature presents benefits when the resin is filled by CNFs, it also evidences that the same are sensitive to the strain rate. There exist some previous works in nano-enhanced resins with CNFs about the strain rate effect on mechanical properties. Zhou et al. [14], for example, observed that in uniaxial tensile tests, neat and CNFs modified epoxy are strain rate dependent materials and the elastic modulus and tensile strength of the materials both increased with higher strain rates between 0.00033 and 0.033 s^{-1}. Proveda et al. [15] observed for a CNFs/epoxy resin, under compression for 5×10^{-3} - 2800 s^{-1} strain rates, that the strength and modulus increased by a maximum of 180.7 and 241.7%, respectively. Nevertheless, for longterm applications, composites based on polymers have the limitation of suffering stress relaxation and creep. According to the open literature, for example, in polymers there are mainly two mechanisms involved in stress relaxation: a) molecular rearrangements that demand little primary breakage or bond

arrangement (physical stress); and b) crosslink formation, scission, or chain scission (chemical stress). On the other hand, creep is the combined result of the viscous flow and elastic deformation and happens because of the molecular rearrangements in the backbone and depends on the stress degree. Therefore, the main goal of this work is to compare sensitive to the strain rate, stress relaxation and creep behaviour of two commercial epoxy resins and understand the influence of CNFs as nano-reinforcements. For this purpose, several percentages by weight of CNFs were mixed in two different resins by the technique of mechanical agitation and simultaneously the application of ultrasound. Both resins are widely used in the automotive and aeronautical sector. The bending mode was selected for this study because is the type of analysis with greater sensitivity and one of the most employed in the field.

4.2. Materials and experimental procedure

Two types of epoxy resin were used to produce nanocomposites enhanced by CNFs. For this purpose, an epoxy resin SR 8100 and a hardener SD 8822, both supplied by Sicomin, and an epoxy resin AH 150 and a hardener IP 430, both supplied by Ebalta, were selected due to their different viscosities, as reported in Table 4.1.

Epoxy-based materials are very interesting from an engineering point of view because of their properties and characteristics are directly controlled by their molecular structures. Epoxy resins thanks to their two main components implementation are available in a range of molecular structures, suitable for reaction with a large variety of different curing agents, for a multitude of end uses. Therefore, in order to control and understand the mechanical behaviour of these materials is a key factor to know their composition (chemical structures), and relative quantities of their components. In this work, both epoxy materials were purchased from a private company and part of the data is protected by intellectual property. Unfortunately, not all the components and quantities are disclosed in their technical datasheet to the general public. For the Sicomin SR 8100/SD 8824 the information was more detailed than for the Ebalta AH 150/IP 430, as the resin relative composition and the hardener chemical components were not indicated for the latter one. In this sense, Table 4.2 summarizes all the known relevant information about the chemical compositions of the two resin formulas obtained from the datasheet, and Figure 4.1 shows their chemical structures.

Regarding the CNFs, their technical specifications are summarized in Table 4.3 and Figure 4.2 shows the SEM images of the CNFs used in this study. In terms of dimensions, as shown, the average diameter is about 130 nm, the length ranges from 20 to 200 μm and the average specific surface area around 54 m^2/g.

In terms of manufacture process, and after weighing, CNFs were added to the epoxy resin and several contents by weight were studied: 0.25, 0.5, 0.75 and 1%. The dispersion into the resin was conducted using, simultaneously, a high-speed shear mixer at a shear rate of 1000 rpm and sonication (using an ultrasonic bath with a frequency of 40 kHz) for 3 hours at RT.

Table 4.1: Main mechanical and physical properties of the epoxy resins.

Property		Sicomin SR 8100 / SD 8824	Ebalta AH 150/ IP 430
Colour		Light yellow liquid	Opaque
Viscosity (@ 25 °C)	[mPa×s]	285 ± 60	250 ± 50
Density at 20 °C	[g/cm^3]	-	1.13 ± 0.02
Modulus of elasticity	[N/mm^2]	2970	3400 ± 300
Maximum resistance	[N/mm^2]	108	125 ± 1.2
Elongation at max. load	[%]	4.9	-
Elongation at break	[%]	11.8	5.9 ± 0.1
Charpy impact strength	[kJ/m^2]	52	60 ± 6
Glass transition/DCC	[°C]	63	-
Water absorption 48 hours/70 °C	[%]	1.2	-

Table 4.2: Chemical composition of the epoxy resins, diluent and hardeners used in this study based on the data known from their technical datasheets.

Type of component	Identification number	Sicomin SR 8100 / SD 8824	Ebalta AH 150/ IP 430
Resin	CAS: 1675-54-3	bisphenol A epoxy resin (DGEBA)	
	EC: 216-823-5	Composition: 10 <= x % < 25	Composition: % not specified MW≤700
	CAS: 9003-36-5	bisphenol F epoxy resin (DGEBF)	
	EC: 500-006-8	Composition: 50 <= x % < 100	Composition: % not specified MW≤700
Diluent	CAS: 16096-31-4	1,6-bis(2,3-epoxypropoxy)hexane	
	EC:240-260-4	Composition: 10 <= x % < 25	Composition: % not specified
Hardener: amines	CAS: 15520-10-2 EC: 239-556-6	2-methylpentane-1,5-diamine Composition: 25 <= x % < 50	Composition: Molecules and % not specified
	CAS: 1477-55-0 EC: 216-032-5	m-phenylenebis(methylamine) Composition: 25 <= x % < 50	
	CAS: 39423-51-3 EC: 500-105-6	trimethylolpropane tris[poly(propylene glycol), amine terminated] ether Composition: 2.5 <= x % < 10	

This procedure took another 10 minutes, with a rotation speed of just 150 rpm, to mix the hardener into the system. The low rotation speed aimed to minimize the formation of air bubbles and to promote only a homogeneous mixture of the hardener into the system. The rotation speed and time of mixture were optimized in previous studies. The mixture was again degassed in a vacuum oven to remove remaining air bubbles and then poured into a cardboard mould with dimensions of 100 × 130 × 3 mm^3. Finally, all nanocomposites produced with Sicomin resin were cured at RT for 24 hours and subjected to a post-cure at 40 °C for 24 hours, while those that were produced with Ebalta resin were cured at RT for 48 hours and subjected to a post-cure at 80 °C for 5 hours.

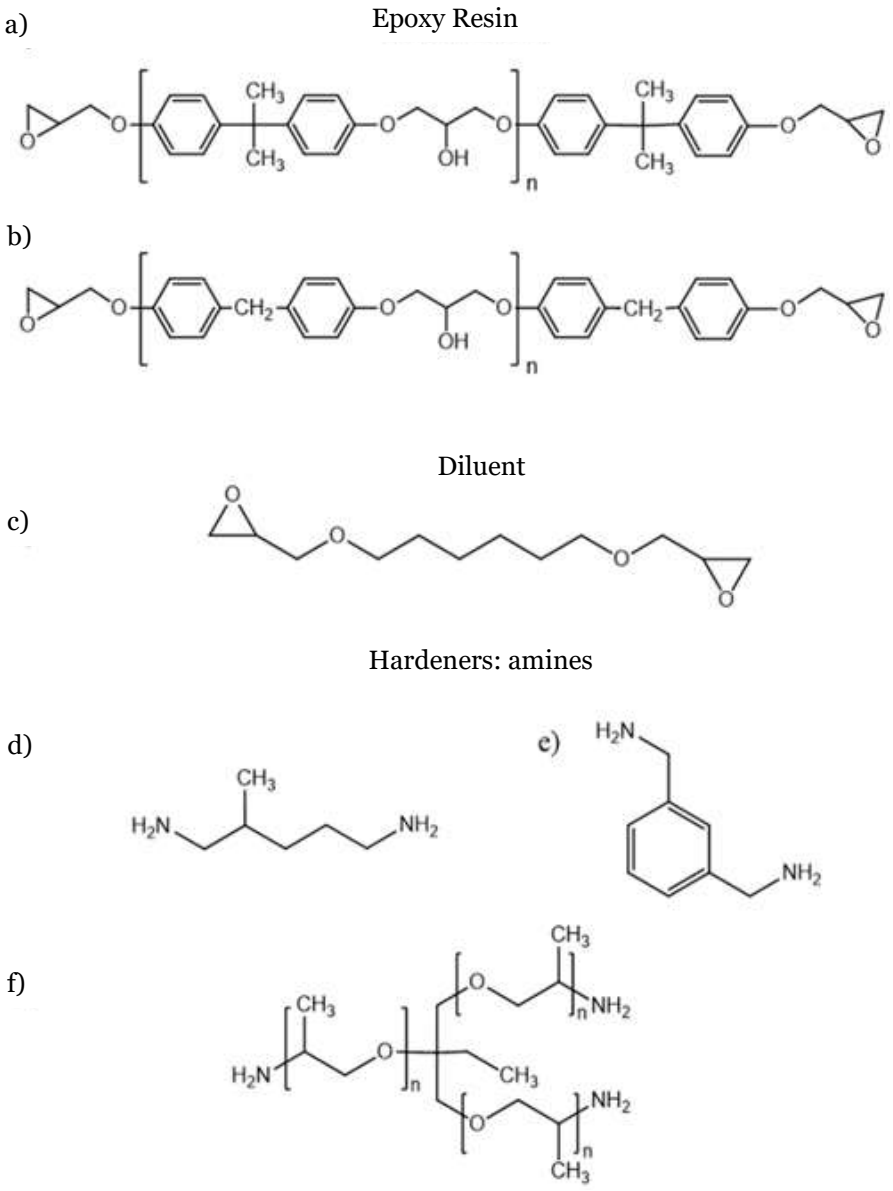

Figure 4.1: Chemical structures of: a) Bisphenol A epoxy resin (DGEBA); b) Bisphenol F epoxy resin (DGEBF); c) 1,6-bis(2,3-epoxypropoxy)hexane; d) 2-methylpentane-1,5-diamine; e) m-phenylenebis(methylamine); f) trimethylolpropane tris[poly(propylene glycol), amine terminated] ether.

For the tests to be performed, the samples were obtained from the original plates to specimens with the dimensions and geometry shown in Figure 4.3. Following the recommendations of the European Standard EN ISO 178:2003, three-point bending (3PB) static tests were carried out at RT and using a span length of 50 mm. An Autograph AGS-X universal testing machine, from Shimadzu, with a 10 kN load cell and a displacement rate of 2 mm/min was used to test six different samples for each configuration.

Table 4.3: Technical specifications of the CNFs used in this study.

Property	Value
Assay	> 98% carbon basis
Form	Platelets (conical) powder
Diameter × length	100 nm × 20 - 200 μm
Average diameter	130 nm
Impurities	< 14,000 ppm iron content
Pore size	0.12 cm^3/g average pore volume 89.3 Å average pore diameter
Surface area	Average specific surface area 54 m^2/g
Mp	3652 - 3697 °C
Density	1.9 g/mL at 25 °C
Bull density	0.5 - 3.5 lb/cu.ft

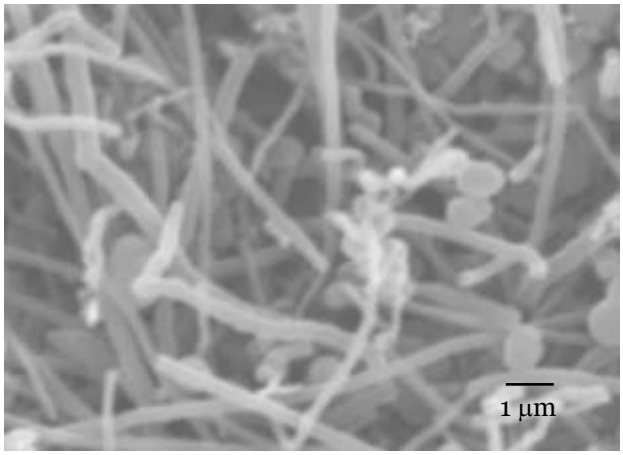

Figure 4.2: SEM images of the CNFs used in this study.

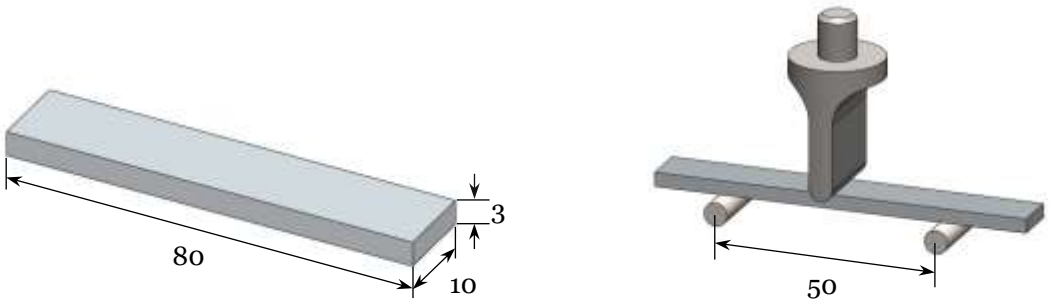

a) b)

Figure 4.3: a) Geometry of the specimens; b) Three-point bending apparatus. All dimensions in mm.

The bending strength was obtained from the nominal stress at the central span section by:

$$\sigma = \frac{3\,P\,L}{2\,b\,h^2} \tag{4.1}$$

where P is the load, L the span length, b the width and h the thickness of the specimen. The stiffness modulus was determined from the linear elastic bending beams theory relationship:

$$E = \frac{\Delta P\, L^3}{48\, \Delta u\, I} \tag{4.2}$$

where I, ΔP and Δu are, respectively, the moment of inertia of the cross-section, the load range and bending displacement range in the middle span for an interval in the linear region of the load versus displacement plot. Finally, the bending strain was calculated according to the European Standard EN ISO 178:2003 by the following equation:

$$\varepsilon_f = \frac{6\, S\, h}{L^2} \tag{4.3}$$

where S is the deflexion, L the span length and h the thickness of the specimen. Displacement rates of 200, 20, 2, 0.2 and 0.02 mm/min were employed, which corresponds to strain rates ($\dot{\varepsilon}$) of 9.7×10^{0}, 9.7×10^{-1}, 9.7×10^{-2}, 9.7×10^{-3}, 1.3×10^{-4} s^{-1} according to equation (4.4):

$$\dot{\varepsilon} = \frac{d\varepsilon_f}{dt} = \frac{6\, V_T\, b}{L^2} \tag{4.4}$$

In this equation $\dot{\varepsilon}$ is the peripheral fibre strain, t is the time, V_T is the crosshead speed, L the span length and h the thickness of the specimen. For each condition, six specimens were tested.

Finally, the same machine was used to carried out stress relaxation and creep tests, at RT and with similar samples to those shown in Figure 4.3. For the first tests a fixed displacement was applied, and the stress recorded during the loading time, while for creep tests a fixed stress was applied and the displacement registered during the loading period. For both resins, a bending stress of 50 MPa was considered in order to ensure that all tests were carried out on the elastic region of the bending stress-strain curve.

4.3. Results and discussion

Static bending tests were performed according to the experimental procedure described in the previous section and with a strain rate ($\dot{\varepsilon}$) of 9.7×10^{-2} s^{-1} (corresponding to a displacement rate of 2 mm/min), in order to find the best amount of nano reinforcement to maximize the bending properties. In this context, Figure 4.4 presents typical bending stress-strain curves obtained for different conditions, but they are representative of all curves obtained in this analysis.

In all curves, a linear increase in the bending stress with the strain (linear elastic region) is observed, followed by a nonlinear performance where the maximum bending stress is reached. After the peak load, the bending stress drop significantly, evidencing the imminent collapse of the nanocomposites. Figure 4.5 summarizes the main bending properties, obtained from these curves, in terms of average values (symbols) and respective maximum and minimum values

(dispersion bands). For both resins, it is noticed that the increase in CNFs promotes higher values of bending strength, but after a certain content of nanoparticles these values decrease due to the aggregates/agglomerates that have occurred due to intermolecular interactions (van der Waals forces and chemical bonds). While the maximum bending stress occurs with 0.75 wt.% of CNFs for the Sicomin resin, this property reached its maximum for 0.5% of CNFs when the Ebalta resin is considered. In comparison with the control samples (neat resin), an increase around 11.7% was observed for both resins.

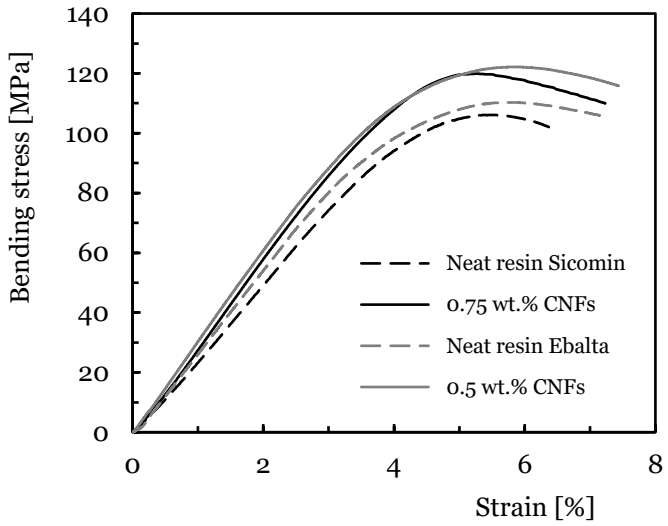

Figure 4.4: Representative bending stress-strain curves obtained for 9.7×10^{-2} s^{-1}. Comparison between neat and the best nano-enhanced resin.

In fact, according to the open literature, agglomerations/aggregations are expected for higher filler contents, which, in addition to being treated as defects, are responsible for significant concentrations of stresses in nanocomposites [16–18]. They also reduce the interfacial area between the polymeric matrix and nanoparticles, which reduces the mechanical involvement of polymeric chains in the nanoparticles [19]. On the other hand, only a few polymer molecules can penetrate between the nanoparticles, which promotes an exceptional increase in viscosity, even for relatively low filler contents [20]. However, due to the higher viscosity of the Sicomin resin (compared to Ebalta), it was expected to obtain the highest bending strength with lower content of CNFs. Regardless of Fiedler et al. [21] report that the low viscosity of a resin allows a better organization of the nanoparticles, they also consider that the manufacturing process as well as the properties of the particles and matrix are determinants in the interfacial strength of the composite and dispersibility of the fillers during the production.

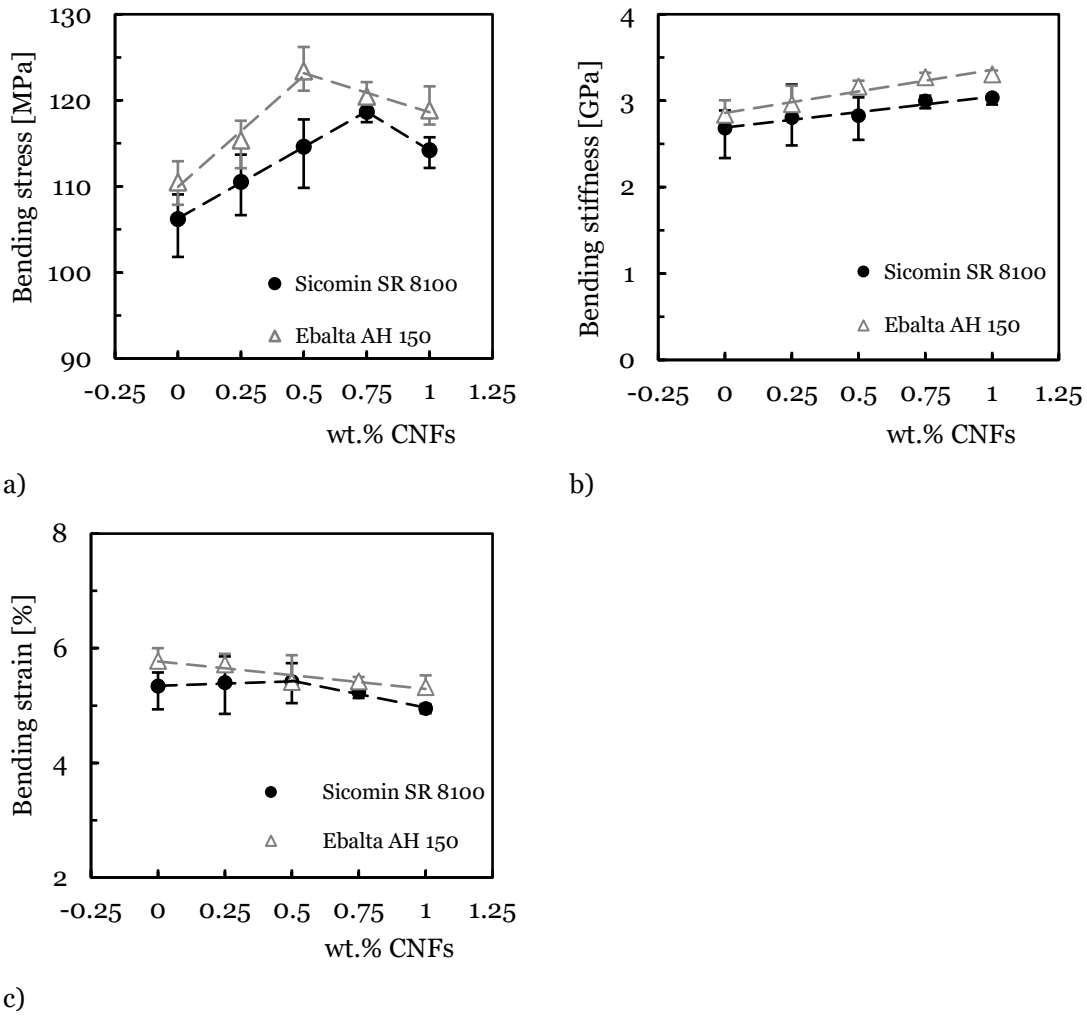

Figure 4.5: Nano-enhanced resin Sicomin SR 8100 and Ebalta AH 150 with different percentages of CNFs: a) Bending stress; b) Bending stiffness; c) Bending strain.

Although CNFs are considered ideal materials for reinforcing polymers due to their excellent mechanical properties, a good interaction between reinforcement CNFs and polymer matrix is necessary to obtain composites with optimal properties. For that reason, the knowledge of the chemical composition of resins and hardeners is essential to understand the physicochemical interactions between the matrix and the fillers, in order to overcome possible incompatibilities and to optimize the composite mechanical behaviour [22]. However, from the chemical point of view, both resins are based on the same components, bisphenol A (DGEBA) and bisphenol F epoxy resin (DGEBF), respectively. The most relevant and employed epoxy resin is the DGEBA, which results from the chemical reaction of bisphenol A with epichlorohydrin. Manufactured DGEBA resin usually presents a distribution of molecular weight and a certain preference to have a crystalline solid material when is stored at RT. But DGEBF is usually less viscous and once cured has greater toughness and flexibility. Nonetheless, although the use of both resins is indicated in their technical datasheets, there exists a lack of information about the exact proportion of both components and their molecular weight in the final commercial products (Sicomin SR 8100 and Ebalta AH 150). These differences in the epoxy resin compositions (DGEBF/DEBA), molecular

weights and the quantity of diluent [1,6-bis(2,3-epoxypropoxy)hexane] probably explain the different viscosity referenced for Sicomin Sr 8100 (285 ± 60 mPa×s) and Ebalta AH 150 (250 ± 50 mPa×s) resins at 25 ºC in their datasheets. With respect to hardeners, the situation is more difficult because there was no information about the composition in the Ebalta technical datasheet. As it was explained before, hardeners based on amines as curing agents become part of the chemical structure of the solid epoxy through cross-linking after reacting with a resin. Therefore, the influence in the general properties of the materials is at least as much important as the resins. For instance, to obtain the best properties it is necessary an optimum curing reaction, which implies that the amount of curing reagent employed must be stoichiometric. The number of epoxy groups and reactive hydrogens of the hardener must be equal, which is the amine molecular weight divided by the number of hydrogens (amine-equivalent weight, AEW) [23].

The curing process and the chemical phenomena of cross-linking are responsible for many of the properties of the solidstate in epoxy derived materials. The cross-link density is the spacing between successive cross-link sites, and normally, when the cross-link density increases, the glass transition temperature, thermal stability, and chemical resistance increase, but the fracture toughness and the strain to failure decreases [24]. Therefore, during the curing reaction was observed a difference of colour with a naked eye between the two resin materials, light yellow liquid (Sicomin SR 8100/SD 8824) and opaque (Ebalta AH 150/IP 430). This difference of colour can be explained because of the different hardeners formulations since both resin products are based on the same two polymers (DGEBA and DGEBF). The introduction of new molecular chains of different lengths, with pendant groups, aliphatic or aromatic elements, vary many physicochemical and solid-state properties of the composites. For example, heterocyclic and aromatic curing reagents are responsible for higher temperature stabilities than their aliphatic amine alternatives [25]. An increment in the flexible amine content decreases the tensile and flexible strength related to a reduced crosslinking density [26]. In summary, the higher modulus of elasticity and maximum resistance of the Ebalta AH 150/IP 430 over the Sicomin SR 8100/SD 8824, referenced in these neat cured resins, could be explained from the different chemical relative composition (DGEBA/DGEBF) of both resins, and for their different hardeners employed.

In the case of epoxy resins reinforced with CNFs the introduction of CNFs was aimed to enhance the mechanical properties of the two epoxy materials. Properties of composites are ruled not only by the carbon fibre, the resin matrix, but also are influenced by the interface formed between the two constituents. Favourable interfacial adhesion can efficiently transfer stress from matrix to fillers, which plays a key role in the mechanical properties as well as the reliability [27]. Although carbon nanofibres are increasingly used in various industries, these materials present some drawbacks. The smooth pristine surface of carbon fibre is non-polar and affects the interfacial adhesion between carbon fibres and resin matrix, which has a negative effect on the overall performance. The composite interfacial shear strength reflects the load transfer efficiency between the nanofibres and the resin, and has a relevant function in the mechanical properties.

The general idea is to reach an efficient load transfer between both constituents to strengthen the nanofibre-matrix interface to overcome the lack of good interfacial bonding limited by the non-polar and smooth surface of CNFs. The fillers-resin adhesion may require strengthened by treating the fillers with a coupling agent or functionalization that bridges their molecules together. Then, the creation of covalent bonds or van der Waals forces of attraction would enhance the adhesion between the two materials (fillers/matrix) [28,29].

Advances in interfacial improvement have been made, but the mechanisms of interfacial adhesion are difficult to be fully understood. The most common explanations for enhancement mechanisms by fillers are: a) stiffer matrix/fibres interfaces with a higher shear modulus are formed, which promotes the stress transfer; b) the presence of fibres in the interface assists in holding back excessive stress spreading in the flaw and provides a crack deflection mechanism; c) chemical interaction among CNFs, sizing and resin matrix can be improved when the nanoparticles are modified with a surface modifier. In this context, a uniform dispersion and good wetting of the nanofibres within the matrix are necessary to ensure maximum utilization of the nanofibres' characteristics, because a good CNFs dispersion can be critical to obtaining a homogeneous dispersion. High shear mixing, ultrasonication, the employment of surfactants, or the dilution method are some of the alternatives [30,31]. According to the results, 0.75 wt.% of CNFs is the content that promotes the maximum bending stress for the Sicomin resin, while for Ebalta resin is 0.5 wt.% of CNFs. Since the mixture and dispersion procedure was exactly the same, in both commercial pre-cured resins, the difference in the filler percentage values can be attributed to variation in the matrix-fibre interfaces that modify the stress transfer and spreading in the flaws and crack deflection. Normally, the variation in the interfaces can be explained by different factors, such as a) diverse aggregation formation, b) different chemical composition of the polymer matrixes and hardeners, and c) the effect of fillers on the kinetics of epoxy cure.

As was explained previously, in this work both commercial matrixes have very similar compositions, the same two epoxy materials and diluent. The exact composition is not known because are protected by copyrights, but to the best of our knowledge are analogous due to the information disclosed in datasheets. Probably, the variation in their relative compositions is responsible for the different viscosity previous curing. In theory, in less viscous fluids (Ebalta) a uniform dispersion of the nanofibres within the matrix would be easier to perform, limiting the tendency to form CNFs agglomerates, which are responsible for an excessive stress concentration and origin of flaws. Nonetheless, from our results, the difference in viscosities does not seem a relevant parameter, because the maximum percentage in Ebalta (0.5%) is lower than in Sicomin (0.75%). Therefore, the difference in filler acceptance from the matrix should be attributed to greater physicochemical compatibility of the Sicomin and not the viscosity. What is different is the hardener chemical formula composed of different types of amine molecules. The difference in composition affects clearly many parameters in pristine epoxies and it is more relevant when the parameter of fillers appears.

Surface polarity is one of the most important physicochemical attributes of both materials that affect the interface quality of the filler/matrix. However, due to their important polarity and attractive forces formed between the resin and the other material, epoxies adhere satisfactorily to multiple surfaces. Normally, strong polar attractions or direct bonds that can be formed between reactive sites in the resin and polar sites on the surface of the filler. Most inorganic materials (metals, minerals, glasses, ceramics) have some polarity so they have high surface energy, whereas organic polymer surfaces are generally less polar (more covalent) and lower surface energy [32,33].

In a very wide range of epoxy resins, polarity varies depending the molecules and curing conditions involved. The nonepoxy part of the chemical structures presents multiple possibilities, because it may have aromatic, cycloaliphatic and/or aliphatic molecules that vary its polarity and general properties. In the same way for the amines, i.e., cross-linking and chain extension reagents. The amino group shows some polar character because the N–H bonds are more electronegative than the C–H bonds [34]. On the other hand, pristine CNFs are basically non-polar materials, i.e., a molecule where the electrons between the two atoms are equally shared or where the polar bonds of the global structure are symmetrically disposed. Therefore, despite the great properties of these nanofibres, CNFs/epoxy composites can have unsatisfactory mechanical properties because CNFs have poor interfacial adhesion due to their non-polar surface. In short, the different hardeners (several amine molecules) could affect the overall polarity of the epoxy cured materials which as a relevant effect in the fillers/resin compatibility. In the optimum based nanocomposites (0.5%), the matrix/fibres interface interaction is worse than in Sicomin (0.75%), which has an impact on the CNFs percentage that can accept before having a detrimental Effect on the mechanical characteristics, such as bending stress.

Other possible explanation, apart from polarity mismatch, is the effects of CNFs fillers on the curing processes, since it is accepted that the physicochemical and thermo-mechanical characteristics of the cured epoxy resin depend on the curing reaction conditions (temperature and time), degree of cure (curing extent) and network of crosslinking. Since the overall characteristics arises in great part from the curing reactions, their curing kinetics should be studied by differential scanning calorimetry (DSC). For example, Tao et al. [35] reported that CNTs are able of modifying the curing process, initiating the curing reactions at inferior temperatures with respect to a neat epoxy resin. The presence of CNTs modified the curing kinetics, reduced the crosslinking density and the glass transition temperature [36]. Silanized CNFs exhibited lower peak temperature as well as higher heat of cure, and maximization in the cure reaction rates at the very initial stage of the reaction compared to those without the pristine CNFs. The curing and post-cure procedures for Sicomin and Ebalta resins in terms of temperature and time were obtained from their datasheets and were optimized from the manufacturers for neat epoxy formulas, i.e., without fillers, in this case, CNFs. That means the curing mechanism should be corroborated and maybe optimized for each filler content [37].

In this context, because the resin was the only different variable in this study, it is possible to conclude that Ebalta enables the formation of stronger covalent bonds and/or polar interactions between the resin and the CNFs. On the other hand, higher specific surface area already encourages the formation of agglomerates due to the intermolecular interactions. In terms of bending stiffness, and for Sicomin neat resin, the maximum valour is about 2.68 GPa, while for similar resin filled by 0.75 wt.% CNFs this value is about 2.99 GPa (11.76% higher). For Ebalta neat resin, these values are around 2.84 GPa and resin filled by 0.5 wt.% CNFs this value is about 3.16 GPa, respectively (11.3% higher).

The strain rate effects on the bending properties are shown in Figure 4.6. Typical bending stress versus bending strain curves, for all strain rates, are plotted in Figures 4.6.a) and 4.6.b), respectively, for Sicomin SR 8100 with 0.75 wt.% CNFs and Ebalta AH 150 with 0.5 wt.% CNFs. Both curves exhibit two different regimens, a quasi-linear zone, which is followed by a nonlinear region where the maximum bending stress occurs. However, it is noticed that for higher strain rates the linear region is longer for both systems and considerably affect bending properties. For example, independently of the resin, higher values of strain rate promote higher bending stress and stiffness, but the highest values are always obtained when CNFs are added to the resin. A linear model, as suggested by the literature [38–40], can be fitted to the data according with the following equations:

$$\sigma = c + d \times \dot{e} \tag{4.5}$$

$$E = c + d \times \dot{e} \tag{4.6}$$

where σ is the maximum bending stress, E is the bending modulus, $\dot{e}$ is the logarithm of strain rate and c and d constants presented in Table 4.4. From this table, it is possible to conclude that those linear relationships between the logarithm of strain rate ($\dot{\varepsilon}$) and the mechanical properties present good accuracy, and they can be used as models to predict the strain rate effect on the bending properties.

Apart from high stiffness and strength, the matrix should present viscoelastic and/or viscoplastic behaviour to eliminate brittle fracture of the composite. Good dispersion and adequate introduction of CNFs with the interfacial area and high aspect ratio into an epoxy matrix controls the long-term deformability and strength of the composite, and decrease the rate of creep strain [41]. The addition of a certain quantity of CNFs or CNTs could enhance the efficiency of interfacial stress transfer thanks to an improvement in the interlaminar shear strength. However, in case of poor quality of adhesion, the damage process of the bulk resin can be accelerated, especially under shear loading, because of the increase in the number of dissipation sites, i.e., CNFs/epoxy interfaces.

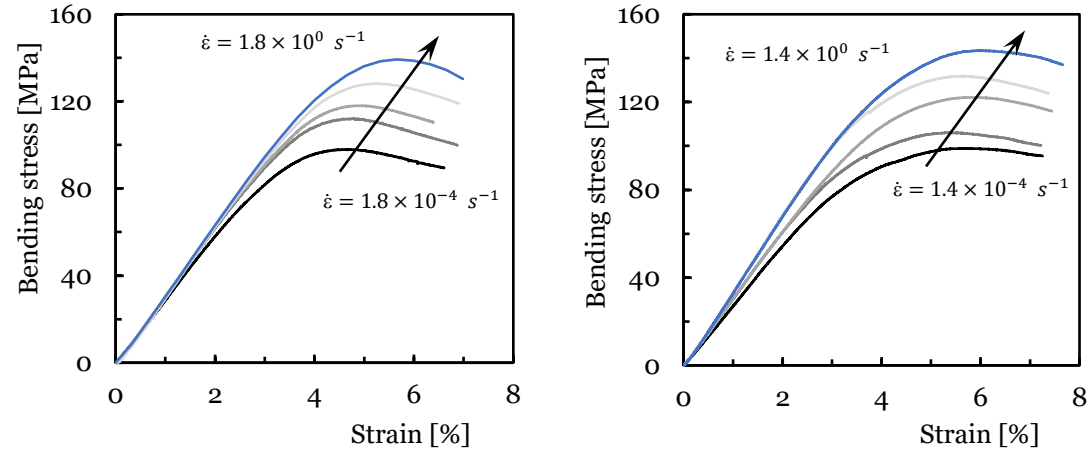

a)

b)

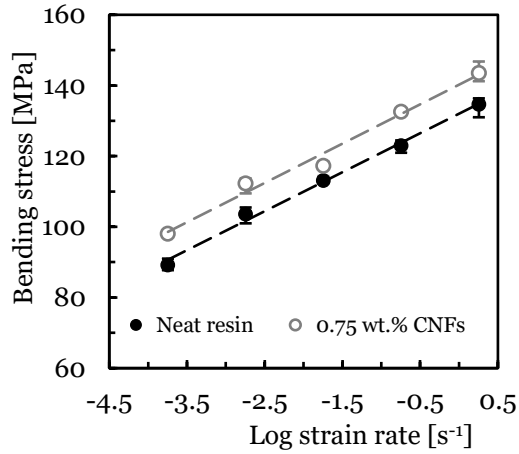

c)

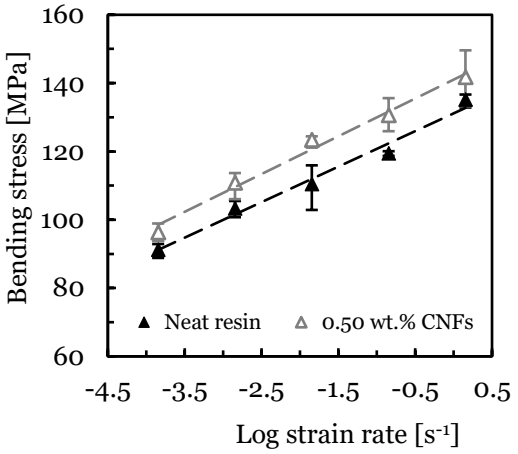

d)

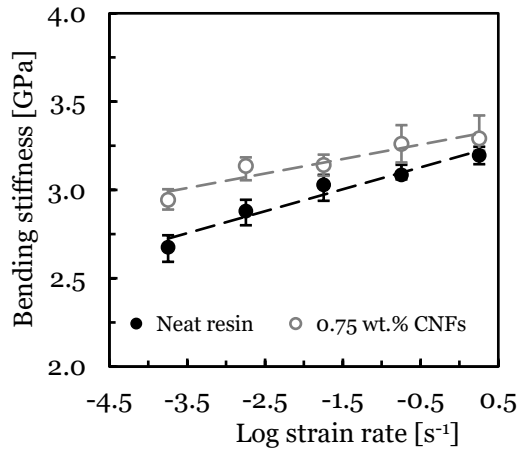

e)

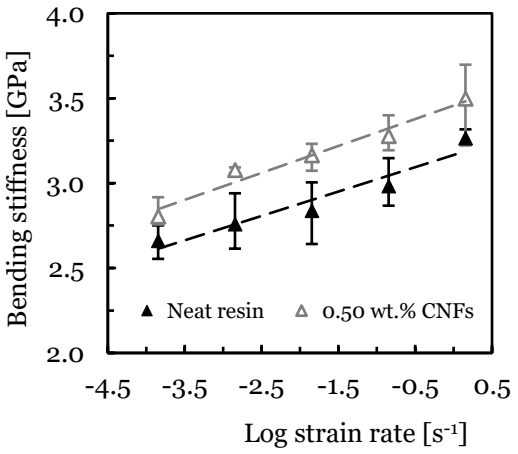

f)

Figure 4.6: Effect of the strain-rate: a) For resin Sicomin SR 8100 with 0.75 wt.% CNFs; b) For resin Ebalta AH 150 with 0.5 wt.% CNFs; c) Bending stress Sicomin; d) Bending stress Ebalta; e) Bending stiffness Sicomin; f) Bending stiffness Ebalta; g) Bending strain Sicomin; h) Bending strain Ebalta.

Table 4.4: Parameters of the equations that fits the effect of the strain-rate on the nanocomposites.

Material	Properties	Parameters		Stdev
		c	*d*	
Neat Sicomin resin	Bending stress (σ)	133.12	11.04	0.997
	Bending modulus (*E*)	3.20	0.124	0.977
Sicomin + 0.75 wt.% CNFs	Bending stress (σ)	141.34	11.12	0.992
	Bending modulus (*E*)	3.31	0.082	0.947
Neat Ebalta resin	Bending stress (σ)	131.13	10.40	0.991
	Bending modulus (*E*)	3.17	0.144	0.963
Ebalta + 0.5 wt.% CNFs	Bending stress (σ)	141.02	11.06	0.994
	Bending modulus (*E*)	3.46	0.159	0.982

Stdev = Standard deviation.

With respect to viscoelastic behaviour, Figure 4.7 shows the stress relaxation curves for both neat resins (Ebalta and Sicomin) and their respective CNFs nanocomposites. In these graphs, the average bending stress versus time are plotted, where σ is the bending stress at any specific instant of the test and σ_0 is the initial bending stress. For all samples tested, it was noticed that, independently of the resin type and CNFs percentage, the stress decreases with time, but the neat Sicomin resin has an inferior tendency to stress relaxation than Ebalta resin. For instance, after 180 min and for neat Sicomin resin, this drop is about 10%, while for the same resin with 0.75 wt.% CNFs is about 7.9%. For Ebalta neat resin this decrease is around 14.8%, and for Ebalta resin with 0.5 wt.% CNFs is about 13.2%.

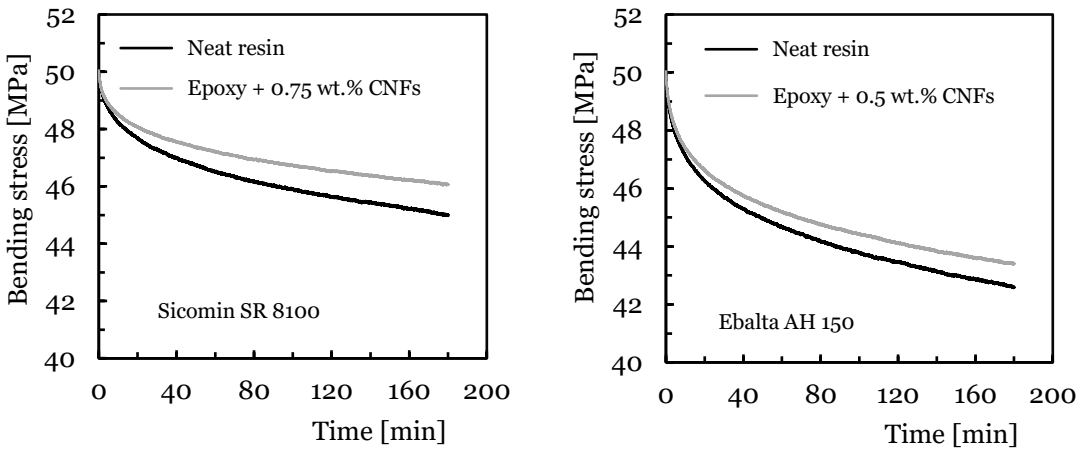

a) b)

Figure 4.7: Relaxation curves for: a) Neat Sicomin SR 8100 and nano-enhanced resin with 0.75 wt.% CNFs, bending stress of 50 MPa; b) Neat Ebalta AH 150 and nano-enhanced resin with 0.5 wt.% de CNFs, bending stress of 50 MPa.

For the neat resins, in the literature essentially two mechanisms are referenced that can induce stress relaxation: a) chemical stress relaxation due to chain scission and crosslinking formation

or scission, and b) physical stress relaxation due to molecular rearrangements that involve little primary bonding formation or breakage [42]. However, the CNFs presence demonstrated an effective enhancement of the mechanical properties with increasing filler content, up to 0.75% for Sicomin and 0.5% for Ebalta [43]. Nonetheless, the degree of improvement showed in the results is lower than expected because the increase in mechanical performance is restricted by a concentration limit, and the great properties of CNFs are not fully achieved. In epoxy composites, a good load transfer efficiency combined with the dispersion state plays a relevant role in the enhancement of performance. A suboptimal dispersion state and the CNFs random orientation during the fabrication may result in an ineffective reinforcement or even negative effect. In general, the load transfer reflects the interfacial interactions: weak fillers/polymer van der Waals interactions and polymer matrix, ionic or covalent bonding when chemical treatments are applied, and the mechanical interlocking caused by unsmooth fibre surfaces. Since in this work CNFs were not chemically treated the interfacial adhesion is originated from the non-bonded interactions, which produces inefficient load transfer. Due to the fact that both cured epoxy matrixes are not the same and present important differences, their different results showed in their relaxation curves can be attributed to their different interfacial adhesion and the different physical interactions turned out from the non-identical polarity of both resins.

Regarding the creep behaviour, Figure 4.8 shows typical curves obtained from the experimental tests, where the displacement is the result measured at any moment of the test (D) divided by its first value (D_o). In all curves is observed an instantaneous displacement, which depends on the stress level, and is followed by primary and secondary creep stages that are typical in creep curves. For these settings, the third stage occurs only for extended periods of time or higher stress values.

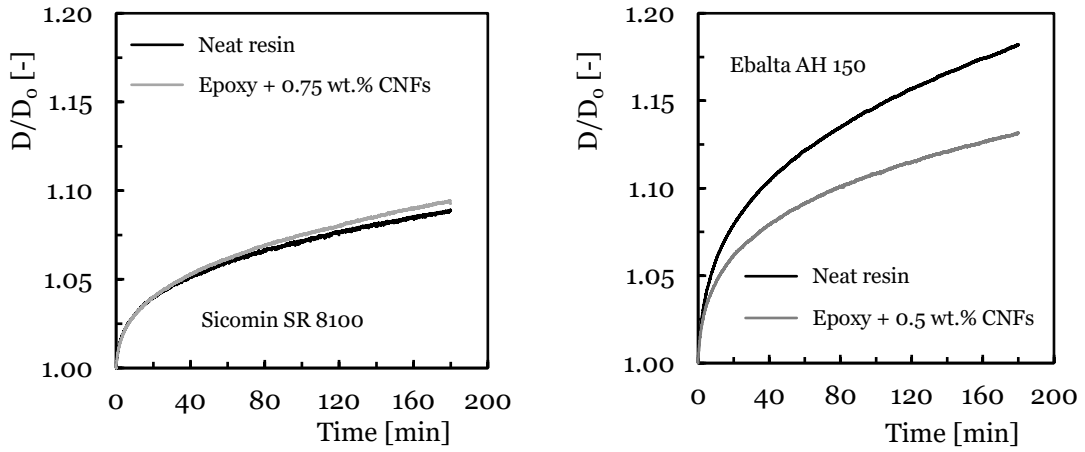

Figure 4.8: Creep curves for: a) Neat Sicomin SR 8100 and nano-enhanced resin with 0.75 wt.% CNFs, at bending stress of 50 MPa; b) Neat Ebalta AH 150 and nano-enhanced resin with 0.5 wt.% CNFs, at bending stress of 50 MPa.

In detail, Figure 4.8.b) shows that Ebalta resin with 0.5 wt.% CNFs presents greater creep displacements than neat Ebalta resin. For example, the creep strain increases about 18.2% after

180 min for Ebalta resin with 0.5 wt.% CNFs and 13.2% for neat Ebalta resin. Similarly, for neat Sicomin resin and Sicomin resin with 0.75 wt.% CNFs, this value increases 8.6% and 9.4%, respectively.

In this case, for neat resins, the creep is a consequence of the combining effect of viscous flow and elastic deformation [41]. According to Bouafif et al. [44], molecular motions in the backbone polymer arrangement is responsible for the creep phenomenon, and it is conditioned by the stress level. Jian et al. [45] suggested that there is a quantitative connection between molecular mobility and macroscopic deformation. A relatively low quantity of CNFs has a hindrance effect on polymer chain mobility of the epoxy matrix, as well as the chain disentanglement and slippage. It was mentioned that the presence of CNFs can hinder the motion of the epoxy polymer chains leading to an improved creep performance but depending on the filler concentration a contradictory response to the above said have also been detailed. CNFs-epoxy nanocomposites tend to exhibit time-dependent deformations on account of the inherent viscoelastic behaviour of polymers, over a wide range of temperatures which can be depicted by creep for a constant load. The presence of fillers can lead to a relevant improvement in the creep resistance. However, in the case of local aggregation of CNTs or CNFs, the creep resistance does not increase continuously with growing the filler weight fraction in particular at elevated percentages [46]. The creep response in an epoxy nanocomposite is affected by an irregular dispersion of CNFs in the matrix and a weakened filler/polymer interfacial region derived from the bad compatibility between both materials. Hassanzadeh-Aghdam et al. [46] explained that an increment in the interface thickness appeared to improve the nanocomposite creep resistance because the interface had lower compliance. The reinforcing capability in nanocomposites is weaker with higher weight fraction and creep loads as the agglomeration occurs and the filler/epoxy adhesion deteriorates [45]. However, na increment in filler weight fraction with good dispersion may result in a perceptible reduction of creep displacements. Thus, a greater comprehension of the creep deformation and the reinforcing mechanism of creep resistance in nanocomposites at the molecular level is still imperative because the creep response is a matter of concern for long-term durability of these materials [47].

One the one hand, from the comparison of the creep curves for neat Sicomin SR 8100 and nano-enhanced resin with 0.75 wt.% de CNFs it can be observed that the effect of the filler presence is almost irrelevant, neither positive nor detrimental. there was a slight increment of creep displacement, especially after 50-75 minutes, which shows a slightly negative effect of the CNFs in the long-term durability. One the other hand, for the neat Ebalta AH 150 and the nano-enhanced resin with 0.5 wt.% de CNFs, it can be clearly observed the negative effect of the fillers in the overall creep behaviour. The Ebalta based nanocomposite creep displacement increases noticeably respect to the pristine resin meaning that the creep resistance decreases in an important way. The harmful effects of a weakened filler/polymer interfacial region and/or the bad state of dispersion of CNFs into the polymer matrix are detected in the Ebalta sample. The reason

may come from the different physical interactions yield from the distinctive polarities of both resins since their chemical compositions are not identical.

4.4. Conclusions

Different percentages of CNFs were used to improve the mechanical properties of two commercial epoxy resin, particularly their static and viscoelastic properties. It was possible to observe that, independently of the epoxy resin, higher values of CNFs added to the resin promoted higher bending stress and modulus. The best weight content was 0.75% for Sicomin SR 8100 and 0.5% for Ebalta AH 150.

Regarding the strain-rate sensitivity, independently of the resin and nanocomposite, it was possible to observe that both materials are strain-rate sensitivity. The bending stress and modulus increase for higher values of strain rate. Finally, from the stress relaxation tests, it is clear that stress is reduced over time, but when the CNFs are added to the resins, they are less prone to stress relaxation. In the case of creep response, the displacement increases with time for all systems, but, in this case, nanocomposites are more prone to creep.

Bibliography

[1] Kancherla KB, Subbappa DB, Hiremath SR, Raju B, Roy Mahapatra D. Enhancing mechanical properties of glass fabric composite with surfactant treated zirconia nanoparticles. Composites Part A: Applied Science and Manufacturing 2019;118:131–41. https://doi.org/10.1016/j.compositesa.2018.12.023.

[2] Balasubramaniam B, Sathiyan G, Palani GS, Iyer NR, Gupta RK. Fiber Reinforced Polymer Nanocomposites for Structural Engineering Applications. Materials Science and Technology 2019:1–20. https://doi.org/10.1002/9783527603978.mst0452.

[3] Licari JJ, Swanson DW. Chapter 3 - Chemistry, Formulation, and Properties of Adhesives. Adhesives Technology for Electronic Applications, Elsevier; 2011, p. 75–141. https://doi.org/10.1016/B978-1-4377-7889-2.10003-8.

[4] Fiore V, Valenza A. Epoxy resins as a matrix material in advanced fiber-reinforced polymer (FRP) composites. Advanced Fibre-Reinforced Polymer (FRP) Composites for Structural Applications, Elsevier; 2013, p. 88–121. https://doi.org/10.1533/9780857098641.1.88.

[5] Takeichi T, Furukawa N. Epoxy Resins and Phenol-Formaldehyde Resins. Polymer Science: A Comprehensive Reference, vol. 5, Elsevier; 2012, p. 723–51. https://doi.org/10.1016/B978-0-444-53349-4.00157-6.

[6] Reis PNB, Ferreira JAM, Santos P, Richardson MOW, Santos JB. Impact response of Kevlar composites with filled epoxy matrix. Composite Structures 2012;94:3520–8. https://doi.org/10.1016/j.compstruct.2012.05.025.

[7] Kaybal HB, Ulus H, Demir O, Şahin ÖS, Avcı A. Effects of alumina nanoparticles on dynamic impact responses of carbon fiber reinforced epoxy matrix nanocomposites. Engineering Science and Technology, an International Journal 2018;21:399–407. https://doi.org/10.1016/j.jestch.2018.03.011.

[8] Shen M-Y, Chang T-Y, Hsieh T-H, Li Y-L, Chiang C-L, Yang H, et al. Mechanical Properties and Tensile Fatigue of Graphene Nanoplatelets Reinforced Polymer Nanocomposites. Journal of Nanomaterials 2013;2013:1–9. https://doi.org/10.1155/2013/565401.

[9] Gao X, Lan J, Jia X, Cai Q, Yang X. Improving interfacial adhesion with epoxy matrix using hybridized carbon nanofibers containing calcium phosphate nanoparticles for bone repairing. Materials Science and Engineering: C 2016;61:174–9. https://doi.org/10.1016/j.msec.2015.12.033.

[10] Liu X, Yue D, Yang C, Li N, Gao S, Liu Y, et al. Fluorinated carbon nanofiber/polyimide composites: Electrical, mechanical, and hydrophobic properties. Surface and Coatings Technology 2019;361:206–11. https://doi.org/10.1016/j.surfcoat.2019.01.033.

[11] Liu W, Wang Y, Wang P, Li Y, Jiang Q, Hu X, et al. A biomimetic approach to improve the dispersibility, interfacial interactions and toughening effects of carbon nanofibers in epoxy composites. Composites Part B: Engineering 2017;113:197–205. https://doi.org/10.1016/j.compositesb.2017.01.040.

[12] Gantayat S, Rout D, Swain SK. Structural and mechanical properties of functionalized carbon nanofiber/epoxy nanocomposites. Materials Today: Proceedings 2017;4:9060–4. https://doi.org/10.1016/j.matpr.2017.07.259.

[13] Buchanan JP, Reed-Gore ER, Jefcoat JA, Moser RD, Klaus KL, Peel HR, et al. Increasing mechanical resilience and enhanced electrical conductivity through the incorporation of CNF reinforcing additives in PA6 nanocomposites. Structural Chemistry 2019;30:341–9. https://doi.org/10.1007/s11224-018-1236-8.

[14] Zhou Y, Akanda SR, Jeelani S, Lacy TE. Nonlinear constitutive equation for vapor-grown carbon nanofiber-reinforced SC-15 epoxy at different strain rate. Materials Science and Engineering A 2007;465:238–46. https://doi.org/10.1016/j.msea.2007.04.042.

[15] Poveda RL, Gupta N. Change in failure mode of carbon nanofibers in nanocomposites as a function of loading rate. Journal of Materials Science 2016;51:4917–27. https://doi.org/10.1007/s10853-016-9796-8.

[16] Zare Y. The roles of nanoparticles accumulation and interphase properties in properties of polymer particulate nanocomposites by a multi-step methodology. Composites Part A: Applied Science and Manufacturing 2016;91:127–32. https://doi.org/10.1016/j.compositesa.2016.10.003.

[17] Oberdisse J. Aggregation of colloidal nanoparticles in polymer matrices. Soft Matter 2006;2:29–36. https://doi.org/10.1039/B511959F.

[18] Padmanabhan V, Frischknecht AL, Mackay ME. Effect of Chain Stiffness on Nanoparticle Segregation in Polymer/Nanoparticle Blends Near a Substrate. Macromolecular Theory and Simulations 2012;21:98–105. https://doi.org/10.1002/mats.201100048.

[19] Ma X, Zare Y, Rhee KY. A Two-Step Methodology to Study the Influence of Aggregation/Agglomeration of Nanoparticles on Young's Modulus of Polymer Nanocomposites. Nanoscale Research Letters 2017;12:621. https://doi.org/10.1186/s11671-017-2386-0.

[20] Shaffer MSP, Fan X, Windle AH. Dispersion and packing of carbon nanotubes. Carbon 1998;36:1603–12. https://doi.org/10.1016/S0008-6223(98)00130-4.

[21] Fiedler B, Gojny FH, Wichmann MHG, Nolte MCM, Schulte K. Fundamental aspects of nano-reinforced composites. Composites Science and Technology 2006;66:3115–25. https://doi.org/10.1016/j.compscitech.2005.01.014.

[22] Liu S, Chevali VS, Xu Z, Hui D, Wang H. A review of extending performance of epoxy resins using carbon nanomaterials. Composites Part B: Engineering 2018;136:197–214. https://doi.org/10.1016/j.compositesb.2017.08.020.

[23] Ignatenko VY, Ilyin SO, Kostyuk A V., Bondarenko GN, Antonov S V. Acceleration of epoxy resin curing by using a combination of aliphatic and aromatic amines. Polymer Bulletin 2020;77:1519–40. https://doi.org/10.1007/s00289-019-02815-x.

[24] Garcia FG, Soares BG, Pita VJRR, Sánchez R, Rieumont J. Mechanical properties of epoxy networks based on DGEBA and aliphatic amines. Journal of Applied Polymer Science 2007;106:2047–55. https://doi.org/10.1002/app.24895.

[25] Baig Z, Akram N, Zia KM, Saeed M, Khosa MK, Ali L, et al. Influence of amine-terminated additives on thermal and mechanical properties of diglycidyl ether of bisphenol A (DGEBA) cured epoxy. Journal of Applied Polymer Science 2020;137:48404.

https://doi.org/10.1002/app.48404.

[26] Cai H, Li P, Sui G, Yu Y, Li G, Yang X, et al. Curing kinetics study of epoxy resin/flexible amine toughness systems by dynamic and isothermal DSC. Thermochimica Acta 2008;473:101–5. https://doi.org/10.1016/j.tca.2008.04.012.

[27] Nie Y, Hübert T. Effect of carbon nanofiber (CNF) silanization on the properties of CNF/epoxy nanocomposites. Polymer International 2011;60:1574–80. https://doi.org/10.1002/pi.3124.

[28] Bal S. Experimental study of mechanical and electrical properties of carbon nanofiber/epoxy composites. Materials & Design (1980-2015) 2010;31:2406–13. https://doi.org/10.1016/j.matdes.2009.11.058.

[29] Wu Q, Zhao R, Ma Q, Zhu J. Effects of degree of chemical interaction between carbon fibers and surface sizing on interfacial properties of epoxy composites. Composites Science and Technology 2018;163:34–40. https://doi.org/10.1016/j.compscitech.2018.05.013.

[30] Prolongo SG, Burón M, Gude MR, Chaos-Morán R, Campo M, Ureña A. Effects of dispersion techniques of carbon nanofibers on the thermo-physical properties of epoxy nanocomposites. Composites Science and Technology 2008;68:2722–30. https://doi.org/10.1016/j.compscitech.2008.05.015.

[31] Zhu J, Wei S, Ryu J, Budhathoki M, Liang G, Guo Z. In situ stabilized carbon nanofiber (CNF) reinforced epoxy nanocomposites. Journal of Materials Chemistry 2010;20:4937–48. https://doi.org/10.1039/c0jm00063a.

[32] Wang J, Gong J, Gong Z, Yan X, Wang B, Wu Q, et al. Effect of curing agent polarity on water absorption and free volume in epoxy resin studied by PALS. Nuclear Instruments and Methods in Physics Research Section B: Beam Interactions with Materials and Atoms 2010;268:2355–61. https://doi.org/10.1016/j.nimb.2010.04.010.

[33] Sandler SR, Berg FR. Effect of polarity of bisphenol a epoxy resins on adhesion at cryogenic and elevated temperatures. Journal of Applied Polymer Science 1965;9:3707–19. https://doi.org/10.1002/app.1965.070091118.

[34] Wilson AD, Stewart FF. Structure-function study of tertiary amines as switchable polarity solvents. RSC Advances 2014;4:11039–49. https://doi.org/10.1039/c3ra47724j.

[35] Tao K, Yang S, Grunlan JC, Kim YS, Dang B, Deng Y, et al. Effects of carbon nanotube fillers on the curing processes of epoxy resin-based composites. Journal of Applied Polymer Science 2006;102:5248–54. https://doi.org/10.1002/app.24773.

[36] Seyhan AT, Sun Z, Deitzel J, Tanoglu M, Heider D. Cure kinetics of vapor grown carbon nanofiber (VGCNF) modified epoxy resin suspensions and fracture toughness of their resulting nanocomposites. Materials Chemistry and Physics 2009;118:234–42. https://doi.org/10.1016/j.matchemphys.2009.07.045.

[37] Dutta A, Ryan ME. Effect of fillers on kinetics of epoxy cure. Journal of Applied Polymer Science 1979;24:635–49. https://doi.org/10.1002/app.1979.070240302.

[38] Ingram J, Zhou Y, Jeelani S, Lacy T, Horstemeyer MF. Effect of strain rate on tensile behavior of polypropylene and carbon nanofiber filled polypropylene. Materials Science and Engineering: A 2008;489:99–106. https://doi.org/10.1016/j.msea.2008.01.010.

[39] Delhaye V, Clausen AH, Moussy F, Othman R, Hopperstad OS. Influence of stress state and strain rate on the behaviour of a rubber-particle reinforced polypropylene. International Journal of Impact Engineering 2011;38:208–18. https://doi.org/10.1016/j.ijimpeng.2010.11.004.

[40] Reis PNB, Gorbatikh L, Ivens J, Lomov SV. Strain-rate sensitivity and stress relaxation of hybrid self-reinforced polypropylene composites under bending loads. Composite Structures 2019;209:802–10. https://doi.org/10.1016/j.compstruct.2018.11.030.

[41] Glaskova-Kuzmina T, Aniskevich A, Zarrelli M, Martone A, Giordano M. Effect of filler on the creep characteristics of epoxy and epoxy-based CFRPs containing multi-walled carbon nanotubes. Composites Science and Technology 2014;100:198–203. https://doi.org/10.1016/j.compscitech.2014.06.011.

[42] Reis PNB, Silva MP, Santos P, Parente JM, Valvez S, Bezazi A. Mechanical performance of an optimized cork agglomerate core-glass fibre sandwich panel. Composite Structures

2020;245:112375. https://doi.org/10.1016/j.compstruct.2020.112375.

[43] Jian W, Lau D. Understanding the effect of functionalization in CNT-epoxy nanocomposite from molecular level. Composites Science and Technology 2020;191:108076. https://doi.org/10.1016/j.compscitech.2020.108076.

[44] Bouafif H, Koubaa A, Perré P, Cloutier A. Creep behaviour of HDPE/wood particle composites. International Journal of Microstructure and Materials Properties 2013;8:225. https://doi.org/10.1504/IJMMP.2013.055385.

[45] Jian W, Lau D. Creep performance of CNT-based nanocomposites: A parametric study. Carbon 2019;153:745–56. https://doi.org/10.1016/j.carbon.2019.07.069.

[46] Hassanzadeh-Aghdam MK, Mahmoodi MJ, Ansari R. Creep performance of CNT polymer nanocomposites -An emphasis on viscoelastic interphase and CNT agglomeration. Composites Part B: Engineering 2019;168:274–81. https://doi.org/10.1016/j.compositesb.2018.12.093.

[47] Nomula SSR, Rathore DK, Ray BC, Prusty RK. Creep performance of CNT reinforced glass fiber/epoxy composites: Roles of temperature and stress. Journal of Applied Polymer Science 2019;136:1–15. https://doi.org/10.1002/app.47674.

Chapter 5

Effect of carbon nanofibres on the viscoelastic response of epoxy resins[4]

Abstract

Two epoxy resins with different viscosities were enhanced up to 1 wt.%, applying a simple method with carbon nanofibres (CNFs). These were characterized in terms of static bending stress, stress relaxation, and creep tests. In bending, the contents of 0.5 wt.% and 0.75 wt.% of CNFs on Ebalta and Sicomin epoxies, respectively, promote higher relative bending stress (above 11.5% for both) and elastic modulus (13.1% for Sicomin and 16.2% for Ebalta). This highest bending stress and modulus occurs for the lower viscosity resin (Ebalta) due to its interfacial strength and dispersibility of the fillers. Creep behaviour and stress relaxation for three stress levels (20, 50, and 80 MPa) show the benefits obtained with the addition of CNFs, which act as a network that contributes to the immobility of the polymer chains. A long-term experiment of up to 100 hours was successfully applied to fit the Kohlrausch-Williams-Watts (KWW) and Findley models to stress relaxation and creep behaviour with very good accuracy.

5.1. Introduction

Epoxy resins, in addition to playing the important role of matrix in composite materials, are an important class of thermosetting polymers due to their excellent mechanical properties, high adhesiveness to many substrates, and good thermal and chemical resistances [1–3].

However, due to this cross-linked structure, the epoxy has low toughness, stiffness, and impact resistance [4]. The addition of a small amount of inorganic nanofiller in the epoxy matrix improves the mechanical properties of the net epoxy, particularly its toughness and stiffness [5]. Different studies refer to the benefit of adding micro and nano ceramic particles, as an example, 1 vol.% of Al_2O_3 improves by more than 15% the bending strength and stiffness [6]; 2 wt.% of $CaCO_3$ increments the tensile strength and the toughness by 22% and 37%, respectively [7]; the tensile strength increases by 32% and fracture toughness by 45% with the loading of 4 wt.% of TiO_2 [8]; adding 3 wt.% of SiO_2, the tensile and impact strength doubles [9,10]; the tensile

[4] Based on the work published in the Polymers, Santos, P.; Silva, A.P.; Reis, P.N.B. Effect of Carbon Nanofibers on the Viscoelastic Response of Epoxy Resins. *Polymers* **2023**, *15*, 821. https://doi.org/10.3390/polym15040821

strength and the fracture toughness increases by 50% and 106%, respectively, with the introduction of 4 wt.% of Fe_2O_3 [11].

Moreover, epoxy enhanced by graphene-based nanomaterials has been widely explored and are more attractive because of their unique physical properties [12,13]. It is often functionalized to get the desired characteristics, namely, to improve the surface ionic bonds and the interfacial van der Waals interactions. The carbon nanotubes (CNTs) fundamentally come in three variations: singular-walled CNTs (SWCNTs), double-walled CNTs (DWCNTs), and multi-walled CNTs (MWCNTs). They have a typical one-dimensional (1D) cylindrical fibrous structure, diameters ranging from fractions to tens of nanometres and lengths up to several micrometres and can be considered a cylindrical graphene sheet covered by fullerene-like structures. Their reported surface areas range from 150 to 1500 $m^2\ g^{-1}$, which is a basis for serving as good sorbents [14]. Carbon nanofibres (CNFs) have lengths in the order of micrometres, diameters ranging from ten to hundreds of nanometres (50–200 nm), specific surface area up to 1877 $m^2\ g^{-1}$, and aspect ratio greater than 100. The cylindrical nanostructures of CNFs have a different chemical structure of graphene sheets, such as stacked platelet, ribbon, spiral, fishbone hollow core, fishbone solid, ribbon, stacked cup, and amorphous CNFs without graphene layers [14,15]. CNFs typically used as reinforcements have diameters of several micrometres and are produced from petroleum-based precursors, such as high-strength polyacrylonitrile (PAN) and mesophase pitch (MPP) [16,17].

The relative enhancement in mechanical properties mainly depends on the shape, surface area, and the quality of the interface between matrix and CNFs. Their large surface-to-volume ratio leads to agglomeration, and their chemically inert nature leads to poor interfacial interactions [18]. Thus, different functionalization and dispersion methodologies correspond to different loadings optimizations and consequently, to different strengths, stiffness, and other enhanced properties. Thus, different wt.% loadings of CNFs result in different strengths and stiffness levels. For example, reinforcement with CNTs is typically done with loads up to 2 wt.%, but there are also reinforcements carried out with more than 10 wt.% [13]. In many cases, very low CNTs loads of 0.1-0.5 wt.% promote very significant improvements: tensile strength and elongation-to-break increases by 12.6% and 25.4%, respectively, with 0.1 wt.% [12]; and tensile strength increases 68% with 0.3 wt.% [13]. In addition, smaller loads facilitate manufacturing, especially in optimizing simple, low-cost, and technologically easy-to-implement techniques.

In previous works, applying a manual lay-up process, known to be a simple method and particularly suitable for large components, it was verified that the use of CNFs benefits the mechanical properties of the epoxy resins [3,19]. In addition, other works with benefits from the use of CNFs in epoxy are referred to in the literature. Shokrieh et al. [20] studied the reinforcing effect of CNFs (up to 1 wt.% by weight) of an epoxy resin using a mechanical stirrer and sonication. The maximum improvements in tensile strength and bending strength occurring for 0.25 wt.% of CNFs were 23 and 10%, respectively. Sun et al. [21] carried out a study of the static and dynamic

mechanical behaviour of epoxy nanocomposites with CNFs. The results show the highest tensile strength (8%) and the maximum Young's modulus (17%) are found for 1 wt.% of CNFs.

However, most published work characterizes the mechanical performance of these nano-reinforced systems at the level of quasi-static properties and mainly in tensile mode. Nevertheless, in many engineering applications, knowledge of the viscoelastic response (stress relaxation and creep) of materials is crucial due to the requirement for long-term dimensional stability of structures/components. Therefore, in addition to the experimental studies, it is also possible to find several models in literature to predict the viscoelastic response. Although the simplest models are based on a spring or dashpot to represent a purely elastic or ideal fluidic material, they are not applicable to most materials used in engineering because they are neither purely elastic nor ideally fluidic. For these conditions, models involving springs and dashpots with different arrangements are suggested, and among others, it is possible to find the Maxwell model, Voigt model, Boltzmann model, Burgers model, Kelvin model, etc. A review and comparability of these models can be found in [22]. To obtain predictions with better accuracy, and for specific materials, literature also suggests the Kohlrausch-Williams-Watts (KWW) model, an empirical "stretched exponential" function [23].

Therefore, the main goal of this work is to apply a manual lay-up process, known to be a simple, low-cost, and technologically easy-to-implement method, to study the viscoelastic behaviour of two epoxy resins with different viscosities and nano reinforced with low loads of CNFs. Thus, stress relaxation and creep for short periods are assessed through a detailed and comparative methodology of mechanical tests, and the KWW and Findley models are proposed to predict the viscoelastic behaviour of the two nano-enhanced epoxy resins based on experimental static bending stress results for long-term service.

5.2. Materials and experimental procedure

Nanocomposites were produced with two different epoxy resins, which were enhanced with carbon nanofibres (CNFs). For this purpose, an epoxy resin, SR 8100, and a hardener, SD 8822, both supplied by Sicomin, and an epoxy resin, AH 150, and a hardener, IP 430, both supplied by Ebalta, were used due to their different viscosities: Ebalta resin with lower viscosity than Sicomin of 250 ± 50 and 390 mPa × s, respectively, according to the technical data sheet of the resins. In terms of CNFs, they were supplied by Sigma-Aldrich, and according to the manufacturer's datasheet, they have an average diameter of around 130 nm, a length between 20–200 μm, and an average specific surface area of around 54 m^2/g. Several contents by weight were studied (0.25, 0.5, 0.75, and 1 wt.%). More details about the resins and CNFs can be found in [3]. For example, for Sicomin resin with 0.75 wt.% CNFs, 150 g of resin, 33 g of hardener, and 1.37 g of CNFs were used. The weight content of CNFs was selected according to the literature and from the perspective of mechanical performance, where typical values of those used in this study can be found [16]. It should be noted the electrical performance is outside the scope of this work because, according to Farzaneh et al. [24], electrical conductivity increases with increasing carbon-based

nano reinforcement content due to the formation of a continuous network and the facilitation of free electron mobility.

These nanocomposites were produced by adding CNFs to the epoxy resins (see procedure in Figure 5.1), and the mixture was carried out at room temperature (RT) in a mixer, LBX STIV-020-001, with a shear rate of 1000 rpm for 3 hours, followed by 10 min at 150 rpm to disperse the hardener into the system. All of the procedure was combined with sonication, Ultrasonic Cleaner model AU-65, (using an ultrasonic bath with a frequency of 40 kHz) to improve the dispersion of the nanofibres [19,25] in which the temperature was controlled not to exceed the glass transition temperature (T_g) of the resins. Finally, the mixture was degassed in a vacuum oven, Bacoeng Vacuum Chamber, with the aid of a vacuum pump, VEVOR 3CFM, to remove air bubbles and was poured into a cardboard mould with dimensions of 100 × 200 × 3 mm^3. The nanocomposite-manufacturing process ends with the cure and post-cure suggested in the technical datasheets. While nanocomposites produced with Sicomin resin were cured at RT for 24 hours and subjected to post-cure at 40 °C for 24 hours, those involving Ebalta resin were cured at RT for 48 hours and subjected to post-cure at 80 °C for 5 hours.

Figure 5.1: Methodology used to produce the nano-enhanced resins with CNFs.

The samples used in the experiments were cut from these thin plates into specimens with dimensions of 80 × 10 × 3 mm^3 (Figure 5.2.a)) and tested in a Shimadzu machine, model Autograph AGS-X, equipped with a 10 kN load cell. The static characterization was performed in bending mode and for this purpose, in accordance with the European Standard EN ISO 178:2003; three-point-bending (3PB) static tests were carried out at RT and using a span length of 50 mm (Figure 5.2.b)). For each condition, at least five specimens were tested at a displacement rate of 2 mm/min, and the main properties for bending strength, bending modulus, and bending strain were obtained according to Equations (5.1) to (5.3), respectively.

$$\sigma = \frac{3\,P\,L}{2\,b\,h^2} \tag{5.1}$$

$$E = \frac{\Delta P\,L^3}{48\,\Delta u\,I} \tag{5.2}$$

$$\varepsilon_f = \frac{6\,S\,h}{L^2} \tag{5.3}$$

where P is the load, L is the span length, b is the width, h is the thickness of the specimen, I is the moment of inertia of the cross-section, ΔP and Δu are, respectively, the load range and bending displacement range in the middle span for an interval in the linear region of the load versus displacement plot, and S is the deflexion. The error is the standard deviation.

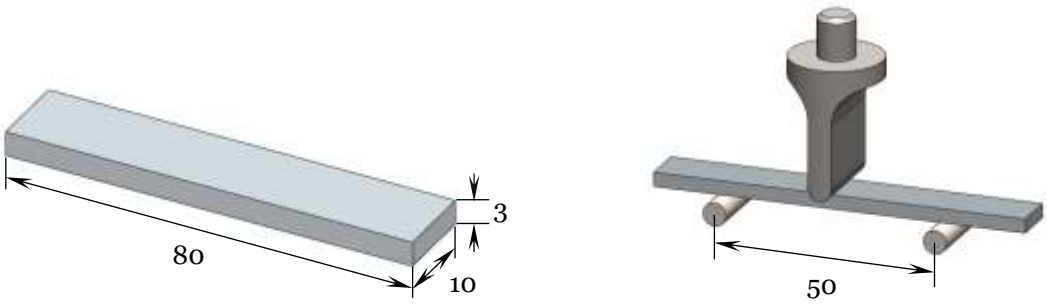

Figure 5.2: a) Geometry of the specimens; b) Schematic view of the three-point bending apparatus. All dimensions in mm.

Stress-relaxation tests were performed at RT and in accordance with ASTM E328-13 standard in the same machine. A fixed strain was applied (correspondent to 20, 50, and 80 MPa), and the stress was recorded during the loading time (180 min). On the other hand, the creep tests were performed at RT and in accordance with ASTM D2990-09 standard where a fixed bending stress was applied (with similar values to those previously reported), and the displacement was recorded during the loading time (180 min). The values used in both tests with at least five specimens were selected to ensure all viscoelastic tests were performed within the elastic regime. The maximum and minimum values reported were as extremes (error) of the solution envelope.

5.3. Results and discussion

To evaluate the benefits obtained with the CNFs in both resins as well as to select the values used in the creep and stress relaxation tests, static bending tests were carried out. This is important to ensure all tests are performed within the elastic regime of the nanocomposites. Therefore, Figure 5.3 presents typical bending stress–strain curves for Ebalta resin, which are representative of all curves obtained in this study (including for Sicomin resin).

Regardless of the weight content of CNFs, all curves evidence a linear increase in bending stress with strain, followed by a non-linear behaviour in which the maximum bending stress is reached. For both resins and all conditions analysed, the bending stress decreases until the imminent collapse occurs. It is notorious that the lowest value of the bending strength occurs for neat resin, which increases with the weight content of CNFs until reaching a maximum value. After this maximum, this property is significantly affected by the filler content, and similar behaviour was observed for Sicomin resin but for a different weight content of CNFs.

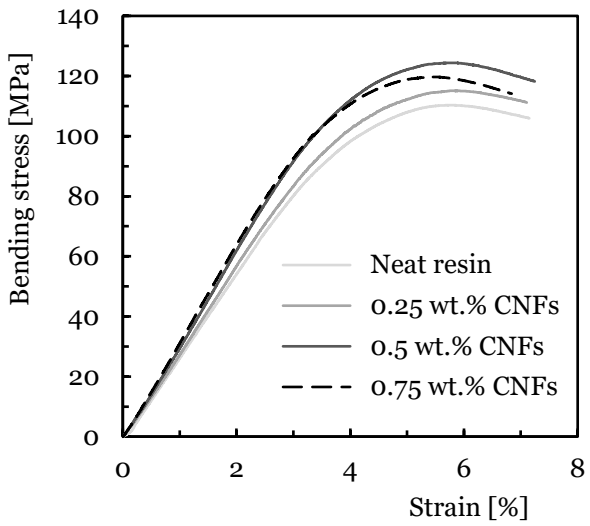

Figure 5.3: Average bending stress-strain curves for Ebalta resin with different CNFs contents.

This evidence can be seen in Figure 5.4, which summarizes the main bending properties resulting from these curves. Symbols represent the average values and the dispersion bands respective of the maximum and minimum values. Black symbols are related to the bending stress, grey symbols represent the average values of bending stiffness, and blue symbols represent the bending strain. Quantitative analysis for the Sicomin resin (Figure 5.4.a)) reveals an increase of about 11.8% in the bending strength when comparing the values obtained for the neat resin (106.2 MPa) and those obtained for 0.75 wt.% (118.7 MPa). Subsequently, the bending strength decreases from 118.7 MPa to 114.2 MPa when the filler content increased up to 1 wt.% of CNFs.

On the other hand, the same analysis for the Ebalta resin shows the maximum bending stress is reached for 0.5 wt.% of CNFs with a value of 123.4 MPa, which is 11.7% higher than that obtained for neat resin (110.5 MPa). Regarding the bending modulus and for both resins, an increase was observed with increasing filler content. While for the Sicomin resin, the increase was around 13.1% and between the neat resin (2.68 GPa) and the nanocomposite reinforced with 1 wt.% of CNFs (3.03 GPa), for the Ebalta resin this value is around 16.2% (from 2.84 GPa to 3.3 GPa). However, when the bending stiffness obtained for the highest bending stress is compared with that of the neat resin, an increase of 11.9% is observed for Sicomin resin and 11.3% for Ebalta. Finally, the bending strain decreases with the increase of filler content for the Ebalta resin, around 6.4% between the value obtained for the neat resin (5.78%) and that of the nanocomposite with 0.5 wt.% of CNFs (5.41%), while for the Sicomin resin, it appears to be constant up to 0.5 wt.% and then decreases.

The reported increase, according to Farzaneh et al. [24], can be explained by the higher modulus of the nanofillers compared to the polymer as well as to the promotion of microphase separation and the formation of harder domains in the presence of the nanofillers. For these authors, the well-controlled microphase separation explains the mechanism responsible for the improvements in strength and modulus.

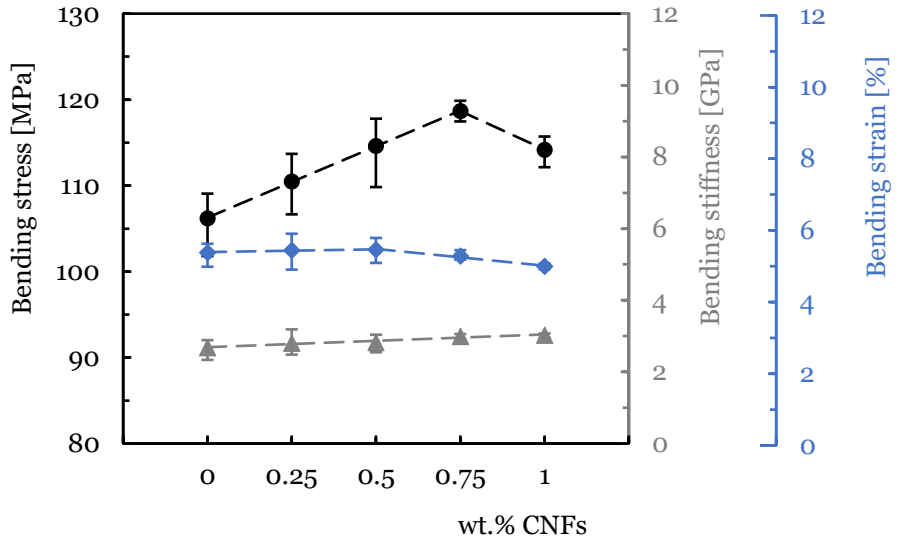

a)

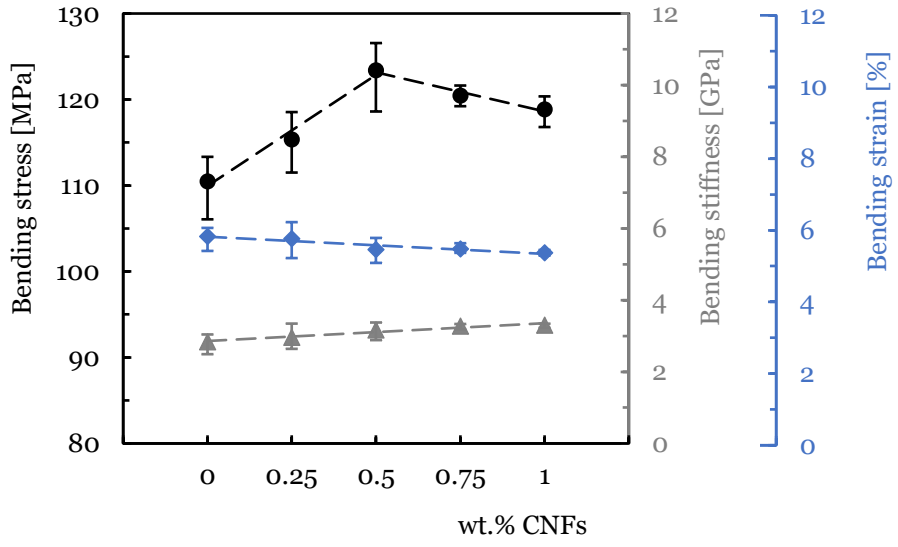

b)

Figure 5.4: Bending properties versus weight content of CNFs for: a) Sicomin resin; b) Ebalta resin.

On the other hand, the presence of nanofillers and the formation of the filler network limited the chain mobility and consequently, a decrease in the ultimate bending strain [24]. Furthermore, these results agree with the literature because for higher filler contents, agglomerations/aggregations (corresponding to defects) are observed (see Figure 5.5), which act as stress concentration points in nanocomposites [26–28]. The SEM images shown in Figure 5.5 refer to the fracture surfaces of the samples tested with the Ebalta resin but are also representative of the Sicomin resin with 0.75 and 1 wt.% of CNFs. A good dispersion of the nano-fillers is evident for 0.5 wt.% of CNFs (Figure 5.5.a)), while for 0.75 wt.%, the previously reported agglomerations/aggregations are visible (Figure 5.5.b)). Moreover, the interfacial area between the polymer matrix and nanoparticles also decreases and consequently, the mechanical involvement of polymer chains with the nanoparticles [29]. In this context, because only a few polymer molecules can penetrate between the nanoparticles, the viscosity also increases

substantially [30]. Finally, according to Fiedler et al. [31], resins with low viscosity promote a better organization of nanoparticles and consequently, better mechanical properties for lower filler contents. This evidence is confirmed in this study because the highest bending stress and modulus were obtained with the Ebalta resin (the one with the lowest viscosity).

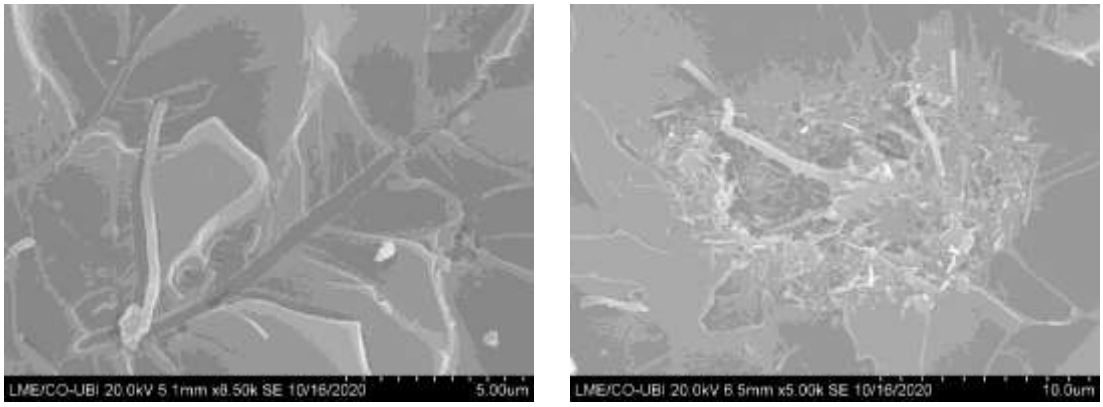

a) b)

Figure 5.5: SEM pictures for the Ebalta resin with: a) 0.5 wt.% of CNFs; b) 0.75 wt.% of CNFs.

Therefore, the proposed study on stress relaxation and creep will only consider configurations that maximized the bending strength. This is due to the fact that higher levels of CNFs promote agglomerations of nanoparticles with a consequent negative effect on the creep response of nanocomposites [32]. In this case, for the creep tests, a fixed bending stress was applied with values of 20, 50, and 80 MPa for both resin and filler contents, and the displacement was recorded during the loading time (180 min). Therefore, from the experimental tests, the curves shown in Figure 5.6 were obtained where D is the bending displacement obtained at any instant of the test, and D_o is the initial bending displacement. These results are representative of the creep behaviour of the other conditions analysed.

All curves clearly show three regions, an instantaneous deformation followed by the first stage and an unfinished secondary one. Inevitably, under these conditions, the third stage is not observed because the creep rupture or failure is out of consideration in this study. In other words, this work focuses on short-term tests that prove to be an easy, fast, and reliable methodology to predict long-term behaviour [33]. The first region is time independent, and the elongation/displacement is attributed to the elastic and plastic deformation of the polymer under a constant applied load but strongly dependent on its magnitude [32,34,35]. For all materials, an increase in instantaneous displacement is evident with increasing applied load as well as for all creep displacements. For example, when comparing the creep displacement between neat resins for the bending stress of 80 MPa, it is observed that after 180 min, the Ebalta resin presents values 14.2% higher than the Sicomin resin. In fact, the creep displacement increases nonlinearly with time, even at RT, as shown in Figure 5.6 and at stress levels much lower than the ultimate strength due to the combination of elastic strain and viscous flow [36–38].

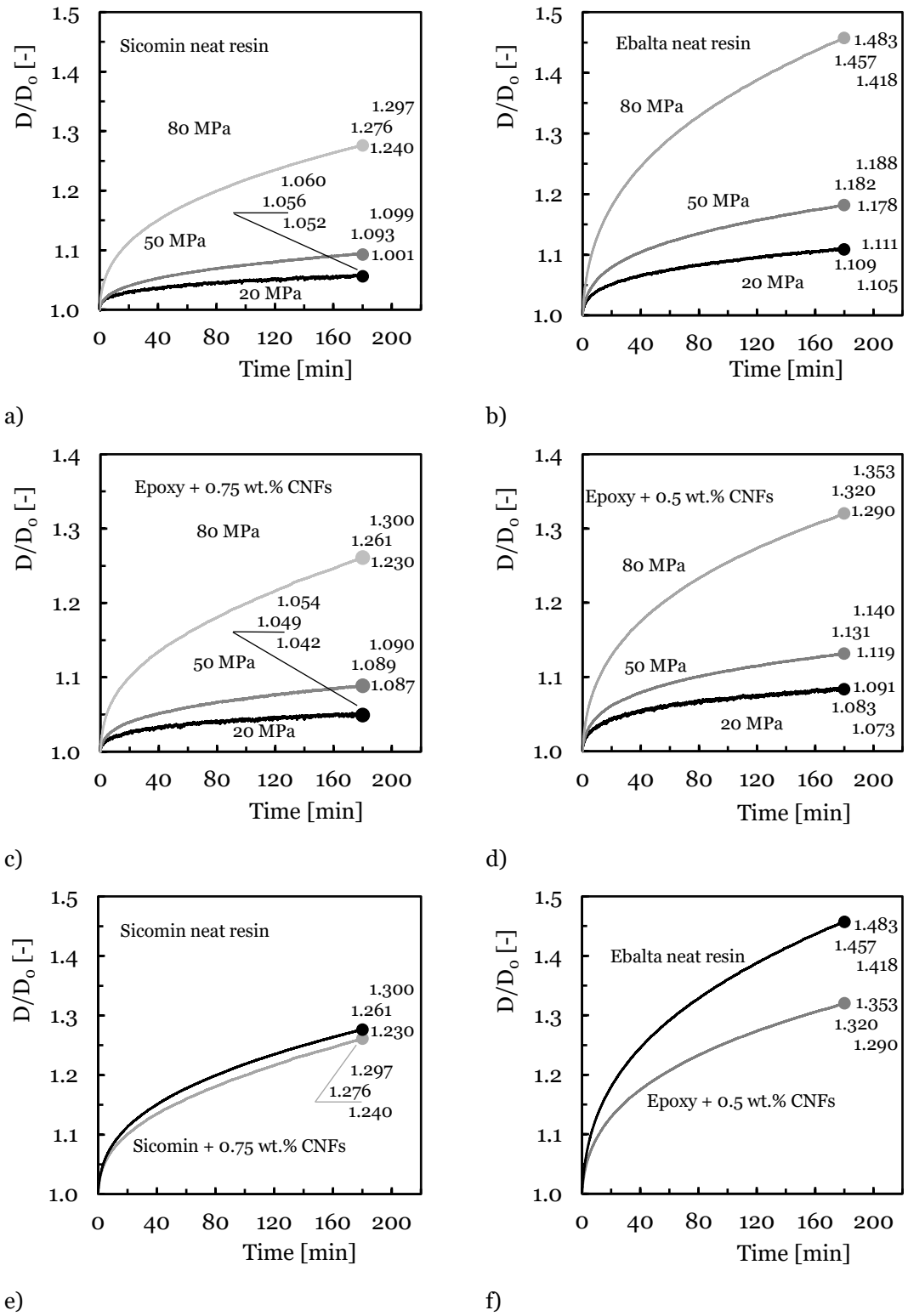

Figure 5.6: Creep curves for: a) Sicomin neat resin and different bending stresses; b) Ebalta neat resin and different bending stresses; c) Sicomin resin with 0.75 wt.% of CNFs and different bending stresses; d) Ebalta resin with 0.5 wt.% of CNFs and different bending stresses; e) Sicomin neat resin and with 0.75 wt.% of CNFs for bending stress of 80 MPa; f) Ebalta neat resin and with 0.5 wt.% of CNFs for bending stress of 80 MPa.

However, there is a quantitative relationship between molecular mobility and macroscopic deformation [39], which explains the 14.2% difference reported above. On the other hand, according to Bouafif et al. [40], creep is due to molecular motion in the backbone polymer arrangement and depends on the stress level. This explains the different values observed. For example, comparing the values for 180 min and 20 MPa test, while the creep displacement for the Sicomin resin increases by about 3.5% for 50 MPa and 20.8% for 80 MPa, these values are 6.6% and 31.4%, respectively, for the Ebalta resin. These values also show the higher sensitivity to the loading level of the Ebalta resin in relation to Sicomin one due to its higher molecular mobility [39]. In this context, Vlasveld et al. [41] even reported the deformation process in polymers under load is strongly dependent on the mobility of the chains and not only dependent on temperature.

Another evidence observed in Figure 5.6 is the benefits achieved by filling the resins with carbon nanofibres. In terms of Ebalta resin, CNFs improve the creep resistance by 10.4%, while for Sicomin resin it is around 1.2%. In this context, the large number of dispersed nanoparticles binds to the matrix via interphase, bridging segments and junctions to support the load and improve the immobility of the polymer chains [35]. This immobility is related to the restriction to slippage, realignment, and motion of polymeric chains that CNFs cause [32], and three mechanisms can contribute to this: (i) good interfacial strength between CNFs/matrix, (ii) CNFs act as blocking sites, and (iii) high aspect ratio of CNFs [42]. Furthermore, below T_g, the molecular weight has a very small influence on the creep behaviour because only the local motion of the chain segments is involved in the glassy state [41]. Therefore, the higher creep resistance observed for Ebalta resin can be explained by the stronger interfaces that were established between CNFs/polymer. All these facts are summarized in Figure 5.7 where the difference between initial and final bending displacement (ΔD) is shown. It is possible to compare the load effect on the creep behaviour previously reported, both for neat resins and for the respective nanocomposites as well as the CNFs effect for each resin.

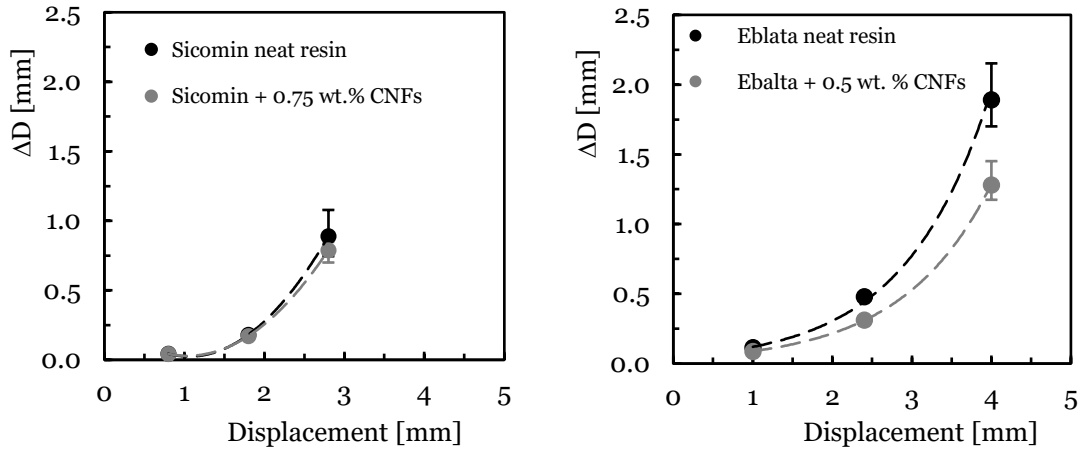

Figure 5.7: Difference between initial and final bending displacement for: a) Sicomin resin; b) Ebalta resin.

An increase in creep displacement for higher loads is visible as well as increased creep resistance when resins are reinforced with CNFs. However, this difference is more expressive for higher stresses because at lower load levels there are no clearly visible benefits for resins filled with CNFs. According to Yang et al. [35], higher loads increase viscous flow and can even activate non-linear viscoelasticity mechanisms for very high loads. Finally, it is also visible that the benefits achieved for the Ebalta resin are more expressive due to higher interaction between CNFs/polymer.

In terms of stress relaxation, Figure 5.8 shows the average bending stress versus time curves, where σ0 is the bending stress at any given moment of the test, and σ is the initial bending stress. The final values represent the average, maximum, and minimum values obtained for all conditions analysed after 180 min of testing. For comparability, bending displacements corresponding to the same values of bending stress used in the creep tests (20, 50, and 80 MPa) were used. It is notorious that all materials show a decrease in stress over time, and because this study focuses on short-term tests, as reported above, it would not be expected to reach a constant value for bending stress. This will only occur for higher stress values or longer tests.

Another evidence reported by the curves is the existence of an initial stage where the bending stress decreases considerably compared to the remaining time [43,44]. For example, considering only the resins filled with CNFs and bending stress of 80 MPa (Figures 5.8.c), 5.8.d)), the Sicomin one reveals a decrease of about 8.2% in the first 30 min, while the remaining time it decreases (between 30 and 180 min) about 6.3%. These values for the Ebalta resin are 12.5% and 8.5%, respectively. According to the literature, stress relaxation occurs due to physical and/or chemical phenomena. In the first case, it results from molecular rearrangements that require little formation or rupture of the primary bonds, while the second one is due to chain scission, crosslink scission, or crosslink formation [45–47]. However, for resins nano-reinforced, all these processes are delayed because the CNFs act as a network that contributes to the immobility of the polymer chains [32,35,42].

Figure 5.9 compares the differences between initial and final bending stress ($\Delta\sigma$), and it is possible to observe higher stress relaxations for higher bending displacements as well as the benefits achieved with nano-reinforced resins. For example, for Sicomin resin and for the bending displacement corresponding to the highest bending stress (80 MPa), CNFs decreased the stress relaxation by around 21.7% compared to the neat resin, while for the same conditions, this value is about 9.2% for Ebalta resin. It is also noted that with decreasing the bending displacement, the stress relaxation values also decrease, and there is practically no difference between neat and nano-reinforced resins for the smallest bending displacement (corresponding to 20 MPa).

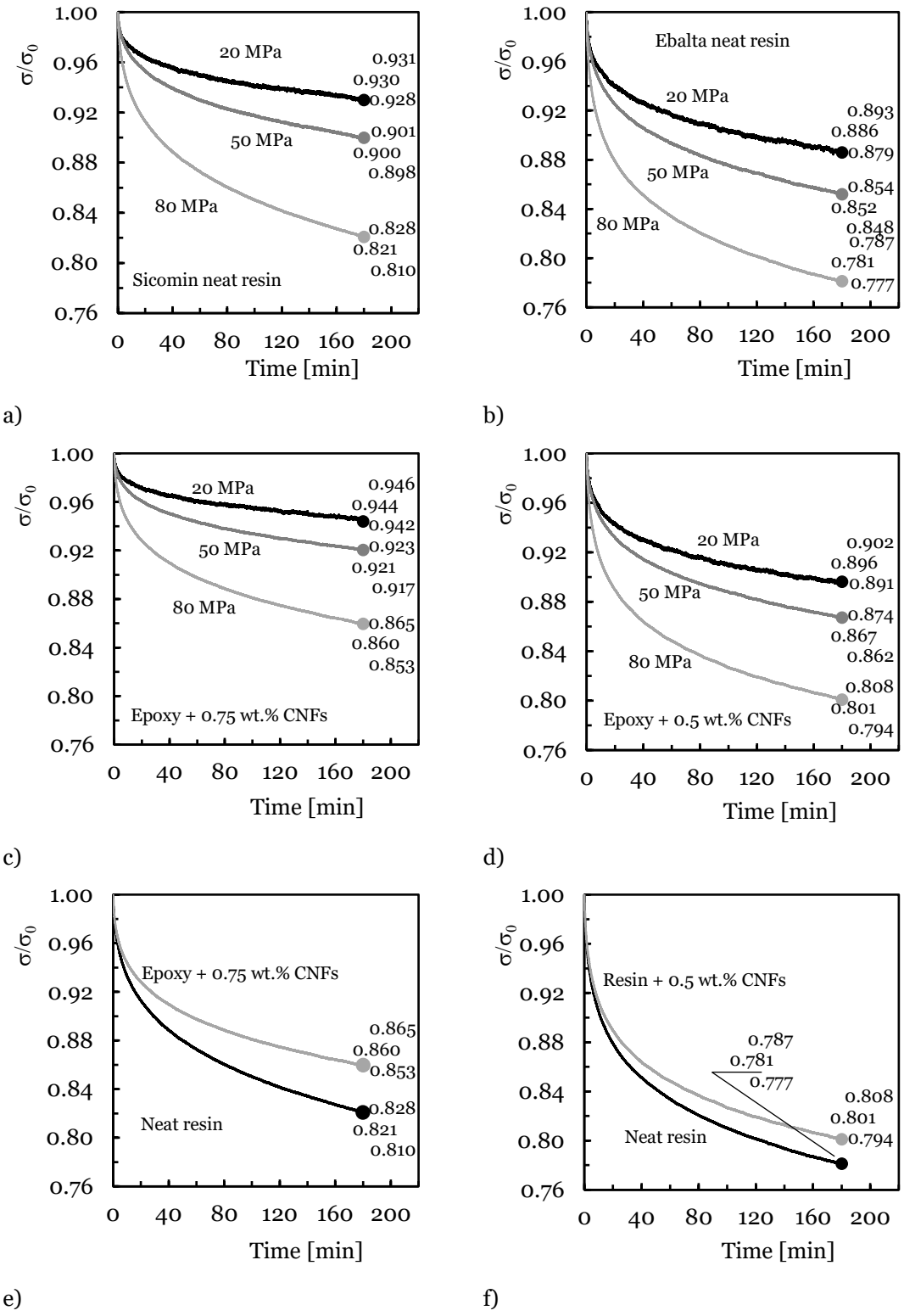

Figure 5.8: Stress relaxation curves for: a) Sicomin neat resin and different bending stresses; b) Ebalta neat resin and different bending stresses; c) Sicomin resin with 0.75 wt.% of CNFs and different bending stresses; d) Ebalta resin with 0.5 wt.% of CNFs and different bending stresses; e) Sicomin neat resin and with 0.75 wt.% of CNFs for bending stress of 80 MPa; f) Ebalta neat resin and with 0.5 wt.% of CNFs for bending stress of 80 MPa.

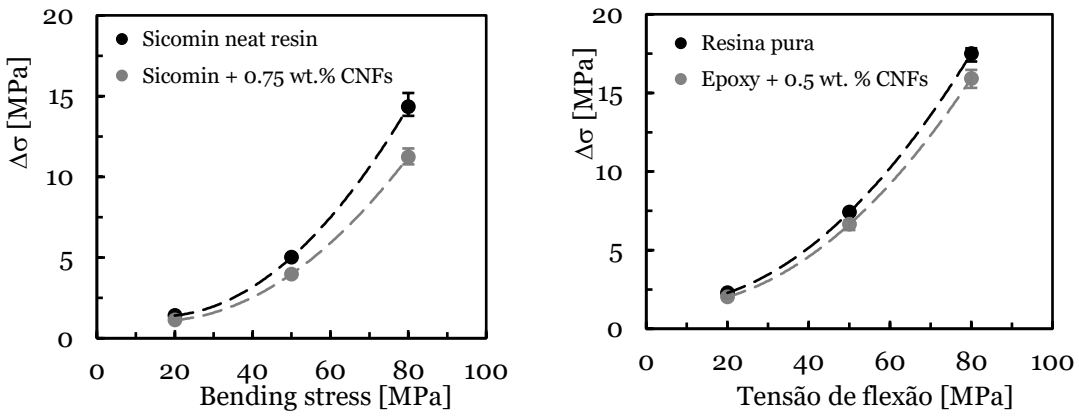

a) b)

Figure 5.9: Difference between initial and final bending stress for: a) Sicomin resin; b) Ebalta resin.

Literature reports several models to predict the viscoelastic response from short-term tests. In terms of creep, Findley's law is widely used to describe the creep response of composite materials [40,48–50] and can even be supported by short-term tests [50–52]. The Findley law is given by:

$$\varepsilon(t) = \varepsilon_0 + At^n \tag{5.4}$$

where $\varepsilon(t)$ is the creep displacement at time, t, ε_0 is the instantaneous elastic displacement, A is the amplitude of transient creep (time-dependent) and n is a constant independent of the stress and generally less than one [52]. All parameters were obtained according to the recommendations of Gupta and Lahiri [51]. However, some studies show that the KWW model estimates the creep response better than the Findley model [23,53]. In this case, for comparability, this model will also be analysed, which is given by the following equation:

$$\varepsilon(t) = \varepsilon_0 e^{\left(\frac{t}{\tau}\right)^{\beta}} \tag{5.5}$$

where $\varepsilon(t)$ is the creep displacement at time, t, ε_0 is the initial displacement when a constant stress is applied, β parameter is the distribution factor related to the breadth of the distribution of creep times, and τ accounts for the mean creep time.

Figure 5.10 compares the experimental results with those obtained by the two models and evaluates the accuracy of each one in predicting results. Although the illustrated results refer to Ebalta resin filled with CNFs, they replicate what was observed for the other materials studied. Tables 5.1 and 5.2 present the parameters of each model for all conditions analysed and the accuracy of each model in relation to the experimental results. Therefore, from Figure 5.10.a), it is possible to observe both models fit the experimental data successfully, denoting a maximum error of less than 0.5%. Furthermore, from Tables 5.1 and 5.2, it is possible to conclude the maximum error observed for all conditions studied after 180 min of testing is 2.75%, which evidences the good accuracy obtained.

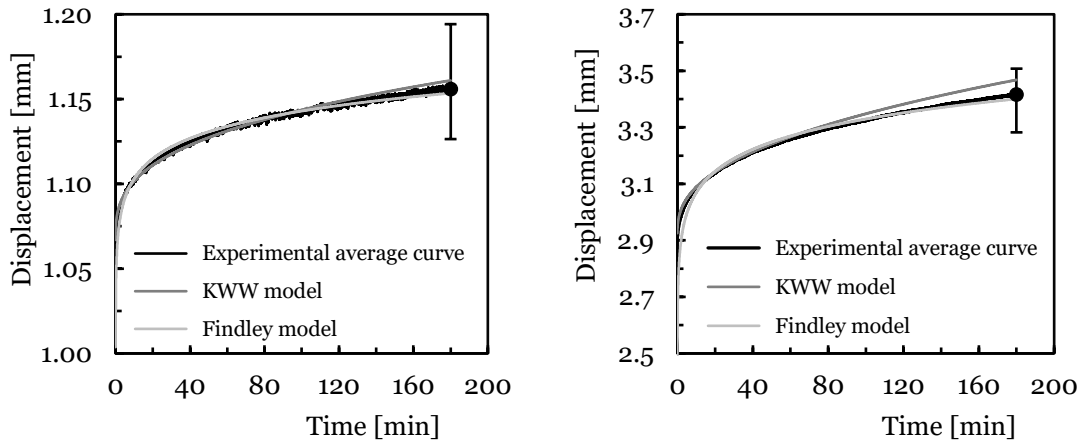

a) b)

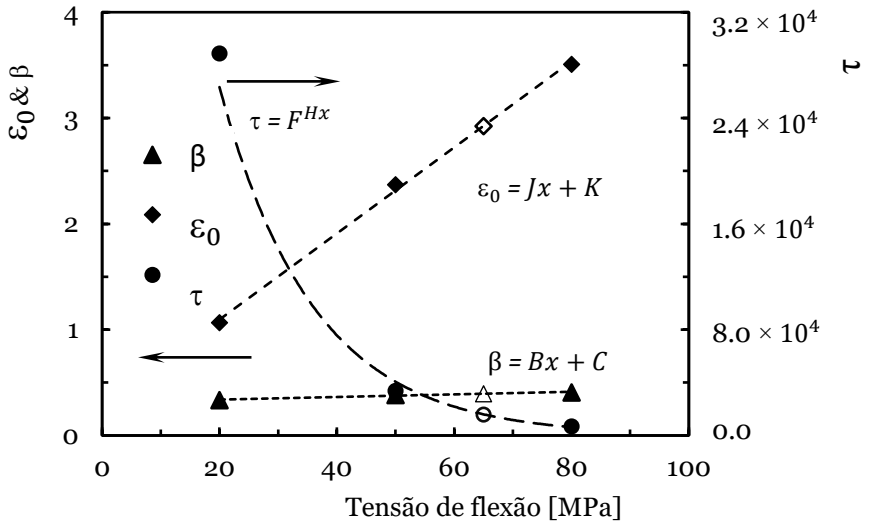

c)

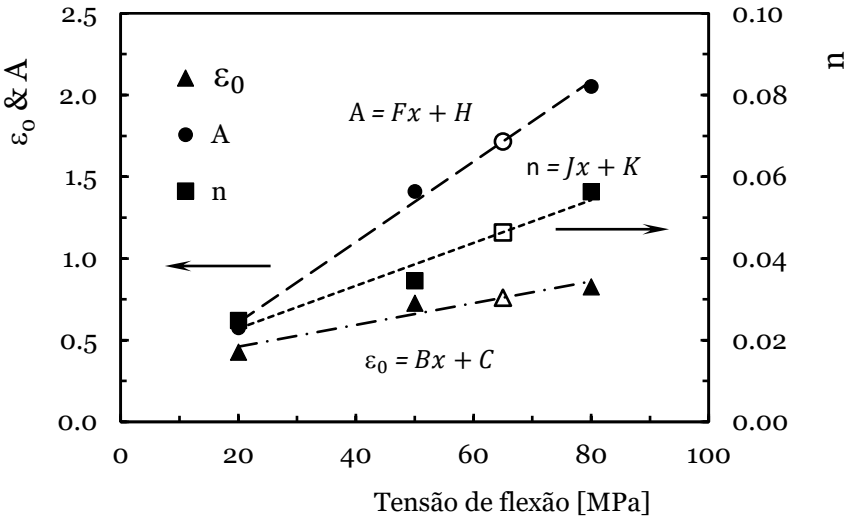

d)

Figure 5.10: a) Comparison between the experimental and theoretical curves for Ebalta resin with 0.5 wt.% of CNFs and bending stress of 20 MPa; b) Model validation for the same material and bending stress of 65 MPa; c) KWW parameters versus bending stress; d) Findley parameters versus bending stress.

Table 5.1: KWW model parameters for creep.

Bending stress [MPa]	ε_0	β	τ	Displacement after 3 hours [mm]		
				Experimental value	KWW value	Error [%]
Sicomin resin						
20	0.892	0.333	1.37×10^{6}	0.936	0.939	0.319
50	2.03	0.392	8.94×10^{4}	2.21	2.22	0.253
80	3.40	0.431	5.12×10^{3}	4.29	4.31	0.409
Sicomin resin + 0.75 wt.% CNFs						
20	0.765	0.318	1.50×10^{6}	0.807	0.809	0.216
50	1.81	0.416	5.44×10^{4}	1.98	1.99	0.437
80	2.86	0.417	4.86×10^{3}	3.64	3.68	0.949
Ebalta resin						
20	1.06	0.362	8.72×10^{4}	1.18	1.18	0.36
50	2.67	0.407	1.27×10^{4}	3.16	3.19	0.954
80	4.02	0.430	1.53×10^{3}	5.83	5.99	2.75
Ebalta resin + 0.5 wt.% CNFs						
20	1.07	0.335	2.89×10^{5}	1.16	1.16	0.444
50	2.37	0.385	3.38×10^{4}	2.68	2.71	0.983
80	3.51	0.409	6.90×10^{3}	4.34	4.39	1.29

Table 5.2: Findley's law parameters for creep.

Bending stress [MPa]	ε_0	A	n	Displacement after 3 hours [mm]		
				Experimental value	Findley value	Error [%]
Sicomin resin						
20	0.406	0.454	0.017	0.936	0.935	0.035
50	0.979	0.873	0.037	2.21	2.21	0.253
80	0.780	1.913	0.063	4.29	4.22	1.67
Sicomin resin + 0.75 wt.% CNFs						
20	0.368	0.367	0.019	0.807	0.806	0.135
50	0.822	0.847	0.033	1.98	1.97	0.600
80	0.792	1.477	0.069	3.64	3.60	1.27
Ebalta resin						
20	0.414	0.563	0.032	1.18	1.17	0.418
50	0.796	1.500	0.048	3.16	3.13	0.829
80	0.932	2.042	0.091	5.83	5.71	2.087
Ebalta resin + 0.5 wt.% CNFs						
20	0.427	0.576	2.49×10^{-2}	1.16	1.15	0.203
50	0.726	1.410	3.45×10^{-2}	2.68	2.67	0.536
80	0.827	2.053	5.63×10^{-2}	4.34	4.29	1.049

Table 5.3: Values of the equations that fit the KWW model.

Material	ε_0			β			τ		
	B	*C*	*R*	*F*	*H*	*R*	*J*	*K*	*R*
Sicomin									
Neat resin	0.042	0.018	0.997	1.64×10^{-3}	0.304	0.993	9.01×10^{6}	-0.093	0.999
Resin + 0.75 wt.% CNFs	0.035	0.069	0.999	1.64×10^{-3}	0.301	0.869	8.74×10^{6}	-0.096	0.996
Ebalta									
Neat resin	0.049	0.120	0.999	1.13×10^{-3}	0.343	0.982	3.46×10^{5}	-0.067	0.999
Resin + 0.5 wt.% CNFs	0.041	0.282	0.999	1.24×10^{-3}	0.314	0.980	9.15×10^{5}	-0.062	0.999

R = Correlation coefficient.

Table 5.4: Values of the equations that fit the Findley model.

Material	ε_0			A			n		
	B	*C*	*R*	*F*	*H*	*R*	*J*	*K*	*R*
Sicomin									
Neat resin	6.24×10^{-3}	0.410	0.643	0.024	-0.136	0.971	7.77×10^{-4}	3.26×10^{-5}	0.997
Resin + 0.75 wt.% CNFs	7.06×10^{-3}	0.308	0.834	0.018	-0.028	0.997	8.35×10^{-4}	-1.43×10^{-3}	0.969
Ebalta									
Neat resin	8.64×10^{-3}	0.282	0.964	0.025	0.136	0.988	9.85×10^{-4}	7.98×10^{-3}	0.964
Resin + 0.5 wt.% CNFs	6.66×10^{-3}	0.327	0.961	0.025	0.116	0.997	5.24×10^{-4}	1.24×10^{-2}	0.976

R = Correlation coefficient.

Other evidence taken from these tables is that the most significant errors occur for the highest level of the applied load. Subsequently, to predict the creep response for any bending stress, Figures 5.10.c), 5.10.d) show the parameters of both models versus bending stress for the Ebalta resin with CNFs, and the value of 65 MPa (corresponding to the white marks) to validate the proposed methodology. For the other materials, Tables 5.3 and 5.4 present the respective parameters of each equation. Considering the parameters shown in Figures 5.10.c), 5.10.d) and the respective values presented in Tables 5.3 and 5.4 for 65 MPa, it is possible to obtain the respective values of the equations to predict the creep response. In this case, the following values were obtained: $\varepsilon_0 = 2.93$, $\beta = 0.395$, and $\tau = 1.60 \times 10^4$ for the KWW model and $\varepsilon_0 = 0.760$, $A = 1.716$, and $n = 4.64 \times 10^{-2}$ for the Findley model, and the estimated curves are compared with the experimental ones in Figure 5.10.b).

It is possible to observe both models estimate the bending stress effect on the creep behaviour with good accuracy. After 180 min of testing, the maximum error obtained with the KWW model is 1.5%, overestimating the creep response, and 0.5% for the Findley model. However, for all materials, the maximum error obtained is 4.8% where the Findley model presented the lowest value. Nevertheless, when these models are used to predict long-term creep responses, Figure 5.11 compares the estimated curves with those obtained experimentally. In this case, 100 hours of testing was considered, a value 33 times more than that used in the short-term tests. Although

this comparison is made for Ebalta resin with 0.5 wt.% of CNFs and bending stress of 65 MPa, it is representative of the others.

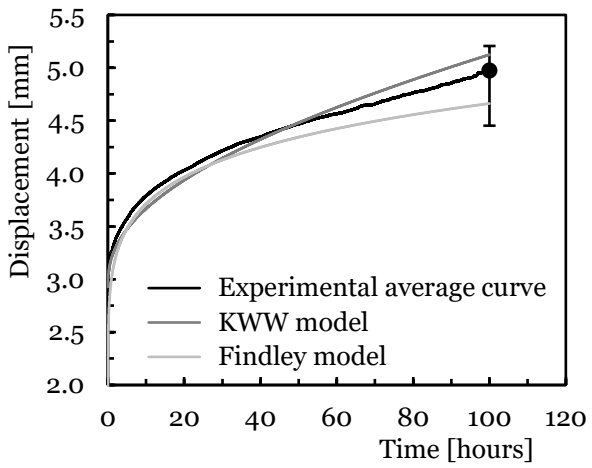

Figure 5.11: Models' validation for 100 hours (Ebalta resin with 0.5 wt.% of CNFs and bending stress of 65 MPa.

It is possible to observe both models present good accuracy in predicting the creep response after 100 hours because the theoretical results obtained are within the dispersion bands resulting from the experimental tests. The errors obtained are around 6.3% obtained with the Findley model and 3% with the KWW model, and while the latter overestimates the experimental result, the Findley model underestimates them. Therefore, the KWW model is more conservative and seems to present better accuracy in relation to the experimental results for longer lives.

In terms of stress relaxation, literature reports several models, but more complex ones than those based on spring-dashpot systems are preferable to obtain predictions with better accuracy [54]. Although the constants have no physical meaning, the Kohlrausch-Williams-Watts model (KWW) can describe the experimental curves very accurately, and it can be used to predict the stress-relaxation response for longer lives [44,55,56]. In this case, the relaxation function ϕ is given by:

$$\phi(t) = \frac{\sigma(t)}{\sigma_0} = e^{-\left(\frac{t}{\tau}\right)^{\beta}} \tag{5.6}$$

where $\sigma(t)$ and σ_0 are, respectively, the stress at time, t, and at t = 0, β is the fractional power exponent, and τ is the KWW relaxation time. In this context, Figure 5.12 compares the experimental and theoretical curves using the KWW model to evaluate its accuracy.

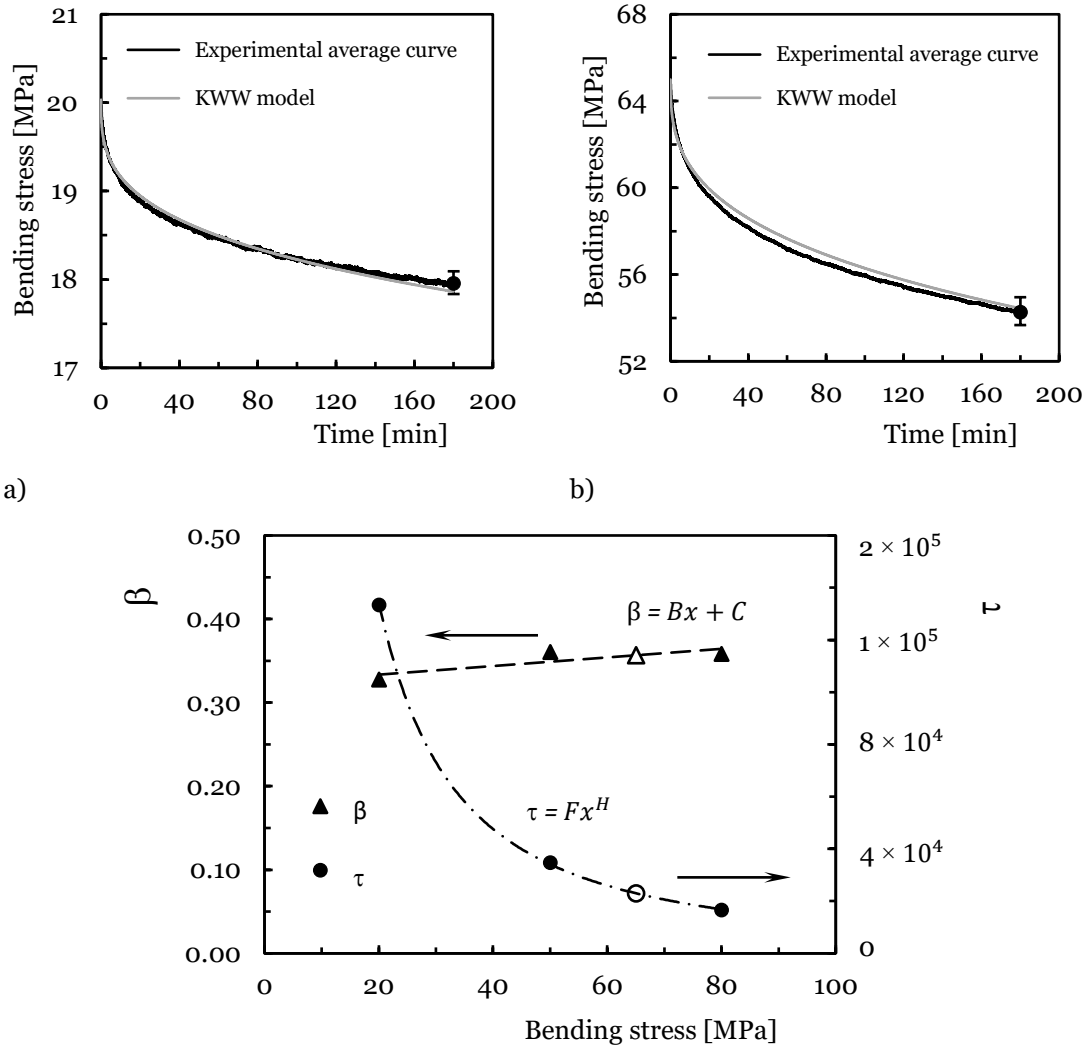

Figure 5.12: a) Comparison between experimental and theoretical curves for Ebalta resin with 0.5 wt.% of CNFs and bending displacement corresponding to a bending stress of 20 MPa; b) model validation for the same material and bending displacement corresponding to a bending stress of 65 MPa; c) KWW parameters versus bending stress that correspond to the bending displacements studied.

It is shown the results for Ebalta resin with 0.5 wt.% of CNFs and for the bending displacement corresponding to bending stress of 20 MPa, but they are representative of the other materials studied. Tables 5.5 and 5.6 present the parameters of the model for all conditions analysed and the accuracy of the model in relation to the experimental results. Therefore, from Figure 5.12.a), it is possible to observe a good accuracy where the error between theoretical and experimental curves is only about 0.52% after 180 min of testing. Considering all materials and conditions, from Table 5.5 it is possible to observe the maximum error is less than 1.3%, which confirms the good accuracy reported above. In addition, to predict the stress relaxation response for any bending displacement, Figure 5.12.c) shows the parameters of the model versus bending stress (corresponding to the analysed bending displacement) for the Ebalta resin with CNFs as well as

the value of 65 MPa (corresponding to the white marks) to validate the prediction. The values of the equations used to predict the stress-relaxation response are shown in Table 5.6.

Table 5.5: Parameters of the KWW model for stress relaxation.

Initial bending stress [MPa]	β	τ	Bending stress after 3 hours [MPa]		
			Experimental value	KWW value	Error [%]
Sicomin neat resin					
20	0.321	6.36×10^{5}	18.62	18.63	0.012
50	0.388	5.56×10^{4}	45.07	44.90	0.378
80	0.394	1.15×10^{4}	66.24	65.88	0.554
Sicomin resin + 0.75 wt.% CNFs					
20	0.312	1.86×10^{6}	18.94	18.97	0.163
50	0.360	1.69×10^{5}	46.07	45.96	0.225
80	0.361	3.04×10^{4}	68.64	68.36	0.059
Ebalta neat resin					
20	0.338	8.57×10^{4}	17.73	17.68	0.299
50	0.376	2.12×10^{4}	42.59	42.33	0.622
80	0.349	8.60×10^{3}	62.47	61.69	1.255
Ebalta resin + 0.5 wt.% CNFs					
20	0.328	1.33×10^{5}	17.96	17.86	0.520
50	0.361	3.48×10^{4}	43.32	43.01	0.523
80	0.359	1.66×10^{4}	66.28	65.66	0.934

Table 5.6: Values of the equations that fit the KWW model.

Material	β			τ		
	B	*C*	*R*	*F*	*H*	*R*
Sicomin						
Neat resin	1.21×10^{-3}	0.307	0.897	2.10×10^{6}	-0.067	0.994
Epoxy + 0.75 wt.% CNFs	8.16×10^{-4}	0.304	0.874	6.55×10^{6}	-0.069	0.995
Ebalta						
Neat resin	1.73×10^{-3}	0.345	0.270	1.19×10^{7}	-1.64	0.998
Epoxy + 0.5 wt.% CNFs	5.14×10^{-4}	0.323	0.838	1.19×10^{7}	-1.49	1.000

R = Correlation coefficient.

Therefore, the following values were used to compare the theoretical results with the experimental ones: β = 0.357, and τ = 2.30×10^{4}. This comparison shown in Figure 5.12.b) reveals a good accuracy where the error for this condition is about 0.32%, but considering all materials, the maximum error observed is less than 3.6%.

Finally, when this model is used to predict the long-term stress-relaxation response, Figure 5.13 confirms its accuracy by showing the error between the theoretical and experimental values is only 4.9%. Furthermore, the predicted values at the end of 100 hours of testing are within the scatter bands, which represent the respective maximum and minimum values obtained from the experimental tests. Therefore, this evidence solidifies the conclusion that the models predict quite well the viscoelastic response of the materials and can be used with good accuracy.

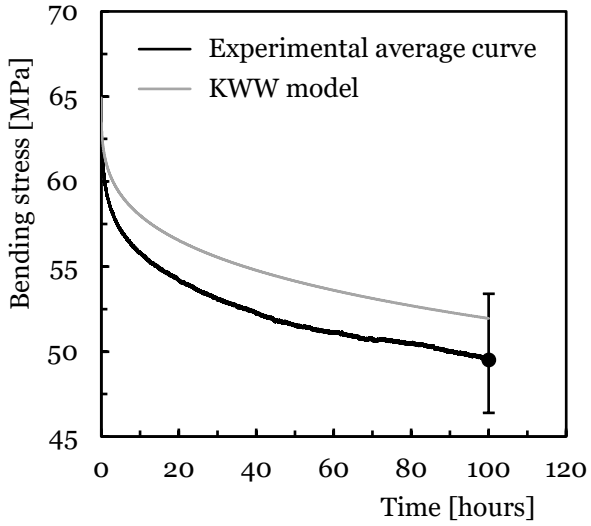

Figure 5.13: Validation of the model for 100 hours and for Ebalta resin with 0.5 wt.% of CNFs and bending displacement corresponding to bending stress of 65 MPa.

Therefore, the benefits observed with nano-reinforced resins is extremely important because these systems can be transferred to composites where the matrix is the phase with the lowest mechanical performance. This is not only evident for the response to static loads but also for the viscoelastic behaviour of structures/components produced by composite materials. It is conveniently reported in the literature that when the fibres are incorporated into the matrix, they hinder the molecular flow and consequently, delay its viscoelastic response. Regardless of this fact and due to the inherent viscoelasticity of the matrix phase, polymeric composites are prone to creep and stress relaxation, becoming a major challenge when used in long-term applications. However, from this study, it is evident the presence of CNFs delays the viscoelastic response of the resins because they act as a network that contributes to the immobility of the polymeric chains and consequently, decreases the viscoelastic response of the composite materials. Finally, the methodology based on the KWW model presented in this study proves to be effective in predicting the viscoelastic response for long-term applications of structures/components produced by composite materials.

5.4. Conclusions

The main goal of this study is to evaluate the benefits of resins reinforced with carbon nanofibres, and for this purpose, two resins with different viscosities were used.

The static-bending performance showed in both cases, higher values of CNFs added to the resins promoted higher bending stress and modulus; however, an ideal value was observed that maximized these properties. While the optimum weight content was 0.75% for Sicomin SR 8100 resin, for Ebalta AH 150 it was 0.5 wt.%. In addition, the highest bending stress and modulus were obtained with the lower viscosity resin (Ebalta resin) because it promoted a better organization of the nanoparticles. On the other hand, it would be expected the resin with higher viscosity would maximize its mechanical properties for lower filler contents, but the compatibility between the properties of the nanoparticles and matrix significantly influenced the interfacial strength and dispersibility of the fillers.

In terms of creep behaviour and stress relaxation, both phenomena were shown to be strongly dependent on the applied load level. Furthermore, because the study was based on short-term tests, the creep tests presented only the first two regimes, and in the case of the relaxation tests, the stress decrease never reached a constant value for the period under study. However, regardless of the resin, the benefits obtained with the nano-reinforcements were evident because CNFs act as a network that contributes to the immobility of the polymer chains. Finally, for both creep and stress-relaxation behaviour, the results were adjusted following the Kohlrausch–Williams–Watts model, evidencing a good accuracy of the model for longer times in both cases. However, for shorter times, the Findley model shows higher accuracy to estimate the creep behaviour.

Bibliography

[1] Jin F-L, Li X, Park S-J. Synthesis and application of epoxy resins: A review. Journal of Industrial and Engineering Chemistry 2015;29:1–11. https://doi.org/10.1016/j.jiec.2015.03.026.

[2] Higgins C, Cahill J, Jolanki R, Nixon R. Epoxy Resins. Kanerva's Occupational Dermatology, vol. 11, Cham: Springer International Publishing; 2018, p. 1–43. https://doi.org/10.1007/978-3-319-40221-5_51-2.

[3] Pina dos Santos PS, Maceiras A, Valvez S, Reis PNB. Mechanical characterization of different epoxy resins enhanced with carbon nanofibers. Frattura Ed Integrità Strutturale 2020;15:198–212. https://doi.org/10.3221/IGF-ESIS.55.15.

[4] Hsieh TH, Kinloch AJ, Masania K, Taylor AC, Sprenger S. The mechanisms and mechanics of the toughening of epoxy polymers modified with silica nanoparticles. Polymer 2010;51:6284–94. https://doi.org/10.1016/j.polymer.2010.10.048.

[5] Cho J, Joshi MS, Sun CT. Effect of inclusion size on mechanical properties of polymeric composites with micro and nano particles. Composites Science and Technology 2006;66:1941–52. https://doi.org/10.1016/j.compscitech.2005.12.028.

[6] Bazrgari D, Moztarzadeh F, Sabbagh-Alvani AA, Rasoulianboroujeni M, Tahriri M, Tayebi L. Mechanical properties and tribological performance of epoxy/Al2O3 nanocomposite. Ceramics International 2018;44:1220–4. https://doi.org/10.1016/j.ceramint.2017.10.068.

[7] Eskizeybek V, Ulus H, Kaybal HB, Şahin ÖS, Avcı A. Static and dynamic mechanical responses of CaCO3 nanoparticle modified epoxy/carbon fiber nanocomposites.

Composites Part B: Engineering 2018;140:223–31. https://doi.org/10.1016/j.compositesb.2017.12.013.

[8] Singh SK, Singh S, Kohli R, Jain A, Kumar A. Effect of TiO2 dispersion on mechanical properties of epoxy polymer. AIP Conference Proceedings 2016;1728. https://doi.org/10.1063/1.4946637.

[9] Yadav PS, Purohit R, Kothari A. Study of friction and wear behaviour of epoxy/nano SiO2 based polymer matrix composites-A review. Materials Today: Proceedings 2019;18:5530–9. https://doi.org/10.1016/j.matpr.2019.07.666.

[10] Molina J, Szczucka-Lasota B, Węgrzyn T, P. Silva A, Maceiras A. Manufacturing and characterization of epoxy resin with Fe3O4 and SiO2 particles. KnE Engineering 2020;2020:117–28. https://doi.org/10.18502/keg.v5i6.7026.

[11] Sun T, Fan H, Wang Z, Liu X, Wu Z. Modified nano Fe2O3-epoxy composite with enhanced mechanical properties. Materials and Design 2015;87:10–6. https://doi.org/10.1016/j.matdes.2015.07.177.

[12] Liu S, Chevali VS, Xu Z, Hui D, Wang H. A review of extending performance of epoxy resins using carbon nanomaterials. Composites Part B: Engineering 2018;136:197–214. https://doi.org/10.1016/j.compositesb.2017.08.020.

[13] Kausar A, Rafique I, Muhammad B. Review of Applications of Polymer/Carbon Nanotubes and Epoxy/CNT Composites. Polymer - Plastics Technology and Engineering 2016;55:1167–91. https://doi.org/10.1080/03602559.2016.1163588.

[14] Zhang B, Zheng X, Li H, Lin J. Analytica Chimica Acta Application of carbon-based nanomaterials in sample preparation : A review. Analytica Chimica Acta 2013;784:1–17. https://doi.org/10.1016/j.aca.2013.03.054.

[15] Huang J, Liu Y, You T. Carbon nanofiber based electrochemical biosensors: A review. Analytical Methods 2010;2:202–11. https://doi.org/10.1039/b9ay00312f.

[16] Feng L, Xie N, Zhong J. Carbon Nanofibers and Their Composites: A Review of Synthesizing, Properties and Applications. Materials 2014;7:3919–45. https://doi.org/10.3390/ma7053919.

[17] Meek N, Penumadu D, Hosseinaei O, Harper D, Young S, Rials T. Synthesis and characterization of lignin carbon fiber and composites. Composites Science and Technology 2016;137:60–8. https://doi.org/10.1016/j.compscitech.2016.10.016.

[18] Lee KM, Lee SE, Lee YS. Improved mechanical and electromagnetic interference shielding properties of epoxy composites through the introduction of oxyfluorinated multiwalled carbon nanotubes. Journal of Industrial and Engineering Chemistry 2017;56:435–42. https://doi.org/10.1016/j.jiec.2017.08.001.

[19] Santos P, Maceiras A, Reis PNB. Influence of manufacturing parameters on the mechanical properties of nano-reinforced CFRP by carbon nanofibers. IOP Conference Series: Materials Science and Engineering 2021;1126:012012. https://doi.org/10.1088/1757-899X/1126/1/012012.

[20] Shokrieh MM, Esmkhani M, Vahedi F, Shahverdi HR. Improvement of mechanical and electrical properties of epoxy resin with carbon nanofibers. Iranian Polymer Journal 2013;22:721–7. https://doi.org/10.1007/s13726-013-0170-2.

[21] Sun L-H, Ounaies Z, Gao X-L, Whalen CA, Yang Z-G. Preparation, Characterization, and Modeling of Carbon Nanofiber/Epoxy Nanocomposites. Journal of Nanomaterials 2011;2011:1–8. https://doi.org/10.1155/2011/307589.

[22] Chen DL, Yang PF, Lai YS. A review of three-dimensional viscoelastic models with an application to viscoelasticity characterization using nanoindentation. Microelectronics Reliability 2012;52:541–58. https://doi.org/10.1016/j.microrel.2011.10.001.

[23] Reis PNB, Silva MP, Santos P, Parente JM, Bezazi A. Viscoelastic behaviour of composites with epoxy matrix filled by cork powder. Composite Structures 2020;234:111669. https://doi.org/10.1016/j.compstruct.2019.111669.

[24] Farzaneh A, Rostami A, Nazockdast H. Mono-filler and bi-filler composites based on thermoplastic polyurethane, carbon fibers and carbon nanotubes with improved physicomechanical and engineering properties. Polymer International 2022;71:232–42.

https://doi.org/10.1002/pi.6314.

[25] Rana S, Alagirusamy R, Joshi M. Mechanical behavior of carbon nanofibre-reinforced epoxy composites. Journal of Applied Polymer Science 2010;48:n/a-n/a. https://doi.org/10.1002/app.30861.

[26] Oberdisse J. Aggregation of colloidal nanoparticles in polymer matrices. Soft Matter 2006;2:29–36. https://doi.org/10.1039/B511959F.

[27] Padmanabhan V, Frischknecht AL, Mackay ME. Effect of Chain Stiffness on Nanoparticle Segregation in Polymer/Nanoparticle Blends Near a Substrate. Macromolecular Theory and Simulations 2012;21:98–105. https://doi.org/10.1002/mats.201100048.

[28] Zare Y. The roles of nanoparticles accumulation and interphase properties in properties of polymer particulate nanocomposites by a multi-step methodology. Composites Part A: Applied Science and Manufacturing 2016;91:127–32. https://doi.org/10.1016/j.compositesa.2016.10.003.

[29] Ma X, Zare Y, Rhee KY. A Two-Step Methodology to Study the Influence of Aggregation/Agglomeration of Nanoparticles on Young's Modulus of Polymer Nanocomposites. Nanoscale Research Letters 2017;12:621. https://doi.org/10.1186/s11671-017-2386-0.

[30] Shaffer MSP, Fan X, Windle AH. Dispersion and packing of carbon nanotubes. Carbon 1998;36:1603–12. https://doi.org/10.1016/S0008-6223(98)00130-4.

[31] Fiedler B, Gojny FH, Wichmann MHG, Nolte MCM, Schulte K. Fundamental aspects of nano-reinforced composites. Composites Science and Technology 2006;66:3115–25. https://doi.org/10.1016/j.compscitech.2005.01.014.

[32] Zhou TH, Ruan WH, Yang JL, Rong MZ, Zhang MQ, Zhang Z. A novel route for improving creep resistance of polymers using nanoparticles. Composites Science and Technology 2007;67:2297–302. https://doi.org/10.1016/j.compscitech.2007.01.015.

[33] Lim SD, Rhee JM, Nah C, Lee S-H, Lyu M-Y. Predicting the Long-term Creep Behavior of Plastics Using the Short-term Creep Test. International Polymer Processing 2004;19:313–9. https://doi.org/10.3139/217.1826.

[34] Zhang Z, Yang J-L, Friedrich K. Creep resistant polymeric nanocomposites. Polymer 2004;45:3481–5. https://doi.org/10.1016/j.polymer.2004.03.004.

[35] Yang J-L, Zhang Z, Schlarb AK, Friedrich K. On the characterization of tensile creep resistance of polyamide 66 nanocomposites. Part I. Experimental results and general discussions. Polymer 2006;47:2791–801. https://doi.org/10.1016/j.polymer.2006.02.065.

[36] Park B-D, Balatinecz JJ. Short term flexural creep behavior of wood-fiber/polypropylene composites. Polymer Composites 1998;19:377–82. https://doi.org/10.1002/pc.10111.

[37] Houshyar S, Shanks RA, Hodzic A. Tensile creep behaviour of polypropylene fibre reinforced polypropylene composites. Polymer Testing 2005;24:257–64. https://doi.org/10.1016/j.polymertesting.2004.07.003.

[38] Wang W-H, Huang H-B, Du H-H, Wang H. Effects of fiber size on short-term creep behavior of wood fiber/HDPE composites. Polymer Engineering & Science 2015;55:693–700. https://doi.org/10.1002/pen.23935.

[39] Jian W, Lau D. Creep performance of CNT-based nanocomposites: A parametric study. Carbon 2019;153:745–56. https://doi.org/10.1016/j.carbon.2019.07.069.

[40] Bouafif H, Koubaa A, Perré P, Cloutier A. Creep behaviour of HDPE/wood particle composites. International Journal of Microstructure and Materials Properties 2013;8:225. https://doi.org/10.1504/IJMMP.2013.055385.

[41] Vlasveld DPN, Bersee HEN, Picken SJ. Creep and physical aging behaviour of PA6 nanocomposites. Polymer 2005;46:12539–45. https://doi.org/10.1016/j.polymer.2005.10.120.

[42] Yang J, Zhang Z, Friedrich K, Schlarb AK. Creep Resistant Polymer Nanocomposites Reinforced with Multiwalled Carbon Nanotubes. Macromolecular Rapid Communications 2007;28:955–61. https://doi.org/10.1002/marc.200600866.

[43] Ferreira JA., Costa JD., Reis PN. Static and fatigue behaviour of glass-fibre-reinforced polypropylene composites. Theoretical and Applied Fracture Mechanics 1999;31:67–74. https://doi.org/10.1016/S0167-8442(98)00068-8.

[44] Reis PNB, Gorbatikh L, Ivens J, Lomov SV. Strain-rate sensitivity and stress relaxation of hybrid self-reinforced polypropylene composites under bending loads. Composite Structures 2019;209:802–10. https://doi.org/10.1016/j.compstruct.2018.11.030.

[45] Varghese S, Kuriakose B, Thomas S. Stress relaxation in short sisal-fiber-reinforced natural rubber composites. Journal of Applied Polymer Science 1994;53:1051–60. https://doi.org/10.1002/app.1994.070530807.

[46] George J, Sreekala MS, Thomas S, Bhagawan SS, Neelakantan NR. Stress relaxation behavior of short pineapple fiber reinforced polyethylene composites. Journal of Reinforced Plastics and Composites 1998;17:651–72. https://doi.org/10.1177/073168449801700704.

[47] Sreekala MS, Kumaran MG, Joseph R, Thomas S. Stress-relaxation behaviour in composites based on short oil-palm fibres and phenol formaldehyde resin. Composites Science and Technology 2001;61:1175–88. https://doi.org/10.1016/S0266-3538(00)00214-1.

[48] Scott DW, Lai JS, Zureick AH. Creep Behavior of Fiber-Reinforced Polymeric Composites: A Review of the Technical Literature. Journal of Reinforced Plastics and Composites 1995;14:588–617. https://doi.org/10.1177/073168449501400603.

[49] Xu Y, Wu Q, Lei Y, Yao F. Creep behavior of bagasse fiber reinforced polymer composites. Bioresource Technology 2010;101:3280–6. https://doi.org/10.1016/j.biortech.2009.12.072.

[50] Georgiopoulos P, Kontou E, Christopoulos A. Short-term creep behavior of a biodegradable polymer reinforced with wood-fibers. Composites Part B: Engineering 2015;80:134–44. https://doi.org/10.1016/j.compositesb.2015.05.046.

[51] Vidya Bhushan Gupta, Lahiri J. Non Linear Viscoelastic Behavior of Polypropylene and Glass Reinforced Polypropylene in Creep. Journal of Composite Materials 1980;14:286–96. https://doi.org/10.1177/002199838001400402.

[52] Almeida JHS, Ornaghi HL, Lorandi NP, Bregolin BP, Amico SC. Creep and interfacial behavior of carbon fiber reinforced epoxy filament wound laminates. Polymer Composites 2018;39:E2199–206. https://doi.org/10.1002/pc.24537.

[53] Reis PNB, Silva MP, Santos P, Parente JM, Valvez S, Bezazi A. Mechanical performance of an optimized cork agglomerate core-glass fibre sandwich panel. Composite Structures 2020;245:112375. https://doi.org/10.1016/j.compstruct.2020.112375.

[54] Vaidyanathan TK, Vaidyanathan J. Validity of predictive models of stress relaxation in selected dental polymers. Dental Materials 2015;31:799–806. https://doi.org/10.1016/j.dental.2015.04.002.

[55] Reis PNB, Neto MA, Amaro AM. Effect of hostile solutions on stress relaxation of carbon/epoxy composites. Polymer Degradation and Stability 2019;165:60–7. https://doi.org/10.1016/j.polymdegradstab.2019.04.026.

[56] Reis PNB, Silva MP, Santos P. Stress Relaxation in Delaminated Carbon/Epoxy Composites. Fibers and Polymers 2019;20:1284–9. https://doi.org/10.1007/s12221-019-8916-x.

Chapter 6

Effect of carbon nanofibres, strain rate, chemical exposure and temperature on bending behaviour and interlaminar shear strength of carbon/epoxy composites[5]

Abstract

The static bending properties, different strain rates and interlaminar shear strength (ILSS) of carbon-fibre-reinforced polymers (CFRPs) with two epoxy resins nano-enhanced with carbon nanofibres (CNFs) are studied. The effect on ILSS behaviour from aggressive environments, such as hydrochloric acid (HCl), sodium hydroxide (NaOH), water and temperature, are also analysed. The laminates with Sicomin resin and 0.75 wt.% CNFs and with Ebalta resin with 0.5 wt.% CNFs show significant improvements in terms of bending stress and bending stiffness, up to 10%. The values of ILSS increase for higher values of strain rate, and in both resins, the nano-enhanced laminates with CNFs show better results to strain-rate sensitivity. A linear relationship between the logarithm of the strain rate was determined to predict the bending stress, bending stiffness, bending strain and ILSS for all laminates. The aggressive solutions significantly affect the ILSS, and their effects are strongly dependent on the concentration. Nevertheless, the alkaline solution promotes higher decreases in ILSS and the addition of CNFs is not beneficial. Regardless of the immersion in water or exposure to high temperatures a decrease in ILSS is observed, but, in this case, CNFs content reduces the degradation of the laminates.

6.1. Introduction

Carbon-fibre-reinforced polymers (CFRPs) are characterized by their low weight, high strength and stiffness and low coefficient of thermal expansion in the fibre direction, making them attractive for a wide range of applications including wind energy generation structures, transportation, aerospace and sports equipment. Superior properties, excellent strength-to-weight ratio and versatility in manufacture/application, particularly in the transport sector, result in reduced energy consumption, which is the main driver for the use of CFRP [1,2].

[5] Based on the work subjected at the Materials journal, Santos, P.; Silva, A.P.; Reis, P.N.B. Effect of Carbon Nanofibers on the Strain Rate and Interlaminar Shear Strength of Carbon/Epoxy Composites. *Materials* **2023**, *16*, 4332, https://doi.org/10.3390/ma16124332

Several methods are used in the manufacture of CFRP for different applications, depending on the final shape, size and geometry of the component or structure. Some of the main methods used to manufacture composites are hand lay-up, vacuum bagging, vacuum-assisted resin transfer moulding (VARTM), vacuum-assisted resin infusion moulding (VARIM), autoclave, compression moulding, pultrusion and filament winding [1–3].

Carbon fibres are an important constituent of CFRP and have played a central role in the production of lightweight high-performance composites due to their inherent properties-high tensile strength, high modulus, low densities, good thermal and electrical conductivity, high thermal and chemical stabilities, low coefficient of thermal expansion, biological compatibility and fatigue resistance-which are imparted into the properties of the final composite [4–6].

As far as the matrix is concerned, the first choice in engineering is epoxy resin, which can be characterized as a molecule containing more than one epoxy group capable of being converted into a thermoset form. It has high electrical resistivity and good performance at elevated temperatures, thanks to both its higher heat deflection temperature and high glass transition temperature (T_g). It also exhibits optimum adhesion to various substrates and to fibres used as reinforcements in composite materials [7,8]. In terms of application, it is very versatile, and for this, epoxy resins are among the mainstream plastic materials for applications such as coatings, adhesives, laminates and structural components. However, when the application is structural, they may prove to be either brittle, notch-sensitive or both. As a result, considerable effort has been devoted to improving the toughness of epoxy resins, particularly in the last two decades [9]. One of their characteristics, especially in the case of low-viscosity liquids, is that their properties can be optimized by mechanical means, as they can be nano-enhanced with nanoparticles.

The reinforcing capacity of nanofibres increases with decreasing their dimensions, i.e., nanofibres have higher reinforcing capacity than microfibres and short fibres due to the increased interfacial area [10,11]. This has the ability to strengthen the fibre/polymer interface and increase matrix stability [12], thereby improving their mechanical, chemical and/or physical properties. Nowadays, the strongest materials available for structural applications are in the form of small particles: nanoparticles (nano-powder, nanoclusters, nanocrystals) are sized less than 100 nm in diameter; nanofibres have diameters less than 100 nm and a high aspect ratio; and nanoplatelets are 2D stacks of nanomaterials that may be made from metals, ceramics or graphene powder (GP).

In addition to being the most expensive, GP is actually the most commonly used in composites manufacturing, for example; it has 1 to 10 nm thick and 1 to 15 μm in diameter, resulting in aspect ratios of up to 1:1000 and surface areas up to 700 m^2/g. Nanocarbon comprises many allotropes; these are the same element, carbon, but with different arrangements of atoms, and include carbon and graphene dots, graphene sheets and platelets, and graphene rolled into high-aspect-ratio carbon nanotubes (CNTs), sphere-like buckyballs/fullerenes and multi-layered nano-onions [13].

On the other hand, carbon nanofibres (CNFs), vapor-grown carbon fibres (VGCFs) or vapor-grown carbon nanofibres (VGCNFs) are cylindrical nanostructures one-dimensional (1D) with graphene layers arranged as stacked cones, cups or plates [14–16]. They contain more reactive carbon edges that can interact with the matrix better, and they are an alternative for manufacturing single-filled, bi-filled and multi-filled synergistic reinforced composite structures for shielding purposes [17]. However, nowadays, CNFs of different morphologies have been synthesized, such as the following: platelet-like CNFs composed of small graphene layers perpendicular to the fibre axis; fishbone-like CNFs or herringbone CNFs where the graphene layers are inclined with respect to the fibril axis; CNFs ribbons are comprised of straight, unrolled graphene layers that are parallel to the fibril axis with noncylindrical cross-sections; stacked-cup CNFs which are a continuous layer of rolled (spiral) graphene along the fibre axis; and thickened tubular CNFs comprising a base structure of one of the previously mentioned catalytic nanofilaments (CNFs or CNTs) with a variable coating of amorphous carbon [18].

CNFs containing carbon with diameters of 50 to 200 nm, with exceptional mechanical and electrical properties, can be prepared mainly by two methods: one is catalytic thermal chemical vapor deposition growth, and the other is electrospinning followed by heat treatment [15,19]; relatively large quantities use a variety of metals either in powder or supported form as catalytic entities. The efficiency of load transfer between nanomaterial and polymer chains is a critical factor for the mechanical properties and consequently for the structural behaviour of the composite. If this transfer is complete and the percentage of nanomaterials dispersed in the polymer is optimized, the behaviour of the composite will be improved due to the increase in its mechanical properties. This enhancement is related to some nano effects of the nanomaterials, such as their high aspect ratio and large interfacial area, which can form a huge interphase between nanomaterials and the matrix and, thus, contribute positively to the load transfer [20].

Numerous studies combine these materials to optimize them, whether for increasingly demanding applications or to replace those already applied. For example, in the investigation by Zhou et al. [21], CNFs were infused in epoxy with a high-intensity ultrasonic irradiation method. The adding of 2.0 wt.% CNFs and using VARTM to produce carbon-fibre-reinforced epoxy composites led to increases of 17.4% in tensile strength and 22.3% in bending strength compared to the control composite. Green et al. [22], applying the VARIM technique, produced laminates of E-glass fibres reinforced with 0.1 wt.% and 1 wt.% of the multiscale fibre-reinforced composites (M-FRCs) based on CNFs dispersed in an epoxy resin. The tests showed that the bending strength increased by 16 and 20%, the modulus increased by 23 and 26% and the ILSS properties increased by 6% and 25%, respectively, for the 0.1 wt.% and 1 wt.% M-FRCs when compared to the control FRCs. Arai et al. [23] produced two types of unidirectional CFRP laminates with interlayers made by CNFs with a volume fraction of about 10%, inserted between the carbon prepregs with sixteen or thirty-two layers using the autoclave technique. The interlaminar strength of unidirectional composites was studied and, by inserting a CNFs interlayer, the critical curve of the damage criterion increased by about 20% in the area where the compression stress acts in the transverse

direction of the beam. In the work by Palmeri et al. [24], 0.69 and 2.0 wt.% CNFs were dispersed in the epoxy matrix phase of carbon-fibre-reinforced composites in unidirectional and quasi-isotropic configurations. Tensile modulus and strength in the quasi-isotropic composites containing CNFs were enhanced without reducing strain to failure, and short-beam shear strength (SBSS) was increased by 15 to 22% with the addition of CNFs in both composite orientations. Bortz et al. [14] dispersed 1 wt.% CNFs in the epoxy matrix first by hand-mixing, and afterwards it was passed through a three-roll calender mill to manufacture a continuous carbon-fibre-reinforced composite via the VARTM technique. Improvements were observed in the bending modulus and bending strength. Tensile failure strain was also found to increase from 10.7% to 11.9%, indicating simultaneous stiffness, strength and toughness enhancements. Zhou et al. [25] used the VARTM technique to fabricate unidirectional carbon/epoxy composites modified with 2.0 wt.% CNFs composites. Composites prepared with CNFs displayed a 15.8% increase in ILSS in comparison to control composites. Ma et al. [26] applied the filtering-membrane-assisted method to obtain composites of carbon/epoxy with high content of CNFs and improve the interlaminar properties. The ILSS of CFRP made by this method increased by up to 55% at 3.0 wt.% CNFs, while the maximum of ILSS increases up to 11% at 1 wt.% CNFs by the no-mem-brane-assisted method. The results of Dhakate et al. [16] indicated that the inclusion of 1.1 wt.% CNFs at the interlaminar region between carbon fibre fabric layers in the epoxy matrix of the carbon laminate improves the mechanical properties compared to control laminate and for higher values of CNFs, the properties are affected. The bending strength increased by 175%, modulus by 200%, and ILSS by 190%. Recently, Senthil et al. [27] in your work CNFs were filled into the glass fibre/unsaturated polyester composite, by a combined hand lay-up technique followed by a filtering membrane vacuum-assisted method. For a concentration of 2 wt.% CNFs reinforcement shows an 89% increase in the ILSS of the composite. The composite with 2 wt.% of CNFs also exhibits enhanced storage elastic modulus and hardness to about 49% and 26%, respectively. In the work by Ramezani et al. [28], cross-ply laminated composite specimens were fabricated with the stacking sequence of [02/906]s using unidirectional E-glass fibres and the effect of adding CNFs on the reduction of matrix cracking was studied. The specimens were tested under tensile loading, and it was concluded that the addition of CNFs fillers into the composite specimens resulted in lower crack densities and less stiffness reduction at certain applied stress levels by adding 0.25 wt.% CNFs into the matrix.

However, due to the rapid growth in the use of composite materials, they can be exposed to a range of corrosive environments and temperature variations during their service life, causing degradation of material properties and affecting their static stability and long-term durability [29–31]. Several immersion aging studies of CFRP composites immersed into water and acidic or alkaline solutions at different temperatures show that degradation adversely affects the mechanical properties and, according to thermal and mechanical analyses, ageing depends on the ageing temperature and the ageing medium, being more pronounced at higher temperatures, mainly in acidic conditions [29,30]. Uthaman et al. [29] attributed the decreases in the properties of the composites to the degradation of the resin matrix and debonding at the fibre–resin

interface. On the other hand, Yang et al. [30] showed that the addition of multi-walled carbon nanotubes (MWCNTs) improves the ageing resistance of CFRPs due to good interfacial interaction and their high barrier property. Nanoclays, in turn, improve the ageing resistance of CFRPs due to their high aspect ratio and moderate interfacial adhesion. In short, CFRPs containing nanofillers reduce the loss of mechanical properties less than pure CFRP. Kojnoková et al. [31] studied how different chemical environments at a given temperature affect the viscoelastic properties of composites when subjected to degradation by immersion and confirmed a synergistic influence caused by degradation changes and a plasticizing effect due to water absorption, which causes a reduction in the modulus of elasticity.

Sinmazçelik et al. [32] studied the ILSS changes in unidirectional carbon-fibre-reinforced polyetherimide (PEI) composites following exposure to various liquid environments, i.e., 0.6 molar NaCl, triple-distilled water (TDW) and petrol, and a temperature of 90 °C for 90 days, highlighting a huge decrease in the results for all samples subjected to liquid environments. For example, the ILSS of control samples was 85.28 MPa, and the results of samples immersed in NaCl environments after 90 days were 63.18 MPa, which represents a decrease of 39.2%. Mahato et al. [33] engaged in various experimental analyses of the effect of thermal shock on ILSS of thermally (above and below the room temperature (RT)) conditioned woven-fabric glass/epoxy and glass/polyester composites, concluding that there is a decrease in ILSS value with an increase in conditioning time. Kopietz et al. [34] studied the impact of different media-water, sodium hydroxide (NaOH) and hydrochloric acid (HCl)-on ILSS of glass-fibre-reinforced plastics (GFRPs), and a negative impact from all media-water, acid and alkaline solutions-was clearly verified on all tested composites.

Zhang et al. [35] studied the influence of environmental factors such as water, seawater, acid, alkali and organic solutions under post-cure and pre-cure curing conditions on the ILSS of cured structural carbon-fibre-reinforced epoxy composite. The results showed a reduction of the ILSS properties, and the control of various contaminants such as water, acids, alkalis, salts and organic solvents can have significant effects on the mechanical performance of laminate composite components during the manufacturing process and their usage. Silva et al. [36] investigated how accelerated ageing under different conditions (distilled water, seawater, UV radiation plus water spray) for up to 3000 h affected SBS of pultruded CFRP rods with epoxy and vinylester matrices. The experimental results showed that resistance SBS was strongly affected by seawater and distilled water ageing. SEM images showed greater fibre/matrix adhesion for the carbon/epoxy composites, extensive degradation and microcracking of the vinylester matrix and debonding of the fibre/matrix interface in the carbon/vinylester rods.

Nowadays, both industry and researchers are faced with new challenges/opportunities on a daily basis. Due to the currently changing climate, the paradigm shift in production/distribution/energy consumption, changes in the way we travel and the need for more protection, both individual and collective, to prevent natural or provoked attacks, the

application/development/optimization of composite materials is topical and requires continuous advancement to respond to all these demands. In the future, advanced materials will be responsible for achieving climate neutrality, thereby boosting the economy through green technologies, the development of sustainable transport and safety in all areas of human endeavor. In this sense, optimized nanocomposite materials will be a very important part of the answer to problems in industrial applications, providing materials that are easier to manufacture in complex shapes, lighter, structurally stronger, corrosion-resistant regardless of the environment, with low thermal conductivity and a longer life cycle, reducing their environmental footprint and recycling issues.

Therefore, in this work, an initial characterization of the static properties in the bending mode of the laminates manufactured with two different epoxy resins will be carried out, and the influence of the strain rate on the mechanical properties is studied, which will allow us to understand the influence of different wt.% CNFs on the composites in response to static demands. The ILSS test will allow us to understand the benefits of adding CNFs and the response of the laminates in terms of adhesion between fibre and matrix. The effect of water temperature, concentration and temperature of HCl and NaOH solutions on ILSS strength after immersion will be analysed.

This study aims to contribute to improving the scientific knowledge of the effect of adding CNFs as a low-cost reinforcement through the application of simple dispersion techniques in composites. It responds to a gap in the literature that does not report studies on the effect of corrosive environments on ILSS strength. Although some studies have investigated the ageing behaviour of CFRP with nanofillers in different solutions, the study of common ageing factors in the industry, such as HCl, NaOH, water and temperature are not frequent. The degradation of the mechanical properties of CFRPs under these different ageing conditions was systematically studied in order to understand their behaviour and mathematical models are proposed to estimate the properties for complementary conditions.

6.2. Materials and methods

6.2.1 Production of composite laminates

Eight plain weaves of carbon fibres at 0 and 90 degrees with 98 ± 4% g/m² in each direction were combined with two different resins (epoxy resin SR 8100 with hardener SD 8824, both supplied by Sicom, Paris, France, and an epoxy resin AH 150 with hardener IP 430, both supplied by Ebalta, Rothenburg, Germany) to produce laminates with overall dimensions of 330 × 330 × t [mm] by hand lay-up technique. After curing, the thickness (h) obtained for each laminate was 1.5 ± 0.1 mm for laminates with Sicomin resin and 1.9 ± 0.1 for the Ebalta resin. The main mechanical and physical properties of the epoxy resins are summarized in Table 6.1, and more details about them can be found in [37]. The systems were placed inside a vacuum bag and subjected to a load of 2.5 kN to obtain a constant fibre volume fraction and uniform laminate thickness. Finally, composites involving the Sicomin matrix were cured at RT for 24 hours and subjected to a post-cure at 40 °C for 24 hours, while those involving the Ebalta matrix were cured

at RT for 48 hours and subjected to a post-cure at 80 °C for 5 hours. During the first 4 hours of the curing process, all composites were subjected to vacuum in order to eliminate any air bubbles.

Table 6.1: Main mechanical and physical properties of the epoxy resins.

Property		Sicomin SR 8100 / SD 8824	Ebalta AH 150/ IP 430
Colour		Light yellow liquid	Opaque
Viscosity (@ 25 °C)	[mPa×s]	285 ± 60	250 ± 50
Density at 20 °C	[g/cm³]	-	1.13 ± 0.02
Modulus of elasticity	[N/mm²]	2970± 280	3400 ± 300
Maximum resistance	[N/mm²]	108 ± 1.1	125 ± 1.2
Elongation at max. load	[%]	4.9 ± 0.2	-
Elongation at break	[%]	11.8± 0.3	5.9 ± 0.1
Charpy impact strength	[kJ/m²]	52 ± 4	60 ± 6
Glass transition/DCC	[°C]	63 ± 3	-
Water absorption 48 hours/70 °C	[%]	1.2 ± 0.2	-

The literature reports that the mechanical properties of commercial resins can be improved by using nano-reinforcements, but this is strongly dependent on the nano-particle content and type of resin [38]. In this context, to evaluate the benefits achieved in terms of bending properties and ILSS, similar composite laminates were produced with different weight contents of CNFs. These values were 0.25, 0.5, 0.75 and 1 wt.%, which are similar to those used by the authors in another study that aimed to maximize the static properties of these nano-reinforced resins [39].

Therefore, in terms of bending response, this study aims to compare the CNFs content that maximized these properties in the commercial resins with that obtained for the composite laminates. In both studies, the CNFs used were supplied by Sigma-Aldrich (Burlington, MA, USA) and are pyrolytically stripped (conical) with an average diameter of 130 nm, a length between 20 and 200 μm and an average specific surface area of 54 m²/g. In terms of manufacturing process, resin and CNFs were initially mixed using a high-speed shear mixer at 1000 rpm at RT for 3 hours, followed by 10 min at 150 rpm for the hardener to disperse into the system. To improve the CNFs dispersion, this process was combined with an ultrasonic bath (with a frequency of 40 kHz). Finally, the system was degassed in a vacuum oven. All this methodology is detailed in [40]. Subsequently, the nano-reinforced resins were combined with the carbon fibre fabrics using the methodology described above and summarized in Figure 6.1.

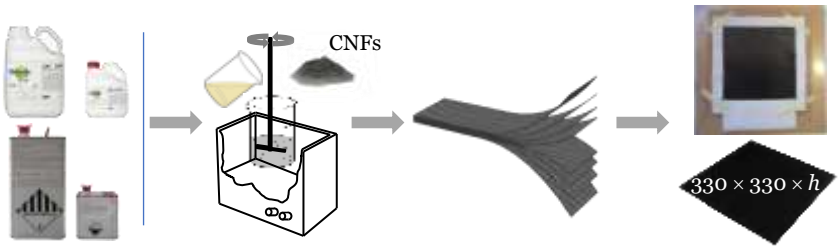

Figure 6.1: Schematic sequence of the manufacturing process of composite laminates with nano-reinforced resins.

6.2.2 Experimental tests

From those laminated plates, two batches of samples were obtained with dimensions of 80 × 10 × h (mm) and 12 × 4 × h (mm) for the bending and interlaminar shear tests, respectively. The static three-point bending (3PB) tests were carried out at RT on a Shimadzu universal testing machine, model Autograph AGS-X (Shimadzu, Kyoto, Japan), equipped with a 10 kN load cell. For each condition, six specimens were tested in accordance with the European Standard EN ISO 178:2003 and at a displacement rate of 2 mm/min. Finally, the bending properties (stress, stiffness and strain) were obtained using the following equations:

$$\sigma = \frac{3\,P\,L}{2\,b\,h^2} \tag{6.1}$$

$$E = \frac{\Delta P\,L^3}{48\,\Delta u\,I} \tag{6.2}$$

$$\varepsilon_f = \frac{6\,S\,h}{L^2} \tag{6.3}$$

where P is the load, L is the span length, b is the width, h is the thickness of the specimen, I is the moment of inertia of the cross-section, ΔP and Δu are, respectively, the load range and bending displacement range in the middle span for an interval in the linear region of the load versus displacement plot and S is the deflexion. The bending modulus was obtained by linear regression of the load-displacement curves considering the interval in the linear segment with a correlation factor higher than 95% [41].

The strain rate effect was analysed only with laminates whose CNFs contents maximized the bending properties and, for this purpose, displacement rates of 200, 20, 2, 0.2 and 0.02 mm/min were used, which correspond to strain rates ($\dot{\varepsilon}$) of 1.2×10^{0}, 1.2×10^{-1}, 1.2×10^{-2}, 1.2×10^{-3} and 1.2×10^{-4} s^{-1} for laminates with a Sicomin matrix and 1.4×10^{-1}, 1.4×10^{-2}, 1.4×10^{-3}, 1.4×10^{-4} and 1.4×10^{-5} s^{-1} for laminates with an Ebalta matrix, values that were obtained by the Equation (6.4):

$$\dot{\varepsilon} = \frac{d\varepsilon_f}{dt} = \frac{6\,V_T\,b}{L^2} \tag{6.4}$$

where $\dot{\varepsilon}$ is the peripheral fibre strain, t is the time, V_T is the crosshead speed, L is the span length and h is the thickness of the specimen.

In terms of ILSS, the short-beam shear (SBS) method is the simplest and most widely used. Therefore, interlaminar shear tests were carried out according to ASTM D2344/D2344M-00 standard using the same equipment (Shimadzu Autograph AGS-X) with a crosshead speed of 1 mm/min. The ILSS value is obtained by Equation (6.5):

$$\tau_S = \frac{3}{4}\frac{P_C}{w\,h} \tag{6.5}$$

where P_C is the maximum load and w and h are, respectively, the width and the thickness of the beam. For each condition, five samples were tested at RT using the same equipment of the 3PB static tests. The nominal dimensions of the specimen for ILSS tests are a length of 12 mm, width (w) and height (h) approximately 4 mm and 2 mm, respectively, and a distance between the supports in the specimens of 10 mm, all a function of the height h of the laminate. The loading rate effect on the ILSS of the laminates was also studied for displacement rates of 0.01, 0.1, 1, 10, 100 and 1000 mm/min.

Figure 6.2 shows the apparatus, schematic view of the tests and respective dimensions of the samples used in the experimental tests.

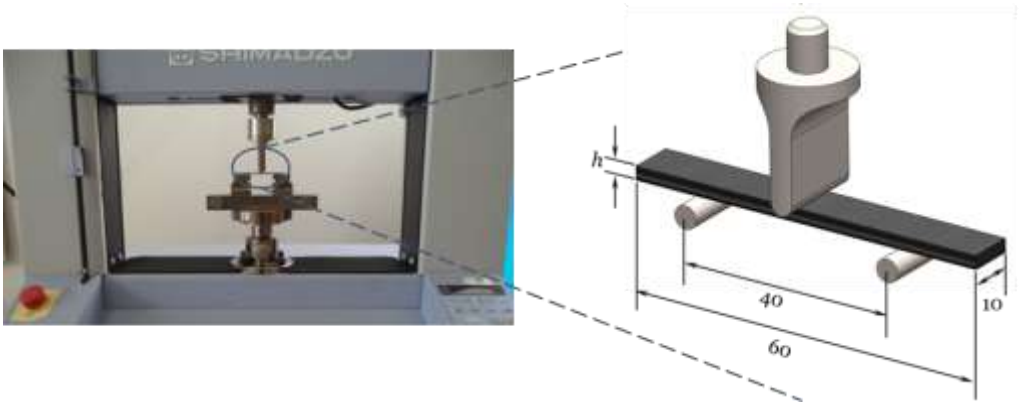

a)

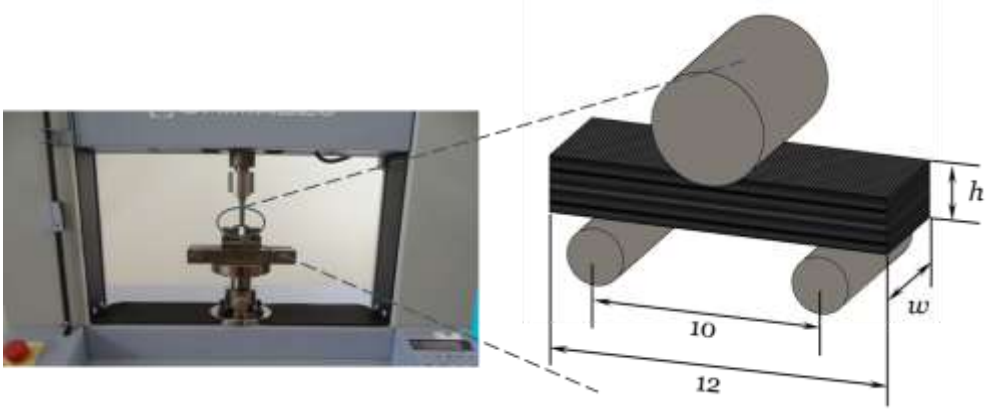

b)

Figure 6.2: Apparatus, schematic view and geometry of the specimens for: a) Three-point bending tests; b) Interlaminar shear tests. All dimensions in mm.

From the batch of samples that were produced for use in the interlaminar shear tests, a part of them was tested as produced, while the other set was immersed into different hostile solutions immediately after production. The hostile solutions selected were HCl and NaOH because they aim to simulate the different environments that can be found in the civil engineering sector or in the chemical and food industry [42] in addition to being among those that most affect the mechanical properties of composite materials [43–45] Therefore, some samples were completely submerged into HCl and NaOH at RT for 20 days. Considering these conditions, concentrations of 5%, 15%, 25% and 35% by weight (wt.%) were analysed for both solutions in order to evaluate

their effect on the ILSS. Finally, the effect of temperature was also analysed and, for this study, the specimens were previously submerged for 20 days at RT, 40 °C and 80 °C into both solutions at a concentration of 15 wt.%. For comparison purposes, some samples were also immersed into distilled water at RT, 40 °C and 80 °C. Finally, before testing, the specimens immersed into the different hostile solutions were washed with clean water and dried at RT.

Table 6.2 summarizes all the tests performed and conditions analysed in this study, while Figure 6.3 schematically shows the methodology adopted to evaluate the effect of different hostile solutions on interlaminar shear strength.

Table 6.2: Summary of all tests performed, and conditions analysed in this study.

Properties/Conditions	Sicomin Resin Reinforced (wt.%)					Ebalta Resin Reinforced (wt.%)				
	0	0.25	0.5	0.75	1	0	0.25	0.5	0.75	1
Static tests										
Bending properties	X	X	X	X	X	X	X	X	X	X
Strain rate effect	X			(a)		X			(a)	
Interlaminar shear tests										
ILSS	X	X	X	X	X	X	X	X	X	X
Strain rate effect	X			(b)		X			(b)	
HCl - concentration effect	X			(b)		X			(b)	
NaOH - concentration effect	X			(b)		X			(b)	
HCl - temperature effect	X			(b)		X			(b)	
NaOH - temperature effect	X			(b)		X			(b)	
Distilled water - temperature effect	X			(b)		X			(b)	

(a) - Only for the CNFs content that maximizes the bending properties. (b) - Only for the CNFs content that maximizes the ILSS.

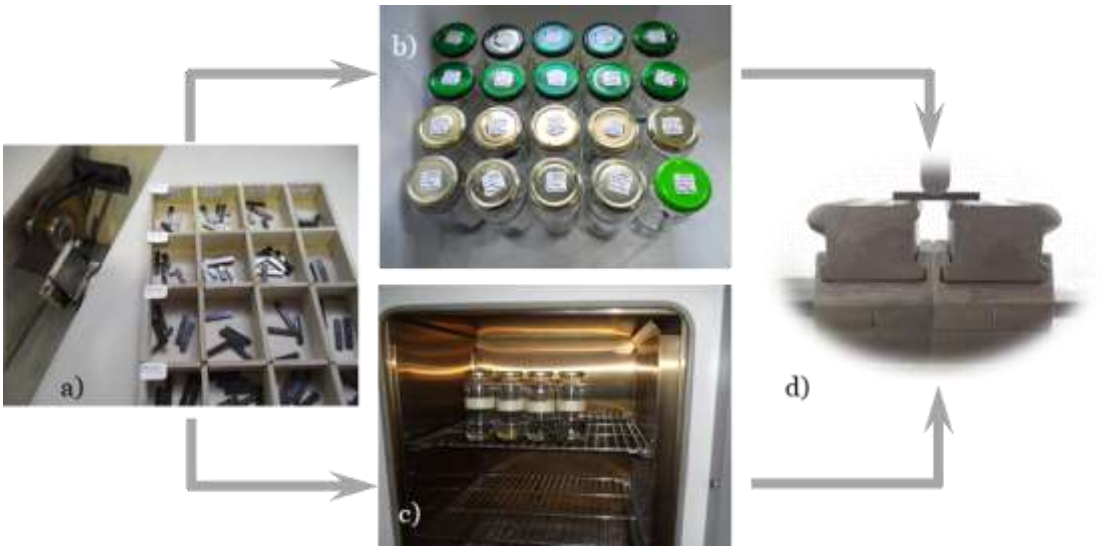

Figure 6.3: a) Specimens after manufacture; b) Specimens immersed into different hostile solutions at RT; c) Oven with specimens inside to study the temperature effect; d) ILSS tests.

6.3. Results and discussion

For all composite laminates produced, 3PB static tests were carried out to evaluate the effect of CNFs content on bending properties. Typical bending stress–strain curves are shown in Figure 6.4, which are representative of all others obtained for the same conditions.

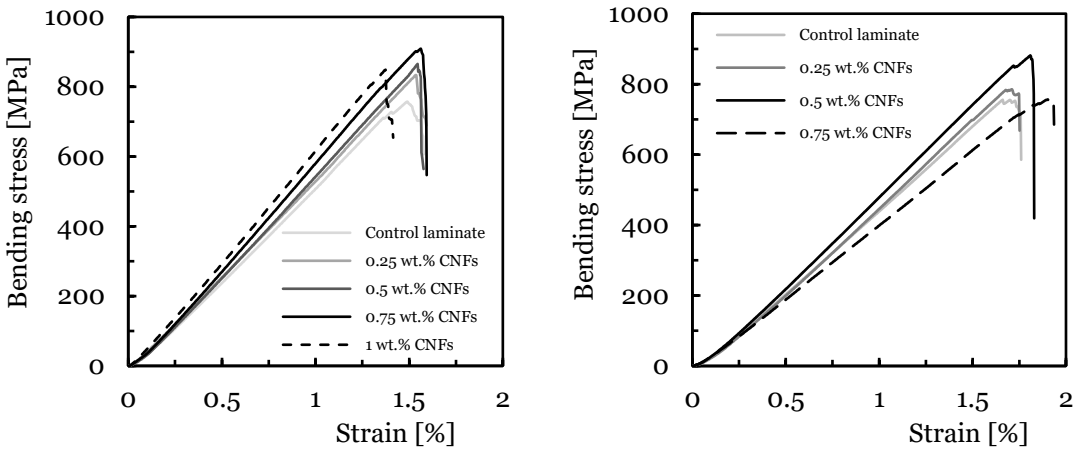

Figure 6.4: Bending stress-strain curves for laminates with: a) Sicomin resin; b) Ebalta resin.

These curves are characterized by a linear increase in bending stress with bending strain (linear elastic region) close to the maximum bending load, followed by an abrupt decrease due to the imminent collapse of the laminates. Figure 6.5 shows the typical damage mechanism observed in all composites, where broken fibres under compression are notorious, accompanied by small delamination's around them. The zigzag aspect observed in some curves is due to progressive breakage of various fibres, while the others show an abrupt collapse due to instantaneous breakage of a significant number of fibres under compression. In fact, it has been reported in the literature that this failure mode is typical of composites containing carbon fibres [46,47] due to the low compressive strength of these fibres. In addition, the high stress concentration that occurs in the contact region with the load pin leads to higher local compressive stresses and, consequently, higher propensity for an imminent collapse [46].

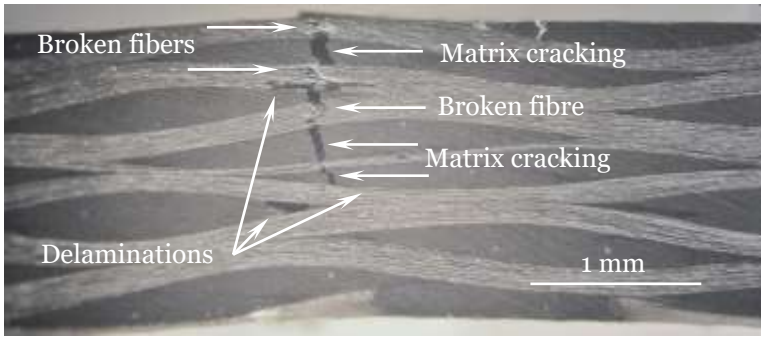

Figure 6.5: Typical failure mode observed for all composites.

Therefore, the main bending properties were obtained from the curves shown in Figure 6.4 and summarized in Figure 6.6 for both resins. Regarding laminates produced with Sicomin resin (Figure 6.6.a), the maximum bending strength (905.3 MPa) is reached for 0.75 wt.% of CNFs, which is 20.4% higher than that obtained for the control samples (752.2 MPa). When the filler content increases up to 1 wt.%, the bending strength decreases to 874.8 MPa. Similar behaviour occurs for laminates produced with Ebalta resin but, in this case, the maximum bending strength (850.9 MPa) is reached for 0.5 wt.% of CNFs and is 12.5% higher than the value obtained for the control samples (756.2 MPa). Concerning the bending modulus, an increase in stiffness (13.8%) is observed with the increase in filler content for laminates with Sicomin resin (from neat resin to 1 wt.% of CNFs), while for laminates with Ebalta resin the maximum bending modulus is reached at 0.5% and is 8.8% higher than the value obtained for the control samples (47.5 GPa). However, when comparing the bending modulus for the maximum bending strength of both laminates, the value obtained for the one produced with Sicomin resin is 18.8% higher than the one produced with Ebalta resin. Finally, as expected, the bending strain decreases with increasing filler content for both resins.

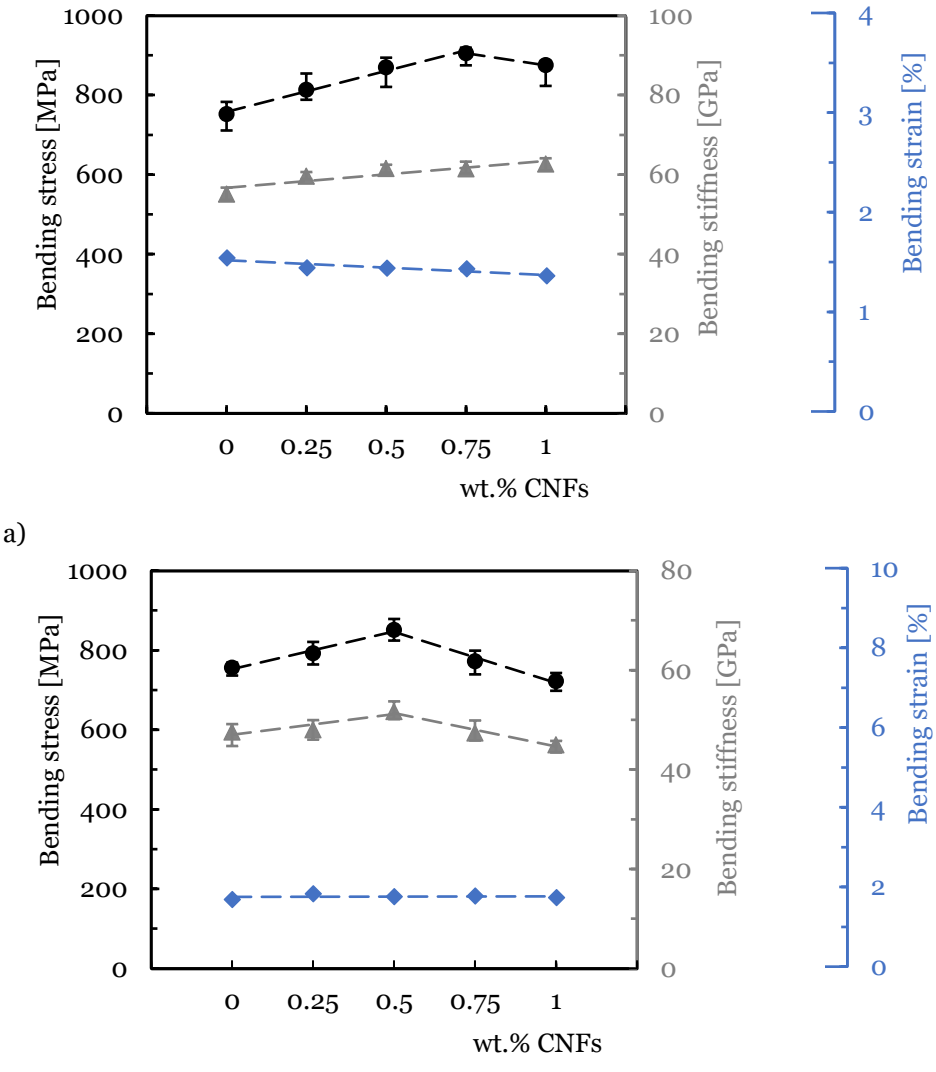

Figure 6.6: Bending properties for laminates produced with: a) Sicomin resin; b) Ebalta resin.

These results are in good agreement with those obtained by Santos et al. [37], for whom the same values for the respective resins enhanced with CNFs were found. In this case, the maximum bending strength was also achieved for the same weight contents shown in Figure 6.6, evidence that maximizing the bending properties of the resins also maximizes the bending properties of the laminates produced with them. This denotes that, in composite materials, the matrix is the weakest phase and any increase in its mechanical properties increases those of the composite. On the other hand, if the use of nanoparticles is an effective strategy to increase strength and stiffness without compromising density, toughness and the manufacturing process [48], it is also observed that the improvements achieved are strongly related to the nano-reinforcement content and resin used [38].

According to Santos et al. [37], due to the higher viscosity of the Sicomin resin, it would be expected that the bending properties would be maximized for lower CNFs contents than those used for the Ebalta resin. This is because the low viscosity of a resin allows better organization of nanoparticles [49]. However, based on the greater physicochemical compatibility of the Sicomin resin (greater acceptance of the filler by the matrix), they justified the values observed for the respective CNFs contents. Finally, as shown in Figure 6.7, higher filler contents promote agglomerations/aggregations, which correspond to defects and act as stress-concentration points in nanocomposites [46,47,50].

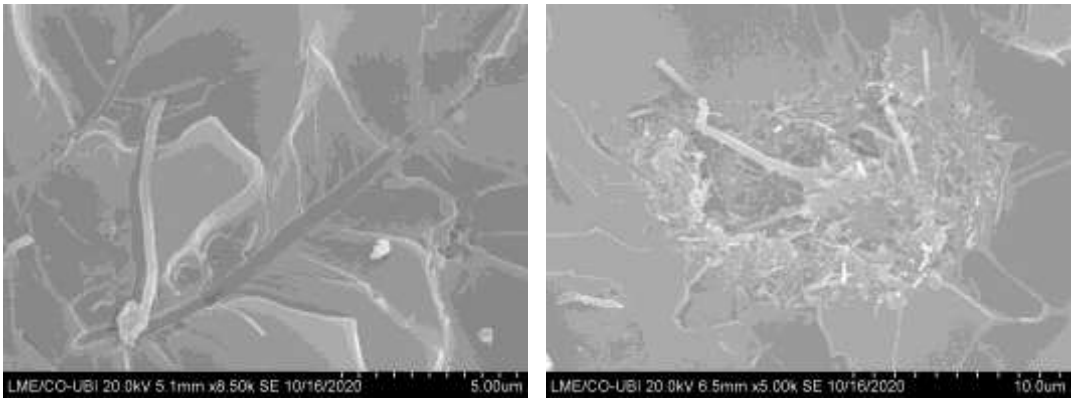

a) b)

Figure 6.7: SEM pictures for the Ebalta resin with: a) 0.5 wt.% of CNFs; b) 0.75 wt.% of CNFs [39].

In addition, the interfacial area between the polymer matrix and the nanoparticles also decreases and only a few polymer molecules can penetrate between the nanoparticles, promoting, in this case, a substantial increase in viscosity [51,52]. This evidence was well-reported in a previous study [39],where SEM images of the fracture surfaces revealed good dispersion for 0.5 wt.% CNFs, while for 0.75 wt.% agglomeration/aggregation occurs. Under these conditions, the mechanical properties are affected, especially in terms of bending strength.

Strain rate is the change in strain (deformation) with respect to time, and for this study the bending properties are analysed only for the conditions that promoted the highest bending

strength, i.e., laminates with Sicomin resin reinforced with 0.75 wt.% of CNFs and Ebalta resin reinforced with 0.5 wt.% of CNFs. Therefore, Figure 6.8 shows representative stress–strain curves for all strain rates obtained with laminates produced with Sicomin resin; however, they also reproduce the behaviour obtained with the Ebalta resin.

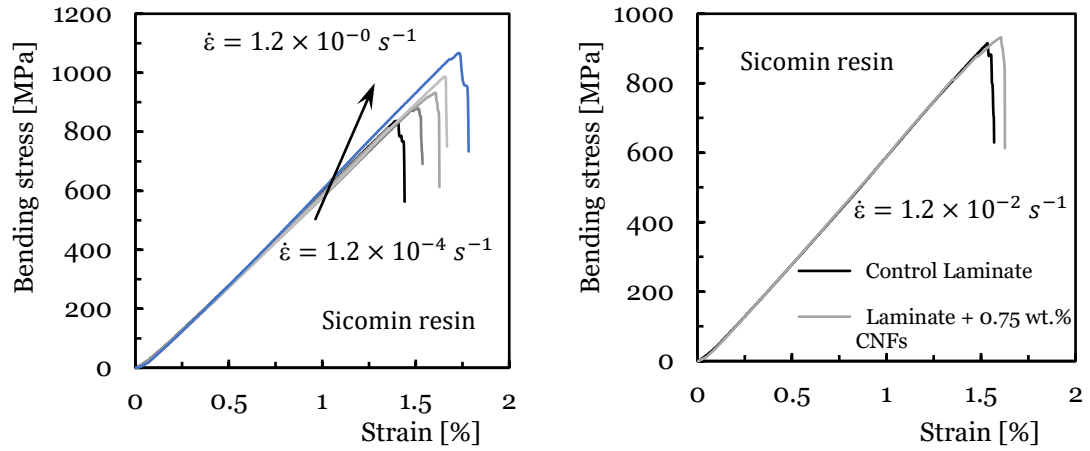

a) b)

Figure 6.8: Bending stress versus strain curves for: a) Laminates produced with Sicomin resin reinforced with 0.75 wt.% of CNFs and different strain rates; b) Comparative curves obtained at 1.2×10^{-2} s^{-1} for control laminates and laminates produced with Sicomin resin reinforced with 0.75 wt.% of CNFs.

It is noticed that the profile of these curves is very similar to that observed in Figure 6.4, evidencing similar damage mechanisms. The bending properties were also obtained, which are summarized in Figure 6.9. Symbols represent the average values, and the dispersion bands are the maximum and minimum values obtained from the experimental tests.

It is possible to observe that the maximum bending stress increases for all laminates with an increase in strain rate, which is in line with the literature [49,53]. For example, considering the laminates produced with Sicomin resin and the range of strain rate studied, it is found that the control laminate increases its bending stress by around 22.7%, while that produced with resin reinforced with 0.75 wt.% of CNFs is 15.4%. On the other hand, the same comparison for Ebalta resin leads to values of 21.6% and 25.8%, respectively. In terms of bending modulus, these values are 7.4% and 6.3% for Sicomin resin, and 3.9% and 18.4% for Ebalta resin. From this analysis, and regardless of resin, it is possible to observe that the control laminates have a very similar sensitivity (22.7% and 21.6%), but when the resins are nano-reinforced, while the laminates produced with Sicomin resin present lower sensitivity to the strain rate (from 22.7% to 15.4%), those produced with Ebalta resin present higher sensitivity (from 21.6% to 25.8%). According to the literature, these increases are related to secondary molecular processes, because an increasing strain rate decreases the molecular mobility of the polymer chains, making the chains stiffer [54].

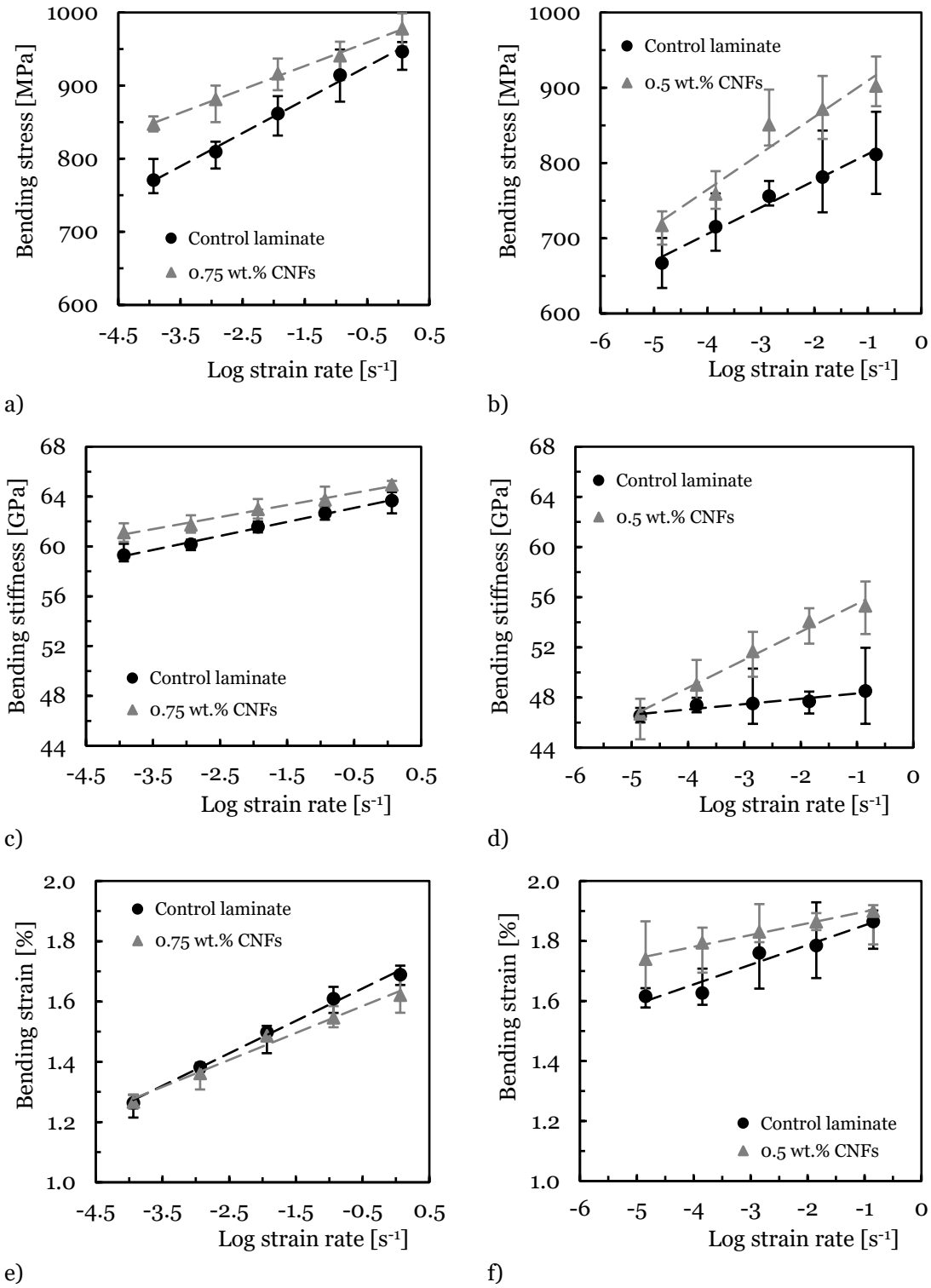

Figure 6.9: Strain rate effect on: a) Bending stress for Sicomin resin; b) Bending stress for Ebalta resin; c) Bending stiffness for Sicomin resin; d) Bending stiffness for Ebalta resin; e) Bending strain for Sicomin resin; f) Bending strain for Ebalta resin.

Finally, as suggested by the literature [55–57], a linear model can be fitted to the data according to Equations (6.6)–(6.8), with which it is possible to obtain the sensitivity to strain rate through the slope of the curves [58].

$$\sigma = c + d \times \dot{e} \quad (6.6)$$

$$E = c + d \times \dot{e} \quad (6.7)$$

$$\varepsilon = c + d \times \dot{e} \quad (6.8)$$

In these equations, σ is the maximum bending stress, E is the bending modulus, ε is the strain at maximum bending stress and $\dot{e}$ is the logarithm of strain rate and c and d constants presented in Table 6.1. Therefore, from Table 6.3, it is possible to observe that the proposed linear relationships (between the logarithm of strain rate and mechanical properties) present good precision (standard deviation (Stdev) higher than 0.951) and can be used as prediction tools.

Table 6.3: Parameters of the equations that fits the effect of the strain rate.

Laminate	Properties	Parameters		Stdev
		c	d	
Sicomin control laminate	Bending stress (σ)	948.94	45.52	0.997
	Bending modulus (E)	63.65	1.12	0.998
	Bending modulus (ε)	1.70	0.108	0.997
Sicomin laminate + 0.75 wt.% CNFs	Bending stress (σ)	974.94	32.05	0.998
	Bending modulus (E)	64.77	0.967	0.995
	Bending modulus (ε)	1.63	0.089	0.992
Ebalta control laminate	Bending stress (σ)	847.30	35.44	0.983
	Bending modulus (E)	48.75	0.424	0.951
	Bending modulus (ε)	1.91	0.066	0.970
Ebalta laminate + 0.5 wt.% CNFs	Bending stress (σ)	957.77	48.29	0.972
	Bending modulus (E)	57.70	2.23	0.993
	Bending modulus (ε)	1.94	0.039	0.994

Stdev = Standard deviation.

The interlaminar shear strength test provides the composite's resistance to delamination under shear forces parallel to the laminate layers. In many cases, the low interlaminar shear strength of polymer composites can be explained by the use of fibres without surface treatment or with inadequate treatments for the matrix used [59]. Therefore, to evaluate the ILSS of the laminates produced with the different resins, as well as the benefits obtained with CNFs, this study used the short-beam shear test for this purpose. In this context, Figure 6.10 shows the load-displacement curves obtained for all configurations studied.

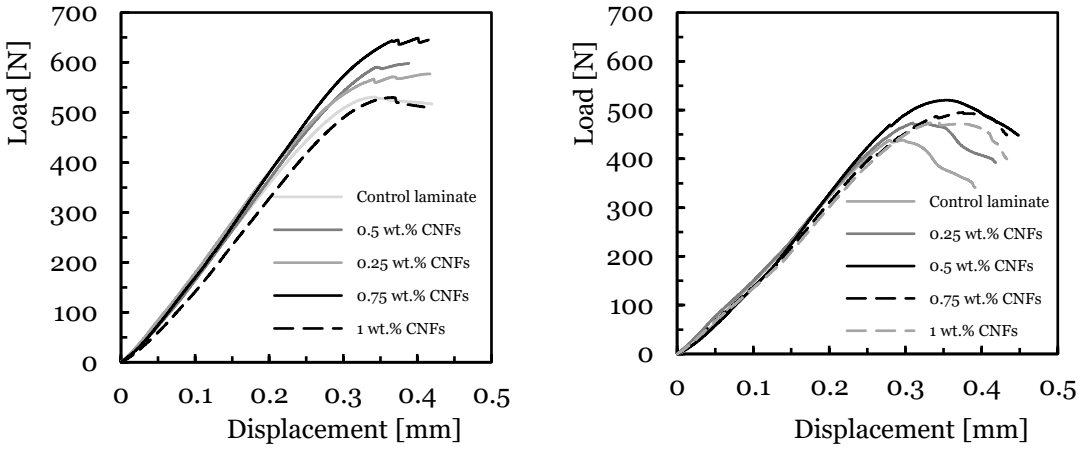

a) b)

Figure 6.10: Typical load versus displacement curves of laminates with: a) Sicomin resin; b) Ebalta resin.

All curves obtained from the short-beam shear tests show a quasi-linear increase in the load with displacement, after which a plateau region appears instead of an abrupt drop in load. However, according to Espadas-Escalante and Isaksson [60], delamination's are more related to curves that show abrupt load drop, while the observed curve shape (containing plateaus) suggests a multi-step failure mode. In this case, delamination zones appear when two longitudinal yarns are in contact or when a longitudinal yarn and a transverse yarn are in contact. On the other hand, zones where two transverse yarns are in contact promote transverse yarn cracking, causing an apparent delamination in interlaminar shear strength. However, the literature also reports that interlaminar shear strength is very similar for both types of failure (different curve shapes) [61]. In this context, Figure 6.11 shows the damage mechanisms observed for laminates with neat Ebalta resin, which are also representative of all other laminates.

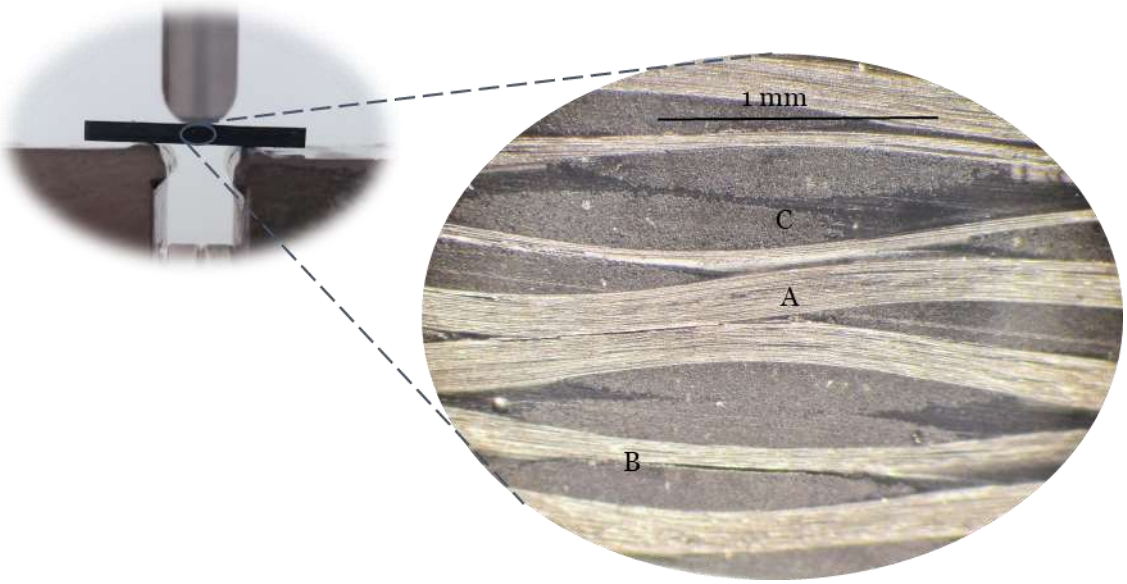

Figure 6.11: Damage mechanisms observed for laminates with neat Ebalta resin.

It is possible to observe delamination's resulting from the contact between two longitudinal yarns (A), another delamination resulting from the contact between a longitudinal yarn and a transverse yarn (B) and transverse yarn cracking (C) in a region where two transverse yarns are in contact. In the last case (C), the crack propagates further into a resin-rich region. These failure mechanisms created a region of coalescence of cracks in which one of them became dominant (A). Therefore, the yarns' interactions and the resin-rich regions (favourable to cracking) prove to be determinants in triggering the damage and confirm what is referred to in the literature [61].

Based on these curves (load-displacement shown in Figure 6.10), He and Gao defined the total fracture work (W_t), as the area under the curve, and verified its dependence with nanoparticle content [62]. A similar effect can be observed in this study, where W_t depends on CNFs content and type of resin. In terms of interlaminar shear strength, its value is also obtained from these curves and Figure 6.12 summarizes the effect of CNFs on this parameter. Symbols represent the mean values, and the scatter bands represent the maximum and minimum values. It is possible to observe that, in terms of laminates produced with neat resins (control laminates), the highest ILSS value is obtained with the Sicomin resin, 3.3% higher than that obtained with the Ebalta resin, evidencing its greater physicochemical compatibility in relation to carbon fibres used (as mentioned above). On the other hand, regarding the CNFs content, its increase is responsible for higher ILSS values until reaching a maximum that depends on the resin and, consequently, on the CNFs content. For example, while the maximum ILSS value is reached with 0.75 wt.% of CNFs in laminates produced with the Sicomin resin, in the case of those involving the Ebalta resin, it is 0.5 wt.%. Moreover, compared to the control laminates, the ILSS value for those using the Sicomin resin reinforced with 0.75 wt.% of CNFs is about 8.6% higher, while for the Ebalta resin reinforced with 0.5 wt.% it is about 9.4% higher.

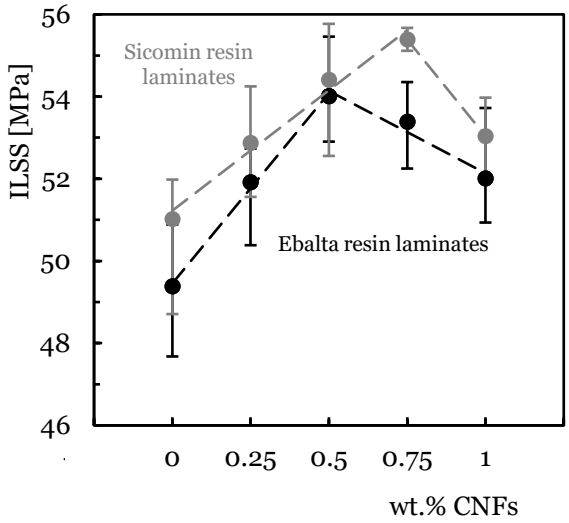

Figure 6.12: Effect of CNFs content on interlaminar shear strength, for two epoxy resins.

These results are similar to those obtained in the static characterization, where the bending strength was also maximized for the same CNFs content. Therefore, it can be concluded that these

CNFs contents (0.75 wt.% for Sicomin resin and 0.5 wt.% for Ebalta resin) simultaneously maximize the static bending strength and interlaminar shear strength. If the benefits obtained at the static level have already been explained above, in terms of ILSS, the literature reports that they are explained by the better interface/interphase bond between the epoxy matrix and carbon fibres [62,63].

In this context, the incorporation of CNFs into the epoxy matrix improves its strength and the interface, increasing the stress transfer and, consequently, the ILSS of the composites. On the other hand, CNFs contents higher than the optimal values promote lower interlaminar shear strength due to weak interactions between nanofillers and epoxy resin, as well as the imminent crack propagation from the agglomerates that act as stress concentration points. As mentioned in the literature [47,64], these agglomerations/aggregations reduce the interfacial area between the matrix/CNFs and, consequently, the mechanical engagement of the polymer chains in the nanoparticles. In addition, only a few polymer molecules penetrate between the CNFs due to the increased viscosity [43,51,52].

The effect of strain rate on interlaminar shear strength was also analysed and the results obtained for the different laminates are shown in Figure 6.13. This study involved only control laminates (with neat resin) and laminates with nano-enhanced resins whose CNFs content maximized the properties studied (0.75 wt.% for the Sicomin resin and 0.5 wt.% for the Ebalta resin). In Figure 6.13, symbols represent the mean values, and the scatter bands represent the maximum and minimum values obtained in the experimental tests. It is possible to observe that higher loading rates promote higher interlaminar shear strength values. In terms of laminates produced with neat Sicomin resin, for example, this increase is around 39.9% (from 43.9 MPa to 61.3 MPa), while for laminates nano-enhanced with 0.75 wt.% of CNFs it is about 44.6% (from 47.3 MPa to 68.4 MPa). These values for laminates produced with the Ebalta resin are 57.1% and 55.4%, respectively. This effect is well-explained in the literature [65–67], where lower loading rates provide enough time for the micro-cracks to propagate along the matrix, while at higher rates the micro-cracks have to break the covalent bond established between the matrix/CNFs or even break the nano-fibres for their propagation and, consequently, higher ILSS values arise. Simultaneously, other energy absorption mechanisms can also occur at high loading rates such as shear delamination's, matrix cracking and translaminar fracture [65,66].

Regardless of the temporal effect on the previously mentioned damage mechanisms, for Agirregomezkorta et al. [65] the loading rate effect is essentially due to the viscoelastic nature of the polymeric matrices. Therefore, based on this dependence, and similar to what was established for the bending tests, a linear model can be fitted to the data according to the following equation:

$$\mathrm{ILSS} = c\ ln(x) + d \tag{6.9}$$

where x is the displacement rate value, and the constants c and d are shown in Table 6.4.

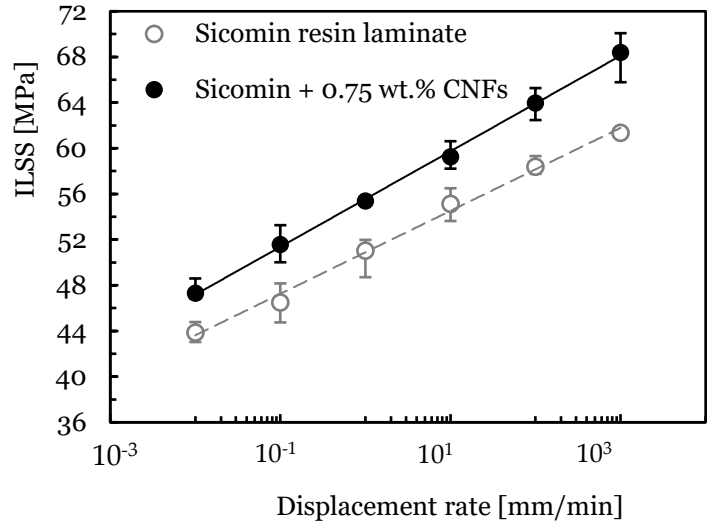

a)

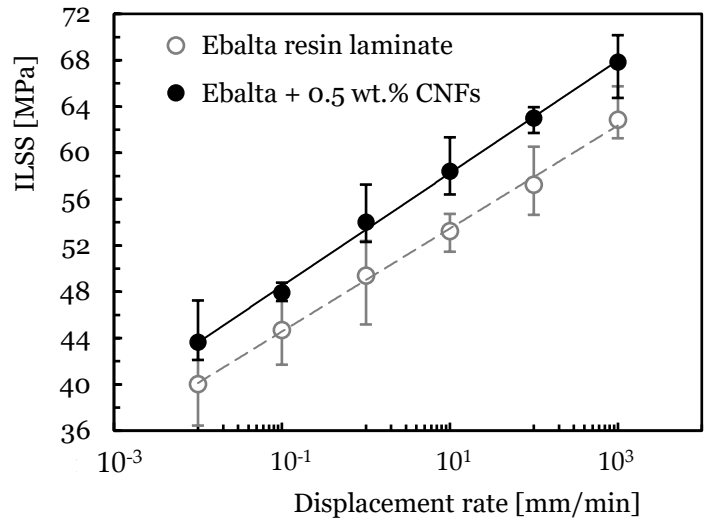

b)

Figure 6.13: ILSS values at different strain rates for laminates with: a) Sicomin resin; b) Ebalta resin.

Table 6.4: Parameters of the equation describing the loading rate effect on the ILSS.

Laminate	ILSS equation parameters		Stdev
	c	*d*	
Sicomin control laminate	1.58	50.89	0.997
Sicomin laminate + 0.75 wt.% CNFs	1.82	55.55	0.999
Ebalta control laminate	1.93	49.01	0.999
Ebalta laminate + 0.5 wt.% CNFs	2.12	53.36	0.999

Stdev = Standard deviation.

From this table it is possible to note that the proposed model presents good accuracy (Stdev higher than 0.997) and can be used as a forecasting tool to estimate the interlaminar shear strength as a function of different loading rates. Regardless of the resin, it can also be seen that, in terms of ILSS, laminates with nano-enhanced resin by CNFs show more sensitivity to the loading rate than

the control laminates (with neat resins). On the other hand, when comparing resins, laminates produced with Sicomin resin have less sensitivity due to greater physicochemical compatibility with the carbon reinforcements. Exposure to hostile environments also affects the mechanical performance due to interaction with composite constituents, essentially at the level of the fibre/matrix interface [68–70]. In this context, the interlaminar shear strength is the ideal parameter to evaluate this effect, which is shown in Figure 6.14 for different solutions (alkaline and acid) and concentrations. From the results obtained, both solutions (HCl and NaOH) affect the interlaminar shear strength of all laminates, and this trend increases with increasing solution concentration.

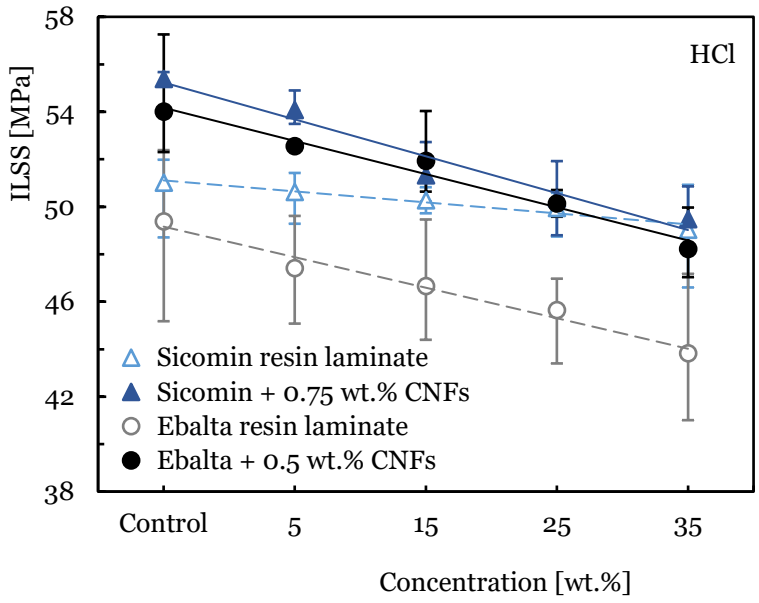

a)

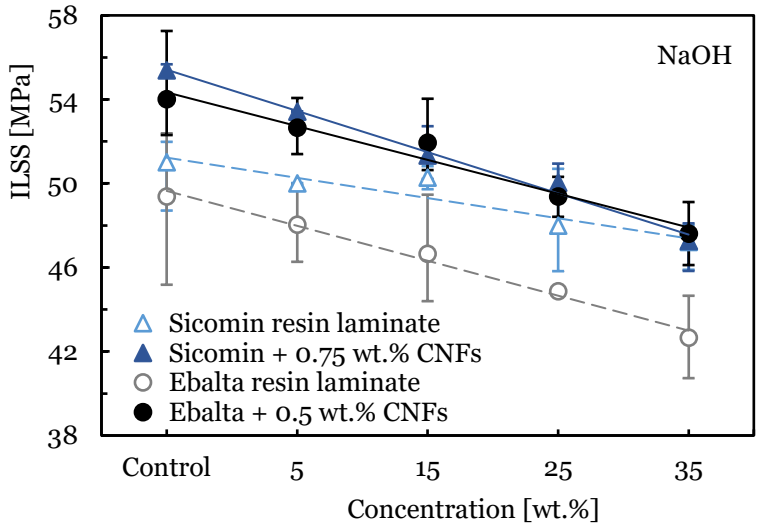

b)

Figure 6.14: Effect of the hostile solution and its concentration on the ILSS for: a) HCl; b) NaOH.

For example, compared to non-immersed laminates, ILSS decreases around 3.9% for laminates produced with neat Sicomin resin and immersed into HCl at 35 wt.% and by about 7.4% for laminates immersed into NaOH for the same concentration. However, when this resin is reinforced with CNFs these values are 10.7% and 14.7%, respectively. The same comparison for laminates produced with Ebalta resin leads, respectively, to values of 11.2% and 13.6% for laminates with neat resin and 10.7% and 11.8% for nano-enhanced laminates. Based on this analysis, it can be noted that the laminates produced with neat Sicomin resin are the least sensitive when exposed to both solutions, but when the resins are reinforced with CNFs the ILSS values approach each other significantly and mitigate the difference found between laminates with neat resins. In fact, according to Agirregomezkorta et al. [65], the interlaminar shear strength depends essentially on the mechanical performance of the resin, but it is also mentioned in the literature that ILSS decreases with exposure to hostile environments [43,71]. Moreover, this effect increases with the pH value [70,72]. Finally, another point of evidence expressed by the ILSS results obtained for both resins is related to the greater severity of the alkaline solution in relation to the acidic one (see Figure 6.14). This is in line with the literature and, as shown in Figure 6.15, is justified by the greater severity of the damage introduced in the laminates [43,44].

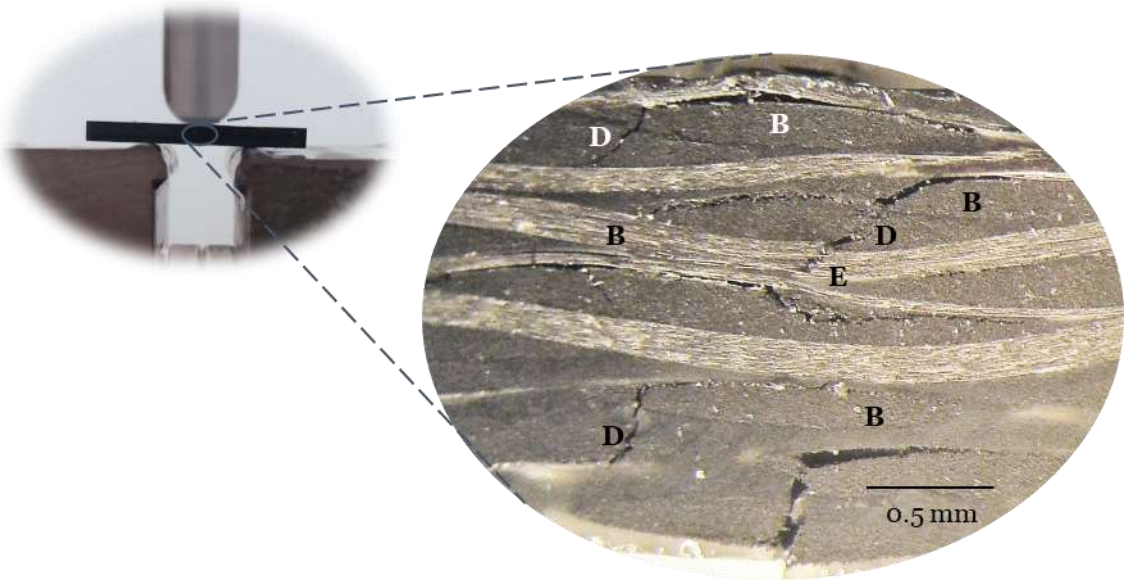

Figure 6.15: Damage mechanisms observed for laminates with neat Ebalta resin immersed into NaOH at 35 wt.%.

These damage mechanisms are relative to the laminates with neat Ebalta resin; however, they are representative of those observed for the other laminates studied. Furthermore, they are similar to those observed in Figure 6.11 but with higher severity. In this context, it is possible to observe several delamination's resulting from the contact between longitudinal and transverse yarns (B), matrix cracking (D) and broken fibres (E). Similar to what was observed above, cracks also occur into resin-rich regions. The observed severity of the damage mechanisms previously reported is a consequence of the absorption, penetration and reaction that occur between solutions and composite constituents [69]. In terms of the fibre/matrix interface,, the degradation is due to

dehydration of the matrix and penetration of solutions through micro-cracks [70,73], crazes or voids in the matrix [68]. Simultaneously, the matrices are also attacked under the combined action of water diffusion and the presence of H^+ (promoting matrix expansion and production of pits/micro-cracks), while the fibres are attacked with consequent cracks on their surface. In this context, the composite's strength is significantly affected [32,74].

The effect of temperature was also analysed, and Figure 6.16 shows the results obtained for samples immersed into distilled water and into both solutions (NaOH and HCl) at concentrations of 15 wt.%. The immersion time was 20 days, and the fluids were at temperatures of 22 °C (RT), 40 °C and 80 °C.

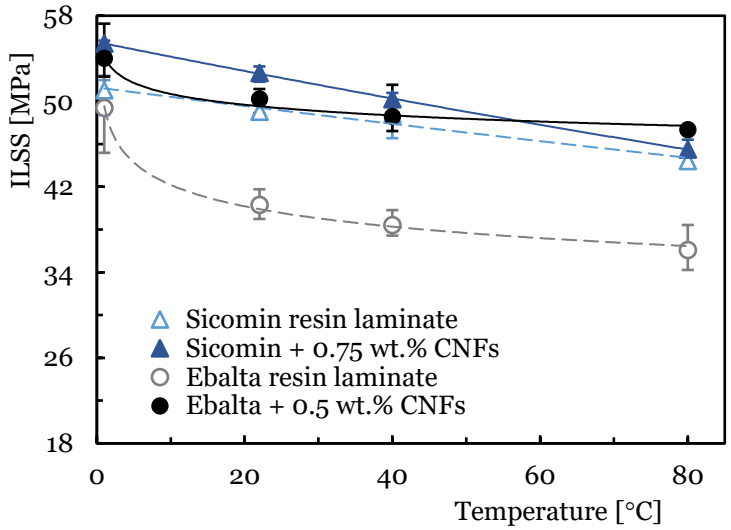

a)

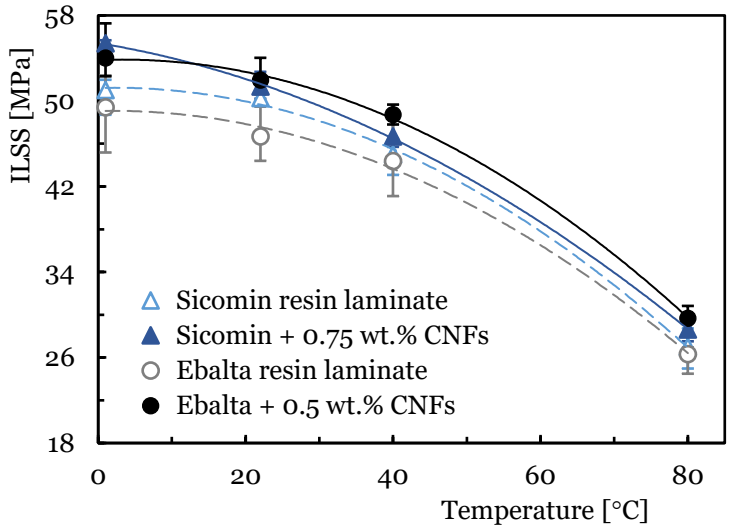

b)

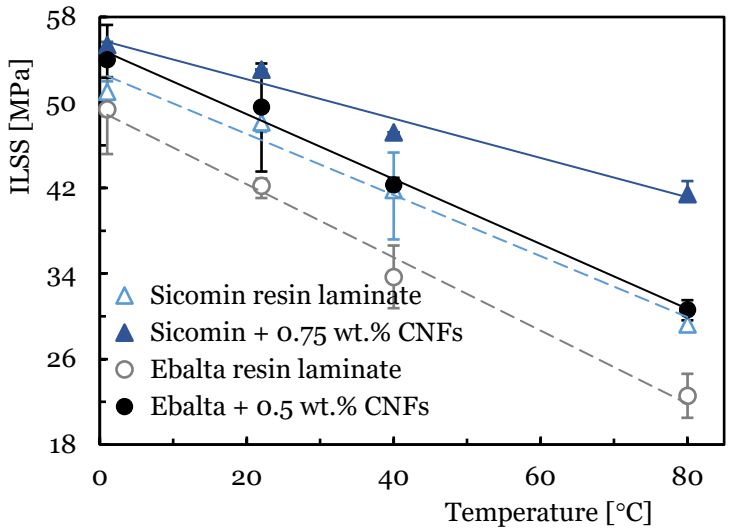

c)

Figure 6.16: Temperature effect on the interlaminar shear strength for laminates immersed into: a) Distilled water; b) HCl; c) NaOH.

It is possible to observe for all laminates and fluids that increasing the temperature decreases the ILSS values. For example, compared to non-immersed laminates, the interlaminar shear strength decreases around 3.9% when laminates produced with neat Sicomin resin are immersed into distilled water at RT, and this value increases to 13% when the temperature increases to 80 °C. These values are, respectively, 4.9% and 17.9% for the same laminates reinforced with CNFs. On the other hand, when the Ebalta resin is considered, these values are around 18.4% and 26.9% for laminates with neat resin, and 7.1% and 12.4% for laminates with nano-reinforced resin, respectively. When the same analysis considers HCl, these values are 1.5% and 47.1% for laminates with neat Sicomin resin and 7.3% and 48.3% when nano-reinforced, while for the Ebalta resin they are 5.6% and 46.7% for laminates with neat resin and 3.8% and 45.1% when nano-reinforced, respectively. Finally, the same comparative analysis for the alkaline solution leads to ILSS values slightly lower than those observed for the acidic solution (consequently higher percentage values relative to the non-immersed laminates), evidencing its higher severity mentioned above.

These results are in line with those discussed based on Figure 6.14, evidencing the fact that laminates with neat Ebalta resin are the most affected by the solutions analysed, but the opposite trend occurs when they are nano-reinforced (higher benefits are obtained than with Sicomin resin). In this context, the resin used has an influence on interlaminar shear strength, confirming what was reported by Banna et al. [75]. Another clear point of evidence reveals that increasing temperature promotes a further decrease in interlaminar shear strength for all laminates. In fact, temperature accelerates the degradation of mechanical properties, and both acid and alkali solutions are more harmful than water at the same temperature, which agrees with the studies developed by Yang et al. [30]. This is explained by the fact that diffusion is a thermally activated process and, in this context, increasing temperature accelerates short-term diffusion and

increases the diffusion coefficient [76]. Consequently, the liquid flow into laminates increases. Furthermore, there are residual stresses at the interface that are responsible for the appearance of micro-voids/micro-cracks due to different coefficients of thermal expansion existing between fibre and matrix [77]. In this context, the aggressive fluids create hydrostatic pressure at the crack tips and hasten crack propagation and damage in the matrix [78]. The acid solution and the alkali solution more strongly damaged CFRPs compared with aqueous water at the same temperature [30].

6.4. Conclusions

Bending tests and interlaminar shear tests were carried out to investigate the behaviour of carbon laminates nano-reinforced with CNFs. Relevant improvements in bending stress (20.4 and 12.5% for Sicomin and Ebalta, respectively) and bending stiffness (13.8 and 8.8% for Sicomin and Ebalta, respectively) were obtained with the incorporation of CNFs. A reduction in bending strain of the carbon laminates is observed with the increasing filler content for both epoxy resins, showing a more brittle behaviour. In terms of strain-rate sensitivity, the bending stress increases for all laminates with an increasing strain rate. For the laminates with Sicomin resin, relative to the control laminates an increase in bending stress of 22.7% was obtained, while that of the laminate with 0.75 wt.% of CNFs increased by 15.4%. The values obtained for bending modulus were 7.4% and 6.3% for Sicomin resin, and 3.9% and 18.4% for Ebalta resin. Nano-reinforced laminates produced with Sicomin resin have a lower strain-rate sensitivity than laminates produced with Ebalta resin. A linear model is proposed as a tool that describes with high precision the evolution of bending stress, bending stiffness and bending strain for all laminates.

In terms of ILSS, the best results coincided with the results of the static bending point, that is, Sicomin resin in laminate with 0.75 wt.% CNFs and Ebalta resin with 0.5 wt.% CNFs. For all laminates studied, the ILSS is strain-rate sensitive; the values increase for higher values of strain rate. Additionally, a linear model describes accurately its behaviour for all laminates. In both resins, the nano-enhanced laminates with the optimal percentage of CNFs show higher results as an answer to strain-rate sensitivity.

The corrosive environments significantly affect the ILSS response, and their effects are strongly dependent on the concentration of the solution. The alkaline solution promotes higher decreases in ILSS than the acid solution. However, Sicomin resin is less sensitive to both solutions than those produced with Ebalta resin. When CNFs were added to the resins, a decrease in ILSS was observed in comparison with laminates produced with neat resin. This effect is more significant in Sicomin because the adhesion between the CNFs and this resin is poor.

Finally, regardless of the epoxy resin or the environment in which the laminates were immersed in solution or water, higher temperatures induced a decrease in ILSS. The addition of CNFs was beneficial as it reduced the degradation of the laminates.

Bibliography

[1] Rajak DK, Pagar DD, Kumar R, Pruncu CI. Recent progress of reinforcement materials: a comprehensive overview of composite materials. Journal of Materials Research and Technology 2019;8:6354–74. https://doi.org/10.1016/j.jmrt.2019.09.068.

[2] Rajak DK, Wagh PH, Linul E. Manufacturing Technologies of Carbon/Glass Fiber-Reinforced Polymer Composites and Their Properties: A Review. Polymers 2021;13:3721. https://doi.org/10.3390/polym13213721.

[3] Pulikkalparambil H, Rangappa SM, Siengchin S, Parameswaranpillai J. Introduction to Epoxy Composites. Epoxy Composites, vol. 2, Wiley; 2021, p. 1–21. https://doi.org/10.1002/9783527824083.ch1.

[4] Edie DD. The effect of processing on the structure and properties of carbon fibers. Carbon 1998;36:345–62. https://doi.org/10.1016/S0008-6223(97)00185-1.

[5] Newcomb BA. Processing, structure, and properties of carbon fibers. Composites Part A: Applied Science and Manufacturing 2016;91:262–82. https://doi.org/10.1016/j.compositesa.2016.10.018.

[6] Wang F. Carbon Fibers and Their Thermal Transporting Properties. Thermal Transport in Carbon-Based Nanomaterials. 1st ed., Elsevier; 2017, p. 135–84. https://doi.org/10.1016/B978-0-32-346240-2.00006-6.

[7] Licari JJ, Swanson DW. Chemistry, Formulation, and Properties of Adhesives. Adhesives Technology for Electronic Applications, Elsevier; 2011, p. 75–141. https://doi.org/10.1016/B978-1-4377-7889-2.10003-8.

[8] Fiore V, Valenza A. Epoxy resins as a matrix material in advanced fiber-reinforced polymer (FRP) composites. Advanced Fibre-Reinforced Polymer (FRP) Composites for Structural Applications, Elsevier; 2013, p. 88–121. https://doi.org/10.1533/9780857098641.1.88.

[9] Unnikrishnan KP, Thachil ET. Toughening of epoxy resins. Designed Monomers and Polymers 2006;9:129–52. https://doi.org/10.1163/156855506776382664.

[10] Endo M, Kim Y., Hayashi T, Nishimura K, Matusita T, Miyashita K, et al. Vapor-grown carbon fibers (VGCFs). Carbon 2001;39:1287–97. https://doi.org/10.1016/S0008-6223(00)00295-5.

[11] Mohammadzadehmoghadam S, Dong Y, Jeffery Davies I. Recent progress in electrospun nanofibers: Reinforcement effect and mechanical performance. Journal of Polymer Science Part B: Polymer Physics 2015;53:1171–212. https://doi.org/10.1002/polb.23762.

[12] Wang Y, Zhu W, Wan B, Meng Z, Han B. Hygrothermal ageing behavior and mechanism of carbon nanofibers modified flax fiber-reinforced epoxy laminates. Composites Part A: Applied Science and Manufacturing 2021;140:106142. https://doi.org/10.1016/j.compositesa.2020.106142.

[13] González C, Vilatela JJ, Molina-Aldareguía JM, Lopes CS, LLorca J. Structural composites for multifunctional applications: Current challenges and future trends. Progress in Materials Science 2017;89:194–251. https://doi.org/10.1016/j.pmatsci.2017.04.005.

[14] Bortz DR, Merino C, Martin-Gullon I. Mechanical characterization of hierarchical carbon fiber/nanofiber composite laminates. Composites Part A: Applied Science and Manufacturing 2011;42:1584–91. https://doi.org/10.1016/j.compositesa.2011.07.002.

[15] Feng L, Xie N, Zhong J. Carbon Nanofibers and Their Composites: A Review of Synthesizing, Properties and Applications. Materials 2014;7:3919–45. https://doi.org/10.3390/ma7053919.

[16] Dhakate SR, Chaudhary A, Gupta A, Pathak AK, Singh BP, Subhedar KM, et al. Excellent mechanical properties of carbon fiber semi-aligned electrospun carbon nanofiber hybrid polymer composites. RSC Advances 2016;6:36715–22. https://doi.org/10.1039/C6RA02672A.

[17] Yilmaz AC, Ozen MS, Sancak E, Erdem R, Erdem O, Soin N. Analyses of the mechanical,

electrical, and electromagnetic shielding properties of thermoplastic composites doped with conductive nanofillers. Journal of Composite Materials 2018:002199831773782. https://doi.org/10.1177/0021998317737826.

[18] Tripathi S. Role of Nanocatalysts in Synthesis of Carbon Nanofiber. Carbon Nanofibers, Wiley; 2021, p. 49–74. https://doi.org/10.1002/9781119769149.ch3.

[19] Baker RTK. Carbon Nanofibers. Encyclopedia of Materials: Science and Technology, Elsevier; 2001, p. 932–41. https://doi.org/10.1016/B0-08-043152-6/00178-9.

[20] Yang J, Zhang Z, Friedrich K, Schlarb AK. Creep Resistant Polymer Nanocomposites Reinforced with Multiwalled Carbon Nanotubes. Macromolecular Rapid Communications 2007;28:955–61. https://doi.org/10.1002/marc.200600866.

[21] Zhou Y, Pervin F, Rangari VK, Jeelani S. Fabrication and evaluation of carbon nano fiber filled carbon/epoxy composite. Materials Science and Engineering: A 2006;426:221–8. https://doi.org/10.1016/j.msea.2006.04.031.

[22] Green KJ, Dean DR, Vaidya UK, Nyairo E. Multiscale fiber reinforced composites based on a carbon nanofiber/epoxy nanophased polymer matrix: Synthesis, mechanical, and thermomechanical behavior. Composites Part A: Applied Science and Manufacturing 2009;40:1470–5. https://doi.org/10.1016/j.compositesa.2009.05.010.

[23] Arai M, Matsushita K, Hirota S. Criterion for interlaminar strength of CFRP laminates toughened with carbon nanofiber interlayer. Composites Part A: Applied Science and Manufacturing 2011;42:703–11. https://doi.org/10.1016/j.compositesa.2011.01.005.

[24] Palmeri MJ, Putz KW, Ramanathan T, Brinson LC. Multi-scale reinforcement of CFRPs using carbon nanofibers. Composites Science and Technology 2011;71:79–86. https://doi.org/10.1016/j.compscitech.2010.10.006.

[25] Zhou Y, Jeelani S, Lacy T. Experimental study on the mechanical behavior of carbon/epoxy composites with a carbon nanofiber-modified matrix. Journal of Composite Materials 2014;48:3659–72. https://doi.org/10.1177/0021998313512348.

[26] Ma L, Wu L, Cheng X, Zhuo D, Weng Z, Wang R. Improving the interlaminar properties of polymer composites using a situ accumulation method to construct the multi-scale reinforcement of carbon nanofibers/carbon fibers. Composites Part A: Applied Science and Manufacturing 2015;72:65–74. https://doi.org/10.1016/j.compositesa.2015.01.023.

[27] Senthil T, Weng Z, Wu L. Interlaminar microstructure and mechanical response of 3D robust glass fabric-polyester composites modified with carbon nanofibers. Carbon 2017;112:17–26. https://doi.org/10.1016/j.carbon.2016.10.087.

[28] Ramezani H, Kazemirad S, Shokrieh MM, Mardanshahi A. Effects of adding carbon nanofibers on the reduction of matrix cracking in laminated composites: Experimental and analytical approaches. Polymer Testing 2021;94:106988. https://doi.org/10.1016/j.polymertesting.2020.106988.

[29] Uthaman A, Xian G, Thomas S, Wang Y, Zheng Q, Liu X. Durability of an Epoxy Resin and Its Carbon Fiber- Reinforced Polymer Composite upon Immersion in Water, Acidic, and Alkaline Solutions. Polymers 2020;12:614. https://doi.org/10.3390/polym12030614.

[30] Yang T, Lu S, Song D, Zhu X, Almira I, Liu J, et al. Effect of Nanofiller on the Mechanical Properties of Carbon Fiber/Epoxy Composites under Different Aging Conditions. Materials 2021;14:7810. https://doi.org/10.3390/ma14247810.

[31] Kojnoková T, Nový F, Markovičová L. The Study of Chemical and Thermal Influences of the Environment on the Degradation of Mechanical Properties of Carbon Composite with Epoxy Resin. Polymers 2022;14:3245. https://doi.org/10.3390/polym14163245.

[32] Sinmazçelik T, Arici AA. Influence of various fluids on the interlaminar shear strength (ILSS) and impact behaviour of carbon/pei composites. Journal of Materials Science 2006;41:3255–62. https://doi.org/10.1007/s10853-005-5475-x.

[33] Mahato KK, Shukla MJ, Kumar DS, Ray BC. In- service Performance of Fiber Reinforced Polymer Composite in Different Environmental Conditions: A Review. Journal of Advanced Research in Manufacturing, Material Science & Metallurgical Engineering 2014;1:55–88.

[34] Kopietz M, Wetzel B. Impact of Aggressive Media on the Interlaminar Shear Strength of

Innovative Glass Fiber Reinforced Polyurea/Polysilicate Hybrid Resins. Procedia Structural Integrity 2018;13:143–8. https://doi.org/10.1016/j.prostr.2018.12.024.

[35] Zhang M, Mason SE. Interlaminar Shear Strength of Carbon Fibre Reinforced Epoxy Composite under the Influence of Environments. Advanced Composites Letters 1998;7:096369359800700. https://doi.org/10.1177/096369359800700104.

[36] da Silva LV, de Menezes EAW, Tarpani JR, Amico SC. Accelerated Ageing Effects on Short-Beam Strength Behavior of Pultruded CFRP Rods. Applied Composite Materials 2022;29:855–69. https://doi.org/10.1007/s10443-021-09985-w.

[37] Pina dos Santos PS, Maceiras A, Valvez S, Reis PNB. Mechanical characterization of different epoxy resins enhanced with carbon nanofibers. Frattura Ed Integrità Strutturale 2020;15:198–212. https://doi.org/10.3221/IGF-ESIS.55.15.

[38] Ferreira JAM, Reis PNB, Costa JDM, Capela C. Assessment of the mechanical properties of nanoclays enhanced low Tg epoxy resins. Fibers and Polymers 2014;15:1677–84. https://doi.org/10.1007/s12221-014-1677-7.

[39] Santos P, Silva AP, Reis PNB. Effect of Carbon Nanofibers on the Viscoelastic Response of Epoxy Resins. Polymers 2023;15:821. https://doi.org/10.3390/polym15040821.

[40] Santos P, Maceiras A, Reis PNB. Influence of manufacturing parameters on the mechanical properties of nano-reinforced CFRP by carbon nanofibers. IOP Conference Series: Materials Science and Engineering 2021;1126:012012. https://doi.org/10.1088/1757-899X/1126/1/012012.

[41] Ferreira J, Reis P, Costa J, Richardson M. Fatigue behaviour of Kevlar composites with nanoclay-filled epoxy resin. Journal of Composite Materials 2013;47:1885–95. https://doi.org/10.1177/0021998312452024.

[42] Reis PNB, Silva MP, Santos P, Parente J, Valvez S. Effect of Hostile Solutions on the Residual Fatigue Life of Kevlar/Epoxy Composites after Impact Loading. Molecules 2021;26:5520. https://doi.org/10.3390/molecules26185520.

[43] Amaro AM, Reis PNB, Neto MA, Louro C. Effects of alkaline and acid solutions on glass/epoxy composites. Polymer Degradation and Stability 2013;98:853–62. https://doi.org/10.1016/j.polymdegradstab.2012.12.029.

[44] Mortas N, Er O, Reis PNB, Ferreira JAM. Effect of corrosive solutions on composites laminates subjected to low velocity impact loading. Composite Structures 2014;108:205–11. https://doi.org/10.1016/j.compstruct.2013.09.032.

[45] Reis PNB, Neto MA, Amaro AM. Effect of hostile solutions on stress relaxation of carbon/epoxy composites. Polymer Degradation and Stability 2019;165:60–7. https://doi.org/10.1016/j.polymdegradstab.2019.04.026.

[46] Oberdisse J. Aggregation of colloidal nanoparticles in polymer matrices. Soft Matter 2006;2:29–36. https://doi.org/10.1039/B511959F.

[47] Zare Y. The roles of nanoparticles accumulation and interphase properties in properties of polymer particulate nanocomposites by a multi-step methodology. Composites Part A: Applied Science and Manufacturing 2016;91:127–32. https://doi.org/10.1016/j.compositesa.2016.10.003.

[48] Reis PNB, Ferreira JAM, Zhang ZY, Benameur T, Richardson MOW. Impact response of Kevlar composites with nanoclay enhanced epoxy matrix. Composites Part B: Engineering 2013;46:7–14. https://doi.org/10.1016/j.compositesb.2012.10.028.

[49] Rana D, Sauvant V, Halary JL. Molecular analysis of yielding in pure and antiplasticized epoxy-amine thermosets. Journal of Materials Science 2002;37:5267–74. https://doi.org/10.1023/A:1021012721619.

[50] Padmanabhan V, Frischknecht AL, Mackay ME. Effect of Chain Stiffness on Nanoparticle Segregation in Polymer/Nanoparticle Blends Near a Substrate. Macromolecular Theory and Simulations 2012;21:98–105. https://doi.org/10.1002/mats.201100048.

[51] Shaffer MSP, Fan X, Windle AH. Dispersion and packing of carbon nanotubes. Carbon 1998;36:1603–12. https://doi.org/10.1016/S0008-6223(98)00130-4.

[52] Ma X, Zare Y, Rhee KY. A Two-Step Methodology to Study the Influence of

Aggregation/Agglomeration of Nanoparticles on Young's Modulus of Polymer Nanocomposites. Nanoscale Research Letters 2017;12:621. https://doi.org/10.1186/s11671-017-2386-0.

[53] Richeton J, Ahzi S, Daridon L, Rémond Y. A formulation of the cooperative model for the yield stress of amorphous polymers for a wide range of strain rates and temperatures. Polymer 2005;46:6035–43. https://doi.org/10.1016/j.polymer.2005.05.079.

[54] Richeton J, Ahzi S, Vecchio KS, Jiang FC, Adharapurapu RR. Influence of temperature and strain rate on the mechanical behavior of three amorphous polymers: Characterization and modeling of the compressive yield stress. International Journal of Solids and Structures 2006;43:2318–35. https://doi.org/10.1016/j.ijsolstr.2005.06.040.

[55] Mckown S, Cantwell WJ. Investigation of Strain-rate Effects in Self-reinforced Polypropylene Composites. Journal of Composite Materials 2007;41:2457–70. https://doi.org/10.1177/0021998307084173.

[56] Zabihzadeh SM. Flexural properties and orthotropic swelling behavior of bagasse/thermoplastic composites. BioResources 2010;5:650–60. https://doi.org/10.15376/BIORES.5.2.650-660.

[57] Silva MP, Santos P, Sousa NN, Reis PNB. Strain rate effect on composites with epoxy matrix filled by cork powder. Material Design & Processing Communications 2019;1:e47. https://doi.org/10.1002/mdp2.47.

[58] Reis PNB, Gorbatikh L, Ivens J, Lomov SV. Strain-rate sensitivity and stress relaxation of hybrid self-reinforced polypropylene composites under bending loads. Composite Structures 2019;209:802–10. https://doi.org/10.1016/j.compstruct.2018.11.030.

[59] Monjon A, Santos P, Valvez S, Reis PNB. Hybridization Effects on Bending and Interlaminar Shear Strength of Composite Laminates. Materials 2022;15:1302. https://doi.org/10.3390/ma15041302.

[60] Espadas-Escalante JJ, Isaksson P. A study of induced delamination and failure in woven composite laminates subject to short-beam shear testing. Engineering Fracture Mechanics 2019;205:359–69. https://doi.org/10.1016/j.engfracmech.2018.10.015.

[61] Fan Z, Santare MH, Advani SG. Interlaminar shear strength of glass fiber reinforced epoxy composites enhanced with multi-walled carbon nanotubes. Composites Part A: Applied Science and Manufacturing 2008;39:540–54. https://doi.org/10.1016/j.compositesa.2007.11.013.

[62] He H, Gao F. Resin modification on interlaminar shear property of carbon fiber/epoxy/nano-CaCO 3 hybrid composites. Polymer Composites 2017;38:2035–42. https://doi.org/10.1002/pc.23775.

[63] Nayak RK, Mahato KK, Routara BC, Ray BC. Evaluation of mechanical properties of Al 2 O 3 and TiO 2 nano filled enhanced glass fiber reinforced polymer composites. Journal of Applied Polymer Science 2016;133:1–13. https://doi.org/10.1002/app.44274.

[64] Vinay SS, Sanjay MR, Siengchin S, Venkatesh C V. Effect of <scp> Al $_2$ O $_3$ </scp> nanofillers in basalt/epoxy composites: Mechanical and tribological properties. Polymer Composites 2021;42:1727–40. https://doi.org/10.1002/pc.25927.

[65] Agirregomezkorta A, Zurbitu J, Aretxaga G, Sarrionandia M, Aurrekoetxea J. Strain rate effect on interlaminar shear strength of carbon fibre reinforced pCBT and epoxy composites. ICCM International Conferences on Composite Materials 2009.

[66] Nayak RK, Rathore D, Ray BC, Routara BC. Inter Laminar Shear Strength (ILSS) of Nano Al2O3 Filled Glass Fiber Reinforced Polymer (GFRP) Composite - A Study on Loading Rate Sensitivity. Materials Today: Proceedings 2017;4:8688–96. https://doi.org/10.1016/j.matpr.2017.07.217.

[67] Kumar C, Rawat P, Singh KK, Behera RP, Deep A. Combined effect of loading rate and percentage by weight of MWCNTs on inter laminar shear strength (ILSS) and flexural strength of CFRP. IOP Conference Series: Materials Science and Engineering 2018;377:012074. https://doi.org/10.1088/1757-899X/377/1/012074.

[68] Kawada H, Srivastava VK. The effect of an acidic stress environment on the stress-intensity factor for GRP laminates. Composites Science and Technology 2001;61:1109–14.

https://doi.org/10.1016/S0266-3538(01)00008-2.

[69] Mahmoud MK, Tantawi SH. Effect of Strong Acids on Mechanical Properties of Glass/Polyester GRP Pipe at Normal and High Temperatures. Polymer-Plastics Technology and Engineering 2003;42:677–88. https://doi.org/10.1081/PPT-120023102.

[70] Stamenović M, Putić S, Rakin M, Medjo B, Čikara D. Effect of alkaline and acidic solutions on the tensile properties of glass–polyester pipes. Materials & Design 2011;32:2456–61. https://doi.org/10.1016/j.matdes.2010.11.023.

[71] Amaro A, Reis P, Neto M, Louro C. Effect of different acid solutions on glass/epoxy composites. Journal of Reinforced Plastics and Composites 2013;32:1018–29. https://doi.org/10.1177/0731684413483886.

[72] Griffiths R, Ball A. An assessment of the properties and degradation behaviour of glass-fibre-reinforced polyester polymer concrete. Composites Science and Technology 2000;60:2747–53. https://doi.org/10.1016/S0266-3538(00)00147-0.

[73] Stamenović M, Putić S, Drmanić S, Rakin M, Medjo B. The influence of service solutions on the longitudinal and circumferential tensile properties of glass-polyester composite pipes. Materials Science 2011;47:61–9. https://doi.org/10.1007/s11003-011-9368-7.

[74] Hammami A, Al-Ghuilani N. Durability and environmental degradation of glass-vinylester composites. Polymer Composites 2004;25:609–16. https://doi.org/10.1002/pc.20055.

[75] Banna MH, Shirokoff J, Molgaard J. Effects of two aqueous acidic solutions on polyester and bisphenol A epoxy vinyl ester resins. Materials Science and Engineering: A 2011;528:2137–42. https://doi.org/10.1016/j.msea.2010.11.049.

[76] Boukhoulda BF, Adda-Bedia E, Madani K. The effect of fiber orientation angle in composite materials on moisture absorption and material degradation after hygrothermal ageing. Composite Structures 2006;74:406–18. https://doi.org/10.1016/j.compstruct.2005.04.032.

[77] Ray BC. Temperature effect during humid ageing on interfaces of glass and carbon fibers reinforced epoxy composites. Journal of Colloid and Interface Science 2006;298:111–7. https://doi.org/10.1016/j.jcis.2005.12.023.

[78] Abdel-Magid B, Ziaee S, Gass K, Schneider M. The combined effects of load, moisture and temperature on the properties of E-glass/epoxy composites. Composite Structures 2005;71:320–6. https://doi.org/10.1016/j.compstruct.2005.09.022.

Chapter 7

Effect of carbon nanofibres on the viscoelastic response of carbon/epoxy composites[6]

Abstract

Carbon fibre reinforced polymer (CFRP) laminates nano-enhanced with carbon nanofibres (CNFs): 0.75 wt.% and 0.5 wt.% of epoxies Sicomin and Ebalta, respectively, were manufactured and their static and viscoelastic behaviour analysed. After 180 minutes, the bending stress decreases and creep displacement increases over time, with Ebalta nano-enhanced resin laminates with CNFs showing the best results. A strong dependence of creep behaviour and stress relaxation is obtained with the applied stress level. The results show that laminates produced with pure Sicomin resin increased creep displacement by 1%, for a bending stress of 200 MPa, and 2 times greater for the bending stress of 700 MPa. The viscoelastic behaviour of CFRP composites nano-enhanced with CNFs was accurately predicted by the Kohlrausch-Williams-Watts (KWW) model and Findley power law.

7.1. Introduction

Epoxy-based composites, such as, carbon fibre reinforced polymer (CFRP) composites have been widely applied in aerospace, energy, and many other fields where a lightweight material is required, due to their high specific strength and modulus, fatigue resistance, good thermal and electrical conductivities, excellent creep resistance and remarkable design [1–4]. However, their outstanding mechanical performance largely depends on the cohesion between the matrix and fibre reinforcement, also an effective nanoscale reinforcement can be provided by the addition of carbon nanofillers [5–7].

Extensive research has resulted in remarkable property improvements of carbon nanotubes (CNTs) reinforced epoxy composites. It was noted that as the loading of CNTs increased up to 10 wt.%, the failure strength improved slightly [8]. For instance, the addition of up 1 wt.% of CNTs, the failure strength of the composites improves 3 times and the Young's modulus doubled [5,8]. Nevertheless, besides the considerable values reported, considering the properties of the CNTs by themselves, the improvements in these properties are lower than expected. Their large surface-to-volume ratio leads to agglomeration due to the strong attraction between CNTs and the large

[6] Based on the work published in the Journal of Reinforced Plastics and Composites, Santos, P.; Silva, A.P.; Reis, P.N.B. Effect of carbon nanofibers on the viscoelastic response of carbon/epoxy composites, **2023**, *43*, 21–22, https://doi.org/10.1177/07316844231203787

van der Waals forces [9–11]. On the other hand, even with the increase of the body weight ratio of CNTs in the polymer matrix, the properties tend to decrease [12]. Another disadvantage is the chemically inert nature of CNTs leading to poor interfacial interactions with epoxy matrix [10,13]. High energy input and mechanical dispersion are used with success to improve the dispersion of CNTs. Advances in chemical modification and functionalization of CNTs also improve the surface bonds and facilitate the transfer of stress between the CNTs and the polymer matrix [5,13,14]. This improvement was related with C–F covalent, semi-ionic, ionic and van der Waals interactions which brings about enhanced interfacial interactions [10,14]. These difficulties are mainly felt in the multi-walled carbon nanotubes (MWCNTs) due to their strong inter-tube interaction and large surface area [15].

The addition of CNTs into an epoxy matrix significantly reduces the creep deformation; as an example, when adding 0.25 wt.% of CNTs, a reduction of up to 30% in the creep strain is observed. However, the creep improvement is only evident for small levels of reinforcement. When the nanotube fraction is increased to more than 1% by weight, the creep performance deteriorates rapidly due to poor quality dispersion of the nanotubes in the epoxy resin [16].

In previous works [17] it was verified that the use of carbon nanofibres (CNFs) benefits the mechanical properties of the epoxy resins. The improvements are mainly attributed to enhanced interfacial properties [17–19]. Applying a simple manufacturing process, that can be implemented in the automotive, aeronautics, military, and green energy production industries, is intended to optimise CFRP carbon fabric with an ideal percentage of CNFs to respond to new structural requirements. These functions are often related to load bearing and dynamic loading applications to increase the durability of this hierarchical laminate and predict the response in viscoelasticity and temperature dependence, therefore it is very important to evaluate the response to stress relaxation and creep strength [20–22].

In this work, the static bending response of several laminates involving matrices with different viscosities (285 ± 60 mPa×s for Sicomin resin and 250 ± 50 mPa×s for Ebalta resin) and reinforced with different CNFs contents (0.25, 0.5; 0.75 and 1 wt.% of CNFs) was analysed. Subsequently, considering the few studies found in the literature, a study will be carried out to evaluate the benefits of nano-reinforcements on the viscoelastic response of laminated composites. For this purpose, only the laminates involving the neat resin (resins without CNFs) and those containing the CNFs content that maximized the static properties will be subjected to stress relaxation and creep tests for different periods of time (3 hours and 100 hours). Finally, based on the experimental results for 3 hours, the analytical Kohlrausch-Williams-Watts (KWW) and Findley models will be fitted and subsequently validated for 100 hours by comparability with those obtained experimentally.

7.2 Materials and methods

Composite laminates involving two different resins were studied in this work. For this purpose, an epoxy resin SR 8100 with hardener SD 8824, both supplied by Sicomin, and an epoxy resin AH 150 with hardener IP 430, both supplied by Ebalta, were combined with eight layers of bidirectional carbon fibre 195-1000P (195 g/m²) using the hand lay-up technique. The plain weave used consists of carbon fibres at 0 and 90 degrees with 98 ± 4% g/m² in each direction, and more details about the resins can be found in previous work [23]. All layers were placed in the same direction to obtain plates with overall dimensions of 330 × 330 × h (mm), where t is the thickness of the laminates after curing (h = 1.5 ± 0.1 mm for laminates with Sicomin resin and 1.9 ± 0.1 for the Ebalta resin). Subsequently, they were placed inside a vacuum bag and subjected to a compressive load of 2.5 kN load to obtain a constant fibre volume fraction and uniform laminate thickness. Finally, according to the supplier´s guidelines, the laminates produced with the Sicomin resin were cured at room temperature (RT) for 24 hours and subjected to a post-cure at 40 °C for 24 hours, while the laminates involving the Ebalta resin were cured at RT for 48 hours and subjected to a post-cure at 80 °C for 5 hours. In both composites, the bag remained attached to a vacuum pump for the first 4 hours to eliminate any air bubbles.

To assess the benefits of CNFs on the bending properties of the composite laminates, these resins were nano-enhanced with 0.25%, 0.5%; 0.75% and 1% by weight of CNFs. These nanofibre contents were also used in a previous study to evaluate the value that maximized the static properties of each resin [23], and the results obtained are summarized in Figure 7.1. For this purpose, the carbon nanofibres used were supplied by Sigma-Aldrich which, according to the manufacturer's datasheet, are pyrolytically stripped (conical) with an average diameter of 130 nm, length between 20 and 200 μm and average specific surface area of 54 m²/g.

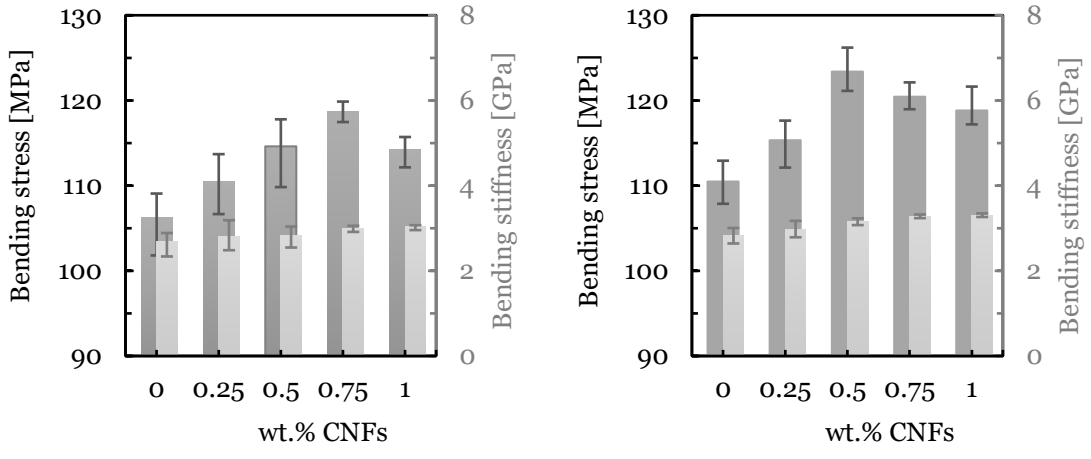

Figure 7.1: Effect of CNFs content on bending stress and bending stiffness for the: a) Sicomin resin; b) Ebalta resin (detailed information can found in previous work [23]).

Their mixture into the resin was conducted using a high-speed shear mixer at 1000 rpm, at RT for 3 hours, followed by 10 minutes at 150 rpm for the hardener to disperse into the system. Simultaneously, this procedure was combined with an ultrasonic temperature-controlled bath (with a frequency of 40 kHz) to improve the dispersion of the nanofibres. Finally, the system was degassed in a vacuum oven. This optimised methodology is conveniently reported in the work of Santos et al. [19]. After ensuring good dispersion of the CNFs into the resins, these systems (resin + CNFs) were combined with the carbon fibres using the procedure described above (similar to that used with the neat resins to produce carbon/epoxy laminates).

The samples used in this study were cut from those plates with the dimensions 80 × 10 × h (mm) and tested in the bending mode (see Figure 7.2). Regarding the three-point bending (3PB) tests, they were carried out at RT in a Shimadzu universal testing machine, model Autograph AGS-X, with a 10 kN load cell, at a displacement rate of 2 mm/min and, for each condition, at least five specimens were tested in accordance with the European Standard EN ISO 178:2003. The span used for all configurations was 40 mm. These tests were also useful for selecting the values used in the creep and stress relaxation tests to ensure that they were performed within the elastic regime of the composites.

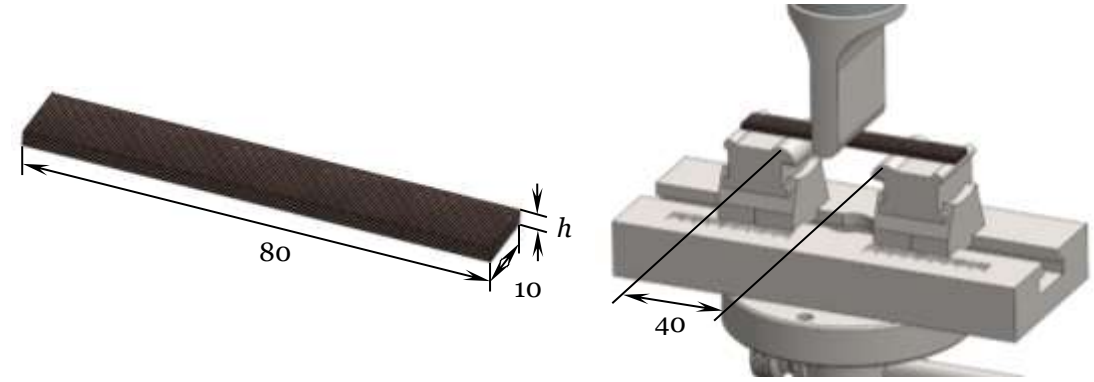

a) b)

Figure 7.2: a) Geometry of the specimens; b) Schematic view of the three-point bending apparatus. All dimensions in mm.

The same equipment was used to perform the stress relaxation and creep tests at RT and with samples similar to those described above. Note that these tests were only performed with laminates whose CNFs content maximized the static properties. Therefore, regarding the stress relaxation tests and according to the recommendations described in ASTM E328-13, a fixed strain was applied (corresponding to 200 MPa, 450 MPa and 700 MPa for composites involving the Sicomin resin, and 190 MPa, 380 MPa and 570 MPa for those involving the Ebalta resin) and the stress recorded during the loading time of 3 hours. In terms of creep tests, they were carried out according to the recommendations described in ASTM D2990-09 standard. In this case, a fixed bending stress was applied (with values similar to those previously reported), and the displacement recorded during 3 hours of loading. A 40 mm span was used in all the tests and at least three specimens were tested.

Finally, for the execution of this work plan about forty days elapsed between production and the beginning of the last test, but to guarantee that all samples were tested under the same conditions, they were stored in controlled environmental conditions (no sun exposure, RT (22-24 °C) and relative humidity between 55% and 60%). Subsequently, during testing, all specimens were also subjected to the same laboratory conditions (RT (22-24 °C) and relative humidity between 55% and 60%).

7.3. Results

7.3.1. Static characterization

From the static tests performed to evaluate the CNFs content to maximize the bending properties, Figure 7.3 shows the typical curves obtained and which are representative of all others obtained in this study.

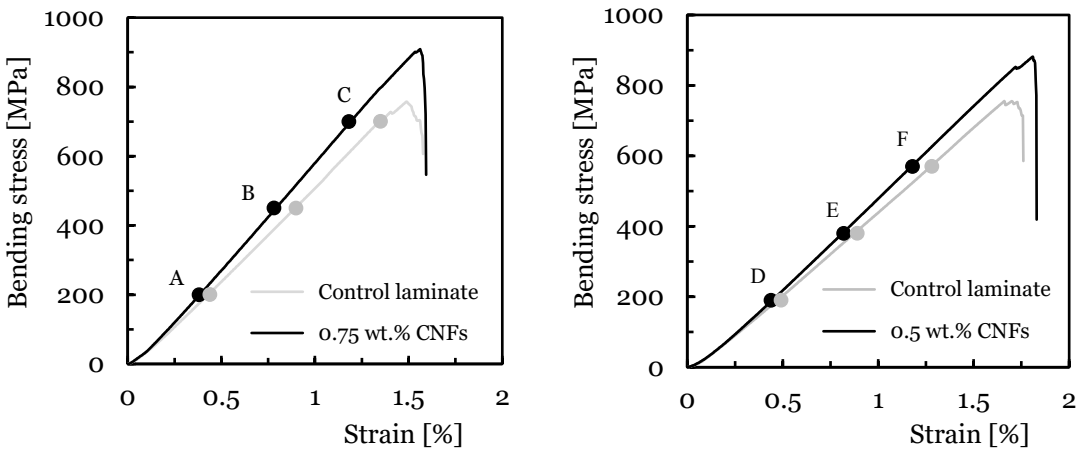

a) b)

Figure 7.3: Bending stress-strain curves for composite laminates with: a) Sicomin matrix; b) Ebalta matrix.

It is possible to observe that both composites show a quasi-brittle behaviour, where the bending stress increases linearly with the strain, culminating in a sudden drop after reaching the peak stress. Figure 7.4 shows the damage mechanism common to all composites, where it is possible to observe the existence of broken fibres under compression, accompanied by small delamination around them. Note that at the top of the image, due to the applied loading, there is a region subject to compression while the bottom is in tensile. According to the literature, this damage mechanism is typical of composites involving carbon fibres [17,24], due to their low compressive strength, in addition to high compressive stress concentration in the pin load contact region [24].

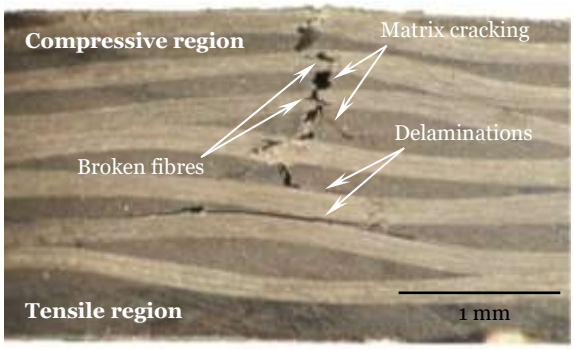

Figure 7.4: Typical failure damage observed for control laminates.

From these curves (Figure 7.3), the bending properties shown in Figure 7.5 are obtained. In terms of bending strength, for example, average values of 752.2 ± 15.0 MPa and 756.2 ± 13.9 MPa were found for laminates with neat Sicomin and Ebalta resins (resins without CNFs), respectively. Furthermore, the bending strength was maximized when the resins were filled with 0.75 wt.% and 0.5 wt.% of CNFs, respectively, and these values were about 20.4% (from 752.2 MPa to 905.3 MPa) and 12.5% (from 756.2 MPa to 850.9 MPa) higher than those obtained with the control laminates.

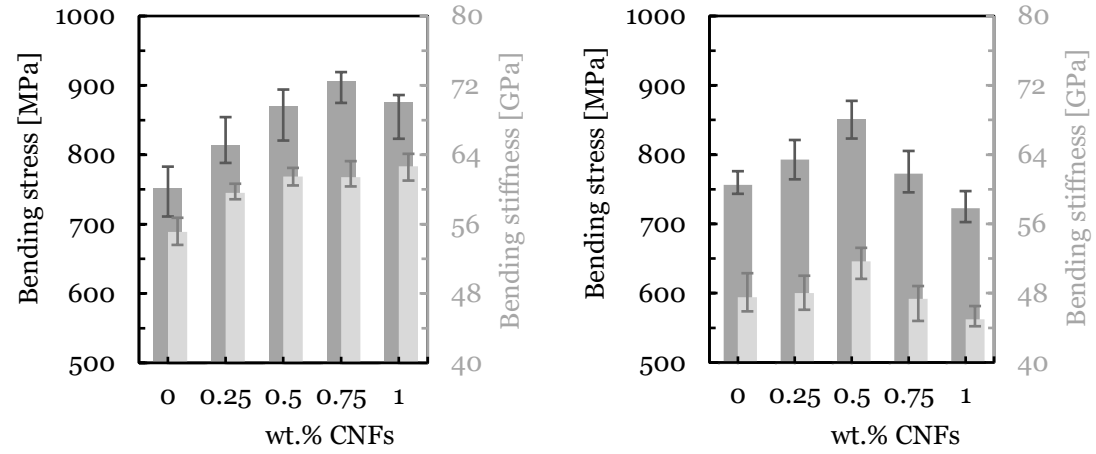

Figure 7.5: Bending stress and bending stiffness for laminates produced with different wt.% CNFs for: a) Sicomin resin; b) Ebalta resin.

These results also highlight that the bending strength was maximized for the same CNFs content observed in the previous study (see Figure 7.1) involving these resins and the same nano-reinforcements [23]. In the previous mentioned study, it was observed that higher values of CNFs promoted agglomerates, which drastically affected the mechanical properties. Moreover, the difference in viscosities (250 ± 50 mPa×s for the Ebalta resin and 390 mPa×s for the Sicomin resin) was not relevant, given the higher physicochemical compatibility between Sicomin resin and CNFs [23].

In terms of creep and stress relaxation tests, these were performed involving control laminates (with neat resins) and laminates whose CNFs content maximized the bending strength (0.75 wt.% and 0.5 wt.% of CNFs for Sicomin and Ebalta resins, respectively). Figure 7.3 also shows the different bending stress levels used in the creep and stress relaxation tests. To ensure that all tests were performed within the elastic regime, stresses of 200 MPa (A), 450 MPa (B) and 700 MPa (C) were selected for laminates involving the Sicomin resin and for the Ebalta resin 190 MPa (D), 380 MPa (E) and 570 MPa (F). These values are close to 25%, 50% and 75% of the maximum bending stress for each laminate, respectively.

7.3.2. Stress relaxation

According to the bibliography, stress relaxation in polymer systems is based on physical and/or chemical processes. While molecular rearrangements that require little formation or rupture of primary bonds are expected in the first case, chain scission, crosslink scission or crosslink formation occur in the second case [25–27]. However, when the polymers are reinforced with fibres, these hinder the molecular flow and delay the relaxation process, as shown in Figure 7.6.

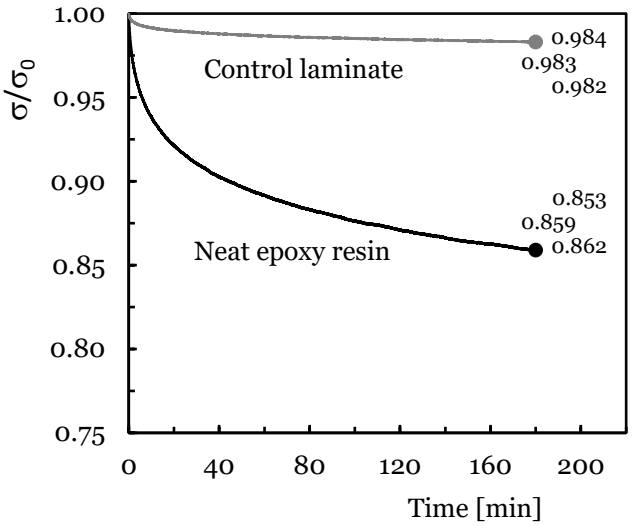

Figure 7.6: Stress relaxation curves obtained with samples produced with neat Ebalta resin (obtained from [28]) and carbon/epoxy laminates produced with neat Ebalta resin.

This figure depicts the benefits obtained with the introduction of carbon fibres, where σ represents the bending stress at any given moment of the test and σ_0 represents the initial bending stress. This analysis involves only resin without nano-enhancements (CNFs) and the values shown in Figure 7.6 at the end of each curve represent the quotient between the average value of the bending stress after 180 min and the initial value of the bending stress used in the test, as well as the respective average values corresponding to the maximum and minimum obtained.

It is possible to observe that the epoxy resin relaxes much more than the composite, showing that the latter is 8.3 times less sensitive than the resin to the stress relaxation phenomenon. The fibres hinder the molecular flow and delay the relaxation process, although, the interface properties are

very relevant because relaxation processes can occur due to the breaking of bonds and respective propagation [22]. Therefore, in composites, the stress relaxation phenomenon is a consequence of two mechanisms: matrix phase relaxation and fibre/matrix debonding zones with the respective crack propagation [27,29].

Regarding the benefits obtained with resins reinforced with CNFs, Figure 7.7 presents the average bending stress versus time curves for all laminates and bending strains. Again, σ represents the bending stress at any given moment of the test and σ_0 represents the initial bending stress. The values presented for 180 min represent the average value and respective maximum and minimum values observed in each test/condition.

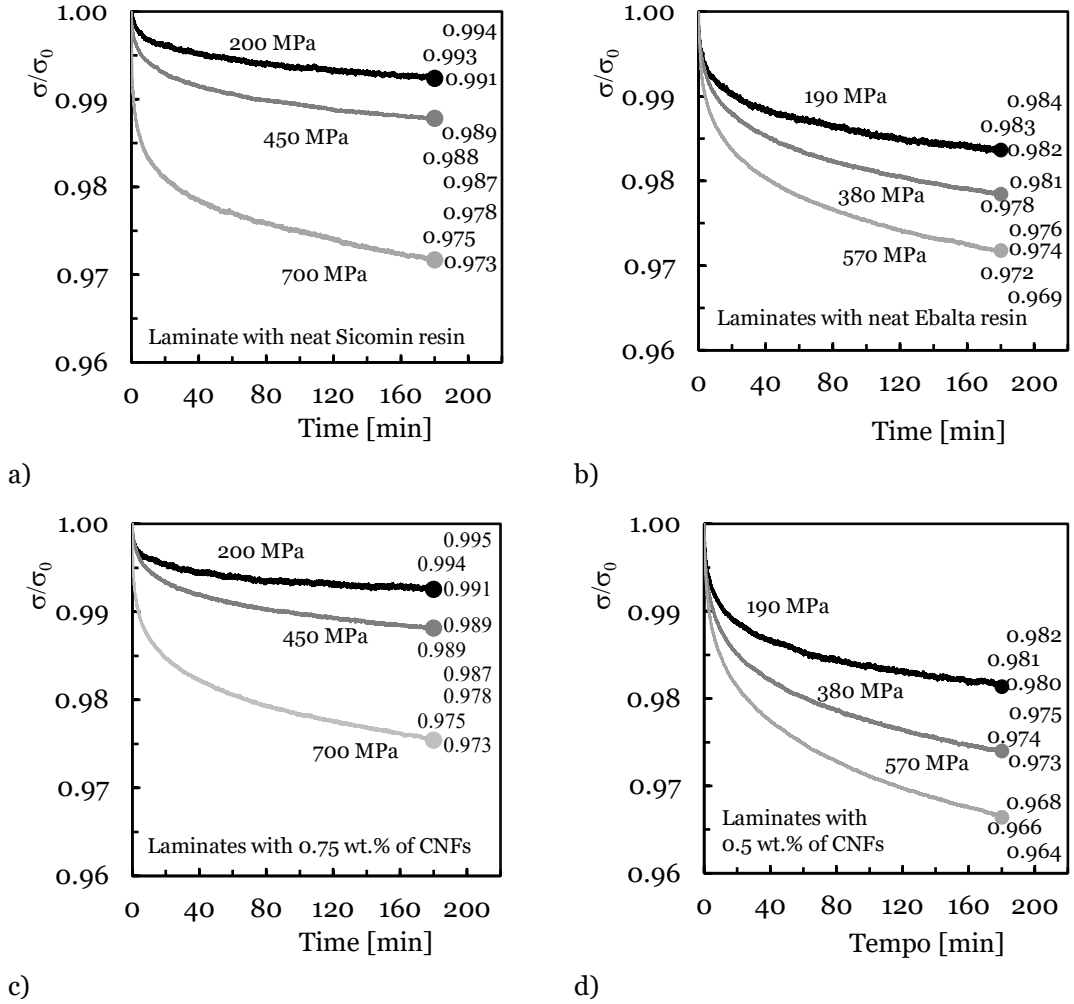

Figure 7.7: Stress relaxation curves for all bending strains and laminates with: a) Neat Sicomin resin; b) Neat Ebalta resin; c) Sicomin resin enhanced with 0.75 wt.% of CNFs; d) Ebalta resin enhanced with 0.5 wt.% of CNFs.

Regardless of resins and bending strain levels, it is possible to observe a decrease in bending stress with time. The bending stress never reached a constant value because this study focuses on short-term tests. In fact, they are an easy, fast and reliable method to predict the behaviour for longer periods of time [29,30]. It is also noticed that higher bending strains promote higher stress

relaxation values. Referring only to the values corresponding to laminates produced with neat Sicomin resin, the bending stress decreases by only 0.8% for the bending stress of 200 MPa, but this value is already 2.9% for the bending stress of 700 MPa (3.6 times higher). However, this evidence also extends to the other configurations analysed. What´s more, as reported in literature [29,31–34], it is also noted that there is an initial period in which the decrease in bending stress is higher compared to the remaining time. For example, considering laminates produced with Sicomin resin nano-enhanced by 0.75 wt.% of CNFs (Figure 7.7.c)), there is a decrease around 0.4%, 0.8% and 2.0% in the first 30 minutes for the bending strains corresponding to bending stresses of 200 MPa, 450 MPa and 700 MPa, respectively, while the remaining decrease (between 30 and 180 min) is only about 0.3%, 0.4% and 0.8%, respectively. Again, this evidence also extends to all configurations analysed. Therefore, as previously reported, the stress relaxation response is due to the matrix phase relaxation and fibre/matrix debonding zones with the respective crack propagation [27,29]. However, Figure 7.7 also shows that laminates with Ebalta resin show higher stress relaxation values than those observed for laminates produced with Sicomin resin. As reported by Santos et al. [23], this can be attributed to their different interfacial adhesion and different physical interactions resulting from the non-identical polarity of both resins. On the other hand, according to Vlasveld et al. [35] and Jian and Lau [36], the deformation process in polymers under load is strongly dependent on the mobility of the chains and not only dependent on temperature. Finally, the CNFs effect is also shown in Figure 7.7, and considering the expected experimental variation and measurement errors, the almost identical results that are observed for the same resin typology reveal that CNFs do not have a deleterious effect on the relaxation behaviour of the laminates. This denotes that the dispersed nanoparticles bind to the matrix via interphases, bridging segments and junctions to support the load, but are not in sufficient quantity to promote immobility of the polymer chains [37–39]. Furthermore, it should also be emphasized that the bending stresses used in these tests are the same for each type of resin, giving laminates with nano-reinforced resins a slight advantage due to their higher bending strength compared to laminates with neat resin.

Literature presents several models to predict the behaviour of stress relaxation based on results obtained in short-term tests. In this context, Kohlrausch-Williams-Watts model (KWW) is preferable to those based on spring-dashpot systems, because it promotes more accurate predictions [40]. Although the constants involved in this model have no physical significance, it fits the experimental curves quite accurately and can be used to predict the stress relaxation response for longer lives [29,32,33,41]. According to this model, the relaxation function ϕ is given by:

$$\phi(t) = \frac{\sigma(t)}{\sigma_0} = e^{-\left(\frac{t}{\tau}\right)^{\beta}} \tag{7.1}$$

where $\sigma(t)$ and σ_0 are the stress at time t and at $t = 0$, respectively, β a fractional power exponent (known as non-exponential factor) and τ the KWW relaxation time. The β-term represents the degree of non-exponentially of the relaxation function.

The comparison between the experimental and theoretical curves is shown in Figure 7.8 for the laminate produced with Ebalta resin reinforced with 0.5 wt.% CNFs. However, this comparison is representative of all conditions analysed, where the final bands represent the maximum and minimum values obtained in each condition analysed. Table 7.1 summarizes all constants of the KWW model and respective error in relation to the experimental results, while Table 7.2 presents the constants of the equations that fit the KWW model (Figure 7.8.b)). In detail, Figure 7.8.a) shows the good accuracy obtained with this model, in which the error between the theoretical and experimental curves is only 0.05% after 180 min of testing. However, this evidence can be generalized to all conditions and materials because, as shown in Table 7.1, the maximum error obtained with this model is less than 0.13%. In terms of prediction, Reis et al. [29,32,41] suggested that when the parameters of the KWW model are presented against the applied stresses, it is possible to fit a function capable of being used as a prediction tool to predict the stress relaxation response for any bending displacement.

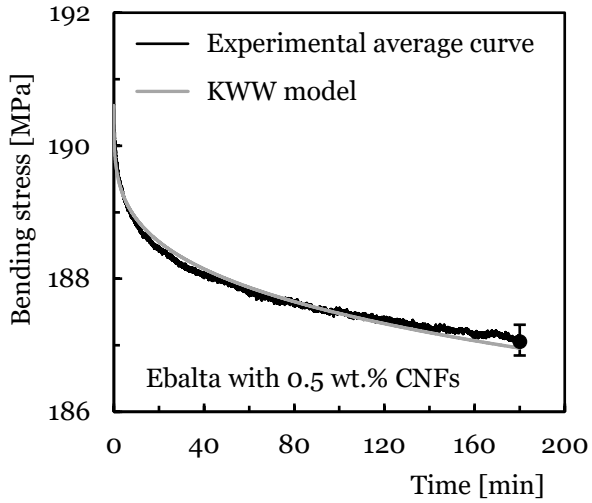

a)

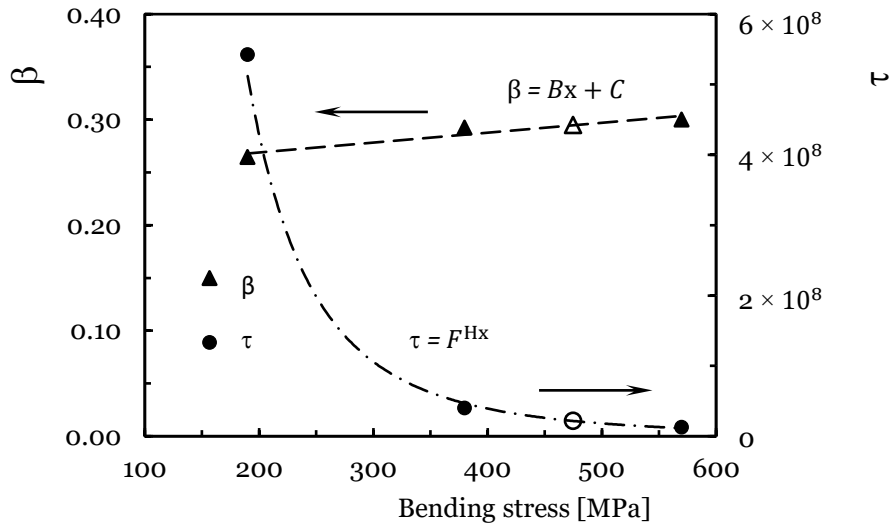

b)

Figure 7.8: a) Comparison between experimental and theoretical curves for laminates with Ebalta resin reinforced with 0.5 wt.% CNFs and bending stress of 190 MPa; b) KWW parameters versus bending stress for laminates with Ebalta resin reinforced with 0.5 wt.% CNFs.

In this context, Figure 7.8.b) illustrates this methodology for laminates produced with Ebalta resin reinforced with 0.5 wt.% of CNFs, as well as the bending stress value of 475 MPa (corresponding to the white marks: $\beta = 0.291$ and $\tau = 2.17\times10^{7}$) that will be used for validation. This procedure was applied to all laminates and the values of the respective equations used to predict the stress relaxation response are shown in Table 7.2. Therefore, considering the values shown in Figure 7.8.b) ($\beta = 0.291$ and $\tau = 2.17\times10^{7}$), it is possible to conclude that the error obtained with the methodology described above is less than 0.23%. However, when all materials are considered, the maximum error observed is only 0.87%, which reveals the good accuracy of this methodology (see Table 7.2).

Table 7.1: Constants of the KWW model for stress relaxation.

Material	Initial bending stress [MPa]	β	τ	Bending stress after 3 hours [MPa]		
				Experimental value	KWW value	Error [%]
Sicomin control laminate	200	0.228	3.61×10^{11}	199.30	199.27	0.013
	450	0.282	1.00×10^{9}	445.13	445.05	0.019
	575 (*)	0.252	1.48×10^{9}	560.67	565.58	0.871
	700	0.240	8.41×10^{8}	683.49	683.23	0.038
Sicomin laminate + 0.75 wt.% CNFs	200	0.344	2.41×10^{8}	198.95	198.91	0.020
	450	0.282	9.69×10^{8}	445.18	444.99	0.043
	575 (*)	0.239	3.09×10^{9}	566.96	565.04	0.339
	700	2.000	8.63×10^{9}	680.09	679.97	0.0175
Ebalta control laminate	190	0.263	9.67×10^{8}	187.56	187.48	0.044
	380	0.299	5.66×10^{7}	372.30	372.03	0.074
	475 (*)	0.300	3.42×10^{7}	463.16	463.36	0.043
	570	0.306	2.15×10^{7}	555.13	554.42	0.129
Ebalta laminate + 0.5 wt.% CNFs	190	0.265	5.42×10^{8}	187.05	186.96	0.050
	380	0.293	4.00×10^{7}	370.79	370.44	0.092
	475 (*)	0.291	2.17×10^{7}	461.65	460.62	0.223
	570	0.300	1.27×10^{7}	551.46	550.98	0.086

(*) Values used in the forecast.

Table 7.2: Parameters of the equations that fit the KWW model.

Material (Initial bending stress)		β			τ		
		B	*C*	*R*	*F*	*H*	*R*
Sicomin (575 MPa)	Control laminate	2.36×10^{-5}	0.239	0.044	1.58×10^{12}	-0.012	0.771
	Laminate + 0.75 wt.% CNFs	-2.86×10^{-4}	0.404	0.994	5.05×10^{7}	7.16×10^{-3}	0.984
Ebalta (475 MPa)	Control laminate	1.12×10^{-4}	0.247	0.857	9.70×10^{16}	-3.53	0.986
	Laminate + 0.5 wt.% CNFs	9.38×10^{-5}	0.250	0.901	3.77×10^{16}	-3.45	0.986

R = Correlation coefficient.

Finally, the ability of this model to predict the structural behaviour for longer periods of time was also analysed and, for this purpose, the reasonable accuracy obtained is shown in Figure 7.9 for a bending stress of 475 MPa and 100 hours of testing (33.4 times longer than the time used in short-term tests). In this case, the observed error is less than 0.6%, and although the theoretical curves lead to lower values of stress relaxation than those obtained experimentally, they are within the scatter of the experimental results. Therefore, the reasonable accuracy obtained shows that the methodology used to estimate the effect of bending stress on stress relaxation for long periods of time can be used with some confidence. Nonetheless, further studies for other materials and longer periods of time will be needed to confirm the robustness of the model.

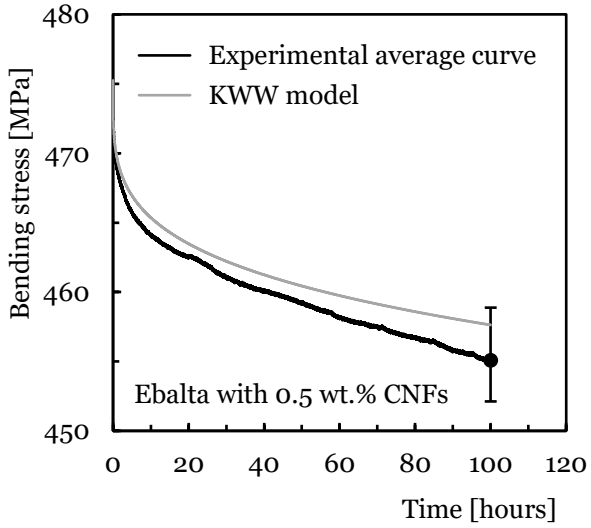

Figure 7.9: Comparison between experimental and theoretical curves for 100 hours and a bending stress of 475 MPa.

7.3.3. Creep

In terms of creep, this phenomenon in polymers happens even at RT and for low stress levels as a consequence of the molecular motion in backbone polymer arrangement [21,42–44]. However, as shown in Figure 7.10, the creep process is delayed by the presence of carbon fibres because the elastic deformation and viscous flow are retarded. Inevitably, the fibre/matrix interface proves to

be very important because the bonds' breakage and their propagation control the creep displacement [6,21].

Similar to what was observed for stress relaxation, these curves also show that the resin exhibits a higher creep displacement than the composite. For example, after 180 minutes, the resin has a creep deformation almost 11 times higher than the composite, which evidences that carbon fibres retard the elastic deformation and the viscous flow of the matrix [6,21].

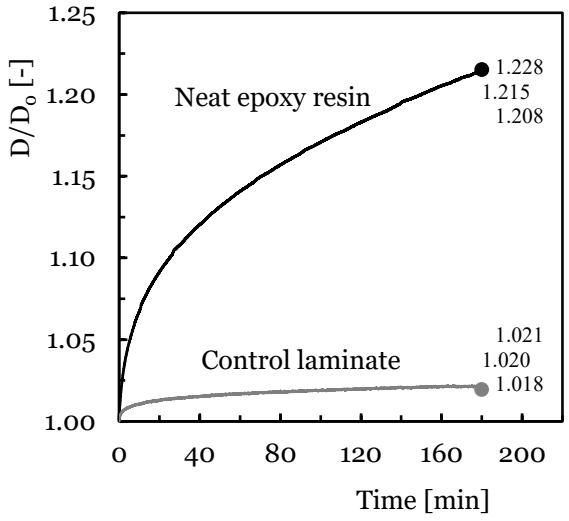

Figure 7.10: Creep curves obtained with samples produced with neat Ebalta resin (obtained from [28]) and carbon/epoxy laminates produced with neat Ebalta resin.

In relation to the benefits obtained with resins reinforced with CNFs, Figure 7.11 presents the average creep displacement versus time curves for all laminates and bending stresses, where the displacement presented is the displacement at any time of the test (D) divided by its initial value (D_o). The values presented for 180 min represent the average value and respective maximum and minimum values observed in each test/condition. For all laminates and bending stresses, it is possible to observe an increase in creep displacement over time. In detail, all curves present an instantaneous displacement, which depends on the stress level, followed by the primary and secondary creep regimes that characterise the typical creep curves. However, for the analysed conditions, the third regime is expected to occur only for higher bending stresses or longer periods of time. On the other hand, there is a strong dependence of the creep behaviour with the applied stress level. Considering the control laminates produced with neat Sicomin resin, for example, while creep displacement increases around 1% for a bending stress of 200 MPa, this value is about 2 times higher for the bending stress of 700 MPa. These values for laminates produced with Ebalta resin are 2% and 1.4 times higher, respectively, for bending stresses of 190 MPa and 570 MPa. Furthermore, comparing both laminates, the creep displacements are higher for laminates produced with Ebalta resin due to the higher mobility of their polymer chains [35,36]. Finally, similar to what was observed in the stress relaxation behaviour, CNFs do not have a noxious effect on the creep behaviour of the laminates when considering the observed experimental variation

and no measurement errors occurred. The dispersed CNFs bind to the matrix via interphase, bridging segments and junctions to support the load, but are not sufficient to improve the restriction to slippage, realignment and motion of polymeric chains [37–39].

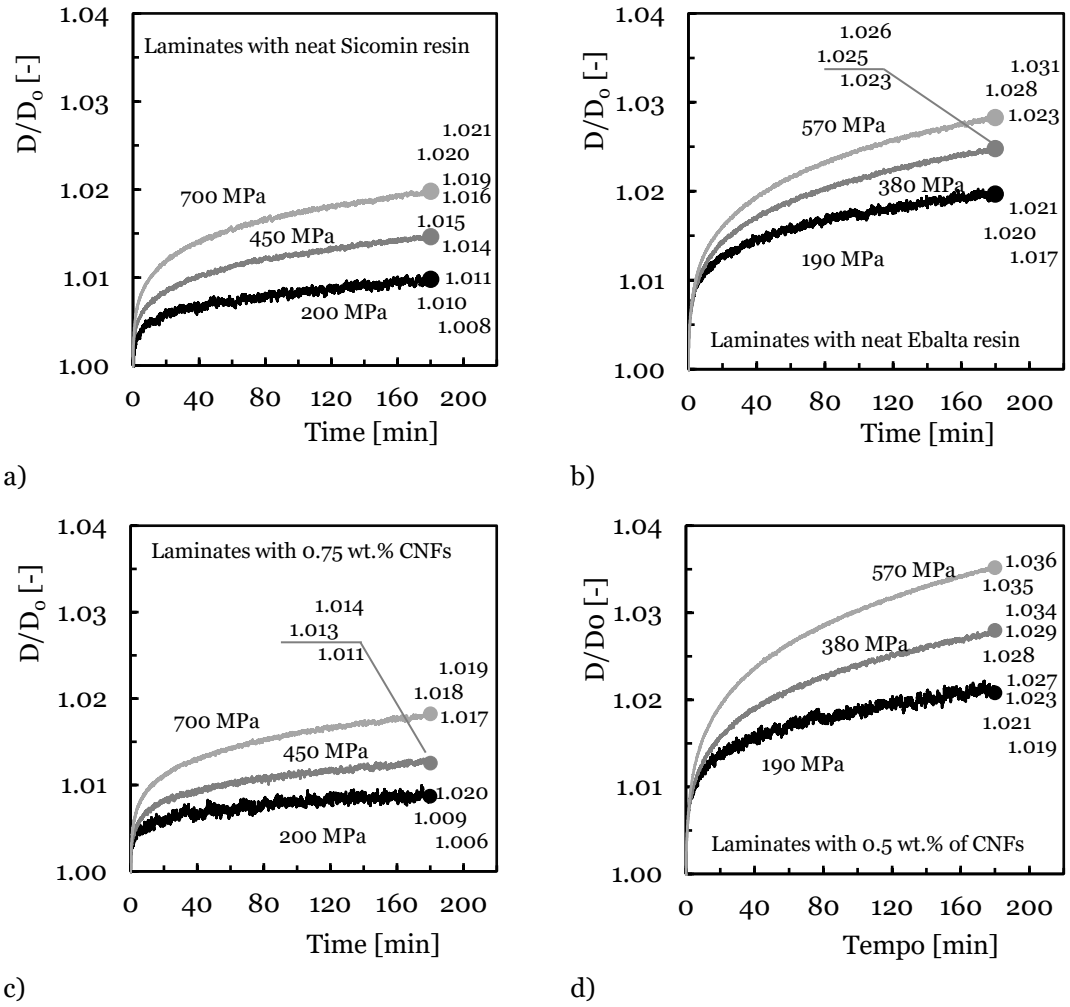

Figure 7.11: Creep curves for all bending stresses and laminates with: a) neat Sicomin resin; b) neat Ebalta resin; c) Sicomin resin enhanced with 0.75 wt.% of CNFs; d) Ebalta resin enhanced with 0.5 wt.% of CNFs.

In terms of creep prediction, two models will be compared. Findley law (equation 7.2) is widely used to describe the creep behaviour of composite materials [20,43,45,46] and in some studies it is applied to short-term creep tests [46–48], which is given by:

$$\varepsilon(t) = \varepsilon_0 + At^n \tag{7.2}$$

where $\varepsilon(t)$ is the creep displacement at time t, ε_0 is the instantaneous elastic displacement or time-independent, A is the amplitude of transient creep (time-dependent), and n is a constant independent of the stress and generally less than one.

The other one is the KWW equation [29], which is given by:

$$\varepsilon(t) = \varepsilon_0 e^{\left(\frac{t}{\tau}\right)^{\beta}} \quad (7.3)$$

where, ε is the displacement, t the time, ε_0 is the initial displacement when a constant stress is applied, the β parameter is the distribution factor, and it is related to the breadth of the distribution of creep times or relaxation times, and τ accounts for the mean creep time.

In this context, Figure 7.12 compares the experimental and theoretical curves obtained with the KWW and Findley models for laminates produced with Ebalta resin reinforced with 0.5 wt.% CNFs. This evaluation is representative of all analysed conditions, where the final bands represent the maximum and minimum values obtained in each analysed condition. Tables 7.3 and 7.4 summarise all the constants of Findley's law and the KWW model, respectively, while Table 7.5 and 6 present the constants of the equations that fit the two models (Figures 7.12.b) and 7.12.c)).

From Figure 7.12.a), it is possible to observe the good accuracy obtained with both models, in which the errors between the theoretical and experimental curves are 0.014% and 0.064% after 180 min of testing and for Findley's law and the KWW model, respectively. However, this evidence can be generalized to all conditions and materials because, as shown in Tables 7.3 and 7.4, the maximum error obtained with these models is less than 0.6%. In terms of prediction, a methodology similar to that used for stress relaxation is utilised to predict the creep response for any bending stress [29]. In this context, Figures 7.12.b) and 12.c) illustrate this methodology for laminates produced with Ebalta resin reinforced with 0.5 wt.% of CNFs, as well as the bending stress value of 475 MPa (corresponding to the white marks) that will be used for validation. Nevertheless, this procedure was applied to all materials and the values of the respective equations used to predict the creep displacement are shown in Tables 7.5 and 7.6.

Considering the values shown in Figure 7.12.b) (ε_0 = 1.83, β = 0.313 and τ = 7.26×10^6) and Figure 7.12.c) (ε_0 = 0.572, A = 0.970 and n = 9.25×10^{-3}), it is possible to conclude that the error obtained is less than 0.26%. However, when all materials are considered, after 180 minutes the maximum error observed is only 0.544%, which reveals the good accuracy of this methodology (see Tables 7.5 and 7.6).

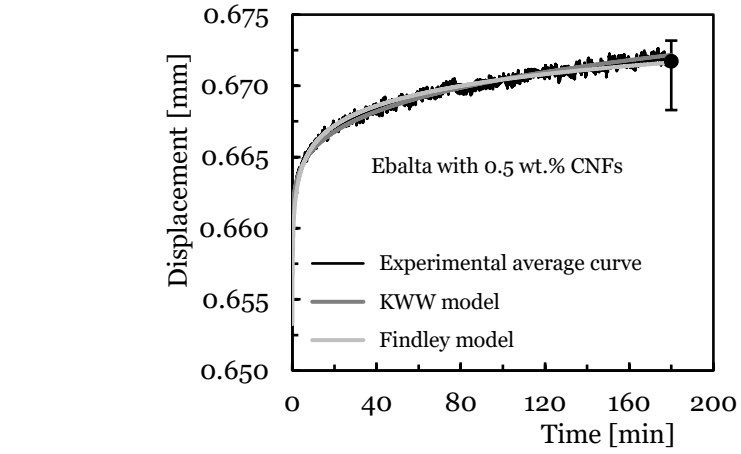

a)

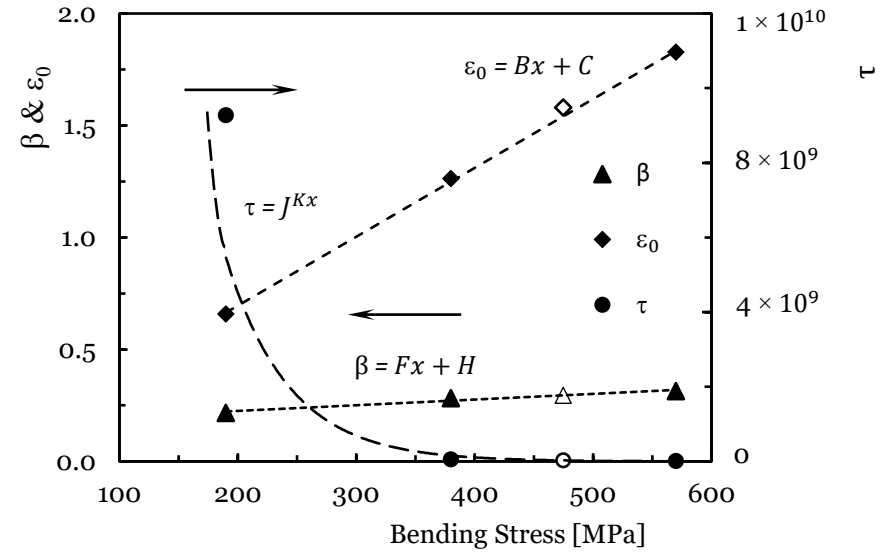

b)

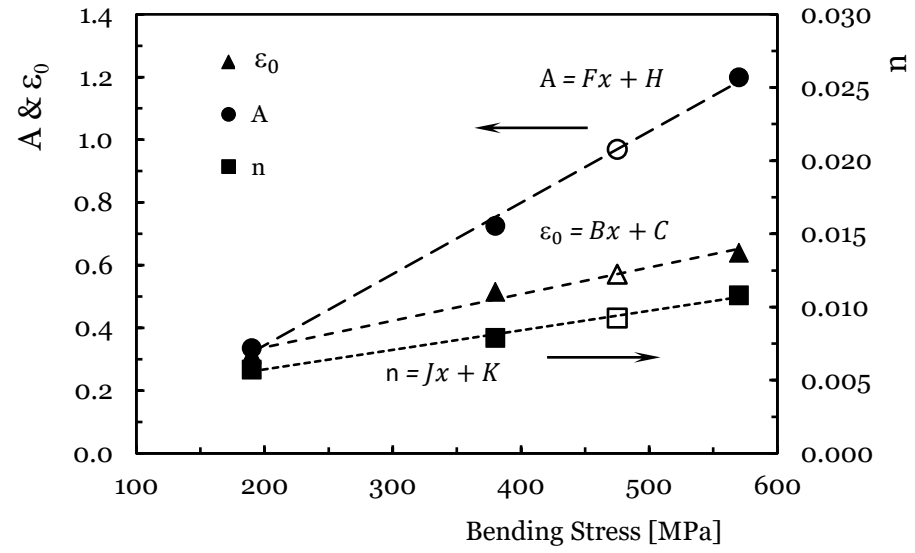

c)

Figure 7.12: a) Comparison between experimental and theoretical curves for laminates with Ebalta resin reinforced with 0.5 wt.% CNFs and a bending stress of 190 MPa; b) KWW parameters versus bending stress; c) Findley parameters versus bending stress.

Table 7.3: Constants of the Findley's law for creep.

Material	Initial bending stress [MPa]	ε_0	A	n	Displacement after 3 hours [mm]		
					Experimental value	Findley value	Error [%]
Sicomin control laminate	200	0.329	0.351	3.04×10^{-3}	0.690	0.690	0.055
	450	0.535	0.802	3.91×10^{-3}	1.37	1.37	0.051
	575 (*)	0.631	1.03	4.89×10^{-3}	1.70	1.71	0.544
	700	0.729	1.26	4.59×10^{-3}	2.05	2.05	0.054
Sicomin laminate + 0.75 wt.% CNFs	200	0.316	0.329	3.34×10^{-3}	0.656	0.656	0.0008
	450	0.636	0.710	4.53×10^{-3}	1.38	1.38	0.056
	575 (*)	0.952	0.779	5.37×10^{-3}	1.78	1.77	0.278
	700	1.22	0.883	6.50×10^{-3}	2.16	2.16	0.056
Ebalta control laminate	190	0.330	0.354	5.34×10^{-3}	0.703	0.702	0.042
	380	0.531	0.754	6.80×10^{-3}	1.33	1.33	0.084
	475 (*)	0.655	0.883	7.79×10^{-3}	1.60	1.60	0.065
	570	0.772	1.034	8.80×10^{-3}	1.89	1.89	0.041
Ebalta laminate + 0.5 wt.% CNFs	190	0.317	0.336	5.73×10^{-3}	0.672	0.672	0.014
	380	0.515	0.726	7.89×10^{-3}	1.30	1.30	0.103
	475 (*)	0.572	0.970	9.25×10^{-3}	1.63	1.62	0.258
	570	0.640	1.199	1.08×10^{-2}	1.96	1.96	0.105

(*) Values used in the forecast.

Finally, the ability of these models to predict the structural behaviour for longer periods of time was evaluated and the good accuracy obtained is shown in Figure 7.13 for a bending stress of 475 MPa and 100 hours of testing (33.4 times longer than the time used in short-term tests). It is possible to observe that the error obtained by Findley's law is around 0.2% and by the KWW model is about 0.4%. Furthermore, it is noticed that Findley's law leads to creep displacements slightly higher than the experimental values, while with the KWW model they are slightly lower. However, in both cases, the theoretical values are within the experimental scatter, revealing that this methodology can be used to estimate the effect of bending stress on the creep response for longer periods of time with good accuracy. However, similar to the results observed for stress relaxation, further studies for other materials and longer periods of time will be needed to confirm the robustness of the models.

Table 7.4: Constants of the KWW model for creep.

Material	Initial bending stress [MPa]	ε_0	β	τ	Displacement after 3 hours [mm]		
					Experimental value	KWW value	Error [%]
Sicomin control laminate	200	0.683	0.260	9.83×10^{9}	0.690	0.690	0.012
	450	1.35	0.266	1.38×10^{9}	1.37	1.37	0.024
	575 (*)	1.68	0.259	1.19×10^{9}	1.70	1.71	0.496
	700	2.01	0.255	8.03×10^{8}	2.05	2.05	0.041
Sicomin laminate + 0.75 wt.% CNFs	200	0.648	0.198	7.17×10^{11}	0.656	0.656	0.036
	450	1.36	0.265	1.14×10^{9}	1.38	1.38	0.098
	575 (*)	1.74	0.248	2.74×10^{9}	1.78	1.77	0.100
	700	2.12	0.246	2.03×10^{9}	2.16	2.16	0.027
Ebalta control laminate	190	0.689	0.224	7.10×10^{9}	0.703	0.703	0.041
	380	1.30	0.273	1.32×10^{8}	1.33	1.34	0.049
	475 (*)	1.57	0.276	9.92×10^{7}	1.60	1.61	0.261
	570	1.84	0.285	4.58×10^{7}	1.89	1.90	0.085
Ebalta laminate + 0.5 wt.% CNFs	190	0.658	0.217	9.27×10^{9}	0.673	0.672	0.064
	380	1.26	0.283	5.29×10^{7}	1.29	130	0.086
	475 (*)	1.58	0.295	2.55×10^{7}	1.63	1.63	0.016
	570	1.83	0.313	7.26×10^{6}	1.91	1.92	0.144

(*) Values used in the forecast.

Table 7.5: Constants of the equations that fit the Findley model.

Material (Initial bending stress)	ε_0			A			n		
	B	C	R	F	H	R	J	K	R
Sicomin (575 MPa)									
Control laminate	8.00×10^{-4}	0.171	0.998	1.82×10^{-3}	-0.014	0.998	3.69×10^{-6}	2.29×10^{-3}	0.999
Laminate + 0.75 wt.% CNFs	1.81×10^{-3}	-0.092	0.986	1.11×10^{-3}	0.142	0.977	6.32×10^{-6}	1.94×10^{-3}	0.990
Ebalta (475 MPa)									
Control laminate	1.16×10^{-3}	0.102	0.998	1.79×10^{-3}	0.034	0.995	9.11×10^{-6}	3.52×10^{-3}	0.996
Laminate + 0.5 wt.% CNFs	8.49×10^{-4}	0.168	0.991	2.27×10^{-3}	-0.110	0.998	1.33×10^{-5}	3.07×10^{-3}	0.996

R = Correlation coefficient.

Table 7.6: Constants of the equations that fit the KWW model.

Material (Initial bending stress)	ε_0			β			τ		
	B	*C*	*R*	*F*	*H*	*R*	*J*	*K*	*R*
Sicomin (575 MPa)									
Control laminate	2.65×10^{-3}	0.154	1	-9.20×10^{-6}	0.265	0.438	2.11×10^{10}	-5.01×10^{-3}	0.950
Laminate + 0.75 wt.% CNFs	2.95×10^{-3}	0.047	1	9.64×10^{-5}	0.193	0.700	2.33×10^{12}	-1.17×10^{-2}	0.823
Ebalta (475 MPa)									
Control laminate	3.04×10^{-3}	0.124	1	1.61×10^{-4}	0.200	0.943	5.42×10^{10}	-1.33×10^{-2}	0.998
Laminate + 0.5 wt.% CNFs	3.08×10^{-3}	0.080	1	2.54×10^{-4}	0.175	0.979	1.95×10^{11}	-1.88×10^{-2}	1

R = Correlation coefficient.

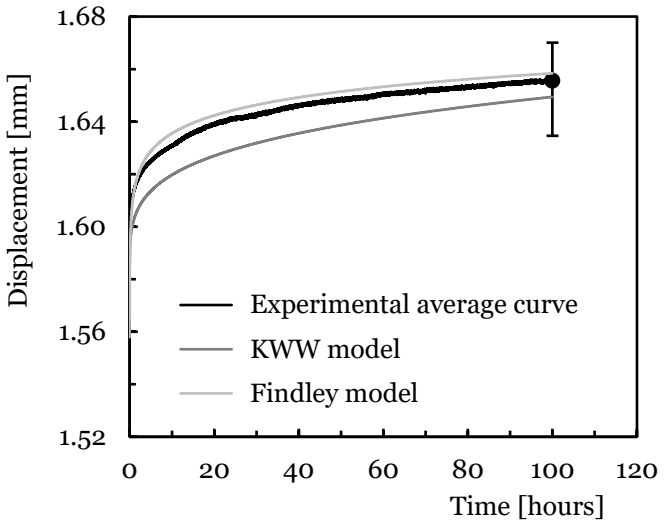

Figure 7.13: Comparison between experimental and theoretical curves for 100 hours and a bending stress of 475 MPa.

7.4 Conclusions

In the present work the viscoelastic properties of CFRP composite laminates produced by hand lay-up technique, with two epoxies resins Sicomin and Ebalta, nano-enhanced by CNFs were studied. From the results of the different characterization tests, the main conclusions were drawn. Static tests show a quasi-brittle behaviour, and the bending stress was maximized when the epoxies resins Sicomin and Ebalta were filled with 0.75 wt.% and 0.5 wt.% of CNFs, respectively. These values are about 20.4% (from 752.2 MPa to 905.3 MPa) and 12.5% (from 756.2 MPa to 850.9 MPa) higher than those obtained with the control laminates. Stress relaxation and creep tests show that, for both resins, a strong dependence of the viscoelastic behaviour with the applied stress level. However, identical results were obtained between the filled and the control laminates. The addition of CNFs does not have a deleterious effect on the relaxation behaviour of the laminates. This denotes that the dispersed nanoparticles bind to the matrix via interphases, bridging segments and junctions to support the load, but are not in sufficient quantity to promote

immobility of the polymer chains. The viscoelastic behaviour of CFRP composites nano-enhanced with CNFs was accurately predicted by the Kohlrausch-Williams-Watts (KWW) model and Findley power law, where a maximum error of 0.9% and 0.6% for stress relaxation and creep, respectively, was obtained.

Bibliography

[1] Alberto M. Introduction of Fibre-Reinforced Polymers – Polymers and Composites: Concepts, Properties and Processes. Fiber Reinforced Polymers - The Technology Applied for Concrete Repair, InTech; 2013, p. 3–40. https://doi.org/10.5772/54629.

[2] Che D, Saxena I, Han P, Guo P, Ehmann KF. Machining of carbon fiber reinforced plastics/polymers: A literature review. Journal of Manufacturing Science and Engineering 2014;136. https://doi.org/10.1115/1.4026526.

[3] Aamir M, Tolouei-Rad M, Giasin K, Nosrati A. Recent advances in drilling of carbon fiber–reinforced polymers for aerospace applications: a review. International Journal of Advanced Manufacturing Technology 2019;105:2289–308. https://doi.org/10.1007/s00170-019-04348-z.

[4] Marques A, Mocanu A, Tomić N, Balos S, Stammen E, Lundevall A, et al. Review on Adhesives and Surface Treatments for Structural Applications: Recent Developments on Sustainability and Implementation for Metal and Composite Substrates. Materials 2020;13:5590. https://doi.org/10.3390/ma13245590.

[5] Kim MT, Rhee KY, Lee JH, Hui D, Lau AKT. Property enhancement of a carbon fiber/epoxy composite by using carbon nanotubes. Composites Part B: Engineering 2011;42:1257–61. https://doi.org/10.1016/j.compositesb.2011.02.005.

[6] Georgakilas V, Perman JA, Tucek J, Zboril R. Broad Family of Carbon Nanoallotropes: Classification, Chemistry, and Applications of Fullerenes, Carbon Dots, Nanotubes, Graphene, Nanodiamonds, and Combined Superstructures. Chemical Reviews 2015;115:4744–822. https://doi.org/10.1021/cr500304f.

[7] Basheer B V., George JJ, Siengchin S, Parameswaranpillai J. Polymer grafted carbon nanotubes—Synthesis, properties, and applications: A review. Nano-Structures & Nano-Objects 2020;22:100429. https://doi.org/10.1016/j.nanoso.2020.100429.

[8] Kausar A, Rafique I, Muhammad B. Review of Applications of Polymer/Carbon Nanotubes and Epoxy/CNT Composites. Polymer - Plastics Technology and Engineering 2016;55:1167–91. https://doi.org/10.1080/03602559.2016.1163588.

[9] Son SY, Um SH, Jang HS, Jeon SK, Nahm SH, Kim HW, et al. Effective disentangling method of bundled multi-walled carbon nanotubes into individual multi-walled carbon nanotubes by magnetic-field induction. Journal of Industrial and Engineering Chemistry 2017;46:28–34. https://doi.org/10.1016/j.jiec.2016.09.030.

[10] Lee KM, Lee SE, Lee YS. Improved mechanical and electromagnetic interference shielding properties of epoxy composites through the introduction of oxyfluorinated multiwalled carbon nanotubes. Journal of Industrial and Engineering Chemistry 2017;56:435–42. https://doi.org/10.1016/j.jiec.2017.08.001.

[11] Han CL, Wang GD, Li N, Wang M, Liu X liang, Ma J he. Study on interlaminar performance of CNTs/epoxy film enhanced GFRP under low-temperature cycle. Composite Structures 2021;272:114191. https://doi.org/10.1016/j.compstruct.2021.114191.

[12] Siddiqui NA, Khan SU, Kim JK. Experimental torsional shear properties of carbon fiber reinforced epoxy composites containing carbon nanotubes. Composite Structures 2013;104:230–8. https://doi.org/10.1016/j.compstruct.2013.04.033.

[13] Geng Y, Liu MY, Li J, Shi XM, Kim JK. Effects of surfactant treatment on mechanical and electrical properties of CNT/epoxy nanocomposites. Composites Part A: Applied Science and Manufacturing 2008;39:1876–83. https://doi.org/10.1016/j.compositesa.2008.09.009.

[14] González-Domínguez JM, Martínez-Rubí Y, Díez-Pascual AM, Ansón-Casaos A, Gómez-Fatou M, Simard B, et al. Reactive fillers based on SWCNTs functionalized with matrix-based moieties for the production of epoxy composites with superior and tunable properties. Nanotechnology 2012;23. https://doi.org/10.1088/0957-4484/23/28/285702.

[15] Ali F, Ishfaq N, Said A, Nawaz Z, Ali Z, Ali N, et al. Fabrication, characterization, morphological and thermal investigations of functionalized multi-walled carbon nanotubes reinforced epoxy nanocomposites. Progress in Organic Coatings 2021;150:105962. https://doi.org/10.1016/j.porgcoat.2020.105962.

[16] Zhang W, Joshi A, Wang Z, Kane RS, Koratkar N. Creep mitigation in composites using carbon nanotube additives. Nanotechnology 2007;18. https://doi.org/10.1088/0957-4484/18/18/185703.

[17] Amaro AM, Reis PNB, Moura MFSF. Residual strength after low velocity impact in carbon-epoxy laminates. Materials Science Forum 2006;514–516:624–8. https://doi.org/10.4028/www.scientific.net/msf.514-516.624.

[18] Zhu J, Wei S, Ryu J, Budhathoki M, Liang G, Guo Z. In situ stabilized carbon nanofiber (CNF) reinforced epoxy nanocomposites. Journal of Materials Chemistry 2010;20:4937–48. https://doi.org/10.1039/c0jm00063a.

[19] Santos P, Maceiras A, Reis PNB. Influence of manufacturing parameters on the mechanical properties of nano-reinforced CFRP by carbon nanofibers. IOP Conference Series: Materials Science and Engineering 2021;1126:012012. https://doi.org/10.1088/1757-899X/1126/1/012012.

[20] Scott DW, Lai JS, Zureick A-H. Creep Behavior of Fiber-Reinforced Polymeric Composites: A Review of the Technical Literature. Journal of Reinforced Plastics and Composites 1995;14:588–617. https://doi.org/10.1177/073168449501400603.

[21] Park BD, Balatinecz JJ. Short term flexural creep behavior of wood-fiber/polypropylene composites. Polymer Composites 1998;19:377–82. https://doi.org/10.1002/pc.10111.

[22] Obaid N, Kortschot MT, Sain M. Understanding the stress relaxation behavior of polymers reinforced with short elastic fibers. Materials 2017;10:1–15. https://doi.org/10.3390/ma10050472.

[23] Pina dos Santos PS, Maceiras A, Valvez S, Reis PNB. Mechanical characterization of different epoxy resins enhanced with carbon nanofibers. Frattura Ed Integrità Strutturale 2020;15:198–212. https://doi.org/10.3221/IGF-ESIS.55.15.

[24] Reis PNB, Ferreira JAM, Antunes FV, Costa JDM. Flexural behaviour of hybrid laminated composites. Composites Part A: Applied Science and Manufacturing 2007;38:1612–20. https://doi.org/10.1016/j.compositesa.2006.11.010.

[25] Varghese S, Kuriakose B, Thomas S. Stress relaxation in short sisal-fiber-reinforced natural rubber composites. Journal of Applied Polymer Science 1994;53:1051–60. https://doi.org/10.1002/app.1994.070530807.

[26] George J, Sreekala MS, Thomas S, Bhagawan SS, Neelakantan NR. Stress relaxation behavior of short pineapple fiber reinforced polyethylene composites. Journal of Reinforced Plastics and Composites 1998;17:651–72. https://doi.org/10.1177/073168449801700704.

[27] Sreekala MS, Kumaran MG, Joseph R, Thomas S. Stress-relaxation behaviour in composites based on short oil-palm fibres and phenol formaldehyde resin. Composites Science and Technology 2001;61:1175–88. https://doi.org/10.1016/S0266-3538(00)00214-1.

[28] Santos P, Silva AP, Reis PNB. Effect of Carbon Nanofibers on the Viscoelastic Response of Epoxy Resins. Polymers 2023;15:821. https://doi.org/10.3390/polym15040821.

[29] Reis PNB, Silva MP, Santos P, Parente JM, Bezazi A. Viscoelastic behaviour of composites

with epoxy matrix filled by cork powder. Composite Structures 2020;234:111669. https://doi.org/10.1016/j.compstruct.2019.111669.

[30] Lim SD, Rhee JM, Nah C, Lee S-H, Lyu M-Y. Predicting the Long-term Creep Behavior of Plastics Using the Short-term Creep Test. International Polymer Processing 2004;19:313–9. https://doi.org/10.3139/217.1826.

[31] Ferreira JA., Costa JD., Reis PN. Static and fatigue behaviour of glass-fibre-reinforced polypropylene composites. Theoretical and Applied Fracture Mechanics 1999;31:67–74. https://doi.org/10.1016/S0167-8442(98)00068-8.

[32] Reis PNB, Neto MA, Amaro AM. Effect of hostile solutions on stress relaxation of carbon/epoxy composites. Polymer Degradation and Stability 2019;165:60–7. https://doi.org/10.1016/j.polymdegradstab.2019.04.026.

[33] Reis PNB, Gorbatikh L, Ivens J, Lomov SV. Strain-rate sensitivity and stress relaxation of hybrid self-reinforced polypropylene composites under bending loads. Composite Structures 2019;209:802–10. https://doi.org/10.1016/j.compstruct.2018.11.030.

[34] Monticeli FM, Ornaghi HL, Neves RM, Odila Hilário Cioffi M. Creep/recovery and stress-relaxation tests applied in a standardized carbon fiber/epoxy composite: Design of experiment approach. The Journal of Strain Analysis for Engineering Design 2020;55:109–17. https://doi.org/10.1177/0309324719892710.

[35] Vlasveld DPN, Bersee HEN, Picken SJ. Creep and physical aging behaviour of PA6 nanocomposites. Polymer 2005;46:12539–45. https://doi.org/10.1016/j.polymer.2005.10.120.

[36] Jian W, Lau D. Creep performance of CNT-based nanocomposites: A parametric study. Carbon 2019;153:745–56. https://doi.org/10.1016/j.carbon.2019.07.069.

[37] Yang J-L, Zhang Z, Schlarb AK, Friedrich K. On the characterization of tensile creep resistance of polyamide 66 nanocomposites. Part I. Experimental results and general discussions. Polymer 2006;47:2791–801. https://doi.org/10.1016/j.polymer.2006.02.065.

[38] Zhou TH, Ruan WH, Yang JL, Rong MZ, Zhang MQ, Zhang Z. A novel route for improving creep resistance of polymers using nanoparticles. Composites Science and Technology 2007;67:2297–302. https://doi.org/10.1016/j.compscitech.2007.01.015.

[39] Yang J, Zhang Z, Friedrich K, Schlarb AK. Creep resistant polymer nanocomposites reinforced with multiwalled carbon nanotubes. Macromolecular Rapid Communications 2007;28:955–61. https://doi.org/10.1002/marc.200600866.

[40] Vaidyanathan TK, Vaidyanathan J. Validity of predictive models of stress relaxation in selected dental polymers. Dental Materials 2015;31:799–806. https://doi.org/10.1016/j.dental.2015.04.002.

[41] Reis PNB, Silva MP, Santos P. Stress Relaxation in Delaminated Carbon/Epoxy Composites. Fibers and Polymers 2019;20:1284–9. https://doi.org/10.1007/s12221-019-8916-x.

[42] Houshyar S, Shanks RA, Hodzic A. Tensile creep behaviour of polypropylene fibre reinforced polypropylene composites. Polymer Testing 2005;24:257–64. https://doi.org/10.1016/j.polymertesting.2004.07.003.

[43] Bouafif H, Koubaa A, Perré P, Cloutier A. Creep behaviour of HDPE/wood particle composites. International Journal of Microstructure and Materials Properties 2013;8:225. https://doi.org/10.1504/IJMMP.2013.055385.

[44] Wang W-H, Huang H-B, Du H-H, Wang H. Effects of fiber size on short-term creep behavior of wood fiber/HDPE composites. Polymer Engineering & Science 2015;55:693–700. https://doi.org/10.1002/pen.23935.

[45] Xu Y, Wu Q, Lei Y, Yao F. Creep behavior of bagasse fiber reinforced polymer composites. Bioresource Technology 2010;101:3280–6. https://doi.org/10.1016/j.biortech.2009.12.072.

[46] Georgiopoulos P, Kontou E, Christopoulos A. Short-term creep behavior of a biodegradable polymer reinforced with wood-fibers. Composites Part B: Engineering 2015;80:134–44. https://doi.org/10.1016/j.compositesb.2015.05.046.

[47] Almeida JHS, Ornaghi HL, Lorandi NP, Bregolin BP, Amico SC. Creep and interfacial behavior of carbon fiber reinforced epoxy filament wound laminates. Polymer Composites 2018;39:E2199–206. https://doi.org/10.1002/pc.24537.

[48] Vidya Bhushan Gupta, Lahiri J. Non Linear Viscoelastic Behavior of Polypropylene and Glass Reinforced Polypropylene in Creep. Journal of Composite Materials 1980;14:286–96. https://doi.org/10.1177/002199838001400402.

Chapter 8

The effect of carbon nanofibres on the interlaminar fracture toughness of carbon composites with different epoxy resins

Abstract

The improvement of two commercial epoxy matrices (Sicomin and Ebalta) through the addition of one-dimensional (1D) carbon nanofibres (CNFs) represents a strategy to improve both Mode I and Mode II interlaminar fracture toughness (ILFT) in multiscale carbon fibre reinforced polymer (CFRP). Two experimental techniques were used to assess delamination behaviour. The double cantilever beam (DCB) method was utilized for measuring Mode I fracture toughness, while the end-notched flexure (ENF) method was employed for evaluating interlaminar Mode II fracture toughness. The obtained results indicated that the ILFT of the nanocomposite laminates surpassed that of the control CFRP laminates. Additionally, the optimal CNFs weight percentage was determined, showing dependency on the specific type of epoxy matrix used. The results revealed significant improvements in Mode I (9.86%) and Mode II (23.9%) fracture toughness by adding 0.75 wt.% and 1 wt.% CNFs to Sicomin epoxy matrix, respectively. Similarly, Mode I (14.87%) and Mode II (21.78%) fracture toughness enhancements were achieved by incorporating 0.5 wt.% CNFs into Ebalta epoxy matrix.

8.1. Introduction

The global demand for lightweight and resistant composite materials is experiencing rapid growth, particularly in primary and secondary structures applications. Carbon fibres are the preferred choice due to their favourable cost-to-mechanical properties ratio, excellent fatigue and creep resistance, as well as high strength, modulus, temperature and corrosion resistance, electrical and thermal conductivity, and low density. Carbon fibre reinforced polymer (CFRP) composites have extensive applications in the automotive, aerospace, naval industries, structures for trains and energy production, leading to reduced structural weight and more efficient energy consumption [1–3]. As far as matrices are concerned, epoxy resins are an excellent choice for many engineering applications due to their excellent properties, but proper cross-linking is crucial for achieving high mechanical, thermal, and chemical resistance [4]. However, optimizing the cross-linking process is essential to prevent void formation, which could reduce fracture toughness and increase internal stresses [5]. Petroleum-based epoxy monomers present exceptional characteristics, including high tensile strength, stiffness, and electrical strength,

rendering them suitable for applications in materials like CFRP. CFRP leverages the advantageous properties of epoxy, such as robust mechanical strength, dimensional stability, excellent wetting capability, fire and chemical resistance, as well as minimal cure shrinkage [4,6,7]. Carbon/epoxy composites have excellent in-plane properties, but their out-of-plane properties are comparatively poor due to their laminar structure. In addition, the out-of-plane properties of carbon/epoxy composites are matrix dependent. This laminar structure makes them susceptible to delamination, which is the primary failure mode, and to delamination growth over the life of the structures [8].

The development of internal damage in composites is known to involve three fundamental stages: crack initiation, crack propagation, and crack localization leading to ultimate failure. In multidirectional composites, matrix cracking is the primary mode of damage. Local stress concentrations can occur in heterogeneous microstructures, leading to microcrack initiation even at very low loads. Microcracks in different regions gradually propagate and interact with each other as the load increases [9].

The fibre, as the primary load bearing component, plays a critical role in inhibiting crack propagation. As a result, specific crack orientations become more prevalent, tending to propagate along the easiest paths, i.e., through the matrix, the lowest resistance constituent of the composite material, which in itself justifies the maximisation of its properties through the addition of nanoparticles. Severe damages can lead to further fibre fractures or macroscopic delaminations. Fibre fracture typically results from applied stresses that exceed its mechanical strength, while delamination involves matrix cracks between highly anisotropic layers [9].

In recent times, a wide range of different nano-sized materials has become available for high-performance applications: as carbon allotropes [10–14], metal nanoparticles [15], nano clays [16], nano silica [17] and/or the conjugation of several nanomaterials in different weight fraction. One of the most significant types of nanomaterials is carbon nanofibres (CNFs), one-dimensional (1D) structures made up of carbon, exhibiting a complex arrangement. CNFs belong to the category of linear, sp^2-based materials, characterized by discontinuous filaments where the aspect ratio surpasses 100 [18]. In general, CNFs are less expensive compared to other nano-reinforcements (such as graphene and carbon nanotubes), offering several advantages including high yield, a high aspect ratio, low cost, strong thermal and electrical conductivity, and the adaptability to tailor processing parameters based on desired mechanical properties, making them an excellent option for reinforcing epoxy matrices [19,20]. However, challenges such as poor dispersion, clusters, phase separation, and weak interfacial bonding with the matrix result in inadequate load transfer across the interface [5].

Delamination, for example, is the most prevalent failure mode in the CFRP and can be caused by defects induced during manufacturing, which subsequently propagate throughout the life of the material (like matrix deficit, poor fibre impregnation, air bubbles between layers), accidents (falling bodies during maintenance), natural factors (impact of a bird, tree branches, hail or

lightning) and geometric construction restrictions (such as curved free edge, external ply drop, corner, skin stiffener interaction, solid-sandwich transition, internal ply drop and straight free edge) [21,22]. Delamination takes place when a crack develops and propagates between two consecutive layers of reinforcement (fibre) usually filled with a thermosetting resin [21,23,24]. As already mentioned, the matrix is the lowest strength constituent of a composite, which, once cracked, tends to cause delamination to spread quickly [21,25]. In the study of the fracture mechanics of composite materials, the most common and effective approach mainly relies on Mode I and Mode II loading conditions, where two consecutive layers of a laminate are made opening or sliding one over the other, respectively.

Under Mode I loading conditions, the fibre/matrix adhesion properties of composites are assessed using the double cantilever beam (DCB) configuration, a standard geometry to determine the critical energy release rate (G_{Ic}). In contrast, Mode II loading conditions, which entail crack sliding or in-plane shear, evaluate the critical energy release rate (G_{IIc}). The end-notched flexure (END) specimen is commonly employed for this purpose [26]. Therefore, interlaminar fracture toughness (ILFT) depends not only on the matrix properties, but also on the properties of the fibre/matrix interfaces. Furthermore, no less important is the composite manufacturing process, especially in the case of hand lay-up process, a technique widely used industrially and by many researchers due to its simplicity/versatility, where the operator can be an element influencing the final properties of the composite: (i) if the matrix distribution is not uniformly along the woven layer and/or along the fibre length, delamination may occur between layers; (ii) dragging the matrix along the layer, may promote small air bubbles that lodge into the composite; (iii) the type and density of the reinforcing fabric may make it difficult for the matrix to impregnate; and (iv) if the surrounding area is not perfectly clean during manufacturing, small foreign particles may lodge into the composite and affect its final properties [27,28].

Therefore, it is not surprising that the literature reports the incorporation of a ductile and nanofibrous interlayer, even at a low weight content of CNFs, to reduce crack initiation and propagation and, consequently, the emergence of delaminations. This approach is extremely valuable both from the point of view of structural integrity and multifunctionality [29–31]. In this context, there are several studies where CNFs were added to an epoxy matrix to improve the ILFT properties. In these studies, various manufacturing methods, diverse approaches for nanoparticles manipulation, CNFs alignment/orientation methods, and the conjugation of CNFs with other particles were explored to obtain improved composites properties. For example, Arai et al. [32] investigated unidirectional CFRP prepregs laminates with a vapor grown carbon nanofibre (VGCNFs) epoxy interlayer of 50-200 μm, varying this interlayer thickness, applied by hand after making a paste of the CNFs with a small amount of solvent (ethanol). The Mode I ILFT for laminates with CNFs is about 50% higher than the CFRP control laminate, and the Mode II ILFT for laminates with CNFs is 2–3 times higher than the CFRP control laminate. Kostopoulos et al. [33] applied CNFs and lead zirconate titanate (PZTs) piezoelectric particles in the reinforcement of the matrix of CFRP. The results showed that adding 1 wt.% CNFs doubling of

the G_{IC} compared with the neat epoxy matrix composites (0.39 to 0.79 kJ/m²). In terms of Mode II fracture energy, authors observed that CNFs require more energy to be broken and pulled out leading to higher G_{IIc} values when compared to the control laminates (1.724 to 2.626 kJ/m²).

Arai et al. [31] manufactured unidirectional CFRP laminates composed of 20 prepreg layers using the autoclave process. The CNFs (VGCF, VGCF-S) were inserted between prepregs interlayers of the CFRP with an area density of 10, 20 and 30 g/m². In regions where opening mode prevails, the fracture toughness of CFRP with CNFs interlayers increased from 1.3 to 2.3 times compared to the control CFRP laminate. In regions where shearing mode predominates, the fracture toughness of CFRP/CNFs reached 3.6 times that of the control laminate. In another study, Arai et al. [34] used carbon fibre twill woven fabric and epoxy resin as base materials for CFRP laminates with 10 layers made by vacuum-assisted resin transfer moulding (VARTM) process and, CNFs (VGCF) were used as nano reinforcements with an area density of 5, 10 and 20 g/m². The influence of the VGCF interlayers on the fracture toughness G_{IC} is almost 20% compared to the control laminate (density of 10 g/m²). Wang et al. [35] studied the ILFT of CFRP laminates involving an epoxy matrix enhanced with pristine and functionalized SCCNFs (H_2SO_4 and HNO_3 manufactured by hand lay-up process. The results showed that the highest increases in Mode I (13.6%) and Mode II (45.3%) fracture toughness were obtained with the addition of 0.5 wt.% and 1 wt.% functionalized nanofibres, respectively, relative to the values obtained with the control laminates. Ladani et al. [36] used 12-layer unidirectional carbon fibre/epoxy prepreg laminates manufactured via an autoclave process in which liquid resin mixed with CNFs acted as an adhesive layer. The liquid epoxy resin, CNFs, and a surfactant were simultaneously dispersed using a three-roll mill. An alternating current (AC) electric field was applied to align the CNFs prior to curing of the nano-enhanced epoxy resin. The results demonstrate that the incorporation of 1.6 wt.% aligned CNFs significantly increases the fracture energy, G_{IC}, by around 17 times (from 134 to 2345 J/m²). This increases the values to seven orders of magnitude above the fracture energy of the unmodified epoxy. When compared to randomly oriented CNFs, the alignment of the CNFs resulted in a 27% increase in fracture energy. In another study, Ladani et al. [37] compared the increases in fracture energy of epoxy nanocomposites consisting of 12 layers of unidirectional carbon fibre, reinforced by one-dimensional CNFs or two-dimensional graphene nanoplatelets (GNPs). They employed a calendaring process and an AC electric field during the initial phase of the resin cure cycle to orient the nano-reinforcements in the through-thickness direction of the epoxy nanocomposite layer before the resin began to gel. The fracture energy values, G_{IC}, of the nanocomposites containing 0.5 wt.% randomly oriented CNFs or GNPs improved by around 200% when compared to the control epoxy. Furthermore, the alignment of the nano-reinforcement transverse to the crack growth direction led to an additional increase of approximately 40% in fracture energy.

Ravindran et al. [38] analysed the effect of hybridization of CNFs with short carbon fibres (SCFs) for concentrations ranging up to 1 wt.% and 1.5 wt.%, respectively. They also studied the effect of aligning these fillers to improve Mode I ILFT by positioning them perpendicular to the crack

growth direction through the application of an AC electric field. It was found that CNFs exhibited more effectiveness than SCFs in increasing the G_{IC} value, but when alignment of CNFs or SCFs was performed, bith led to a considerable increase in G_{IC}. In another work, Ravindran et al.[39] studied the Interlaminar Fracture Toughness (ILFT) of 12-layer carbon-epoxy laminates using a single type of nanofiller, either 1D (such as CNTs or CNFs) or 2D (such as GNPs), at a concentration of 1 wt.%, prepared by hand mixing and three-roll milling. They also compared laminates with z-pins, reinforced with a combination of carbon nanofiller and z-pins, and observed that the 1D nanofillers induced a synergistic effect. The addition of CNFs increased the fracture energy, G_{IC}, by approximately 91% (from 0.73 to 1.4 kJ/m^2) and G_{IIC} by about 42% (from 2.04 to 2.88 kJ/m^2), while the 2D nanofiller showed virtually no effect. Ekhtiyari et al. [40] analysed the influence of the loading rate, from quasi-static to 200 mm/s, on Mode I for unidirectional E-glass/epoxy laminates with neat and nano-enhanced resin with 0.25 wt.% CNFs, observing that the nanoreinforcements led to an increase of 32.8% and 13.5% in the quasi-static values of initiation and propagation ILFT values, respectively, and for the higher loading rates the propagation fracture toughness was reduced to 8%. Ravindran et al. [41] used CNFs and SCFs at a concentration of 1 wt.% in an epoxy matrix to increase the ILFT in 20-layer CFRP laminates manufactured by hand lay-up process and subsequently consolidated using high-pressure compression moulding. Both fillers contributed to increasing ILFT values of Mode I and Mode II, although CNFs demonstrated higher effectiveness for the weight fraction used in their study. However, with the hybridization of nanoparticles, although an improvement was observed in Mode I fracture toughness, it was in Mode II that it was most noticeable due to the synergistic effect. In terms of structural properties of CFRP composite T-joints incorporating 1 wt.% of CNFs, CNTs, or GNPs into the epoxy matrix phase, Ravindran et al. [42] found that CNFs and CNTs were most effective at improving the steady-state Mode I and Mode II ILFT, respectively, while CNTs and GNPs were less effective in enhancing steady-state Mode I and Mode II ILFT, respectively.

Another important consideration is the fracture surface of the tested laminates. For example, Arai et al. [32] observed that the fracture surface of control laminates shows a typical brittle fracture of Mode I deformations, and as the CNFs area density increases, the fracture surface acquires an irregular aspect. On the other hand, the fracture surface regains a brittle aspect when the CNFs area density exceeds the adequate quantity limit of 20 g/m^2. Observation of the SEM images of the fracture surface of Mode II delamination indicates that energy absorption due to plastic deformation on the fracture surface has produced the “sawtooth” typical hackle pattern. In particular, the number of hackle markings increases significantly at a CNFs area density of 20 g/m^2. These fracture surface results illustrate that optimum toughness occurs at a CNFs area density of 20 g/m^2. Kostopoulos et al. [33] concluded from observing the fracture of Mode I images that the entangled and interspersed CNFs in the matrix can inhibit crack propagation due to the extra energy required for interfacial failure. This interfacial failure leads to frictional sliding and/or plastic deformation at the interface and ultimately to CNFs fracture or pull-out and crack bridging. Wang et al. [35], by observing the Mode I fracture surfaces of the control CFRP, identify

the debonding of carbon fibres and several smooth grooves are in the rupture surface. These smooth grooves suggest that the cracks can propagate easily through the carbon fibre/epoxy interface. For the CFRP laminate with 1 wt.% SCCNFs, the retained fibres show a disordered pattern, and it is possible to identify the pull-out and breakage of carbon fibres. It can be concluded that the strength of the epoxy properties is improved by incorporating the SCCNFs into the carbon laminates. In terms of Mode II fracture morphologies, in the control CFRP laminates the epoxy fractures into fragments and only a small amount of fragments are retained between the carbon fibres. On the other hand, the surface with 0.5 wt.% SCCNFs/CFRP laminates shows that a large amount of epoxy fragments is retained. The Mode II failure characteristics are dominated by the sliding shear of the interlaminates, where the shear fracture of the SCCNFs helps to prevent crack movement. After pullout or fracture of the SCCNFs, the SCCNFs can still act as a barrier in the crack surface. Ladani et al. [37] observed a smooth and featureless crack surface indicative of brittle fracture in the neat epoxy DCB specimens. In comparison, the samples containing CNFs exhibited stick-slip crack propagation with pronounced stress whitening of the epoxy at the crack initiation and arrest regions. The stress-whitening is due to plastic deformation associated with the crack initiation process, as the lengths of these stress-whitening bands increased with increasing nano-strengthening concentration, correlating with the observed increases in their fracture energy values. Fractographic analysis of DCB specimens by Ravindran et al. [41] showed that CNFs increased Mode I fracture toughness through intrinsic and extrinsic toughening mechanisms. Intrinsically, before the crack tip, CNFs facilitated interfacial debonding from the epoxy matrix, resulting in plastic void growth. Extrinsically, behind the crack tip, toughening mechanisms included fibre pull-out, bridging and fracture. The dominant mechanism was plastic void growth in the epoxy matrix, particularly in CNFs-reinforced composites, due to a triaxial stress state. This resulted in a higher Mode I initiation toughening effect for CNFs, with voids approximately 5 to 7 times the diameter of the CNFs. In addition, fibre bridging and pull-out contributed significantly to extrinsic toughening in CNFs-reinforced composites. Under Mode II loading, the analysis revealed the initiation of echelon or wedge microcracks due to shear stresses in the process zone near the crack tip. These microcracks grew at approximately 45° to the crack propagation direction as local Mode I (tensile) cracks, eventually coalescing to drive delamination crack propagation. In nano-enhanced laminates, CNFs debonded from the epoxy matrix within the process zone under high stresses prior to the crack tip, leading to echelon crack formation. Due to their small size, fibrous morphology and random orientation, the CNFs bridged the echelon cracks between the continuous carbon fibres/tows, limiting their growth and increasing the Mode II fracture toughness.

Based on the studies presented, it can be observed that there is already relatively robust knowledge about the effect of CNFs on the interlaminar fracture resistance of composite materials, but regarding the interaction of the effect of CNFs with the viscosity of the resin, this is not yet well consolidated in the authors' opinion. This is important because viscosity is a physical property that ultimately affects the resin's resistance to movement. For this purpose, two resins were chosen (Sicomin and Ebalta) with different viscosities, molecular structures, chemical

polarity and consequent compatibility with both nanoparticles and carbon fibres. For example, in other studies the authors found that Sicomin SR 8100 resin maximized the bending strength for 0.75 wt.% while Ebalta AH 150 for 0.5 wt.% CNFs. The highest bending stress and modulus occurred in the resin with the lowest viscosity (Ebalta) due to its interfacial resistance and the dispersibility of the CNFs. On the other hand, the highest viscosity resin (Sicomin), due to its better physic-chemical compatibility with the nanoparticles, significantly influenced the interfacial resistance and the dispersibility of the CNFs, promoting lower mechanical properties at lower filler contents compared to the resin with the lowest viscosity. When CNFs are added, regardless of the resin, in terms of sensitivity to strain rate, the highest values of bending stress and stiffness are always obtained with the addition of CNFs, and they are also less prone to tension relaxation and creep [43,44].

In line with the results obtained for epoxy matrices, also in carbon fibre laminates, the optimum weight content for Sicomin resin was 0.75%, for Ebalta it was 0.5 wt.%. In addition, the highest bending stress and modulus were also obtained for the lower viscosity resin (Ebalta) due to promote a better organization of the nanoparticles. In terms of strain-rate sensitivity, the addition of CNFs contributes to the increase in bending stress and bending modulus in both resins, being that the nano-reinforced laminates produced with Sicomin resin have a lower strain-rate sensitivity than laminates produced with Ebalta resin. Regarding ILSS, the best results coincided with the results of the static bending point, that is, Sicomin resin in laminate with 0.75 wt.% CNFs and Ebalta resin with 0.5 wt.% CNFs [45]. Laminates stress relaxation and creep tests show that for both resins, the addition of CNFs does not have a deleterious effect on the relaxation behaviour of the laminates. This indicates that the dispersed CNFs bind to the matrix via interphases, bridging segments and junctions to support the load, but are not present in sufficient quantities to promote immobility of the polymer chains [46].

The current study investigates the influence of two commercial nano-enhanced epoxy resins with different viscosities, molecular structures, chemical polarity and different compatibility with both nanoparticles and carbon fibres, containing CNFs on the delamination resistance of CFRP/CNFs laminates, applying simple methods, both for the addition of CNFs to the resins and for manufacturing composite laminates. Therefore, the aim is to use these methodologies to develop processes that can be easily implemented on an industrial scale and to optimize the toughness resistance of the laminates. The research assessed the impact of varying weight percentages of CNFs on the Mode I and Mode II ILFT properties of the laminates. The inclusion of CNFs aims to enhance resistance against interlaminar cracking and delamination, ultimately improving the fracture toughness of CFRP composite laminates. As a complement to the static tests, DCB and ENF tests were conducted to analyse their interlaminar properties, and a detailed analysis of the fracture surface was carried out to characterize the failure modes of the laminates.

8.2. Materials and experimental procedure

8.2.1. Production of composite laminates

In the production of carbon fibre composites reinforced with CNFs, were applied an epoxy resin SR 8100 and a hardener SD 8824, both supplied by Sicomin, in a weight ratio of resin to hardener 100:22 and an epoxy resin AH 150 and a hardener IP 430, both supplied by Ebalta, in a weight ratio of resin to hardener 100:30. How do matrices have different viscosities, divers weight contents of CNFs (i.e., 0.25, 0.5, 0.75 and 1 % wt.%) have been added, to achieve the maximum mechanical properties and compare with respective control laminate. In the CNFs supplied by Merck, in terms of dimensions, the average diameter is about 130 nm, the length ranges from 20 to 200 μm and the average specific surface area around is 54 m^2/g. More details on the technical specifications of the matrices are summarized in Table 8.1 and the CNFs properties, can be found in [43]. Laminates with eight layers, all in the same direction, of bidirectional carbon plain fabric 195-1000P (195 g/m^2) with a thickness of 0.25 (± 15%) mm, density of 1.76 g/cm^3, average tensile strength of 3.53 GPa, and tensile modulus of 230 GPa, were manufacture by hand lay-up technique.

Table 8.1: Main mechanical and physical properties of the epoxy resins.

Property		Sicomin SR 8100 / SD 8824	Ebalta AH 150/ IP 430
Colour		Light yellow liquid	Opaque
Viscosity (@ 25 °C)	[mPa×s]	285 ± 60	250 ± 50
Density at 20 °C	[g/cm^3]	-	1.13 ± 0.02
Modulus of elasticity	[N/mm^2]	2970	3400 ± 300
Maximum resistance	[N/mm^2]	108	125 ± 1.2
Elongation at max. load	[%]	4.9	-
Elongation at break	[%]	11.8	5.9 ± 0.1
Charpy impact strength	[kJ/m^2]	52	60 ± 6
Glass transition/DCC	[°C]	63	-
Water absorption 48 hours/70 °C	[%]	1.2	-

To produce the laminates nano-enhanced, in the first stage CNFs were added to the epoxy resin, and the mixture was conducted using a high-speed shear mixer at a shear rate of 1000 rpm for 3 hours at room temperature (RT) (22 ± 1°C), followed by 10 minutes at 150 rpm to disperse the hardener in the system homogeneously. This whole process was combined with sonication (using an ultrasonic bath with a frequency of 40 kHz) and the bath temperature was controlled to improve the dispersion of the nanofibres. After degassing the mixture in a vacuum oven to remove air bubbles in the second stage, the laminates were manufactured. This step is important because, the mixing of the resin with the hardener produces highly reactive volatile vapor bubbles at the initial stages of the reaction, which could detrimentally affect the properties of the laminates by creating voids.

The nano-enhanced epoxy matrices were evenly distributed and interspersed with the layers of carbon fibre woven perfectly aligned, to evenly impregnate the eight layers one by one. In the intermediate layers of the laminate was introduced a 25 μm PTFE film (Teflon) during moulding to generate the starter crack. The assembly was subsequently positioned within a vacuum box and subjected to a pressure of approximately - 0.9 ± 0.1 bar. This step aims to eliminate the maximum quantity of small air bubbles trapped within the layers of the carbon fibre fabric mesh, resulting from the specific manufacturing process, and ensure the uniform distribution of matrix among the multiple fibre layers. The assembly was placed between two release agent films, and an absorbent fabric was placed around the carbon layers to absorb some excess matrix and create an air extraction path.

This assembly was then placed inside a vacuum bag, heat sealed, and subjected to a 2.5 kN load in a hydraulic press to maintain a constant fibre volume fraction and uniform laminate thickness during the curing time, which was followed according to epoxy resins datasheet, and reported in [43]. During the first 4 hours, the bag remained attached to a vacuum pump to eliminate any air bubbles existing in the laminate. This procedure proved to be promising for obtaining good results, as proven in [47], some manufacturing parameters influence the final mechanical properties of laminates.

After manufacture, the laminates had a dimension of 330 × 330 × h (mm) (where h is the thickness), and the specimens' geometries presented in Figure 8.1.a) to DCB tests and Figure 8.2.a) to ENF tests, respectively, were cut from these same boards using a diamond disc saw and water-cooled. The cutting speed was controlled to ensure that no pulling out of material from the test specimens would occur. Stainless steel piano hinges were adhesively bonded with the epoxy Araldite HY 4076 to the laminates, allowing the application of the load for the DCB tests. After cutting the specimens, an optical inspection was carried out to ensure their integrity and a dimensional inspection to ensure that their dimensions were the minimum to comply with the respective test standards. The DCB and ENF specimens were tested respectively at a crack opening displacement rate and a three-point bending loading rate of 1 mm/min using a Shimadzu machine, model Autograph AGS-X, equipped with a 10 kN load cell. For each test condition, at least five specimens were tested at RT. Given values are the average and standard deviation was used as error.

8.2.2. DCB test configuration and method

Experimental DCB tests with load requests in Mode I were carried out in accordance with the recommendations described in ASTM D5528-13. The ASTM D-5528 standard was initially devised for evaluating unidirectional fibre systems. However, the standard acknowledges the potential utilization of woven fabrics, recognizing that these fabrics often encounter run-arrest phenomena attributable to matrix-rich pockets formed between the warp and weft strands within the weave structure. The DCB specimens were prepared with the geometry and dimensions indicated in Figure 8.1.a). Figure 8.1.b) shows the experimental setup of the DCB specimen. A

sharp crack tip was achieved by carefully wedging the crack opening from the tip of the Teflon film and the load versus displacement (P–δ) typical curves of the quasi-static specimens were obtained during the test, Figure 8.1.c) [42,48,49]. Figure 8.1.c) shows the result of interpreting the experimental data collected during the study based on the information from the literature analysis [42,48]. At the initial loading stage, the P–δ curves, show a linear increase stage with displacement increasing. However, a nonlinear increase can be found when the load reaches a relatively higher value. When the peak load is reached, there is a non-linear decreasing.

Additionally, crack length measurements were conducted during the experiments by a paper ruler which was glued to the samples. High-resolution images, measuring 5328 × 4000 pixels, were captured utilizing a Canon EOS 80D digital SLR camera to facilitate a clear visualization of the crack length.

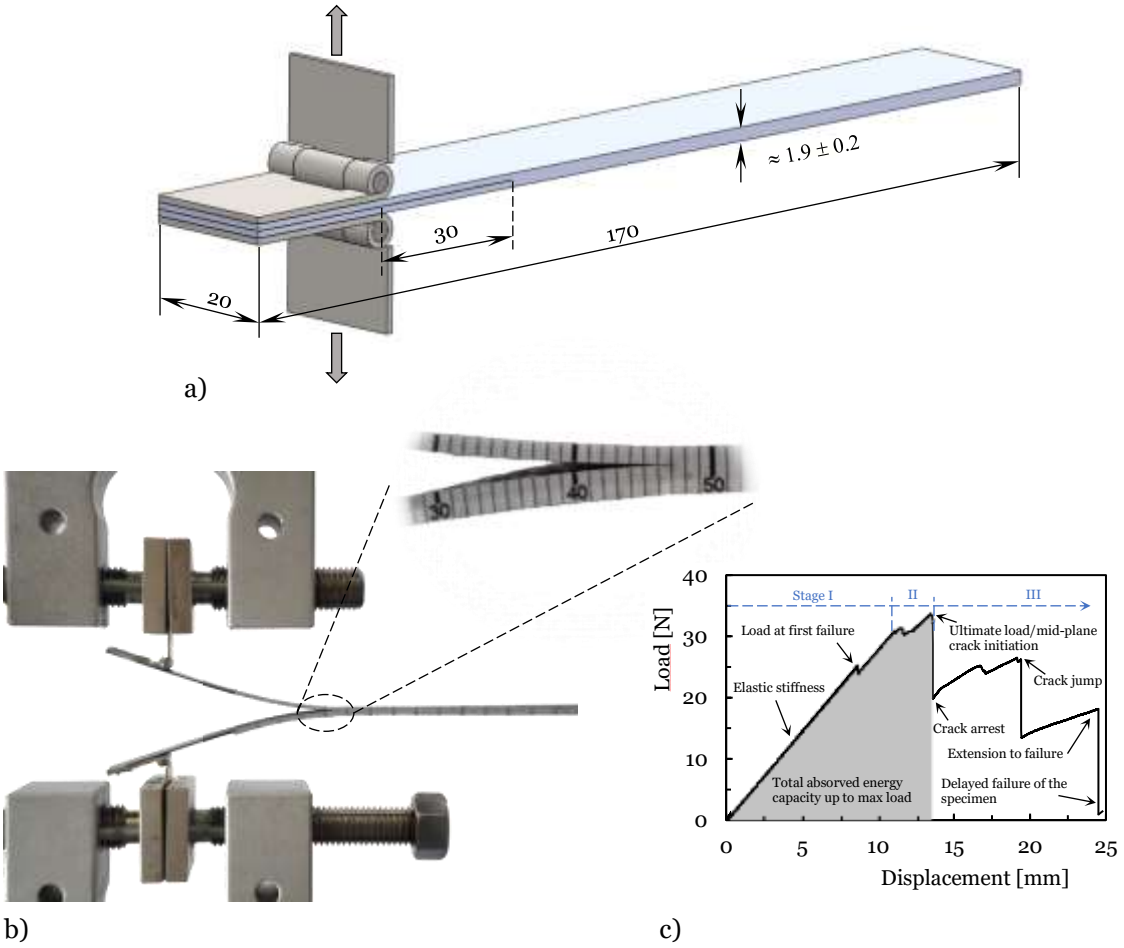

Figure 8.1: DCB test: a) Schematic specimen geometry (Dimensions in mm); b) Experimental test specimen, apparatus, and detail of the ongoing delamination stage; c) Example of load versus displacement curve test of control Sicomin epoxy control laminate.

Mode I strain energy release rate, G_I was calculated by means of the modified beam theory (MBT) method, the compliance calibration (CC) method and the modified compliance calibration (MCC) method, using equations (8.1), (8.2) and (8.3), respectively:

$$G_I = \frac{3P\delta}{2b(a + |\Delta l|)} \tag{8.1}$$

$$G_I = \frac{n\,P\delta}{2\,b\,a} \tag{8.2}$$

$$G_I = \frac{3P^2C^{2/3}}{2\,A_1\,b\,h} \tag{8.3}$$

where P is the load, δ is the load point displacement, b is the specimen width, h is the thickness, a is the delamination length, C is the compliance, Δ is the modulus of a correction factor obtained experimentally by generating the least squares plot of the cube root of the compliance C against the delamination length a (Δ the value for $C^{1/3}$ equal to zero), n is a correction factor given by the slope of the straight line generated by the least squares plot of the log of the compliance C against the log of the delamination length a and A_1 is a correction factor given by the slope of the straight line generated by the least squares plot of a/h against $C^{1/3}$ [50].

One significant advantage of the DCB setup lies in its simple construction and moderate cost. However, when tested on universal testing equipment, it encounters certain challenges, such as maintaining symmetrical opening of the specimen and accurately measuring the crack length to prevent oscillations in the load signal [51].

8.2.3. ENF test configuration and method

In the ENF tests of ILFT with load request in Mode II, specimens with geometry and dimensions shown in Figure 8.2.a) were used. The tests were carried out according to the procedure described in the ASTM D7905/D7905M-14 standard. Figure 8.2.b) illustrates the experimental scheme for the 3PB ENF test. The test stand was additionally equipped with a camera tracking the front of the propagating crack and the crack length was measured using a paper ruler which was glued to the samples. Typical load versus displacement curves were obtained, Figure 8.2.c), whose interpretation of results was based on the study of literature [52–54]. In the first stage, the P-δ curve increases linearly, except for the gap closure at the beginning of the load. In the second stage the P-δ curve continues to rise but in a non-linear fashion, the visual initiation of delamination occurs somewhere in this stage and a non-linear fracture process zone develops ahead of the crack tip where the visual initiation of delamination occurs. Once the P_{max} value is reached, the pre-crack propagates abruptly with a dislocation movement of the upper and lower cantilever beams. A significant drop can be seen from the P-δ curve, stage three. The crack extension stops at the central loading area where the local effects of compressive stress hinder the crack propagation, a minimum point is reached. In the stage IV, the specimen bears the post-bending load, and the P-δ curve rises again.

Mode II strain energy release rate, G_{II} was calculated, according to the experimental compliance method (ECM), simple beam theory (SBT) and the compliance calibration method (CCM) using the equations (8.4), (8.5) and (8.6), respectively:

$$G_{II} = \frac{3P^2\, a^2 m}{2b} \tag{8.4}$$

$$G_{II} = \frac{9P^2\, a^2}{4b^4\, h^3\, E_1} \tag{8.5}$$

$$G_{II} = \frac{9P\delta\, a^2}{2b(2L^3 + 3a^3)} \tag{8.6}$$

where m is a correction factor given by the slope of the straight line generated by the least squares plot of the compliance C against the cube of the delamination length, a^3, E_1 can be deduced from the slope (i.e. 0.00171/(N$^{1/3}$ × mm$^{2/3}$)) of the linear regression to the $C^{1/3}$ versus free length L_{free}, obtained by experimentally performing the clamp calibration procedure, and L is the half-support span length of the ENF test fixture [50,55]. For each test condition, at least five specimens were tested at RT and at a displacement rate of 1 mm/min. Given values are the average and standard deviation was used as error. For each specimen, the values of P, δ and a were monitored and recorded during the tests. The same Shimadzu universal testing machine, model Autograph AGS-X, was used and to acquire the results, the software Trapezium X, version 1.4.0.

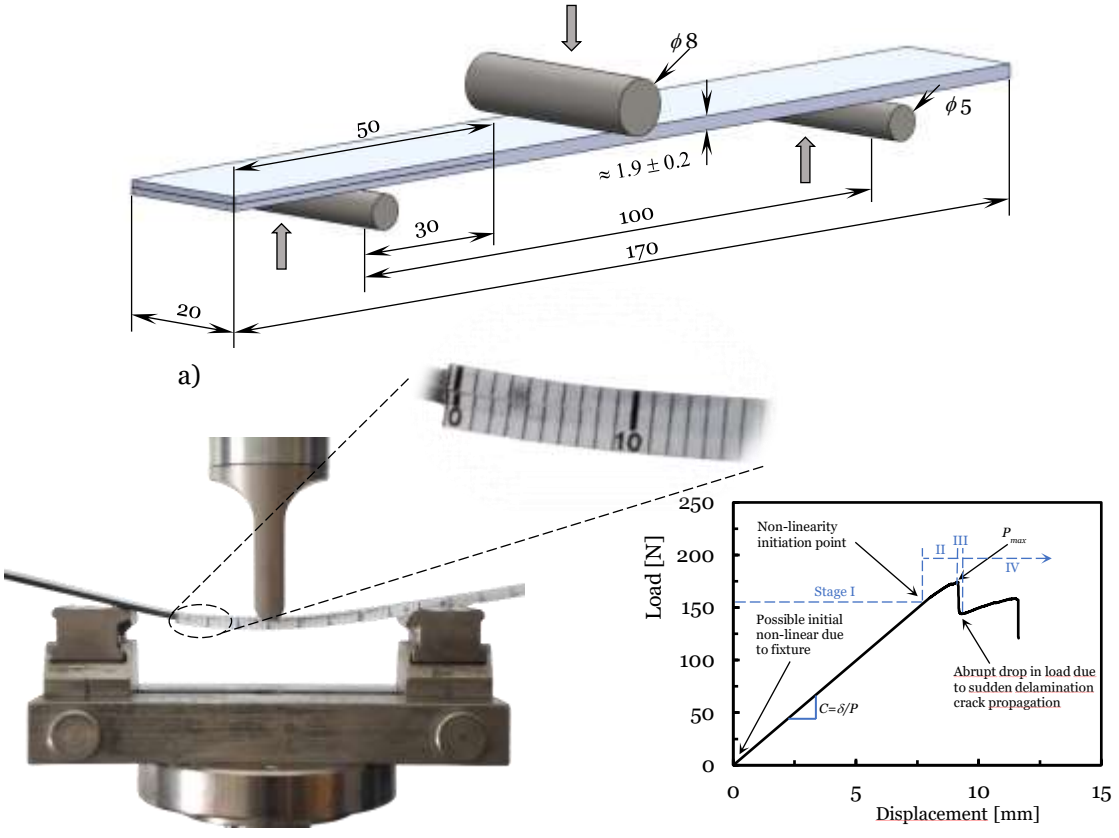

Figure 8.2: ENF test: a) Schematic specimen geometry (Dimensions in mm); b) Experimental test specimen, apparatus, and detail of the delamination stage; c) Example of the load versus displacement curve of control Sicomin epoxy control laminate.

8.3. Results and discussion

8.3.1. Microstructure analysis

The Figure 8.3.a) is representative of the laminates under study, where one can observe in the cross-section the various fibre layers (plain weave fabric), epoxy matrix-rich regions and the Teflon layer, a defect caused for crack initialization. The formation of epoxy matrix-rich regions is common to most laminates processed using the manufacture by hand lay-up technique and the type of fabric used [56].

In structural applications, achieving high-strength and stiffness laminates relies on factors such as layer stacking sequence, compaction during the curing cycle, and the cutting operation during final manufacturing. Epoxy matrix-rich regions appear between layers in many laminates processed through stacking, contributing to stabilization during curing. The thickness of these regions varies based on material selection and manufacturing conditions. Plain weave style, the simplest among different fabric types for composites, involves warp and weft yarns alternately passing above and below, creating voids filled by epoxy matrix during curing. Depending on laminate thickness, epoxy matrix regions can negatively affect mechanical properties, potentially initiating delamination failures. This phenomenon occurs between layers, at layer edges, interfacial flaws near epoxy matrix-rich zones, or through a combination of microcracks within the epoxy matrix.

Figure 8.3.b) shows the fracture origin region located between the end of the pre-crack simulated by the Teflon insert and the beginning of delamination originating from the applied load. The detail of Figure 8.3.b) presents a representative image of the upper and lower surfaces of the transitional region existing between the simulated failure end by the Teflon insert and the origin of the delamination front resulting from the applied static loading.

The figure refers to the region at the beginning of the fracture process in one of the several epoxy matrix-rich areas, specifically identified as an epoxy matrix concentration, which settled in the vicinity of the imaginary vertical line indicating the boundary of the Teflon insert. The figure depicts the typical configuration of the interweaving of carbon fibre bundles in the plain weave fabric. It also accurately indicates that the direction of delamination propagation in the image occurred from left to right, that the interlaminar debonding partially compromised the fibre integrity at the raised positions of the fibre bundle interweaving, and that the phenomenon of fibre bridging, commonly found in continuous unidirectional tape composites, did not manifest in this textile-configured composite. The epoxy matrix concentration is directly associated with the thickness of the Teflon insert and the processing conditions of the laminates. Furthermore, it must be taken into account that the matrix concentration was augmented by the matrix portion distributed along the interlaminar regions of the composite due to the vacuum and pressure parameters acting during laminate formation. In the formation of the matrix concentrations, the matrix naturally retained in the interstices of the interweaving of weft and warp fibre bundles located near the insert's end must also be considered.

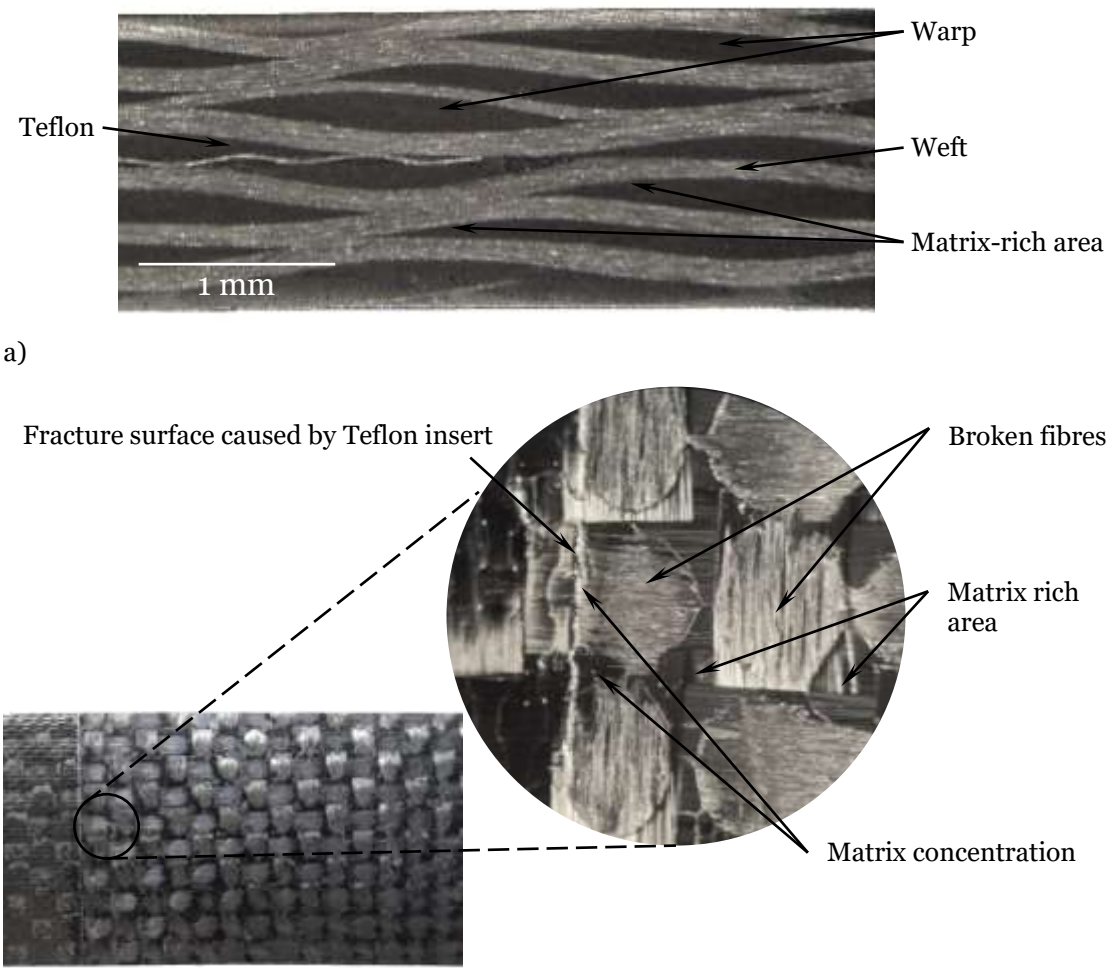

Figure 8.3: Sicomin control laminate: a) Cross-section of the specimen showing the layer distribution along the length of the specimen; b) Regions with broken fibres and other matrix-rich.

At the moment when the tensile load was applied to induce the opening of the specimen, there was simultaneous rupture of the epoxy matrix and interfacial debonding between fibre and matrix within the mentioned matrix concentrations, initiating the delamination failure process. Furthermore, Figure 8.3.b) reveals evidence of plastic deformation of the epoxy matrix, which occurred at the end of the concentration along with the failure displacement and partial fibre rupture.

The delamination front propagated through the development of shear stresses within the laminate's failure plane during loading. The combination of applied tensile stress with the tensile component of interlaminar stresses led to a progressive increase in the opening angle of the specimen, resulting in uniform debonding along the laminate's failure plane. The predominant feature observed on the delaminated surfaces corresponds to river line marks (Figure 8.4) imprinted in the epoxy matrix concentration, oriented at various angles under different fracture levels, typical in this type of request for composite laminates [57,58].

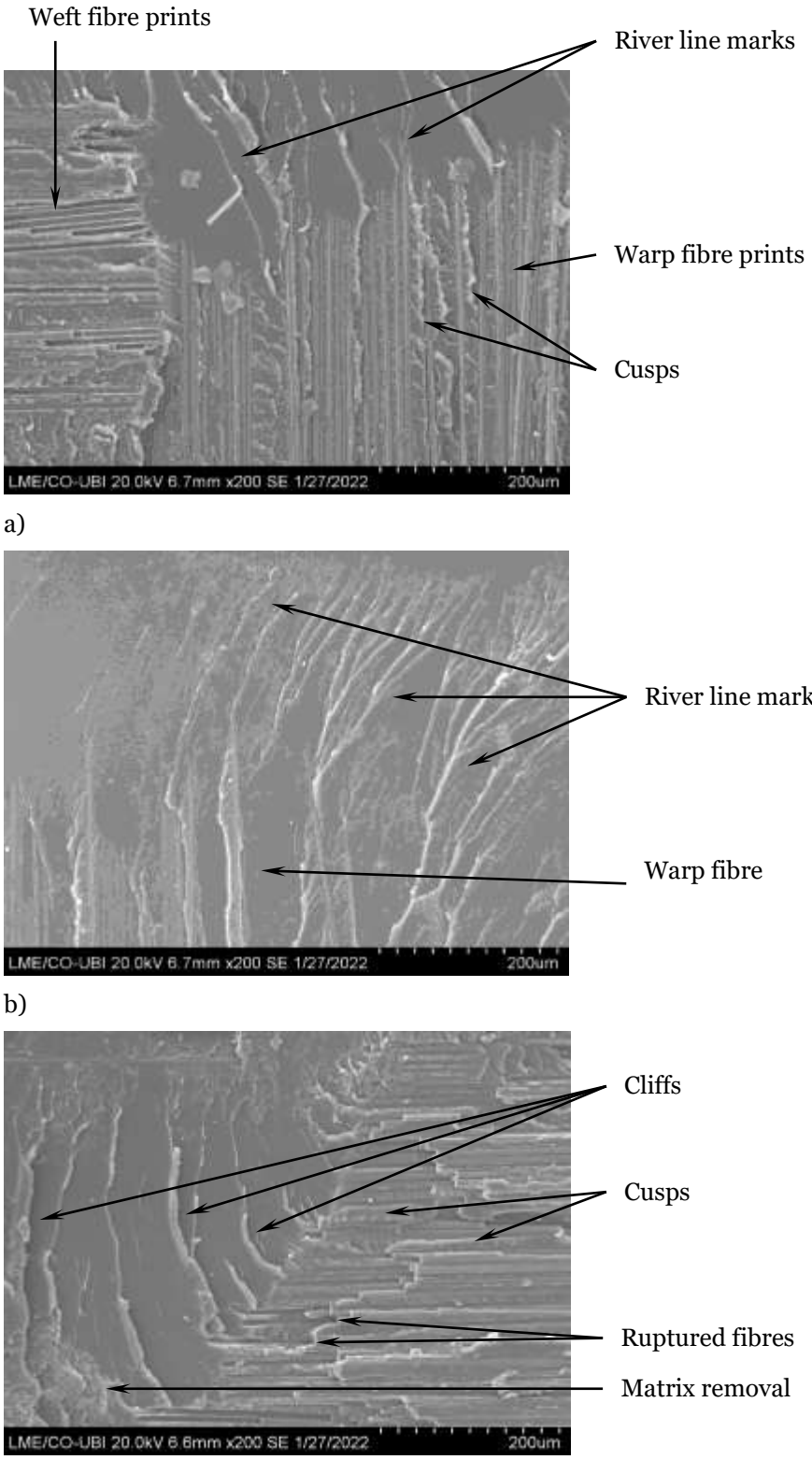

Figure 8.4: Fracture surface of control Sicomin carbon/epoxy laminate under Mode I loading: a) Detail of the formation of river lines marks from the impressions of the warp fibre surfaces retained in the epoxy matrix; b) Detail of the formation of river lines in the mirror region of the fracture from the residual matrix covering the warp fibres; c) Scarp formation and epoxy matrix peeling on the fracture surface of a matrix-rich area.

These river line marks are essentially fracture edges formed by the gradual merging of numerous neighbouring, very small, and disordered fracture planes during failure, from which the flow direction can be used to determine the direction of failure propagation. Figure 8.4.a) illustrates how river line marks originated from the imprint of the fibre surface retained in the matrix and angled towards the fibre imprint. This process is repeatedly observed in other parallel fibre imprints, as depicted in Figure 8.4.b) [48,49].

The Figures 8.4.a) and 8.4.c) also display the occurrence of matrix fracture in irregular lamellar shapes known as shear cusps [48,49]. The presence of these cusps occupying the space between neighbouring fibres of the weave is induced by loads applied on the surface of these fibres during the specimen opening process, leading to transverse interlaminar shearing at the fibre/matrix interface. The partial formation of the cusp mechanism along the weft yarn, where the resistance to delamination growth is considerably higher, accounts for the observed increase in fracture toughness in the woven laminate structures [24].

Also, in Figure 8.4.c), some fractographic aspects can be observed, such as cusps between the weft fibres and roughly perpendicular cliffs to the impressions of the weft fibre, pulling out of the matrix and rupture of the fibres.

8.3.2. Mode I ILFT

The DCB test is characterised by a significant amount of local bending and large displacement of the sample even before the initial crack starts to propagate. The load versus displacement curves can be divided in two stages: the linear increasing stage and the nonlinear decreasing stage. The load increases sharply before reaching the maximum value, with the displacement gradually increasing, for both control and nano-enhanced with CNFs specimens, as shown in Figure 8.5. The small thickness of CFRP sample in combination with its low elastic modulus is the main cause for this nonlinearity.

Figure 8.5 exhibits a sequence of captured images illustrating the progression of visual crack propagation in a specimen containing 0.25 wt.% CNFs, along with plotted data representing the load and opening displacement. In general, the following remarks can be made. At the initial loading stage, the curve shows a typical linear increase stage with displacement increasing (from A to B points). With increasing of the applied displacement, the crack enters in the propagation stage. However, for the specimen with 0.25 wt.% CNFs, a nonlinear increase can be found when the load reaches a relatively higher value (from B to C points) which confirms the effect of the expected increase in toughness.

The initial loading step is terminated immediately after a sudden drop in force at the maximum point, when the maximum load value is reached the first delamination occurs (point C). After the maximum force point, the curve represents the first step corresponding to the observed crack growth during the test (from C to D points). From point D, the delamination propagates progressively (from point D to point H). It should be noted that as delamination increases, the

force required to cause new delamination decreases and tends to remain constant (points F, G and H). Typical behaviour of carbon laminates, widely reported in the literature [59,60].

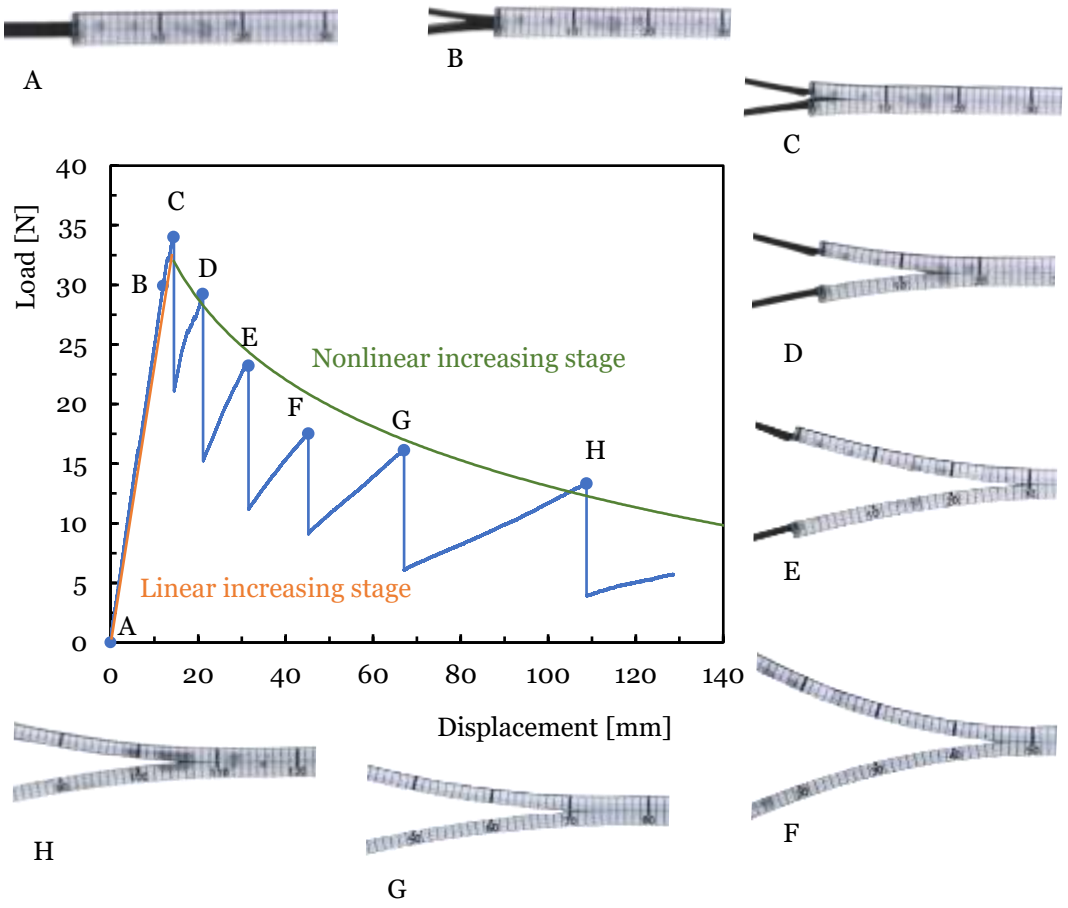

Figure 8.5: Representative load versus displacement curve of DCB test of a 0.25 wt.% CNFs Sicomin matrix laminate and associated crack propagation.

Figure 8.6 shows the typical force-displacement curves of the Mode I interfacial fracture toughness test for laminates with different matrices modified with CNFs, compared to the respective control laminates. All experiments exhibited the typical load-displacement curves for DCB specimen. Up to approximately 16 mm for Sicomin matrix (Figure 8.6.a)) and 12 mm for Ebalta matrix (Figure 8.6.b)) in vertical extension, a linear relationship is observed in the curves for all composites. This linearity corresponds to the absence of resistance to crack propagation until the crack reaches the end of the pre-crack. Beyond the pre-crack length, the curve becomes nonlinear, indicating the onset of resistance to crack propagation. This resistance could be attributed to the matrix intervening between the fibre layers or may be due fibres/nano-fillers bridging along the crack propagation, or a combination of both factors. Notably, the load at the onset of nonlinearity is highest for CNFs reinforced laminates compared to their respective control laminates. This may be due to the toughening effect of the nano-fillers, which makes crack propagation more difficult [48].

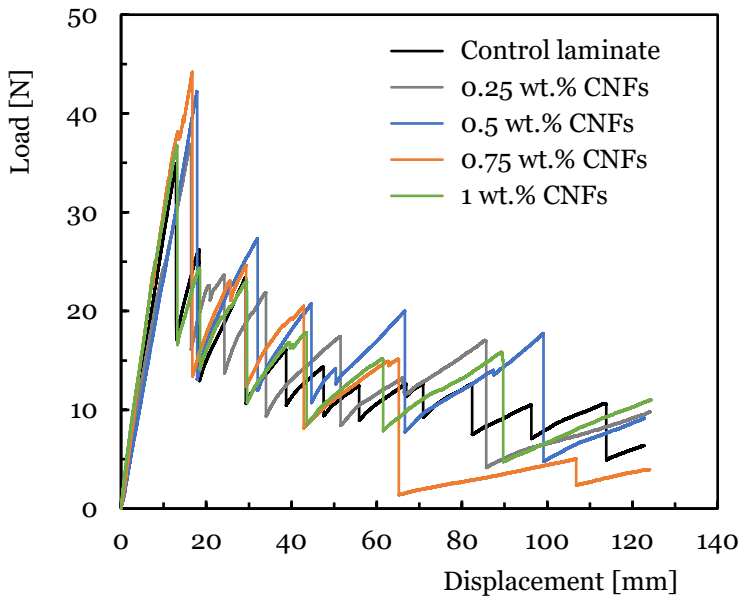

a)

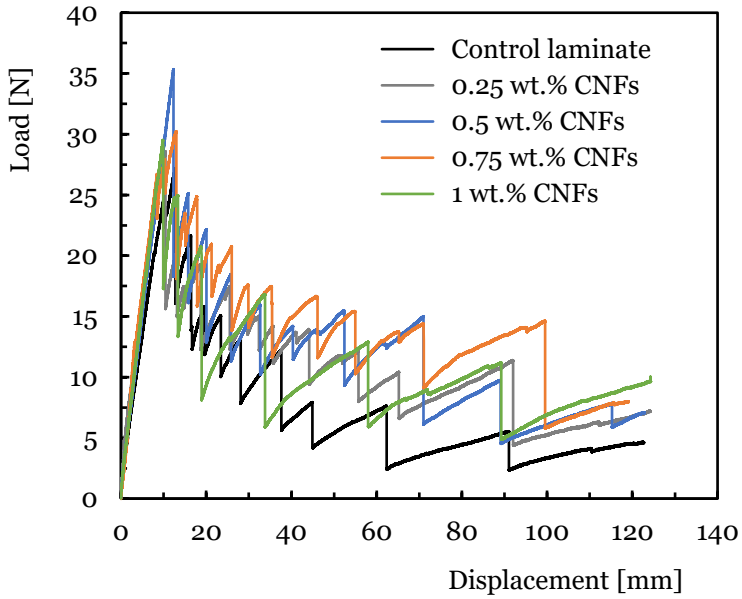

b)

Figure 8.6: Load versus displacement curves for DCB tests of carbon laminates containing different wt.% CNFs: a) Sicomin epoxy matrix; b) Ebalta epoxy matrix.

As observed in the figures, all representative curves have the same trend until the first force drop, in which the crack start to propagate. Among the laminates with Sicomin matrix, Figure 8.6.a), the crack in the CNFs modified laminates onset to propagate later than the control laminate, as the quantity of CNFs increased to an optimal value of 0.75 wt.% CNFs, shortly thereafter decreasing to 1 wt.% CNFs. Similar behaviour was obtained for Ebalta matrix, Figure 8.6.b), the crack in the CNFs modified laminates onset to propagate more later as the quantity of CNFs increased to an optimal value of 0.5 wt.% CNFs, shortly thereafter decreasing to 0.75 and 1 wt.% CNFs. Note that all curves, regardless of matrix or weight percent of CNFs, show unstable or "stick-slip" propagation occurring intermittently with force values appropriate for both crack

initiation and crack arrest for a given displacement. According to the Figure 8.6, for both matrices, the slope of the initial linear elastic part of the curves for all specimens increases as higher weight percent of CNFs were added to the matrix.

Two values were defined, namely $G_{IC,}$init, where the load and displacement started to deviate from the straight line for the first load, and $G_{IC,}$ prop, where the load and displacement started to deviate from the straight line for the second load [61]. Table 8.2 presents the average values of maximum load (P_{max}), fracture initiation energy in Mode I ($G_{IC,}$init) and fracture propagation energy ($G_{IC,}$prop), calculated by three different methods: MBT, CC and MCC. The results are analysed for laminates with different concentrations of CNFs, using two distinct epoxy matrices: Sicomin and Ebalta.

In the case of the Sicomin matrix, an increase in maximum load with CNFs content is observed, reaching a peak at 0.75 wt.% CNFs (38.09 N, a 14.8% improvement on the control value). At 1 wt.% CNFs, a slight reduction is evident, suggesting potential saturation or difficulties in dispersing the CNFs. In contrast, the Ebalta matrix demonstrates a more erratic response, exhibiting an initial increase up to 0.5 wt.% CNFs (30.0 N, representing a 21.6% enhancement), followed by a decline at higher CNFs concentrations. This behaviour may suggest that elevated levels of CNFs reduce of local plasticity and damage mechanisms in the fracture process zone.

At the fracture initiation energy, $G_{IC,}$init, for the Sicomin matrix, all the methods indicate a progressive increase in the initiation energy up to 0.75 wt.% CNFs, with values higher than the control, especially in the MCC method. However, in the laminate with 1 wt.% CNFs, there is a reduction, suggesting possible fragility due to the agglomeration of CNFs. In laminates with Ebalta matrix, there is a similar behaviour, but with smaller variations. The peak occurs at 0.5 wt.% CNFs, followed by a significant drop at 1 wt.% CNFs, especially in the MCC method. For the fracture propagation energy, $G_{IC,}$prop, in the Sicomin matrix, a progressive increase in propagation energy is observed up to 0.75 wt.% CNFs. In the Ebalta matrix, the $G_{IC,}$prop values follow a similar pattern, with an increase up to 0.5 wt.% CNFs and subsequent reduction.

For the control laminates, the average $G_{IC,}$init and $G_{IC,}$prop were 331.66 J/m² and 616.20 J/m², respectively to Sicomin laminate and 351.66 J/m² and 560.20 J/m², respectively to Ebalta laminate, calculated by means of the MBT. The results calculated by the CC and the MCC methods show slight differences. Considering the addition of CNFs in different percentages by weight, 0.25, 0.5, 0.075 and 1 wt.% and according to the results obtained, for example, calculated by means of the MBT, the $G_{IC,}$init increased by 7.41%, 10.43%, 17.46% and 13.15% respectively for the Sicomin matrix.

Table 8.2: Average values of maximum load, G_{IC} initiation and G_{IC} propagation calculate by different methods.

Composite	P_{max} [N]		MBT method [J/m²]				CC method [J/m²]				MCC method [J/m²]			
			$G_{IC,}$init		$G_{IC,}$prop		$G_{IC,}$init		$G_{IC,}$prop		$G_{IC,}$init		$G_{IC,}$prop	
	Mean	Var. (%)	Mean	Var. (%)	Mean	Var. (%)	Mean	Var. (%)	Mean	Var. (%)	Mean	Var. (%)	Mean	Var. (%)
Sicomin laminates														
Control	33.19 ± 1.66	-	331.66 ± 10	-	616.20 ± 12	-	412.01 ± 8	-	519.39 ± 20	-	334.07 ± 12	-	605.53 ± 23	-
0.25 wt.% CNFs	35.71 ± 1.52	7.6	356.23 ± 56	7.41	632.23 ± 12	2.60	452.25 ± 10	9.77	523.23 ± 8	0.74	357.23 ± 23	6.93	615.85 ± 14	1.70
0.5 wt.% CNFs	36.55 ± 0.69	10.1	366.25 ± 45	10.43	652.32 ± 10	5.86	463.63 ± 12	12.53	536.01 ± 10	3.20	365.85 ± 14	9.51	648.52 ± 10	7.10
0.75 wt.% CNFs	38.09 ± 4.13	14.8	389.58 ± 36	17.46	678.47 ± 8	10.11	489.85 ± 36	18.89	556.56 ± 12	7.16	389.23 ± 10	16.51	689.23 ± 5	13.82
1 wt.% CNFs	36.64 ± 0.35	10.4	375.28 ± 24	13.15	652.85 ± 9	5.95	479.45 ± 23	16.37	547.96 ± 14	5.50	352.14 ± 8	5.41	665.23 ± 6	9.86
Ebalta laminates														
Control	24.67 ± 4.01	-	351.66 ± 10	-	560.20 ± 12	-	421.01 ± 10	-	529.39 ± 8	-	344.17 ± 2	-	615.13 ± 2	-
0.25 wt.% CNFs	27.58 ± 4.64	11.8	366.23 ± 8	4.14	601.23 ± 12	7.32	452.25 ± 11	7.42	543.45 ± 10	2.66	357.83 ± 12	3.97	635.35 ± 10	3.29
0.5 wt.% CNFs	30.00 ± 4.40	21.6	384.25 ± 10	9.27	620.96 ± 9	10.85	483.63 ± 12	14.87	566.52 ± 12	7.01	375.05 ± 10	8.97	678.02 ± 8	10.22
0.75 wt.% CNFs	27.77 ± 2.36	12.6	359.58 ± 6	2.25	618.73 ± 8	10.45	459.85 ± 24	9.23	546.23 ± 10	3.18	339.03 ± 8	1.49	659.73 ± 8	7.25
1 wt.% CNFs	27.49 ± 2.87	11.4	335.28 ± 2	-4.66	598.24 ± 9	6.79	439.45 ± 23	4.38	537.14 ± 4	1.46	312.14 ± 8	9.31	635.63 ± 5	3.33

For laminates with Ebalta matrix, for the same percentages and with the same method, there is an increase of 4.14%, 9.27%, 2.25% from 0.25 to 0.75 wt.% CNFs and a decrease of 4.66% for 1 wt.% CNFs. It should also be noted that the variations in $G_{IC,}$init calculated by the CC and MCC methods are similar, as shown in Table 8.2.

For both matrices, the results obtained were consistent with the static properties previously studied, suggesting that the fracture energy was initially dominated by the matrix strength and that with the addition of CNFs, up to an optimum percentage, the initial fracture toughness properties of the laminates improved, which agrees with the results obtained by other authors [35,36].

The crack propagation energy, $G_{IC,}$prop, is slightly higher than the initiation fracture energies due to the presence of CNFs. Compared to the control sample, $G_{IC,}$prop calculated by MBT showed increases of 2.6%, 5.86%, 10.11% and 5.95% for Sicomin laminates with 0.25, 0.5, 0.075 and 1 wt.% CNFs added respectively. Similarly, for the Ebalta matrix laminates, the $G_{IC,}$prop calculated by MBT showed increases of 7.32%, 10.85%, 10.45% and 6.79%, respectively, for the same weight percentages of CNFs. It is worth noting that for both matrices and regardless of the percentage of CNFs added, there were large load drops at the crack growth stages, which are characteristic of high toughness matrices due to their high potential energy prior to crack initiation. When a large amount of potential energy is released, it triggers large crack growth and results in a large load drop [61]. The sudden release of a higher energy which stored in the modified sample may eventually cause the large instability and irregular fracture in the crack plane [35].

As mentioned above, for Mode I the strain energy release rate, G_I, was calculated using the MBT, CC and MCC methods and plotted against delamination length for all laminates in the study. Figure 8.7.a) and b) show representative plots for the cases of a neat Sicomin epoxy matrix and a matrix filled with 0.75 wt.% CNFs, respectively, and Figure 8.7.c) and d) show representative plots for the cases of a pure Ebalta epoxy matrix and a matrix filled with 0.5 wt.% CNFs, respectively. The values of the ILFT obtained by means of the three different calculation methods are similar for the ten materials, there being none that stands out. In accordance with the hypothesis, the ILFT tends to a stabilised value for long delamination lengths. The average value of G_I in the stabilised region was assumed to be G_{IC}. Reduced differences between G_I values obtained by the three methods were obtained [50].

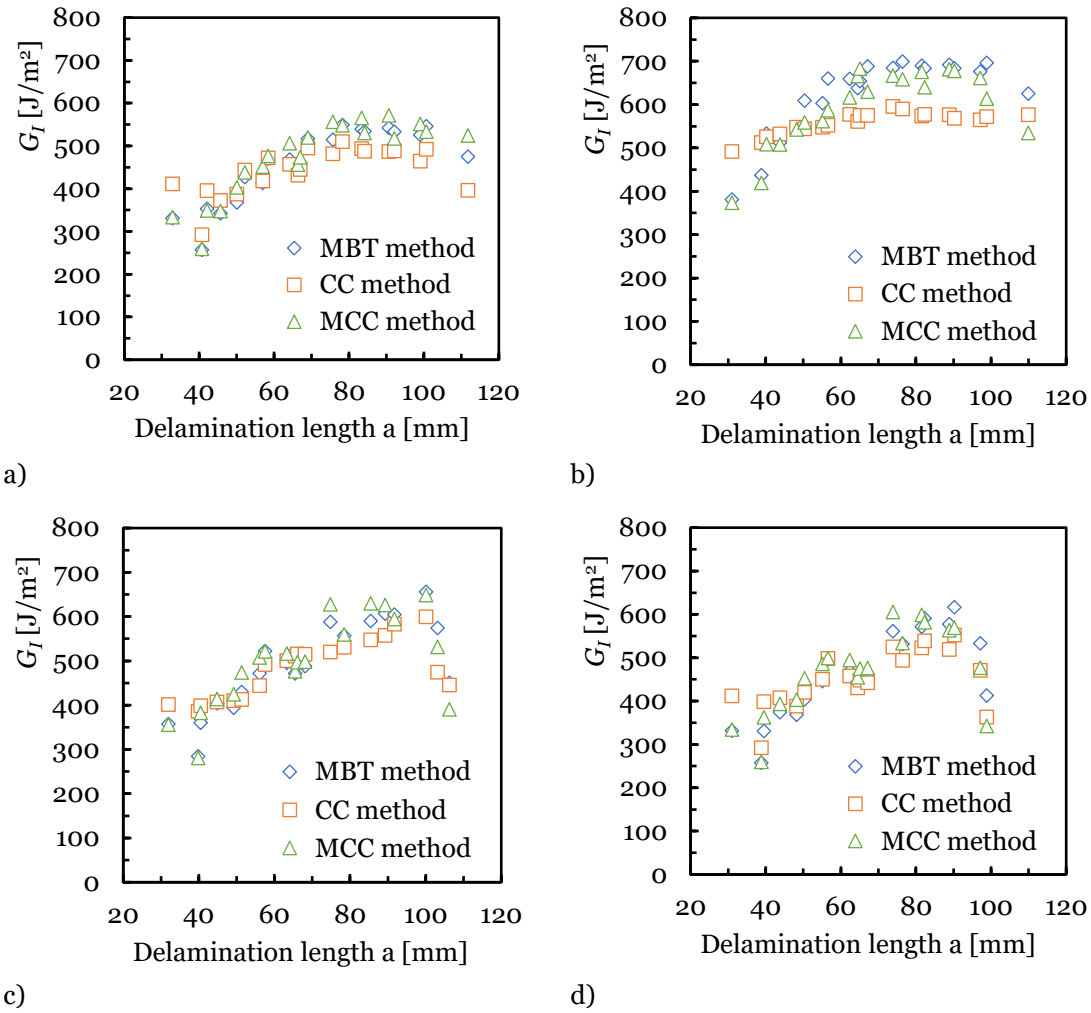

Figure 8.7: Mode I, ILFT versus delamination length for: Sicomin control laminate; b) and with 0.75 wt.% CNFs; c) Ebalta control laminate; d) and with 0.5 wt.% CNFs.

8.3.3. Mode II ILFT

Delamination in Mode II ILFT arises from shear forces acting between the separating plies. This phenomenon involves two mechanisms: cohesive fracture occurring within the matrix material between two plies, and fibre/matrix interface debonding at the interface of the matrix and a single ply. The interplay of these mechanisms leads to delamination. In the case of a Teflon insert, the initial major failure is expected to happen at the tip of the pre-crack due to stress concentration. Delamination onset becomes visually noticeable in a region positioned between the non-linear initiation point and the peak stress. Once the strain energy attains the critical value for Mode II crack propagation, the crack abruptly starts to propagate, leading to a sudden load drop. Subsequently, the load increases again as the two separated halves continue to bear the bending load until eventual crushing or tensile failure occurs at the top or bottommost extreme fibres [52].

In Mode II delamination growth, the initiation of crack growth occurs when the applied load remains below the maximum capacity, and no evident load drop is observed. Subsequently, a process zone is established, characterised by the formation of cusps, striations, and microcracks

in the immediate vicinity of the crack tip. This process continues until the occurrence of coalescence, at which point crack growth becomes discernible along the sides of the specimen. It is only upon the attainment of coalescence that a decline in the load is discernible in the load versus displacement history [56].

Mode II was characterized by a three-point ENF test and the load versus displacement curves were also obtained, as shown in Figure 8.8. At the initial loading stage, the curves of all specimens show a linear increase stage with displacement increasing, followed by a nonlinear increase when the load reaches a relatively higher value.

As illustrated in Figure 8.8.a), the representative load-displacement curves of the END test of a neat Sicomin matrix laminate and with different percentages of CNFs where crack propagation is associated are shown. Similarly, Figure 8.8.b) shows the load-displacement curves from Mode II fracture toughness tests on CFRP composite laminates with varying CNFs content compared to the control laminate curve.

The Mode I fracture mode is largely dependent on the fibre/epoxy interface strength, and the interface strength has not been significantly improved during this work. These failure mechanisms may cause the Mode II fracture toughness improvement to be more sensitive than Mode I fracture toughness. But the Mode II mode is mainly due to the sliding shear of the laminates, which is a matrix dominated process, and the CNFs modified epoxy shows the prominent effect in increasing the fracture toughness [35,62].

As illustrated in Figure 8.8.a), the Sicomin matrix demonstrates that the control laminate demonstrates the lowest resistance when compared to laminates modified with CNFs. Conversely, the maximum load increases in proportion to the percentage of CNFs, reaching its highest value at 1 wt.% CNFs, as does the laminates' stiffness. Unlike Sicomin matrix, Ebalta matrix shows a slightly different behaviour in terms of maximum load. The laminate reinforced with 0.5 wt.% CNFs shows the highest strength compared to all other percentages of CNFs. On the other hand, the control laminate shows an abrupt failure indicating a lower toughness compared to the CNF reinforced composites as shown in Figure 8.8.b). In summary, the findings indicate that laminates with Sicomin matrix demonstrate a propensity for the maximum load to undergo a continuous increase with the CNF content. Conversely, laminates with an Ebalta matrix exhibit a resistance peak with 0.5 wt.% CNFs, followed by a decline for higher concentrations. The analysis indicates that Sicomin matrix promotes enhanced adhesion and resistance to crack growth, leading to an increase of the interlaminar fracture with 1 wt.% CNFs. In contrast, Ebalta matrix appears to have attained a maximum strength limit at lower concentrations. These findings underscore the pivotal role of matrix choice in dictating the strength and mechanical behaviour of CNFs reinforced carbon laminates, thereby influencing Mode II fracture toughness.

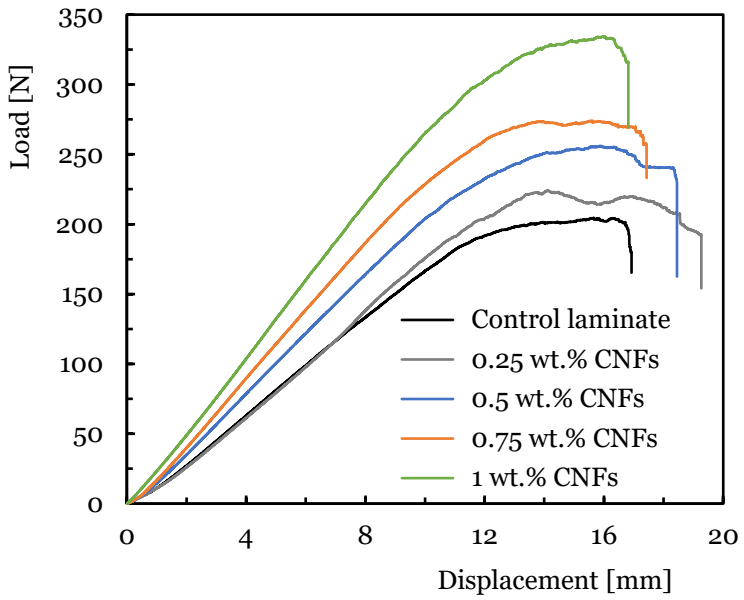

a)

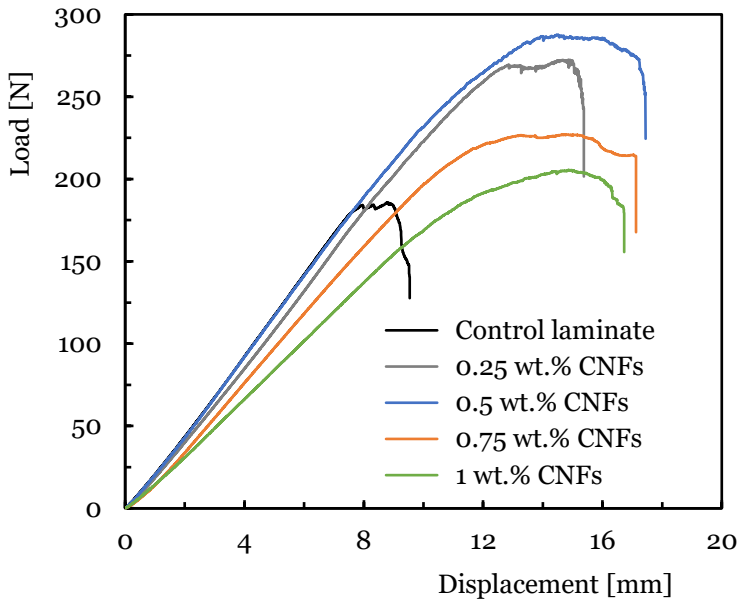

b)

Figure 8.8: Load versus displacement curves for END tests of carbon laminates containing different wt.% CNFs: a) Sicomin epoxy matrix; b) Ebalta epoxy matrix.

Table 8.3 shows the average values of stiffness (K), maximum load (P_{max}) and fracture energy propagation in Mode II ($G_{IIC,}$prop) for the ECM method, SBT method and CCM method. In laminates with Sicomin matrix, there is a progressive increase in stiffness with the CNFs content, reaching a maximum value of 36.15 GPa for 1 wt.% CNFs, representing an increase of approximately 5.5% in relation to the value of the control laminate. In laminates with Ebalta matrix, the stiffness shows a different behaviour, with a peak in the laminate nano-enhanced with 0.5 wt.% CNFs (31.65 GPa) and a reduction for higher percentages, reaching a drop of 10.2% for 1 wt.% CNFs. This behaviour may indicate difficulties in the homogeneous dispersion of CNFs at higher concentrations, as reported in previous studies.

With regard to the maximum load, for Sicomin matrix, the maximum load increases significantly with the CNF content, reaching a 51% increase for 1 wt.% CNFs. This behaviour suggests better mechanical resistance to interlaminar failure with the addition of CNFs. In the case of Ebalta matrix, the behaviour is different, with a maximum load peak for 0.5 wt.% CNFs (286.10 N, 61.7% compared to the control laminate) followed by a reduction for higher percentages, reaching a decrease for 1 wt.% CNFs of 16.2%. This may indicate a possible weakening of the matrix for higher concentrations of CNFs, indicating that the optimum value is 0.5 wt.% CNFs

Fracture energy was assessed using three different methods: ECM, SBT and CCM. In laminates with Sicomin matrix, there is a systematic increase with the addition of CNFs in all methods, reaching maximum values at 1 wt.% CNFs, with variations up to 23.9% in the CCM method. For laminates made with Ebalta matrix, the behaviour shows a maximum at 0.5 wt.% CNFs, followed by a decrease at higher contents, especially in the CCM method, where there is a decrease of 1.48% at 1 wt.% CNFs. These values are also related to the difficulty of dispersion and possible agglomeration of CNFs at higher percentages, leading to the formation of failure points and consequently a reduction in interlaminar fracture.

Figure 8.9 shows the Mode II strain energy release rate, G_{II}, obtained by the ECM, SBT and CCM methods versus delamination length for the neat Sicomin matrix and with 1 wt.% CNFs (Figure 8.9.a) and b), respectively) and the neat Ebalta matrix and with 0.5 wt.% CNFs (Figure 8.9.c) and d), respectively). Similar to other works, the strain energy release rate tends towards a stabilised value for crack lengths above 40 mm. In fact, it is known that during shear mode crack propagation, a large fracture process zone is formed in front of the crack. This fracture process zone affects the measured toughness values due to the amount of energy dissipated [50].

For the Sicomin control laminate, Figure 8.9.a), the three methods show a tendency for G_{II} to increase with delamination length, indicating typical stable fracture growth behaviour. The ECM method shows slightly lower values compared to SBT and CCM, suggesting less sensitivity in the detection of fracture energy. Figure 8.9.b) shows that the addition of 0.75 wt.% CNFs results in a significant increase in G_{II}, especially for delamination lengths greater than 35 mm. The values obtained by the SBT and CCM methods are virtually identical, confirming the reliability of these method.

The ECM method, although showing a similar trend, gives lower values which may be related to the way the fracture energy is estimated in this method. In the control laminate with Ebalta matrix, the G_{II} values are significantly lower than those observed in the laminate with Sicomin matrix, indicating a lower resistance to delamination propagation. The SBT method gives slightly higher values than CCM and ECM, suggesting a possible overestimation of this method for the material analysed. The scatter of the points indicates a more significant variation of the interlaminar strength along the crack growth, Figure 8.9.c). Also, in the Ebalta matrix, Figure 8.9.d), the incorporation of 0.5% wt.% CNFs results in a significant improvement in delamination resistance, as evidenced by the increase in G_{II} values.

Table 8.3: Average values of laminate stiffness, maximum load and G_{IIC} propagation calculate by different methods.

Composite	K [GPa] at a_o = 30 mm		P_{max} [N]		$G_{IIC,}$prop (ECM) [J/m²]		$G_{IIC,}$prop (SBT) [J/m²]		$G_{IIC,}$prop (CCM) [J/m²]	
	Mean	Var. (%)	Mean	Var. (%)	Mean	Var. (%)	Mean	Var. (%)	Mean	Var. (%)
Sicomin laminates										
Control	34.12 ± 1.65	-	214.05 ± 9.12	-	1822.2 ± 0.56	-	2366.0 ± 0.36	-	2226.6 ± 0.21	-
0.25 wt.% CNFs	34.18 ± 1.22	0.2	224.52 ± 13.12	4.9	1952.6 ± 0.12	7.14	2456.4 ± 0.56	3.80	2389.4 ± 0.36	7.32
0.5 wt.% CNFs	35.02 ± 1.15	2.6	251.50 ± 9.59	17.5	2014.0 ± 0.36	10.54	2569.1 ± 0.78	8.58	2456.3 ± 0.52	10.33
0.75 wt.% CNFs	35.94 ± 1.21	5.3	273.89 ± 0.94	28.0	2145.1 ± 0.26	17.73	2654.6 ± 0.96	12.17	2612.1 ± 0.14	17.34
1 wt.% CNFs	36.15 ± 1.60	5.5	323.28 ± 10.55	51.0	2236.8 ± 0.52	22.72	2845.3 ± 0.32	20.25	2758.6 ± 0.39	23.90
Ebalta laminates										
Control	31.22 ± 1.90	-	176.89 ± 19.01	-	1524.4 ± 0.30	-	2035.2 ± 0.34	-	1926.9 ± 0.36	-
0.25 wt.% CNFs	30.14 ± 1.69	- 3.5	261.15 ± 7.45	47.6	1625.6 ± 0.24	6.63	2106.6 ± 0.21	3.49	2014.1 ± 0.24	4.57
0.5 wt.% CNFs	31.65 ± 0.88	1.4	286.10 ± 10.80	61.7	1856.3 ± 0.15	21.78	2350.5 ± 0.12	15.48	22365.8 ± 0.12	16.12
0.75 wt.% CNFs	30.42 ± 1.4	- 2.6	227.42 ± 19.32	28.6	1725.2 ± 0.28	13.19	2258.4 ± 0.29	10.96	2158.9 ± 0.31	12.05
1 wt.% CNFs	28.05 ± 0.64	- 10.2	205.55 ± 20.54	16.2	1632.9 ± 0.12	7.09	2158.1 ± 0.15	6.04	19545.8 ± 0.10	1.48

The SBT method continues to show the highest values, while CCM and ECM show an intermediate but more conservative trend. The addition of CNFs contributes to an increase in fracture growth stability, reducing data scatter, especially for delamination values above 35 mm.

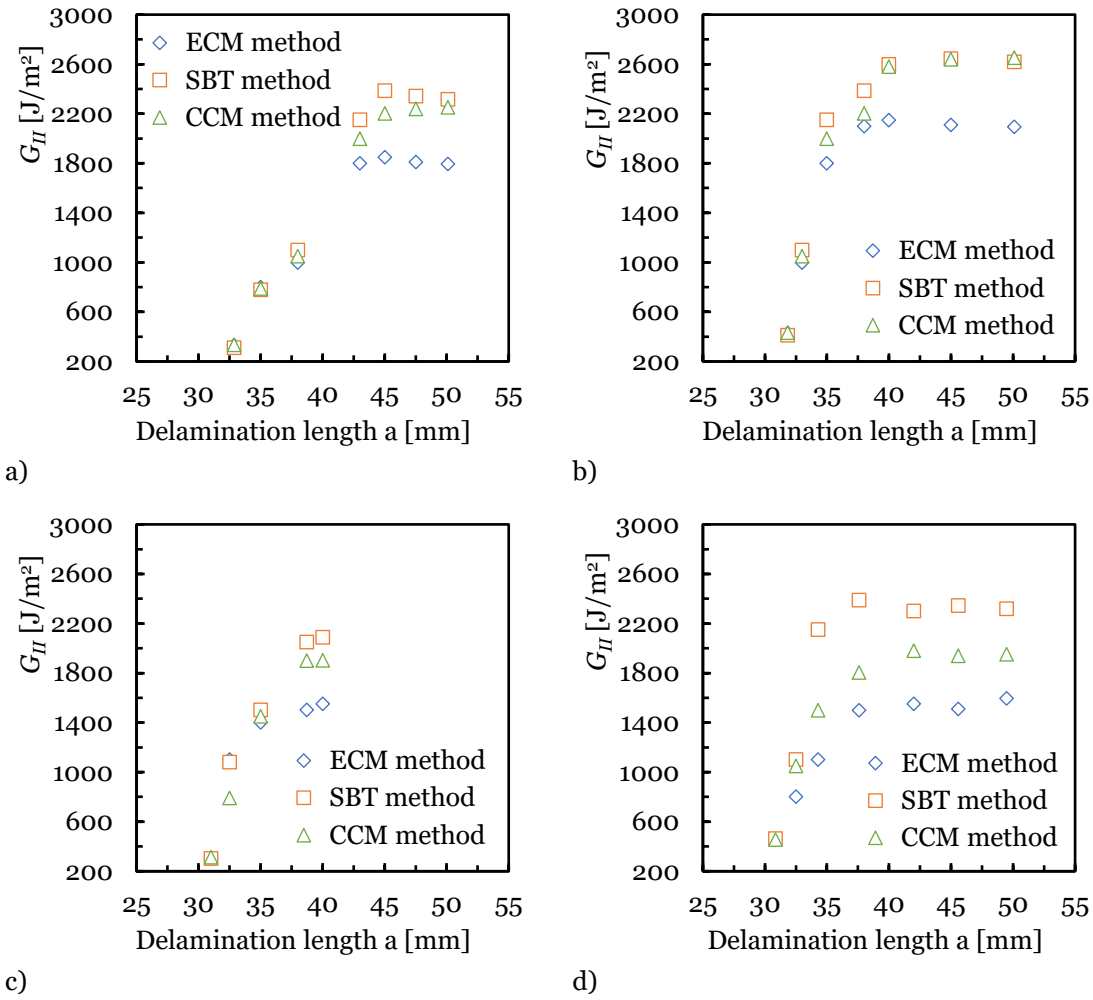

Figure 8.9: Mode II, ILFT versus delamination length for: Sicomin control laminate; b) and with 0.75 wt.% CNFs; c) Ebalta control laminate; d) and with 0.5 wt.% CNFs.

8.4. Conclusions

The interlaminar fracture toughness of CFRP laminates has been investigated under Mode I and Mode II loading, where two different epoxy matrices (Sicomin and Ebalta) have been reinforced with different weight percentages of CNFs.

In the DCB tests, the addition of CNFs improved the mechanical strength and toughness of the laminates, especially for the Sicomin matrix, which showed more consistent increases in all the parameters analysed. The best performance was observed for 0.75 wt.% CNFs (16.51% improvement in $G_{IC,}$init and 13.82% improvement in $G_{IC,}$prop), while for 1 wt.% CNFs there were noticeable downward trends, probably due to difficulties in the homogeneous dispersion of the CNFs. When calculating the results, the MCC method showed the highest $G_{IC,}$prop values, indicating greater sensitivity in detecting resistance to crack propagation. For the Ebalta matrix,

the results indicate that reinforcement with CNFs can be beneficial, but there is a critical concentration limit, 0.5 wt.% CNFs (14.87% improvement in $G_{IC,}$init and 7.01% improvement in $G_{IC,}$prop, results calculated by the CC method), beyond which structural performance can be compromised.

Regarding the ENF tests, the addition of CNFs has a positive effect on the stiffness, maximum load and fracture energy of carbon laminates, but the behaviour is highly dependent on the type of matrix used. The Sicomin matrix showed better compatibility with CNFs, with progressive increases in the three parameters analysed up to 1 wt.% CNFs (improvements of 23.9%). The Ebalta matrix showed optimum behaviour at 0.5 wt.% CNFs (21.78% improvement), with reductions at higher concentrations. The MCC method gave the highest G_{IIC} values, indicating greater sensitivity in detecting resistance to crack propagation.

According to the results obtained, the CNFs are effective in load transfer due to their large surface area and high aspect ratio. Thus, the choice of matrix and the optimum concentration of CNFs are critical factors in optimising the mechanical performance of carbon laminates with respect to Mode II delamination.

Bibliography

[1] Pusch J, Wohlmann B. Carbon Fibers. Inorganic and Composite Fibers, Elsevier; 2018, p. 31–51. https://doi.org/10.1016/B978-0-08-102228-3.00002-5.

[2] Rubino F, Nisticò A, Tucci F, Carlone P. Marine Application of Fiber Reinforced Composites: A Review. Journal of Marine Science and Engineering 2020;8:26. https://doi.org/10.3390/jmse8010026.

[3] Hagnell MK, Kumaraswamy S, Nyman T, Åkermo M. From aviation to automotive - a study on material selection and its implication on cost and weight efficient structural composite and sandwich designs. Heliyon 2020;6:e03716. https://doi.org/10.1016/j.heliyon.2020.e03716.

[4] Paluvai NR, Mohanty S, Nayak SK. Synthesis and Modifications of Epoxy Resins and Their Composites: A Review. Polymer - Plastics Technology and Engineering 2014;53:1723–58. https://doi.org/10.1080/03602559.2014.919658.

[5] Aziz I, Duran H, Saleem M, Yameen B, Arshad SN. The role of interface on dynamic mechanical properties, dielectric performance, conductivity, and thermal stability of electrospun carbon nanofibers reinforced epoxy. Polymer Composites 2021;42:4366–79. https://doi.org/10.1002/pc.26154.

[6] Kumar S, Krishnan S, Mohanty S, Nayak SK. Synthesis and characterization of petroleum and biobased epoxy resins: a review. Polymer International 2018;67:815–39. https://doi.org/10.1002/pi.5575.

[7] Sukanto H, Raharjo WW, Ariawan D, Triyono J, Kaavesina M. Epoxy resins thermosetting for mechanical engineering. Open Engineering 2021;11:797–814. https://doi.org/10.1515/eng-2021-0078.

[8] Mirsalehi SA, Youzbashi AA, Sazgar A. Enhancement of out-of-plane mechanical properties of carbon fiber reinforced epoxy resin composite by incorporating the multi-walled carbon nanotubes. SN Applied Sciences 2021;3:630.

https://doi.org/10.1007/s42452-021-04624-2.

[9] Qu Z, Zhao C, An L. A micromechanics perspective on the intralaminar and interlaminar damage mechanisms of composite laminates considering ply orientation and loading condition. Composite Structures 2024;347:118454. https://doi.org/10.1016/j.compstruct.2024.118454.

[10] Al-Saleh MH, Sundararaj U. Review of the mechanical properties of carbon nanofiber/polymer composites. Composites Part A: Applied Science and Manufacturing 2011;42:2126–42. https://doi.org/10.1016/j.compositesa.2011.08.005.

[11] Chen Q, Zhao Y, Zhou Z, Rahman A, Wu XF, Wu W, et al. Fabrication and mechanical properties of hybrid multi-scale epoxy composites reinforced with conventional carbon fiber fabrics surface-attached with electrospun carbon nanofiber mats. Composites Part B: Engineering 2013;44:1–7. https://doi.org/10.1016/j.compositesb.2012.09.005.

[12] Eskizeybek V, Yar A, Avcı A. CNT-PAN hybrid nanofibrous mat interleaved carbon/epoxy laminates with improved Mode I interlaminar fracture toughness. Composites Science and Technology 2018;157:30–9. https://doi.org/10.1016/j.compscitech.2018.01.021.

[13] Wable V, Biswas PK, Moheimani R, Aliahmad N, Omole P, Siegel AP, et al. Engineering the electrospinning of MWCNTs/epoxy nanofiber scaffolds to enhance physical and mechanical properties of CFRPs. Composites Science and Technology 2021;213:108941. https://doi.org/10.1016/j.compscitech.2021.108941.

[14] Jain V, Bisht A, Jaiswal S, Dasgupta K, Lahiri D. Assessment of Interfacial Interaction in Graphene Nanoplatelets and Carbon Fiber-Reinforced Epoxy Matrix Multiscale Composites and Its Effect on Mechanical Behavior. Journal of Materials Engineering and Performance 2021;30:8913–25. https://doi.org/10.1007/s11665-021-06115-2.

[15] Wu S, Ladani RB, Zhang J, Kinloch AJ, Zhao Z, Ma J, et al. Epoxy nanocomposites containing magnetite-carbon nanofibers aligned using a weak magnetic field. Polymer 2015;68:25–34. https://doi.org/10.1016/j.polymer.2015.04.080.

[16] Gabr MH, Okumura W, Ueda H, Kuriyama W, Uzawa K, Kimpara I. Mechanical and thermal properties of carbon fiber/polypropylene composite filled with nano-clay. Composites Part B: Engineering 2015;69:94–100. https://doi.org/10.1016/j.compositesb.2014.09.033.

[17] Louis BM, Klunker F, Ermanni P. Effect of locally deposited nanosilica particles on interlaminar fracture toughness of high glass-transition temperature epoxy carbon fiber-reinforced composites. Journal of Composite Materials 2019;53:3599–614. https://doi.org/10.1177/0021998319836063.

[18] Barhoum A, Rasouli R, Yousefzadeh M, Rahier H, Bechelany M. Nanofiber Technologies: History and Development. Handbook of Nanofibers, Cham: Springer International Publishing; 2019, p. 3–43. https://doi.org/10.1007/978-3-319-53655-2_54.

[19] Rana S, Alagirusamy R, Joshi M. Effect of carbon nanofiber dispersion on the tensile properties of epoxy nanocomposites. Journal of Composite Materials 2011;45:2247–56. https://doi.org/10.1177/0021998311401076.

[20] Xu S, Akchurin A, Liu T, Wood W, Tangpong X, Akhatov IS, et al. Thermal properties of carbon nanofiber reinforced high-density polyethylene nanocomposites. Journal of Composite Materials 2015;49:795–805. https://doi.org/10.1177/0021998314525980.

[21] Palazzetti R, Zucchelli A. Electrospun nanofibers as reinforcement for composite laminates materials – A review. Composite Structures 2017;182:711–27. https://doi.org/10.1016/j.compstruct.2017.09.021.

[22] Gong Y, Tian D, Cao T, Zhao L, Zhang J, Hu N, et al. An R-curve effect-included delamination growth criterion for mixed-mode I/II delamination predictions of composite laminates. Composite Structures 2022;295. https://doi.org/10.1016/j.compstruct.2022.115846.

[23] Greenhalgh ES, Rogers C, Robinson P. Fractographic observations on delamination growth and the subsequent migration through the laminate. Composites Science and Technology 2009;69:2345–51. https://doi.org/10.1016/j.compscitech.2009.01.034.

[24] Delamination-dominated failures in polymer composites. Failure Analysis and

Fractography of Polymer Composites, Elsevier; 2009, p. 164–237. https://doi.org/10.1533/9781845696818.164.

[25] Al-Khudairi O, Hadavinia H, Waggott A, Lewis E, Little C. Characterising mode I/mode II fatigue delamination growth in unidirectional fibre reinforced polymer laminates. Materials and Design 2015;66:93–102. https://doi.org/10.1016/j.matdes.2014.10.038.

[26] Rikards R, Buchholz FG, Bledzki AK, Wacker G, Korjakin A. Mode I, mode II, and mixed-mode I/II interlaminar fracture toughness of GFRP influenced by fiber surface treatment. Mechanics of Composite Materials 1996;32:439–62. https://doi.org/10.1007/BF02313863.

[27] Xu A, Bao L, Nishida M, Yamanaka A. Molding of PBO fabric reinforced thermoplastic composite to achieve high fiber volume fraction. Polymer Composites 2013;34:953–8. https://doi.org/10.1002/pc.22501.

[28] Elkington M, Bloom D, Ward C, Chatzimichali A, Potter K. Hand layup: understanding the manual process. Advanced Manufacturing: Polymer & Composites Science 2015;1:138–51. https://doi.org/10.1080/20550340.2015.1114801.

[29] Kaynan O, Atescan Y, Ozden-Yenigun E, Cebeci H. Mixed Mode delamination in carbon nanotube/nanofiber interlayered composites. Composites Part B: Engineering 2018;154:186–94. https://doi.org/10.1016/j.compositesb.2018.07.032.

[30] Khan SU, Kim JK. Improved interlaminar shear properties of multiscale carbon fiber composites with bucky paper interleaves made from carbon nanofibers. Carbon 2012;50:5265–77. https://doi.org/10.1016/j.carbon.2012.07.011.

[31] Arai M, Sasaki T, Hirota S, Ito H, Hu N, Quaresimin M. Mixed modes interlaminar fracture toughness of cfrp laminates toughened with CNF interlayer. Acta Mechanica Solida Sinica 2012;25:321–30. https://doi.org/10.1016/S0894-9166(12)60029-9.

[32] Arai M, Noro Y, Sugimoto K, Endo M. Mode I and mode II interlaminar fracture toughness of CFRP laminates toughened by carbon nanofiber interlayer. Composites Science and Technology 2008;68:516–25. https://doi.org/10.1016/j.compscitech.2007.06.007.

[33] Kostopoulos V, Karapappas P, Loutas T, Vavouliotis A, Paipetis A, Tsotra P. Interlaminar Fracture Toughness of Carbon Fibre-Reinforced Polymer Laminates With Nano- and Micro-Fillers. Strain 2011;47:e269–82. https://doi.org/10.1111/j.1475-1305.2008.00612.x.

[34] Arai M, Hirokawa JI, Hanamura Y, Ito H, Hojo M, Quaresimin M. Characteristic of mode i fatigue crack propagation of CFRP laminates toughened with CNF interlayer. Composites Part B: Engineering 2014;65:26–33. https://doi.org/10.1016/j.compositesb.2014.02.025.

[35] Wang P, Liu W, Zhang X, Lu X, Yang J. Enhanced fracture toughness of carbon fabric/epoxy laminates with pristine and functionalized stacked-cup carbon nanofibers. Engineering Fracture Mechanics 2015;148:73–81. https://doi.org/10.1016/j.engfracmech.2015.09.010.

[36] Ladani RB, Wu S, Kinloch AJ, Ghorbani K, Zhang J, Mouritz AP, et al. Improving the toughness and electrical conductivity of epoxy nanocomposites by using aligned carbon nanofibres. Composites Science and Technology 2015;117:146–58. https://doi.org/10.1016/j.compscitech.2015.06.006.

[37] Ladani RB, Wu S, Kinloch AJ, Ghorbani K, Zhang J, Mouritz AP, et al. Multifunctional properties of epoxy nanocomposites reinforced by aligned nanoscale carbon. Materials & Design 2016;94:554–64. https://doi.org/10.1016/j.matdes.2016.01.052.

[38] Ravindran AR, Ladani RB, Wu S, Kinloch AJ, Wang CH, Mouritz AP. Multi-scale toughening of epoxy composites via electric field alignment of carbon nanofibres and short carbon fibres. Composites Science and Technology 2018;167:115–25. https://doi.org/10.1016/j.compscitech.2018.07.034.

[39] Ravindran AR, Ladani RB, Wang CH, Mouritz AP. Hierarchical mode I and mode II interlaminar toughening of Z-pinned composites using 1D and 2D carbon nanofillers. Composites Part A: Applied Science and Manufacturing 2019;124:105470. https://doi.org/10.1016/j.compositesa.2019.05.038.

[40] Ekhtiyari A, Shokrieh MM, Alderliesten R. Loading rate effects on mode-I delamination in

glass/epoxy and glass/CNF/epoxy laminated composites. Engineering Fracture Mechanics 2020;228:106908. https://doi.org/10.1016/j.engfracmech.2020.106908.

[41] Ravindran AR, Ladani RB, Kinloch AJ, Wang CH, Mouritz AP. Improving the delamination resistance and impact damage tolerance of carbon fibre-epoxy composites using multi-scale fibre toughening. Composites Part A: Applied Science and Manufacturing 2021;150:106624. https://doi.org/10.1016/j.compositesa.2021.106624.

[42] Ravindran AR, Ladani RB, Wang CH, Mouritz AP. Strengthening of composite T-joints using 1D and 2D carbon nanoparticles. Composite Structures 2021;255:112982. https://doi.org/10.1016/j.compstruct.2020.112982.

[43] Pina dos Santos PS, Maceiras A, Valvez S, Reis PNB. Mechanical characterization of different epoxy resins enhanced with carbon nanofibers. Frattura Ed Integrità Strutturale 2020;15:198–212. https://doi.org/10.3221/IGF-ESIS.55.15.

[44] Santos P, Silva AP, Reis PNB. Effect of Carbon Nanofibers on the Viscoelastic Response of Epoxy Resins. Polymers 2023;15:821. https://doi.org/10.3390/polym15040821.

[45] Santos P, Silva AP, Reis PNB. Effect of Carbon Nanofibers on the Strain Rate and Interlaminar Shear Strength of Carbon/Epoxy Composites. Materials 2023;16:4332. https://doi.org/10.3390/ma16124332.

[46] Santos P, Silva AP, Reis P. Effect of carbon nanofibers on the viscoelastic response of carbon/epoxy composites. Journal of Reinforced Plastics and Composites 2023;15:821. https://doi.org/10.1177/07316844231203787.

[47] Santos P, Maceiras A, Reis PNB. Influence of manufacturing parameters on the mechanical properties of nano-reinforced CFRP by carbon nanofibers. IOP Conference Series: Materials Science and Engineering 2021;1126:012012. https://doi.org/10.1088/1757-899X/1126/1/012012.

[48] Saurabh S, Dasari S, Chandra Ray B, Kumar Prusty R. Mode I interlaminar fracture toughness improvement of the glass/epoxy composite by using multiscale composite approach. Materials Today: Proceedings 2020;33:5328–33. https://doi.org/10.1016/j.matpr.2020.03.023.

[49] Zhou Y, Cao Y, Cao J, Zhang C, Li J, Wang Z. Fracture toughness and fiber bridging mechanism for mode-I interlaminar failure of spread-tow woven composites. Engineering Fracture Mechanics 2024;298:109957. https://doi.org/10.1016/j.engfracmech.2024.109957.

[50] Silva H, Ferreira JAM, Capela C, Richardson MOW. Mixed Mode interlayer fracture of glass fiber/nano-enhanced epoxy composites. Composites Part A: Applied Science and Manufacturing 2014;64:211–22. https://doi.org/10.1016/j.compositesa.2014.05.011.

[51] May M. Measuring the rate-dependent mode I fracture toughness of composites – A review. Composites Part A: Applied Science and Manufacturing 2016;81:1–12. https://doi.org/10.1016/j.compositesa.2015.10.033.

[52] Sajith S, Arumugam V, Dhakal HN. Effects of curing pressure on mode II fracture toughness of uni-directional GFRP laminates. Polymer Testing 2015;48:59–68. https://doi.org/10.1016/j.polymertesting.2015.09.011.

[53] Mohammadi R, Najafabadi MA, Saghafi H, Zarouchas D. Mode-II fatigue response of AS4/8552 carbon /epoxy composite laminates interleaved by electrospun nanofibers. Thin-Walled Structures 2020;154:106811. https://doi.org/10.1016/j.tws.2020.106811.

[54] Yan X, Guo X, Gao Y, Lin Y, Zhang N, Zhao Q. Mode-II fracture toughness and crack propagation of pultruded carbon Fiber-Epoxy composites. Engineering Fracture Mechanics 2023;279:109042. https://doi.org/10.1016/j.engfracmech.2022.109042.

[55] Li X, Monticeli F, Pascoe J-A, Mosleh Y. Interlaminar fracture behaviour of emerging laminated-pultruded CFRP plates for wind turbine blades. Engineering Fracture Mechanics 2024;308:110353. https://doi.org/10.1016/j.engfracmech.2024.110353.

[56] Mahmood AS, Summerscales J, James MN. Resin-Rich Volumes (RRV) and the Performance of Fibre-Reinforced Composites: A Review. Journal of Composites Science 2022;6:1–16. https://doi.org/10.3390/jcs6020053.

[57] Cholake ST, Moran G, Joe B, Bai Y, Singh Raman RK, Zhao XL, et al. Improved Mode I

fracture resistance of CFRP composites by reinforcing epoxy matrix with recycled short milled carbon fibre. Construction and Building Materials 2016;111:399–407. https://doi.org/10.1016/j.conbuildmat.2016.02.039.

[58] Quan D, Urdániz JL, Ivanković A. Enhancing mode-I and mode-II fracture toughness of epoxy and carbon fibre reinforced epoxy composites using multi-walled carbon nanotubes. Materials & Design 2018;143:81–92. https://doi.org/10.1016/j.matdes.2018.01.051.

[59] Amaral L, Yao L, Alderliesten R, Benedictus R. The relation between the strain energy release in fatigue and quasi-static crack growth. Engineering Fracture Mechanics 2015;145:86–97. https://doi.org/10.1016/j.engfracmech.2015.07.018.

[60] de Paula Santos LF, Monticeli FM, Ribeiro B, Costa ML, Alderliesten R, Botelho EC. Does carbon nanotube buckypaper affect mode-I and II interlaminar fracture toughness under quasi-static loading? Composite Structures 2023;323:117507. https://doi.org/10.1016/j.compstruct.2023.117507.

[61] Ning N, Wang M, Zhou G, Qiu Y, Wei Y. Effect of polymer nanoparticle morphology on fracture toughness enhancement of carbon fiber reinforced epoxy composites. Composites Part B: Engineering 2022;234:109749. https://doi.org/10.1016/j.compositesb.2022.109749.

[62] Liu W, Kong J, Toh WE, Zhou R, Ding G, Huang S, et al. Toughening of epoxies by covalently anchoring triazole-functionalized stacked-cup carbon nanofibers. Composites Science and Technology 2013;85:1–9. https://doi.org/10.1016/j.compscitech.2013.05.009.

Chapter 9

Low-velocity and multi-impact response of carbon fibre composites enhanced with carbon nanofibres

Abstract

The interest and increasing demand for lightweight, cost-effective and optimized structural properties are known. On their own, carbon fibre reinforced polymer (CFRP) composites are chosen by having high strength and excellent stiffness-to-weight ratios over other materials, but its sensitivity and degradation when subjected to impact it's one of your problems. In this chapter, carbon fibre and epoxy resin nano-enhanced by incorporating a very small amount of carbon nanofibres (CNFs), (i.e.,0.5wt.% CNFs) are used to manufacture an optimized composite to respond to low-velocity impact (LVI) loads and to create an attractive material for the composites materials industries. Therefore, this work intends to study the LVI and multi-impact behaviour of composite laminates. For this purpose, LVI tests were carried out with impact energies of 1 J, 3 J, 5 J, 7 J and 9 J. In terms of multi-impact strength, the classic strength - number of impacts (S-N) curves were obtained, obviously the number of impacts to failure varied inversely with the impact energy, and the nano-enhanced laminate with CNFs promoted lives about 5 times higher than the observed on the control laminates.

9.1. Introduction

Carbon fibre reinforced polymer (CFRP) composites have been widely used in the last two decades in several industries such as aeronautical, automotive, railways and also in various sports equipment, due to their high specific strength and stiffness. Therefore, from the perspective of the transportation sector, these materials allow the achievement of more rigid structures associated with greater fuel economy and, consequently, lower greenhouse gas emissions [1–3]. In addition, CFRP exhibit impressive in-plane tensile strength, chemical and corrosion resistance, electrical conductivity, fatigue resistance, high durability, and ease of fabrication, many of which are superior to those of more commonly used metallic materials in engineering applications [4–6]. Nonetheless, CFRP composites have several weaknesses, such as low resistance to compressive loads, limited capacity to withstand interlaminar fibre-matrix cracking, and delamination owing to the constrained fracture toughness inherent in the polymer matrices [4,7]. However, it is the loads applied along the thickness of the laminates that are the most damaging/critical, with special emphasis on low velocity impact (LVI) loads [8,9].

Generally, LVI are events which can be treated as quasi-static, the upper limit of which can vary from 1 to 10 m/s up to a hundred m/s. Abrate in his review of impact on laminated composites stated that LVI occur for impact speeds of less than 100 m/s [10]. On the other hand, Hodgkinson defines LVI when it is between 1 to 10 m/s. Impacts greater than 100 m/s are classified as ballistics tests, while at a speed greater than 1000 m/s they are called hyper-velocity impacts [11]. Too Sjöblom et al. define of LVI as events which can be treated as quasi-static, the upper limit of which can vary from 1 to 10 m/s depending on the target stiffness, material properties and the impactor's mass and stiffness [12].

There are several sources of impact damage to the composite materials, hat may occur during the service of a component, such as: dropping of tools during maintenance or repair on the composite structure, debris or foreign object impact (bird strike, tire debris from burst tires, walking on a structure), natural events (hailstone, lightning strike shock waves) and accidental collision with other handling equipment [13].

CFRP cannot absorb the impact energy through plastic deformation, only via physical damage, which are mostly barely visible impact damage (BVID), which may not be immediately apparent but can increase under cyclic loading, that according to Andrew et al. [8], outlined five primary phases occurring in the following sequence: (I) initiation of matrix cracking and fibre/matrix interface debonding due to elevated transverse shear stresses in the upper layers; (II) development of transverse bending cracks due to increased flexural stresses in the lower layers; (III) occurrence of interlaminar delamination due to cracks constrained and redirected through the interlaminar region; (IV) damage mode involving fibre failure under tension and fibre micro-buckling under compression loading; and (V) penetration.

Understanding these effects will allow better prediction of material life. Understanding how composites absorb and dissipate energy during impact can lead to the design of structures with improved impact energy management, reducing the risk of catastrophic failure. Optimisation with nanoparticle reinforcement shows promise in mitigating the adverse effects of LVI. Detailed studies can optimise nanoparticle type, concentration and dispersion to maximise impact resistance.

The LVI damage tolerance of CFRP composites can also be improved by adding nano-dimensional scale fillers in the polymer matrix, such as, nanoclays, carbon nanotubes (CNTs), multi-walled carbon nanotubes (MWCNTs), graphene nanoplatelets (GNPs) [14–17], and hybrids (at least two nano-sized materials) are gaining space and interest because they impart the different maximum properties to the CFRP composite.

Carbon nanofibres (CNFs) are also effective at increasing impact damage resistance of composites, for example, Bhuiyan et al. [18] investigated the LVI response of sandwich panels with 0.2 wt.% CNFs cores. The impact tests were performed at three different energy levels (15, 29 and 44 J). results showed that nanophase systems absorbed more energy at low energy levels

compared to their neat counterparts, and samples with nanophase foam sustained higher peak loads. Ito et al. [19] investigated the impact damage and residual compressive strength of CNFs/CFRP laminates using drop-weight impact tests. The study found that the damage area was reduced, and the CAI strength increased by inserting a CNFs interlayer, with an optimum VGCF additive amount of about 20 g/m^2. Arai et al. [20] explored increasing the residual compressive strength after impact of CFRP laminates by adding CNFs to the matrix resin. The delamination area of 2.5 vol% CNFs/CFRP laminates is smaller than that of 1.2 vol% laminates. M. Hossain et al. [21] manufactured plain weave E-glass/polyester-CNFs composites and impacted at 10 J, 20 J, and 30 J energy levels. The composite with 0.2 wt.% CNFs gives the highest peak load and lowest absorbed energy compared to the control composite. It was observed that the extent of damage was more severe in the control composite and the composite nano-enhanced impacted at 30 J exhibited lower delamination area compared to control. M. Rahman et al. [22] in their study, the use of 1wt.% oxidised CNFs improved peak load by about 11%, 14% and 17% and reduced the impact damage area of a carbon fibre/epoxy laminate by 30%, 70% and 58% when impacted at energy levels of 10 J, 20 J and 30 J, respectively. Ivañez et al. [23] experimentally investigated the LVI behaviour of repaired sandwich structures with woven carbon/epoxy skins and Nomex honeycomb core. The damaged area of the sandwich panels was repaired with 0.75 wt.% CNFs nano-enhanced resin and a double external patch. The repaired specimens showed similar or even better behaviour compared to the non-repaired specimens. Ravindran et al. [24] investigated the use of multi-scale fibre reinforcement to improve the delamination resistance and impact damage tolerance of carbon fibre-epoxy composites. For impact energies of 10, 20, 30, 40 and 50 J, the nanolaminates reinforced with 1.0 wt.% CNFs showed a reduction in the damaged area of the order of 1.5%, 13%, 17%, 9.9% and 11%, respectively, compared to the control laminate.

The present study intends to identify the influence of a low weight percentage of CNFs to evaluate the LVI impact behaviour and the gap identified in the bibliography, the resistance multi-impact fatigue strength of a carbon fibre/epoxy laminate at room temperature (RT). To achieve this objective, a series of single impacts ranging from 1 J to 9 J will be conducted initially to assess their respective impact on the severity of damage. Following this, a similar analysis will be conducted with multiple impacts until complete perforation is observed. Multiple impacts will be administered at energy levels of 3 J, 5 J, and 9 J. To gain a comprehensive understanding of the phenomenon, the damage analysis will be supplemented with an investigation into the progression of key parameters such as maximum impact load, maximum displacement, restored energy and impact bending stiffness. This approach aims to provide a more comprehensive insight into the evolution of damage under varying impact conditions.

9.2. Materials and experimental procedure

The hand lay-up technique was used to produce laminates with eight layers of woven bidirectional carbon 195-1000P (195 g/m^2), all in the same direction, and an epoxy resin AH 150 combined with the hardener IP 430, both supplied by Ebalta, in a weight ratio of 100:30. More details about the main mechanical and physical properties of the epoxy resin can be found in [25]. Subsequently

this system was placed inside a vacuum bag and subjected to a load of 2.5 kN in a hydraulic press, to maintain a constant fibre volume fraction and uniform laminate thickness, for 48 hours at RT. During the first 4 hours, the bag remained connected to a vacuum pump to eliminate any air bubbles in the laminate. Finally, post-curing was performed at 80°C for 5 hours.

For the nano-reinforced laminates, carbon nanofibres (CNFs) supplied by Merck were used, which have an average diameter of about 130 nm, a length between 20-200 μm and an average specific surface area of around 54 m^2/g. More details about CNFs can be found in [25]. The manufacture of these laminates was similar to that described above, but in this case the CNFs were first mixed with the resin at RT using a shear mixer at 1000 rpm for 3 hours, followed by a further 10 minutes at 150 rpm to homogeneously disperse the hardener in the system. All this process was combined with sonication, using an ultrasonic bath with a frequency of 40 kHz, and the bath temperature was controlled to ensure that the temperature of the resin was lower than its glass transition temperature (T_g). Finally, the mixture was degassed in a vacuum oven to remove any air bubbles resulting from the mixing process and distributed evenly between the eight layers of carbon fibres. It should be noted that a CNFs content of 0.5 wt.% was used because, according to a previous study carried out by the authors [25], this was the value that maximized the mechanical properties of nano-reinforced laminates with CNFs.

The specimens used in the impact tests (see Figure 9.1) were obtained from these plates produced with dimensions of 330 × 330 × 1.9 ± 0.1 (mm), using a diamond disc saw and cooled with dry air to avoid overheating that could affect the structure of the resin. Regarding the LVI tests, they were performed on an IMATEK-IM10 drop weight testing machine and in accordance with ASTM standard D7136. An impactor with a diameter of 10 mm and a mass of 2.823 kg was used, and the tests were performed on square section samples of 75 × 75 mm^2 with the impactor advancing towards the centre of the samples embedded centrally in 100 × 100 mm^2 specimens. More details about the impact machine can be found in [26]. The impact energies used were 1 J, 3 J, 5 J, 7 J, and 9 J, which were chosen to introduce damage of different severities, but without inducing perforation in the specimens. For each condition, five specimens were tested at RT.

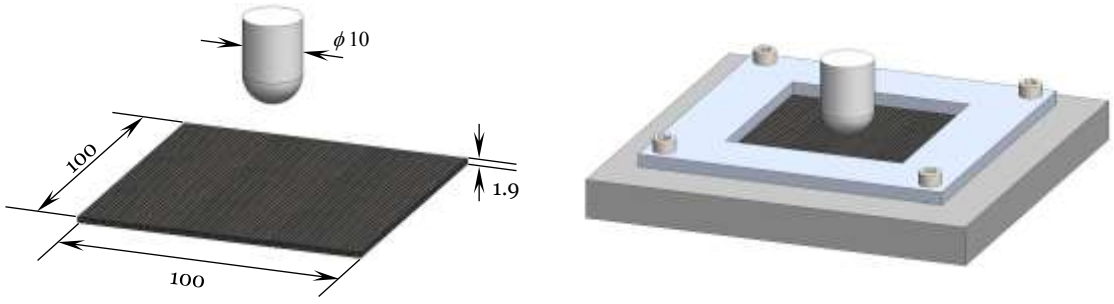

a) b)

Figure 9.1: a) Schematic specimen geometry and dimensions (mm); b) Low-velocity impact and multi-impact testes, apparatus.

9.3. Results and discussion

9.3.1. Low-velocity impact

For both laminates under study, Figure 9.2 shows typical curves load versus displacement (Figures 9.2.a) and 9.2.c)), and load versus time (Figures 9.2.b) and 9.2.d)) of control samples and laminates with 0.5 wt.% of CNFs, for other energies identical curves were obtained. Note that these curves are also representative of the other laminates tested for the other energies at RT, and are in line with those disseminated in the literature [27]. All curves exhibit some oscillations that result from the elastic waves generated by the sample vibrations and the natural vibration modes of the impact system [28,29], which are highly dependent on the stiffness and mass of the specimen and impactor [27,30].

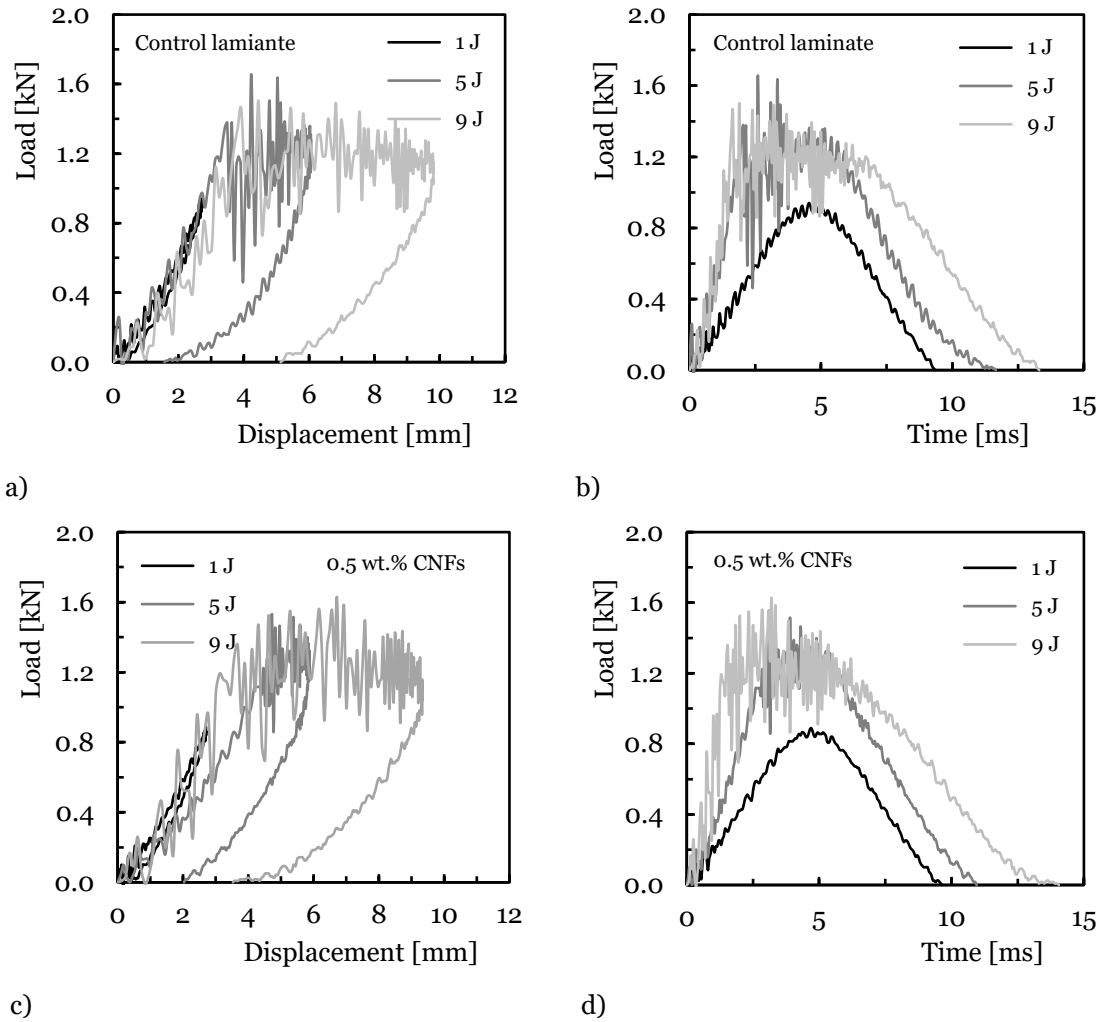

Figure 9.2: Typical curves for the first impact: a) Load vs. displacement control laminate; b) Load vs. time control laminate; c) Load vs. displacement laminate with 0.5 wt.% CNFs; d) Load vs. time laminate with 0.5 wt.% CNFs.

Throughout all tests, the maximum impact energy failed to surpass a threshold sufficient for achieving complete penetration. This was evident as the impactor consistently adhered to the specimens and rebounded subsequently. This phenomenon is discernible in Figures 9.2.a) and

9.2.c), where the initiation of a plateau, subsequent to reaching maximum energy, signifies the disengagement between the impactor and the specimen. The load-displacement curves follow a characteristic pattern of load increase up to a peak load, succeeded by a decline post-peak load. This decline induces matrix cracking, delamination, and subsequent rebounding within the laminate composite. The maximum load, as shown in Figure 9.2a), was 0.928 KN, 1.551 KN, and 1.681 KN when the impact energy was 1 J, 5 J, and 9 J, respectively to the control laminate and 0.902 KN, 1.687 KN and 1.863 KN respectively for the same impact energies and to the laminate with 0.5 wt.% CNFs, as show in Figure 9.2.c). When subjected to LVI, the elastic response observed on the force-displacement curve appears to be independent from the impact energy (Figures 9.2.a) and 9.2.c)). The residual displacement increases with the impact energy. It is well correlated to the non-reversible phenomena (damage, plasticity) [29].

Relatively to Figures 9.2.b) and 9.2.d), it shows the typical load versus time curves, exhibit a common pattern wherein the load progressively rises to a maximum value before declining, indicating the impactor's rebound. As the impact energy increases, both the maximum load and the steepness of the curves demonstrate a noticeable escalation. This signifies that higher impact energies result in greater maximum loads and steeper slopes in the curves. The contact time, as shown in Figure 9.2.b), also increase with the impact energy increase and was 9.73 ms, 11.28 ms, and 12.80 ms when the impact energy was 1 J, 5 J, and 9 J, respectively to the control laminate and 9.20 ms, 10.60 ms and 12.32 ms, respectively, for the same impact energies and to the laminate with 0.5 wt.% CNFs, as show in Figure 9.2.d).

Figure 9.3.a) represents typical energy versus time curves of LVI for an intermediate energy of 5 J, identical curves can be plotted for other impact energies. The increase in impact energy corresponds to a reduction in elastic recovery and, consequently, leads to increased damage.

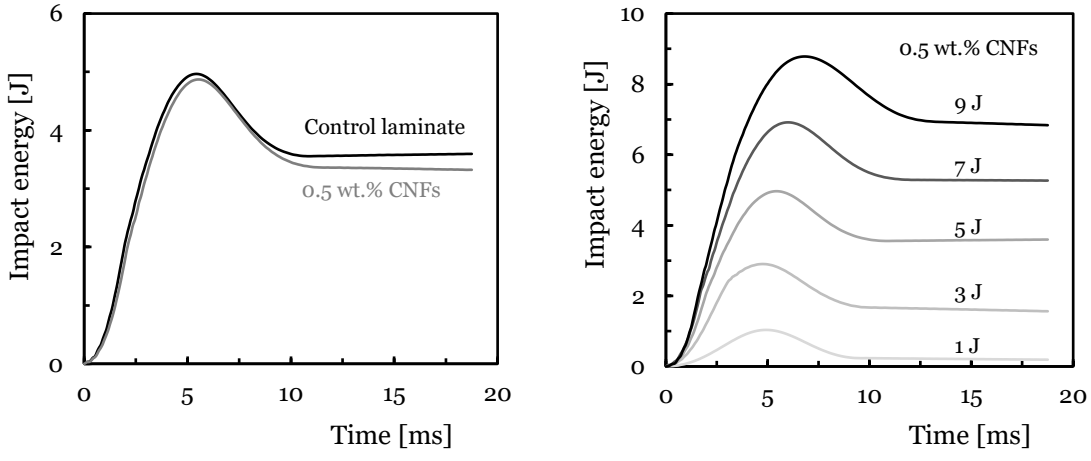

a) b)

Figure 9.3: Typical curves energy versus time: a) Comparison between control laminate and laminate filled by 0.5 wt.% CNFs tested at 5 J; b) Laminate nano-enhanced tested to various impact energies.

The initiation of the plateau phase in the curve aligns with the point where contact between the striker and the specimen is lost, indicating that this energy correlates with that absorbed by the specimen. Essentially, as the impact energy rises, more energy is absorbed by the specimen, resulting in decreased elastic recovery and heightened damage. Overall, the absorbed energy demonstrates a consistent increase with the rise in impact energy, as depicted in Figure 9.3.b). The composite laminates subjected to the lowest impact energy exhibited a moderate level of energy absorption, which is characteristic of carbon composite laminates. At this energy level, no visible damage was observed on the upper face-sheet of the laminate. However, as the impact energy increased, noticeable damage became apparent on the upper face-sheet. Higher impact energies led to a visible increase in damage area and enhanced energy absorption in the composite laminates. This aligns with findings from other studies and underscores the correlation between impact energy levels, damage manifestation, and energy absorption in composite laminates [31,32].

Typical cross-section image of the nano-enhanced laminate sample on impacted at 5 J are shown in Figure 9.4. For this energy, it is already possible to identify delamination's between the intermediate layers of the laminate and minor delamination along the back-face. These internal damages, which are not visible on the outer surface of the laminates, decrease the composite properties and reduce the load carrying capacity of the composite structure by more than 50% [30,33]. It is easy to identify a small indent on the impact surface, typical for this energy level and reported in the bibliography. As proven in the case of thin laminates, the matrix cracking begins on the lowest layer and moves to the upper layer due to bending stresses on the rear surface of the plate, leading to an inverted cone or a reversed pine-tree patterns [34].

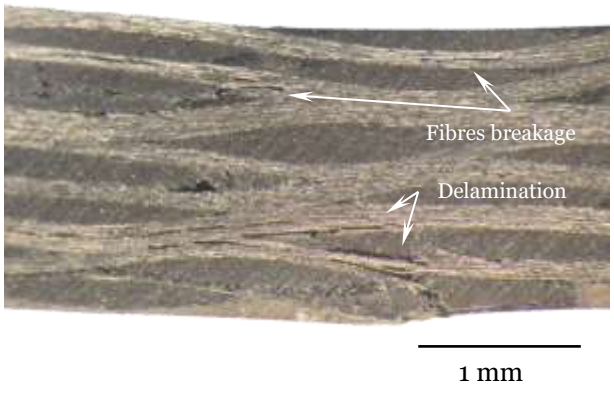

Figure 9.4: Characteristic optical micrographs of laminate cross sections with 0.5 wt.% CNFs impacted at 5 J.

The impact peak load, P_{max} can be defined as the ultimate impact load capacity delineating the threshold at which a composite laminate undergoes substantial damage when subjected to a specific level of impact energy [35]. According to the figures, the value of P_{max} is highly contingent upon the impact energy. Some authors have observed a direct correlation where the maximum load escalates proportionally with higher impact energy levels [35,36] and similar tendency was

observed in this work, for both materials, as shown in Figure 9.5. There were observed increases between 1 and 9 J in the range of approximately 81.3% and 105.5% for the control samples and specimens with epoxy filled by 0.5 wt.% CNFs. The inclusion of CNFs resulted in notably higher maximum impact loads, registering values approximately 8.8% higher for 5 J and 10.9% higher for 9 J compared to the control samples. These results are consistent with studies conducted by Sarasini et al. [17] where, for example, the addition of MWCNTs promoted maximum loads around 8.0% highest than occurred in carbon laminates with pure epoxy matrix. Moumen et al. [15] also found that the maximum load of the carbon fibre/epoxy specimen containing 1.0 wt.% CNTs are improved to 13.16% when compared to the control laminates. Rahman et al. [22] concluded that the impact peak load is substantially improved by 1.0 wt.% oxidized carbon nanofibres (O-CNFs) incorporation in carbon/epoxy composites. An increase in peak load by about 11%, 14% and 17% at 10 J, 20 J and 30 J energy levels, respectively has been observed upon O-CNFs loading into nano-enhanced composites.

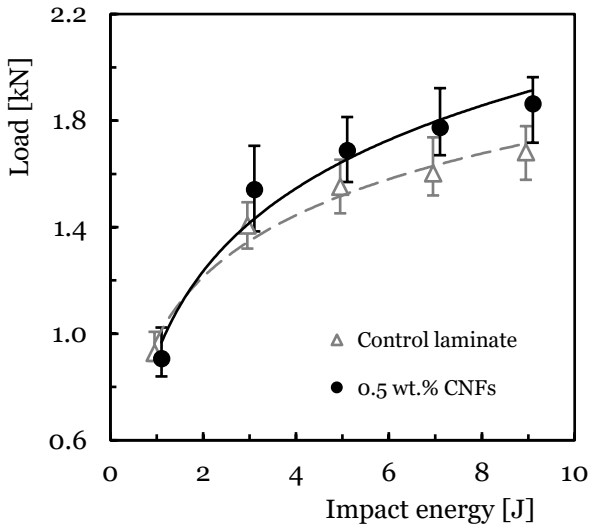

Figure 9.5: Relationship between the maximum load and impact energy.

The average impact duration was also gauged and is depicted in Figure 9.6.a). In all cases, the maximum contact time between the impactor and samples was noted in the control laminates, registering values approximately 6.4% higher for an impact energy of 5 J and 3.4% higher for 7 J, compared to the specimens with matrix filled by CNFs. The relationship between displacement and impact energy is demonstrated in Figure 9.6.b). When CNFs are added to the epoxy matrix, led to a reduction in displacements by approximately 2.3% and 7.4%, respectively, for impact energies of 1 J and 9 J. However, within the energy spectrum studied (ranging from 1 to 9 J), displacements witnessed an increase of about 230.9% and 229.4%, respectively, for control laminates and laminates nano-enhanced with 0.5 wt.% CNFs. Figure 9.6.c) illustrates the comparison of elastic recovery for each laminate, determined by computing the disparity between the absorbed energy and the energy at the peak load. The average values represented, in percentage, show when the CNFs are added to the epoxy matrix better results can be found. The laminates manufactured with epoxy matrix filled by CNFs present best performance in terms of

elastic recuperation. For impact energies of 1 J CNFs improve the elastic recuperation around 8.7% while for 9 J this value increases to 22.1%. However, in the energy range studied (between 1 and 9 J), the elastic recuperation decreases around 304.1% and 282.7% respectively, for control laminates and laminates with epoxy nano-enhanced by CNFs. Finally, the evolution of the impact bending stiffness with the impact energy is presented in Figure 9.6.d).

The stiffness of laminate composites serves as a pivotal parameter in analysing LVI events. This characteristic governs the effective mass of the composite, consequently influencing its dynamic response to impact. In the analysis of thin isotropic plates, the impact of deformation attributed to shear effects is typically negligible, as the bending stiffness significantly outweighs shear stiffness [37]. Upon incorporating CNFs into the pure resin, there is an observed increase in stiffness by approximately 9.6% and 22.9%, respectively, for impact energies of 1 J and 9 J. However, within the studied energy range spanning from 1 to 9 J, the stiffness exhibits an increase of about 17.8% and 32.1%, respectively, for laminates exclusively composed of neat epoxy matrix and laminates with matrix reinforced by CNFs.

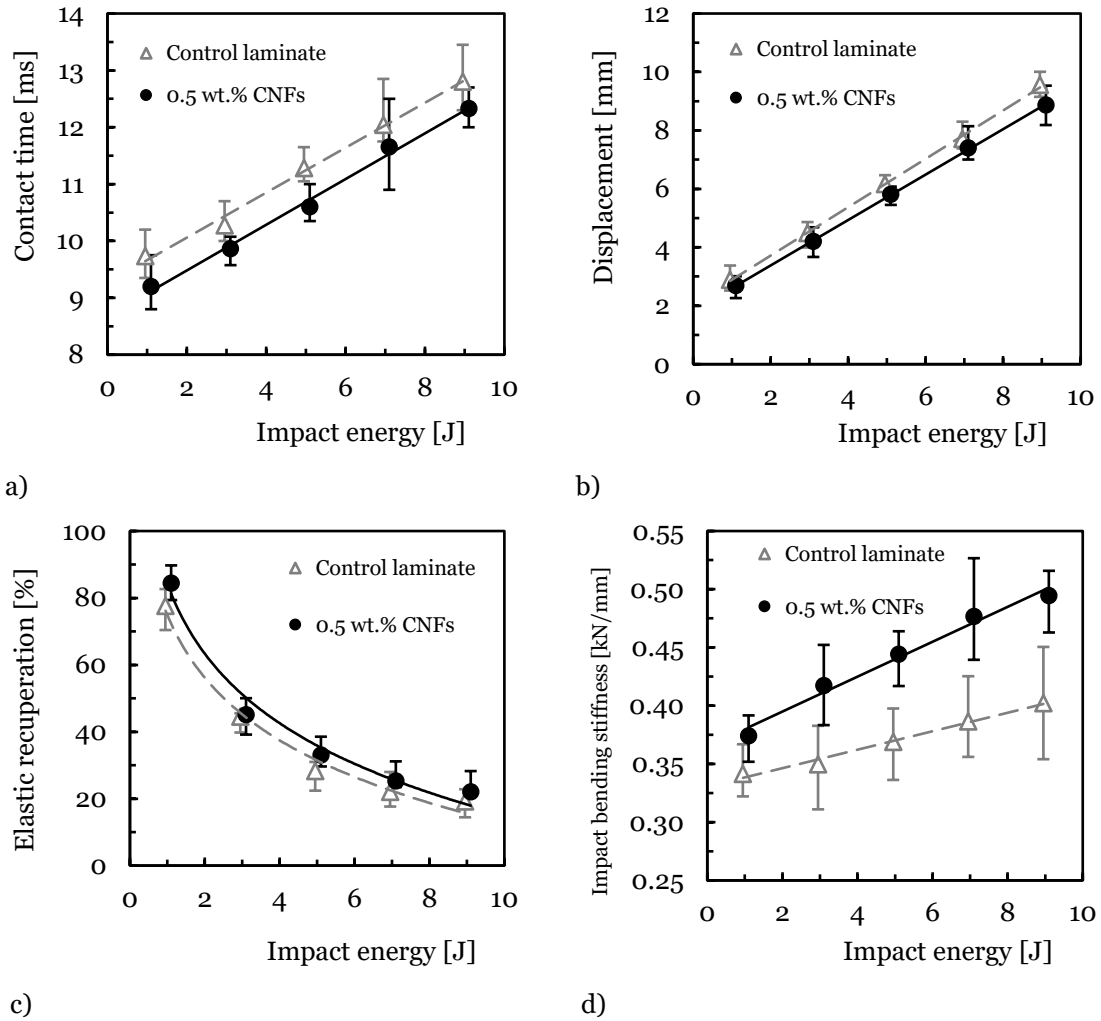

Figure 9.6: a) Evolution of the contact time with the impact energy; b) Evolution of the maximum displacement with the impact energy; c) Evolution of the elastic recuperation with the impact energy; d) Evolution of the impact bending stiffness with the impact energy.

Figure 9.7 displays the energy profile diagram for the laminates investigated in this study. The data points corresponding to the laminates are closely clustered and consistently positioned below the unity curve. This pattern signifies that the absorbed energy consistently falls short of matching the impact energy, indicating that the penetration threshold has not been reached. Within this range, the extent of damage relies on the magnitude of the impact energy, and any surplus energy is directed toward rebounding the impactor rather than causing penetration. The data plotted (Figure 9.7) can be fitted, for each laminate type, by the equation $\Delta E = \alpha E_0^2 + \beta E_0 + \varepsilon$, where ΔE is the energy absorbed, E_0 is the impact energy and $\alpha, \beta, \varepsilon$, constants presented in Table 9.1. This equation is more reasonable than the linear relationship between impact energy and the energy absorbed [14,38].

The penetration thresholds can be found if the data points E_e - E_i (i.e., elastic energy (E_e), and impact energy (E_i)) were represented in a diagram and fitted by polynomial equations. According to bibliography [14,38] the roots of these equations represent the points where $E_i/E_a = 1$ ($E_e = 0$) (i.e., absorbed energy (E_a)) and the higher roots give the penetration thresholds.

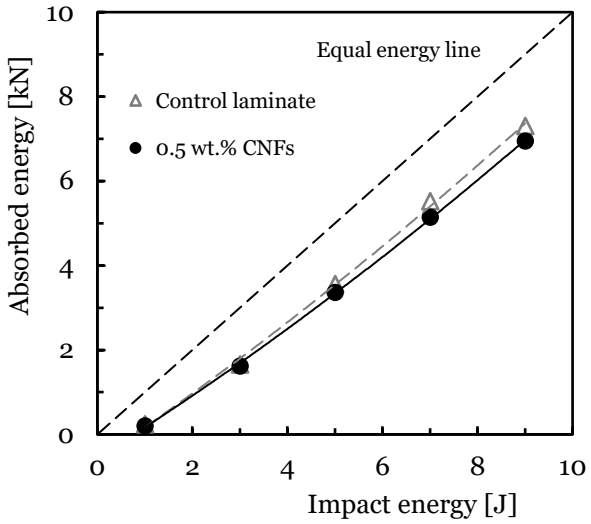

Figure 9.7: Energy profile diagram of the laminates tested.

Table 9.1: Constants of the equation $\Delta E = \alpha E_0^2 + \beta E_0 + \varepsilon$, for the studied laminates.

Laminate	α	β	ε	R
Control laminate	0.0141	0.7588	- 0.6045	0.9986
Laminate + 0.5 wt.% CNFs	0.0145	0.7056	- 0.5533	0.9996

R =Linear correlation coefficient.

The Figure 9.8 shows the penetration threshold for laminates in study and values of 13.2 J and 15.4 J were found, for control laminates, laminates filled by CNFs, respectively, which means that the addition of CNFs to the epoxy matrix promoted an increase of 16.3% in the penetration threshold of carbon laminates.

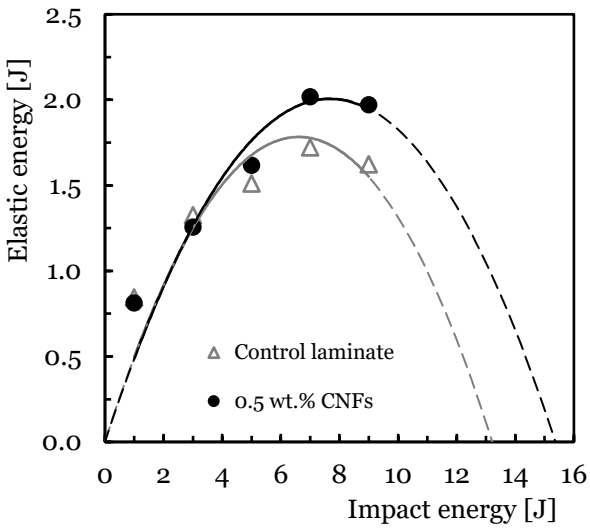

Figure 9.8: Identification of penetration threshold.

9.3.2. Multi-impact

The samples were subsequently subjected to multi-impacts tests considering impact energies of 3 J, 5 J and 7 J. The final failure is considered when full perforation occurs, or in other words, when the impactor crosses the sample transversely, occurs full penetration (E_e = 0). In this context, it was possible to construct the SN fatigue curves, one for the control laminate and other for the laminate nano-enhanced with 0.5 wt.% CNFs and compare the fatigue behaviour by impact of different laminates. In this case, the impact energy is depicted as a function of the number of impacts (N_f), and the resulting curves follow the conventional fatigue behaviour modelled by a power law. Consequently, Figure 9.9 illustrates the impact of energy on the multi-impact response, where the mean curves, fitted to match the experimental results, are overlaid. It's noticeable that the number of impacts until failure exhibits an inverse relationship with the impact energy, aligning with findings reported in existing literature [39–42]. The impact energy versus the number of impacts can be expressed by the following equation (9.1) to the control laminate with R = 0.967 and the equation (9.2) to the nano-enhanced laminate with R = 0.972.

$$E = 6.686 \times N_f^{-0.280} \tag{9.1}$$

$$E = 10.315 \times N_f^{-0.285} \tag{9.2}$$

where, E is the impact energy and N_f the number of impacts to failure. Therefore, this equation can be used to predict the impact response of this laminate.

As anticipated, both laminates exhibit an anticipated trend where lower energies correspond to longer lifespans (N_f). For instance, in comparison to an impact energy of 3 J, achieving full perforation requires approximately 66 - 89 impacts for the nano-enhanced laminate with CNFs, whereas for the control laminates, this requires only 17 - 20 impacts. On average, the nano-enhanced laminate with CNFs yields lifespans approximately five times longer than those observed in the control laminates. This significant difference in lifespans can be attributed to

distinct stiffness characteristics, consequently influencing differing damage mechanisms, as reported by Amaro et al. [43].

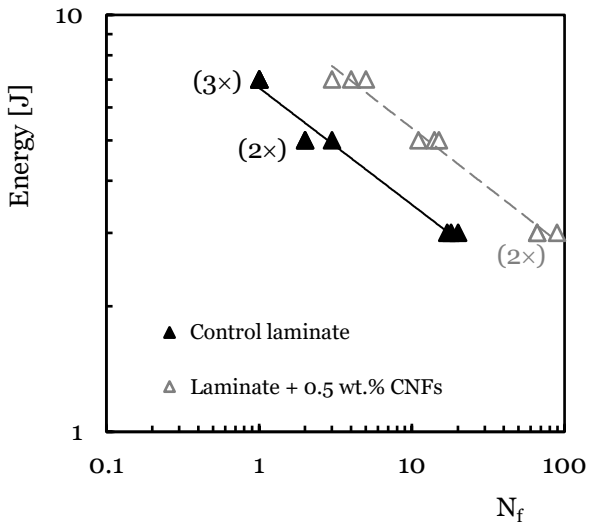

Figure 9.9: Impact energy versus the number of impacts to failure.

Figure 9.10 present the typical evolution of the curves for control laminates and laminates nano-enhanced with 0.5 wt.% CNFs tested at 3 J impact energy subjected to multi-impacts, similar curves can be obtained for the other impact energies studied that they are in good agreement with the literature [44,45]. The Figures 9.10.a) and 9.10.b), show an evolution in curves impact after impact to control laminates and laminates nano-enhanced with 0.5 wt.% CNFs. It can be inferred that the initial impact triggers substantial damage, which is further propagated by subsequent impacts. Consequently, from the second to the final impact, there's an observed increase in contact time values coupled with a decrease in maximum force values. In the context of the control laminates (as illustrated in Figures 9.10.a) and 9.10.b)), there's an approximate decrease of about 39.4% in maximum force from the 1st to 20th impact. Nonetheless, the curve remains bell-shaped from the 1st to 15th impact. After that, the damage caused to the laminate is already considerable and its response decreases, taking the curve to a different geometry. In the 20th impact the load decrease abruptly and the contact time increase, the damage in the laminate is already considerable, which means that perforation of the laminate is imminent. Table 9.2 presents the average values obtained for the first impact and successive for control laminates, in terms of maximum load (P_{max}), maximum displacement and elastic recuperation.

The laminate nano-enhanced with CNFs demonstrates analogous behaviour to the control laminate when subjected to multi-impacts, as depicted in Figures 9.10.c) and 9.10.d). Corresponding to the initial impact, Figure 9.10.d) illustrates load-time curves characterized by an ascent in load to reach a maximum value (P_{max}), succeeded by a decline corresponding to the impactor's rebound.

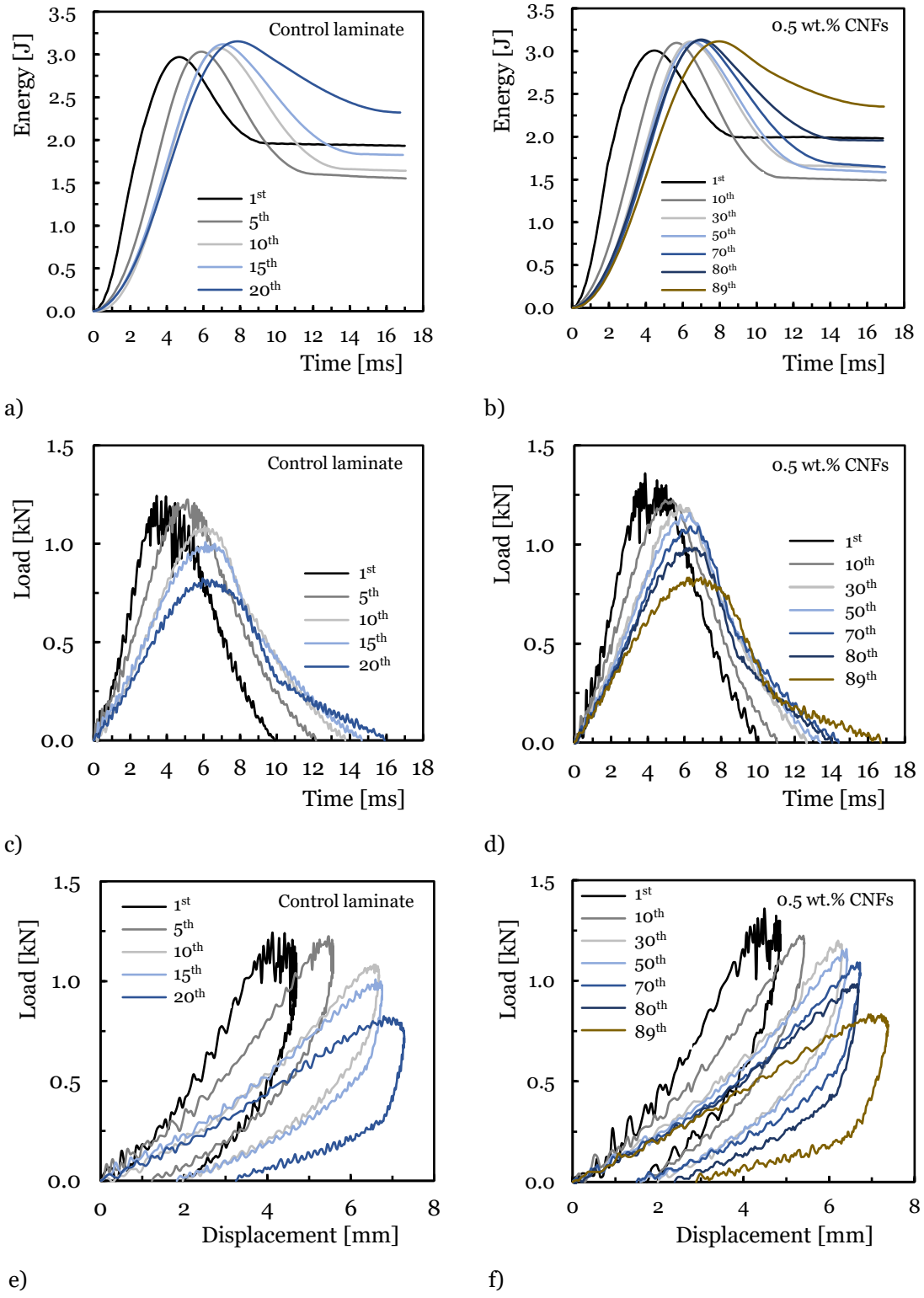

Figure 9.10: Time vs energy curves: a) Control laminate; b) Nano-enhanced with 0.5 wt.% CNFs laminate; Time vs load: c) Control laminate; d) Nano-enhanced with 0.5 wt.% CNFs laminate; Displacement vs. load: e) Control laminate; f) Nano-enhanced with 0.5 wt.% CNFs laminate.

The impact energy applied was insufficient to induce complete penetration, as the impactor consistently adhered to the specimens and rebounded after impact. However, the initiation of the plateau phase signifies the disengagement between the impactor and the specimen. As a result,

the disparity between the maximum energy - representing the maximum load - and the energy corresponding to the plateau denotes the restitution component, which signifies the elastic energy released due to the impactor's rebound. Conversely, during the final impact resulting in full perforation, all the energy is absorbed by the sample, rendering the elastic energy component as zero. The Energy-time curves show us the evolution of the energy absorbed over the various impacts to which the sample is subjected.

Taking the first impact as a reference, it is clear that up to the 30th impact the energy absorbed increases, from the 31th impact to the 80th impact it is always higher than the 1st impact, but it gradually decreases and from the 81th impact to the 89th impact the energy absorbed is lower to the first impact. Table 9.3 presents the average values obtained for the first impact and successive for laminates with CNFs.

Table 9.2: Parameters obtained to control laminates subject to 3 J multiple impacts energy.

Number of impact (N_f)	Max. Load [kN]	Elastic recuperation [%]	Displacement [mm]	IBS [kN/mm]
1st	1.149	32.34	3.955	0.415
5th	1.224	47.24	5.581	0.236
10th	1.082	45.96	6.676	0.191
15th	1.007	41.18	6.753	0.163
20th	0.824	25.98	7.284	0.129

Table 9.3: Parameters obtained to laminate nano-enhanced with 0.5 wt.% CNFs subjected to 3 J multiple impacts energy.

Number of impact (N_f)	Max. Load [kN]	Elastic recuperation [%]	Displacement [mm]	IBS [kN/mm]
1st	1.332	31.29	3.686	0.634
10th	1.222	50.60	5.419	0.254
20th	1.216	51.50	5.695	0.225
30th	1.199	46.59	6.299	0.201
40th	1.174	46.30	6.072	0.203
50th	1.157	47.91	6.425	0.194
60th	1.066	43.35	6.194	0.188
70th	1.091	46.12	6.723	0.173
80th	0.983	37.07	6.683	0.160
89th	0.833	24.45	7.374	0.123

In Figure 9.11, a similar analysis is conducted for the multi-impact study involving the laminate enhanced with 0.5 wt.% CNFs, illustrating parameters concerning the number of impacts (N) at different test stages, along with the count of impacts until failure (N_f). The final impact, resulting

in full perforation (Elastic energy = 0), is not depicted. Mean curves are superimposed and fitted to the experimental data using the least squares method. Overall, the depicted curves exhibit a noteworthy alignment with findings documented in the literature [41].

Across all energy levels, there is a noticeable trend where the maximum load (Figure 9.11.a)) diminishes as the number of impacts increases, attributed to the accumulation of damage and degradation of the laminate. The cumulative damage leads to reduced stiffness values, particularly at the impact point, revealing a significant correlation between parameters such as impact load, displacement, and stiffness. This relationship is further supported by the progression of restored energy and impact bending stiffness (IBS), as depicted in Figures 9.11.c) and 9.11.d), respectively. Both parameters exhibit a direct connection to the severity of damage, affirming their relationship with the progression of damage accumulation and its intensity within the laminate.

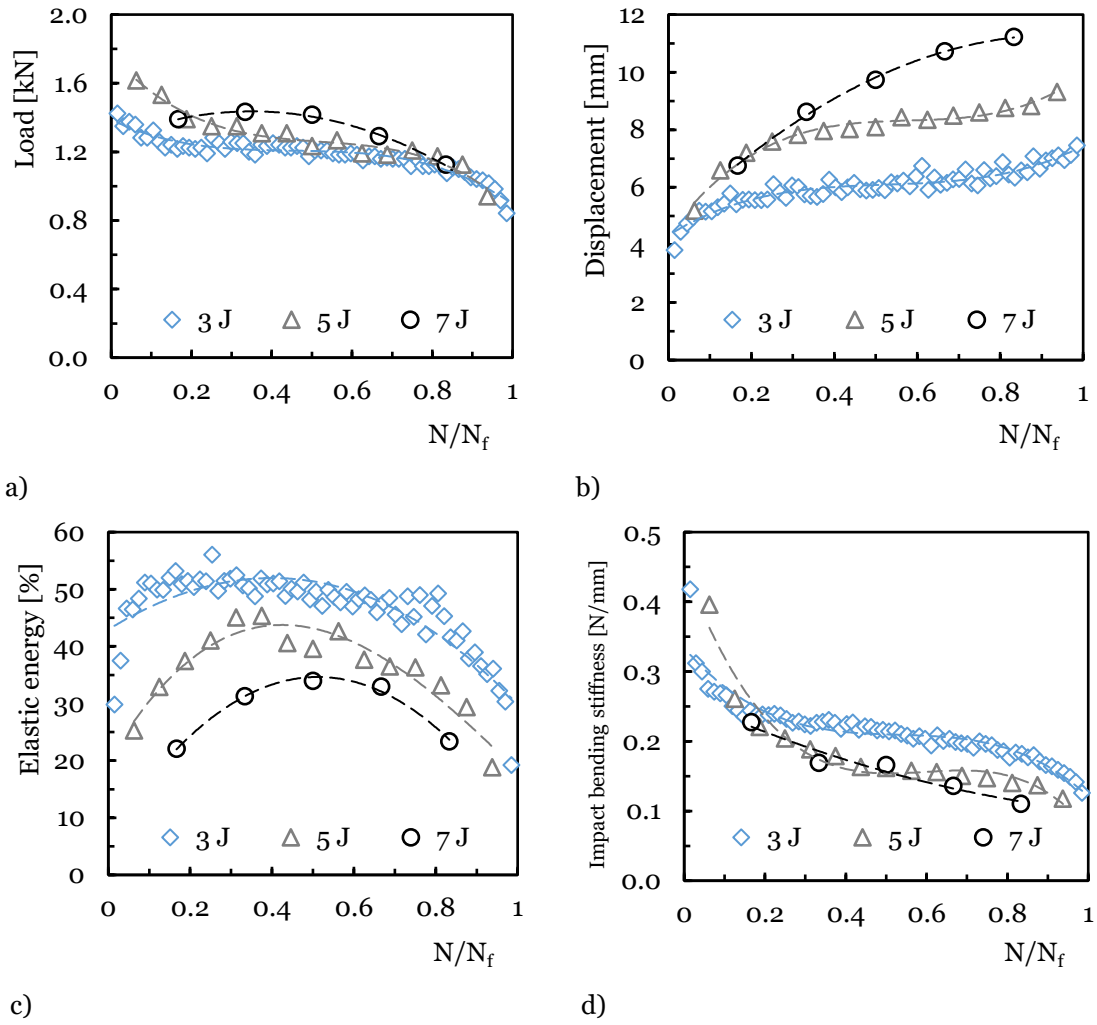

Figure 9.11: Laminate nano-enhanced with 0.5 wt.% CNFs subjected to multiple impacts: a) Maximum impact load versus N/N_f; b) Maximum displacement versus N/N_f; b) Elastic energy versus N/N_f; d) Impact bending stiffness versus N/N_f.

In Figure 9.11.b), the elastic energy was computed as the difference between the absorbed energy and the energy at peak load. The parameter N represents the number of impacts at any specific instance during the test, while N_f signifies the number of impacts leading to failure. Each curve depicted for every studied energy level serves as a representative model encapsulating the characteristics observed across multiple curves obtained for each configuration.

Figure 9.11 allows defining for an association between the severity of damage within the sample and the polynomial degree utilized to fit the experimentally obtained points. Notably, the experimental data acquired at lower impact energies (i.e., 3 J and 5 J) are suitably modeled by a third-order polynomial, while data corresponding to the highest impact energy of 7 J is better represented by a second-order polynomial. This observation aligns with the findings of Azouaoui et al. [46], who delineated three distinct zones in damage progression: initiation and propagation of delamination's (Zone I), stabilization of delamination growth (Zone II), and ply cracking accompanied by fibre fracture (Zone III).

The chronological sequence of damage initiation typically begins with matrix cracking, followed by the appearance of delamination in the first impacts. Delamination initially starts at the interface of the outermost layer and then spreads to create new delaminated surfaces at other interfaces. After a certain number of impacts, a phase characterised by delamination saturation occurs, where the propagation of existing delamination and the formation of new delamination stops or stabilises. This is followed by an acceleration of damage progression leading to ultimate failure, characterised by the ultimate failure of fibres within the material [41,46,47].

9.4. Conclusions

This experimental investigation compares the low-velocity impact strength and the multi-impact behaviour of woven carbon fabric composites and epoxy matrix, produced by hand lay-up technique, with the laminate with epoxy nano-enhanced with 0.5 wt.% CNFs. The analysis commenced by studying the impact of single impacts at five distinct energy levels. Results indicated that in both types of laminates, the maximum load, contact time, maximum displacement, and impact bending stiffness exhibit an increment as the impact energy increases. Notably, the laminate incorporating CNFs demonstrated superior properties compared to the counterpart.

Observations revealed that samples impacted at 1 J and 3 J showed no visible mark at the impact point, while considerable impact damage was evident at 7 J and 9 J. Additionally, the absorbed energy displayed an increase corresponding to the elevation in energy levels.

Subsequently, a similar analysis was conducted to explore the impact of energy on multi-impact life. Employing the classic SN fatigue curve, a typical fatigue behaviour was observed, showcasing an inverse relationship between the number of impacts leading to failure and the impact energy. Irrespective of the energy level applied, a consistent trend emerged: the maximum impact load,

restored energy, and IBS demonstrated a decrease with an increasing number of impacts. Conversely, the maximum displacement exhibited an increase, signifying the exacerbation of damage incurred over time.

This observed severity of damage was further reflected in the polynomial fitting of the experimental data. Specifically, a third-order polynomial fitting was suitable for the lowest impact energies, whereas a second-order polynomial offered a better fit for the highest impact energies. This fitting underscored the varying levels of damage and their manifestation with differing impact energies.

Bibliography

[1] Meek N, Penumadu D, Hosseinaei O, Harper D, Young S, Rials T. Synthesis and characterization of lignin carbon fiber and composites. Composites Science and Technology 2016;137:60–8. https://doi.org/10.1016/j.compscitech.2016.10.016.

[2] Hagnell MK, Kumaraswamy S, Nyman T, Åkermo M. From aviation to automotive - a study on material selection and its implication on cost and weight efficient structural composite and sandwich designs. Heliyon 2020;6:e03716. https://doi.org/10.1016/j.heliyon.2020.e03716.

[3] Harussani MM, Sapuan SM, Nadeem G, Rafin T, Kirubaanand W. Recent applications of carbon-based composites in defence industry: A review. Defence Technology 2022. https://doi.org/10.1016/j.dt.2022.03.006.

[4] Borowski E, Soliman E, Kandil U, Taha M. Interlaminar Fracture Toughness of CFRP Laminates Incorporating Multi-Walled Carbon Nanotubes. Polymers 2015;7:1020–45. https://doi.org/10.3390/polym7061020.

[5] Alam P, Mamalis D, Robert C, Floreani C, Ó Brádaigh CM. The fatigue of carbon fibre reinforced plastics - A review. Composites Part B: Engineering 2019;166:555–79. https://doi.org/10.1016/j.compositesb.2019.02.016.

[6] Bhatia GS, Andrew JJ, Arockiarajan A. Experimental investigation on compressive behaviour of different patch–parent layup configurations for repaired carbon/epoxy composites. Journal of Composite Materials 2019;53:3269–79. https://doi.org/10.1177/0021998318822706.

[7] Liu B, Cao S, Gao N, Cheng L, Liu Y, Zhang Y, et al. Thermosetting CFRP interlaminar toughening with multi-layers graphene and MWCNTs under mode I fracture. Composites Science and Technology 2019;183. https://doi.org/10.1016/j.compscitech.2019.107829.

[8] Andrew JJ, Srinivasan SM, Arockiarajan A, Dhakal HN. Parameters influencing the impact response of fiber-reinforced polymer matrix composite materials: A critical review. Composite Structures 2019;224. https://doi.org/10.1016/j.compstruct.2019.111007.

[9] Zhou J, Liao B, Shi Y, Ning L, Zuo Y, Jia L. Experimental investigation of the double impact position effect on the mechanical behavior of low-velocity impact in CFRP laminates. Composites Part B: Engineering 2020;193:108020. https://doi.org/10.1016/j.compositesb.2020.108020.

[10] Abrate S. Impact on Laminated Composite Materials. Applied Mechanics Reviews 1991;44:155–90. https://doi.org/10.1115/1.3119500.

[11] Hogg PJ, Bibo GA. Impact and damage tolerance. Woodhead Publishing Ltd; 2000. https://doi.org/10.1533/9781855738911.211.

[12] Sjoblom PO, Hartness JT, Cordell TM. On Low-Velocity Impact Testing of Composite

Materials. Journal of Composite Materials 1988;22:30–52. https://doi.org/10.1177/002199838802200103.

[13] Ali M, Joshi SC, Sultan MTH. Palliatives for Low Velocity Impact Damage in Composite Laminates. Advances in Materials Science and Engineering 2017;2017. https://doi.org/10.1155/2017/8761479.

[14] Reis PNB, Ferreira JAM, Santos P, Richardson MOW, Santos JB. Impact response of Kevlar composites with filled epoxy matrix. Composite Structures 2012;94:3520–8. https://doi.org/10.1016/j.compstruct.2012.05.025.

[15] El Moumen A, Tarfaoui M, Lafdi K, Benyahia H. Dynamic properties of carbon nanotubes reinforced carbon fibers/epoxy textile composites under low velocity impact. Composites Part B: Engineering 2017;125:1–8. https://doi.org/10.1016/j.compositesb.2017.05.065.

[16] Rahman AS, Mathur V, Asmatulu R. Effect of nanoclay and graphene inclusions on the low-velocity impact resistance of Kevlar-epoxy laminated composites. Composite Structures 2018;187:481–8. https://doi.org/10.1016/j.compstruct.2017.12.054.

[17] Sarasini F, Tirillò J, Bavasso I, Bracciale MP, Sbardella F, Lampani L, et al. Effect of electrospun nanofibres and MWCNTs on the low velocity impact response of carbon fibre laminates. Composite Structures 2020;234:111776. https://doi.org/10.1016/j.compstruct.2019.111776.

[18] Bhuiyan MA, Hosur MV, Jeelani S. Low-velocity impact response of sandwich composites with nanophased foam core and biaxial braided face sheets. Composites Part B: Engineering 2009;40:561–71. https://doi.org/10.1016/j.compositesb.2009.03.010.

[19] Ito H, Arai M, Takeyama K, Hu N, Quaresimin M. Impact Damage and Residual Compression Strength of CNF/CFRP Hybrid Laminates. Journal of Solid Mechanics and Materials Engineering 2013;7:381–93. https://doi.org/10.1299/jmmp.7.381.

[20] Arai M, Ito H, Nishimura M, Zakoji T, Quaresimin M. CAI strength of cfrp laminates toughened with multi-walled carbon nanofiber. 16th European Conference on Composite Materials, ECCM, Seville, Spain, 22–26 June 2014 2014:22–6.

[21] Hossain ME, Hossain MK, Hosur M, Jeelani S. Low-velocity impact behavior of CNF-filled glass-reinforced polyester composites. Journal of Composite Materials 2014;48:879–96. https://doi.org/10.1177/0021998313480194.

[22] Rahman MM, Hosur M, Hsiao KT, Wallace L, Jeelani S. Low velocity impact properties of carbon nanofibers integrated carbon fiber/epoxy hybrid composites manufactured by OOA-VBO process. Composite Structures 2015;120:32–40. https://doi.org/10.1016/j.compstruct.2014.09.053.

[23] Ivañez I, Sánchez-Saez S, Garcia-Castillo SK, Barbero E, Amaro AM, Reis PNB. Impact response of repaired sandwich structures. Polymer Composites 2020;41:3014–22. https://doi.org/10.1002/pc.25593.

[24] Ravindran AR, Ladani RB, Kinloch AJ, Wang C-H, Mouritz AP. Improving the delamination resistance and impact damage tolerance of carbon fibre-epoxy composites using multi-scale fibre toughening. Composites Part A: Applied Science and Manufacturing 2021;150:106624. https://doi.org/10.1016/j.compositesa.2021.106624.

[25] Pina dos Santos PS, Maceiras A, Valvez S, Reis PNB. Mechanical characterization of different epoxy resins enhanced with carbon nanofibers. Frattura Ed Integrità Strutturale 2020;15:198–212. https://doi.org/10.3221/IGF-ESIS.55.15.

[26] Amaro AM, Reis PNB, Magalhães AG, de Moura MFSF. The Influence of the Boundary Conditions on Low-Velocity Impact Composite Damage. Strain 2011;47:e220–6. https://doi.org/10.1111/j.1475-1305.2008.00534.x.

[27] Panettieri E, Fanteria D, Montemurro M, Froustey C. Low-velocity impact tests on carbon/epoxy composite laminates: A benchmark study. Composites Part B: Engineering 2016;107:9–21. https://doi.org/10.1016/j.compositesb.2016.09.057.

[28] Schoeppner GA, Abrate S. Delamination threshold loads for low velocity impact on composite laminates. Composites Part A: Applied Science and Manufacturing 2000;31:903–15. https://doi.org/10.1016/S1359-835X(00)00061-0.

[29] Vieille B, Pujols-Gonzalez JD, Bouvet C, Breteau T, Gautrelet C. Influence of impact

velocity on impact behaviour of hybrid woven-fibers reinforced PEEK thermoplastic laminates. Composites Part C: Open Access 2020;2:100029. https://doi.org/10.1016/j.jcomc.2020.100029.

[30] Richardson MOW, Wisheart MJ. Review of low-velocity impact properties of composite materials. Composites Part A: Applied Science and Manufacturing 1996;27:1123–31. https://doi.org/10.1016/1359-835X(96)00074-7.

[31] Malhotra A, Guild FJ. Impact damage to composite laminates: Effect of impact location. Applied Composite Materials 2014;21:165–77. https://doi.org/10.1007/s10443-013-9382-z.

[32] Stephen C, Mourad AHI, Shivamurthy B, Selvam R. Energy absorption and damage assessment of non-hybrid and hybrid fabric epoxy composite laminates: experimental and numerical study. Journal of Materials Research and Technology 2021;14:3080–91. https://doi.org/10.1016/j.jmrt.2021.08.108.

[33] Shah SZH, Karuppanan S, Megat-Yusoff PSM, Sajid Z. Impact resistance and damage tolerance of fiber reinforced composites: A review. Composite Structures 2019;217:100–21. https://doi.org/10.1016/j.compstruct.2019.03.021.

[34] Abrate S. Low-Velocity Impact Damage. Impact on Composite Structures, Cambridge University Press; 1998, p. 135–60. https://doi.org/10.1017/CBO9780511574504.005.

[35] Iqbal K, Khan S-U, Munir A, Kim J-K. Impact damage resistance of CFRP with nanoclay-filled epoxy matrix. Composites Science and Technology 2009;69:1949–57. https://doi.org/10.1016/j.compscitech.2009.04.016.

[36] Hosur M V., Adbullah M, Jeelani S. Studies on the low-velocity impact response of woven hybrid composites. Composite Structures 2005;67:253–62. https://doi.org/10.1016/j.compstruct.2004.07.024.

[37] Chai GB, Zhu S. A review of low-velocity impact on sandwich structures. Proceedings of the Institution of Mechanical Engineers, Part L: Journal of Materials: Design and Applications 2011;225:207–30. https://doi.org/10.1177/1464420711409985.

[38] Aktaş M, Atas C, İçten BM, Karakuzu R. An experimental investigation of the impact response of composite laminates. Composite Structures 2009;87:307–13. https://doi.org/10.1016/j.compstruct.2008.02.003.

[39] Ouroua Y, Azouaoui K, Mesbah A, Ouali N, Boukharouba T. Some insights into the impact fatigue damage behaviour in laminated composites. Structures Under Shock and Impact IX, vol. 1, Southampton, UK: WIT Press; 2006, p. 367–76. https://doi.org/10.2495/SU060361.

[40] Azouaoui K, Ouali N, Ouroua Y, Mesbah A, Boukharouba T. Damage characterisation of glass/polyester composite plates subjected to low-energy impact fatigue. Journal of Sound and Vibration 2007;308:504–13. https://doi.org/10.1016/j.jsv.2007.04.014.

[41] Amaro AM, Reis PNB, Neto MA, Cirne JM. Residual impact strength of carbon/epoxy laminates after flexural loadings. Composite Structures 2016;146:69–74. https://doi.org/10.1016/j.compstruct.2016.03.006.

[42] Reis PNB, Neto MA, Amaro AM. Multi-impact behaviour of composite laminates under constant and different energy levels. Composite Structures 2022;294:115788. https://doi.org/10.1016/j.compstruct.2022.115788.

[43] Amaro AM, Reis PNB, de Moura M, Santos JB. Influence of the specimen thickness on low velocity impact behavior of composites. Journal of Polymer Engineering 2012;32:53–8. https://doi.org/10.1515/polyeng-2011-0101.

[44] de Morais WA, Monteiro SN, D'Almeida JRM. Evaluation of repeated low energy impact damage in carbon–epoxy composite materials. Composite Structures 2005;67:307–15. https://doi.org/10.1016/j.compstruct.2004.01.012.

[45] Bora MÖ, Çoban O, Sinmazçelik T, Cürgül I, Günay V. On the life time prediction of repeatedly impacted thermoplastic matrix composites. Materials and Design 2009;30:145–53. https://doi.org/10.1016/j.matdes.2008.04.036.

[46] Azouaoui K. Modelling of damage and failure of glass/epoxy composite plates subject to impact fatigue. International Journal of Fatigue 2001;23:877–85.

https://doi.org/10.1016/S0142-1123(01)00050-0.

[47] Schrauwen B, Peijs T. Influence of matrix ductility and fibre architecture on the repeated impact response of glass-fibre-reinforced laminated composites. Applied Composite Materials 2002;9:331–52. https://doi.org/10.1023/A:1020267013414.

Chapter 10

Influence of carbon nanofibres on low-velocity impact and post-impact behaviour of carbon composites

Abstract

An experimental approach is used to investigate the behaviour of carbon fibre reinforced polymer (CFRP) composites whose matrix has been modified with different weight fractions (wt.%) of carbon nanofibres (CNFs) on the low-velocity impact (LVI) response and the post-impact properties, such as residual strength, the stress relaxation and in the creep behaviour. Composites with different percentage ratios of the CNFs (i.e., 0.25, 0.5, 0.75 and 1 wt.% CNFs) were manufactured by hand lay-up technique and compared with control laminate. Tests were carried out on drop-weight impact with impactor hemispherical end with five impact energy levels of 1 J, 3 J, 5 J, 7 J and 9 J to study the impact response, such as impact force and energy. The study scrutinized the impact response of different laminates, focusing on parameters such as peak load, absorbed energy, time, and deflection at the point of peak load. Furthermore, the structural integrity post-impact and the viscoelastic characteristics of the impacted laminates were assessed through three-point bending (3PB) tests, as well as stress relaxation and creep tests. Relevant improvements were observed for an impact energy of 9 J, the elastic recovery of the laminate with 0.75 wt.% CNFs increases by around 21% and promotes an improvement of more than 5% in terms of bending stress and bending stiffness when compared to the control laminate.

10.1. Introduction

Carbon fibre reinforced polymer (CFRP) composites have found increasing in various industrial sectors, particularly in transport, due to their excellent specific strength and stiffness, with consequent fuel savings, as well as their good response to fatigue, resistance to corrosion and easy manufacturing associated with the respective arrangement of reinforcements in the loading directions [1,2].

One of the main problems, is your sensibility to low-velocity impact (LVI), which appears more frequently during the manufacturing or assembly and maintenance operations of laminated or composite structures, inducing damage only detectable using advanced imaging tools or non-destructive testing and penalizing the behaviour and performance which causes a huge threat to the structure safety of these structures in the long term [3–5].

During LVI, according to some authors, generally an event that occurs in the range of 1 to 10 m/s [6,7], the impactor contact time is long enough for the entire structure to respond to the impact, that dependent on your properties, your stiffness, projectile stiffness, shape and mass.

Under impact loading, the failure mechanism observed in laminates follows a sequential progression characterized by five key phases in the following order: (i) initiation of matrix cracking and fibre/matrix interface debonding due to elevated transverse shear stresses primarily observed in the top layers; (ii) occurrence of transverse bending cracks triggered by intensified bending stresses predominantly in the bottom layers; (iii) development of interlaminar delamination stemming from cracks confined and diverted within the interlaminar region; (iv) manifestation of fibre failure under tension and fibre micro-buckling induced by compression loading, and lastly; (v) penetration. [4,6,8–10].

Widely employed as reinforcement, conventional carbon fibres exhibit diameters spanning several micrometers. These fibres are derived from petroleum-based precursors, notably high-strength polyacrylonitrile (PAN) and mesophase pitch (MPP). The preparation methods involve varied conditions, encompassing the choice of raw materials, the oxidation atmosphere employed, and the heat treatment temperatures, all of which contribute to the manufacturing process [11,12]. The main vantages associated with carbon fibres are high strength, high modulus and high strength-to-weight ratio. As a disadvantage, they are expensive and have poor performance under impact loading.

Among the various types of polymer matrices available for the manufacture of thermoset composites, epoxy resins are currently the first choice due to their desirable properties, especially in high-performance applications. The preponderant factor which makes epoxy resin suitable for application in composites are easy processing, good thermal, and dielectric properties, high mechanical strength, low shrinkage, resistance to corrosion, heat resistance, adhesion and low shrinkage upon cure [13,14].

To mitigate the performance of composites when subjected to LVI phenomena, researchers have explored advanced reinforcement architectures and matrix modifications. The use of 3D fibre reinforcement fabrics and the incorporation of nano-sized particles into the matrix can be used as effective strategies to improve the LVI performance of composites. 3D fibre reinforcement fabrics offer a significant advantage by incorporating fibres in the thickness direction, effectively stitching or weaving the layers together. These fabrics have fibres interwoven in three orthogonal directions, creating a more integrated structure with superior delamination resistance and higher damage tolerance compared to 2D laminates. Different weaving patterns (e.g., orthogonal, angle-interlock) can be tailored to optimize impact performance [15,16]. The incorporation of nano-sized particles, due to their high surface area to volume ratio and unique properties, can significantly influence the behaviour of the matrix at the micro- and nanoscale, leading to improved overall composite performance without compromising on density, toughness, or manufacturing process [17–19]. Nanoparticles can act as reinforcing fillers, increasing the

stiffness, strength and fracture toughness of the matrix, making it more resistant to cracking under impact loading [20]. The presence of nanoparticles can introduce additional energy dissipation mechanisms during impact, such as crack deflection, particle debonding and increased plastic deformation in the matrix [21]. Nanoparticles can act as crack growth inhibitors, preventing matrix crack propagation and delamination, thus limiting the extent of damage [22].

As one of the most promising and wide commercial availability and good property improvements/low-cost ratio, CNFs have been applied as random reinforcing materials in various polymeric systems, to highlight the reinforcement of composites. CNFs possess a distinctive one-dimensional (1D) cylindrical fibrous structure, characterized by lengths on the scale of micrometres and diameters ranging from tens to several hundreds of nanometres (50–200 nm). These nanofibres demonstrate an aspect ratio exceeding 100. Their cylindrical nanostructures exhibit various chemical configurations differing from graphene sheets, such as stacked platelet, herringbone, ribbon, stacked cup or thickened [11,23] CNFs are primarily synthesized through two key methodologies: catalytically vapor deposition growth and electrospinning techniques. Moreover, CNFs showcase a unique array of physical and chemical properties, notably including exceptional electrical conductivity, a large surface area, biocompatibility, distinctive chemical functionalities, and ease of fabrication. These attributes position CNFs as an ideal candidate for various applications aimed at enhancing and optimizing the properties of polymeric composite materials.

Several studies prove the advantages of adding CNFs, M. Hossain et al. [24] in your study, characterized 0.1 to 0.3 wt.% CNFs filled E-glass/polyester composites. LVI tests were performed at 10 J, 20 J, and 30 J energy levels, and it was concluded that the peak load was more in the composites reinforced with 0.2 wt.% CNFs as compared to the control laminate one, and absorbed energy decreased with the infusion of the CNFs. Another interesting conclusion was that the CNFs aided in reducing delamination in the earlier stage by arresting or blunting the crack tip, resulting in a smaller delamination area. A. Ravindran et al. [25] used CNFs and short carbon fibres (SCFs) at a concentration of 1 wt.% respectively in an epoxy matrix to for improving the LVI damage resistance in CFRP laminates. Hybridizing the CNFs with the SCFs improved the impact damage resistance, up to 24%, of the laminates at various impact energies, from 10 to 50 J.

A point less discussed in the open literature is the residual strength after LVI. A. Amaro et al. [26] study the influence of LVI on the residual strength of carbon epoxy laminates, with different stacking sequences under 1.5 J, 2 J, 2.5 J and 3 J impact energies. From the analysis of the experimental results, it is concluded that for higher values of impact energy, the residual strength decreases. Too, Z. Zhang et al. [27] investigated post impact structural integrity, of the LVI induced non-penetration damage in pultruded glass fibre reinforced polyester, under 6.4 J, 8.9 J, 11.5 J, 14.0 J, 16.6 J and 19.0 J impact energies. Subsequent bending property testing following impact, assessed through the 3PB tests, revealed a notable decrease in bending properties attributed to the damage induced from the impact. Furthermore, it was observed that the residual

bending strength is more susceptible to damage in comparison to the residual modulus, signifying differing degrees of susceptibility to impact-induced damage within the composite.

According to several authors, stress relaxation and creep phenomena within CFRP are observed even at room temperature (RT) and for stresses below their ultimate strength. These phenomena are attributed to molecular motion in backbone polymer arrangement [28,29]. Conversely, the fibre/matrix interface assumes significant importance as it regulates creep displacement by controlling bond breakage and their subsequent propagation. This control is critical, as carbon fibres exhibit minimal viscoelastic behaviour in comparison to the behaviour exhibited by the matrix material [30]. When the resin is nano-enhanced with a nano size material, the stress relaxation and creep mechanisms are much more complex, with the objective of decreasing these values in comparison with the control composites by increasing their specific stiffness. Finally, when the composite is subjected to an LVI, which can provoke delamination in its structure, its behaviour is unknown, as well as the response of the nanomaterial to this delamination effect, this phenomenon requires study and characterization to understand the behaviour and categories of these composites.

With regard to creep, impact events can induce microcracking, delamination and other forms of internal damage that can provide pathways for increased creep deformation under subsequent sustained loads [31,32]. The impact process can induce residual stresses within the material that can contribute to or accelerate creep deformation over time [33]. Impact-induced cracks in the viscoelastic polymer matrix can lead to localised stress concentrations, increasing creep in these regions [34]. Impact can weaken the fibre/matrix interface, potentially leading to increased creep as the matrix deforms and load transfer efficiency is reduced over time [35,36]. Similarly, and in terms of stress relations, impact damage can alter the ability of the material to stress relaxation. For example, cracks can hinder the redistribution of stress within the material over time [37]. LVI can cause changes in the stiffness and damping properties of the material, affecting the rate and extent of stress relaxation [38]. Damage at the fibre-matrix interface can modify how stress is transferred and relaxed within the composite structure [36]. The viscoelastic nature of the composite will cause the impact-induced dent to rebound over time, affecting the residual stress state and subsequent stress relaxation behaviour [39]. Y. Tong et al. [40] studied the relaxation of tensile stress for glass fibre reinforced polyvinyl-ester (GFRP) composite with or without LVI damage, induced by energies of 1.4 J, 5 J and 10 J. After testing, they concluded that the existence of LVI damage in the composite increases the overall relaxation and more relaxation was observed at higher impact energy.

The literature survey highlights the need for more comprehensive investigations into the impact response of CNFs composite, particularly concerning post-impact static and viscoelastic behaviour. In order to bridge this gap, the objective of the current study is the nano-enhanced of a commercial epoxy resin with different percentages, i.e., from 0.25 to 1wt.% of CNFs with the aim of optimizing the properties and impact damage tolerance of a laminated CFRP subject to

charging with various energy levels, manufactured using by hand lay-up process. Post impact structural integrity, of the LVI induced non-penetration damage, is studied through the residual static bending strength and the stress relaxation and creep behaviour are evaluated according to the severity of the damage induced after LVI. In an attempt to confirm the potential of the application of CNFs in maximizing LVI and post-impact, static and viscoelastic properties, a simple preparation and manufacturing technique was applied so that it can be implemented industrially.

10.2. Materials and experimental procedure

Composite laminates were produced by hand lay-up technique, which involved eight layers, all in the same direction, of bidirectional carbon fabric 195-1000P (195 g/m^2) and an epoxy matrix (resin SR 8100 and a hardener SD 8824) supplied by Sicomin. The resin was previously nano enhanced with CNFs and, for this purpose, the following weight contents were studied: 0, 0.25, 0.5, 0.75 and 1% wt.%. More details about the epoxy resin and CNFs can be found in [41].

CNFs were initially added to the resin and the mixture was conducted using a high-speed shear mixer at 1000 rpm for 3 hours at RT, followed by 10 minutes at 150 rpm to disperse the hardener into the nano-reinforced epoxy resin homogeneously. This process was combined with sonication (using an ultrasonic bath with a frequency of 40 kHz) and the bath temperature was controlled to improve the nanofibre' dispersion and not exceed the glass transition temperature (T_g) of the resin. Finally, before producing the laminates, the nano-reinforced matrix was degassed in a vacuum oven to remove any air bubbles introduced during the mixing process with CNFs. More details about the manufacturing process can be found in [42].

This procedure was used to produce plates with overall dimensions of 330 × 330 × 1.5 ± 0.1 (mm), which were subsequently cut to obtain, 100 × 100 × 1.5 mm^3 specimens for testing. To ensure a constant fibre volume fraction and uniform laminate thickness, the system was placed inside a vacuum bag, heat sealed and subjected to a 2.5 kN load in a hydraulic press during the curing time.

The curing of the laminates was followed according to manufacturer datasheet, first during 24 hours at RT and the post-cure at 40 ºC for more 24 hours. During the first 4 hours, the bag remained attached to a vacuum pump to eliminate any air bubbles present within the laminate.

These samples were, subsequently, subjected to impact tests carried out in accordance with ASTM D7136 standard and using an IMATEK-IM10 drop weight test machine. More details about the machine can be found in [43]. An impactor with a diameter of 10 mm and a mass of 2823.5 g was used. The tests were performed on square section samples of 75 × 75 mm^2 and the impactor stroke at the centre of the samples was obtained by centrally supporting the 100 × 100 mm^2 specimens. The impact energies used were 1 J, 3 J, 5 J, 7 J and 9 J, previously selected to avoid perforation of the specimens, Figure 10.1.a).

After the impact tests, the same specimens were tested to obtain the residual bending strength and the viscoelastic response in terms of stress relaxation and creep. For this purpose, a Shimadzu universal testing machine, model Autograph AG-X, was used, equipped with a 10 kN load cell. The residual bending strength was obtained according to the ASTM D790 standard and with a displacement rate of 2 mm/min and a span of 70 mm, Figure 10.1.b). According to the literature, this span was used for to ensure that damage caused by the low velocity impact is completely included between the lower supports. For example, Zhang et al. [27], studied the effect on the residual bending properties in pultruded glass fibre reinforced polyester composite with 4 mm of thickness and applied a span of 80 mm, also Santiuste et al. [44], studied the bending after impact behaviour of glass /polyester composite beams with 3 mm of thickness and used a 90 mm span.

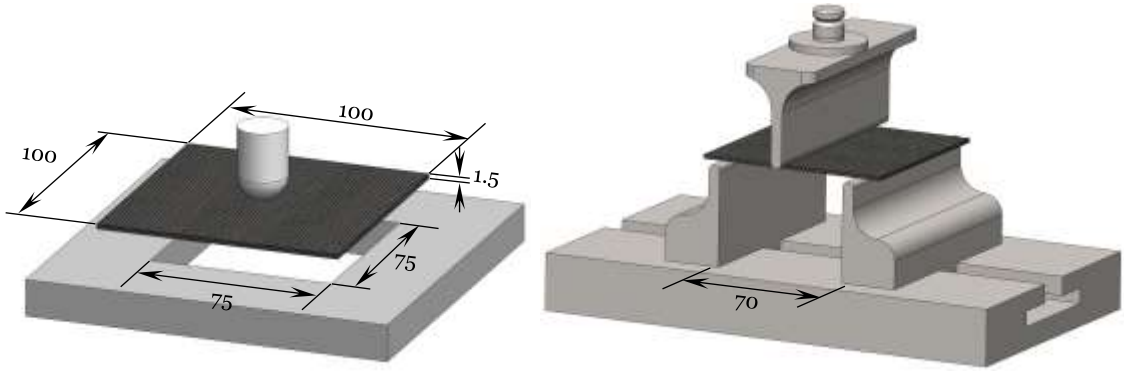

a) b)

Figure 10.1: a) Schematic specimen geometry and dimensions (mm) of LVI apparatus test; b) Three point bending test apparatus.

In terms of stress relaxation tests, they were performed in the same machine, at RT and in accordance with ASTM E328-13 standard. In this case, a fixed displacement was applied correspondent to 0.5% of the residual bending stress, and the stress was recorded during the loading time (180 min). On the other hand, the creep tests were performed also in the same machine, at RT and in accordance with ASTM D2990-09 standard. A fixed bending stress was applied (with equal value as previously reported) and the displacement was recorded during the loading time (180 min). The value used in both tests were selected to ensure that all viscoelastic tests were performed within the elastic regime and for each condition, five specimens were tested. The bending properties were obtained using the following equations:

$$\sigma = \frac{3\,P\,L}{2\,b\,h^2} \tag{10.1}$$

$$E = \frac{\Delta P\,L^3}{48\,\Delta u\,I} \tag{10.2}$$

$$\varepsilon_f = \frac{6\,S\,h}{L^2} \tag{10.3}$$

where P is the load, L the span length, b the width, h the thickness of the specimen, I the second moment of inertia of the cross-section, ΔP and Δu are the load range and bending displacement range, respectively, in the middle span for an interval in the linear region of the load versus displacement plot, and finally S is the deflexion. The bending modulus was obtained by linear regression of the load-displacement curves considering the interval in the linear segment with a correlation factor greater than 95%.

10.3. Results and discussion

10.3.1. Low-velocity impact

Figure 10.2 shows the load and impact energy tested at 9 J versus the time response of control laminate and nano-enhanced with 0.75 wt.% CNFs. These curves represent a typical behaviour for each laminate and agree with the bibliography [45,46]. From the curves, it is possible to observe that the highest values of energies promote smaller elastic recovery and, consequently, higher damages.

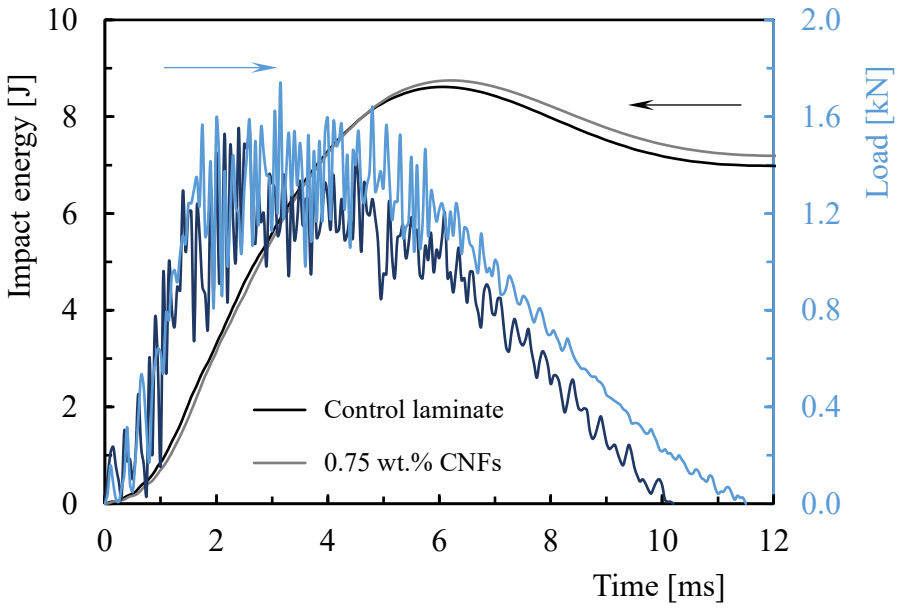

Figure 10.2: Typical curves load-time and impact energy-time of control laminate and laminate nano-enhanced with 0.75 wt.% CNFs tested at 9 J.

Impact tests were conducted, considering variables such as the percentage of CNFs added to the epoxy resin and the applied impact energy. The impact energy-time curves depicted in Figure 10.3.a), demonstrate a consistent behaviour observed across all laminates, encompassing various percentages of CNFs incorporated into the epoxy resin.

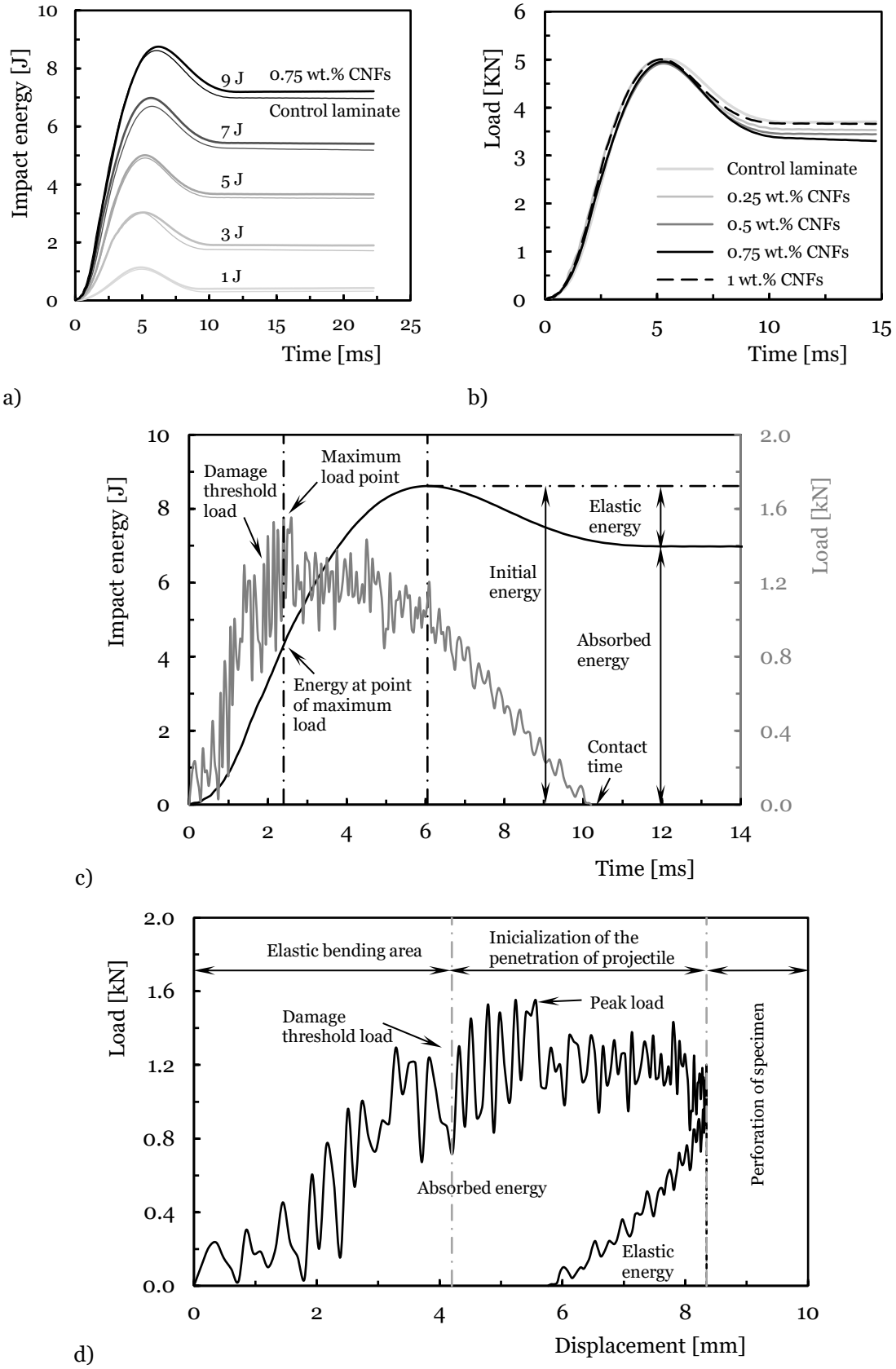

Figure 10.3: Typical curves: a) Impact energy-time of control laminates and nano-enhanced with 0.75 wt.% CNFs, tested to various impact energies; b) Impact energy-time of the different laminates in studies, tested at an energy of 9 J; c) Impact energy-time and load-displacement of control laminate tested at 9 J; d) Load-displacement of control laminate tested at 9 J.

Upon analysing both the control laminates and those with 0.75 wt.% CNFs, it was observed that all applied energy levels induced damage within the samples, albeit not visibly discernible to the naked eye. Even at the highest energy levels, a portion of the energy was allocated to damage formation, while another segment was absorbed by the elastic deformation of the material. This observation suggests the absence of perforation or penetration within the samples. CFRP are characterized as brittle materials, whereby a major portion of the imparted impact energy is utilized for elastic deformation and causing damage to the laminates [46].

Figure 10.3.b) show the representative curves load-time of the impact to different energies of the epoxy laminates with different wt.% CNFs, tested at 5 J, where it is possible to see that the variation of energy with time. The tracing of the curves turns out to be very similar and is guided by the increase in energy with time to a maximum value, later remaining constant after decreasing by a certain amount. The peak represents the impact energy, being the energy supplied to the laminate, and the decrease corresponds to the elastic recovery after impact. If the material were fully elastic, the curve would return to zero again. In this case, part of the impact energy was not elastically absorbed, translating into damage.

Figure 10.3.c) depicts two typical curves of LVI, impact energy-time curve and load-time of control laminate subject to impact energy of 9 J. The observation reveals that initially, the impactor's kinetic energy is entirely absorbed by the carbon laminate. However, during the latter phase of the tests, a fraction of the absorbed energy is discharged back to the impactor due to the carbon laminate's elastic resilience. Consequently, the ultimate energy absorption becomes lower than the initial impact energy. Comparable curves were obtained for the other experimental conditions being investigated.

The load-displacement curve of the control laminate subjected to 9 J quasi-static loading was generated, and it is represented in Figure 10.3.d). For the various laminates in the study, similar curves were generated for the different impact energies tested. We can divide this same curve into three parts, to better understand the mechanical events developed during this study. An initial part of the curve relates to the region of elastic deformation in the laminate due to the applied load which, depending on the impact energy, and the initiation of delamination and the matrix cracking can occur. An intermediate part, where in the beginning, a sudden drop in force corresponds to the matrix cracking due to the indenter impact, and during this section, delamination builds up. Two distinct events can occur: the elastic response of the laminate and its recovery, or the penetration of laminate is initiated and its stiffness of begins to retard. Finally, in the final stage and if penetration occurs, catastrophic damage and complete penetration occur. In this study, this phase is not verified, because the applied energies were not high enough for penetration to occur.

Figure 10.4.a) represents the impact energy-time curves of control laminates and laminates with 0.75 wt.% CNFs, for energies of 1 J, 5 J and 9 J.

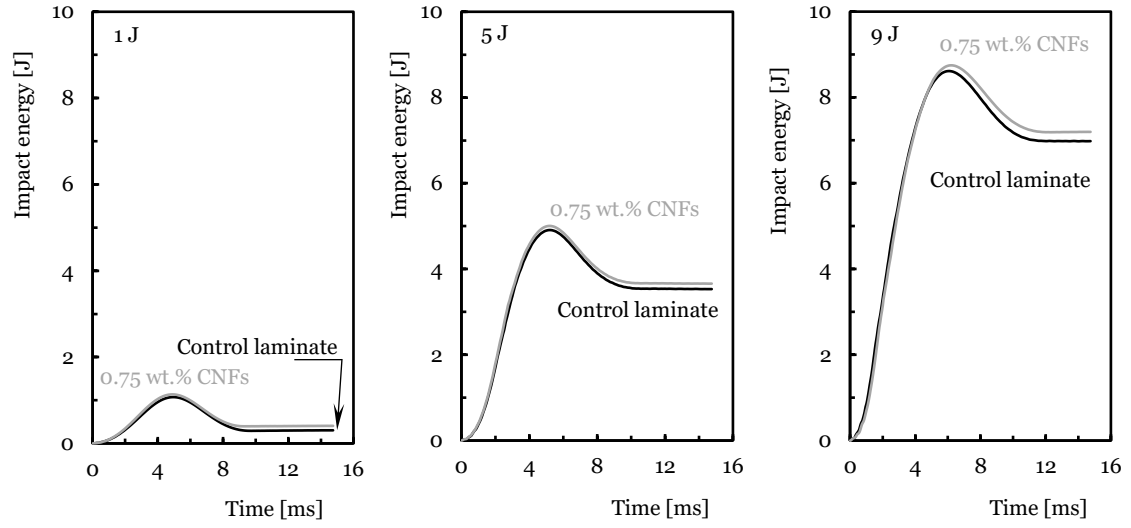

a)

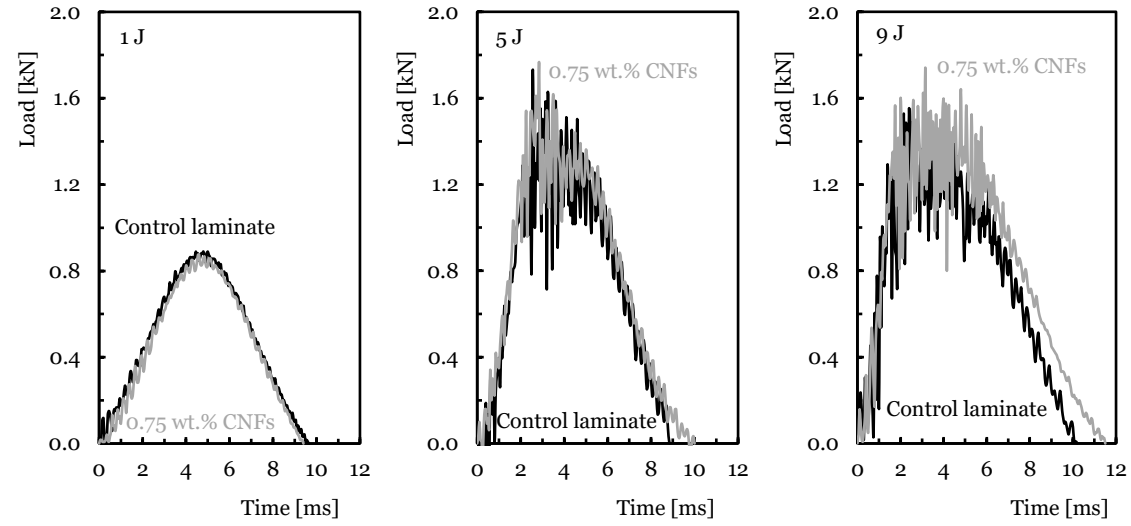

b)

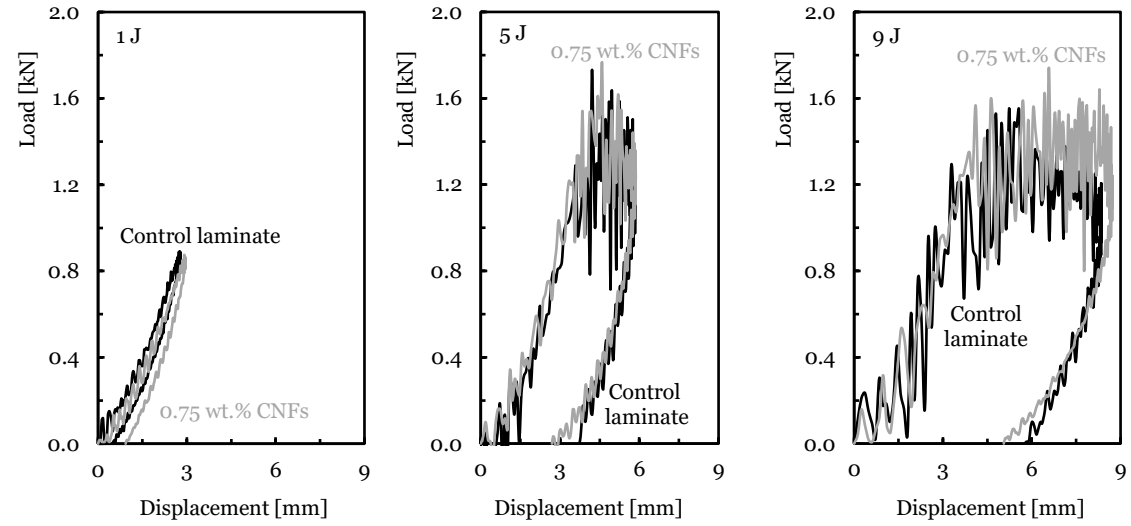

c)

Figure 10.4: Control laminate and with 0.75 wt.% CNFs, tested with 1, 5 and 9 J impact energies, curves: a) energy vs time; b) load vs time; c) load vs displacement.

The observed trend indicates that as the impact energy increases, there is a corresponding reduction in the material's elastic recovery, leading to an escalation in damage. The onset of the curve's plateau aligns with the point where contact between the impactor and the specimen are lost. Therefore, this particular energy value corresponds to the energy absorbed by the specimen.

Figures 10.4.b) and 10.4.c) show the load-time and load-displacement curves for the same laminates, subjected to the same impact energies. The curves exhibit oscillations believed to stem from elastic waves, as per existing literature. These oscillations are generated by the vibrations of the samples and are influenced by the stiffness and mass of both the specimen and impactor. They are induced by the rapid fluctuation of kinetic parameters at the moment of collision [47]. It is possible to observe that, the load increases up to a maximum value (P_{max}), followed by a drop after the peak load. The maximum load decreases with the addition of CNFs. For laminates subjected to 9 J impact energy, subsequent to reaching P_{max}, the load diminishes and stabilizes, while the duration of impact prolongs. These curves indicate the emergence of substantial damage but still within the realm of non-perforating impact events. The impact energy, in this case, was insufficient to penetrate entirely through the material.

Consequently, across all energy levels tested, the impactor induced damage to the laminate surface; however, it consistently rebounded without achieving complete penetration. These curves of Fig 10.3, represent a typical behaviour that occurred for all laminates and agree with the bibliography [46,48,49].

On the other hand, according to the figures, the value of P_{max} is very dependent on the impact energy. As shown in Figure 10.5.a), and mentioned by several authors, the maximum load increases with increasing impact energy [50,51]. Increases, between 1 and 9 J, were observed around 91.9% and 102.5% for control laminate and laminates with 0.75 wt.% CNFs, respectively. The addition of CNFs promoted major maximum impact loads with values, relative to the control samples, around 3.5% higher for 1 J and 9.2% for 9 J.

Another significant evidence from Figure 10.5.a) is the increase of the peak load observed up to an impact energy of 5 J, for both the control laminate and the 0.75 wt.% CNFs composite. Beyond this threshold, the impact energy does not exhibit a substantial influence on the maximum load. Intriguingly, after major damages, the maximum load appears to exhibit a linear increment with rising impact energy [45,51]. Similar results were obtained for laminates, nano-enhanced with other wt.% CNFs.

In both laminates, the increase follows an exponential law, where the maximum load increases around 82% between the energies of 1 J and 5 J and only around 5.4% between 5 J and 9 J for the control laminate and 90.1% and 6.5% at the same intervals for the laminate with 0.75 wt.% CNFs and with a correlation coefficient quite high, in line with the bibliography [51].

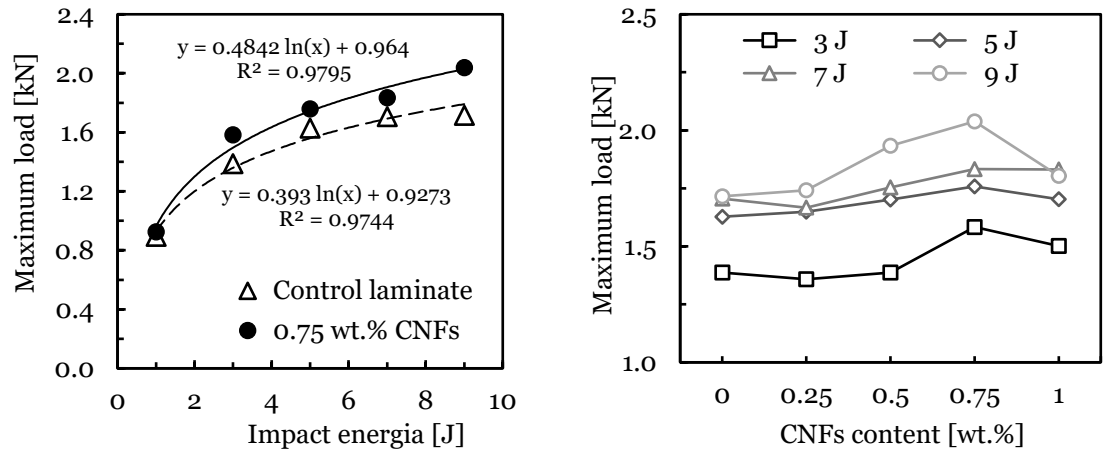

a) b)

Figure 10.5: a) Evolution of the maximum average load with the impact energy; b) Average maximum load vs. CNFs content curves of laminates.

Except for the 1 J impact energy, whose maximum load results do not change, regardless of the wt.% CNFs added, Figure 10.5.b) give the maximum load of all contents of the composite laminates nano-enhanced with CNFs, tested at different impact energies. The 0.75 wt.% sample owns the highest P_{max}, which represents higher impact resistance. It is concluded that, around 0.75 wt.% that the impact resistance improvement effect of CNFs to CFRP composite laminates reaches a maximum level.

In all cases, the maximum contact time between the impactor and samples, as depicted in Figure 10.6, was approximately 1.6% greater, for the control laminate across all impact energy levels in comparison to the specimens containing 0.75 wt.% CNFs.

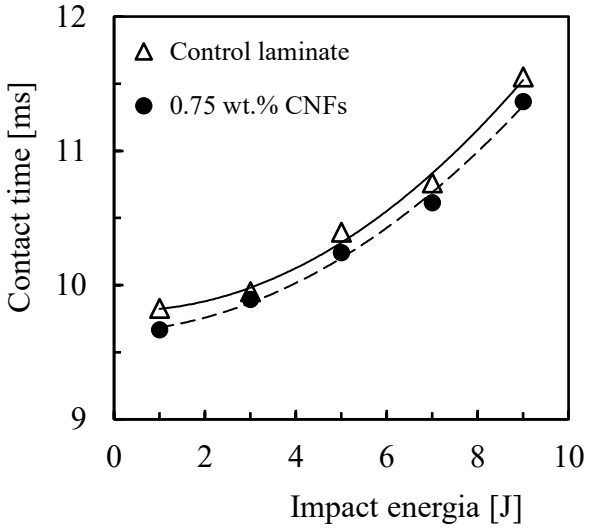

Figure 10.6: Evolution of the contact time with the impact energy.

The trend of displacement concerning impact energy is depicted in Figure 10.7.a) where, when CNFs are added to the neat resin, the displacements decrease around 11.5% and 9.0%,

respectively, for impact energies of 1 J and 9 J. However, in the energy range studied, the displacements increase around 183.8% and 190.4%, respectively to 1 J and 9 J, for the control laminate and the laminate with 0.75 wt.% CNFs. Figure 10.7.b) shows us the displacement of all nano-enhanced laminates with different wt.% CNFs tested with various impact energies. For all energies, the samples with 0.75 wt.% CNFs is the one with the smallest displacement regardless of the impact energy. It is also evident that for all impact energies, with the increasing percentage of CNFs up to 0.75 wt.% CNFs, the displacement decreases, and for 1 wt.% CNFs it increases, which shows that 0.75 wt.% is the optimal percentage of CNFs.

Figure 10.8.a) provides a comparison of elastic recovery among laminates exposed to different impact energy levels. Elastic energy, computed as the discrepancy between absorbed energy and energy at peak load [52,53] was averaged and presented as percentages. The data indicates that higher impact energies correspond to reduced elastic recovery and subsequently, more pronounced damage. Additionally, the incorporation of CNFs yields amplified effects, with the optimal outcome observed at a content of 0.75 wt.% CNFs. In both laminates, the increase follows a polynomial law of grade two and with a correlation coefficient high. Observing the Figure 10.8.b), it is evident that for all studied energies, the laminates with 0.75 wt.% CNFs are the ones with the higher percentage of elastic energy recovered. It is also evident that independently of the impact energies, with the increasing percentage of CNFs up to 0.75 wt.% CNFs, the percentage of elastic energy recovered increases, and for 1 wt.% CNFs these decreases.

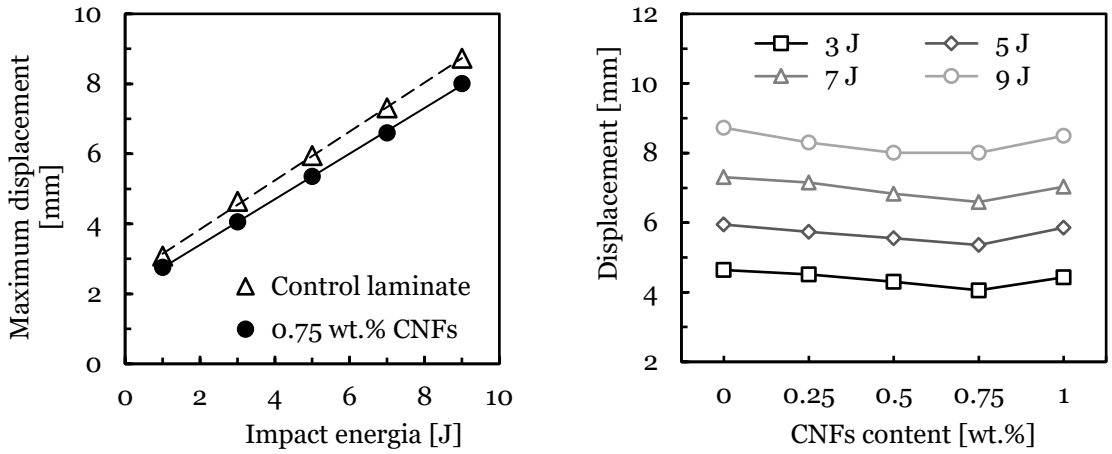

a) b)

Figure 10.7: a) Evolution of the maximum average displacement with the impact energy; b) Trend obtained for displacement vs. wt.% CNFs content of laminates and all impact energies in studied.

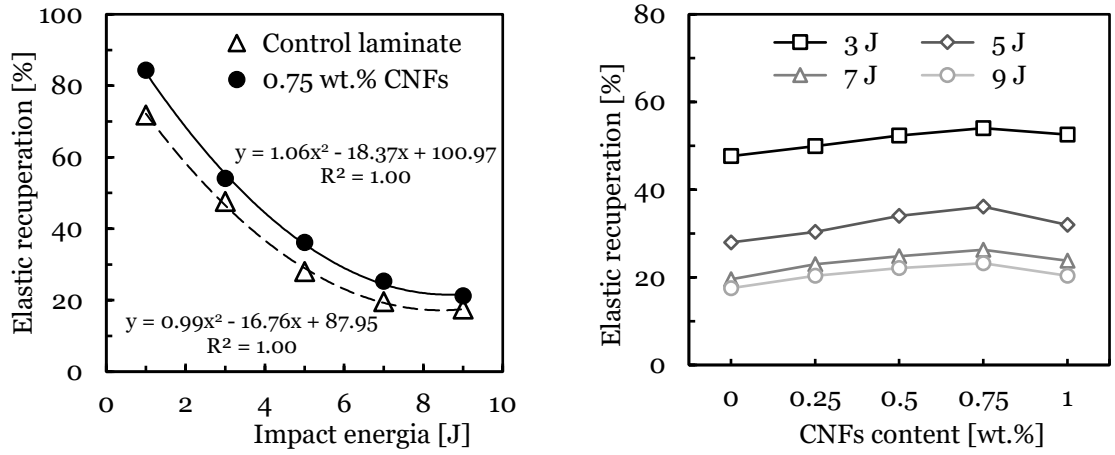

a) b)

Figure 10.8: a) Evolution of the average elastic recuperation with the impact energy; b) Trend obtained for elastic recuperation vs. wt.% CNFs content of laminates and all impact energies in studied.

Figure 10.9 shows the energy profile diagram of the control laminate and laminate with 0.75 wt.%, the other laminates considered in this study have similar trend curves. In the diagram, an equal-energy line, represented by a diagonal, is introduced as a reference for energy absorption capability. The plotted data points for each laminate are close and consistently lie beneath the equal curve. This alignment suggests that the absorbed energy is less than the impact energy, indicating that the penetration threshold has not been attained. In this context, the degree of damage is contingent upon the impact energy, while the surplus energy is utilized for the rebounding action of the impactor [54]. In the control laminate, at 1 J, 3 J, 5 J 7 J and 9 J impact energies, the absorbed energy was 0.31, 1.55, 3.50, 5.40 and 7.22 J, respectively, indicating a rise in the damage by incrementing the energy level. In the laminate with 0.75 wt.% CNFs, subject to the same impact energies, the absorbed energy was 0.27, 1.32, 3.33, 5.26 and 6.94 J, respectively. As suggested by [47,54], the data plotted in Figure 10.9 can be fitted, for each laminate type, by the equation $\Delta E = \alpha E_0^2 + \beta E_0 + \varepsilon$, where ΔE is the energy absorbed, E_0 is the impact energy and $\alpha, \beta, \varepsilon$, constants presented in Table 10.1.

According to the bibliography [54,55], identifying penetration thresholds involves representing the data points $E_e - E_i$ on a diagram and fitting them with polynomial equations. The roots of these equations signify the points where $E_i/E_a = 1$ ($E_e = 0$), with the higher roots indicating the penetration thresholds.

Figure 10.10 illustrates the penetration thresholds determined for all laminates, resulting in values of 12.94 J, 13.35 J, 13.75 J, 14.15 J, and 13.60 J, respectively, for control laminates, 0.25, 0.5, 0.75 and 1 wt.% CNFs. Polynomial fitting was conducted based on five impact energy values, revealing that the incorporation of fillers enhances the penetration threshold, resulting in improved performance. Specifically, the addition of 0.75 wt.% CNFs showcases approximately a 9.4% higher when 0.75 wt.% CNFs are added.

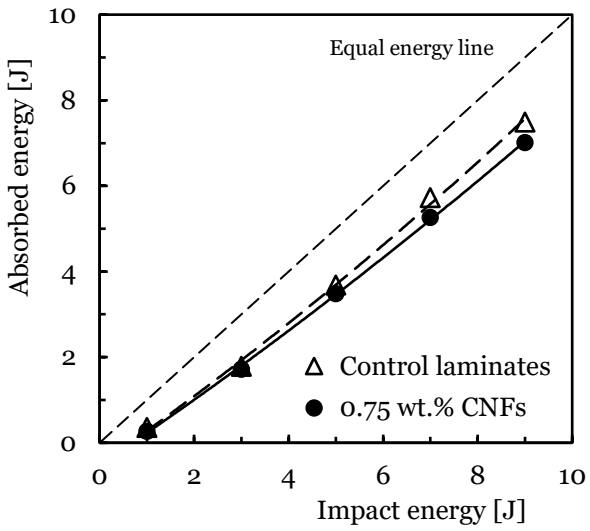

Figure 10.9: Energy profile diagram of the laminates tested.

Table 10.1: Constants of the equation $\Delta E = \alpha E_0^2 + \beta E_0 + \varepsilon$, for different laminates.

Laminate	α	β	ε
Control laminate	0.0145	0.7662	- 0.5001
Laminate + 0.25 wt.% CNFs	0.0128	0.7275	- 0.5439
Laminate + 0.5 wt.% CNFs	0.0129	0.7246	- 0.4642
Laminate + 0.75 wt.% CNFs	0.0112	0.7399	- 0.5194
Laminate + 1 wt.% CNFs	0.0231	0.6263	- 0.3864

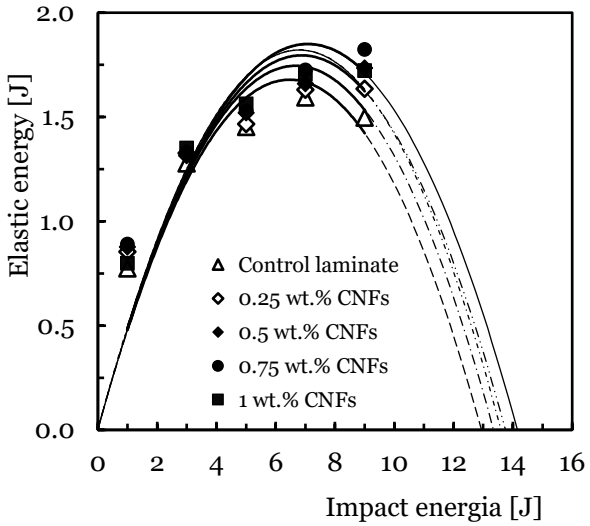

Figure 10.10: Identification of penetration threshold.

Photographs taken of the cross-section of the control laminates on impacted samples are shown in Figure 10.11. Even at this scale, it is possible to identify differences in the mode of damage

induced in the carbon laminates when different energy levels are applied. For impact energy of 1 J, in the transversal section of the laminate, it was not possible to identify any damage, even on the impact surface it is not easy to identify damage since the energy is considerably low.

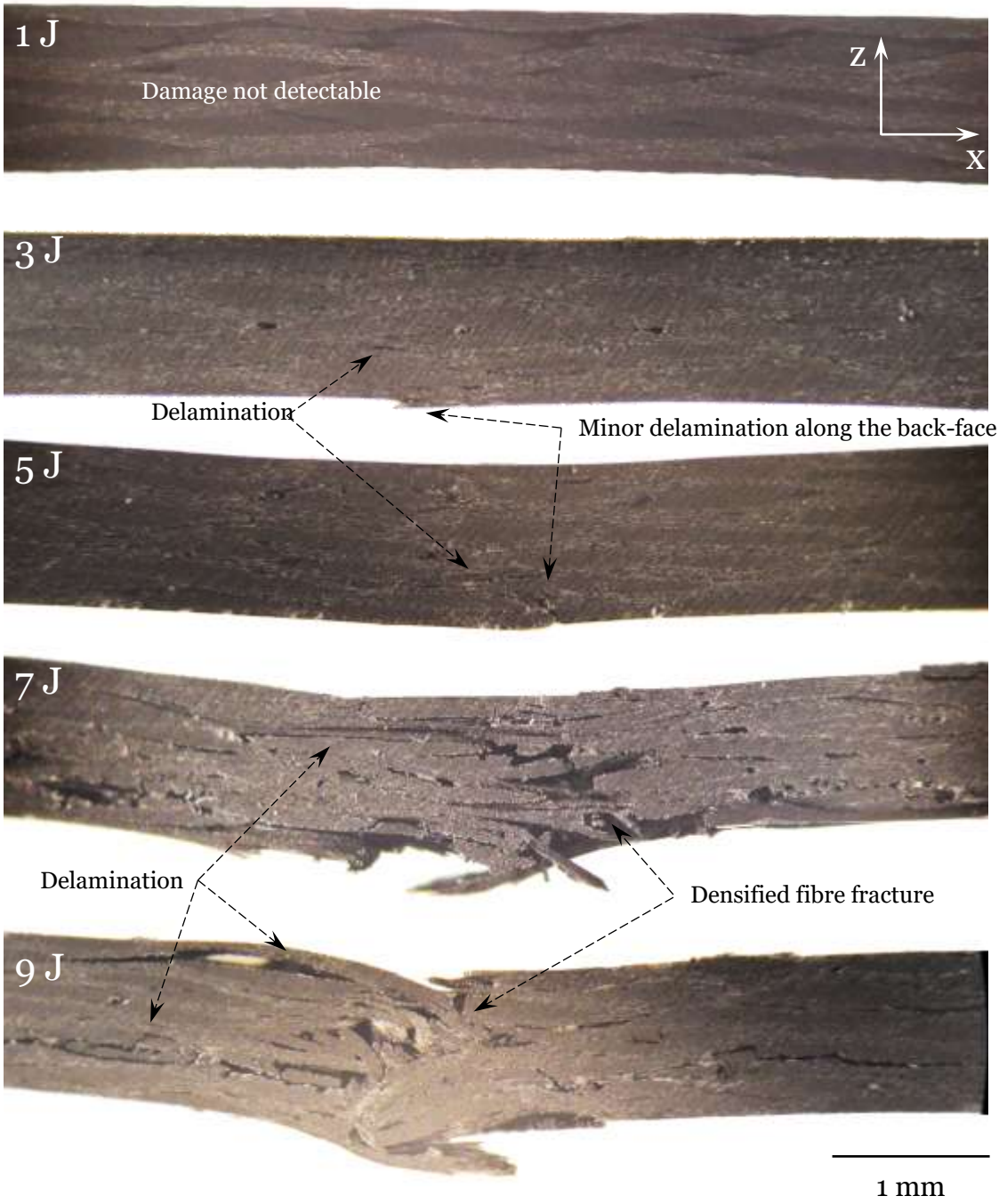

Figure 10.11: Cross-sectional optical images of the control laminates, subjected to different impact energies.

For energies of 3 J and 5 J, it is already possible to identify delamination between the intermediate layers of the laminate and minor delamination along the back face. These internal damages, which are not visible on the surface of laminates, decrease the composite properties and reduce the load-carrying capacity of the composite structure by more than 50% [6,56]. It is easy to identify a small

indent on the impact surface, typical for this energy level and reported in the bibliography. In the context of thin laminates, the initiation of matrix cracking typically commences at the lowermost layer and progresses towards the upper layer. This phenomenon occurs due to bending stresses exerted on the rear surface of the plate, resulting in distinctive patterns akin to an inverted cone or reversed pine-tree configuration [57].

At impact energies of 7 J and 9 J, significantly amplified damage is discernible within the transverse section of the laminate. This damage manifests prominently with the initiation of delamination at the cone's boundaries, fibre fracture, and matrix cracking, predominantly influenced by elevated transverse stresses imparted by the impactor. The indentation on the impact surface becomes prominently visible. As referenced by other authors, it is observed that laminates absorb energy through various mechanisms of damage creation, including delamination, matrix cracking, fibre fracture or pull-out, fibre-matrix debonding, and back-face fibre fracture [24].

10.3.2. Static characterization

3PB tests were conducted after impact across all tested energy levels. The objective was to assess the impact energy's influence on the bending characteristics of nano-enhanced laminates reinforced with CNFs in comparison to the control laminate. Figure 10.12.a) illustrates the stress-strain average curves obtained from the control laminate, employing a strain rate of 2 mm/min.

The Figure 10.12 shows the typical curves of the carbon laminates, initially a linear increase of the bending stress with the strain (linear elastic region) is observed, until the maximum bending load is reached, followed by a decrease in that same bending stress. Due to damage induced by the impact tests, the initiation of crack growth between the lamination layers led to a sudden decrease in load, resulting in the collapse of the laminates. The bending stress decreases by 11.3% and 59.7% when comparing the control laminate with the laminate subjected to impact energy of 1 J and 9 J, respectively. Similar behaviour is observed regarding the bending stiffness, as the impact energy to which the laminate was subjected increases, the stiffness value decreases considerably, as shown in Figure 10.12.b) where the average values (symbols) and respective maximum and minimum values (dispersion bands). The bending stiffness decreases by 1.1% when comparing the control laminate with the laminate subjected to an impact energy of 1 J, from 55.1 GPa to 54.5 GPa and 27.6% for an impact energy of 9 J, i.e., 43.2 GPa. In terms of bending strain for the control laminate, there is a reduction of 14.1% and 24.1%, when compared to laminates impacted with an energy of 1 J and 9 J, respectively, presenting a linear behavior as the impact energy increases, Figure 10.12.c). Similar behaviour is shown by the laminate with 0.75 wt.% CNFs, Figure 10.12.d), for an impact energy of 1 J, there is a decrease of 7.5% and 5.8% in terms of bending stress (from 806 MPa to 750.2 MPa) and bending stiffness (from 61.4 GPa to 58.0 GPa), respectively, when compared to laminate with the same unimpacted load. Comparing the laminate subjected to an impact energy of 9 J with the unimpacted laminate, there is a reduction of 60.6% and 35.0% in terms of bending stress and bending stiffness, respectively.

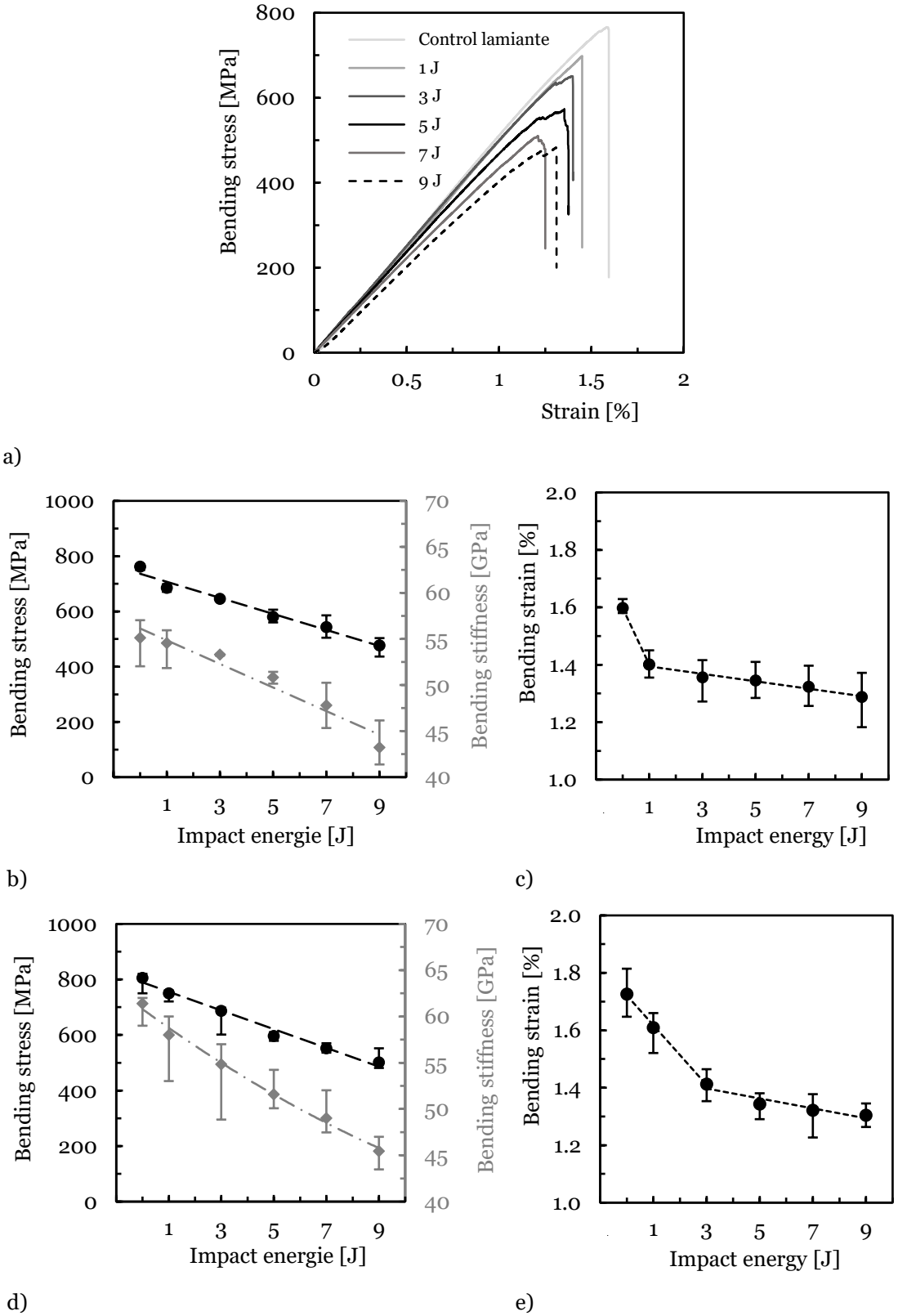

Figure 10.12: Pos-impact 3PB tests of carbon epoxy laminates: a) Typical curves of the control laminates; b) Bending stress and bending stiffness of the control laminates; c) Bending strain of the control laminates; d) Bending stress and bending stiffness of the laminates with nano-enhanced matrix with 0.75 wt.% CNFs; e) Bending strain of the laminates with nano-enhanced matrix with 0.75 wt.% CNFs.

For an impact energy of 1 J and 9 J, the reduction in bending strain was 7.2% and 32.4%, compared to the unimpacted nano-enhanced laminate, Figure 10.12.e). The decrease in bending strain is more pronounced for impact energies between 1 J and 5 J, stabilizing for impact energies between 5 J and 9 J, due to the accumulation of surface and internal damage along the section of the laminates subjected to higher impact energies (Figure 10.12.e)).

10.3.3. Viscoelastic behaviour

Figure 10.13 compares the stress relaxation behaviour for the control laminates after being subjected to different impact energies. For each condition, at least three valid tests were considered, and it is possible to view the average curve, the maximum, and minimum values and the obtained for each condition analysed, after three hours of the test, subject to bending stress of 375 MPa. From the observation of the figure, it can be concluded that the laminate that best responded to stress relaxation was the control laminate, because, unlike laminates subject to impact energy, this laminate does not have any surface or interior damage, and as the impact velocity increases, the stress relaxation of the material also increases. For example, the stress at the end of three hours is 371.8, 371.3 and 366.3 MPa for the control laminate, and laminates subjected to impact energies of 1 J and 9 J, respectively, i.e., a decrease of 0.9%, 1.0% and 2.3%, respectively. The impact energy directly influences the laminate's response to stress relaxation due to introduced damage.

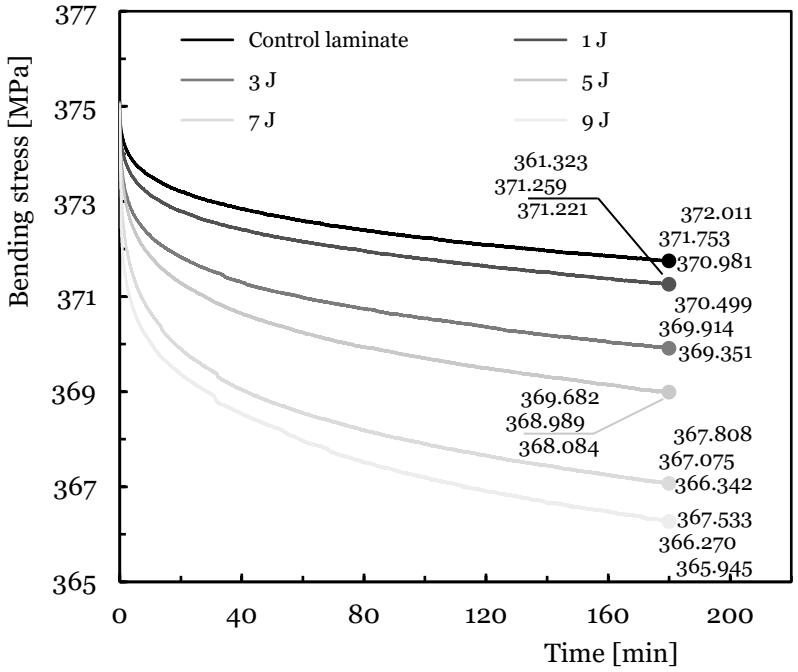

Figure 10.13: Stress relaxation control laminate after LVI Sicomin epoxy matrix.

A similar study was carried out on laminates with nano matrix with different weight percentages of CNFs, subjected to an intermediate impact energy of 5 J and to a bending stress of 375 MPa and compared with the control laminate, Figure 10.14. After three hours, and for an impact energy of 5 J, the stress relaxation of the control laminate and the laminate with 0.25 wt.% CNFs,

increases in both materials from an initial bending stress value of 375 MPa to a final value of 369.0 and 367.9 MPa, respectively. When the value of CNFs rises to 0.5 wt.%, the response of the laminate to stress relaxation is greater, that is, the value after three hours is 368.2 MPa influenced by the presence of a higher percentage of CNFs. In the same sense, when the percentage of CNFs increases to 0.75 wt.%, the response of the laminate to stress relaxation is superior when compared to the lowest added percentages seen so far, with the value after three hours being 369.4 MPa, remaining just below the value of the control laminate, 371.5 MPa reference value, due to the laminate not having any damage mode. We can conclude that the stress relaxation response of the carbon composite nano-enhanced with 0.75 wt.% CNFs after being subjected to impact energy of 5 J is higher than the same laminate after suffering the same phenomenon, but without being nano-enhanced, that is, this optimal percentage of CNFs has a positive influence on the behaviour of the composite.

The creep behaviour of carbon laminates was also studied. Figure 10.15 plots the average displacement versus time, where the displacement is the result measured at any moment of test D divided by its first value D_0. As reported by Reis at al. [58], for all composites and conditions studied, there is an initial regime in which the displacement increased considerably in relation to the remaining time and from an initial value of D_0 to one expected to be constant, which is not achieved because this study focuses on short-term tests.

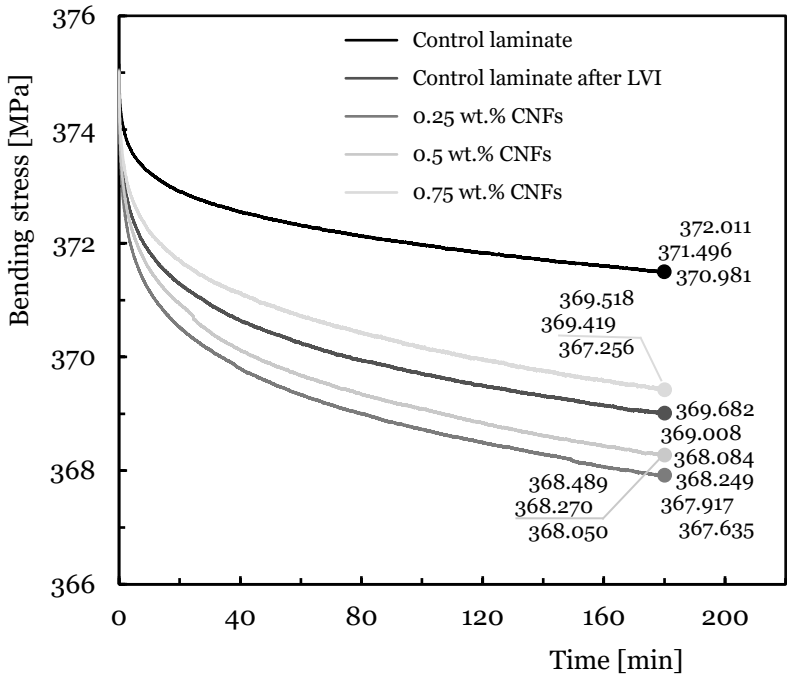

Figure 10.14: Stress relaxation after LVI energy of 5 J Sicomin epoxy matrix nano-enhanced with wt.% CNFs.

Figure 10.15 compares the creep behaviour for the control laminates after being subjected to different impact energies, and it is possible to view the average curve, the maximum, and minimum values and the obtained for each condition analysed, after three hours of the test,

subject to bending stress of 375 MPa. As with stress relaxation, the control laminate has a better response to creep, and as the impact energy increases, the creep value after three hours also increases, because the damage induced in the composite increases with increasing energy.

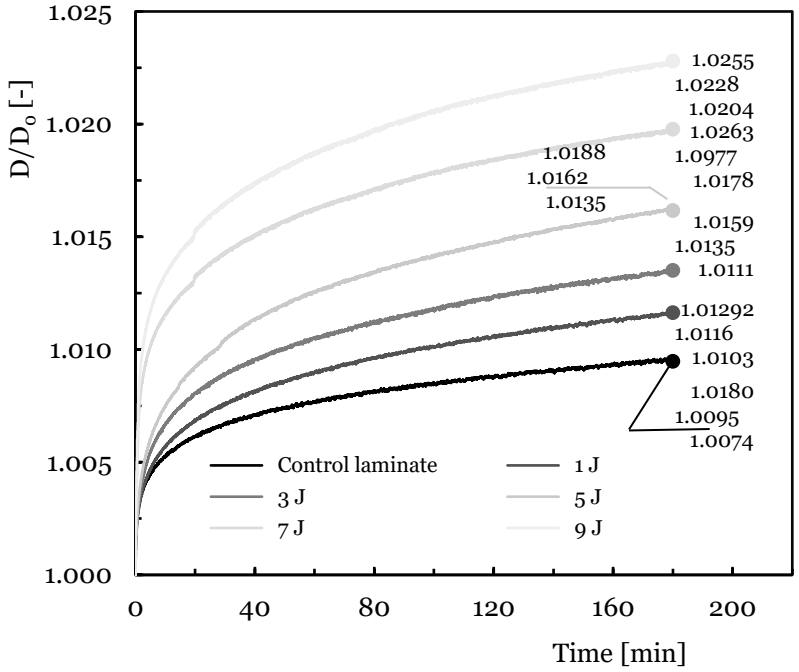

Figure 10.15: Creep control laminate after LVI Sicomin epoxy matrix.

Considering the control laminate, an increase of around 0.95% occurs after three hours, and for the same laminate subjected to an impact energy of 1 J, the value rises to 1.16%. Regarding the control laminate subjected to an impact energy of 9 J (higher energy), this value rises to 2.28%. The strong dependence of creep behaviour with the applied impact energy level to laminate is visible.

Finally, on the laminate's nano-enhanced with different weight percentages of CNFs, equally subjected to an impact energy of 5 J and then to a bending stress of 375 MPa, its creep behaviour was studied and compared with the control laminate, Figure 10.16. Taking as a reference the creep behaviour of the control laminate, given that it was the composite with the best response to this request, with a variation of 0.95%, in the opposite direction we have the same laminate subjected to an impact velocity of 5 J, with a variation of 1.62%, which would be expected given that damage was induced by the LVI action. With the addition of different wt.% CNFs to the matrix, the response of the material tends to improve, that is, the creep variation of the nano laminate with 0.25, 0.5 and 0.75 wt.% CNFs decreased to 1.46%, 1.17% and 1.07%, respectively.

Given the results, it is concluded that the creep response of the carbon composite nano-enhanced with 0.75 wt.% CNFs after being subjected to an impact energy of 5 J is less than the same laminate after suffering the same phenomenon, but without being nano-enhanced, that is, it is notorious that the addition of 0.75 wt.% CNFs significantly reduces creep behaviour of the composite.

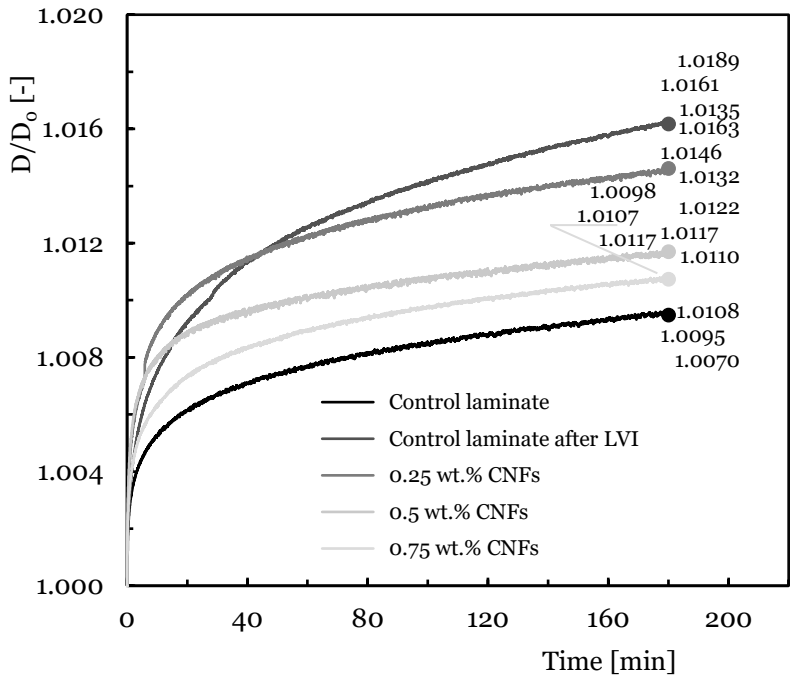

Figure 10.16: Creep after LVI energy of 5 J Sicomin epoxy matrix nano-enhanced with wt.% CNFs.

10.4. Conclusions

The main goal of this study is to assess the advantages conferred by an epoxy resin reinforced with the most effective percentage of CNFs when applied in the production of CFRP under low-velocity impact conditions.

The addition of CNFs to epoxy resin for manufacture of carbon laminates led to an augmentation in the maximum impact load, while conversely, a decrease in displacement was observed, indicating lower values with the inclusion of CNFs. The most favourable outcome concerning elastic recuperation was evident in laminates manufacture using epoxy matrix infused with 0.75 wt.% CNFs. Notably, for an impact energy of 9 J, the elastic recuperation of the CNFs nano-enhanced laminate exhibited an approximately 21.1% increase compared to the control laminate.

The residual strength after low-velocity impact in carbon epoxy laminates, decreases as after low-velocity impact increases, as expected. The bending stress and the bending stiffness, in the control laminate impacted at 1 J decreased by 11.3% and 1.1% respectively and for the energy of 9 J, this decrease is much more evident at 59.7% e 27.6%, respectively. The addition of 0.75 wt.% CNFs and for impact energy of 9 J, promoted an improvement of 5.2% and 5.3% in terms of bending stress and bending stiffness when compared to the control laminate subjected to the same impact energy.

As too expected, higher impact energies induce greater damage, which in turn will contribute to an increase in stress relaxation and creep. After experimental tests were carried out on laminates impacted (5 J) with 0.75 wt.% CNFs, their behaviour in terms of stress relaxation and creep

decreases compared to the control laminate, only there was no improvement when compared to the non-impacted control laminate.

Bibliography

[1] Zhang J, Lin G, Vaidya U, Wang H. Past, present and future prospective of global carbon fibre composite developments and applications. Composites Part B: Engineering 2023;250:110463. https://doi.org/10.1016/j.compositesb.2022.110463.

[2] Hamzat AK, Murad MS, Adediran IA, Asmatulu E, Asmatulu R. Fiber-reinforced composites for aerospace, energy, and marine applications: an insight into failure mechanisms under chemical, thermal, oxidative, and mechanical load conditions. Advanced Composites and Hybrid Materials 2025;8:152. https://doi.org/10.1007/s42114-024-01192-y.

[3] Kurşun A, Şenel M, Enginsoy HM, Bayraktar E. Effect of impactor shapes on the low velocity impact damage of sandwich composite plate: Experimental study and modelling. Composites Part B: Engineering 2016;86:143–51. https://doi.org/10.1016/j.compositesb.2015.09.032.

[4] Bouvet C, Rivallant S. Damage tolerance of composite structures under low-velocity impact. Dynamic Deformation, Damage and Fracture in Composite Materials and Structures, Elsevier; 2016, p. 7–33. https://doi.org/10.1016/B978-0-08-100080-9.00002-6.

[5] Habibi M, Laperrière L, Hassanabadi HM. Influence of low-velocity impact on residual tensile properties of nonwoven flax/epoxy composite. Composite Structures 2018;186:175–82. https://doi.org/10.1016/j.compstruct.2017.12.024.

[6] Richardson MOW, Wisheart MJ. Review of low-velocity impact properties of composite materials. Composites Part A: Applied Science and Manufacturing 1996;27:1123–31. https://doi.org/10.1016/1359-835X(96)00074-7.

[7] Razali N, Sultan MTH, Jawaid M. Impact damage analysis of hybrid composite materials. Durability and Life Prediction in Biocomposites, Fibre-Reinforced Composites and Hybrid Composites, Elsevier; 2019, p. 121–32. https://doi.org/10.1016/B978-0-08-102290-0.00006-4.

[8] Bull DJ, Scott AE, Spearing SM, Sinclair I. The influence of toughening-particles in CFRPs on low velocity impact damage resistance performance. Composites Part A: Applied Science and Manufacturing 2014;58:47–55. https://doi.org/10.1016/j.compositesa.2013.11.014.

[9] Tan R, Xu J, Sun W, Liu Z, Guan Z, Guo X. Relationship between matrix cracking and delamination in CFRP cross-ply laminates subjected to low velocity impact. Materials 2019;12. https://doi.org/10.3390/ma12233990.

[10] Andrew JJ, Srinivasan SM, Arockiarajan A, Dhakal HN. Parameters influencing the impact response of fiber-reinforced polymer matrix composite materials: A critical review. Composite Structures 2019;224:111007. https://doi.org/10.1016/j.compstruct.2019.111007.

[11] Huang J, Liu Y, You T. Carbon nanofiber based electrochemical biosensors: A review. Analytical Methods 2010;2:202–11. https://doi.org/10.1039/b9ay00312f.

[12] Meek N, Penumadu D, Hosseinaei O, Harper D, Young S, Rials T. Synthesis and characterization of lignin carbon fiber and composites. Composites Science and Technology 2016;137:60–8. https://doi.org/10.1016/j.compscitech.2016.10.016.

[13] Jayan JS, Saritha A, Joseph K. Innovative materials of this era for toughening the epoxy matrix: A review. Polymer Composites 2018;39:E1959–86. https://doi.org/10.1002/pc.24789.

[14] Li CP, Chuang CM. Thermal and dielectric properties of cyanate ester cured main chain rigid-rod epoxy resin. Polymers 2021;13:1–19. https://doi.org/10.3390/polym13172917.

[15] Bandaru AK, Patel S, Sachan Y, Alagirusamy R, Bhatnagar N, Ahmad S. Low velocity impact response of 3D angle-interlock Kevlar/basalt reinforced polypropylene composites. Materials & Design 2016;105:323–32. https://doi.org/10.1016/j.matdes.2016.05.075.

[16] Wang C, Su D, Xie Z, Zhang K, Wu N, Han M, et al. Low-velocity impact response of 3D woven hybrid epoxy composites with carbon and heterocyclic aramid fibres. Polymer Testing 2021;101:107314. https://doi.org/10.1016/j.polymertesting.2021.107314.

[17] Rahman MM, Hosur M, Hsiao K-T, Wallace L, Jeelani S. Low velocity impact properties of carbon nanofibers integrated carbon fiber/epoxy hybrid composites manufactured by OOA–VBO process. Composite Structures 2015;120:32–40. https://doi.org/10.1016/j.compstruct.2014.09.053.

[18] Mahdi TH, Islam ME, Hosur M V., Jeelani S. Low-velocity impact performance of carbon fiber-reinforced plastics modified with carbon nanotube, nanoclay and hybrid nanoparticles. Journal of Reinforced Plastics and Composites 2017;36:696–713. https://doi.org/10.1177/0731684417693429.

[19] Sarasini F, Tirillò J, Bavasso I, Bracciale MP, Sbardella F, Lampani L, et al. Effect of electrospun nanofibres and MWCNTs on the low velocity impact response of carbon fibre laminates. Composite Structures 2020;234:111776. https://doi.org/10.1016/j.compstruct.2019.111776.

[20] Ene L, Rafiee MA, Rafiee J, Wang Z, Song H, Yu ZZ, et al. Enhanced Mechanical Properties of Nanocomposites at Low Graphene Content. ACS Nano 2009;3:3884–90.

[21] Jen YM, Chen YJ, Yu TH. Improving the Impact Resistance and Post-Impact Tensile Fatigue Damage Tolerance of Carbon Fiber Reinforced Epoxy Composites by Embedding the Carbon Nanoparticles in Matrix. Polymers 2024;16. https://doi.org/10.3390/polym16243589.

[22] Nik Amrul Faaizol NAN, Mustapha M, Rejab NA, Vahabi H. Multi-walled carbon nanotubes/woven glass/epoxy hybrid nanocomposites: Effect of fabrication methods and types of epoxy matrices. Journal of Reinforced Plastics and Composites 2024. https://doi.org/10.1177/07316844241252321.

[23] Martin-Gullon I, Vera J, Conesa JA, González JL, Merino C. Differences between carbon nanofibers produced using Fe and Ni catalysts in a floating catalyst reactor. Carbon 2006;44:1572–80. https://doi.org/10.1016/j.carbon.2005.12.027.

[24] Hossain ME, Hossain MK, Hosur M, Jeelani S. Low-velocity impact behavior of CNF-filled glass-reinforced polyester composites. Journal of Composite Materials 2014;48:879–96. https://doi.org/10.1177/0021998313480194.

[25] Ravindran AR, Ladani RB, Kinloch AJ, Wang CH, Mouritz AP. Improving the delamination resistance and impact damage tolerance of carbon fibre-epoxy composites using multi-scale fibre toughening. Composites Part A: Applied Science and Manufacturing 2021;150:106624. https://doi.org/10.1016/j.compositesa.2021.106624.

[26] Amaro AM, Reis PNB, Moura MFSF. Residual strength after low velocity impact in carbon-epoxy laminates. Materials Science Forum 2006;514–516:624–8. https://doi.org/10.4028/www.scientific.net/msf.514-516.624.

[27] Zhang ZY, Richardson MOW. Low velocity impact induced damage evaluation and its effect on the residual flexural properties of pultruded GRP composites. Composite Structures 2007;81:195–201. https://doi.org/10.1016/j.compstruct.2006.08.019.

[28] Houshyar S, Shanks RA, Hodzic A. Tensile creep behaviour of polypropylene fibre reinforced polypropylene composites. Polymer Testing 2005;24:257–64. https://doi.org/10.1016/j.polymertesting.2004.07.003.

[29] Reis AK dos, Monticelli FM, Neves RM, de Paula Santos LF, Botelho EC, Luiz Ornaghi Jr H. Creep behavior of polyetherimide semipreg and epoxy prepreg composites: Structure vs. property relationship. Journal of Composite Materials 2020;54:4121–31. https://doi.org/10.1177/0021998320927774.

[30] Qiao P, Barbero EJ, Davalos JF. On the Linear Viscoelasticity of Thin-Walled Laminated Composite Beams. Journal of Composite Materials 2000;34:39–68. https://doi.org/10.1177/002199830003400103.

[31] Li S, Chen C, Zhang F, Yao X. Creep behavior of sandstone containing impact-induced microcracks. Mechanics of Time-Dependent Materials 2022;26:741–60. https://doi.org/10.1007/s11043-021-09510-3.

[32] Barreira-Pinto R, Carneiro R, Miranda M, Guedes RM. Polymer-Matrix Composites: Characterising the Impact of Environmental Factors on Their Lifetime. Materials 2023;16:1–61. https://doi.org/10.3390/ma16113913.

[33] Umarfarooq MA, Shivakumar Gouda PS, Veeresh kumar GB, Banapurmath NR, Edacherian A. Impact of process induced residual stresses on interlaminar fracture toughness in carbon epoxy composites. Composites Part A: Applied Science and Manufacturing 2019;127:105652. https://doi.org/10.1016/j.compositesa.2019.105652.

[34] Fancey KS. Viscoelastically prestressed polymeric matrix composites - Potential for useful life and impact protection. Composites Part B: Engineering 2010;41:454–61. https://doi.org/10.1016/j.compositesb.2010.05.002.

[35] Engelbrecht-Wiggans A, Phoenix SL. A stochastic model based on fiber breakage and matrix creep for the stress-rupture failure of unidirectional continuous fiber composites. vol. 217. Springer Netherlands; 2019. https://doi.org/10.1007/s10704-019-00359-9.

[36] Wu R, Wang XQ, Zhao D, Hou J ao, Wu C, Lau D, et al. Degradation of fiber/matrix interface under various environmental and loading conditions: Insights from molecular simulations. Construction and Building Materials 2023;390:131101. https://doi.org/10.1016/j.conbuildmat.2023.131101.

[37] Musthaq MA, Dhakal HN, Zhang Z, Barouni A, Zahari R. The Effect of Various Environmental Conditions on the Impact Damage Behaviour of Natural-Fibre-Reinforced Composites (NFRCs)—A Critical Review. vol. 15. 2023. https://doi.org/10.3390/polym15051229.

[38] Treviso A, Van Genechten B, Mundo D, Tournour M. Damping in composite materials: Properties and models. Composites Part B: Engineering 2015;78:144–52. https://doi.org/10.1016/j.compositesb.2015.03.081.

[39] Yousaf M, Zhou C. Numerical Study on the Rebound of Low-Velocity Impact-Induced Indentation in Composite Laminate. Aerospace 2022;9. https://doi.org/10.3390/aerospace9110651.

[40] Tong YJ, Xu LH, Li CQ. The stress relaxation of glass fibre composites with low velocity impact damage. Proceedings of the 1st Asia-Pacific Conference on FRP in Structures, APFIS 2007 2007;2:651–6.

[41] Pina dos Santos PS, Maceiras A, Valvez S, Reis PNB. Mechanical characterization of different epoxy resins enhanced with carbon nanofibers. Frattura Ed Integrità Strutturale 2020;15:198–212. https://doi.org/10.3221/IGF-ESIS.55.15.

[42] Santos P, Maceiras A, Reis PNB. Influence of manufacturing parameters on the mechanical properties of nano-reinforced CFRP by carbon nanofibers. IOP Conference Series: Materials Science and Engineering 2021;1126:012012. https://doi.org/10.1088/1757-899X/1126/1/012012.

[43] Amaro AM, Reis PNB, Magalhães AG, de Moura MFSF. The Influence of the Boundary Conditions on Low-Velocity Impact Composite Damage. Strain 2011;47:e220–6. https://doi.org/10.1111/j.1475-1305.2008.00534.x.

[44] Santiuste C, Sanchez-Saez S, Barbero E. Residual flexural strength after low-velocity impact in glass/polyester composite beams. Composite Structures 2010;92:25–30. https://doi.org/10.1016/j.compstruct.2009.06.007.

[45] Iqbal K, Khan S-U, Munir A, Kim J-K. Impact damage resistance of CFRP with nanoclay-filled epoxy matrix. Composites Science and Technology 2009;69:1949–57. https://doi.org/10.1016/j.compscitech.2009.04.016.

[46] Fakhreddini-Najafabadi S, Torabi M, Taheri-Behrooz F. An experimental investigation on the low-velocity impact performance of the CFRP filled with nanoclay. Aerospace Science

and Technology 2021;116:106858. https://doi.org/10.1016/j.ast.2021.106858.

[47] Reis PNB, ZhangFerreira JAM, Zhang ZY, Benameur T, Richardson MOW. Impact response of Kevlar composites with nanoclay enhanced epoxy matrix. Composites Part B: Engineering 2013;46:7–14. https://doi.org/10.1016/j.compositesb.2012.10.028.

[48] Suvarna R, Arumugam V, Bull DJ, Chambers AR, Santulli C. Effect of temperature on low velocity impact damage and post-impact flexural strength of CFRP assessed using ultrasonic C-scan and micro-focus computed tomography. Composites Part B: Engineering 2014;66:58–64. https://doi.org/10.1016/j.compositesb.2014.04.028.

[49] Körbelin J, Derra M, Fiedler B. Influence of temperature and impact energy on low velocity impact damage severity in CFRP. Composites Part A: Applied Science and Manufacturing 2018;115:76–87. https://doi.org/10.1016/j.compositesa.2018.09.010.

[50] Schoeppner GA, Abrate S. Delamination threshold loads for low velocity impact on composite laminates. Composites Part A: Applied Science and Manufacturing 2000;31:903–15. https://doi.org/10.1016/S1359-835X(00)00061-0.

[51] Reis PNB, Santos P, Ferreira JAM, Richardson MOW. Impact response of sandwich composites with nano-enhanced epoxy resin. Journal of Reinforced Plastics and Composites 2013;32:898–906. https://doi.org/10.1177/0731684413478993.

[52] Mortas N, Er O, Reis PNB, Ferreira JAM. Effect of corrosive solutions on composites laminates subjected to low velocity impact loading. Composite Structures 2014;108:205–11. https://doi.org/10.1016/j.compstruct.2013.09.032.

[53] Reis PNB, Ferreira JAM, Zhang ZY, Benameur T, Richardson MOW. Impact strength of composites with nano-enhanced resin after fire exposure. Composites Part B: Engineering 2014;56:290–5. https://doi.org/10.1016/j.compositesb.2013.08.048.

[54] Reis PNB, Ferreira JAM, Santos P, Richardson MOW, Santos JB. Impact response of Kevlar composites with filled epoxy matrix. Composite Structures 2012;94:3520–8. https://doi.org/10.1016/j.compstruct.2012.05.025.

[55] Aktaş M, Atas C, İçten BM, Karakuzu R. An experimental investigation of the impact response of composite laminates. Composite Structures 2009;87:307–13. https://doi.org/10.1016/j.compstruct.2008.02.003.

[56] Shah SZH, Karuppanan S, Megat-Yusoff PSM, Sajid Z. Impact resistance and damage tolerance of fiber reinforced composites: A review. Composite Structures 2019;217:100–21. https://doi.org/10.1016/j.compstruct.2019.03.021.

[57] Abrate S. Low-Velocity Impact Damage. Impact on Composite Structures, Cambridge University Press; 1998, p. 135–60. https://doi.org/10.1017/CBO9780511574504.005.

[58] Reis PNB, Silva MP, Santos P, Parente JM, Bezazi A. Viscoelastic behaviour of composites with epoxy matrix filled by cork powder. Composite Structures 2020;234:111669. https://doi.org/10.1016/j.compstruct.2019.111669.

Chapter 11

Conclusions and future works

11.1. Conclusions

The present work focused on the manufacture and laboratory maximisation of the mechanical and viscoelastic properties of two different commercial epoxy matrices with the addition of the respective weight percentages of optimised carbon nanofibres (CNFs). Based on the experimental results obtained, the same matrices were applied to the preparation of carbon fibre reinforced composites and various properties were also studied. In both cases, simple, low-complexity manufacturing techniques were used, which are easy to transfer and replicate on an industrial scale. After extensive characterisation, processing and analysis of the results, the following conclusions can be drawn:

- CNFs offer unique properties such as exceptional mechanical strength, electrical conductivity and ease of application, providing new ways to enhance the mechanical properties of laminate composites. With their high aspect ratio, lower density and increased modulus, strength and ductility compared to other nanoparticles, CNFs have potential as multifunctional reinforcements. The incorporation of an optimised amount of CNFs into epoxy matrices demonstrates a significant ability to improve the mechanical properties of composites, modifying the viscoelastic behaviour of both epoxy resins and laminates. This addition improves bending strength, interlaminar shear strength, fracture toughness and low-velocity impact resistance. The incorporation of CNFs at the optimum loading, up to 1 wt.%, is beneficial for industrial scale composite manufacture;

- Variables such as mixer rotation speed, CNFs dispersion time and vacuum time, both in the resin after preparation and in the laminate after manufacture, influence the mechanical properties of these materials, for example, the additional step of vacuum promoted improvements of 16.6%. The hand lay-up carbon woven laminate, when impregnated with epoxy resin nano-enhanced with the optimum percentage of CNFs, showed improved properties compared to the control laminate, in particular, improvements of over 16% in terms of bending stress and bending stiffness

- The optimum percentage of CNFs to be added to different commercial epoxy resins depends on their chemical, physical and mechanical properties. Higher percentages of CNFs added to the resin resulted in increased bending stress and bending modulus. As polymeric materials, both resins exhibited strain rate sensitivity regardless of the amount of CNFs added. Bending stress and modulus showed higher values at higher strain rates. Stress relaxation tests showed that

stress decreases with time; however, when CNFs are incorporated into the resins, they show reduced susceptibility to stress relaxation. In terms of creep response, displacement increases with time for all systems; however, the nanocomposites are more susceptible to creep in this scenario. For example, at a bending stress of 50 MPa, the stress relaxation after 180 min for neat Sicomin resin is about 10%, while for the same resin with 0.75 wt.% CNFs it is about 7.9%. For neat Ebalta resin this decrease is about 14.8% and for Ebalta resin with 0.5 wt.% CNFs it is about 13.2%;

- For both resins with different viscosities, an optimal CNFs content was identified that maximized the static properties. For the Sicomin SR 8100 resin, the optimum content was 0.75 wt.% of CNFs, while for the Ebalta AH 150 resin it was 0.5 wt.% of CNFs, in particular, promote higher relative bending stress, 11.5% for both and bending stiffness, 13.1% for Sicomin and 16.2% for Ebalta. Remarkably, the resin with lower viscosity (Ebalta resin) exhibited the highest bending stress and bending modulus due to better nanoparticle organization. This defied the expectation that higher viscosity resins would enhance mechanical properties with lower filler content, underlining the significant influence of nanoparticle-matrix compatibility on interfacial strength and dispersibility. That both creep behaviour and stress relaxation are highly load dependent, yet the incorporation of CNFs offered clear advantages by creating a network that restricted polymer chain mobility. The creep and stress relaxation results were accurately modelled using the Kohlrausch-Williams-Watts model, especially for longer times, while the Findley model showed better accuracy for shorter times in estimating creep behaviour;

- The incorporation of CNFs resulted in significant improvements in bending stress and stiffness of the carbon/epoxy laminates, although this was accompanied by increased brittleness as the bending strain decreased with higher filler content in both epoxy matrix, specifically, improvements in bending stress (20.4 and 12.5% for Sicomin and Ebalta, respectively) and bending stiffness (13.8 and 8.8% for Sicomin and Ebalta, respectively) were obtained with the incorporation of CNFs. The bending stress in all laminates increased with increasing strain rate, with those made with the Sicomin matrix showing less strain-rate sensitivity compared to the Ebalta matrix. For interlaminar shear strength (ILSS), the best results mirrored those for static bending, with ILSS being strain-rate sensitive across all laminates. Compared to the control laminates, the ILSS value is approximately 8.6% higher for those using the Sicomin resin reinforced with 0.75 wt.% CNFs, and approximately 9.4% higher for those using the Ebalta resin reinforced with 0.5 wt.% CNFs. Corrosive environments notably impacted ILSS responses, particularly in alkaline solutions, and the effect was dependent on solution concentration. Alkaline solutions induced a greater decrease in ILSS than acid solutions, with Sicomin matrix showing greater resistance than Ebalta matrix. The addition of CNFs caused a decrease in ILSS when compared to laminates with neat matrix. In addition, elevated temperatures caused a reduction in ILSS regardless of the epoxy matrix or environment, but the inclusion of CNFs mitigated this degradation;

- Stress relaxation and creep tests reveal a strong correlation between viscoelastic behaviour and applied stress levels in both matrices, with similar results for filled and control laminates. The inclusion of CNFs does not adversely affect the relaxation behaviour, suggesting that the nanoparticles interact with the matrix through interfaces, bridging segments, and junctions to carry loads without significantly limiting the mobility of the polymer chains. The viscoelastic response of carbon laminates reinforced with CNFs agrees well with the predictions of the Kohlrausch-Williams-Watts model and the Findley power law, demonstrating the accuracy of these models in describing the behaviour of the material. The application of these models also showed a good correlation between the experimental and theoretical results over long periods of time, demonstrating their applicability in predicting behaviour under stress relaxation or creep in service life situations, in all cases, with an error of less than 0.6%;

- In Mode I, the addition of CNFs significantly improved both strength and interlaminar fracture toughness, particularly in the Sicomin matrix, which consistently showed better mechanical properties. The optimum reinforcement level was 0.75 wt.% CNFs. However, at 1 wt.% CNFs, performance declined, probably due to difficulties in achieving uniform CNFs dispersion. The Ebalta matrix showed a similar trend, with a critical limit of 0.5 wt.% CNFs, above which mechanical properties were negatively affected, in particular, using different methods, the results showed significant improvements in Mode I (9.86%) and Mode II (23.9%) fracture toughness against Sicomin matrix, and Mode I (14.87%) and Mode II (21.78%) fracture toughness improvements against Ebalta matrix. The MCC method proved to be the most sensitive in detecting resistance to crack propagation, giving the highest $G_{IC,\text{prop}}$ values. In Mode II, CNFs reinforcement increased stiffness, ultimate load and fracture energy, although its effectiveness depended on the epoxy matrix used. The Sicomin matrix showed the best compatibility with CNFs, with continuous improvements up to 1 wt.% CNFs, while the Ebalta matrix performed optimally at 0.5 wt.% CNFs, but showed a deterioration in performance at higher concentrations. The MCC method also gave the highest G_{IIC} values, confirming its reliability in measuring crack propagation resistance;

- The low-velocity impact strength of the carbon control laminate and the epoxy nano-enhanced laminate with 0.5 wt.% CNFs (Ebalta matrix) were conducted at different energy levels, revealing that the impact properties such as maximum load, contact time, maximum displacement, and impact bending stiffness increased with higher energy levels for both laminates, with the nano-enhanced laminate showing superior performance. The absorbed energy also increased with energy level. For example, the maximum impact loads were approximately 8.8% higher for 5 J and 10.9% higher for 9 J and the impact bending stiffness was approximately 20.4% higher for 5J and 22.9% higher for 9J compared to the control samples. A subsequent multi-impact analysis based on impact energy was performed, yielding an SN fatigue curve where the number of impacts to failure is inversely correlated with impact energy. At an impact energy of 3 J, the nano-enhanced laminate with CNFs requires approximately 66 - 89 impacts to achieve full perforation, whereas the control laminates require only 17 - 20 impacts. The decreasing recovered energy with

increasing maximum impact load, and impact bending stiffness and maximum displacement highlighted the cumulative damage effect. A cubic polynomial fit was appropriate for lower impact energies, while a quadratic polynomial fit was appropriate for higher energies;

- The addition of CNFs increased the maximum impact load, and the opposite tendency was observed for the displacement, where the CNFs promoted lower values. The best performance in terms of elastic recuperation was obtained for laminates manufactured with epoxy matrix filled with 0.75 wt.% CNFs (Sicomin matrix). The residual strength of the carbon laminates decreased with increasing low-velocity impact energy, resulting in reduced bending stress and stiffness in the impacted control laminate. However, the inclusion of 0.75 wt.% CNFs resulted in improved bending stress and stiffness when compared to the control laminate at the same impact energy. For a laminate with 0.75 wt.% CNFs, there is a reduction in bending stress of 7.5% for an impact energy of 1J and a reduction of 60.6% for an impact energy of 9J. Higher impact energies caused more damage, contributing to increased stress relaxation and creep. After impact tests of laminates with epoxy matrix with 0.75 wt.% CNFs (5 J), the stress relaxation and creep behaviour was decreased compared to the control laminate, although no improvement was observed compared to the non-impacted control laminate;

- Notwithstanding the increase in complexity at specific points in the manufacturing process and the consequent rise in production costs, together with the cost of acquiring and applying CNFs and the analysis of experimental results, it is evident that the application of the ideal amount of CNFs, added to optimise different mechanical properties of commercial epoxy matrices and carbon laminates, which in some cases, the values obtained are found to be several tens of percentage points higher than those recorded in neat matrices and control laminates. This finding serves to provide a robust rationale for the implementation of these materials in a range of industrial sectors, with a particular emphasis on those applications that are either directly or indirectly contingent upon mechanical properties, the safety of the players and operators, the extension of the service life, and the augmentation of the time interval between corrective and/or predictive maintenance are but a few of the notable benefits that have been observed, i.e. in composite primary structures and safety components.

11.2. Future works

As future works, some tasks are proposed that will lead to better design specifications and optimisation of this type of laminate composites. To this end, it is recommended the following future work to be carried out in the short term:

- Numerical simulation - Experimental work should be supported by numerical studies, i.e. digital twins, in order to obtain results more economically and quickly. It is proposed to develop numerical tools capable of predicting the effect of reinforcement with different percentages of CNFs in the different types of characterisation;

- Mechanical characterisation of laminates in tensile and fatigue tests - Future studies should focus on a more detailed mechanical characterisation of CNFs reinforced carbon laminates through tensile and fatigue tests. This will help to understand the long-term durability of these materials under cyclic loading conditions and assess their suitability for structural applications where fatigue resistance is critical;

- Study of hygrothermal effects - The mechanical characterisation performed was carried out at room temperature, during service life, the behaviour/performance of advanced composite/structural materials is influenced by other variations such as temperature and humidity. Therefore, a study of the effect of these parameters on the static and viscoelastic behaviour of composites reinforced with CNFs other than those used in this work would be an interesting topic to develop;

- Prolonged chemical attack by other agents (salt water, various fuels, acids and/or bases) - It is essential to investigate the chemical resistance of CNFs enhanced laminates to prolonged exposure to aggressive environments such as salt water and various fuels. This will provide insight into their potential use in marine, aerospace and automotive applications where exposure to harsh chemicals is common;

- Non-destructive characterisation of epoxy matrices and laminates reinforced with different percentages of CNFs - Further studies should explore advanced non-destructive techniques to assess the structural integrity of epoxy matrices and CNFs reinforced laminates with different CNF concentrations. This will help to optimise the dispersion of the CNFs and assess their effect on the overall mechanical and physical properties of the composite;

- Characterisation of Mode I and Mode II interlaminar fracture toughness in CNFs reinforced CFRP at different temperatures and strain-rate - The investigation of Mode I and Mode II interlaminar fracture toughness at different temperature conditions and loading rates will provide a comprehensive understanding of the failure mechanisms of CNFs reinforced CFRP. This knowledge is crucial for improving the structural reliability of these materials in dynamic and extreme environments;

- Mode III of interlaminar fracture toughness, room temperature, varying temperature and under fatigue - Further studies should examine the interlaminar fracture toughness in mode III, evaluating the effects of temperature variations and fatigue loading. This will allow for a more complete characterization of delamination resistance in real-world applications;

- Low-velocity impact - A more in-depth analysis of low-velocity impact damage should be undertaken, focusing on damage quantification and the influence of environmental factors on impact and post-impact performance. In addition, a thorough study of the post-impact viscoelastic behaviour of CNFs reinforced laminates and their compression after impact (CAI) performance will improve the understanding of their mechanical resilience;

- Investigating electrical properties in the presence of nano-reinforcement - Future research should investigate the electrical properties of CNFs reinforced laminates to explore their potential in multifunctional applications, such as self-sensing materials and electromagnetic shielding. Understanding how nano-reinforcement affects electrical conductivity can open up new possibilities for smart composite structures.

- Investigate the synergistic effect of CNFs with other nanoparticles - For example graphene nanoplatelets, where the distance between the graphene nanoplatelet sheets can be controlled by the presence of CNFs rods.